TECHNISCHE UNIVERSITÄT MÜNCHEN
FAKULTÄT FÜR CHEMIE

Ligand-stabilized Silicon and Germanium Clusters: Prospect for Materials Synthesis

Lorenz Jakob Schiegerl

Vollständiger Abdruck der von der Fakultät für Chemie der
Technischen Universität München
zur Erlangung des akademischen Grades eines

Doktors der Naturwissenschaften (Dr. rer. nat.)

genehmigten Dissertation.

Vorsitzender: apl. Prof. Dr. Wolfgang Eisenreich

Prüfer der Dissertation:

1. Prof. Dr. Thomas Fässler
2. Prof. Dr. Dr. h.c. Bernhard Rieger
3. Prof. Dr. Antti Karttunen

Die Dissertation wurde am 8. Juli 2019 bei der Technischen Universität München eingereicht und durch die Fakultät für Chemie am 6. August 2019 angenommen.

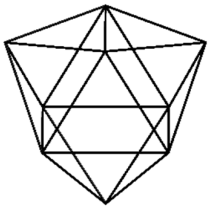

simplicity is the key to brilliance

„Wir verlangen, das Leben müsse einen Sinn haben – aber es hat nur ganz genau so viel Sinn, als wir selber ihm zu geben imstande sind."

– Hermann Hesse –

Diese Arbeit ist meinen Eltern gewidmet.

DANKGSAGUNGEN

Als Erstes danke ich **Prof. Thomas Fässler** für die Möglichkeit in seinem Arbeitskreis zu promovieren, sowie für die interessanten Themenstellungen und die stetige Unterstützung.

Ich bedanke mich bei den Mitgliedern der Arbeitskreise von **Prof. Thomas Fässler** und **Prof. Tom Nilges** für die Zusammenarbeit und die gemeinsame Zeit.

Mein besonderer Dank gilt:

- **Manuela Donaubauer** für ihre Geduld und die zahlreichen Hilfestellungen bei organisatorischen Angelegenheiten,

- **Kerstin Mayer** für die Betreuung meiner Masterarbeit und die stets angenehme Zusammenarbeit,

- **Felix Geitner** für produktive Zusammenarbeit im Rahmen des Silicium-Instituts,

- **Benedikt Witzel** für musikalische Untermalung der gemeinsamen Arbeit im Labor und die kollegiale Zusammenarbeit,

- **Wilhelm Klein** und **Viktor Hlukhyy** für die Geduld und Unterstützung bei kristallographischen Angelegenheiten,

- **Ingrid Werner** und **Christina Fischer** für die reibungslose Zusammenarbeit im Rahmen der Betreuung des Massenspektrometers,

- **Henrik Eickhoff**, **Michael Giebel**, **Christoph Wallach** und **Maria Müller** für Hilfestellungen in zahlreichen Angelegenheiten,

- **Ebru Üzer** und **Katharina Freitag** für Bereicherung der gemeinsamen Zeit im Büro,

- **Tassilo Restle** und **David Müller** für die Bereicherung der Mittagspausen mit angeregten Diskussionen,

- Meinen Mitstreitern **Kevin Frankiewicz**, **Brigita Bratic**, **Hussayn Ahmed**, **Simon Krebs**, **Michael Huber** und **Corvin Lossin** für Unterstützung und Zusammenarbeit.

Des Weiteren bedanke ich mich bei allen **Kooperationspartnern**, die mich während meiner Promotion unterstützt haben.

Mein besonderer Dank gilt:

- Der **WACKER CHEMIE AG** für die Aufnahme in das WACKER-INSTITUT FÜR SILICIUMCHEMIE. **Dr. Thomas Renner**, **Dr. Richard Weidner**, **Dr. Jan Tillmann und Dr. Elke Fritz-Langhals** für die nette Betreuung im Rahmen des Instituts und die interessanten Einblicke in die chemische Industrie.

- **Prof. Antti Karttunen** (AALTO UNIVERSITY, FINLAND) for the fruitful cooperation regarding computational studies and his outstanding support and patience.

- **Prof. Guy Bertrand** (UNIVERSITY OF CALIFORNIA, SAN DIEGO) for the opportunity to visit his group for a research stay. Further I thank his group members **Mohand Melaimi**, **Michèle Soleilhavoup** and **Daniel Tolentino** for the collaborative atmosphere and the support.

Mein weiterer Dank gilt allen Mitarbeitern der TECHNISCHEN UNIVERSITÄT MÜNCHEN, die meine Arbeit unterstützt haben.

Mein besonderer Dank gilt:

- **Prof. Wolfgang Eisenreich**, **Dr. Gabriele Raudaschl-Sieber** und **Maria Matthews** für zahlreiche Hilfestellungen im Rahmen von NMR Messungen,

- **Ulrike Ammari** für die stets zuverlässige und zeitnahe Messung von Elementaranalysen,

- **Meinen Kollegen im WACKER-INSTITUT FÜR SILICIUMCHEMIE** für die spannende Zeit sowie die Zusammenarbeit,

- **Prof. Shigeyoshi Inoue** für die Hilfestellungen und die Inspiration, sowie seinem Arbeitskreis für die Unterstützung und die kollegiale Zusammenarbeit.

Mein abschließender Dank gilt meinen Freunden und Bekannten.

Besonderer Dank gilt:

- meinen **Freunden aus der Heimat,** die mir stets zur Seite stehen und immer an mich glauben,

- All den **Freunden**, **die ich in München hinzugewinnen durfte**,

- meinen Freunden und ehemaligen Studienmistreitern **Sebastian Ghanbari**, **Jakob Timmermann**, **Manuel Rondelli** und **Severin Merget**.

Danke an meine Familie für die stetige Unterstützung und das Verständnis für all meine Entscheidungen.

Danke an die Wichtigsten: Meine Geschwistern **Anna** und **Clemens Schiegerl** und meine Eltern **Isabelle** und **Christoph Schiegerl**.

ABSTRACT

The utilization of the intermetallic precursors K_4Ge_9 and $K_{12}Si_{17}$ as cluster sources for material building blocks is central topic of this thesis. Silicon- and germanium-based materials are key components in nowadays high-tech industry and find application in a wide range of products as *e.g.* in electronics, batteries and photovoltaics. Due to increasing demand for novel material sources, synthetic access to preformed silicon and germanium structures, such as those contained in binary $K_{12}Si_{17}$ (1x Si_9^{4-} and 2x Si_4^{4-}) and K_4Ge_9 (1x Ge_9^{4-}) solids, is of central interest with focus on the synthesis of tailored cluster species with tunable properties for future use in fabrication. Such precursor materials can be obtained by simple fusing of the elements, and the utilization of K_4Ge_9 as a cluster source was developed during the last decades by the synthesis of cluster-based Ge_9 structures *via* reactions of K_4Ge_9 with *e.g.* chlorosilanes or alkynes. A transfer of such reactions to Si_9 clusters from $K_{12}Si_{17}$ has not been achieved before and was one central ambition of this work.

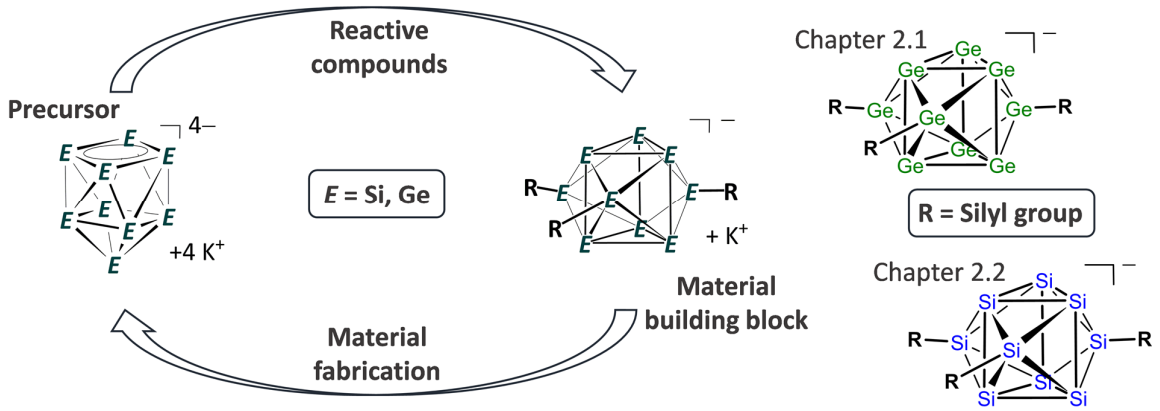

Herein, new silylation reactions of Ge_9 clusters from K_4Ge_9 were explored by reactions with SiR_3Cl/$SiHR_2Cl$ chlorosilanes in acetonitrile or thf. ESI-MS detections of $[(SiR_3)_3Ge_9]^-$ (R = Ph, ^{i}Bu, ^{i}Pr, Et) and Si–H-functionalized $[(SiHR_2)_3Ge_9]^-$ (R = Ph, ^{i}Pr) clusters extended the feasible cluster silylations. NMR (^{1}H, ^{13}C, ^{29}Si) investigations manifested the presence of $[(SiR_3)_3Ge_9]^-$ (R = Ph, ^{i}Bu) in bulk materials and confirmed the attachment of three covalently bonded silyl groups at a Ge_9 core. All species were obtained by single-step reactions in solution, which yielded stable species including Si–H silyl-functionalization.

The role of the electronic and steric properties of the silyl groups in obtained cluster compounds was revealed by silyl-ligand cleavage from $[(SiR_3)_3Ge_9]^-$ (R = Ph, ^{i}Bu) resulting in $[(Si^iBu_3)_2Ge_9]^{2-}$, and after subsequent reaction in form of the twofold copper-bridged metal complex $[Cu(P^iPr_3)]_4[(SiPh_3)_2Ge_9]_2$. The copper cluster complex bears a novel structural arrangement comprising η^1-, η^3- and η^4-coordination modes between clusters and copper atoms. Further cluster metal complexes were obtained in form of $[M(L)][\{Si(TMS)_3\}_3Ge_9]$ {$M(L)$ = $Cu(P^iPr_3)$, $Zn(Cp^*)$, Cu(carbene) with carbene = CAAC, MIC} and $[Cu(CAAC)]_2[\{Si(TMS)_3\}_2Ge_9]$. Au^+-bridged Ge_9 clusters were found in the molecular structure of $\{[K\text{-}18c6]\text{-}[Au\{(Si^iBu_3)_3Ge_9\}_2]\}_\infty$. The Ge_9 metal complexes are readily soluble in nonpolar solvents and accessible by simple reaction pathways in good yields. Metal- as well as ligand-depending divergences were found for the obtained structures by Ge–Ge bond elongations within the η^3-metal-coordinated prism faces of the Ge_9 cluster cores.

Comprehensive investigations of $K_{12}Si_{17}$ precursor material in solid-state allowed the measurement of ^{29}Si MAS NMR shifts for contained Si_4^{4-} and Si_9^{4-} clusters consistent with computational studies. Solubility experiments with $K_{12}Si_{17}$ showed the functioning of NH_3/222crypt precursor "*activation*" as the key step for the formation of soluble Si_9 clusters. "$K_{12}Si_{17}$ (*activated*)" was transferred to pyridine and ethylenediamine solutions under formation of $[H_2Si_9]^{2-}$ clusters, which were characterized by ESI-MS, Raman and NMR (^1H, ^{29}Si) experiments under usage of ^{29}Si-enriched precursor material. Investigations showed that $[H_2Si_9]^{2-}$ clusters boast outstanding properties with novel characteristics if compared to known molecular silicon species including a dynamic Si_9 core with deshielded hydrogen atoms, which are scrambling at the cluster surface.

NMR (^1H, ^{29}Si) and ESI-MS reactivity studies of $[H_2Si_9]^{2-}$ in ethylenediamine, aiming Si_9 cluster vinyl-functionalization with TMS-C≡C-TMS, indicated the formation of a $[(CH_2CH)_xSi_9]^{(4-x)-}$ species consistent with established reactions with Ge_9 clusters. Furthermore, the transfer of known silylation reactions from Ge_9 to Si_9 clusters succeeded by formation of the anionic siliconoids $[(ER_3)_3Si_9]^-$ {ER_3 = $Si(TMS)_3$, SiH^tBu_2, Si^iPr_3, $SnCy_3$,} in single-step reactions of "$K_{12}Si_{17}$ (*activated*)" with the respective chlorosilane and chlorostannane compounds in thf. ESI-MS and NMR (^1H, ^{13}C, ^{29}Si) investigations verified ligand-stabilized Si_9 cluster species bearing three covalently bonded -ER_3 groups and six ligand-free cluster atoms within a wide ^{29}Si NMR shift range of +18.0 to −361 ppm. Intrinsic bond orbitals analysis (IBO) confirmed delocalized species with multicenter (5centre-6e$^-$/3centre-2e$^-$) bonds. A reactivity experiment of the Si–H-functionalized $[(SiH^tBu_2)_3Si_9]^-$ cluster with (2-butene)Si^tBu_2 silirane indicated a synthetic modification by extension of the cluster reactant with four SiH^tBu_2 units to $[(Si(^tBu_2)_7Si_9]^-$ in ESI-MS.

Single crystals, which were obtained from crystallization of isolated $[(ER_3)_3Si_9]^-$ bulk materials, revealed the molecular structures of $[(ER_3)_2Si_9]^{2-}$ {ER_3 = $Si(TMS)_3$, SiH^tBu_2, Si^iPr_3, $SnCy_3$,}. The species form under loss of one of the respective cluster substituents along with partial cluster bond localization (IBO) and bear twofold negatively charged cluster surfaces. Si–Si bond length analysis of the structures showed elongations for the bonds that include ligand-free Si atoms in agreement with reported siliconoid clusters, and thus, a new synthetic protocol for the synthesis of siliconoid building blocks from a cluster precursor was firstly developed.

In a nutshell, the synthesis of cluster-based material building blocks from binary K_4Ge_9 was expanded and for the first time successfully transferred to $K_{12}Si_{17}$. Processing of the precursors yields tailored building blocks by simple synthetic procedures and offers a new prospect for the future fabrication of silicon- and germanium-based materials.

KURZFASSUNG

Die Nutzung der intermetallischen Precursoren K_4Ge_9 und $K_{12}Si_{17}$ als Clusterquellen für Materialbausteine ist zentraler Inhalt dieser Arbeit. Silicium- und germaniumbasierte Materialien sind Schlüsselkomponenten in der heutigen Hightechindustrie und finden Anwendung in einem breiten Produktspektrum, wie z.B. in elektronischen Geräten, Batterien und Photovoltaiken. Aufgrund der steigenden Nachfrage für neue Materialquellen ist der synthetische Zugang zu vorgeformten Silicium- und Germaniumstrukturen, wie sie in binären $K_{12}Si_{17}$ (1x Si_9^{4-} und 2x Si_4^{4-}) und K_4Ge_9 (1x Ge_9^{4-}) Festkörpern enthalten sind, von zentralem Interesse mit Fokus auf die Synthese maßgeschneiderter Clusterspezies mit abstimmbaren Eigenschaften für zukünftige Verarbeitungen. Solche Precursormaterialien können durch simples verschmelzen der Elemente erhalten werden, und die Nutzung von K_4Ge_9 als Clusterquelle wurde über die letzten Jahrzehnte durch die Synthese von clusterbasierten Ge_9-Strukturen, die aus Reaktionen von K_4Ge_9 mit beispielsweise Chlorsilanen oder Alkinen erhalten wurden, entwickelt. Der Transfer solcher Reaktionen zu Si_9-Clustern aus $K_{12}Si_{17}$ wurde zuvor noch nicht erreicht und war ein zentrales Ziel dieser Arbeit.

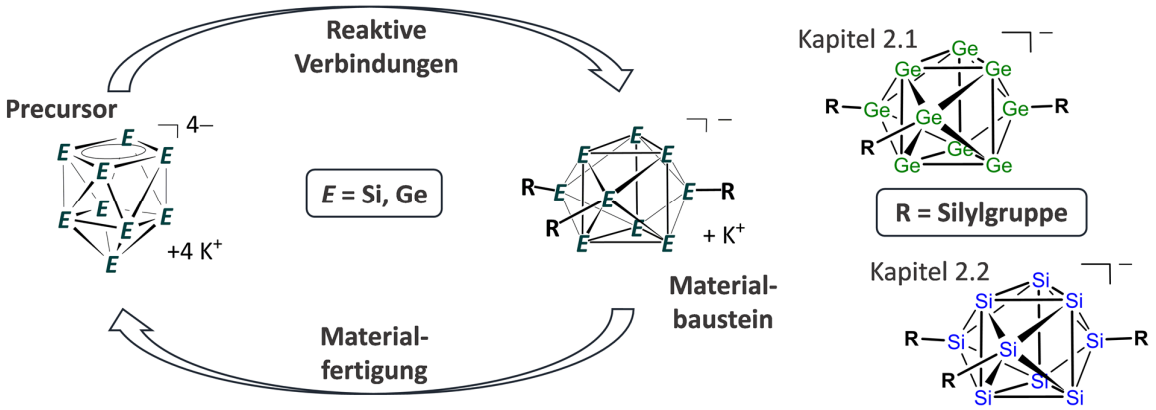

Im Rahmen dieser Arbeit wurden neue Silylierungen von Ge_9-Clustern aus K_4Ge_9 durch Reaktionen mit SiR_3Cl/$SiHR_2Cl$ Chlorsilanen in Acetonitril oder THF ergründet. Dazu erweiterten ESI-MS Nachweise von $[(SiR_3)_3Ge_9]^-$ (R = Ph, ^{i}Bu, ^{i}Pr, Et) und Si–H-funktionalisierten $[(SiHR_2)_3Ge_9]^-$ (R = Ph, ^{i}Pr) Clustern nutzbare Clustersilylierungen. NMR (^{1}H, ^{13}C, ^{29}Si) Untersuchungen manifestierten des Vorliegen von $[(SiR_3)_3Ge_9]^-$ (R = Ph, ^{i}Bu) in isolierten Feststoffen und bestätigten die Anbindung von drei kovalent gebundenen Silylgruppen an einem Ge_9-Kern. Alle Spezies wurden durch einstufige Reaktion in Lösung erhalten, wobei stabile Spezies einschließlich Si–H-Funktionalisierung hervorbracht wurden.

Ein Einfluss der elektronischen und sterischen Eigenschaften der Silylgruppen in erhaltenen Clusterverbindungen wurde durch Abspaltung eines Silylliganden von $[(SiR_3)_3Ge_9]^-$ (R = Ph, ^{i}Bu) unter Bildung von $[(Si^iBu_3)_2Ge_9]^{2-}$, sowie durch den nach Reaktion erhaltenen doppelt kupferverbrückten Metallkomplex $[Cu(P^iPr_3)]_4[(SiPh_3)_2Ge_9]_2$, identifiziert. Der Kupferkomplex bringt eine neuartige strukturelle Anordnung hervor, die η^1-, η^3- and η^4-Koordinationsmoden zwischen Clustern und Kupferatomen beinhaltet. Weitere Metallkomplexe wurden mit $[M(L)][\{Si(TMS)_3\}_3Ge_9]$ {$M(L)$ = $Cu(P^iPr_3)$, $Zn(Cp^*)$, Cu(Carben) mit Carben = CAAC, MIC} und $[Cu(CAAC)]_2[\{Si(TMS)_3\}_2Ge_9]$ erhalten.

Au^+-verbrückte Ge_9 Cluster wurden in der Molekülstruktur von $\{[K\text{-}18c6][Au\{(Si^iBu_3)_3Ge_9\}_2]\}_\infty$ gefunden. Die Cluster-Metallkomplexe sind löslich in unpolaren Lösungsmitteln und durch einfache Reaktionspfade in guten Ausbeuten verfügbar. Abweichungen innerhalb der gefundenen Strukturen zeigen metall- sowie ligandenabhängige Ge–Ge Bindungsverlängerungen in den η^3-metallkoordinierten Dreiecksflächen der Ge_9-Clusterkerne.

Umfassende Untersuchungen von $K_{12}Si_{17}$ Precursor-Material im Festkörper erlaubten die Messung von ^{29}Si MAS NMR Signalen für die enthaltenden Si_4^{4-} und Si_9^{4-} Cluster und deren Bestätigung mit rechnerischen Studien. Löslichkeitsexperimente mit $K_{12}Si_{17}$ zeigten, dass NH_3/222crypt Precursor-"*Aktivierung*" als der Schlüsselschritt für die Bildung löslicher Si_9-Cluster fungiert. "$K_{12}Si_{17}$ (*aktiviert*)" wurde unter Bildung einer $[H_2Si_9]^{2-}$ Spezies in Pyridin- und Ethylendiamin-Lösung überführt, die durch ESI-MS, Raman- und NMR- (^1H, ^{29}Si) Experimente mit Hilfe von ^{29}Si-angereichertem Precursormaterial charakterisiert wurde. Untersuchungen zeigten, dass $[H_2Si_9]^{2-}$ Cluster, im Vergleich zu bekannten Silicium-Molekülspezies, einzigartige Eigenschaften mit neuartigen Charakteristiken aufweisen, die einen dynamischen Si_9-Kern mit entschirmten Wasserstoffatomen die auf der Clusteroberfläche wandern, beinhalten.

NMR (^1H, ^{29}Si) und ESI-MS Reaktivitätsstudien in Ethylendiamin, die auf Si_9-Clustervinylierungen mit TMS-C≡C-TMS abzielten, deuteten die Bildung einer $[(CH_2CH)_xSi_9]^{(4-x)-}$ Spezies in Analogie zu etablierten Reaktionen mit Ge_9-Clustern an. Der Transfer bekannter Silylierungsreaktionen von Ge_9 zu Si_9 Clustern gelang durch den Aufbau der anionischen Siliconoide $[(ER_3)_3Si_9]^-$ {ER_3 = $Si(TMS)_3$, SiH^tBu_2, Si^iPr_3, $SnCy_3$,} mittels einstufiger Reaktion von "$K_{12}Si_{17}$ (*aktiviert*)" mit der jeweiligen Chlorsilan- und Chlorstannan-Verbindung in THF. ESI-MS und NMR (^1H, ^{13}C, ^{29}Si) Untersuchungen verifizierten ligandstabilisierte Si_9 Clusterspezies mit drei kovalent gebundene -ER_3 Gruppen und sechs ligandfreien Clusteratomen in einem weiten ^{29}Si NMR Verschiebungsbereich von +18.0 bis −361 ppm. Analyse der intrinsische Bindungsorbitale (IBO) bestätigte delokalisierte Spezies mit Multizentrenbindungen (5Zentren-6e^-/3Zentren-2e^-). Ein Reaktivitätsexperiment des Si–H-funktionalisierten $[(SiH^tBu_2)_3Si_9]^-$ Clusters mit dem Siliran (2-Buten)Si^tBu_2 deutete eine synthetische Modifikation mittels Erweiterung des Cluster-Reaktanten mit vier SiH^tBu_2 Einheiten zu $[(SiH^tBu_2)_7Si_9]^-$ in ESI-MS-Experimenten an.

Erhaltende Einkristalle von der Kristallisation isolierter $[(ER_3)_3Si_9]^-$ Feststoffe offenbarten die Molekülstrukturen $[(ER_3)_2Si_9]^{2-}$ {ER_3 = $Si(TMS)_3$, SiH^tBu_2, Si^iPr_3, $SnCy_3$,}. Die Spezies bilden sich unter jeweiliger Abspaltung eines Clustersubstituenten zusammen mit partieller Bindungslokalisierung im Clusterkern (IBO) und weisen zweifach negativ geladene Clusteroberflächen auf. Analyse der Si–Si Bindungslängen in den Strukturen zeigte Bindungsverlängerung für Bindungen die ligandfreie Si-Atome beinhalten, was in Übereinstimmung mit literaturbekannten Siliconoid-Clustern ist. Das zeigt, dass ein neuer Zugang zur Synthese von Siliconoid-Bausteinen, ausgehend von einem Clusterprecursor, entwickelt werden konnte.

Zusammengefasst wurde die Synthese von clusterbasierten Materialbausteinen aus intermetallischen K_4Ge_9 erweitert und zum ersten Mal auf $K_{12}Si_{17}$ übertragen. Precursorverarbeitung liefert maßgeschneiderte Bausteine durch einfache Reaktionen und bietet einen neuen Ausblick für die zukünftige Herstellung von silicium- und germaniumbasierten Materialen.

DECLARATION

This dissertation is written as publication-based thesis. The bibliographic data of articles published in peer-reviewed journals is compiled in chapter 6. In case of unpublished work, corresponding manuscripts are included as prepared *manuscripts for publication*. The relevance of this work for science and research, as well as the scope and outline, are presented as introductory part in chapter 1. The results and their discussion are presented in chapter 2, which is divided into the two sub-chapters 2.1 (Ge_9 clusters) and 2.2 (Si_9 clusters). The sub-chapters are structured as follows: i) review of relevant literature; ii) summary of the results of the corresponding manuscripts along with further information about investigations and discussions across the respective topics; iii) discussions of the sub-chapters on a broader scope. Summary and conclusions are given in chapter 3. The experimental section in chapter 4 gives details on the cooperation projects, assistances, as well as synthesis, chemicals and characterization of materials. The literature that is cited within this thesis is summarized in chapter 5. Content and contributions from co-authors as well as cooperation partners to the manuscripts are explicitly stated in the manuscript section in chapter 6.

TABLE OF ABBREVIATIONS

Abbreviation	Meaning	Abbreviation	Meaning
18c6	1,4,7,10,13,16-Hexaoxacyclooctadecane	MAS	Magic-angle spinning
222crypt	4,7,13,16,21,24-Hexaoxa-1,10-diazabicyclo[8.8.8]hexacosan	Me	Methyl
A	Alkali metal	Mes	1,3,5-Trimethylbenzene (mesityl)
Å	Angstrom [10^{-10} m]	MIC	Mesoionic carbene
CAAC	Cyclic(alkyl)amino carbene	NHC	*N*-heterocyclic carbene
Cp	Cyclopenta-1,3-diene	NHC^{Dipp}	1,3-Bis-(2,6-di-*iso*-propylphenyl)imidazole-2-ylidene
Cp^*	1,2,3,4,5-Pentamethylcyclopentadienyl	NMR	Nuclear magnetic resonance spectroscopy
Cy	Cyclohexyl	NP	Nanoparticle
Dipp	2,6-Di(*iso*-propyl)phenyl	Pentenyl	$–(CH_2)_3–CH=CH_2$
dppe	1,2-Bis(diphenylphosphino)ethan	Ph	Phenyl
E	Tetrel element	ppm	Parts per million
e^-	Electron	PXRD	Powder X-ray diffraction
EDX	Energy dispersive X-ray spectroscopy	R	Rest / Substituent
eq.	Equivalent	RT	Room temperature (25 °C)
ESI-MS	Electro spray ionization mass spectrometry	SC-XRD	Single crystal X-ray diffraction
Et	Ethyl	SPS	Solvent purification system
eV	Electronvolt	^{t}Bu	*tert*-Butyl
FT-IR	Fourier-transform infrared spectroscopy	thf	Tetrahydrofuran
HMBC	Heteronuclear multiple bond correlation	Tip	2,4,6-Tri-(*iso*-propyl)phenyl
^{i}Bu	*iso*-Butyl	TMS	Trimethylsilyl

TABLE OF ABBREVIATIONS

INEPT	Insensitive nuclei enhanced by polarisation transfer	UV/VIS	Ultraviolet-visible spectroscopy
^{i}Pr	*iso*-Propyl	Vinyl	–CH=CH_2
IR	Infrared spectroscopy	λ	Wavelength
J	*J*-Couplings (indirect dipole–dipole coupling)	*δ*	Chemical shift
L	Ligand	Δ	Difference
m/z	Mass-to-charge ratio	θ	Bragg angle

TABLE OF CONTENTS

1 INTRODUCTION

1.1 The Elements Silicon and Germanium

Silicon (symbol: Si; atomic number: 14) and germanium (symbol: Ge; atomic number: 32) are listed in the 14th group of the periodic table of elements (Figure 1). They are tetrel elements of the 3rd and 4th period, respectively, and thus, they are located in between the elements carbon and tin. Silicon was discovered in 1824 by *Jöns Jacob Berzelius*, germanium later in 1886 by *Clemens Winkler*. Both elements are non-toxic and silicon functions as an essential element for biological organisms, whereas germanium does not according to the current state of knowledge. Both are greyish crystalline semimetals with high melting points of 1414 °C (Si) and 937 °C (Ge).[1-2]

Period \ Group	13.	14.	15.	16.
2.	5 B Boron 10.881 2.0	6 C Carbon 12.011 2.6	7 N Nitrogen 14.007 3.0	8 O Oxygen 15.999 3.4
3.	13 Al Aluminum 26.982 1.6	14 Si Silicon 28.086 1.9	15 P Phosphorus 30.974 2.2	16 S Sulphur 32.065 2.6
4.	31 Ga Gallium 69.723 1.8	32 Ge Germanium 72.64 2.0	33 As Arsenic 74.922 2.2	34 Se Selenium 78.96 2.6
5.	49 In Indium 114.82 1.8	50 Sn Tin 118.71 2.0	51 Sb Antimony 121.76 2.1	52 Te Tellurium 127.60 2.1

Figure 1. Section of the periodic table of the elements (horizontal: groups 13–16; vertical: periods 2–5). Background coloration: metals in red, semimetals in orange, non-metals uncolored. Fonts: element's name, symbol and atomic number in black, standard atomic weights in blue, electronegativities in red (*Pauling* values). The elements silicon and germanium are highlighted in a black frame.[2-3]

The content of silicon and germanium in the earth's crust is determined with 26.3 mass percent (Si) and 0.00014 mass percent (Ge), respectively. Thereby, silicon is the second most abundant element behind oxygen (48.9 mass percent).[4] Oxidation states of −4 to +4 are known for both elements, in nature silicon occurs mainly as oxide compounds due to its high oxophilicity and germanium mostly as sulfide compounds. The elements Si and Ge are semimetals and appear primarily as α-modifications with a diamond-cubic crystal system. Therein, the Si–Si bond lengths are clearly

shorter with 2.35 Å if compared to the Ge–Ge bonds with 2.45 Å, most conclusively due to the smaller atomic radius of silicon. Si consists naturally of the three stable isotopes ^{28}Si, ^{29}Si and ^{30}Si with an abundancy ratio of 92.2 : 4.67 : 3.10% (^{28}Si:^{29}Si:^{30}Si), thereof, the ^{29}Si isotope is detectable by NMR spectroscopy (nuclear spin: I = 1/2). Germanium consist naturally of the four stable isotopes ^{70}Ge, ^{72}Ge, ^{73}Ge and ^{74}Ge with an abundancy ratio of 20.5 : 27.4 : 7.80 : 36.5% (^{70}Ge:^{72}Ge:^{73}Ge:^{74}Ge).[2]

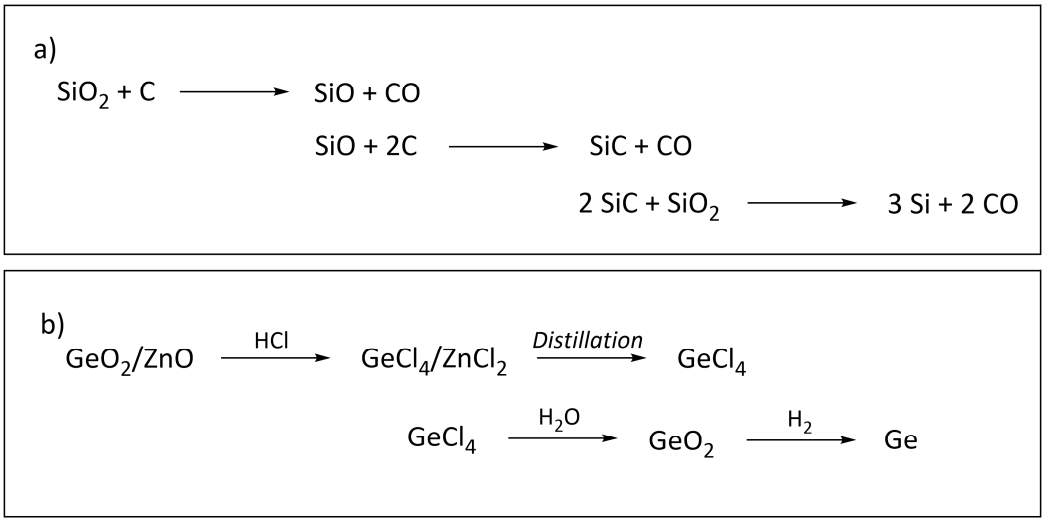

Scheme 1. Technical production routes for elemental Si (a) and Ge (b) by starting from their oxides.[2]

Elemental silicon is produced on industrial scale by reduction of SiO_2 (quartz) with carbon at around 2000 °C (Scheme 1a). Thereby, SiC (silicon carbide) is initially formed from SiO. Elemental crude (metallurgic) Si is finally obtained in the process by reaction of SiC and SiO_2. It normally contains 1–2 mass percent impurities (mainly iron and aluminum). Purified, polycrystalline silicon (polysilicon) can be obtained by thermic reduction of purified $HSiCl_3$. Ultrapure silicon monocrystals are pulled *e.g.* in the *Czochralski* process (Figure 4b, details in chapter 1.2.1).

Elemental germanium is industrially synthesized from GeO_2, which is previously obtained as mixture with ZnO from the processing of zinc (Scheme 1b). For their separation, the oxides are transformed to chlorides and multiply distilled (boiling point $GeCl_4$: 83 °C; boiling point $ZnCl_2$: 756 °C). In the next step, purified GeO_2 is obtained by hydrolyzation and its subsequent reduction with hydrogen yields elemental crude (metallurgic) Ge. Ultrapure, monocrystalline Ge can be obtained from the zone melting process.[2, 5]

Abundancy and production costs of crude Si and Ge are dominating for their prices on the market. Thereby, the price developments of the elements are shown in Figure 2 from 2010 to 2017. Si was listed with price of 2278 $/t in 2017, and thus, was approximately 340 times cheaper if compared to Ge with a price of 776 $/kg in 2017. Properties and performance of both elements are of central interest for a broad range of applications. Both elements are key components for nowadays high-tech products as set out in chapter 1.2.1. Due to its low price and abundancy, silicon is also processed to products on larger scale for the market (see chapter 1.2.2).[2, 6-8]

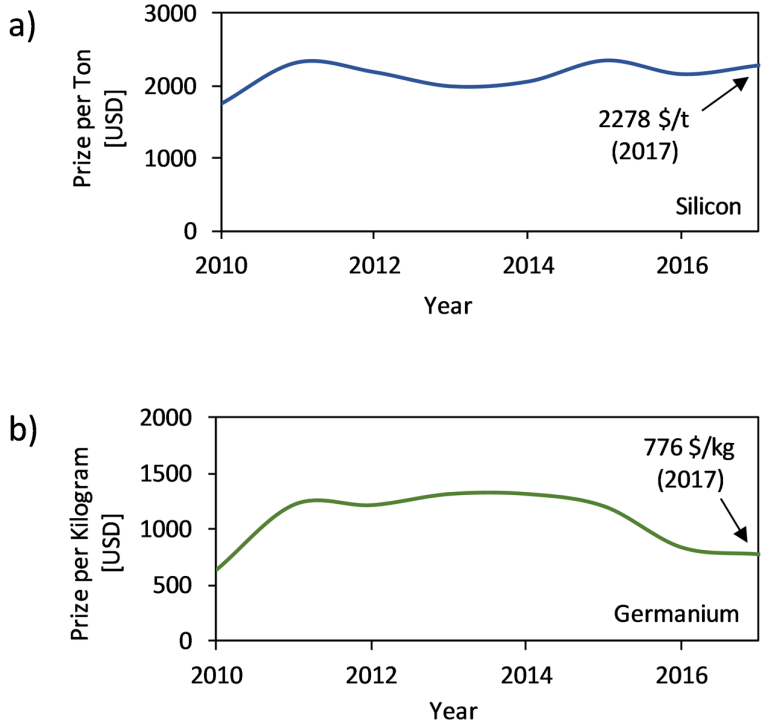

Figure 2. Prize developments for crude silicon [tons] (a; blue line) and crude germanium [kilograms] (b; green line) on the market in the years 2010 to 2017.[6-7]

1.2 Industrial Applications of Silicon and Germanium

1.2.1 Si-and Ge-based High-tech Products

The properties of the elements Si and Ge are of central interest for their applications. Both elements are semimetals with semiconducting properties. The intrinsic band gap of Ge is with a value of 0.62 eV decisively smaller if compared to Si with 1.06 eV (300 K).[9-10] Monocrystalline materials of the elements, which productions have a high demand of energy, are required for semiconducting applications. A view on the market sales of semiconductors in 2017 (Figure 3a) shows that Asia is dominating with a share of 77%. The biggest market by country is China with 47%. The end markets for semiconductor applications in 2017 (Figure 3b) show that electronic devices have a large share of 46% including computers with 19% and smartphones with 27%.[2, 5]

Silicon is the key component for current high-tech products and finds *i.a.* application in electronics devices, photovoltaics and transistors (as *doped* Si).[2] As mentioned in chapter 1.1, Polysilicon can be obtained by thermic reduction of purified $HSiCl_3$. Ultrapure, monocrystalline Si is required for high-tech applications, which is obtained from melted polysilicon in the *Czochralski* process (alternative: floating zone process) as single crystals with a radius up to 300 mm and a weight up to 500 kg. The single crystals are pulled from the melt under rotation with a seed crystal (see in Figure 4). The obtained Si is the purest industrial large-scale product with a purity of 99.99999999%.[5]

Silicon wafers are manufactured from the obtained single crystals by multiple processing steps including *e.g.* wire sawing and polishing (simplified scheme in Figure 4a). Silicon wafers are the starting material for the production of silicon-based microchips with integrated circuits (Figure 4b).[13]

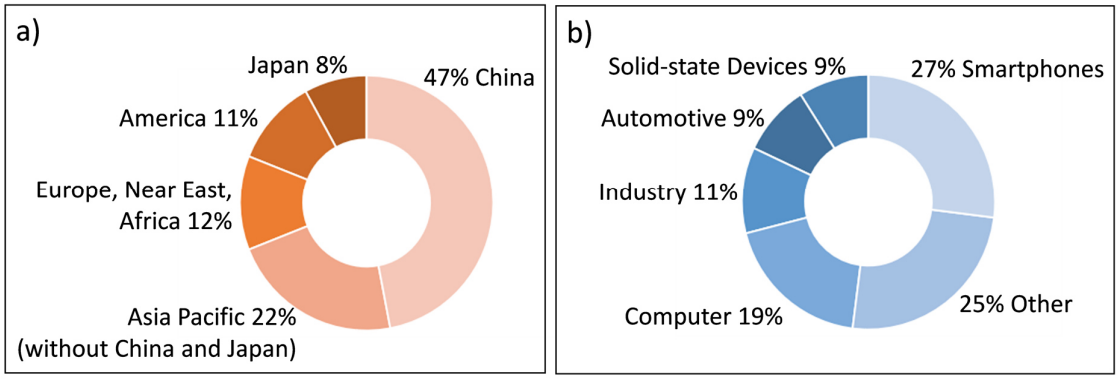

Figure 3. a) Worldwide sale of semiconductors in 2017 (total volume: 430 billion $);[11-12] b) End markets for semiconductor applications in 2017.[13-14]

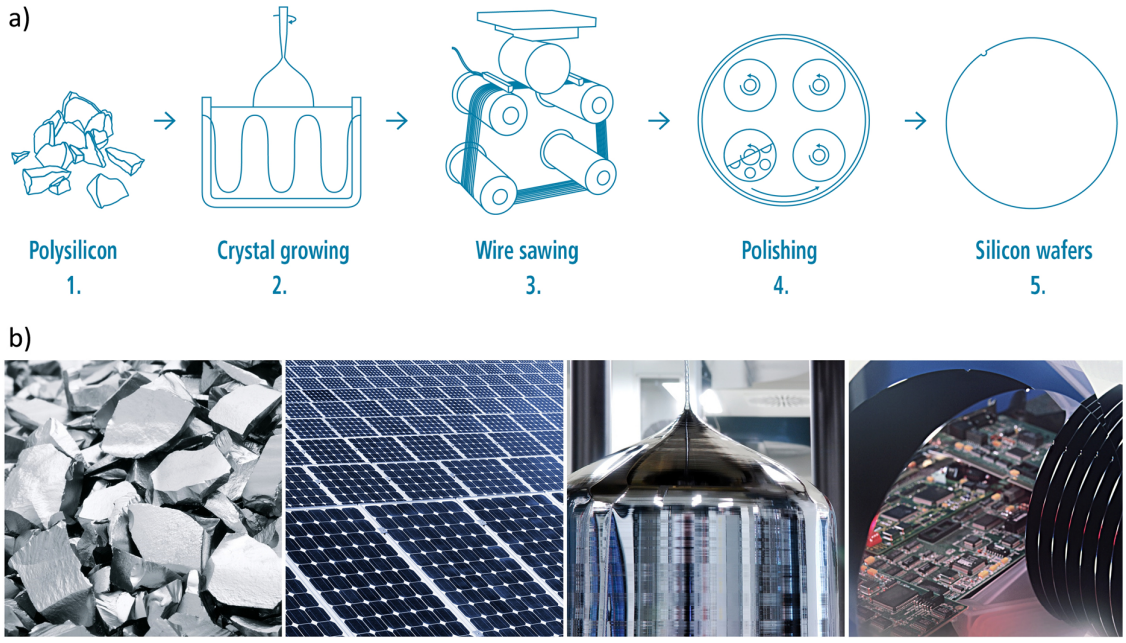

Figure 4. Top: Simplified processing scheme of polysilicon to silicon wafers;[21] Bottom (from left to right): i) Polysilicon as starting material, ii) silicon photovoltaic cells, iii) ultrapure silicon monocrystal from the *Czochralski* process, iv) silicon wafers with mirrored silicon chips on a circuit board.[22]

Besides the breakthrough of silicon-based materials during the last decades, also germanium-based materials have been on the rise. Due to the decisively higher price of Ge if compared to Si (Figure 2), Ge-based applications are focused on high performance materials, what has been triggered by the strong potential for deep submicron (sub 45 nm) technologies in the recent years.[15] The procession and purification of elemental Ge is described in chapter 1.1 and its materials find

broad application at the high-tech market as for example in transistor technology, optical devices and superconductors. Moreover, magnesium germanate is utilized as fluorescent materials. Due to the high performance of germanium-based materials, their application in photovoltaics, batteries as well as device physics is of central interest.[2, 15-20]

Regarding the current switch at the energy market from fossil energy sources towards the usage of renewable energy sources, silicon- and germanium-based materials are suitable for a wide range of applications that promote this switch. Photovoltaics are the interface for the utilization of solar energy and batteries as well as computer chips are fundamental for energy storage and the operation of high-tech electronics. Besides currently applied silicon chips, gallium arsenide chips with higher performance are dominating on the market but have the drawbacks of higher costs and less stability. However, properties of Si- and Ge-based materials are suitable for a wide range of key applications, which markets are constantly growing. This leads to tremendous effort that is put into the development and improvement of such materials nowadays resulting in steady progress.[2, 15-20, 23-28]

1.2.2 Chlorosilanes and Si-based Polymers

Due to its abundancy and low costs, silicon is also processed to industrial products on larger scale for the market. Besides its common use as alloying component, it is also starting material for numerous chemical products as *e.g.* polysiloxanes, polysilanes and silicas. Also germanium has applications in products on a larger scale as *e.g.* in special alloys or fluorescent materials, but the scales are decisively smaller if compared to silicon.[2]

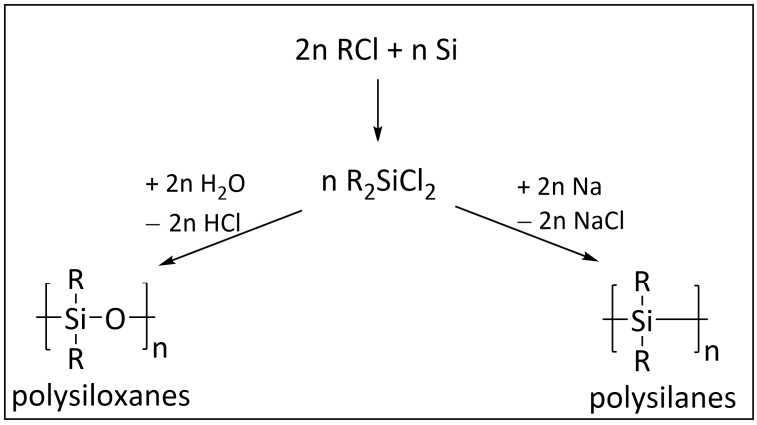

Scheme 2. Technical production routes for polysiloxanes (left reaction pathway) and polysilanes (right reaction pathway) *via* R_2SiCl_2 chlorosilanes from the direct process (R = Me, Ph).[2, 32, 34-35]

The large-scale synthesis of chlorosilanes is key prerequisite for the production of polysiloxanes (so-called silicones) and polysilanes (Scheme 2). Polysiloxanes were discovered and described for the first time by *Frederic S. Kipping*,[2, 29-30] the first description of a polysilane high polymer, synthesized from R_2SiCl_2 (R = Me, Ph) compounds, goes back to *Charles A. Burkhard*.[31-32] The technical

production of both polymers (or oligomers) is mainly based on chloro(methyl)silanes. Other silanes as *e.g.* chloro(phenyl)silanes find application as well, but on smaller scale. Moreover, functionalized chloro(methyl)(vinyl)silanes are used for example as cross-linkers in silicone elastomers.

Chloro(methyl)silanes and chloro(phenyl)silanes can be synthesized by the direct process of *Müller/Rochow* by reaction of silicon with methyl or phenyl chloride. Copper catalysts and promotors are used in the process under (assumed) formation of the silicide Cu_3Si as intermediate. The industrial process in industry is optimized to generate the dichlorosilanes R_2SiCl_2 (R = Me, Ph) as main products, but also $R_{4-x}SiCl_x$ (x = 0, 1, 3, 4) and oligosilanes form as side-products and have to be separated or further processed. Such side-products are further utilized to synthesize products that are separately distributed on the market, *e.g.* highly disperse silicic acid can be obtained from $SiCl_4$.[2, 33]

As mentioned, the most produced chlorosilane in industry is Me_2SiCl_2, which is obtained from the direct process and further processed to *e.g.* polysiloxanes and polysilanes (Scheme 2). The industrial syntheses of so-called silicones (oligo- or polysiloxanes) are versatile and depend *inter alia* on the process parameters, the catalyst, as well as the presence of cross-linkers and $RSi(OH)_3$ and $R_3Si(OH)$ silanols that branch or terminate the oligomer or polymer chains (R = organic rest). The formation of $–[Si(R_2)–O–]_n$ silicone chains is formally based on the condensation of $R_2Si(OH)_2$ silanols which are formed by hydrolysis of chlorosilanes. The properties of silicone materials can be fine-tuned to obtain tailor-made products for the market. Due to their high temperature-, oxygen- and water-resistance, their gas- and electricity-permeability, as well as their mechanical and physical properties, silicones find a wide range of applications as for example in synthetics, materials (*e.g.* as elastomers) and additives.[2, 32-34]

Polysilanes (or polysilylenes) consist of $–[Si(R_2)–]_n$ chains. Thus, their polymer chain consists exclusively of silicon atoms bearing organic side-groups (R = organic rest). The standard method for their synthesis is based on the so-called *Wurtz* reaction and includes the treatment of R_2SiCl_2 with sodium metal, usually above the melting point of sodium (Scheme 2). A main application of polysilanes is their usage as precursors for the synthesis of silicon carbide ceramics. Furthermore, they serve as photoresists in the manufacturing of microelectronics. The cumulated Si–Si bonds in the polysilane chains extensive the occurrence of electron delocalization resulting in exceptional electronic and photochemical properties of these materials. Thus, they are also of interest as materials in electric fields and or for applications in electrophotography, printing technology and display devices.[32, 35-41]

1.3 Utilization of Silicon and Germanium *Zintl* Precursor Materials

Silicon- and germanium-based materials are widely used in industrial applications as set out in the chapter before. Regarding the utilization of larger molecular frameworks, Si-based materials find prominent applications, whereas comparable Ge-based compounds are not broadly established yet.[42-43] Due to an increasing demand for new material sources, the synthesis of Si and Ge material precursors is fundamental for the future fabrication of materials. Thereto, defined homoatomic

structures of both elements are performed in known intermetallic *Zintl* phases. The utilization of such *Zintl* compounds as cluster sources opens a new synthetic protocol for the synthesis of material building blocks, and thus, for the fabrication of Si- and Ge-based materials. The state of current knowledge regarding *Zintl* precursor utilization is presented in the following.

1.3.1 Defined Homoatomic Si and Ge Structures in *Zintl* Precursors

Regarding the accessibility of homoatomic Si and Ge building blocks, a wide range of structures was reported for intermetallic *Zintl* phases. Among other examples, such phases are formed with main group elements and prominent representatives consist *e.g.* of discrete, deltahedral tetrel (group 14) or pentel (group 15) cluster polyanions along with alkali or alkaline earth metal cations. Thereby, the electronegativity difference of the involved elements is large enough to describe them as $[M_n^{x+}][(E_m)^{x-}]$ (M = alkali or alkaline metal; E = tetrel element) binary compounds with formal electron transfer. Therein, the contained metal cations are separated from the polyanionic substructures under formation of salt-like *Zintl* phase solids.[2, 44-49]

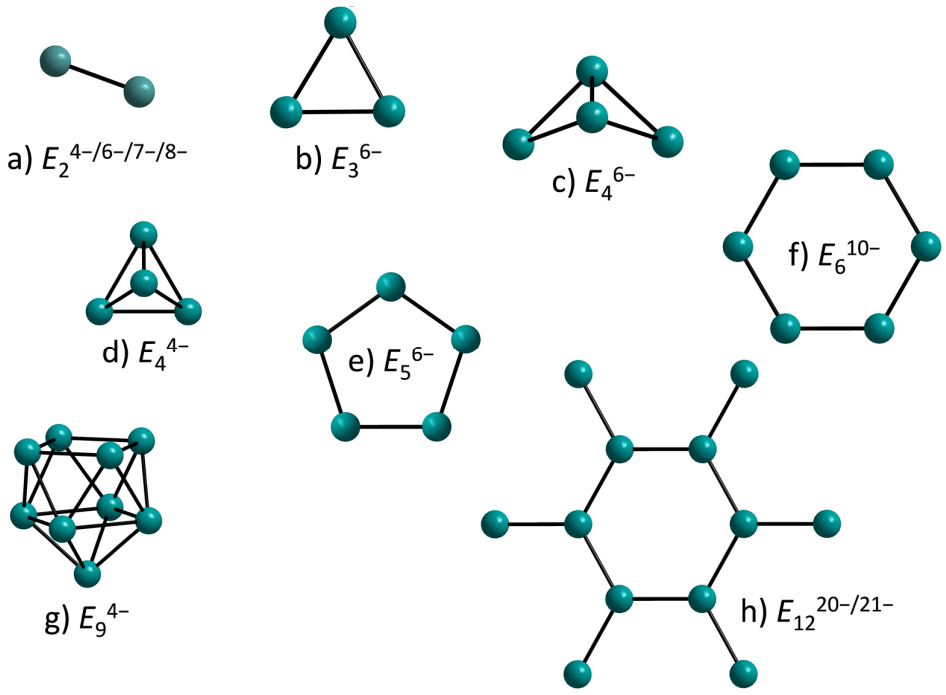

Figure 5. Examples for polyanionic silicon and germanium substructures as they appear in *Zintl* phase materials:[46] a) Ge_2^{4-}, Si_2^{6-} and $E^{4-/6-/7-/8-}$ (E = Si, Ge) dumbbells;[50-54] b) E_3^{6-} triangle (E = Si);[55] c) E_4^{6-} butterfly unit (E = Si, Ge);[56-58] d) E_4^{4-} tetrahedron (E = Si, Ge);[59-63] e) five-membered E_5^{6-} ring (E = Si);[64] f) six-membered E_6^{10-} ring (E = Si, Ge);[65-67] g) E_9^{4-} mono-capped square antiprism (E = Si, Ge);[68-74] h) $E_{12}^{20-/21-}$ ring system (E = Si).[75] E atoms are shown as turquoise spheres.

Examples for polyanionic Si and Ge building blocks in *Zintl* phase materials are shown in Figure 5 and demonstrate that versatile homoatomic E_x^{n-} structures (E = Si, Ge; x = number of atoms; n =

charge value) with varying numbers of atoms and negative charges are accessible. As mentioned, the polyanionic substructures are readily formed in *Zintl* phase materials. Besides two-atomic E_2 dumbbells,[50-51] also larger frameworks consisting solely of Si and Ge atoms are known as *e.g.* E_3 triangles,[55] E_4 butterflies[56-58] and tetrahedral[61-63] structures. In analogy to carbon structures, five- and six-membered E_5 and E_6 rings[64-67] are known along with an six-membered E_{12} ring system[75] and E_9 clusters deriving from a mono-capped square antiprism.[46, 68-73] The salt-like charge separation in binary *Zintl* compounds can be described by the *Zintl-Klemm-Busmann* concept by transfer of the electrons to the electronegative component following the (8–*N*) rule for the polyanionic substructure.[76]

As presented, Si and Ge substructures (Figure 5) are accessible from *Zintl* precursor materials. Structures, as well as properties of these materials are of central interest for material building blocks because contained cluster anions carry Si and Ge atoms with zero or negative oxidation state what results in the formation of low-valent structures as discussed in the following chapter.

1.3.2 *Zintl* Precursors as Si and Ge Cluster Sources

Binary *Zintl* phases that readily provide homoatomic silicon or germanium clusters are central content of this work. Such phases appear as dark-greyish intermetallic compounds with high melting points and low electrical conductance.[2]

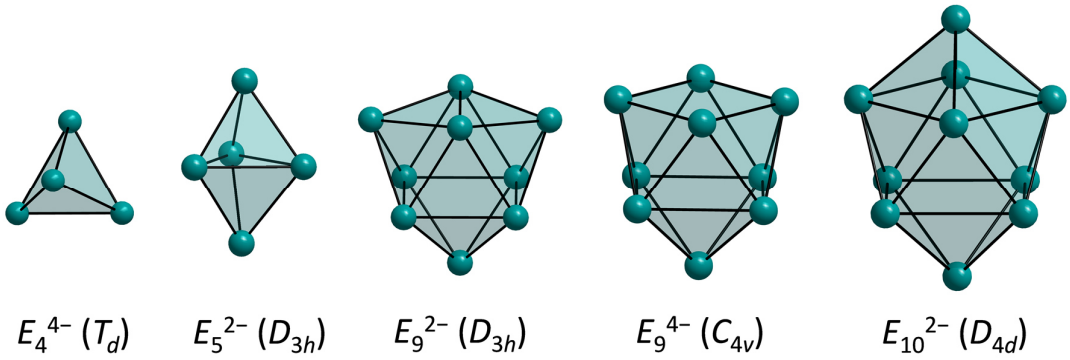

Figure 6. Examples for homoatomic clusters (*E* = Si, Ge) with their point groups (*E* atoms and cluster polyhedra in turquoise,). Ge_9^{4-} clusters are contained in the precursor K_4Ge_9, Si_4^{4-} and Si_9^{4-} clusters in the precursor $K_{12}Si_{17}$ in a 2:1 ratio.[45, 47, 71, 77-81]

The presence of numerous cluster types in *Zintl* phases is known. Within this work, the focus lies on silicon and germanium phases that contain fourfold negatively charged four- and nine-atomic cluster types (Figure 6) along with potassium cations. Considering the *Zintl-Klemm-Busmann* concept,[76] the formal transfers of valence electrons from the electropositive alkali metals to the electronegative group 14 element substructure bears E_9^{4-} cluster anions in case of the composition A_4E_9 (*A* = Na–Cs; *E* = Ge–Pb). In $A_{12}E_{17}$ phases (*A* = K–Cs; *E* = Si–Sn) E_4^{4-} and E_9^{4-} cluster anions occur in a ratio of 2:1 per unit, so that the phase can be rewritten as $(A_4E_4)_2(A_4E_9)$. The presence of the clusters in *Zintl* materials was confirmed by X-ray structure determinations (Figure 7).[2, 44, 48-49]

To overcome an electron deficit, tetrel elements are capable to form multiple bonds or multicenter bonds occurring in cluster systems. The structures of *Zintl* cluster polyanions can frequently be predicted by *Wade's* rules[82-84] with the 2x+n (x = number of vertices, n = negative charge) concept. *Wade's* rules are well-known for the structural arrangement in boranes, in case of the tetrel clusters the radial B–H bonds are formally substituted by an electron lone pair at the cluster vertex atoms. Each tetrel vertex atom contributes two of its four valence electrons to the cluster skeletal bonding. The homoatomic bonds in the clusters are elongated by a maximum of 5% if compared to interatomic distances in modifications of the elements. Due to their negative charges and the occurrence of several lone pairs, low-valent *Zintl* clusters boast an ambivalent character as nucleophilic species in coexistence with an unsaturated bonding system. This combination of properties is outstanding if compared to the vast range of reported molecular silicon and germanium compounds.[2, 8, 45-48]

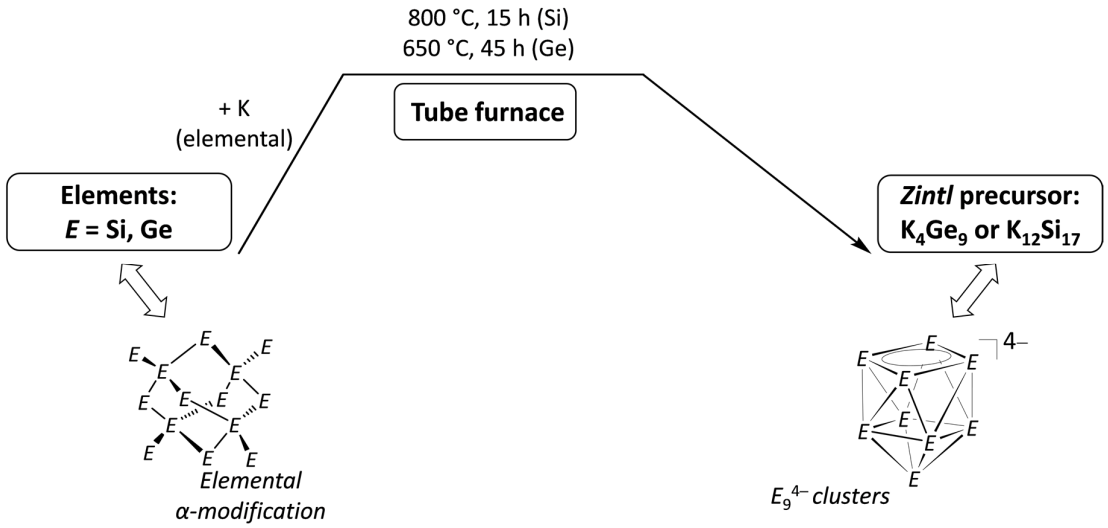

Scheme 3. Reaction pathway for the synthesis of the *Zintl* precursor materials K_4Ge_9 and $K_{12}Si_{17}$ containing E_9^{4-} (*E* = Si, Ge) cluster species.[68, 70, 72-73]

As shown in Scheme 3, Ge_9^{4-} clusters in the *Zintl* precursor K_4Ge_9 can be synthesized from direct solid-state reaction of the elements K and Ge at 650 °C.[68, 73] Up to date the formation of an according "K_4Si_9" phase is not known, but Si_9^{4-} clusters are accessible in the $K_{12}Si_{17}$ precursor along with Si_4^{4-} clusters in a ratio of 1:2 by solid-state reaction of K and Si at 800 °C.[70, 72] Due to moisture and air-sensitivities of the *Zintl* phase materials, syntheses are carried out under dry inert gas atmosphere. $K_{12}Si_{17}$ and K_4Ge_9 compounds can be obtained in quantitative yields (Figure 7) and the formed clusters have a high synthetic potential as building blocks for the further fabrication of nanostructured Si- and Ge-based materials.

Current research is focused on the utilization of such precursors as cluster sources by transfer to cluster solutions. Due to the applicable solubility of K_4Ge_9, the formation of larger Ge_9-based morphologies, as *e.g.* cluster polymers and layers that are suitable for photovoltaics, was already achieved.[20, 85] The state of knowledge regarding the utilization of A_4Ge_9 and $A_{12}Si_{17}$ precursor materials to soluble Si and Ge cluster-based building blocks is presented in the following.

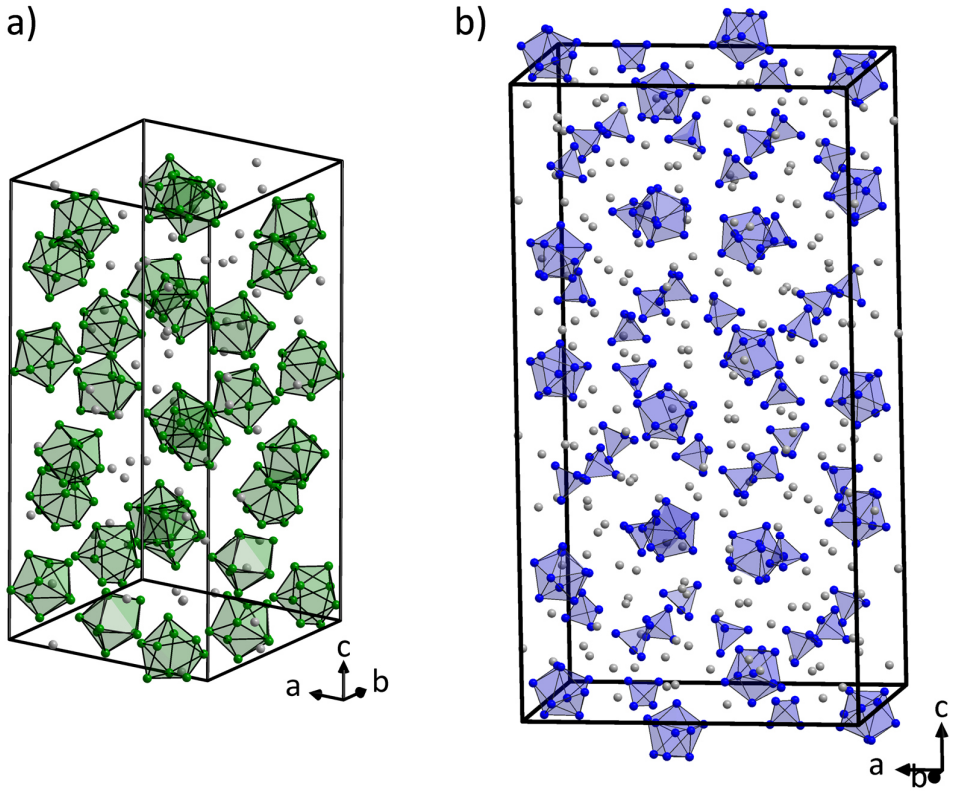

Figure 7. Unit cells of *Zintl* phase precursor materials with E_9^{4-} clusters (*E* = Si, Ge): a) Cs_4Ge_9 containing Ge_9^{4-} clusters;[69] b) $K_{12}Si_{17}$ containing Si_4^{4-} and Si_9^{4-} clusters in a ratio of 2:1.[72] (Ge atoms in green; Si atoms in blue; K and Cs atoms in gray; Ge_9 and Si_9 clusters are shown as green and blue polyhedra, respectively)

1.3.3 Solubility, Linkage and Metal Complexation of Si and Ge Clusters

Regarding the solubility of germanium and silicon *Zintl* precursors, A_4Ge_9 (*A* = alkali metal) phases showed up to be sufficiently soluble in polar organic amine solvents like *e.g.* ethylenediamine or liquid ammonia. In contrast, the solubility of $A_{12}Si_{17}$ (*A* = alkali metal) phases is rather limited to liquid ammonia.[47] Due to this circumstance, reports on synthesized species that contain silicon clusters from $A_{12}Si_{17}$ *Zintl* phases are rare and were limited to the metal complexes $[(CuMes)_2Si_4]^{4-}$,[86] $[(ZnPh)Si_9]^{3-}$,[87] $[\{Ni(CO)_2\}_2(Si_9)_2]^{8-}$,[88] and $[\{Cu(NHC^{Dipp})\}Si_9]^{3-}$ [89] before this thesis (molecular structures are shown in Figure 8). Moreover, solvate crystals containing Si_9^{4-} and Si_4^{4-} clusters units[90-92] have been known as well as cluster oxidations of the Si_9^{4-} units to Si_9^{3-} [78, 93] and Si_9^{2-} [81] species, which were reported along with the unexpected formation of Si_5^{2-} clusters (Figure 6).[78-79]

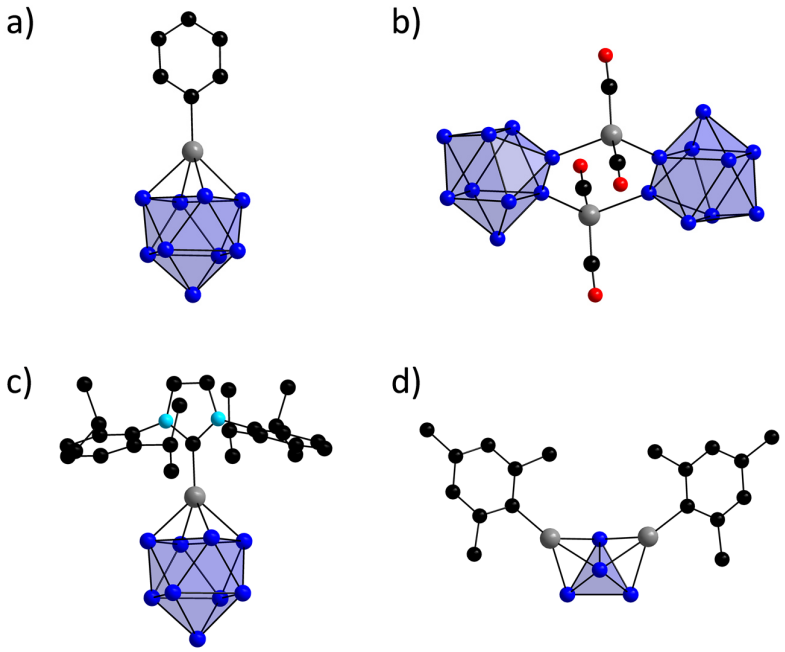

Figure 8. Molecular structures of transition metal complexes with silicon clusters from $A_{12}Si_{17}$ (*A* = alkali metal) *Zintl* precursor material: a) $[(PhZn)Si_9]^{3-}$;[87] b) $[\{Ni(CO)_2\}_2(Si_9)_2]^{8-}$;[88] c) $[\{Cu(NHC^{Dipp})\}Si_9]^{3-}$;[89] d) $[(MesCu)_2Si_4]^{4-}$.[86] Si atoms are shown in blue, *M* atoms in gray (*M* = Cu, Ni), C atoms in black, O atoms in red, N atoms in turquoise, H atoms are omitted, Si_9 clusters are shown as blue polyhedra.

Promoted by the solubility of A_4Ge_9 precursor phases in polar solvents (*e.g.* liquid ammonia, ethylenediamine and dimethylformamide), a versatile chemistry was established for Ge_9 clusters during the last decades. On the one hand, numerous examples for transition metal complexes were reported as mirrored by structures of $[\{Cu(PR_3)\}Ge_9]^{3-}$ (R = ^{i}Pr, Cy),[94] $[Zn(Ge_9)_2]^{6-}$ [95] and $[\{M(CO)_5\}_3Ge_9]^{4-}$ (*M* = Cr, Mo, W)[96] among many others, as well as by the larger cluster species $[Au_3(Ge_9)_5]^{9-}$.[97] On the other hand, chain structures of Ge_9 clusters[98] were synthesized by cluster couplings in reports on $(Ge_9–Ge_9)^{6-}$ dimers,[99-101] $(Ge_9=Ge_9=Ge_9)^{6-}$ trimers,[102-103] $(Ge_9=Ge_9=Ge_9=Ge_9)^{8-}$ [104-105] and $[Hg_3(Ge_9)_4]^{10-}$ [106] tetramers, as well as polymeric $_\infty(Ge_9–)^{2-}$ [85] and $_\infty(Ge_9Zn–)^{2-}$ [107] molecules (Figure 9). The reports demonstrate that *Zintl* precursors can be utilized to form larger cluster-based structures for material building blocks. Furthermore, the transition

metals nickel and palladium, which are prominent for their application in catalysis, were inserted into Ge_9 clusters under formation of endohedrally filled structures as mirrored by $[Ni@\{(Ni\text{-}CCPh)Ge_9\}]^{3-}$,[108] $[Ni@\{Pd(PPh_3)Ge_9\}]^{2-}$,[109] $[(Ni\text{-}Ni\text{-}Ni)@(Ge_9)_2]^{4-}$ [110] and the dimerized Ge_9 species $[(Pd\text{-}Pd)@(Ge_9)_2]^{4-}$.[111]

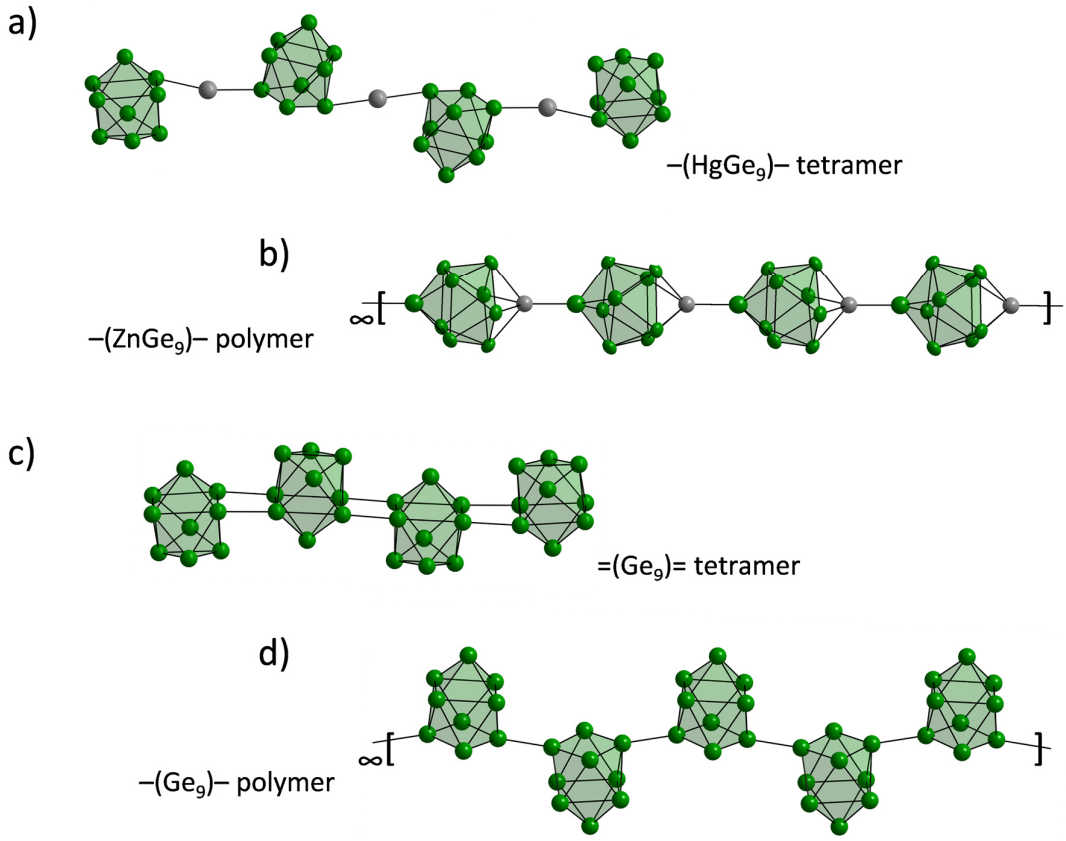

Figure 9. Chain structures of Ge_9 clusters synthesized from intermetallic *Zintl* precursors [Ge atoms in green, *M* atoms in gray (*M* = Zn, Hg), Ge_9 clusters as green polyhedra]: a) $[Hg_3(Ge_9)_4]^{10-}$ tetramer;[106] b) $[ZnGe_9]^{2-}$ polymer;[107] c) $[(Ge_9)_4]^{8-}$ tetramer;[104] d) Ge_9^{2-} polymer.[85]

1.3.4 Silicon NPs and Syntheses with *Zintl* Compounds

The utilization of silicon *Zintl* precursors is also promoted by synthetic achievements to nanoscaled silicon particles. Frequent synthetic progress to nanoparticles (NPs) revealed their high application potential, which dominantly depends on crystallinity, size distribution and morphology. Thus, the tailoring of these properties became matter of central interest for application-focused Si NPs syntheses.

Achievements to defined NPs were initially driven by the exploration of crystalline CdS/CdSe[112-115] and InP/InAs[116-121] NPs that were for example obtained by growth in solution from molecular precursors. Synthetic preparations were intensively developed under variation of nucleation and

growth processes revealing a critical dependence on precise kinetics.[113-115, 122] Steady synthetic effort on morphological control and size-selecting methods[123-125] yielded semiconductor NPs, nanocrystals (NCs) and so-called quantum dots (QDs). Obtained species revealed remarkable characteristics that differ from their bulk counterparts as *e.g.* novel catalytic, electronic and optical properties including optical absorption and photoluminescent response.[126-128] Properties of obtained NPs were intensively studied and understood, but application limitations came up due to electrochemical activity and toxicity.[129] Consequently, Si NPs came into focus because silicon is a bioinert semiconductor with electrochemical stability.[130-133] In contrast to application limitations of silicon bulk materials in optoelectronics, photoluminescence was found for nanostructured silicon and demonstrated an overcoming of the barrier of inefficient emissions.[134-135]

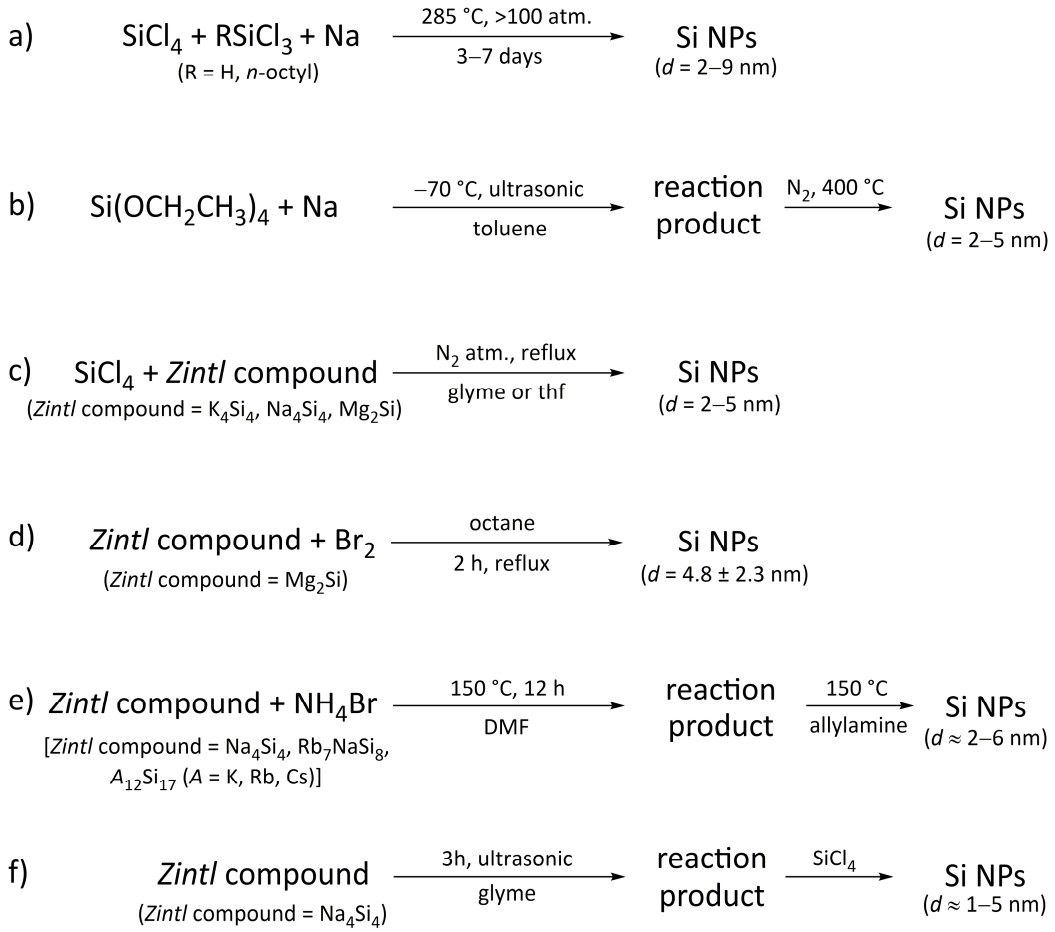

Scheme 4. Solution-based synthesis pathways for preparations of tailored Si NPs.[136-146]

As mentioned, size distribution, crystallinity, and surface chemistry determine the properties of NPs, and thus, preparative methods to tailor these properties were targeted for Si NP syntheses. Versatile silicon nanostructures were reported including porous silicon[147] and discrete crystalline Si nanoparticles, which are in focus of interest because of their unique chemical and optical characteristics.[136, 148] The synthetic effort on Si NPs resulted in a variety of promising approaches, most prominently represented by physical methods, precursor thermolysis and pyrolysis as well as solution-based (Scheme 4) pathways.

Solution-based procedures that involve precursor reduction are well-known for metal and semiconductor NP syntheses and allow the simultaneous tailoring of particle size and surface chemistry. Hereto, a synthesis route for Si NPs is reported by a heterogeneous reaction mixture that contains a sodium dispersion to simultaneously reduce $SiCl_4$ and $RSiCl_3$ (R = H and *n*-octyl). The reaction product contained size polydisperse particles of d = 2–9 nm with Si–O, Si–Cl and Si–H surface termination.[137] Variation of this "alkali metal reduction approach" was reported for sonication under usage of tetraethyl orthosilicate. Subsequent temperature treatment of the reaction product at 400 °C yielded silicon NPs with diameters of 2–5 nm (Scheme 4a, b).[138]

Additionally, silicon *Zintl* compounds were utilized for the synthesis of Si NPs (Scheme 4c–f). K_4Si_4, Na_4Si_4 and Mg_2Si *Zintl* compounds were used to reduce $SiCl_4$ in glyme solutions yielding nanocrystalline silicon particles,[139-140] and for Mg_2Si photoluminescent Si NPs were found.[141] Moreover, Na_4Si_4, Rb_7NaSi_8, and $A_{12}Si_{17}$ (*A* = K, Rb, Cs) *Zintl* compounds were used as precursors for Si NPs of $d \approx$ 2–6 nm, which were obtained from reaction with NH_4Br in dimethylformamide (DMF) and subsequently capped with allylamine.[142] The synthetic potential of Mg_2Si as starting material was further promoted by reaction with Br_2 under refluxing in octane or glyme yielding nanocrystalline silicon particles of d = 4.8 ± 2.0 nm.[143-144] Moreover, ultrasonication of Na_4Si_4 in glyme yielded polydisperse, chloride surface terminated, crystalline Si NPs ($d \approx$ 1–5 nm). The obtained NPs are photoluminescent and emit blue and white light depending on sonication time.[136, 145-146]

1.4 Silicon and Germanium Cluster Compounds

1.4.1 Molecular Bottom-up Reactions for Si and Ge Clusters

Besides the formation of Si and Ge clusters in *Zintl* solids, the exploration of Si and Ge cluster compounds emerged from "molecular bottom-up" approaches which were induced by the reports on stable Si=Si and Ge=Ge double bonds.[149-152] This initiated the discovery of a wide range of unsaturated species and established the field of low-valent Si and Ge compounds, which still undergoes constant progress. Synthetic milestones were *e.g.* achieved by the synthesis of stable silaethenes[153-154] and germaethenes,[155] as well as a silicon-silicon triple bond.[156] Furthermore, stable silylenes[157] and germylenes were isolated,[158] as well as an aromatic hexasilabenzene isomer in $(Tip)_6Si_6$.[159] Rapid synthetic progress in this field outlines the versatility of low-valent Si and Ge compounds in analogy to prominent carbon compounds.

Regarding the tailoring of Si and Ge cluster compounds as material building blocks, also the formation of cluster structures is possible with molecular precursors. Reported examples include achievements for the synthesis of smaller (Figure 10) and larger (Figure 11) Si and Ge cluster compounds. The obtained clusters are stabilized by (bulky) organic ligands bonding at the Si and Ge atoms. Triangular E_3 clusters were *e.g.* synthesized with $(CAAC)_3Si_3$ [160] and R_6Ge_3 (R = 2,3-dimethylphenyl)[151] species, tetrahedral E_4 clusters were *e.g.* obtained in $(Si^tBu_3)_4Si_4$ [161] and $(Si^tBu_3)_4Ge_4$ [162] (Figure 10).

Along with these achievements, the synthesis of Si and Ge clusters that bear unsubstituted, and thus, ligand-free cluster atoms started to accelerate. Besides the anionic tetrahedral $[(SiMeDis_2)_4Si_4]^-$ {Dis = $CH(SiMe_3)_2$}[163] and the $(Tip)_6Si_5$[164] silicon clusters, bearing one unsubstituted Si atom each, also two unsubstituted *E* atoms were obtained in six-atomic $(Tip)_6Si_6$[165] (Figure 31f) and $(Tip)_6Si_4Ge_2$[166] (Figure 11b) clusters.

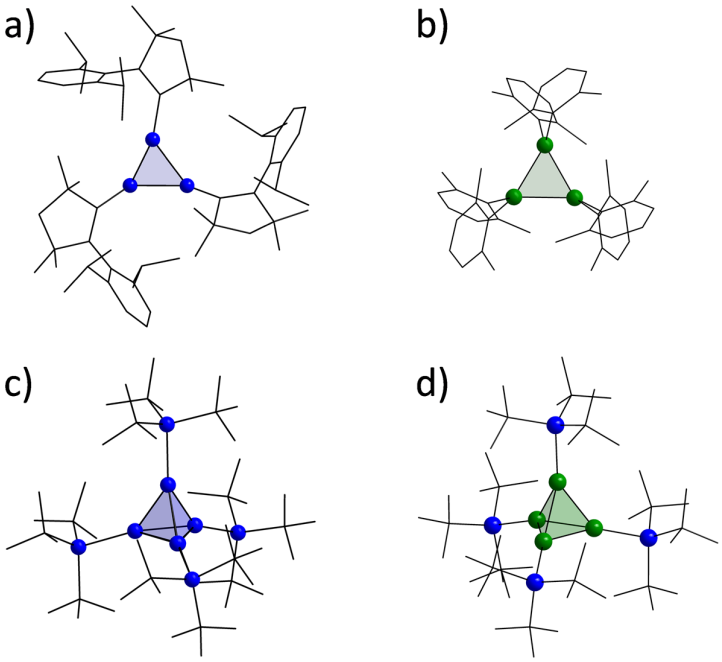

Figure 10. Examples for smaller silicon cluster species with 3 and 4 silicon cluster atoms: a) a triangular Si_3 cluster in $(CAAC)_3Si_3$;[160] b) a triangular Si_3 cluster in R_6Si_3 (R = 2,3-dimehtylphenyl);[151]c) a tetrahedral Si_4 cluster in $(Si^tBu_3)_4Si_4$;[161] c) a tetrahedral Si_4 cluster in $(Si^tBu_3)_4Ge_4$;[162] (Si and Ge atoms in blue and green, respectively; C atoms as wire-sticks; H atoms are omitted; silicon and germanium clusters as blue and green polyhedra, respectively).

Three unsubstituted Si atoms are present in the anionic species $[(Tip)_5Si_6]^-$ [167] (Figure 11a), which showed up to be suitable for cluster expansion until an eight-atomic silicon clusters.[168] Unsubstituted Si and Ge atoms were also found in spirocyclic clusters as *e.g.* $(Si^tBu_3)_6Si_9Cl_2$ [169] (Figure 11c) and $(^tBu)_4(^tBu_2MeSi)_4Si_2Ge_9$ [170] (Figure 11d), as well as in the Si_{11} cluster $(Tip)_8HSi_{11}$ (Figure 11e).[171] Two unsubstituted Si atoms are present in $(Tip)_8HSi_{11}$, whereas a decisively higher number of 12 unsubstituted Ge atoms was found for the Ge_{18} cluster of $\{Si(TMS)_3\}_6Ge_{18}$[172] which was synthesized from the K_4Ge_9 *Zintl* precursor (Figure 11f, more synthesis details in chapter 1.4.2.3,).

By definition,[167, 173] partially substituted – und thus unsaturated – silicon rich clusters are collected in the category of so-called siliconoid clusters. In such clusters at least one exposed atom with a hemispheroidal coordination sphere (Figure 12) is present that is entirely free of bonds other than those to the adjacent vertices. This category can be understood as an intermediate between known "fully substituted" silicon clusters and "fully exposed" silicon clusters such as polyanionic silicon *Zintl* clusters.

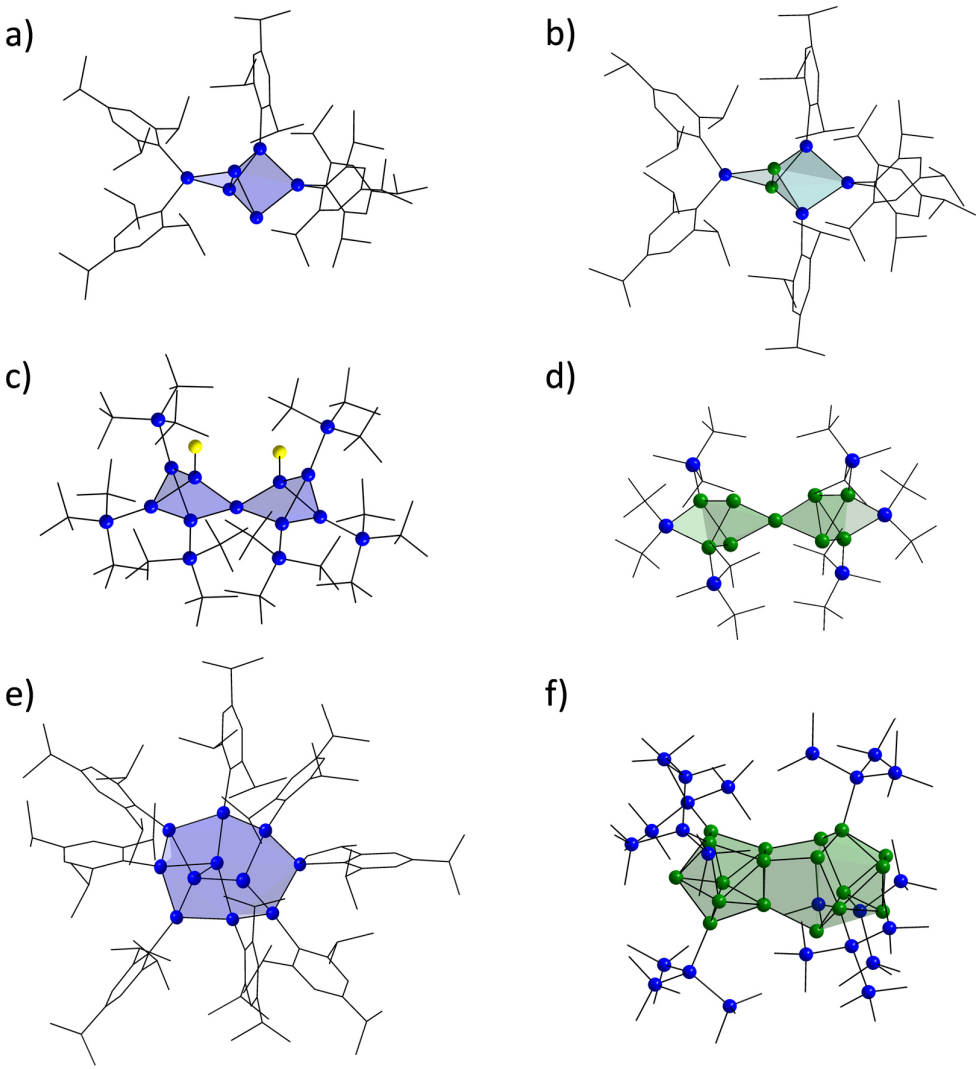

Figure 11. Examples for larger Si and Ge clusters in literature with unsubstituted cluster atoms: a) the anionic siliconoid Si_6 cluster $(Tip)_5Si_6^-$;[167] b) the Si_4Ge_2 cluster $(Tip)_6Si_4Ge_2$;[166] c) the spirocyclic Si_9 siliconoid cluster $(Si^tBu_3)_6Si_9Cl_2$;[169] d) the spirocyclic Si_2Ge_9 cluster $(^tBu)_4(^tBu_2MeSi)_4Si_2Ge_9$;[170] e) the Si_{11} siliconoid cluster $(Tip)_8HSi_{11}$;[171] f) the Ge_{18} cluster $\{Si(TMS)_3\}_6Ge_{18}$.[172] Si and Ge atoms in blue and green, respectively; C atoms as wire-sticks; H atoms are omitted; silicon and germanium clusters as blue and green polyhedra, respectively.

Prominent examples for siliconoids bearing differing numbers of exposed silicon atoms are shown in Figure 12. The idea to synthesize such siliconoid cluster species from silicon *Zintl* precursor, which *e.g.* readily contain the polyanionic Si_4^{4-} and Si_9^{4-} clusters (see chapter 1.3), was already suggested in 1993 in the report on the tetra-substituted $(Si^tBu_3)_4Si_4$ [161] species, but repeatedly discarded due to the strong reducing properties of such polyanions.[161, 173] Thus, the state of research regarding the utilization of silicon *Zintl* precursor materials for material building blocks remained limited to the formation of four transition metal complexes before this work (molecular structures in Figure 8). In contrast, the utilization Ge_9^{4-} clusters from *Zintl* precursor materials could be established by substitution reactions on the cluster vertex atoms as presented in the following.

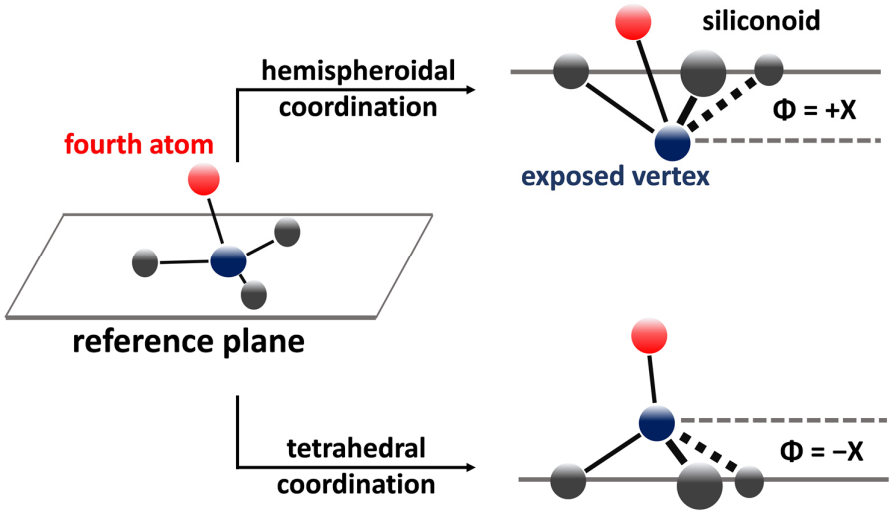

Figure 12. Concept of the hemispheroidality parameter ϕ for the definition of siliconoid clusters: A reference plane is defined by the three bonded atoms (sum of bond angles is closest to 360°). Per convention: the deviation from this plane for the fourth atom of the coordination sphere is set to be a negative value. The hemispheroidality parameter ϕ is defined as the deviation of the "exposed" vertex from the reference plane in comparison to the (mentioned) fourth atom. A positive value of ϕ is defined as hemispheroidal tetra-coordination. In the borderline case of ϕ = 0 the corresponding vertex is planar (tetra-coordinated).[173]

1.4.2 Ge_9 Cluster Compounds from *Zintl* Precursors

Regarding the attachment of covalently bonded ligands at Ge_9 clusters, numerous examples for cluster substitutions have been reported and promote the utilization of *Zintl* precursors for the synthesis of material building blocks. The substituents are attached at the cluster vertex atoms under reduction of the cluster charge yielding soluble species.

1.4.2.1 Substitution of Ge_9 with Organic Main Group Compounds

Synthetic achievements concerning the synthesis of ligand-free Ge_9 cluster metal complexes and aggregated Ge_9 structures from precursor materials were presented in chapter 1.3.3. Despite major progress in this field, the overcome of solubility limitations due to multiple negative charges of synthesized cluster species remained a challenging issue. A promising approach to lower the negative cluster charges in obtained cluster compounds emerged with the attachment of covalently bonded ligands, what firstly succeeded by substitutions with organic main group compounds R_xSL (R = organic rest; S = C, Sn, Ge, P, Sb, Bi; *L* = leaving group). Meanwhile, numerous mono-, di- and tri-substituted cluster species were obtained by such reactions. Thereby, one negative charge of the cluster polyanion can be removed by the attachment of one positively charged substituent along with substitution of a leaving group *L* (mostly chloride) at the main group atom S of the $-SR_x$ group by the cluster nucleophile (Scheme 5 and Scheme 7).

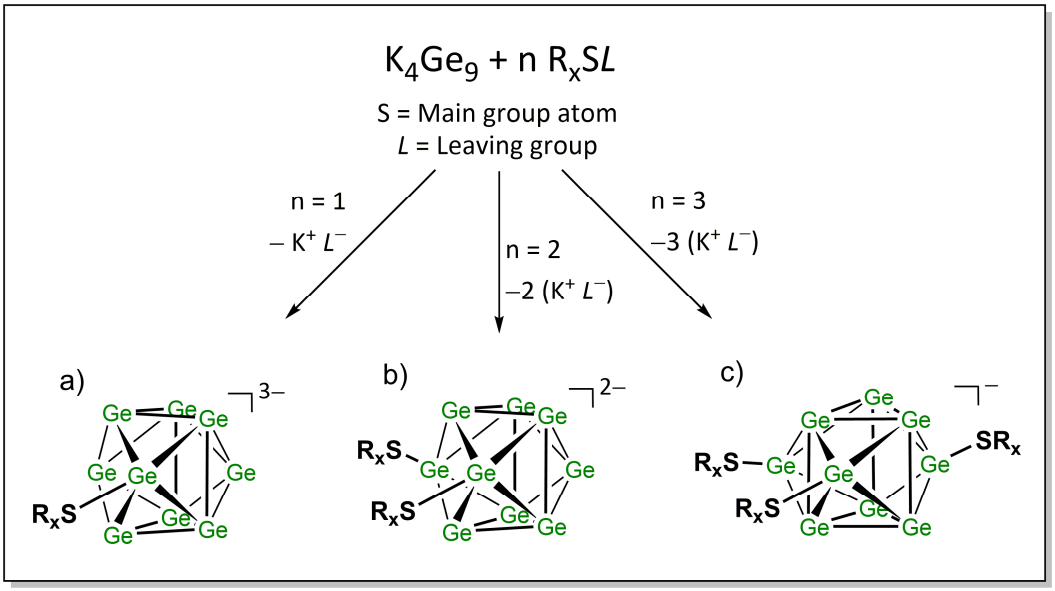

Scheme 5. Reaction scheme for K_4Ge_9 with R_xSL main group compounds (R = organic rest, S = main group atoms, *L* = leaving group) yielding mono- (a), di- (b) and tri-substituted (c) Ge_9 cluster species. One negative cluster charge is removed per formation of a covalent cluster *exo*-bond with a $[SR_x]^+$ group.

Regarding the formation of covalent *exo*-bonds at Ge_9 cluster vertex atoms with -SR_x groups, attachments of organyl, stannyl, phosphinyl, germenyl and stibyl groups are reported. $[RGe_9]^{3-}$ (R = $SnPh_3$, $SnMe_3$)[174], $[R_2Ge_9]^{2-}$ (R = $BiPh_2$, $GePh_3$, $SnMe_3$, $SnPh_3$, $SbPh_2$, Ph)[174-176], $[R_3Ge_9]^-$ {R = Sn^{i}Pr$_3$, $SnCy_3$, $GePh_3$ P(N^{i}Pr)$_2$, P(N^{i}Pr)^{t}Bu}[177-180] and also coupled $[R–Ge_9–Ge_9–R]^{4-}$ (R = $SbPh_2$, ^{t}Bu, ^{s}Bu, ^{n}Bu, 2-methylbutanyl)[174, 176, 181] cluster species were synthesized by reactions of *Zintl* precursors with organic main group compounds in solution. The high versatility of obtained species shows that the attachment of substituents at cluster vertex atoms is as fruitful synthetic approach (examples for molecular structures in Figure 13).

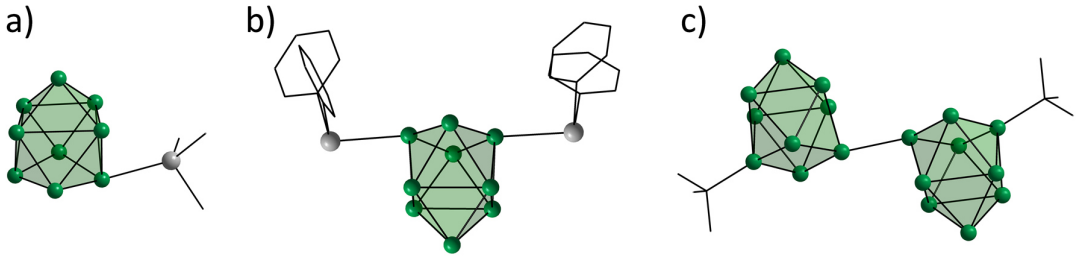

Figure 13. Examples for Ge_9 cluster species with covalently bonded substituents: a) the mono-substituted species $[(SnMe_3)Ge_9]^{3-}$;[174] b) the di-substituted species $[(BiPh_2)_2Ge_9]^{2-}$;[175] c) the coupled alkylated species $[^t Bu–Ge_9–Ge_9–^t Bu]^{4-}$.[181]

The attachment of covalently bonded substituents at the Ge_9 cluster vertex atoms influences the cluster symmetry. The analyzed symmetries in molecular structures are close to idealized point groups. “Bare” unsubstituted Ge_9^{4-} clusters are best described by C_{4v} symmetry, di-substituted species are close to C_{2v} symmetry, and D_{3h} symmetric clusters, in which a capped prism forms, are

observed for tri-substituted species (see Figure 6 and Scheme 5).[45] The observations show that the attachment of substituents has a measurable influence on the atomic Ge_9 cluster arrangement, induced by electronic and steric properties of the substituents. Substituted cluster species are obtained as defined molecules in solution. The species boast significantly less reducing strength if compared to bare clusters due to the lower cluster charges, and thus, increased solubility in organic solvents. Furthermore, the attachment of functionalized substituents at Ge_9 clusters sets a starting point for their further modifications as *e.g.* metal complexation, polymerization and surface grafting. Thereto, approaches are described in the following.[182-183]

1.4.2.2 Vinylation of Ge_9 with Alkyne Compounds

Regarding the synthesis of functionalized Ge_9 clusters, conversions of K_4Ge_9 with alkyne compounds revealed the formation of mono- (a) and di-vinylated (d), as well as coupled (c) and linked vinylated (b) cluster species (Scheme 6 and Figure 14). In addition to the presented species in Scheme 6 also indications for the formation of tri-vinylated species were reported from NMR experiments.[184] Reports to cluster vinylations are commonly based on reactions in ethylenediamine due to specific reaction mechanisms including the solvent.

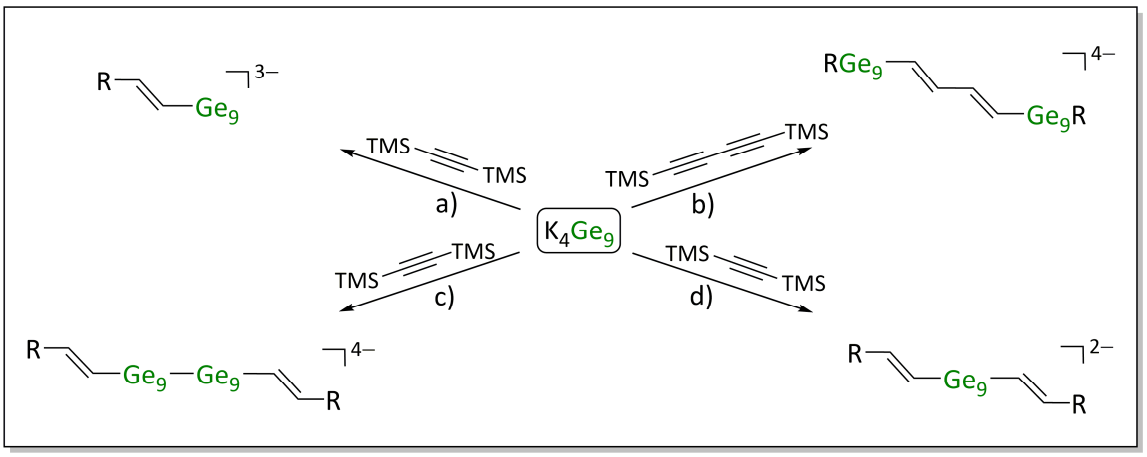

Scheme 6. Reaction pathways for the synthesis of vinyl-functionalized Ge_9 cluster molecules in ethylenediamine starting from K_4Ge_9 *Zintl* material: a) mono-vinylated Ge_9 clusters;[184] b) vinyl-linked Ge_9 clusters;[185] c) coupled, vinylated Ge_9 clusters;[186] d) di-vinylated Ge_9 clusters.[182]

Cluster vinylations proceed by addition of a Ge_9^{4-} cluster at the C≡C triple bond of the alkyne reactant along with a hydrogenation step with ethylenediamine that yields a C=C double bond that is attached at the cluster core. Obtained mono-vinylated $[(R{-}CH{=}CH{-})Ge_9]^{3-}$,[184] di-vinylated $[(R{-}CH{=}CH{-})_2Ge_9]^{2-}$,[182, 184, 187] and $[R{-}CH{=}CH{-}Ge_9{-}Ge_9{-}CH{=}CH{-}R]^{4-}$ species with coupled clusters,[186] as well as vinyl-linked $[R{-}Ge_9{-}CH{=}CH{-}CH{=}CH{-}Ge_9{-}R]^{4-}$ species[185, 188] (R = H or organic rest) show that vinylation reactions of Ge_9 clusters are particularly useful to synthesize vinyl-functionalized Ge_9 clusters (Figure 14). Further investigations of the functionalized clusters species revealed their water stability and the accessibility of the double bonds at the clusters for further reactions,

and thus, the synthetic potential of vinyl-functionalized Ge_9 clusters as material building blocks.[183, 189-190]

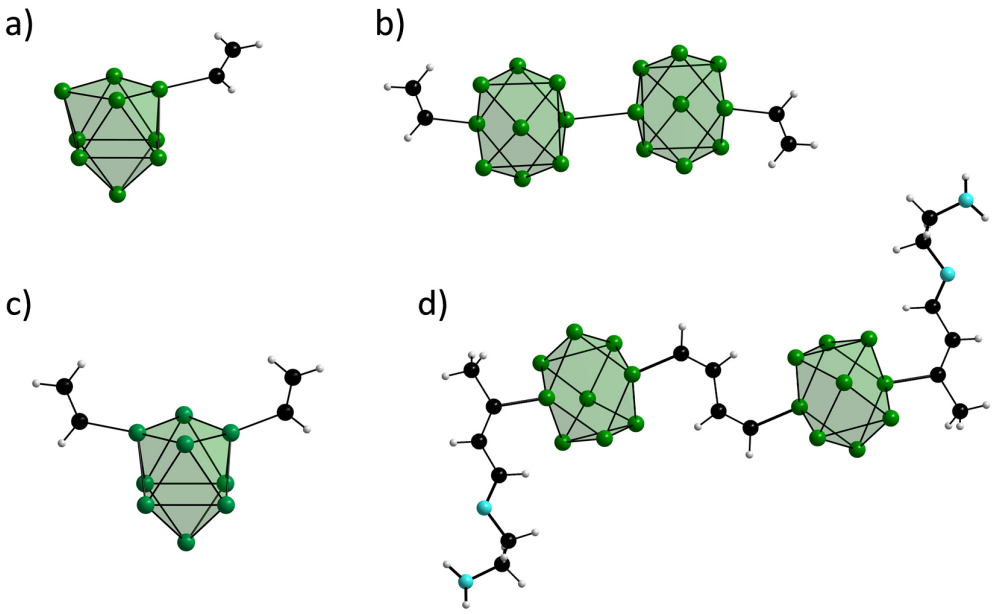

Figure 14. Examples for vinyl-functionalized Ge_9 cluster species: a) the mono-vinylated species $[(CH_2{=}CH)Ge_9]^{3-}$;[184] b) the coupled, vinylated species $[(CH_2{=}CH)Ge_9{-}Ge_9(CH_2{=}CH)]^{4-}$;[186] c) the di-vinylated species $[(CH_2{=}CH)_2Ge_9]^{2-}$;[184] d) the vinyl-linked species $[R{-}Ge_9{-}CH{=}CH{-}CH{=}CH{-}Ge_9{-}R]^{4-}$ {R = (2Z,4E)-7-amino-5-aza-hepta-2,4-dien-2-yl}.[185] Ge atoms in green, N atoms in turquoise, C atoms in black, H atoms in gray, Ge_9 clusters are shown as green polyhedra.

1.4.2.3 Silylation of Ge_9 with Chlorosilane Compounds

Most recently, synthetic progress for the formation of Ge_9 cluster building blocks was promoted by heterogeneous silylations of K_4Ge_9 precursor material by reaction with chlorosilanes. Thereto, the starting point was set by the synthesis of the first silylated Ge_9 cluster species $[\{Si(TMS)_3\}_3Ge_9]^-$,[191] which can be obtained by a single-step reaction of K_4Ge_9 with $Si(TMS)_3Cl$ in acetonitrile solution in good yield (Scheme 7).[177]

During the reaction, three silyl ligands are attached at a Ge_9 core under formation of covalent *exo*-bonds along with a triple reduction of the negative charge of the cluster core in a single-step reaction. $[\{Si(TMS)_3\}_3Ge_9]^-$ shows remarkable stability and is finely soluble in organic solvents such as acetonitrile, thf and toluene. Within the molecular structure, the six unsubstituted Ge_9 cluster atoms of the D_{3h} symmetric cluster core form a prism, and the three silyl ligands are attached at the three prism square capping Ge atoms (Figure 15a). Discovery of this species and its characterization in solution paved the way for rapid progress in the field of silylated Ge_9 clusters. Synthetic achievements for the tailoring and utilization of silylated Ge_9 clusters from K_4Ge_9 are constantly reported and promote their application as cluster-based building blocks (Scheme 7).

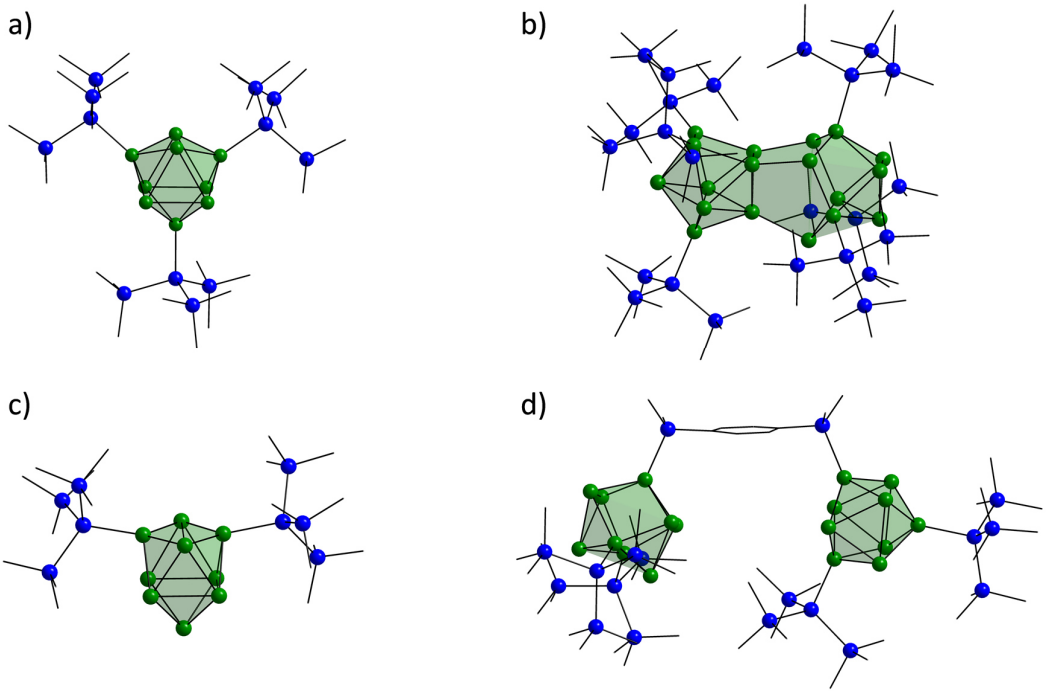

Figure 15. Examples for molecular structures of reported silylated Ge_9 cluster species: a) the tri-silylated species $[\{Si(TMS)_3\}_3Ge_9]^-$;[177] b) the dimerized $[\{Si(TMS)_3\}_3Ge_9]^-$ cluster species $\{Si(TMS)_3\}_6Ge_{18}$;[172] c) the di-silylated species $[\{Si(TMS)_3\}_2Ge_9]^{2-}$;[192] d) the silyl-bridged cluster species $\{Si(TMS)_3\}_2Ge_9–SiMe_2–(C_6H_4)–SiMe_2–\{Si(TMS)_3\}_2Ge_9$.[193]

Among other achievements, complexations with transition metals revealed to be extraordinarily successful for cluster couplings as mirrored by $[\{Si(TMS)_3\}_3Ge_9–M–Ge_9\{Si(TMS)_3\}_3]^x$ (*M* = Zn, Cd, Hg, Mn, x = 0;[194-195] *M* = Cu, Ag, Au,[196-197] x = −1; *M* = Pd,[198] x = −2), $Si(TMS)_3Zn–\{Si(TMS)_3\}_3Ge_9–Pt–\{Si(TMS)_3\}_3Ge_9–ZnSi(TMS)_3$[199] and $\{Si(TMS)_3\}_3Ge_9–Cu–\{Si(TMS)_3\}_3Ge_9–\{Cu(PPh_3)\}$.[198] In all cases η^3-coordination modes of the bare prismatic cluster faces with the metal atoms are present. Regarding the formation of larger, ligand-stabilized cluster species from the K_4Ge_9 precursor, also the direct dimerization of two $[\{Si(TMS)_3\}_3Ge_9]^-$ units to $\{Si(TMS)_3\}_6Ge_{18}$ by oxidation was successful yielding an uncharged Ge_{18} cluster compound (Figure 11f and Figure 15b).[172]

Initiated by the report on $[\{Si(TMS)_3\}_3Ge_9]^-$,[177] a wealth of further reactions with this species was reported in a remarkably short time period, what underlines its high synthetic potential (see Scheme 7). For example, the uncharged transition metal compounds $[M(NHC^{Dipp})]$-$[\{Si(TMS)_3\}_3Ge_9]$ (*M* = Cu, Ag, Au),[200] and [Ni(dppe)] $[\{Si(TMS)_3\}_3Ge_9]$[195] were obtained and feature carbene and phosphine ligands at the metal centers. Besides, a fourth substituent can be attached at the cluster cores forming uncharged compounds as demonstrated by synthesis of $[\{Si(TMS)_3\}_3Ge_9(L)]$ {*L* = PCy_3, P^iPr_3;[201] R = Et, Sn^nBu_3, Tl;[202] R = $SnPh_3$[203]}. The fourth cluster substitution step initiated the synthesis of olefin-functionalized clusters $[\{Si(TMS)_3\}_3Ge_9(Olefin)]$ (olefin = vinyl, pentenyl).[204] Moreover, an example for a tetra-substituted metal complex was found with $[Pd(PPh_3)][\{Si(TMS)_3\}_3Ge_9Et]$,[205] as well as cluster expansion of $[\{Si(TMS)_3\}_3Ge_9]^-$ units by η^4-coordinated transition metal moieties in the structures of $[M(PPh_3)][\{Si(TMS)_3\}_3Ge_9]$ (*M* = Ni, Pt)[206] and $\{[Cr(CO)_n][\{Si(TMS)_3\}_3Ge_9]\}^-$ (n = 3, 5).[207]

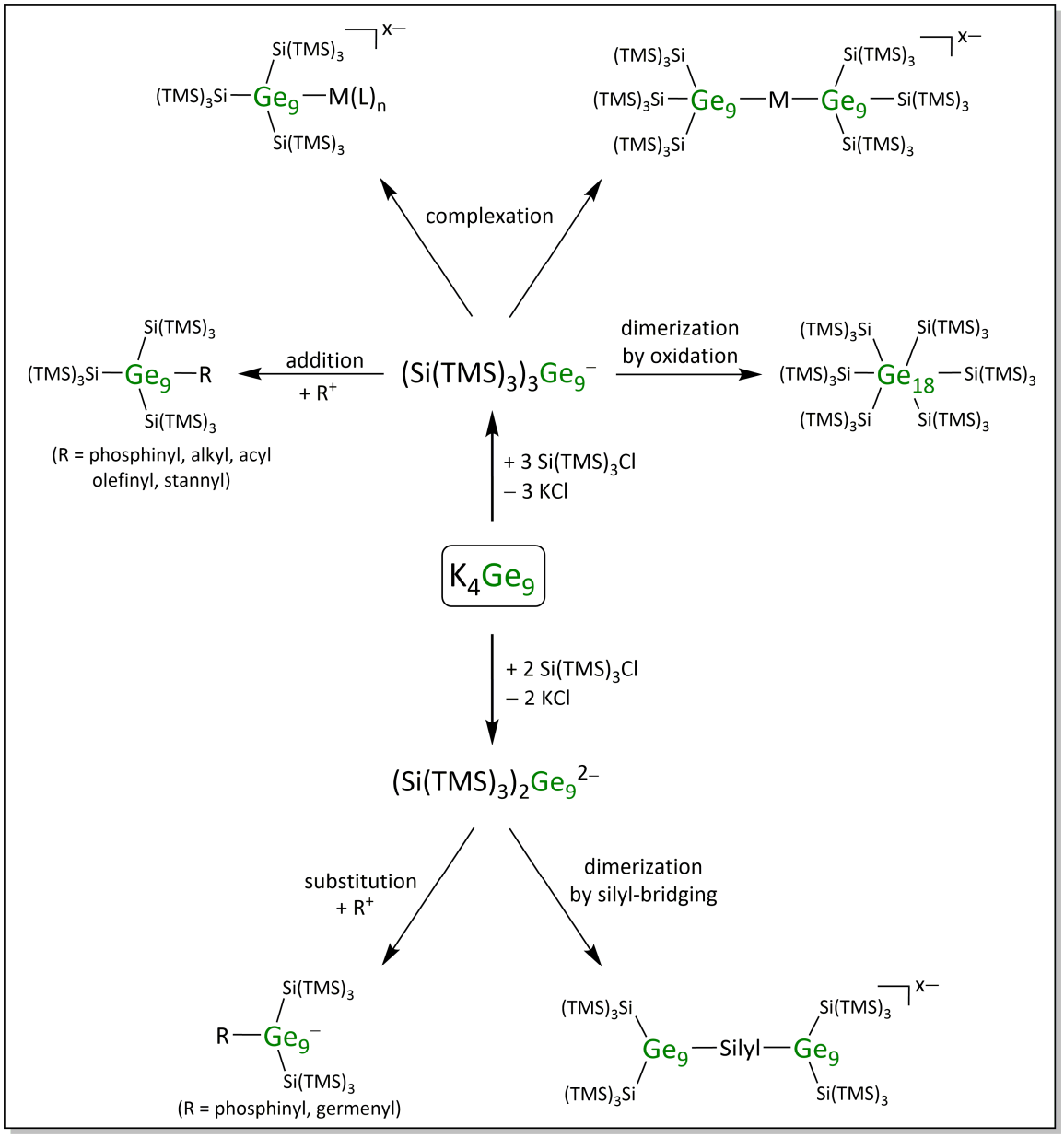

Scheme 7. Reaction pathways for synthesis and tailoring of silylated Ge_9 cluster species (selected examples).

In further reports, the steric impact of the silyl ligands at the Ge_9 cores was modified and the (bulky) tri-silylated derivatives $[\{Si(TMS)_2SiPh_3\}_3Ge_9]^-$ [208] and $[(SiH^tBu_2)_3Ge_9]^-$ [209] were synthesized. However, a synthetic breakthrough was achieved by isolation of the di-silylated Ge_9 species $[\{Si(TMS)_3\}_2Ge_9]^{2-}$ (Figure 15c).[192] Comparison to the tri-silylated derivative $[\{Si(TMS)_3\}_3Ge_9]^-$ in Figure 15a shows that one of the prism square capping Ge vertex atoms remains unsubstituted. Consequently, $[\{Si(TMS)_3\}_2Ge_9]^{2-}$ boasts seven unsubstituted Ge atoms including a further reactive position for ligand attachment. This initiated the synthesis of mixed-substituted Ge_9 clusters as demonstrated with $[\{Si(TMS)_3\}_2(P^tBu_2)Ge_9]^-$ [201] and $[\{Si(TMS)_3\}_2\{Ge(TMS)_3\}Ge_9]^-$,[210] as well as silyl-bridging of two $[\{Si(TMS)_3\}_2Ge_9]^{2-}$ cluster units in $\{Si(TMS)_3\}_2Ge_9–SiMe_2–(C_6H_4)–SiMe_2–\{Si(TMS)_3\}_2Ge_9$[193] (Figure 15d).

1.5 Motivation and Outline of the Thesis

The industrial relevance of silicon- and germanium-based materials has been pointed out. Both elements are key players for nowadays high-tech applications as mirrored by electronics,[15, 211-212] photovoltaics[19, 213-214] and batteries.[18, 24, 215] Due to its abundancy, silicon is also processed to industrial products on larger scale as *e.g.* polysiloxanes (silicones).[2, 32-34] Due to a constantly increasing demand on Si and Ge materials, access to preformed building blocks as contained in *Zintl* precursor materials is of central interest with focus on the synthesis of cluster-based building blocks with tunability for future material fabrication (Figure 16).[15-16, 139, 216-218]

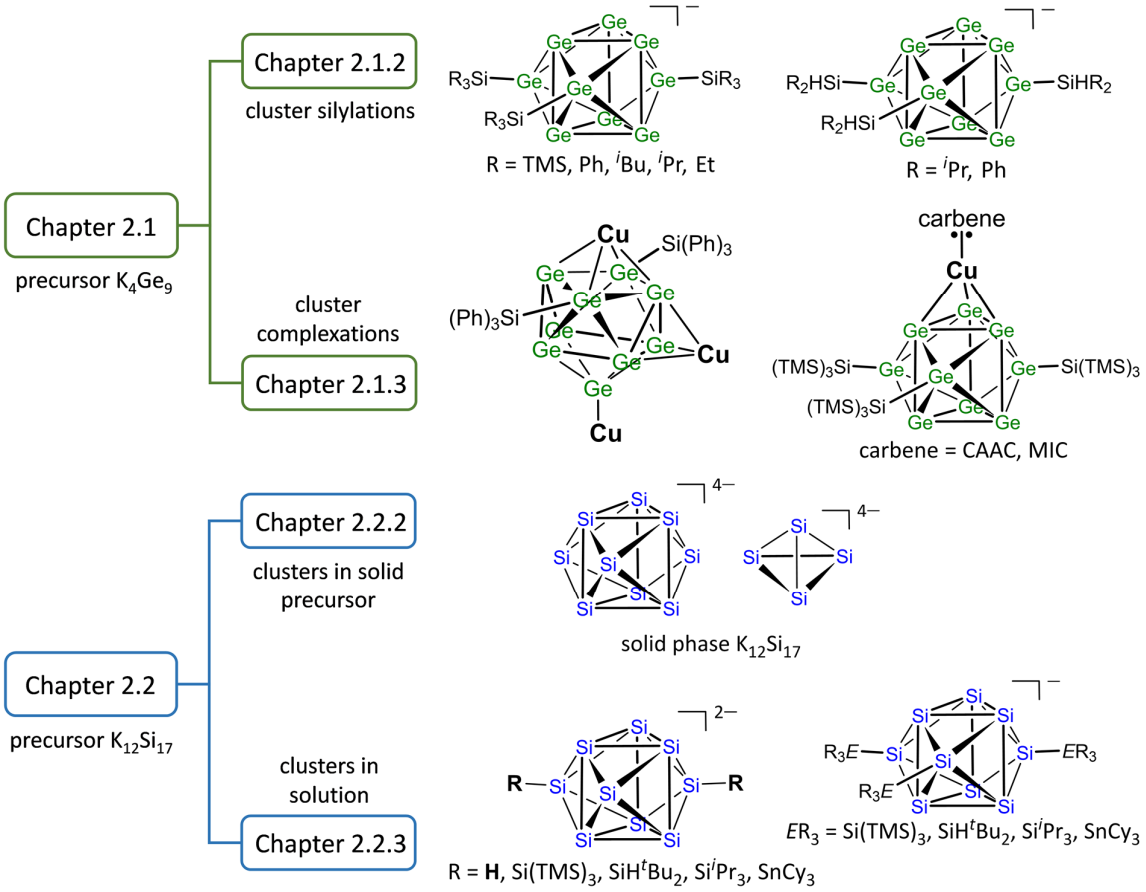

Figure 16. Outline of the results within this doctoral thesis presented in chapter 2 and based on the publications in chapter 6.

Hereto, *Zintl* precursor materials can play a key role as cluster sources because they readily contain low-valent clusters of silicon and germanium. The prominent precursor materials $K_{12}Si_{17}$ and K_4Ge_9 provide low-valent Si_9^{4-}/Si_4^{4-} or Ge_9^{4-} clusters, respectively, along with separated potassium cations in salt-like *Zintl* compounds. They can by synthesized in quantitative yields by direct fusing of the contained elements in solid-state reactions. For their utilization as building blocks, their transformation to cluster solutions is of central interest. Initially, solubility limitations of the clusters were induced by their polyanionic character, and the solubility of the precursors was rather limited to polar amine-based solvents. Thereto, the development of practicable reaction pathways aiming

soluble (functionalized) cluster species is of central interest for future fabrications and their further development is central content of this work.[44-45, 47, 71, 77]

Investigations with the precursor K_4Ge_9 are shown in chapter 2.1 (Reactions with Ge_9 Clusters from K_4Ge_9 Precursor Material). Here, the attachment of versatile silyl groups with varying steric and electronic properties including Si–H-functionalizations is reported in chapter 2.1.2 (Exploration of Silylation Reactions with Ge_9 Clusters). Changing of the silyl ligand's properties resulted in versatile obtained transition metal complexes as presented in 2.1.3 (Exploration of Metal Complexations with Ge_9 Clusters) with application-relevant, organic ligands at the metal atoms.

Synthetic achievements were transferred from Ge_9 to Si_9 clusters in chapter 2.2 (Reactions with Si_9 Cluster from $K_{12}Si_{17}$ Precursor Material). The transfer was initiated by new insights into the nature of the contained silicon clusters in the precursor material $K_{12}Si_{17}$ in solid-state interplaying with computational studies (chapter 2.2.2, Silicon Clusters in Intermetallic $K_{12}Si_{17}$ Precursor Material).

Utilization of the $K_{12}Si_{17}$ precursor material is presented in chapter 2.2.3 (Utilization of Si_9 Clusters from $K_{12}Si_{17}$ Precursor Material). "*Activation*" of the $K_{12}Si_{17}$ precursor (chapter 2.2.3.1, Activation of $K_{12}Si_{17}$ Precursor Material) paved the way for the synthesis of protonated Si_9 clusters in solution in chapter 2.2.3.2 (Investigation of $[H_2Si_9]^{2-}$ in Pyridine and Ethylenediamine Solution). Moreover, Ge_9 cluster silylations could be transferred to Si_9 clusters under formation of siliconoid clusters (chapter 2.2.3.3, Formation of $[(ER_3)_3Si_9]^-$ Siliconoid Clusters). The results were complemented by synthesis and discussion of molecular Si_9 siliconoid clusters in chapter 2.2.3.4 (Molecular Structures of $[(ER_3)_2Si_9]^{2-}$ Siliconoid Clusters), which introduce the formation of siliconoid material building blocks from $K_{12}Si_{17}$ precursor material.

2 RESULTS AND DISCUSSION

2.1 Reactions with Ge_9 Clusters from K_4Ge_9 Precursor Material

Reactions of Ge_9 clusters from the precursor K_4Ge_9 are described in this subchapter. Experimental details can be found in chapter 4. Results of the following manuscripts (see attached in chapter 6) are outlined herein. Experimental data as well as further background, discussion and conclusions of the results can be found in the manuscripts.

List of manuscripts to chapter 2.1:

i) see chapter 6.1: Schiegerl, L. J.; Geitner, F. S.; Fischer, C.; Klein, W.; Fässler, T. F., Functionalization of $[Ge_9]$ with Small Silanes:$[Ge_9(SiR_3)_3]^-$ (R = *i*Bu, *i*Pr, Et) and the Structures of $(CuNHC^{Dipp})[Ge_9\{Si(iBu)_3\}_3]$, (K-18c6)Au$[Ge_9\{Si(iBu)_3\}_3]_2$, and (K-18c6)$_2[Ge_9\{Si(iBu)_3\}_2]$. *Z. Anorg. Allg. Chem*. 2016, *642* (24), 1419-1426.

ii) see chapter 6.2: Mayer, K.; Schiegerl, L. J.; Fässler, T. F., On the Reactivity of Silylated Ge_9 Clusters: Synthesis and Characterization of $[ZnCp^*(Ge_9\{Si(SiMe_3)_3\}_3)]$, $[CuPiPr_3(Ge_9\{Si(SiMe_3)_3\}_3)]$, and $[(CuPiPr_3)_4\{Ge_9(SiPh_3)_2\}_2]$. *Chem. Eur. J*. 2016, *22* (52), 18794-18800.

iii) see chapter 6.3: Schiegerl, L. J.; Klein, W.; Fässler, T. F., Utilization of Si_9 Clusters from $K_{12}Si_{17}$ Precursor Material for Subsequent Reactions. *Manuscript for Publication.* 2019.

iv) see chapter 6.4: Schiegerl, L. J.; Melaimi, M.; Tolentino, D. R.; Klein, W.; Bertrand, G.; Fässler, T. F., Silylated Ge_9 Clusters as New Ligands for Cyclic (Alkyl)amino and Mesoionic Carbene Copper Complexes. *Inorg. Chem*. 2019, *58* (5), 3256-3264.

2.1.1 Motivation and Outline of Relevant Literature for Germanium Clusters

Due to their high performance, germanium-based materials are of central interest for high-tech applications as *e.g.* batteries, *nano*-devices, optoelectronics and photovoltaics.[15-20] Thereby, the tailoring of defined structures, as present for Ge_9 clusters (Figure 17a) from the *Zintl* phase precursor K_4Ge_9, plays a key role for the design of novel material building blocks (chapters 1.3 and 1.4). The synthesis of the precursor material is well-established[68, 73] and the compound can be synthesized in quantitative yield by fusing a stochiometric mixture of elemental germanium and potassium (Scheme 3). Therein, low-valent Ge_9^{4-} polyanions are readily preformed in conjunction with potassium cations. It was pointed out that the contained clusters are accessible to a wide range of further transformations in solution.[68, 73] In the scope of knowledge to known germanium structures, these clusters are outstanding because they boast a combination of unsaturated (bonding situation[82-84]) and nucleophilic (multiple negative charge) properties.[45, 47]

For a long time, the main drawback for an application of Ge_9 clusters was their limited solubility due to their polyanionic charge. However, it was already shown that the cluster charges can be reduced by numerous synthetic approaches under transformation of the precursor to molecular cluster species in solution. Reactions of A_4Ge_9 (*A* = alkali metal) in the polar amine solvent ethylenediamine show that the compound can serve as precursor for the synthesis of Ge_9 polymers (Figure 9d), as well as for films with defined nanomorphologies.[20, 85] Despite these achievements, the development of straight-forward syntheses for cluster compounds, which are soluble in common organic solvents and suitable for further modifications, is still of crucial interest and central content of this work. Thereby, the synthesis of soluble Ge_9 cluster compounds was explored with focus on the attachment of covalently bonded silyl groups.

For the synthesis of Ge_9 cluster compounds with decreased charges, the attachment of covalently bonded ligands was found to be a promising synthetic approach to obtain tailored building blocks (Scheme 5). The cluster solubility is enhanced under formation of ligand-stabilized Ge_9 species. Numerous mono-, di and tri-substituted Ge_9 species were reported by reactions of Ge_9 with main group compounds. Organyl, stannyl, phosphinyl, germenyl and stibyl groups were attached at the clusters under formation of substituted $[RGe_9]^{3-}$ (R = $SnPh_3$, $SnMe_3$)[174], $[R_2Ge_9]^{2-}$ (R = $BiPh_2$, $GePh_3$, $SnMe_3$, $SnPh_3$, $SbPh_2$, Ph)[174-176] and $[R_3Ge_9]^-$ {R = Sn^iPr_3, $SnCy_3$, $GePh_3$, $P(N^iPr)_2$, $P(N^iPr)^tBu$}[177-180] species in solution.

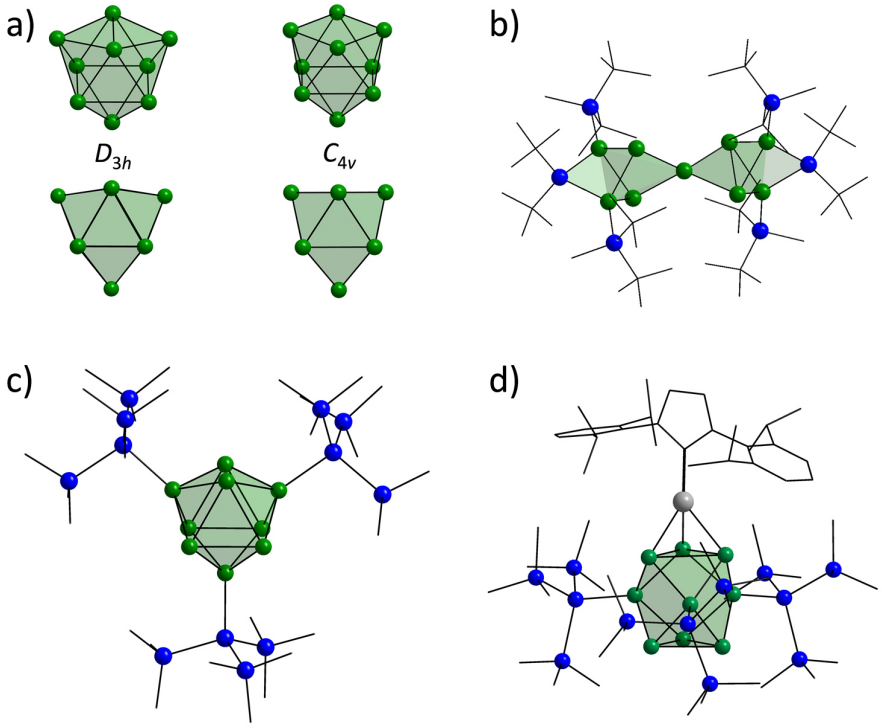

Figure 17. Structures of germanium cluster species: a) D_{3h} symmetric (left) and C_{4v} symmetric (right) Ge_9 clusters; b) the spirocyclic Si_2Ge_9 cluster $(^tBu)_4(^tBu_2MeSi)_4Si_2Ge_9$;[170] c) the tri-silylated Ge_9 cluster $[\{Si(TMS)_3\}_3Ge_9]^-$;[177, 191] d) the Ge_9 copper carbene complex $[Cu(NHC^{Dipp})][\{Si(TMS)_3\}_3Ge_9]$ with a NHC ligand.[200] Ge atoms are shown in green, Si atoms in blue, C and N atoms as wire-sticks, Cu atoms in gray, H atoms are omitted, Ge_9 clusters are shown as green polyhedra.

Regarding the formation of germanium cluster compounds, syntheses also succeeded from "molecular bottom-up" approaches. Besides the formation of smaller Ge_3 and Ge_4 clusters (Figure 10),[151, 162] also larger Ge clusters were reported as *e.g.* the spirocyclic species $(^t Bu)_4(^t Bu_2MeSi)_4Si_2Ge_9$ [170] with five ligand-free Ge atoms (Figure 17b). Anyhow, approaches with molecular precursors require multi-step synthesis what is hindering for applications. Hereto, the utilization of K_4Ge_9 precursor material was most recently promoted by single-step reactions of K_4Ge_9 with SiR_3Cl (R = organic rest) chlorosilane compounds that yielded silyl-stabilized Ge_9 species. The reactions yielded tri-silylated $[R_3Ge]^-$ (R = silyl group) species by heterogenous conversion in acetonitrile or thf. The first reported silylated Ge_9 cluster species is $[\{Si(TMS)_3\}_3Ge_9]^-$ [177, 191] (Figure 17c). The three hypersilyl groups are attached at the Ge_9 core under formation of covalent cluster *exo*-bonds. The molecular species boasts only one negative charge along with an (bulky) organic environment around the cluster core what induces excellent solubility and stability in organic solvents. It was further shown that the steric impact of attached silyl groups can be modified and the tri-silylated derivatives $[\{Si(TMS)_2SiPh_3\}_3Ge_9]^-$ [208] and $[(SiH^tBu_2)_3Ge_9]^-$ [209] were subsequently obtained.

The tri-silyated species $[\{Si(TMS)_3\}_3Ge_9]^-$ set the starting point for rapid progress in the field of silylated Ge_9 clusters. η^3-Coordinations of the bare, prismatic cluster faces at coinage metal atoms revealed to be extraordinarily successful for the synthesis of *e.g.* metal-bridged $[\{Si(TMS)_3\}_3Ge_9–M–\{Si(TMS)_3\}_3Ge_9]^-$ [196-197] dimer species (Scheme 7) and uncharged monomer $[M(NHC^{Dipp})][\{Si(TMS)_3\}_3Ge_9]$ [200] (Figure 17d) complexes bearing carbene ligands at the metal atoms (*M* = Cu, Ag, Au). Oxidation of $[\{Si(TMS)_3\}_3Ge_9]^-$ also yielded the dimerized, uncharged cluster compound $\{Si(TMS)_3\}_6Ge_{18}$ with the high number of 12 naked Ge atoms (Figure 15b) what demonstrates a simple synthetic approach for cluster expansion.[172]

Triggered by the rapid synthetic success to reactions of Ge_9 clusters with chlorosilanes, new silylation were investigated in chapter 2.1.2 to further explore the tailoring of silylated Ge_9 clusters including Si–H functionalization *via* silylation. The synthetic potential of silylated Ge_9 clusters was further explored in chapter 2.1.3 by transition metal (copper, zinc) complexation with versatile organic ligands at the metal atoms including cyclic(alkyl)amino (CAAC) and mesoionic (MICs) carbenes. The investigations further explore synthetic pathways to utilize K_4Ge_9 precursor materials for the formation of Ge_9-based material building blocks.

2.1.2 Exploration of Silylation Reactions with Ge_9 Clusters

As described in chapter 2.1.1, the tri-silylated cluster species $[\{Si(TMS)_3\}_3Ge_9]^-$,[177, 191] $[\{Si(TMS)_2SiPh_3\}_3Ge_9]^-$,[208] and $[(SiH^tBu_2)_3Ge_9]^-$ [209] were obtained by direct, heterogeneous reactions of the precursor K_4Ge_9 with chlorosilane compounds (see Scheme 5). In the scope of this this work, the steric as well as electronic impact of covalently bonded silyl groups at the cluster cores was diversified. Thereby, silylations of K_4Ge_9 were tested with the chlorosilanes SiR_3Cl (R = ^{t}Bu, Ph, ^{i}Bu, ^{i}Pr, Et, N^{i}Pr$_2$, Me) to gain systematic knowledge about the stability of silylated cluster species with respect to the steric and electronic impact of the silyl groups. The reactions were carried out in analogy to syntheses of previously reported silylated Ge_9 species by heterogeneous reactions in

thf or acetonitrile solution and under usage of at least three equivalents of the respective chlorosilane reactant.

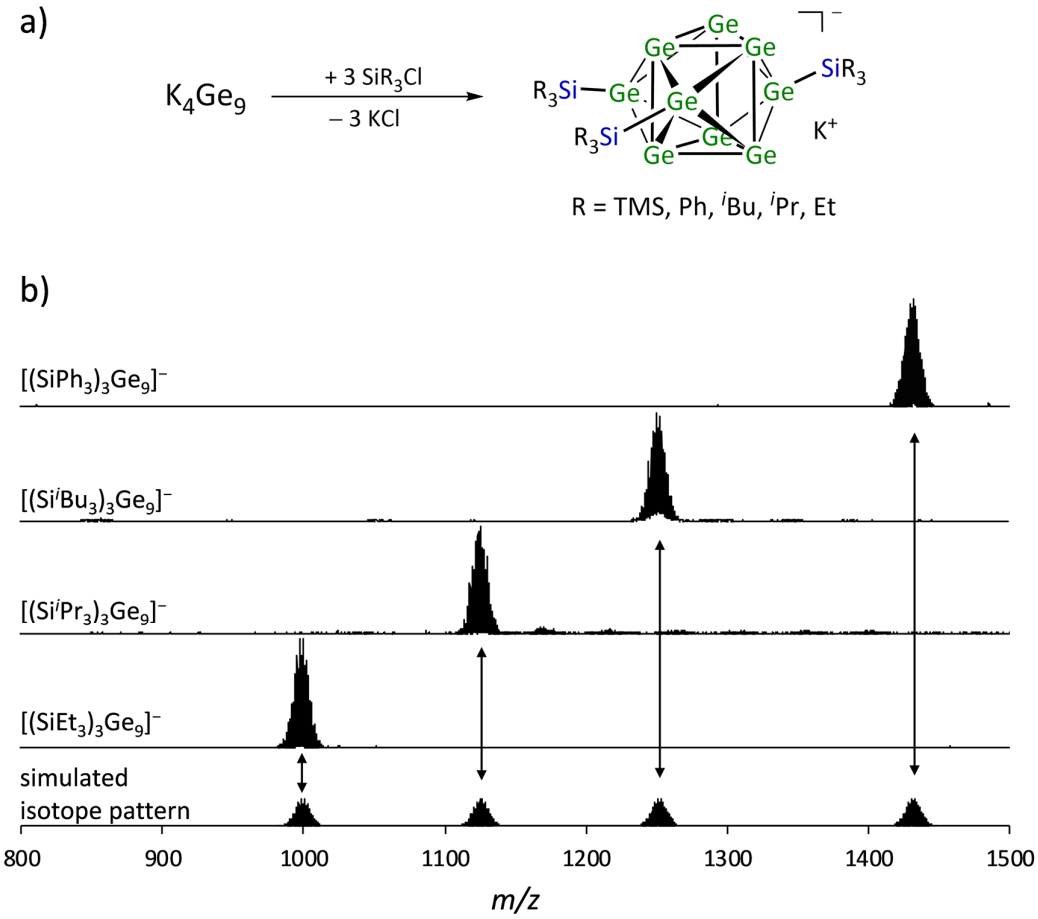

Figure 18. a) Reaction scheme for the silylation of Ge_9 clusters from the precursor K_4Ge_9 with chlorosilanes under formation of tri-silylated cluster species; b) ESI-MS spectra of obtained tri-silylated cluster species $[(SiR_3)_3Ge_9]^-$ (R = Ph, ^{i}Bu, ^{i}Pr, Et) in solution.

Reactions of K_4Ge_9 with SiR_3Cl (R = Ph, ^{i}Bu, ^{i}Pr, Et) chlorosilanes yielded the tri-silylated species $[(SiR_3)_3Ge_9]^-$ (R = Ph, ^{i}Bu, ^{i}Pr, Et) in solution and their formation was confirmed by ESI-MS investigations (Figure 18a). Moreover, bulk material was isolated in the case of R = Ph, ^{i}Bu and characterized by NMR spectroscopy as analytically pure compounds. For SiR_3Cl (R = N^{i}Pr$_2$, Me) the formation of colored reaction solutions was observed, what is indicative for the formation of silyated Ge_9 species in solution, but ESI-MS measurements did not reveal the formation of (stable) silylated Ge_9 cluster species.

Reaction of K_4Ge_9 with Si^{t}Bu$_3$Cl did not reveal the formation of silylated Ge_9 species either, and it is assumed that three organic ^{t}Bu groups at silyl atoms are too bulky for cluster silylation whereas three Me groups in -SiMe$_3$ might be not bulky enough. In case of -SiPh$_3$ groups, which bears the lowest electron density at the silyl atom, also the di-silylated $[(SiPh_3)_2Ge_9]^{2-}$ cluster species was obtained by stochiometric reaction of the reactants in acetonitrile. The species was identified in

ESI-MS and NMR spectra. Interestingly, formations of all obtained $[(SiR_3)_3Ge_9]^-$ (R = Ph, ^{i}Bu, ^{i}Pr, Et) cluster were observed to proceed slower in thf than in acetonitrile solutions.[219-222]

Growing of single crystals from solutions that contain the tri-silylated clusters species $[(SiR_3)_3Ge_9]^-$ (R = Ph, ^{i}Bu, ^{i}Pr, Et) was tested by various attempts under variation of solvents and temperature. In the cases of R = Ph, ^{i}Pr, Et the decoloring of the solutions indicated repeatedly decomposition of the cluster species after several days whereas for R = ^{i}Bu yellow single crystals formed from a toluene/hexane solvent mixture under usage of the sequestering agent 18c6. Single crystal X-ray diffraction revealed the di-silyated structure of $[(Si^iBu_3)_2Ge_9]^{2-}$ (Figure 19) with two η^3-coordinated $[K\text{-}18c6]^+$ units at the cluster [Ge–Si bond lengths in the molecular structure: 2.381(1) Å each]. The crystals were further characterized by ^{1}H NMR and ESI-MS and the presence of di-silylated cluster cores was manifested in solution. A cleavage of one silyl group during crystallization was not observed for silylated Ge_9 clusters before and indicates the lability of one Ge–Si bond within the $[(Si^iBu_3)_3Ge_9]^-$ derivative in the non-polar solvent mixture toluene/hexane.

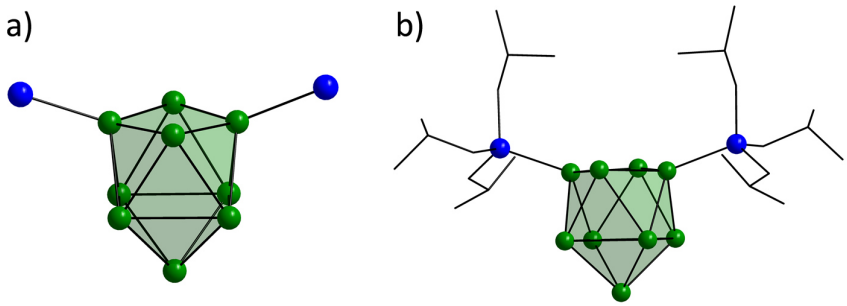

Figure 19. Molecular structure of $[(Si^iBu_3)_2Ge_9]^{2-}$ in the compound $[K\text{-}18c6]_2[(Si^iBu_3)_2Ge_9]$. a) Ge atoms in green, Ge_9 cluster as green polyhedron, C and H atoms are omitted; b) Ge atoms in green, Ge_9 cluster as green polyhedron, C atoms as wire-sticks, H atoms are omitted.

Initiated by the successful synthesis of silylated Ge_9 clusters by reaction of K_4Ge_9 with SiR_3Cl (R = TMS, Ph, ^{i}Bu, ^{i}Pr, Et) chlorosilanes, Ge_9 cluster Si–H functionalization *via* silylation was investigated with the $SiHR_2Cl$ (R = Me, ^{i}Pr, Ph) chlorosilanes in a mass spectrometric study. Regarding the trifunctionalization of Ge_9 clusters from K_4Ge_9 *via* silylation, only a few examples have been reported before with the Si–H functionalized $[(SiH^tBu_2)_3Ge_9]^-$ [209] species and the olefin-functionalized $[\{SiPh_2(\textit{Olefin})\}_3Ge_9]^-$ (olefin = vinyl, pentenyl)[223] species.

ESI-MS examinations of reaction mixtures with K_4Ge_9 / $SiHR_2Cl$ (R = Me, ^{i}Pr, Ph) in acetonitrile revealed mass peaks for tri-functionalized $[(SiHR_2)_3Ge_9]^-$ (R = ^{i}Pr, Ph) cluster species, obtained in single-step synthesis (Figure 20). In the case of R = Me a silylated cluster species was not detected. Most conclusively the -$SiHMe_2$ groups do not boast enough steric impact for the formation of stable silylated cluster molecules as also observed for -$SiMe_3$ groups before. If compared to $[(SiH^tBu_2)_3Ge_9]^-$,[209] $[(SiHR_2)_3Ge_9]^-$ species (R = ^{i}Pr, Ph) provide less shielded cluster cores due to the less bulky organic rests, what might result in a more favorable applicability for future synthetic modifications. Furthermore, formations of mono Si–H-functionalized Ge_9 clusters were tested. Thereto, $SiHR_2Cl$ (R = ^{i}Pr, Ph) chlorosilanes were reacted with the di-silylated $[\{Si(TMS)_3\}]_2Ge_9]^{2-}$ cluster species in acetonitrile solution (Figure 20). The formation of mono-functionalized Ge_9 clusters was indicated in ESI-MS measurements by detection of $[\{Si(TMS)_3\}_2(SiHR_2)Ge_9]^-$ (R = ^{i}Pr, Ph) mass peaks.

Summarized, the results for Si–H functionalized Ge_9 clusters add to olefin-functionalized Ge_9 clusters from silylation reactions in literature that yielded the derivatives $[\{Si(TMS)_3\}_2\{SiPh_2(Olefin)\}Ge_9]^-$ (olefin = vinyl, pentenyl)[223] and extend the accessibility of Ge_9 cluster species that are suitable for further reactions as *e.g.* surface linking and cluster couplings.

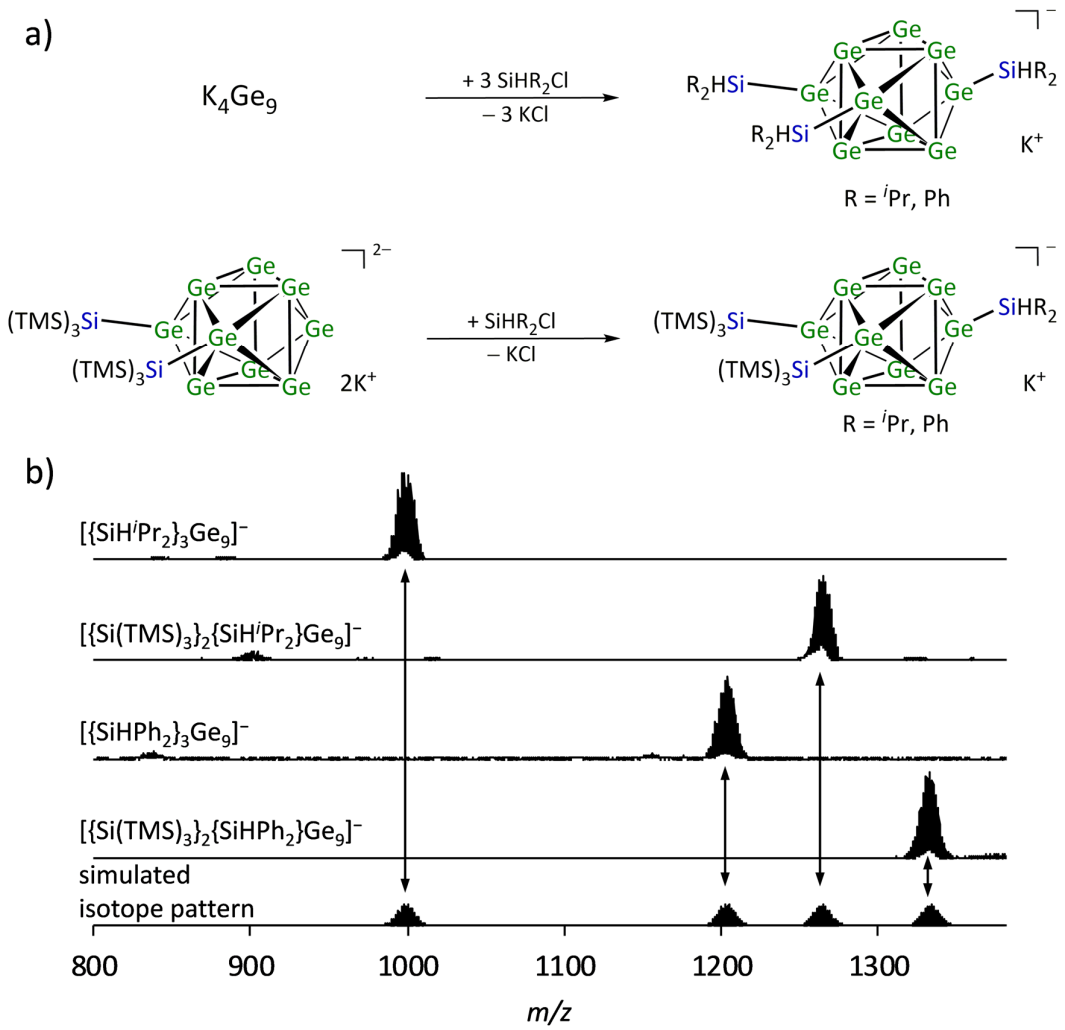

Figure 20. a) Synthesis of Si–H functionalized Ge_9 cluster species by reaction of K_4Ge_9 and $[\{Si(TMS)_3\}]_2Ge_9]^{2-}$ with $SiHR_2Cl$ (R = ^{i}Pr, Ph) chlorosilanes in acetonitrile; b) ESI-MS spectra of obtained Ge_9 cluster species in solution.

2.1.3 Exploration of Metal Complexations with Ge_9 Clusters

Metal complexation of $[\{Si(TMS)_3\}_3Ge_9]^-$ clusters (see chapter 1.4.2.3) showed up to be a fruitful synthetic approach for cluster modification. This initiated investigations to complexations of silylated Ge_9 clusters with Cu(I) and Zn(II) compounds bearing versatile organic ligands at the metal atoms including carbenes (CAAC and MIC).

2.1.3.1 Monomeric and Dimeric Ge_9 Cluster Metal Complexes

The compounds $Cu(P^iPr_3)Cl$, $ZnCl_2$ and $Zn(Cp^*)_2$ were tested for cluster metal complexation with $[\{Si(TMS)_3\}_3Ge_9]^-$ (Scheme 8). Reaction of $[\{Si(TMS)_3\}_3Ge_9]^-$ with $Zn(Cp^*)_2$ in toluene yielded the compound $[Zn(Cp^*)][\{Si(TMS)_3\}_3Ge_9]$ with a η^5-coordinated Cp^* at a Zn atom that is η^3-coordinated by a tri-silylated Ge_9 cluster. The uncharged cluster complex was characterized by NMR and ESI-MS studies in solution. Its structure was determined from single crystals obtained from toluene solution (Figure 21e). In contrast, reaction of $[\{Si(TMS)_3\}_3Ge_9]^-$ with $ZnCl_2$ in acetonitrile yielded the dimeric cluster compound $Zn[\{Si(TMS)_3\}_3Ge_9]_2$ with two η^3-coordinated Ge_9 cluster ligands at a Zn atom after substitution of both of the chloride ligands through a silylated cluster ligand (Scheme 8). Single crystals from a toluene/Et_20 solvent mixture revealed the molecular structure of the compound, which was previously reported by another synthetic approach (Figure 21a).[194] Reaction of $[\{Si(TMS)_3\}_3Ge_9]^-$ with $Cu(P^iPr)_3Cl$ in acetonitrile yielded the compound $[Cu(P^iPr_3)][\{Si(TMS)_3\}_3Ge_9]$ that bears a η^1-coordinated P^iPr_3 ligand and a η^3-coordinated tri-silylated Ge_9 cluster ligand at a Cu atom (Figure 21d). Structure determination succeeded with single crystals from a toluene solution and characterization in solution by NMR and ESI-MS.

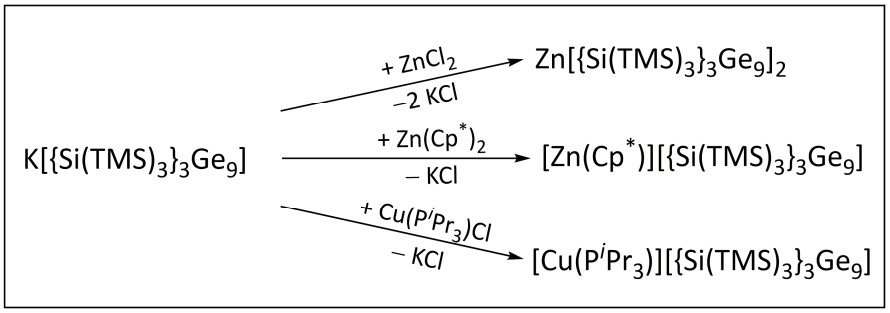

Scheme 8. Formation of transition metal complexes with $[\{Si(TMS)_3\}_3Ge_9]^-$ as they were found in molecular structures (see Figure 21).

In contrast to substitutions of chloride ligands by silylated Ge_9 cluster ligands at metal atoms, syntheses of the compounds $[Zn(Cp^*)][\{Si(TMS)_3\}_3Ge_9]$ and $[Cu(P^iPr_3)]$-$[\{Si(TMS)_3\}_3Ge_9]$ show that electron donating ligands can be retained at the metal atoms in cluster complexes. For further insights, the newly obtained tri-silylated $[(SiR_3)_3Ge_9]^-$ (R = Ph, ^{i}Bu) species were tested upon their reactivity with coinage metal compounds (Scheme 9).

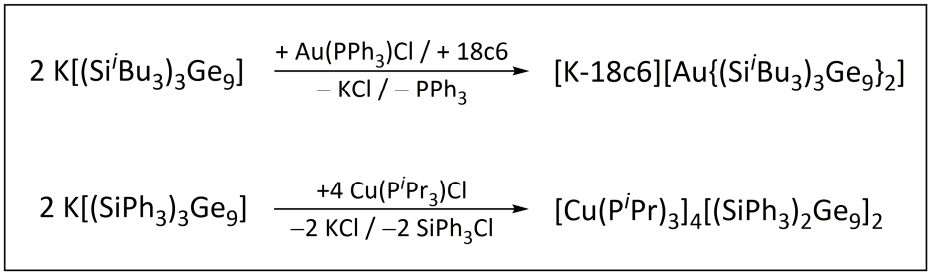

Scheme 9. Formation of coinage metal complexes with $[(SiR_3)_3Ge_9]^-$ (R = Ph, ^{i}Bu) as they were found in molecular structures. Molecular structures are shown in Figure 21.

Thereby, the dimeric cluster species $[Au\{(Si^iBu_3)_3Ge_9\}_2]^-$ was found in single crystals from complexation of $[(Si^iBu_3)_3Ge_9]^-$ with $Au(PPh)_3Cl$ in acetonitrile and forms by cluster substitution of chloride and PPh_3 ligands at the Au^+ atom. In the structure, two $[(Si^iBu_3)_3Ge_9]^-$ ligands are η^3-bridged by one Au^+ atom (Figure 21b). Interestingly, a polymeric arrangement of the $[Au\{(Si^iBu_3)_3Ge_9\}_2]^-$ dimer units is formed in the single crystal structure by η^3-bridging of the bare prismatic cluster faces with $[K\text{-}18c6]^+$ units.

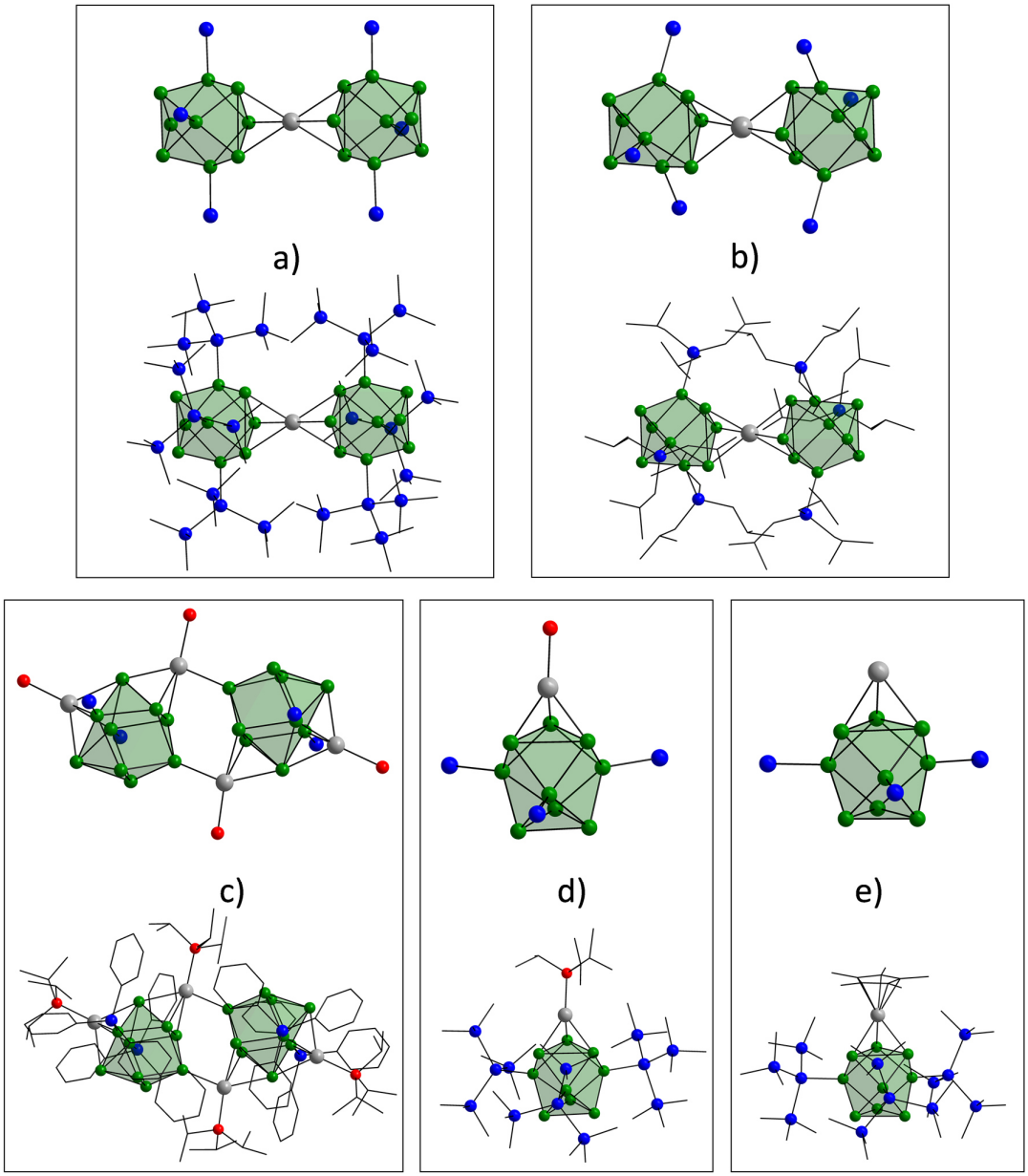

Figure 21. Molecular structures of transition metal complexes with silylated Ge_9 clusters: a) $Zn[\{Si(TMS)_3\}_3Ge_9]_2$; b) $[Au\{(Si^iBu_3)_3Ge_9\}_2]^-$; c) $[Cu(P^iPr_3)]_4[(SiPh_3)_2Ge_9]_2$; d) $[Cu(P^iPr_3)][\{Si(TMS)_3\}_3Ge_9]$; e) $[Zn(Cp^*)][\{Si(TMS)_3\}_3Ge_9]$. Ge atoms in green, Si atoms in blue, P atoms in red, Zn and Cu atoms in gray, Ge_9 clusters as green polyhedra, H atoms are omitted; Top views: TMS, Ph, ^{i}Bu, ^{i}Pr groups are omitted; bottom views: Si_{TMS} atoms in blue and Ph, ^{i}Bu, ^{i}Pr groups as wire-sticks.

In analogy to the di-silyated cluster complex $[(Si^{i}Bu_3)_2Ge_9]^{2-}$ (Figure 19) that forms in single crystals from $[(Si^{i}Bu_3)_3Ge_9]^{-}$, a di-silyated $[Cu(P^{i}Pr_3)]_4[(SiPh_3)_2Ge_9]_2$ cluster complex forms by cleavage of one -$SiPh_3$ substituent from $[(SiPh_3)_3Ge_9]^{-}$. Its synthesis succeeded by reaction of $[(SiPh_3)_3Ge_9]^{-}$ with $Cu(P^{i}Pr_3)Cl$ in acetonitrile. Four $[Cu(P^{i}Pr_3)]^{+}$ moieties are connected with two $[(SiPh_3)_2Ge_9]^{2-}$ cluster units under formation of a novel structural arrangement comprising η^1-, η^3- and η^4-coordination modes between the clusters and the copper atoms (Figure 21c). Thereby, a doubly copper-bridged cluster dimer arised in single crystals from a toluene/hexane solution. In analogy to the phosphine ligands in $[Cu(P^{i}Pr_3)][\{Si(TMS)_3\}_3Ge_9]$ (Figure 21d), the $P^{i}Pr_3$ groups are retained at the copper atoms. The Ge–$SiPh_3$ bond lengths in the structure have an average value of 2.41 Å, what is slightly elongated if compared to an average value of 2.38 Å in $[Cu(P^{i}Pr_3)][\{Si(TMS)_3\}_3Ge_9]$ and $[Zn(Cp^{*})][\{Si(TMS)_3\}_3Ge_9]$ each.

The Ge–Ge bonds within the η^3-coordinated cluster prism faces show characteristic elongations for complexations with different transition metal moieties. Analysis shows a Ge–Ge bond elongation to 2.88 Å (average value) for $[Cu(P^{i}Pr_3)]^{+}$ moieties in $[Cu(P^{i}Pr_3)][\{Si(TMS)_3\}_3Ge_9]$ and to 2.74 Å (average values) in $[Cu(P^{i}Pr_3)]_4[(SiPh_3)_2Ge_9]_2$. The Ge–Ge bond elongations were found to be more pronounced for the $[Zn(Cp^{*})]^{+}$ moiety in $[Zn(Cp^{*})][\{Si(TMS)_3\}_3Ge_9]$ (avg. Ge–Ge distance: 2.96 Å), as well as for the bridging atoms Zn^{2+} in $Zn[\{Si(TMS)_3\}_3Ge_9]_2$ (avg. Ge–Ge distance: 2.90 Å) and Au^{+} atoms in $[Au\{(Si^{i}Bu_3)_3Ge_9\}_2]^{-}$ (avg. Ge–Ge distance: 2.95 Å). Regarding the Ge_9 cluster symmetries, tri-silylated Ge_9 metal complexes bear clusters whose shape is best described as D_{3h} symmetric, whereas the di-silylated clusters in $[Cu(P^{i}Pr_3)]_4[(SiPh_3)_2Ge_9]_2$ and $[(Si^{i}Bu_3)_2Ge_9]^{2-}$ (Figure 19) are best described by C_{2v} symmetry deriving from a mono-capped square antiprism.

2.1.3.2 Ge_9 Cluster Complexes with Copper Carbenes

The firstly reported Ge_9 copper carbene complex is the uncharged $[Cu(NHC^{Dipp})][\{Si(TMS)_3\}_3Ge_9]$ compound (see chapters 2.1.1 and Figure 17).[200] The complex was obtained from acetonitrile solution besides its silver and gold derivatives and under retention of electron-donating NHCs at the metal atoms. The uncharged compounds boast excellent solubility and stability in non-polar solvents such as toluene. This triggered investigations with cyclic(alkyl)amino {$CAAC^{Dipp,Et}$ = [:C(N-Dipp)(CMe_2)(CH_2)(CEt_2)]} and mesoionic {$MIC^{Dipp,Ph}$ = [:C(C-Ph)(N-Dipp)(N)(N-Dipp)]} carbene copper chlorides with the ambition to modify the carbene ligands in Ge_9 copper carbene compounds. Hereto, the CAAC ligand provides one quaternary carbon atom next to the carbene center instead of a nitrogen atom resulting in a stronger σ-donation strength if compared to NHCs. The MIC is based on triazoles and known to have a σ-donation strength between NHCs and CAACs.[224-230]

In analogy to the synthesis of $[Cu(NHC)][\{Si(TMS)_3\}_3Ge_9]$, the compounds $[Cu(CAAC)][\{Si(TMS)_3\}_3Ge_9]$ and $[Cu(MIC)][\{Si(TMS)_3\}_3Ge_9]$ were obtained by reaction of $[\{Si(TMS)_3\}_3Ge_9]^{-}$ with the respective copper carbene chlorides (Scheme 10). NMR and ESI-MS characterizations in solution revealed the formation of analytically pure compounds. Single crystals, obtained from toluene solutions, confirmed the retention of the carbene ligands at the copper atoms in molecular structures and revealed an influence of the nature of the carbene on the cluster geometries in the molecular structures (Figure 22).

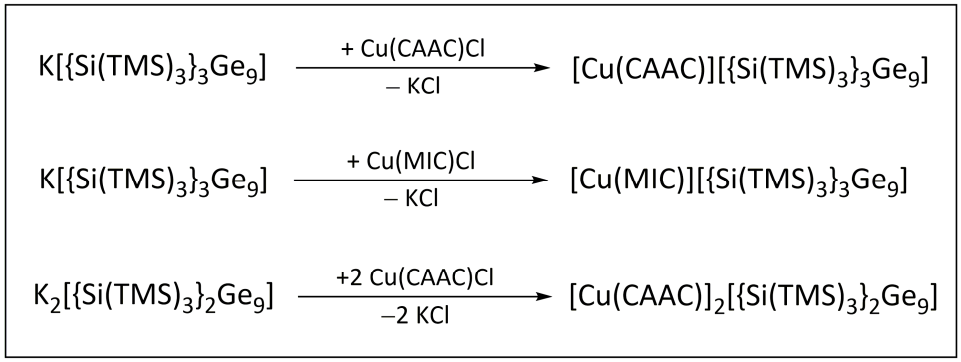

Scheme 10. Synthesis of copper carbene compounds with silylated Ge_9 clusters by reactions of $[\{Si(TMS)_3\}_3Ge_9]^-$ and $[\{Si(TMS)_3\}_2Ge_9]^{2-}$ with Cu(carbene)Cl (carbene = CAAC, MIC). Molecular structures are shown in Figure 22.

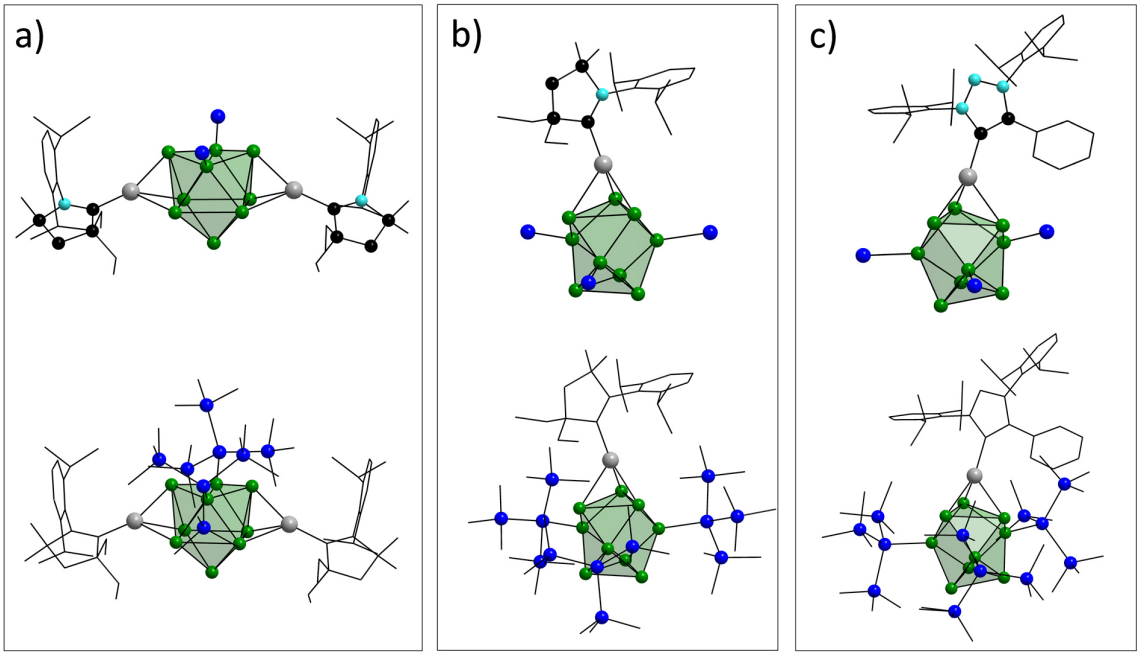

Figure 22. Molecular structures of Ge_9 copper carbene compounds (carbene = CAAC, MIC): a) $[Cu(CAAC)]_2[\{Si(TMS)_3\}_2Ge_9]$; b) $[Cu(CAAC)][\{Si(TMS)_3\}_3Ge_9]$; c) $[Cu(MIC)][\{Si(TMS)_3\}_3Ge_9]$. Ge atoms in green, Si atoms in blue, Cu atoms in gray, C atoms in black, N atoms in turquoise, Ge_9 clusters as green polyhedra, H atoms are omitted; top views: TMS are omitted, Dipp, Ph, Et, Me groups as wire-sticks; bottom views: C and N atoms are shown as wire-sticks.

η^3-Coordinations of silylated Ge_9 clusters at copper atoms are present in all cases (carbene = NHC, CAAC, MIC), and such coordination modes were not known for CAAC and MIC compounds before. Further reactions of CAAC and MIC copper chlorides with the di-silylated cluster species $[\{Si(TMS)_3\}_2Ge_9]^{2-}$ in acetonitrile yielded an isolable product in the case of CAAC (Scheme 10). The formed compound $[Cu(CAAC)]_2[\{Si(TMS)_3\}_2Ge_9]$ was isolated and characterized in solution by NMR and ESI-MS. Single crystals were obtained from toluene solution and revealed a structural arrangement in which two $[Cu(CAAC)]^+$ moieties are η^3-bridged by two opposing prism faces of a

$[\{Si(TMS)_3\}_2Ge_9]^{2-}$ cluster unit under formation of an uncharged compound (Figure 22a). This species represents the third known example that consists of one silyated Ge_9 cluster unit which is complexed with two transition metal moieties besides the reported structures of $[Cu(NHC)]_2[\{Si(TMS)_3\}_2Ge_9]$[231] and $[Ni(dppe)]_2[\{Si(TMS)_3\}_3Ge_9]$.[195]

The Ge–Ge bonds in the η^3-coordinated germanium cluster prism faces become elongated by the coordinated Cu(carbene) moieties and have an average values of 2.92 Å in [Cu(MIC)]-$[\{Si(TMS)_3\}_3Ge_9]$, 2.83 Å in $[Cu(CAAC)][\{Si(TMS)_3\}_3Ge_9]$ and 2.76 Å in $[Cu(CAAC)]_2$-$[\{Si(TMS)_3\}_2Ge_9]$. If compared with NHC derivatives in literature,[200, 231] the overall Ge–Ge bond elongations show a trend of "MIC > NHC > CAAC" what correlates with the reported catalytic activities of carbene species in "click chemistry",[232] even though no obvious connection could be found. In agreement to found cluster symmetries in metal complexes in chapter 2.1.3.1, the di-silylated Ge_9 cluster core in $[Cu(CAAC)]_2[\{Si(TMS)_3\}_2Ge_9]$ is best described by C_{2v} symmetry, whereas the tri-silylated cluster cores in $[Cu(carbene)][\{Si(TMS)_3\}_3Ge_9]$ (carbene = CAAC, MIC) are best described as D_{3h} symmetric.

2.1.4 Discussion of the Results with K_4Ge_9 Precursor Material

The field of silylated Ge_9 cluster species was further explored. Thereto, the new tri-silylated derivates $[(SiR_3)_3Ge_9]^-$ (R = Ph, ^{i}Bu, ^{i}Pr, Et) were obtained in analogy to the established benchmark species $[\{Si(TMS)_3\}_3Ge_9]^-$ [177, 191] by single-step reaction of K_4Ge_9 precursor material with the respective chlorosilane compound. The obtained species represent accessible, silyl-stabilized cluster species that boast remarkable solubility. Along with variation of steric and electronic properties of the silyl groups, cleavages of -SiR_3 (R = Ph, ^{i}Bu) groups from the cluster cores were found in molecular structures underlining the synthetic potential for further synthetic modification. Regarding the functionalization of Ge_9 clusters *via* silylation, as recently established for olefin-functionalizations,[223] known reactions were expanded by the synthesis of the triple and mono Si–H-functionalized cluster species $[(SiHR_2)_3Ge_9]^-$ and $[\{Si(TMS)_3\}_2(SiHR_2)Ge_9]^-$ (R = ^{i}Pr, Ph), respectively. Cluster functionalization *via* silylation paves the way for future cluster modification towards material fabrication as *e.g.* by hydrosilylation or insertion reactions.[233-237]

Complexations with transition metal compounds revealed the formation of versatile structural arrangements in monomeric and dimeric Ge_9 cluster metal complexes. Molecular structures of $[Cu(P^iPr_3)][\{Si(TMS)_3\}_3Ge_9]$, $[Zn(Cp^*)][\{Si(TMS)_3\}_3Ge_9]$, $[Cu(CAAC)][\{Si(TMS)_3\}_3Ge_9]$, [Cu(MIC)]-$[\{Si(TMS)_3\}_3Ge_9]$ and $[Cu(CAAC)]_2[\{Si(TMS)_3\}_2Ge_9]$ represent Ge_9 metal complexes with application relevant, organic ligands at metal atoms.

Analysis of the Ge–Ge bond elongations within the η^3-coordinated cluster prism faces reveals ligand- and metal-depending differences in the Ge_9 cluster geometries. Overall, elongations by Zn^{2+} and Au^+ metal coordination were found to be stronger if compared to Cu^+ atoms. Also the organic ligands at the metal atoms influence the Ge–Ge elongations as detected by stronger bond elongation by the $[Zn(Cp^*)]^+$ moiety if compared to a cluster-bridging Zn^{2+} atom. Divergences were further determined for the carbene ligands in $[Cu(carbene]^+$ moieties (carbene = CAAC, MIC, NHC) following the trend of "MIC > NHC > CAAC" for elongations within the η^3-coordinated cluster prism faces.

Obtained metal cluster compounds are readily soluble in non-polar solvents and accessible by simple syntheses. Cluster coupling by metal complexation was found in the molecular structures of $Zn[\{Si(TMS)_3\}_3Ge_9]_2$, $[Au\{(Si^iBu_3)_3Ge_9\}_2]^-$ and $[Cu(P^iPr_3)]_4[(SiPh_3)_2Ge_9]_2$, whereas the latter revealed a novel structural arrangement comprising η^1-, η^3- and η^4-coordination modes under formation of a twofold copper-bridged cluster dimer.

Summarized, the synthetic potential of the intermetallic precursor K_4Ge_9 towards the formation of silyl-stabilized and functionalized Ge_9 clusters as well as metal complexes of those was expanded. As pointed out, such molecular species are of central interest as material building blocks for targeted, solution-based material fabrication. Thus, the results offer a new prospect for the formation of germanium-based materials and set a starting point for the transfer of precursor utilization to $K_{12}Si_{17}$ material. Thereto, investigations and results are presented in the following chapter.

2.2 Reactions with Si_9 Clusters from $K_{12}Si_{17}$ Precursor Material

Investigations of silicon clusters in the precursor $K_{12}Si_{17}$ and reactions of contained Si_9 clusters are described in this subchapter. Experimental details can be found in chapter 4. Results of the following manuscripts (see attached in chapter 6) are outlined herein. Experimental data as well as further background, discussion and conclusions of the results can be found in the manuscripts.

List of manuscripts to chapter 2.2

i) see chapter 6.3: Schiegerl, L. J.; Klein, W.; Fässler, T. F., Utilization of Si_9 Clusters from $K_{12}Si_{17}$ Precursor Material for Subsequent Reactions. *Manuscript for Publication.* 2019.

ii) see chapter 6.5: Schiegerl, L. J.; Karttunen, A. J.; Tillmann, J.; Geier, S.; Raudaschl-Sieber, G.; Waibel, M.; Fässler, T. F., Charged Si_9 Clusters in Neat Solids and the Detection of $[H_2Si_9]^{2-}$ in Solution: A Combined NMR, Raman, Mass Spectrometric, and Quantum Chemical Investigation. *Angew. Chem. Int. Ed*. 2018, *57* (39), 12950-12955.

iii) see chapter 6.6: Schiegerl, L. J.; Karttunen, A. J.; Klein, W.; Fässler, T. F., Anionic Siliconoids from Zintl Phases: $R_3Si_9^-$ with Six and $R_2Si_9^{2-}$ with Seven Unsubstituted Exposed Silicon Cluster Atoms (R=Si(*t*Bu)$_2$H). *Chem. Eur. J.* 2018, *24* (72), 19171-19174.

iv) see chapter 6.7: Schiegerl, L. J.; Karttunen, A. J.; Klein, W.; Fässler, T. F., Silicon slusters with six and seven unsubstituted vertices *via* a two-step reaction from elemental silicon. *Chem. Sci.* 2019 (DOI: 10.1039/C9SC03324F).

2.2.1 Motivation and Outline of Relevant Literature for Silicon Clusters

Silicon is a key component in modern high-tech products such as batteries, solar cells and electronic devices.[139, 213-218, 238] Due to its abundancy, silicon is also processed to industrial products on larger scale as *e.g.* silicones[2, 32-34] and the field of applications for silicon-based materials is constantly growing. Due to an increasing demand for novel material sources, synthetic access to silicon clusters from the *Zintl* precursor $K_{12}Si_{17}$ is of interest with focus on future material fabrication.

$K_{12}Si_{17}$ contains homoatomic silicon clusters (1x Si_9^{4-} and 2x Si_4^{4-}) along with potassium cations (Figure 23a).[70, 72] $K_{12}Si_{17}$ was further investigated within this work for its potential to serve as source for ligand-stabilized silicon clusters. Si_4^{4-} and Si_9^{4-} clusters are low-valent species that have outstanding properties due to the possessed combination of unsaturated clusters bonds[82-84] and nucleophilicity induced by their polyanionic character (Figure 23a).[45, 47]

In contrast to A_4Ge_9 precursors containing Ge_9^{4-} clusters, the solubility of $A_{12}Si_{17}$ phases (A = alkali metal) was found to be limited to liquid ammonia and crystal structures of solvates containing Si_4^{4-} [91-92] and Si_9^{4-} [90-91, 93] units were reported before this thesis. It was further demonstrated that silicon clusters from $A_{12}Si_{17}$ are accessible to further transformation by complexation with transition metal compounds. Anyhow, only four examples (all structures in Figure 8) were obtained from such reactions up to date with $[(CuMes)_2Si_4]^{4-}$ (Figure 23b),[86] $[(PhZn)Si_9]^{3-}$,[87] $[\{Ni(CO)_2\}_2(Si_9)_2]^{8-}$ [88] and

[{Cu(NHC^{Dipp})}Si_9]$^{3-}$ (Figure 23c).[89] Furthermore, oxidized Si_9^{4-} clusters were obtained from solutions of $A_{12}Si_{17}$ precursors revealing Si_9^{3-} [78, 93] and Si_9^{2-} [81] along with the unclarified formation of Si_5^{2-} [78-79] units. Regarding NMR investigations of $A_{12}Si_{17}$ precursor phases, only a plausible ^{29}Si NMR signal for Si_4^{4-} clusters[239] from liquid ammonia solution was reported, and thus, the question – which cluster species readily appear in solution – remained unclear before this work. In contrast, the synthesis of single-phase $A_{12}Si_{17}$ precursor material was confirmed by Raman spectroscopy and X-ray diffraction.[70-72, 239]

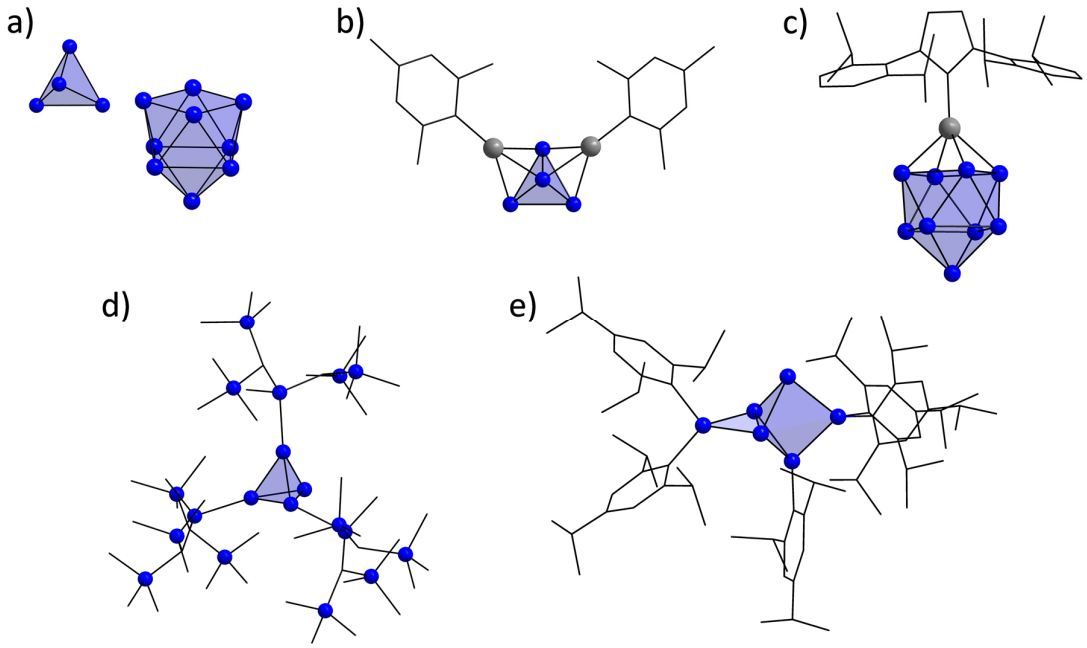

Figure 23. Examples for silicon clusters: a) Si_4^{4-} and Si_9^{4-} clusters as present in the intermetallic precursor *Zintl* phase $K_{12}Si_{17}$;[90-93] b) the Si_4 cluster complex $[(CuMes)_2Si_4]^{4-}$;[86] c) the Si_9 cluster complex [{Cu(NHC^{Dipp})}Si_9]$^{3-}$;[89] d) the Si_4 cluster species $[(SiMeDis_2)_4Si_4]^-$ {Dis = $CH(SiMe_3)_2$};[163] the siliconoid cluster $[(Tip)_5Si_6]^-$.[167] Si atoms are shown in blue, Cu atoms in gray, C and N atoms as wire-sticks, H atoms are omitted, silicon clusters are shown as blue polyhedra.

Apart from silicon *Zintl* clusters, constant progress for the formation of low-valent silicon cluster compounds was promoted by syntheses from "molecular bottom-up" approaches. Starting from molecular precursors, defined silicon clusters can be obtained by their stabilization with (bulky) organic substituents. The substituents allow the formation of silicon clusters with solely substituted silicon atoms as *e.g.* in the triangular Si_3 cluster in $(CAAC)_3Si_3$[160] and in the tetrahedral Si_4 cluster $(Si^tBu_3)_4Si_4$[161] (Figure 10).

The synthesis of partially substituted silicon clusters bearing naked Si atoms yielded *e.g.* the tetrahedral $[(SiMeDis_2)_4Si_4]^-$ {Dis = $CH(SiMe_3)_2$} [163] and the spirocyclic $(Si^tBu_3)_6Si_9Cl_2$[169] clusters with one exposed Si atom each (Figure 11c and Figure 23d). The class of so-called siliconoid clusters comprises partially substituted silicon clusters, which have at least one exposed silicon atom in hemispheroidal coordination sphere (see Figure 12 and chapter 1.4.1).[167, 173] Prominent examples are the six-atomic $(Tip)_6Si_6$ [165] (Figure 31f) and $[(Tip)_5Si_6]^-$ [167] (Figure 23e) clusters with two and three exposed Si atoms, respectively. The high synthetic potential of siliconoid species as building blocks

for material fabrication was for example demonstrated by substitutions of unsubstituted clusters Si atoms, as well as by further modification and expansion of such clusters.[167-168, 171]

The synthesis of siliconoid clusters finally linked "molecular bottom-up" approaches for ligand-stabilized clusters with ("bare") fully unsubstituted clusters as contained in *Zintl* phases.[173] The idea to synthesize ligand-stabilized species from *Zintl* precursors was already proposed by *Wiberg et al.* in 1993[161] and further promoted by calculations that suggest the formation of siliconoids with Si_9^{4-} clusters.[240] Moreover, the constant synthetic progress regarding the utilization of Ge_9 clusters from the K_4Ge_9 precursor (chapters 1.4.2 and 2.1) offers starting points for a transfer to Si_9 clusters. However, synthetic effort to obtain ligand-stabilized silicon clusters from *Zintl* precursors was not successful before this work. This initiated the presented investigations with the intermetallic $K_{12}Si_{17}$ precursor material in chapter 2.2.2 to clarify detection methods for Si_9 clusters. The utilization of $K_{12}Si_{17}$ is presented in chapter 2.2.3 and became feasible by "*activation*" of the precursor in chapter 2.2.3.1. This allowed solubility experiments in pyridine and ethylenediamine (chapter 2.2.3.2) and paved the way for investigations to ligand-stabilized Si_9 clusters (chapters 2.2.3.3 and 2.2.3.4) with the idea to synthesize Si_9 cluster-based material building blocks from a *Zintl* precursor.

2.2.2 Silicon Clusters in Intermetallic $K_{12}Si_{17}$ Precursor Material

Reports on $A_{12}Si_{17}$ (*A* = alkali metal) precursors revealed the presence of Si_4^{4-} and Si_9^{4-} clusters by Raman spectroscopy and X-ray diffraction structure determination (clusters are shown in Figure 26).[70-72, 239] Herein, the characterization of contained silicon clusters in $K_{12}Si_{17}$ was further explored. Investigations with $K_{12}Si_{17}$ were compared to Si_4^{4-} clusters from K_4Si_4 (containing solely Si_4^{4-} clusters), as well as to detailed computational studies on Si_9^{4-}, Si_9^{2-}, Si_5^{2-} and Si_4^{4-} cluster aiming for acquisition of systematic data sets.

$K_{12}Si_{17}$ and K_4Si_4 materials were synthesized by fusing of the elemental K and Si in tantalum ampoules (synthesis details in chapter 4.1.4). A slight excess of silicon (if referred to the stochiometric ratio of K:Si = 12:17) was observed to be favorable for the synthesis of $K_{12}Si_{17}$ to avoid of the formation of the K_4Si_4 phase. Moreover, ^{29}Si-enriched $K_{12}Si_{17}$ material was synthesized as for NMR investigations.

The silicon precursors were obtained as black greyish solids in nearly quantitative yields and their purity was verified by powder X-ray diffraction in comparison to literature data (diffractograms in Figure 33, Figure 35 and Figure 36).[62, 72] Raman spectroscopic vibrations of the contained silicon clusters in $K_{12}Si_{17}$ were assigned by comparison to a measurement of K_4Si_4 and literature values,[70-72, 239] as well as by calculated silicon cluster vibrations (Figure 24). The specific vibrations of Si_4^{4-} and Si_9^{4-} clusters in the *Zintl* phase material $K_{12}Si_{17}$ revealed the presence of a single main vibration for Si_9^{4-} clusters at 390 cm^{-1} and three main Si_4^{4-} cluster vibrations at 281, 354 and 482 cm^{-1} (Figure 24b).

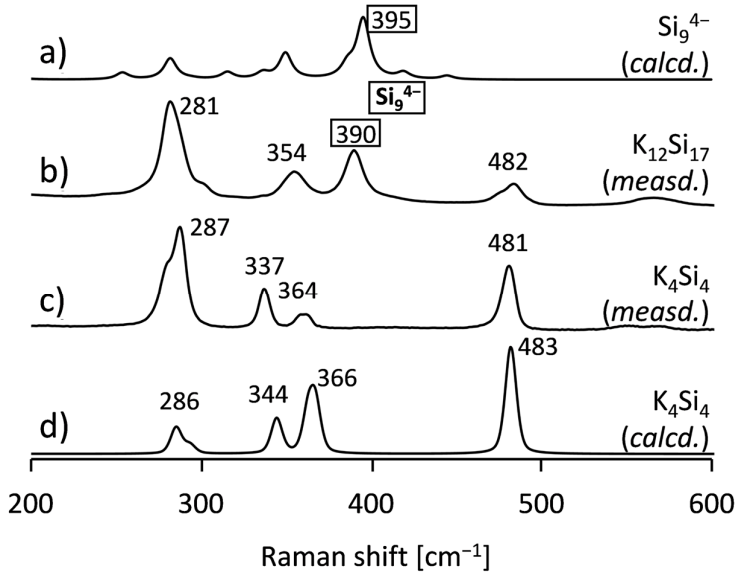

Figure 24. Raman investigations to silicon cluster vibrations in the precursor materials K_4Si_4 and $K_{12}Si_{17}$ in solid-state in comparison to calculated spectra.

A ^{29}Si MAS NMR (solid-state) measurement of ^{29}Si-enriched $K_{12}Si_{17}$ material revealed that the silicon clusters cause seven broad peaks within a shift range of −316 to −344 ppm, and thus, in a strongly upfield shifted ppm area as expected for polyanionic species. A good match of measured ^{29}Si MAS NMR shifts for K_4Si_4 solid material with calculated shifts and literature data[241] verified the accuracy of the applied methods (Table 1).

Table 1. ^{29}Si NMR investigations of *Zintl* precursor materials in solid-state: Measured ^{29}Si MAS NMR silicon cluster shifts in comparison with calculated values. [a] Wyckoff position 24*i*; [b] Wyckoff position 8*e*; [c] averaged values, signals within a range of 18 ppm were collected in bins. Assignment of the measured shifts (1–7) in Figure 25. All values in [ppm].

Precursor material	Silicon cluster	^{29}Si MAS NMR shifts (*measured*)	^{29}Si NMR shifts (*calculated*)
K_4Si_4	Si_4^{4-}	−323	−326[a]
		−346	−353[b]
$K_{12}Si_{17}$	Si_4^{4-}	−316 (**1**)	−281[c]
		−317 (**2**)	−300[c]
		−326 (**3**)	−337[c]
	Si_9^{4-}	−320 (**4**)	−308[c]
		−322 (**5**)	−326[c]
		−331 (**6**)	−344[c]
		−344 (**7**)	−362[c]

Quantum chemical calculations to $K_{12}Si_{17}$ (solid-state) ^{29}Si NMR shifts finally allowed an assignment of the measured signals to the contained Si_4^{4-} and Si_9^{4-} clusters in the precursor (Table 1, Figure 25). The assignment succeeded by a histogram plot of the multitude calculated NMR signals (peaks within a range of 18 ppm were collected into bins) arising from the symmetry independent Si atoms in the single crystal structure of $K_{12}Si_{17}$.[72] The match of the histogram plot with measured intensities and arrangement of the signals is satisfactory whereas the ppm distribution range differs. The broader distribution in the histogram is traced back to the circumstance that the calculations were carried out for 0 K, and that the atoms were kept at their experimental X-ray positions.

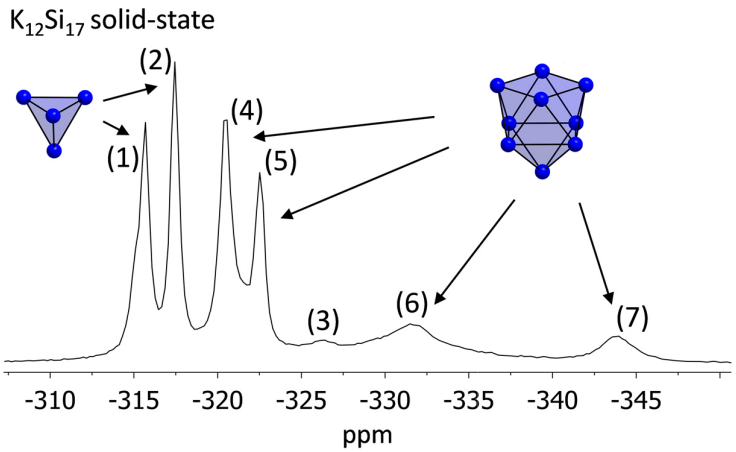

Figure 25. ^{29}Si MAS NMR (solid-state) spectrum of $K_{12}Si_{17}$ precursor material with Si_9^{4-} and Si_4^{4-} cluster assignment (arrows) from quantum chemical studies (Table 1).

2.2.3 Utilization of Si_9 Clusters from $K_{12}Si_{17}$ Precursor Material

2.2.3.1 Activation of $K_{12}Si_{17}$ Precursor Material

Silicon clusters from $K_{12}Si_{17}$ were firstly detected by ^{29}Si NMR methods in solid-state (chapter 2.2.2). In further investigations, a transfer of Si_9 clusters from solid-state into solution was aimed to release the synthetic potential of the clusters. As discussed in the chapters 2.2.1 and 1.3.3, the solubility of $A_{12}Si_{17}$ phases (A = alkali metal) was observed to be limited to the rather impracticable solvent liquid ammonia. Different silicon cluster species were found from $A_{12}Si_{17}$ solutions and the question – which species readily appear in solution – remained unclarified before this work (Figure 26a).[78-79, 81, 90-93]

The solubility of $K_{12}Si_{17}$ was tested in liquid ammonia. Figure 26b shows that the precursor forms a red solution in liquid ammonia (−78 °C), addition of 222crypt as potassium sequestering agent boosts the solubility of the solid phase material. The brown solid "$K_{12}Si_{17}$ (*activated*)" was obtained after removal of liquid ammonia. Solubility experiments of "$K_{12}Si_{17}$ (*activated*)" revealed that the solid is (partly) soluble in pyridine, ethylenediamine, acetonitrile and 1,2-difluorobenzene.

Thereby, the best solubilities were observed in pyridine and ethylenediamine, and for this reason filtrates obtained with these solvents were investigated in further experiments.

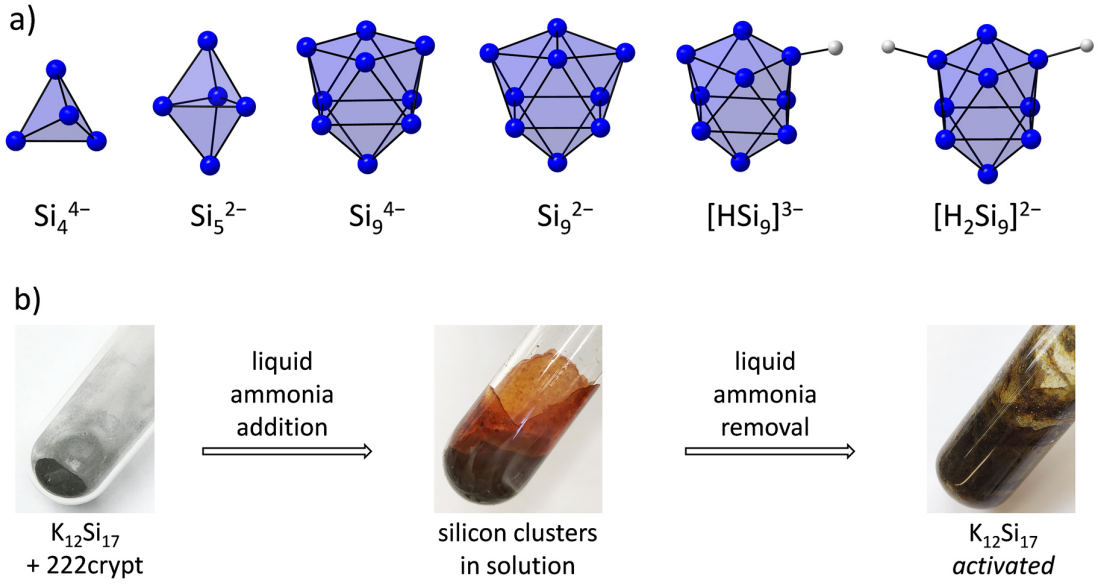

Figure 26. a) Polyanionic silicon cluster species from liquid ammonia solutions and computational studies (NMR investigations in Table 2). Si atoms are shown in blue, H atoms in gray, silicon clusters as blue polyhedra; b) transformation of intermetallic $K_{12}Si_{17}$ precursor material to "$K_{12}Si_{17}$ (*activated*)" by liquid ammonia treatment under usage of the potassium sequestering agent 222crypt.

2.2.3.2 Investigation of $[H_2Si_9]^{2-}$ in Pyridine and Ethylenediamine Solution

Dissolving of "$K_{12}Si_{17}$ (*activated*)" (chapter 2.2.3.1) in pyridine and ethylenediamine yielded red and orange filtrates, respectively. A red bulk material was isolated from pyridine solutions after purification and subsequently dissolved for ESI-MS and NMR investigations. In the case of ethylenediamine, obtained solutions were investigated without further purification.

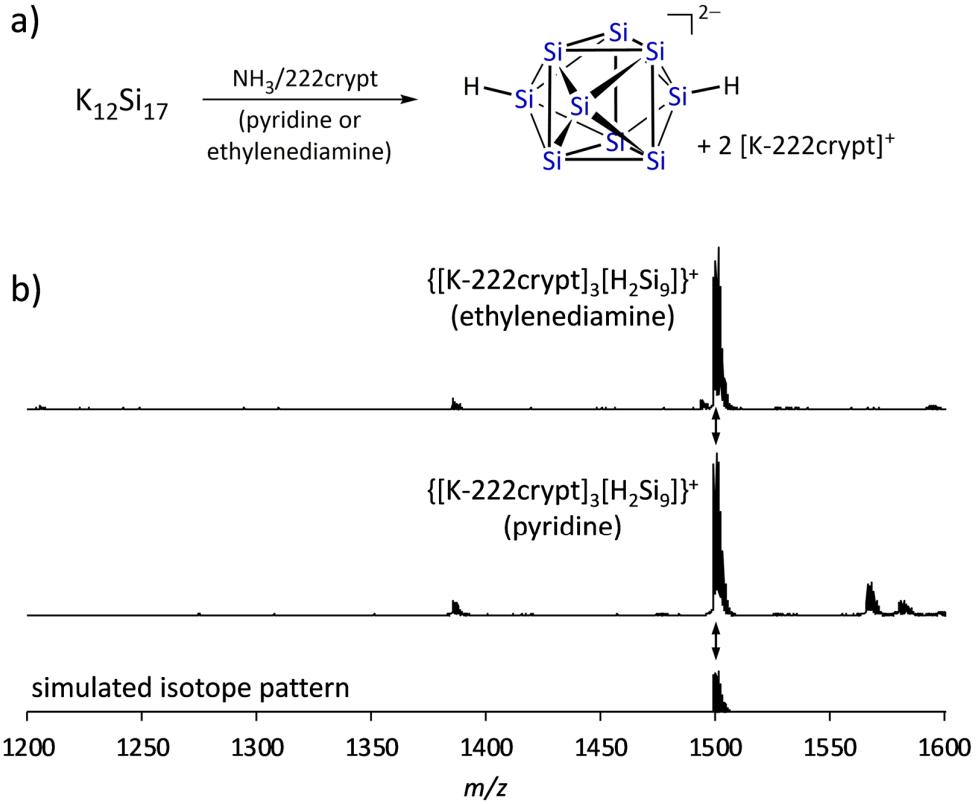

Figure 27. a) Reaction scheme for the transfer of $K_{12}Si_{17}$ precursor material to $[H_2Si_9]^{2-}$ in solution; b) ESI-MS spectra of $[H_2Si_9]^{2-}$ in positive ionization mode as $\{[K\text{-}222crypt]_3[H_2Si_9]\}^+$ mass peaks.

ESI-MS investigation of pyridine and ethylenediamine solutions revealed the presence of di-protonated $[H_2Si_9]^{2-}$ cluster species as $\{[K\text{-}222crypt]_3[H_2Si_9]\}^+$ mass peak in both cases (Figure 26a and Figure 27). Si_4^{4-} clusters species were not detected in ESI-MS measurements and their solubility in organic solvents is expected to be limited due to the higher negative charge per atom. The arising of di-protonated Si_9 clusters in solution was verified by NMR (^1H, ^{29}Si) experiments including investigations with ^{29}Si-enriched $K_{12}Si_{17}$ precursor material (Figure 28).

^1H and ^{13}C NMR spectra confirmed the presence of $[H_2Si_9]^{2-}$ along with $[K\text{-}222crypt]^+$ cations. ^1H NMR shifts of $[H_2Si_9]^{2-}$ were detected within a negative ppm area at −0.7 ppm in pyridine-*d5*/thf *d8* and at −1.5 ppm in ethylenediamine (Figure 28a and b) and match well a calculated value for $[H_2Si_9]^{2-}$ at −1.3 ppm. Moreover, the ^1H NMR signal splitting is in good accordance with a simulated splitting pattern for protons coupling with nine Si atoms and suggest hydrogen scram-

bling at the Si_9 cluster surface. The signal splitting pattern show remarkably small $J(^{29}Si–^{1}H)$ coupling constants of 19.7 Hz (pyridine) and 20.4 Hz (ethylenediamine), respectively. $^{29}Si–^{1}H$ coupling was further confirmed by ^{29}Si decoupled ^{1}H NMR experiments and NMR investigations with ^{29}Si-enriched $K_{12}Si_{17}$ precursor material (Figure 28c). Thereby, a comparison to ^{1}H NMR splitting pattern with ^{29}Si-enriched material (15% ^{29}Si) could verify the hydrogen shifts of $[H_2Si_9]^{2-}$ as well as hydrogen scrambling at the Si_9 cluster surface.

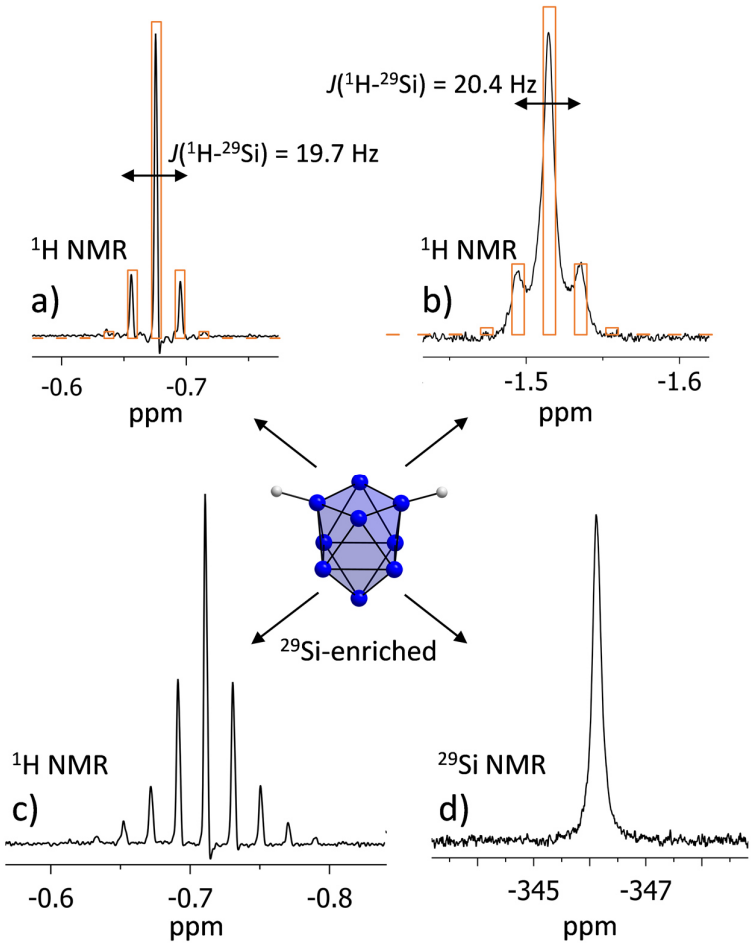

Figure 28. NMR investigations of $[H_2Si_9]^{2-}$ obtained from solutions of "$K_{12}Si_{17}$ (*activated*)": a) ^{1}H NMR spectrum of $[H_2Si_9]^{2-}$ in pyridine in comparison with its simulated ^{1}H-^{29}Si splitting pattern (orange); b) ^{1}H NMR spectrum of $[H_2Si_9]^{2-}$ in ethylenediamine in comparison with its simulated ^{1}H-^{29}Si splitting pattern (orange); c) ^{1}H NMR spectrum of $[H_2Si_9]^{2-}$ with 15% ^{29}Si enrichment; d) ^{29}Si NMR spectrum of $[H_2Si_9]^{2-}$ at −40 °C with 15% ^{29}Si enrichment. A comparison of ^{29}Si NMR shifts for Si_9 cluster species is shown in Table 2 in chapter 2.2.3.3.

The negative ^{1}H NMR shits [ppm] are indicative for hydrogen cores with stronger shielding if compared to literature known cluster-bonded H_{Si} atoms as *e.g.* in $(Tip)_8HSi_{11}$ [171] (H_{Si}: +5.68 ppm), and thus, is better comparable to protons in boranes[242]. ^{29}Si NMR measurements revealed a broad, averaged $[H_2Si_9]^{2-}$ clusters signal, which sharpens at lower temperature (−40 °C) to a broad peak at −346 ppm (Figure 28d). Calculated ^{29}Si NMR cluster shifts revealed a good match for calculations

to $[H_2Si_9]^{2-}$ (*calcd.* shift: −348 ppm, see also Table 2). The temperature-dependent behavior of the shift is not corresponding to typical coalescence behavior, but indicative for the presence of a dynamic Si_9 cluster core in the $[H_2Si_9]^{2-}$ species (Figure 26a).

Reactivity experiments of "$K_{12}Si_{17}$ (*activated*)" in ethylenediamine solutions indicated a reactivity of Si_9 clusters with bis(trimethylsilyl)acetylene (TMS-C≡C-TMS) in analogy to vinylation reactions of K_4Ge_9 (chapter 1.4.2.2). As mentioned, the solvent ethylenediamine plays a key role for the cluster vinylation mechanism, and thus, for the formation of vinyl-functionalized cluster species.[182-184, 187]

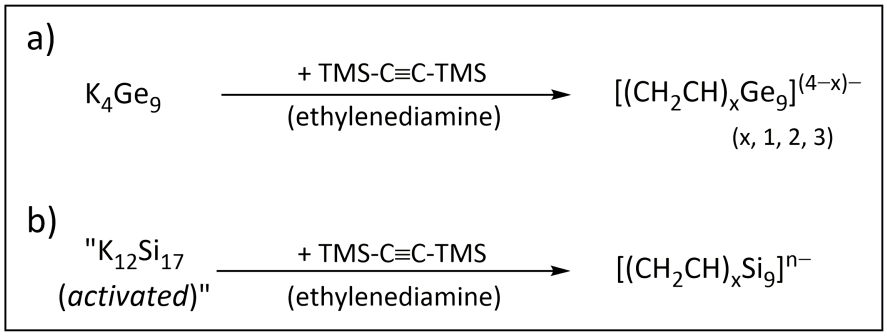

Scheme 11. a) Vinyl-functionalization of Ge_9 clusters from K_4Ge_9 under formation of $[(CH_2CH)_xGe_9]^{(4-x)-}$;[182-184] b) vinyl-functionalization of Si_9 clusters from "$K_{12}Si_{17}$ (*activated*)" under formation of $[(CH_2CH)_xSi_9]^{(4-x)-}$.

NMR (^1H, ^{29}Si) investigations revealed conclusive signals for a $[(CH_2CH)_xSi_9]^{(4-x)-}$ main species. One set of ^1H NMR vinyl shifts with characteristic "doublet of doublet" splitting was found and matches well reported values for $[(CH_2CH)Ge_9]^{3-}$ and $[(CH_2CH)_2Ge_9]^{2-}$ species.[182-184] A ^{29}Si NMR measurement shows two signals, plausible for partially substituted Si_9 cluster cores (substituted atoms Si_{Vinyl}: −38.9 ppm, ligand-free atoms Si_{Si}: −342 ppm). Although the formation of a single $[(CH_2CH)_xSi_9]^{(4-x)-}$ species was suggested by NMR measurements, the number of attached vinyl groups at the Si_9 cluster cores could not be determined by literature comparison, because reaction solutions of vinylated Ge_9 species contain mono-, bis- and also tri-vinylated cluster species simultaneously.[184]

2.2.3.3 Formation of $[(ER_3)_3Si_9]^-$ Siliconoid Clusters

As presented in this thesis, the attachment of *exo*-bonded substituents on Ge_9 clusters is a fruitful approach to obtain tailored, cluster-based building blocks from the K_4Ge_9 precursor. The formation of Si_9 cluster *exo*-bonds was not known before this work and was promoted by detection of the molecular $[H_2Si_9]^{2-}$ species in solution (chapter 2.2.3.2 and Figure 29a). Thereto, the reactivity of "$K_{12}Si_{17}$ (*activated*)" was tested with the chlorostannane $SnCy_3Cl$, the chlorogermane $GePh_3Cl$ and the chlorosilanes SiH^tBu_2Cl, Si^iPr_3Cl and $Si(TMS)_3Cl$ in pyridine and thf solutions [these reactants were found to be suitable for substitutions of Ge_9 clusters from the precursor K_4Ge_9 (chapter 1.4.2)[177, 180, 209]]. ESI-MS measurements of obtained bulk materials from the reactions with "$K_{12}Si_{17}$ (*activated*)"revealed formations of $[(ER_3)_3Si_9]^-$ {ER_3 = SiH^tBu_2, Si^iPr_3, $Si(TMS)_3$, $SnCy_3$} (Figure 30 and Figure 29) species in analogy to known reactions with K_4Ge_9. By contrast, conclusive germanylated Si_9 species from reaction with $GePh_3Cl$ were not found.

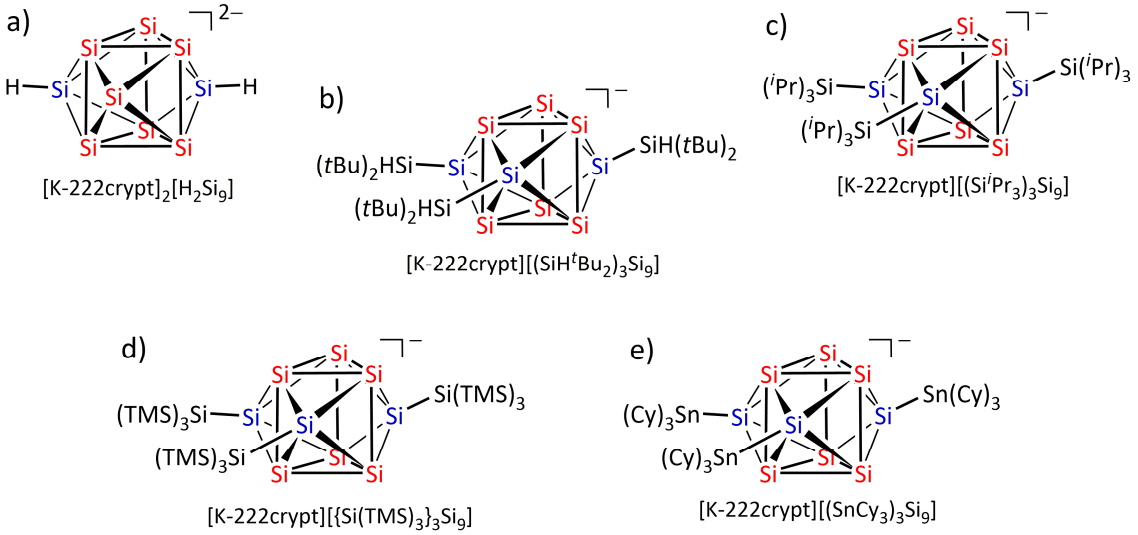

Figure 29. The protonated Si_9 cluster $[H_2Si_9]^{2-}$ (a) and ligand-stabilized Si_9 cluster (b–e) as obtained from the precursor $K_{12}Si_{17}$ in solution. Substituted Si atoms are shown in blue, exposed Si atoms in red.

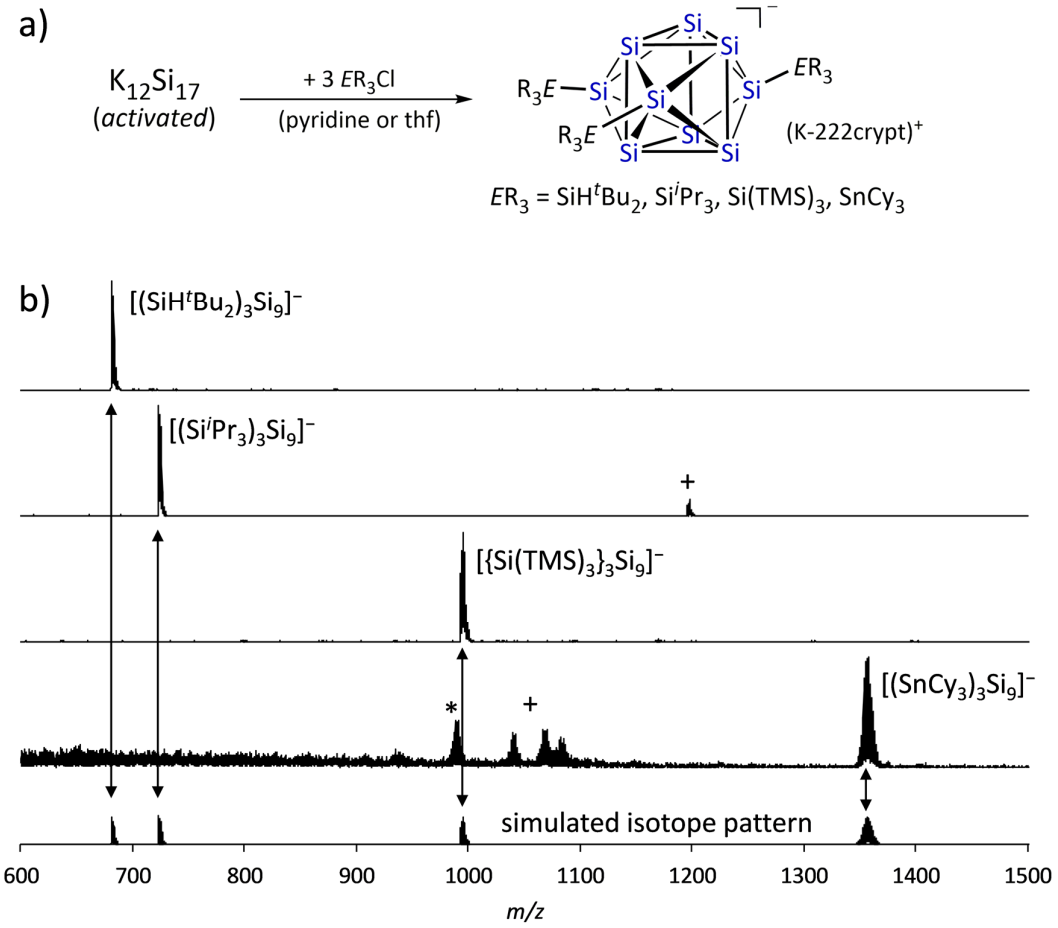

Figure 30. a) Reaction scheme for the transformation of "$K_{12}Si_{17}$ (*activated*)" to silyl- and stannyl-stabilized Si_9 siliconoid clusters; b) ESI-MS spectra of the obtained tri-substituted Si_9 siliconoid clusters in solution (*: $[(SnCy_3)_2Si_9]^{2-}$; +: side-species).

^{29}Si NMR investigations of the $[(ER_3)_3Si_9]^-$ {ER_3 = SiH^tBu_2, $Si(TMS)_3$, $SnCy_3$} containing bulk materials proved the formation of tri-substituted, D_{3h} symmetric silicon cluster cores in solution by presence of conclusive ^{29}Si cluster signals ($Si_{unsubstituted}$ and $Si_{substituted}$) in the shift range of −100 to −361 ppm (Table 2). ^{1}H and ^{13}C NMR spectra of the bulk materials showed the presence of $[K\text{-}222crypt]^+$ cations along with one set of signals for the organic -ER_3 {ER_3 = SiH^tBu_2, $Si(TMS)_3$, $SnCy_3$} substituents. Conclusive NMR shifts were also found for bulk material containing $[(Si^iPr_3)_3Si_9]^-$ that was not isolated as analytically pure.

Table 2. ^{29}Si NMR investigations of silicon clusters in solution: ^{29}Si NMR shifts for exposed and substituted silicon cluster atoms in comparison with calculated values. Selected molecular structures are shown in Figure 31. All values in [ppm].

Silicon *Zintl* clusters	^{29}Si NMR shifts (*measured*)	^{29}Si NMR shifts (*calculated*)	Siliconoid clusters	^{29}Si NMR shifts (*measured*)	^{29}Si NMR shifts (*calculated*)
Si_4^{4-}	-	−484	$[(SnCy_3)_3Si_9]^-$	*substituted:* −100 *exposed:* −336	-
HSi_4^{3-} [80]	*substituted:* −328 *exposed:* −405	*substituted:* −386 *exposed:* −490	$[(SiH^tBu_2)_3Si_9]^-$	*substituted:* −175 *exposed:* −359	*substituted:* −184 *exposed:* −385
Si_5^{2-} [80]	+342 −365	+349 −348	$[\{Si(TMS)_3\}_3Si_9]^-$	*substituted:* −175 *exposed:* −361	-
Si_9^{4-}	-	*averaged:* −403	$[(Tip)_5Si_6]^-$ [167]	*substituted:* +152 to +12 *exposed:* −72 to −233	-
Si_9^{2-}	*averaged:* −309	*averaged:* −308	$(Tip)_6Si_6$ [165]	*substituted:* +175 to −7.5 *exposed:* −274	*substituted:* +207 to +20.4 *exposed:* −267
HSi_9^{3-} [243]	*substituted:* −159 *exposed:* −359	*substituted:* −148 *exposed:* −358	$[(Tip)_5Si_7]^-$ [168]	*substituted:* +284 to +10.8 *exposed:* −66.1 to −196	*substituted:* +292 to +18.1 *exposed:* −73.1 to −205
$H_2Si_9^{2-}$	*averaged:* −346	*averaged:* −348	$(Tip)_5(Cp^*)Si_7$ [168]	*substituted:* +182 to +2.6 *exposed:* −138 to −242	*substituted:* +10.6 to +180 *exposed:* −139 to −256

In analogy to Ge_9 cluster substitutions, the substituents are attached at the three prism-capping Si cluster atoms of the Si_9 cores under formation of anionic siliconoids (Figure 29) in single-step reactions. The six exposed Si atoms within the prism faces originate ^{29}Si NMR shifts in the shift range −336 to −361 ppm (high field shift record for siliconoids). The ^{29}Si NMR shift range for substituted Si cluster atoms in the Si_9 siliconoids is clearly shifted downfield (−100 to −175 ppm) if compared to the exposed Si atoms and shows an electronic influence of the ligands on the cluster atoms. A comparison to ^{29}Si NMR shifts of siliconoids in literature (Table 2) shows that the Si_9 siliconoids are overall shifted more upfield what indicates stronger core shielding for those species.

Moreover, ^{29}Si NMR signal shifts and cluster core symmetries were confirmed by calculations on $[(SiH^tBu_2]_3Si_9]^-$. A ^{29}Si HMBC NMR measurement of $[(SiH^tBu_2]_3Si_9]^-$ showed $J(^1H–^{29}Si)$ couplings of the H_{Si} silyl atoms with all Si_9 cluster atoms of the siliconoid. In a nutshell, the ligand-stabilized Si_9 species $[(ER_3)_3Si_9]^-$ {ER_3 = SiH^tBu_2, $Si(TMS)_3$, $SnCy_3$} add as novel representatives, boasting the highest known number of exposed Si atoms, to reported siliconoids in literature (further definition for siliconoids is shown in Figure 12).

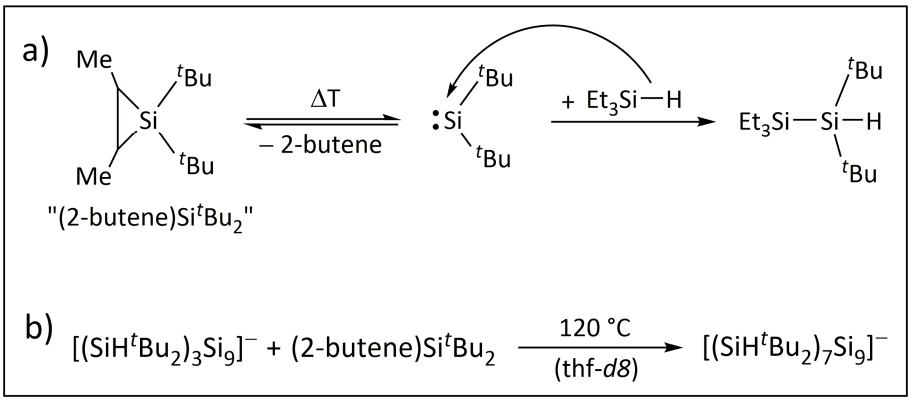

Scheme 12. a) Thermic formation of the $^tBu_2Si$: silylene and Si–H insertion reaction with Et_3SiH; [244-246] b) formation of $[(SiH^tBu_2)_7Si_9]^-$ from reaction of $[(SiH^tBu_2)_3Si_9]^-$ with (2-butene)Si^tBu_2 silirane as indicated by ESI-MS.

Regarding functionalized Si_9 siliconoids, $[(SiH^tBu_2)_3Si_9]^-$ [247] has three Si–H bonds at the silyl ligands and its reactivity was initially tested in an experiment with the (2-butene)Si^tBu_2 silirane.[244-245] This silirane forms $^tBu_2Si$: silylene by thermic treatment in solution (Scheme 12a), which is *e.g.* feasible for Si–H σ-bond insertion,[246, 248] but also for numerous other reactions including methanol insertion and cycloaddition with substituted alkenes are known.[244] Reaction of the reactants at 120 °C (Scheme 12b) revealed signal changes along with the disappearance of the $[(SiH^tBu_2)_3Si_9]^-$ reactant signals in NMR monitoring. An ESI-MS measurement of the obtained reaction solution showed a mass peak corresponding to a $[(SiH^tBu_2)_7Si_9]^-$ main signal. Fragmentation of the mass peak in ESI-MS revealed the cleavage of four SiH^tBu_2 (*m/z* = 143) units from $[(SiH^tBu_2)_7Si_9]^-$ under reformation of the $[(SiH^tBu_2)_3Si_9]^-$ reactant, and thus, suggests an extension of the reactant by four of these units although the molecular structure of such a species could not be determined within this work.

2.2.3.4 Molecular Structures of $[(ER_3)_2Si_9]^{2-}$ Siliconoid Clusters

Attempts to grow single crystals of $[(ER_3)_3Si_9]^-$ {ER_3 = $SnCy_3$, SiH^tBu_2, Si^iPr_3, $Si(TMS)_3$} siliconoid clusters from fluorobenzene/hexane solvent mixtures led to the isolation of single crystals containing di-substituted $[(ER_3)_2Si_9]^{2-}$ {ER_3 = $SnCy_3$, SiH^tBu_2, Si^iPr_3, $Si(TMS)_3$} cluster dianions (Figure 31, framed) along with [K-222crypt]$^+$ cations, although the presence of tri-substituted Si_9 species was verified for the isolated bulk materials before (Figure 29 and Figure 30).

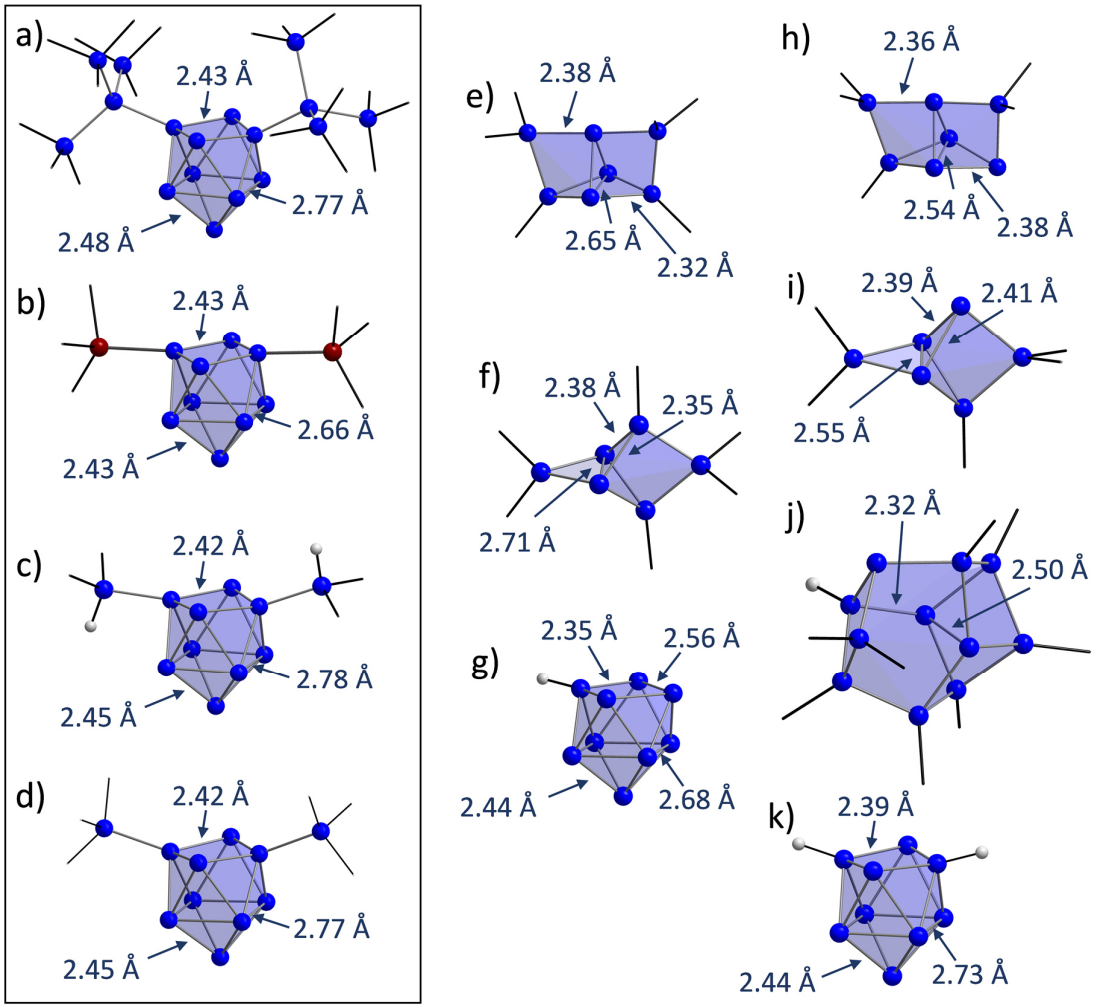

Figure 31. Molecular structures of silicon cluster species with Si–Si bond length comparison: a) $[\{Si(TMS)_3\}_2Si_9]^{2-}$ from crystallization of $[\{Si(TMS)_3\}_3Si_9]^-$; b) $[(SnCy_3)_2Si_9]^{2-}$ from crystallization of $[(SnCy_3)_3Si_9]^-$; c) $[(SiH^tBu_2)_2Si_9]^{2-}$ from crystallization of $(SiH^tBu_2)_3Si_9]^-$; d) $[(Si^iPr_3)_2Si_9]^{2-}$ from crystallization of $[(Si^iPr_3)_3Si_9]^-$; e) $(Tip)_5(Cp^*)Si_7$ from $[(Tip)_5Si_6]^-$;[168] f) $(Tip)_6Si_6$ from hexasilabenzene;[165] g) $[HSi_9]^{3-}$ from liquid ammonia solution of $A_{12}Si_{17}$;[93] h) $[(Tip)_5Si_7]^-$ from $(Tip)_5(Cp^*)Si_7$;[168] i) $[(Tip)_5Si_6]^-$ from hexasilabenzene;[167] j) $(Tip)_8HSi_{11}$ from $(Tip)_3Si_3Cl_3$;[171] k) $[H_2Si_9]^{2-}$ from computational studies. Si atoms in blue, Sn atoms in brown, H_{Si} atoms in gray, Si_9 clusters as blue polyhedra, organic substituents are simplified as black sticks.

The presence of di-silylated $[(ER_3)_2Si_9]^{2-}$ {ER_3 = $SnCy_3$, SiH^tBu_2, Si^iPr_3, $Si(TMS)_3$} clusters was determined by single crystal X-ray diffraction (Figure 31a–d) in all cases. Thus, the loss of one of the

covalently bonded substituents during crystallization becomes plausible for the formation of di-anionic siliconoids bearing exposed cluster surfaces consisting of seven Si atoms. As discussed in chapter 2.1.2, a similar circumstance was found for the formation of the Ge_9 cluster derivative $[(Si^iBu_3)_2Ge_9]^{2-}$, which was formed during crystallization of the tri-silylated species $[(Si^iBu_3)_3Ge_9]^-$ (Figure 21c) in toluene/hexane.

Bond lengths comparison of the ligand-stabilized $[(ER_3)_2Si_9]^{2-}$ clusters with siliconoid clusters in literature reveals a trend for the Si–Si distances within the silicon clusters (Figure 31). The Longest Si–Si distances are found for bonds between two exposed Si atoms, Si–Si bonds including one or two substituted Si atoms are clearly shorter. Conclusively, the averaged Si–Si distances are longer in Si_9 siliconoids due to the higher number of exposed silicon cluster atoms. Within the Si_9 cluster cores of $[(ER_3)_2Si_9]^{2-}$ {ER_3 = $SnCy_3$, SiH^tBu_2, Si^iPr_3, $Si(TMS)_3$}, $[H_2Si_9]^{2-}$ (calculated values) and $[HSi_9]^{3-}$,[93] a comparable bond length distribution is found whereby the longest Si–Si distances are located in the capped cluster squares solely consisting of exposed Si atoms with hemispheroidal coordination (range: 2.52 to 2.78 Å). For siliconoids in literature, Si–Si distances between exposed Si atoms (Figure 31) range between 2.38 to 2.71 Å and confirm elongations for bonds comprising exposed Si atoms with hemispheroidal coordination (Figure 12).

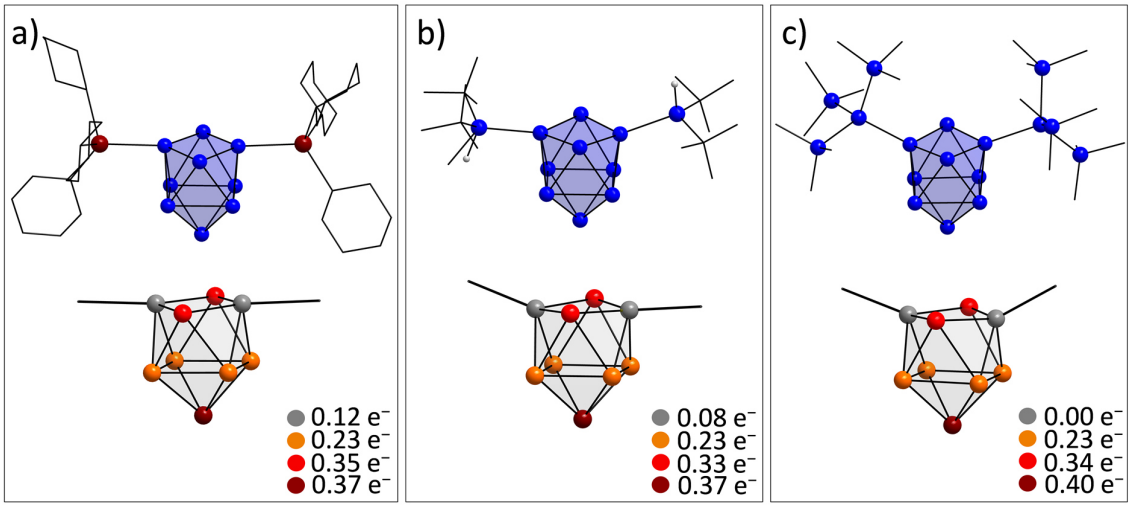

Figure 32. Molecular structures (top) and their partial atomic charge distributions (bottom) of di-substituted Si_9 siliconoid cluster species: a) the di-stannylated species $[(SnCy_3)_2Si_9]^{2-}$; b) the di-silylated species $[(SiH^tBu_2)_2Si_9]^{2-}$; c) the di-silylated species $[\{Si(TMS)_3\}_2Si_9]^{2-}$ (Molecular structures are also shown in Figure 31).

The substituents in the structures of $[(ER_3)_2Si_9]^{2-}$ {ER_3 = $SnCy_3$, SiH^tBu_2, $Si(TMS)_3$} boast versatile steric and electronic properties influencing the Si–Si bond lengths and Si_9–ER_3 arrangements in the molecular structures. Interestingly, the Sn atoms of the -$SnCy_3$ ligands (Figure 32a) are almost in plane with the non-capped cluster square indicating a certain degree of through space interaction of the tin atoms with the silicon cluster atoms, as it was also found in NMR experiments for the tin substituents in the disilene $(Tip)_3(Sn^tBu_2Cl)Si_2$.[249] Such an interaction is further supported by the reported formation of $(SnPh_3)Ge_9^{3-}$ in which the stannyl ligand is bonded to two Ge_9 cluster atoms.[250]

The electronic influence of the -*E*R$_3$ substituents on the Si$_9$ cluster cores was investigated by quantum chemical calculations to the partial atomic distributions [e$^-$] in the siliconoid molecules (Figure 32, bottom). Comparison of the overall charge distributions shows that lower partial charges are located at substituted silicon atoms. In accordance to the stronger shielding of the exposed Si$_9$ cluster atoms in ^{29}Si NMR investigations, higher negative partial charges were found to be located at ligand-free silicon cluster atoms. The lowest partial charges are located at the substituted silicon cluster atoms that form the *exo*-bonds, ligand-specific differences underline an electronic influence of the respective organic rests at the silyl groups on the cluster atoms (partial atomic charges: SnCy$_3$ > SiH^{t}Bu$_2$ > SiTMS$_3$).

An IBO (intrinsic bond orbitals) analysis of [(Si(TMS)$_3$)$_3$Si$_9$]$^-$ and [(Si(TMS)$_3$)$_2$Si$_9$]$^{2-}$ manifested a decisive influence of a third substituent on the bonding situation within the Si$_9$ cluster core comprising 2c–2e (2centre–2electron) and delocalized 3c–2e and 5c–6e multicenter bonds. The bonding situation in the D_{3h} symmetric cluster core of [(Si(TMS)$_3$)$_3$Si$_9$]$^-$ is stronger delocalized if compared to the C_{2v} core in [(Si(TMS)$_3$)$_2$Si$_9$]$^{2-}$. Three 5c–6e bonds are found within the three ligand-bearing capped prism square faces of [(Si(TMS)$_3$)$_3$Si$_9$]$^-$. Two 5c–6e bonds are repealed by release of one ligand and the formation of [(Si(TMS)$_3$)$_2$Si$_9$]$^{2-}$ (one single 5c–6e bond within the exposed capped square face of the cluster). Furthermore, Raman spectroscopic vibrations of the Si$_9$ clusters in [(*E*R$_3$)$_2$Si$_9$]$^{2-}$ {*E*R$_3$ = SnCy$_3$, Si(TMS)$_3$} single crystals could be assigned by comparison to calculated spectra. The assignments revealed the appearance of multiple Si$_9$ cluster vibrations and underline a versatile bonding situation within the silicon cores.

2.2.4 Discussion of the Results with $K_{12}Si_{17}$ Precursor Material

Synthetic approaches for the synthesis of vinylated and silylated Ge$_9$ clusters with K$_4$Ge$_9$ precursor material were successfully transferred to Si$_9$ clusters from the K$_{12}$Si$_{17}$ precursor for the first time.

Fundamental investigations with K$_{12}$Si$_{17}$ precursor material in solid-state revealed ^{29}Si MAS NMR shifts for the contained, polyanionic Si$_9^{4-}$ and Si$_4^{4-}$ silicon clusters in single-phase K$_{12}$Si$_{17}$ material in interplay with computational studies. "*Activation*" of the K$_{12}$Si$_{17}$ material with NH$_3$/222crypt paved the way for its transfer to the molecular [H$_2$Si$_9$]$^{2-}$ clusters species in pyridine and ethylenediamine solutions. NMR investigations of [H$_2$Si$_9$]$^{2-}$ show an outstanding dynamic behavior of this species that bears novel properties if compared to reported molecular silicon compounds boasting a dynamic Si$_9$ cluster core with scrambling hydrogen atoms at the cluster surface.[251]

Later reported NMR spectroscopic investigations of Rb$_6$K$_6$Si$_{17}$ precursor material in liquid ammonia solution further verified the results by revealing the presence of dynamic [HSi$_9$]$^{3-}$ and [HSi$_4$]$^{3-}$ species.[80, 243] Feasible NMR measurements of [HSi$_9$]$^{3-}$ [243] and [HSi$_4$]$^{3-}$ [80] at lower temperature (−70 °C) if compared to [H$_2$Si$_9$]$^{2-}$ (−40 °C) resulted in the formation of rigid Si–H cluster bonds under origination of two ^{29}Si NMR shifts for [HSi$_9$]$^{3-}$ (Si$_H$: –159 ppm; Si$_8$ –359 ppm), which are consistent with the average shift of [H$_2$Si$_9$]$^{2-}$ at −346 ppm in pyridine. The reported ^{1}H NMR shift for [HSi$_9$]$^{3-}$ at –2.9 ppm is in good accordance with the detected [H$_2$Si$_9$]$^{2-}$ shifts at –0.7 ppm (pyridine) and –1.5 ppm (ethylenediamine). The small J(^{29}Si–^{1}H) coupling constants for [H$_2$Si$_9$]$^{2-}$ (19.7 Hz in pyridine and 20.4 Hz ethylenediamine) are in agreement with small values for [HSi$_9$]$^{3-}$ (3 Hz) and [HSi$_4$]$^{3-}$

(<3 Hz) although the NMR shift ranges for $[HSi_4]^{3-}$ clearly differ due to the higher negative charge per atom in Si_4^{4-} clusters (see Table 2).

Initiated by the successful transfer of Si_9 clusters to ethylenediamine solution, a NMR reactivity study targeting cluster vinylations of Si_9 with the alkyne reactant TMS-C≡C-TMS indicated the formation of a $[(CH_2CH)_xSi_9]^{(4-x)-}$ species in analogy to Ge_9 cluster vinylations in ethylenediamine.[182-184, 187] Regarding the formation of ligand-stabilized Si_9 clusters from the $K_{12}Si_{17}$ precursor, the anionic siliconoids $[(ER_3)_3Si_9]^-$ {ER_3 = $Si(TMS)_3$, SiH^tBu_2, Si^iPr_3, $SnCy_3$,} were synthesized by attachment of three covalently *exo*-bonded substituents at the Si_9 cluster cores as reported for Ge_9 clusters before and further explored in the scope of this thesis.[177, 208-209] The formations proceeded by single-step reaction of "$K_{12}Si_{17}$ (*activated*)" precursor material with the respective chlorosilane or chlorostannane compound. The Si_9 siliconoids were obtained as D_{3h} symmetric cluster species in solution and bear six exposed and three substituted silicon cluster atoms. An initializing reactivity test of $[(SiH^tBu_2)_3Si_9]^-$ with the (2-butene)Si^tBu_2 silirane indicated the first synthetic modification of a silylated Si_9 siliconoid in ESI-MS by extension of the cluster reactant with four SiH^tBu_2 units to a $[(SiH^tBu_2)_7Si_9]^-$ species.

Crystallization of obtained bulk material containing $[(ER_3)_3Si_9]^-$ {ER_3 = $Si(TMS)_3$, SiH^tBu_2, Si^iPr_3, $SnCy_3$,} yielded single crystals of di-substituted $[(ER_3)_2Si_9]^{2-}$ {ER_3 = $Si(TMS)_3$, SiH^tBu_2, Si^iPr_3, $SnCy_3$,} cluster species in all cases. This indicates the loss of one of the substituents during crystallization under formation of exposed silicon cluster surfaces in the molecular structures. Therein, the exposed silicon cluster atoms bear higher partial atomic charges if compared to the substituted Si cluster atoms, and the two extra negative charges of the Si_9 molecules are versatile distributed within the cluster cores as verified by calculations. The Si–Si bond lengths are elongated for bonds including exposed Si atoms and add to reported siliconoids in literature.[165, 168]

Summarized, the application of the silicon cluster precursor $K_{12}Si_{17}$ became feasible in the field of low-valent silicon molecules. The precursor was transferred to molecular cluster species in solution, which are now accessible for investigations in the scope of materials science. Moreover, the presented investigations open a simple synthetic protocol for the synthesis of soluble anionic siliconoids with high numbers of exposed silicon atoms. IBO (intrinsic bond orbitals) analysis revealed delocalized cluster cores for Si_9 siliconoids with multicenter bonds. Thus, knowledge to accessible siliconoid compounds was enhanced by outstanding properties of Si_9 clusters that boast a combination of nucleophilicity (negative charges) and low-valence (unsaturated bonding situation). The high synthetic potential of siliconoids was already demonstrated in literature[165, 171, 173, 252-257] and also indicated for $[(SiH^tBu_2)_3Si_9]^-$ herein. The presented investigations within this work pave the way for the transfer of the fruitful chemistry with Ge_9 clusters to Si_9, and thus, for the synthesis of cluster-based material building blocks from an intermetallic precursor.

3 SUMMARY AND CONCLUSIONS

The precursor materials K_4Ge_9 (chapter 2.1) and $K_{12}Si_{17}$ (chapter 2.2) were investigated as cluster sources for building blocks towards the fabrication of germanium- and silicon-based materials. Both precursors contain nine-atomic clusters of Si or Ge, respectively, and the release of their synthetic potential was explored by their transformation to defined molecular species in solution. Whereas the synthesis of ligand-stabilized Ge_9 clusters from K_4Ge_9 was already successful, such reactions were not known for Si_9 clusters from $K_{12}Si_{17}$ before this thesis. The herein presented investigations promote the application potential of the K_4Ge_9 precursors and show that a transfer to $K_{12}Si_{17}$ is possible.

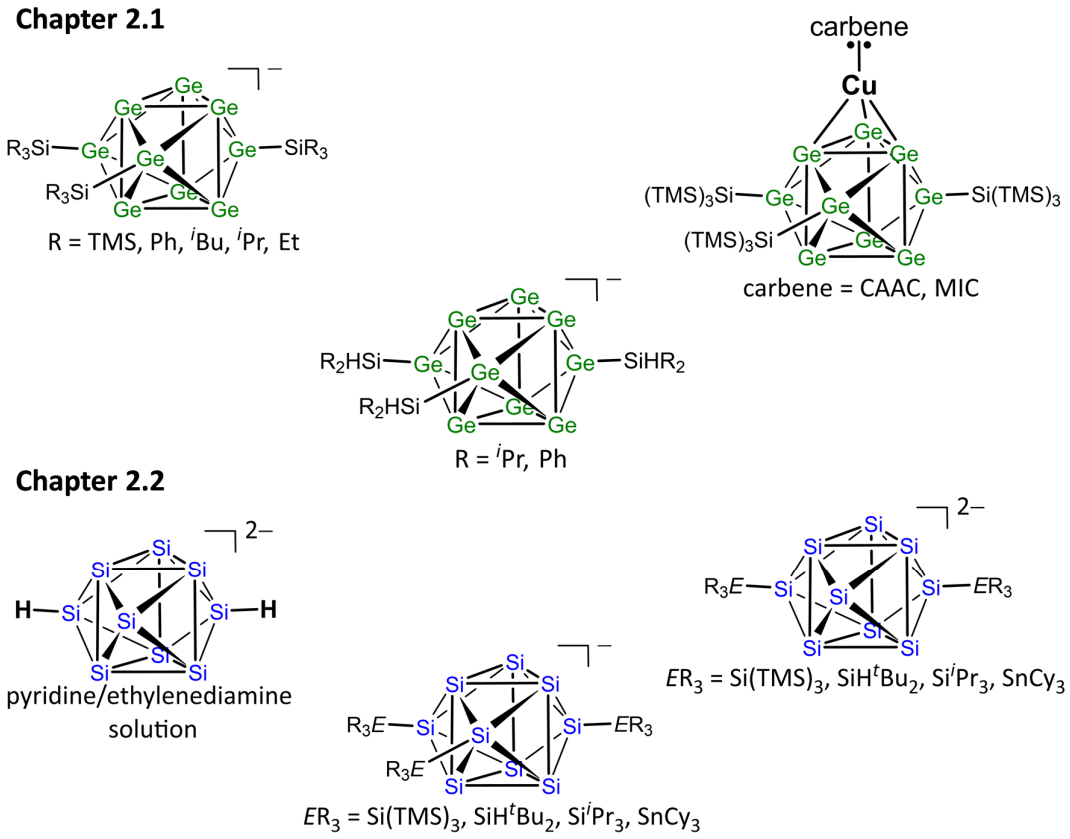

In chapter 2.1.2 (Exploration of Silylation Reactions with Ge_9 Clusters) new silylations of Ge_9 clusters from K_4Ge_9 material were explored by reactions with versatile chlorosilanes. Therewith, knowledge on silylation reactions was extended by obtained tri-silylated $[(SiR_3)_3Ge_9]^-$ (R = Ph, ^{i}Bu, ^{i}Pr, Et) and Si–H-functionalized $[(SiHR_2)_3Ge_9]^-$ (R = ^{i}Pr, Ph) cluster species. Si–H-functionalization prepares the base for further cluster modifications as *e.g.* by insertion or hydrosilylation reactions.

The attachment of three covalently bonded silyl groups at a Ge_9 core proceeds by single-step reaction and yields stable species with differing silyl groups at the deltahedral clusters. The impact of electronic and steric properties of the silyl groups was revealed by -Si^{i}Bu$_3$ group loss in crystallization and by -$SiPh_3$ group substitution in metal complexation. As a result, versatile structures of transition metal complexes with silylated Ge_9 clusters were found in obtained single crystals as

presented in chapter 2.1.3 (Exploration of Metal Complexations with Ge_9 Clusters). Application relevant organic phosphine and carbene (carbene = CAAC, MIC) ligands were obtained in cluster metal complexes by simple reaction pathways and promote the utilization of K_4Ge_9 precursor material for catalytic reactions.

Studies of the $K_{12}Si_{17}$ silicon cluster precursor in chapter 2.2.2 (Silicon Clusters in Intermetallic $K_{12}Si_{17}$ Precursor Material) in solid-state revealed the detection of ^{29}Si MAS NMR shifts for contained Si_4^{4-} and Si_9^{4-} clusters. Utilization of the precursor material succeeded initially by transferring Si_9^{4-} clusters to pyridine and ethylenediamine solutions after prior NH_3/222crypt "*activation*" of the precursor. Thereby, a soluble $[H_2Si_9]^{2-}$ cluster species (chapter 2.2.3.2: Investigation of $[H_2Si_9]^{2-}$ in Pyridine and Ethylenediamine Solution) was detected and characterized. The species boasts outstanding properties including a dynamic Si_9 core with scrambling hydrogen atoms at its cluster surface. Moreover, the transfer of established cluster vinylations from Ge_9 to Si_9 clusters in ethylenediamine solution was indicated.

These insights paved the way for the synthesis of anionic $[(ER_3)_3Si_9]^-$ {ER_3 = $Si(TMS)_3$, SiH^tBu_2, Si^iPr_3, $SnCy_3$,} siliconoids by silylation reactions of $K_{12}Si_{17}$ material with chlorostannane and chlorosilane compounds in chapter 2.2.3.3 (Formation of $[(ER_3)_3Si_9]^-$ Siliconoid Clusters). In analogy to tri-substituted Ge_9 clusters, the species form by attachment of three covalently bonded -ER_3 (*E* = Si, Sn; R = organic rest) groups at a Si_9^{4-} core from the precursor. An reactivity experiment of $[(SiH^tBu_2)_3Si_9]^-$ with a silirane indicated an extension of the reactant to a $(SiH^tBu_2)_7Si_9^-$ species, and thus, the possibility for further molecular transformations of such cluster species. Crystallization of the species (chapter 2.2.3.4: Molecular Structures of $[(ER_3)_2Si_9]^{2-}$ Siliconoid Clusters) yielded di-anionic $[(ER_3)_2Si_9]^{2-}$ {ER_3 = $Si(TMS)_3$, SiH^tBu_2, Si^iPr_3, $SnCy_3$,} siliconoids by cleavage of one of the substituents and under formation of negatively charged, exposed cluster surfaces. The species advance synthetic pathways for siliconoid clusters by few-step synthesis and under usage of precursor material for the first time.

Summarized, a starting point for the utilization of Si_9 clusters from $K_{12}Si_{17}$ precursor material was set by simple syntheses of cluster-based material building blocks. Their accessibility, synthetic fine-tuning and good solubility makes them suitable for material fabrications as pursued in future research.

4 EXPERIMENTAL SECTION

Experiments were carried out in laboratories of the TECHNICAL UNIVERSITY OF MUNICH (Garching b. München, Germany, DEPARTMENT OF CHEMISTRY, CHAIR OF INORGANIC CHEMISTRY WITH FOCUS ON NOVEL MATERIALS, *Prof. Thomas Fässler*). CAAC and MIC carbene compounds were synthesized in laboratories of the UNIVERSITY OF CALIFORNIA, SAN DIEGO in the United States of America (DEPARTMENT OF CHEMISTRY, *Prof. Guy Bertrand*). Computational studies were carried out in cooperation with the AALTO UNIVERSITY in Finland (DEPARTMENT OF CHEMISTRY AND MATERIALS SCIENCE, *Prof. Antti Karttunen*). The investigations within this work were organized in cooperation with the WACKER CHEMIE AG (CONSORTIUM FÜR ELEKTROCHEMISCHE INDUSTRIE, Munich, Germany) within the framework of the WACKER INSTITUTE FOR SILICON CHEMISTRY (TECHNICAL UNIVERSITY OF MUNICH).

4.1 Experimental Procedures

4.1.1 Materials and Equipment

If not stated otherwise, all reactions were carried out in an oxygen and moisture free argon Ar4.8 atmosphere (WESTFALEN AG; purity: 99.998%) using a *Schlenk* line equipped with a rotary vane vacuum pump (VACUUBRAND GMBH & CO RZ 5; average vacuum $4 \cdot 10^{-2}$ mbar) and a mercury pressure control valve or in a glovebox (MBRAUN INTERTGAS-SYSTEME GMBH, average oxygen value < 0.1 ppm; average H_2O value < 0.1 ppm). The Ar4.8 gas was purified by passing a *BTS* catalyst, molecular sieve, silica gel with indicator ("orange gel") and phosphorous pentoxide with H_2O indicator before usage. Glassware was stored in a drying oven (FRANZ BINDER GMBH; ED115) at 120 °C. Reactions were carried out in *Schlenk* tubes or *Schlenk* flasks equipped with a glass valve and a glass stopper using either silicon-based grease (DOW CORNING INC) or *Teflon* paste (CARL ROTH GMBH) as lubricants. Before usage, reaction vessels were heated to 650 °C using a heat gun (STEINEL AMERICA INC) in dynamic vacuum and subsequently purged with argon gas (*Schlenk* line, procedure was repeated three times). Glassware was cleaned in an *iso*-propanol/KOH bath after usage. Plastic syringes and metal cannulas were purged with argon gas three times before usage. Further equipment (NMR tubes, agate mortars, *Teflon* tubing, *Whatman* filters, *Teflon* syringe filters, *Pasteur* pipettes and stirring bars) were stored in a drying oven for at least 2 h before usage.

4.1.2 Filtration Techniques

Filtrations under exclusion of air and moisture were carried out at the *Schlenk* line using *Whatman* filters (*Whatman*, GD 1 µm) attached to *Teflon* tubings with *Teflon* tape (VWR INTERNATIONAL GMBH) or in the glovebox using either *Whatman* filters (WHATMAN PLC, GD 1 µm) packed *Pasteur* pipettes or *Teflon* syringe filters (VWR INTERNATIONAL GMBH: diameter 2.5 cm, pore size 0.2 µm).

4.1.3 Reactants and Solvents

The solvents acetonitrile, diethyl ether, tetrahydrofuran, toluene, and hexane were obtained from a solvent purification system (MB-SPS; MBRAUN INTERTGAS-SYSTEME GMBH). Fluorobenzene and 1,2-difluorobenzene were dried over CaH_2 prior to usage. All solvents including deuterated solvents were stored over molecular sieves (3 Å) prior to usage. The molecular sieves were dried under dynamic vacuum (*Schlenk* line) at 500 °C for at least 12 h prior to usage. For working with dry liquid ammonia, a *Schlenk* line consisting exclusively of glass components was used. Ammonia (WESTFALEN AG; 99.999%) was condensed from a gas cylinder into an *iso*-propanol/dry ice cooled solvent trap containing elemental sodium and stored there for at least 1 h. The formation of a blue solution (solvated electrons) in the solvent trap indicated that liquid ammonia was dry. For subsequent reactions, *Schlenk* tubes including the reactants were attached at the respective adapters of the Schlenk line and liquid ammonia was condensed into the cooled reaction vessels (−78 °C; *iso*-propanol/dry ice) in static vacuum.

Commercially available chemicals were used as received unless stated otherwise. Table 3 summarizes all commercially available reactants and solvents used within this work and provides information about physical state, purity, supplier/producer and storage of the respective chemical.

Table 3. List of commercially available chemicals used within this work.

Substance	Physical state	Purity [%]	Supplier/ Producer	Storage
acetonitrile	liquid	SPS	VWR International GmbH	laboratory
1,2-difluorobenzene	liquid	98%	Chempur Feinchemikalien und Forschungsbedarf GmbH	laboratory
18c6	solid	sublimated	Merck KGaA	glovebox
222crypt	solid	99% (*vacuum* dried)	Merck KGaA	glovebox
5-bromo-1-pentene	liquid	95%	Merck KGaA	glovebox
acetonitrile-*d3*	liquid	99.8%	Deutero GmbH	glovebox
ammonia	gas	99.999 (Na dried)	Westfalen AG	cylinder
argon	gas	9999.8%	Westfalen AG	cylinder
benzene-*d6*	liquid	99%	Deutero GmbH	glovebox
bromobenzene	liquid	≥ 99.5%	Sigma Aldrich by Merck KGaA	laboratory
calcium hydride	solid	for synthesis	Merck KGaA	laboratory
Chloro(dimethyl) vinylsilane	liquid	97%	Sigma Aldrich by Merck KGaA	glovebox
chlorodi(*iso*-propyl) silane	liquid	95%	Acros Organics by Thermo Fisher Scientific Inc	glovebox

chlorodi(methyl) silane	Liquid	> 96%	Acros Organics by Thermo Fisher Scientific Inc	glovebox
chlorodi(phenyl) silane	liquid	90%	Alfa Aesar by Thermo Fisher Scientific Inc	glovebox
chlorodi(*tert*-butyl) silane	liquid	99%	Sigma Aldrich by Merck KGaA	glovebox
chloroform-*d1*	liquid	99.80%	Deutero GmbH	glovebox
chlorotri(*iso*-butyl) silane	liquid	99%	Sigma Aldrich by Merck KGaA	glovebox
chlorotri(*iso*-propyl) silane	liquid	97%	Sigma Aldrich by Merck KGaA	glovebox
chlorotriethylsilane	Liquid	> 98%	Alfa Aesar by Thermo Fisher Scientific Inc	glovebox
chlorotrimethyl-silane	Liquid	> 98%	Alfa Aesar by Thermo Fisher Scientific Inc	glovebox
chlorotriphenyl-silane	solid	96%	Alfa Aesar by Thermo Fisher Scientific Inc	glovebox
chlorotris(trimethylsi-lyl) silane	solid	95%	TCI Deutschland GmbH	glovebox
copper(I) chloride	solid	97%	Alfa Aesar by Thermo Fisher Scientific Inc	glovebox
diethyl ether	liquid	SPS	Brenntag AG	laboratory
dichlorodiphenyl-silane	liquid	97%	Sigma Aldrich by Merck KGaA	glovebox
ethyl acetate	liquid	99.90%	VWR International GmbH	laboratory
fluorobenzene	liquid	99%	Chempur Feinchemikalien und Forschungsbedarf GmbH	laboratory
germanium	solid	99.999%	Evochem Advanced Materials GmbH	glovebox
iodine	solid	99.8%	VWR International GmbH	glovebox
magnesium cuttings	solid	for synthesis	Merck KGaA	laboratory
n-hexane	liquid	SPS	Brenntag AG	laboratory
potassium	solid	≥ 98% (hexane washed)	Sigma Aldrich by Merck KGaA	glovebox
pyridine	liquid	max. 0.0075% H_2O	Merck KGaA	glovebox
pyridine-*d5*	liquid	99.5%	Deutero GmbH	glovebox
polysilicon	Solid (ball-milled)	99.99%	WACKER Chemie AG	glovebox
silicon (^{29}Si)	solid	99.34% (^{29}Si)	Isoflex USA Inc	glovebox

sodium	solid	99%	Merck KGaA	laboratory
tetrahydrofuran	liquid	SPS	Kraft Chemical Company Inc	laboratory
tetrahydrofuran-*d8*	liquid	99.5%	Deutero GmbH	glovebox
toluene	liquid	SPS	Brenntag AG	laboratory
trichlorovinylsilane	liquid	97%	Sigma Aldrich by Merck KGaA	glovebox
tricyclohexyltin chloride	solid	95%	Sigma Aldrich by Merck KGaA	glovebox
triphenylgermanium chloride	solid	99%	Sigma Aldrich by Merck KGaA	glovebox
zinc(II) chloride	solid	98%	Alfa Aesar by Thermo Fisher Scientific Inc	glovebox

4.1.4 Synthesis of the Intermetallic Precursors and $K_{12}Si_{17}$ Activation

Synthesis of the germanium *Zintl* precursor K_4Ge_9:[73]

Potassium (1.05 g, 26.9 mmol) and germanium (4.00 g, 55.1 mmol) were weighed into a stainless-steel cylinder (length: 7 cm, diameter: 1.5 cm) in a glove box (cylinder filling: K at bottom, Si at top). The cylinder was placed in a stainless-steel autoclave (length: 9 cm, diameter: 2.5 cm, see Figure 34). The autoclave was closed in a glovebox with a stainless-steel screw cap and placed in a corundum tube which was closed with a lubricated glass cap equipped with a rubber balloon for pressure balance (length: 60 cm, diameter: 4 cm). Argon atmosphere in the corundum tube was ensured by three-time evacuating and argon flushing at a *Schlenk* line prior to starting of the solid-state reaction. The corundum tube with the contained steel autoclave was vertically placed in a tube furnace (HTM REETZ GMBH) equipped with a temperature controller (EUROTHERM DEUTSCHLAND GMBH).

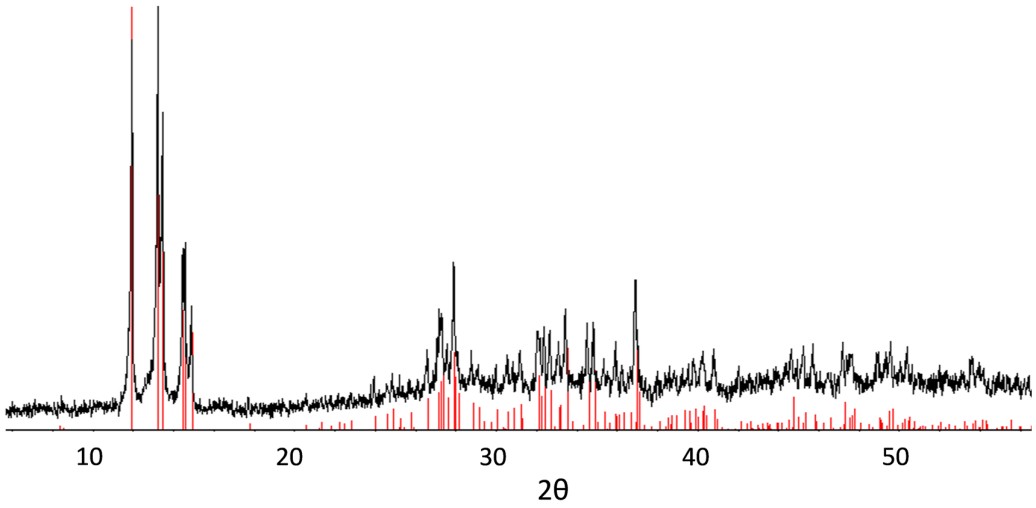

Figure 33. Powder X-ray diffractogram of the precursor *Zintl* phase K_4Ge_9 (black, top) in comparison to a theoretical diffractogram (red, bottom).[73]

The furnace was heated to the target temperature of 650 °C with a rate of 2 °C/min and kept at this temperature for 46 h before it was cooled to ambient temperature with a rate of 1 °C/min. Subsequently, the steel autoclave was removed from the corundum tube and rapidly brought into a glovebox. The product *Zintl* phase K_4Ge_9 was removed from the autoclave and finely grounded using an agate pestle and mortar. The obtained black greyish solid was examined for phase-purity by PXRD in wax sealed glass capillaries prior to usage (PXRD analysis in Figure 33).

Figure 34. Stainless-steel autoclave (for K_4Ge_9) and tantalum ampoule (for K_4Si_4 and $K_{12}Si_{17}$) as used for the solid-state syntheses of *Zintl* precursor phases.

Synthesis of the silicon *Zintl* precursors $K_{12}Si_{17}$ and K_4Si_4:[72, 241]

For the syntheses, the reactants were filled in tantalum ampoules (Figure 34) which were fabricated by cutting tantalum tubes (CHANGSHA SOUTH TANTALUM NIOBIUM CO LTD, Ø: 10 mm or 12.7 mm, wall strength: 0.5 mm) in small cylinders (height approx. 5 cm). The ampoules were cleaned by sonication in acetic acid, water and acetone before they were dried in a drying oven (FRANZ BINDER GMBH; ED115) at 120 °C and stored in the glovebox prior to usage. The cylinders were closed prior to filling in a glovebox (Ar atmosphere) at one end with a tantalum cap and sealed after filling by arc melting in an arc furnace (*MAM 1* EDMUND BÜHLER GMBH). For the solid-sate reaction, the ampoules were placed in a quartz tube (length: 80 cm, diameter: 4 cm; two ampoules per quartz tube), which was closed with a lubricated glass cap, evacuated (*Schlenk* line), and vertically placed in a tube furnace (0.75 m, HTM REETZ GMBH) equipped with a temperature controller (EUROTHERM DEUTSCHLAND GMBH).

Synthesis of K_4Si_4: Potassium (1.19 g, 30.4 mmol) and silicon (0.84 g, 29.8 mmol) were weighed into a tantalum ampoule (Ø: 10 mm, height approx. 5 cm) in a glovebox and the ampoule transferred into a quartz tube after sealing (ampoules filling: K at bottom, Si at top). The furnace was heated to the target temperature of 500 °C at a rate of 5 °C/min and was kept at this temperature for 1 h. Subsequently, it was further heated to 600 °C for 30 h and cooled to room temperature at a rate of 5 °C/min. The ampoule was removed from the quartz tube and brought into a glovebox. The product *Zintl* phase K_4Si_4 was brought out of the ampoules and finely grounded using an agate

pestle and mortar. Subsequently, the obtained black greyish solid was examined for phase purity by PXRD in wax sealed glass capillaries prior to usage (PXRD analysis in Figure 35).

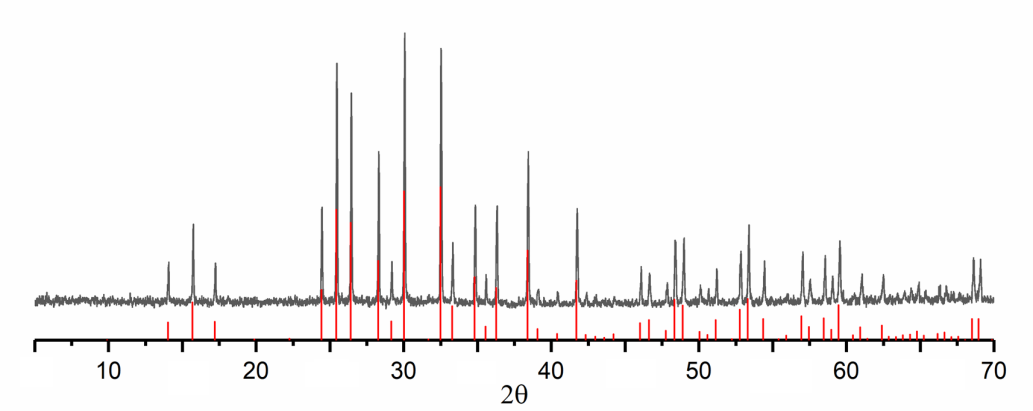

Figure 35. Powder X-ray diffractogram of the precursor *Zintl* phase K_4Si_4 (gray, top) in comparison to a theoretical diffractogram (red, bottom).[62]

Synthesis of $K_{12}Si_{17}$: Potassium (0.55 g, 14.0 mmol) and silicon (0.59 g, 21.0 mmol) [alternative synthesis for Ø 10 mm tantalum (height: 5cm) ampules: potassium (0.38 g, 9.78 mmol) and silicon (0.39 g, 13.9 mmol)] were weighed into a tantalum ampoule (Ø 12.7 mm, height: 5cm) in a glovebox and the ampoule was transferred into a quartz tube after sealing (ampoules filling: K at bottom, Si at top). The furnace was heated to the target temperature of 800 °C at a rate of 2 °C/min and was kept at this temperature for 15 h before it was cooled to ambient temperature at a rate of 0.5 °C/min. The ampoules were removed from the quartz tube and brought into a glovebox. The product *Zintl* phase $K_{12}Si_{17}$ was brought out of the ampoules and finely grounded using an agate pestle and mortar. Subsequently, the obtained black greyish solid was examined for phase purity by PXRD in wax sealed glass capillaries prior to usage (PXRD analysis in Figure 36).

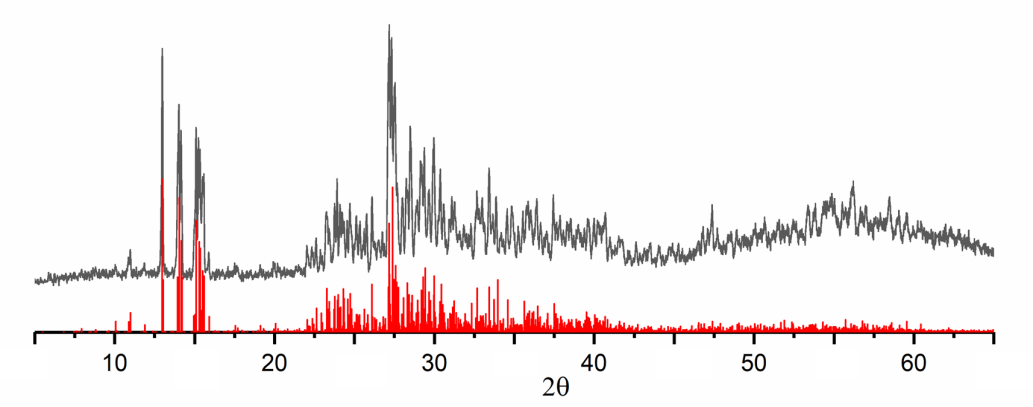

Figure 36. Powder X-ray diffractogram of the precursor *Zintl* phase $K_{12}Si_{17}$ (gray, top) in comparison to a theoretical diffractogram (red, bottom).[72]

Synthesis of "$K_{12}Si_{17}$ (*activated*)": For "*activation*" of the precursor, $K_{12}Si_{17}$ (0.20 g, 0.21 mmol) and 222crypt (0.15 g, 0.39 mmol) were weighed into a Schlenk tube and liquid ammonia was added at

−78 °C (*iso*-propanol/CO_2) yielding a dark red solution (Figure 26b). The mixture was stirred at −78 °C for 2 h and "$K_{12}Si_{17}$ (*activated*)" was obtained as a brown solid after removal of the liquid ammonia and used without further purification.

4.2 Characterization Methods

4.2.1 Nuclear Magnetic Resonance Spectroscopy

Solution NMR spectroscopy: The samples were filled into *Norell ST500* NMR Tubes (NORELL INC) or *Deutero 300* NMR tubes with *Young PTFE Valve* (DEUTERO GMBH). ^{1}H, ^{13}C and ^{29}Si NMR spectra were recorded on a *Bruker AVIII Ultrashield* 400 MHz, a *Bruker AVIII* 500 MHz *Cryo* system or a *Bruker AVIII HD Ultrashield* 500 MHz. ^{119}Sn NMR spectra were recorded on a *Bruker AVIII* 300 MHz (all spectrometers from BRUKER INC). The signals of the ^{1}H and ^{13}C spectra were calibrated on the rest proton signal of the used deuterated solvent (acetonitrile-*d3*, thf-*d8*, benzene-*d6*, pyridine-*d5*, chloroform-*d1*, toluene-*d8*). Chemical shifts are given in δ values by parts per million [ppm]. The coupling constants *J* are stated in Hz. Signal multiplicities are abbreviated as follows: s – singlet, d – doublet, t – triplet, q – quartet, m – multiplet. The spectra were evaluated and visualized with MestReNova.[258]

Solid-state MAS NMR spectroscopy: Magic-angle spinning (MAS) ^{29}Si NMR spectra were recorded on a *Bruker Advance* 300 MHz spectrometer (BRUKER INC) operating at 7.04 T at ambient temperature with single-pulse technique. Samples were packed in 4 mm ZrO_2 MAS NMR probes and rotated with frequencies of 8 and 12 kHz. MestReNova[258] was used for the evaluated and visualization of the spectra. $Si(Si(CH_3)_3)_4$ was used as extern (secondary) standard for referencing. The measurements were carried out by *Dr. Gabriele Raudaschl-Sieber* (TECHNICAL UNIVERSITY OF MUNICH).

4.2.2 Electrospray Ionization Mass Spectrometry

Samples were prepared in a glovebox in 500 µl syringes (HAMILTON GERMANY GMBH). The spectra were measured on an *HCT* instrument (BRUKER INC). Data were analyzed using the program *Bruker Compass Data Analysis 4.0 SP 5* (BRUKER INC). The dry gas temperature was adjusted to 125 or 300 °C and the injection speed to 240 $\mu L \cdot s^{-1}$. Visualization of the spectra was done with the programs *OriginPro* (ORIGIN LAB INC) or *Microsoft Excel* (MICROSOFT INC).

4.2.3 Powder X-Ray Diffraction

Data were collected at room temperature on a Stadi P diffractometer (Ge(111) monochromator (STOE & CIE GMBH; Cu Kα_1 radiation λ = 1.54056 Å or Mo Kα_1 radiation λ = 0.70930 Å) with a *Mythen*

1K detector (DECTRIS AG) in *Debye-Scherrer* geometry. Samples were sealed in glass capillaries (Ø 0.5 mm or 0.7 mm) for the measurements. Raw data were processed and visualized with the software *WinX-POW*[259] or *OriginPro* (ORIGIN LAB INC).

4.2.4 Single Crystal X-Ray Diffraction

Single crystal preparation: For data collection, the air and moisture sensitive crystals were fixed on a glass capillary and positioned in a cold stream of N_2 gas. The single crystals were either transferred from the mother liquor into a perfluoropolyalkyl ether oil at 213 K under a cold N_2 atmosphere and subsequently fixed on a glass capillary or prepared analogously in Ar atmosphere in a glove box.

Data collection: Data were collected using a *Diffraction Xcalibur3* diffractometer (OXFORD INSTRUMENTS PLC; Mo K_α radiation; λ = 0.71073 Å) equipped with a *Sapphire 3* detector or a *StadiVari* (STOE & CIE GMBH; Mo K_α radiation; λ = 0.71073 Å) diffractometer equipped with a *Dectris Pilatus 300K* detector.

Structure refining: Structures were solved by *Direct Methods* and refined by full-matrix least-squares calculations against F^2 (*SHELXL 2014*).[260] The positions of the hydrogen atoms were calculated and refined using the *Riding Model*.[261] Unless otherwise stated, all non-hydrogen atoms were treated with anisotropic displacement parameters. In special cases the electron density of disordered solvent molecules was taken care of by the *Platon* [262] squeeze function. Supplementary crystallographic data for the molecular structures reported in this thesis have been deposited with the *Cambridge Structural* database and are available free of charge *via www.ccdc.cam.ac.uk/data_request/cif*. For visualization, the structures have been plotted with *Diamond 3.2k*.[263] Structure refinements and submissions were done under assistance of *Dr. Wilhelm Klein* (TECHNICAL UNIVERSITY OF MUNICH).

4.2.5 Energy Dispersive X-Ray Analysis

Compounds were analyzed with a *SWIFT-ED-TM* (OXFORD INSTRUMENTS PLC) and a *TM-1000 Tabletop* microscope (HITACHI HIGH-TECHNOLOGIES INC) with the *INCA* system software or a *JEOL 5900LV* scanning electron microscope equipped with an energy dispersive X-ray analyzer (OXFORD INSTRUMENTS PLC). EDX measurements were carried out by *Maria Müller* (TECHNICAL UNIVERSITY OF MUNICH).

4.2.6 Fourier-Transform Infrared Spectroscopy

FT-IR spectra were recorded on a Bruker Alpha FT-IR spectrometer with an *ATR* geometry using a diamond *ATR* unit (BRUKER INC). Sample preparations and measurements were carried out in a glovebox. Samples were measured by *David Mayer* (TECHNICAL UNIVERSITY OF MUNICH).

4.2.7 Raman Spectroscopy

Raman spectra were recorded with an *inVia Raman Microscope RE04* with a *CCD* detector and 500 mW maximal power (RENISHAW PLC; Software: *WiRE 4.2 build 5037*) at λ = 532 nm. Samples were sealed in glass capillaries in a glovebox and measured by *Dr. Sebastian Geier* or *Dr. Herta Slavik* (TECHNICAL UNIVERSITY OF MUNICH).

4.2.8 Elemental Analysis

Elemental analyses were carried out in the microanalytical laboratory at the CATALYTIC RESEARCH CENTER of the TECHNICAL UNIVERSITY OF MUNICH. The elements C, H and N were determined by combustion analysis with an *Euro EA CHNSO Elemental Analysator* (HEKATECH LTD), Si and P were detected photometrically with a *UV-160* at 410 nm or 810 nm (SHIMADZU DEUTSCHLAND GMBH*)*, K and Cu were detected by atom absorption spectroscopy with a *AAS-280FS* (AGILENT TECHNOLOGIES INC).

4.2.9 Quantum Chemical Calculations

Quantum-chemical calculations at the *DFT-PBE0/TZVP* level of theory were carried out using the *TURBOMOLE* program package.[264-268] For solid-state Raman calculations, the *CRYSTAL* program was used (DFT-PBE0/SVP).[269] NMR calculations to silicon clusters (chapter 6.5) were done with the *CFOUR* program (*CCSD(T)/cc-pVTZ*),[270-271] and for solid-state NMR calculations with the *CASTEP* program (*DFT-PBE/USPP*) was used.[272-274] Quantum chemical calculations were carried out by *Prof. Antti Karttunen* (AALTO UNIVERSITY, FINLAND) and evaluated in cooperation. Details can be found in the Supporting Information of the respective manuscript (see chapter 6).

5 REFERENCES

1. Pfannhauser, W., *Essentielle Spurenelemente — Entdeckung, Aufnahme, Metabolismus und Bioverfügbarkeit*. Springer Berlin, Heidelberg: 1988.

2. Wiberg, N., *Holleman Wiberg — Lehrbuch der Anorganischen Chemie (102. Auflage)*. Walter de Gruyter: Berlin, 2007.

3. Kohler, H.; Fischer, H., *Periodensystem der Elemente*. Oldenbourg Wissenschaftsverlag: 2012.

4. Wolfram Research Inc., *WolframAlpha*: 2018, see online *via*: https://www.wolframalpha.com/examples/science-and-technology/chemistry/chemical-elements/

5. Wenski, G.; Hohl, G.; Storck, P.; Crößmann, I., *Chem. Unserer Zeit* 2003, *37* (3), 198.

6. Annual Report of the Wacker Chemie AG 2017.

7. Statisica GmbH, see online *via*: https://de.statista.com/statistik/daten/studie/260427/umfrage/durchschnittspreise-ausgewaehlter-mineralischer-rohstoffe/ (Sources: EIA, OPEC, Asian Metal; Status: December 2018).

8. Jutzi, P.; Schubert, U., *Silicon Chemistry: From the Atom to Extended Systems*. Wiley: Weinheim, 2007.

9. Dash, W. C.; Newman, R., *Phys. Rev.* 1955, *99* (4), 1151.

10. Bludau, W.; Onton, A.; Heinke, W., *J. Appl. Phys.* 1974, *45* (4), 1846.

11. Annual Report of the Infineon AG 2018.

12. IHS Markit Technology Group - Application Market Forecast Tool - Q3 2018 (Septempber 2018).

13. HGB Hamburger Geschäftsberichte GmbH for Siltronic AG, Annual Report 2017.

14. IHS Markit Technology Group - Semiconductor Silicon Forecast Tool - Q4 2017 Update.

15. Claeys, C.; Simoen, E., *Germanium-Based Technologies: From Materials to Devices*. Elsevier Science: 2007.

16. Stein, A., *Nature* 2006, *441*, 1055.

17. Pillarisetty, R., *Nature* 2011, *479*, 324.

18. Eickhoff, H.; Strangmüller, S.; Klein, W.; Kirchhain, H.; Dietrich, C.; Zeier, W. G.; van Wüllen, L.; Fässler, T. F., *Chem. Mater.* 2018, *30* (18), 6440.

19. Müller-Buschbaum, P.; Thelakkat, M.; Fässler, T. F.; Stutzmann, M., *Adv. Energy Mater.* 2017, *7* (16), 1700248.

20. Bentlohner, M. M.; Waibel, M.; Zeller, P.; Sarkar, K.; Müller-Buschbaum, P.; Fattakhova-Rohlfing, D.; Fässler, T. F., *Angew. Chem. Int. Ed.* 2016, *55* (7), 2441.

21. Picture source: HGB Hamburger Geschäftsberichte GmbH for Siltronic AG Annual Report 2017 (published with permission).

22. Picture source: Wacker Chemie AG (published with permission).

23. Obrovacz, M. N.; Christensen, L., *Electrochem. Solid-State Lett.* 2004, *7* (5), A93.

24. Su, X.; Wu, Q.; Li, J.; Xiao, X.; Lott, A.; Lu, W.; Sheldon, B. W.; Wu, J., *Adv. Energy Mater.* 2014, *4* (1), 1300882.

25. Lankhorst, M. H. R.; Ketelaars, B. W. S. M. M.; Wolters, R. A. M., *Nat. Mater.* 2005, *4*, 347.

26. Park, S. R.; Peng, H.; Ling, X. S., *Small* 2007, *3* (1), 116.

27. Borchard-Tuch, C., *Chem. Unserer Zeit* 2003, *37* (5), 362.

28. Adachi, S., *J. Appl. Phys.* 1985, *58* (3), R1.

29. Kipping, F. S.; Sands, J. E., *J. Chem. Soc.* 1921, *119* (0), 830.

30. Kipping, F. S., *J. Chem. Soc., Trans.* 1924, *125* (0), 2291.

31. Burkhard, C. A., *J. Am. Chem. Soc.* 1949, *71* (3), 963.

32. Mitra, A.; Atwood, D. A., *Polysiloxanes & Polysilanes in Encyclopedia of Inorganic Chemistry*. Wiley: 2006.

33. Schliebs, R.; Ackermann, J., *Chem. Unserer Zeit* 1987, *21* (4), 121.

34. Ackermann, J.; Damrath, V., *Chem. Unserer Zeit* 1989, *23* (3), 86.

35. Miller, R. D.; Michl, J., *Chem. Rev.* 1989, *89* (6), 1359.

36. Sato, Y.; Shiobara, E.; Onishi, Y.; Yoshikawa, S.; Nakano, Y.; Hayase, S.; Hamada, Y., *J. Vac. Sci. Technol., B* 2002, *20* (3), 909.

37. Yokoyama, K.; Notsu, S.; Yokoyama, M., *J. Chem. Soc., Chem. Commun.* 1990, (11), 805.

38. Li, X.; Edirisinghe, M. J., *Chem. Mater.* 2004, *16* (6), 1111.

39. Narisawa, M.; Okamura, K.; Iseki, T.; Oka, K.; Dohmaru, T., *Polysilane-Based Precursors for SiC/SiC Composites*. American Ceramic Society: 2006.

40. Song, Y. C.; Wang, J.; Liu, J.; Feng, C. X., *J. Mater. Sci. Lett.* 2003, *22* (9), 679.

41. Abkowitz, M. A.; Stolka, M.; Weagley, R. J.; McGrane, K. M.; Knier, F. E., *Electronic Transport in Polysilylenes*. American Chemical Society: 1989; Vol. 224, p 467.

42. Manners, I., *Angew. Chem. Int. Ed.* 1996, *35* (15), 1602.

43. Wang, D.; Chang, Y.-L.; Liu, Z.; Dai, H., *J. Am. Chem. Soc.* 2005, *127* (33), 11871.

44. Schäfer, H.; Eisenmann, B.; Müller, W., *Angew. Chem. Int. Ed.* 1973, *12* (9), 694.

45. Fässler, T. F., *Coord. Chem. Rev.* 2001, *215* (1), 347.

46. Nesper, R., Structural and Electronic Systematics in Zintl Phases of the Tetrels. In *Silicon Chemistry*, Jutzi, P.; Schubert, U., Eds. 2007.

47. Scharfe, S.; Kraus, F.; Stegmaier, S.; Schier, A.; Fässler, T. F., *Angew. Chem. Int. Ed.* 2011, *50* (16), 3630.

48. Fässler, T. F., *Zintl Ions - Principles and Recent Developments*. Springer: 2011.

49. Corbett, J. D., *Prog. Inorg. Chem.* 1976, *21*, 129.

50. Scherf, L. M.; Karttunen, A. J.; Pecher, O.; Magusin, P. C. M. M.; Grey, C. P.; Fässler, T. F., *Angew. Chem. Int. Ed.* 2016, *55* (3), 1075.

51. Takayuki, H.; Yamane, H.; Becker, N.; Dronskowski, R., *J. Solid State Chem.* 2015, *230*, 390.

52. Axel, H.; Schäfer, H.; Weiss, A., *Angew. Chem. Int. Ed.* 1965, *4* (4), 358.

53. Hopf, V.; Müller, W.; Schäfer, H., *Z. Naturforsch. B* 1972, *27* (10), 1157.

54. Schäfer, H.; Axel, H.; Weiss, A., *Z. Naturforsch. B* 1965, *20* (10), 1010.

55. Wengert, S.; Willems, J. B.; Nesper, R., *Chem. Eur. J.* 2001, *7* (15), 3209.

56. Zürcher, F.; Nesper, R., *Angew. Chem. Int. Ed.* 1998, *37* (23), 3314.

57. Eisenmann, B.; Janzon, K. H.; Schäfer, H.; Weiss, A., *Z. Naturforsch. B* 1969, *24* (4), 457.

58. Aydemir, U.; Ormeci, A.; Borrmann, H.; Böhme, B.; Zürcher, F.; Uslu, B.; Goebel, T.; Schnelle, W.; Simon, P.; Carrillo-Cabrera, W.; Haarmann, F.; Baitinger, M.; Nesper, R.; von Schnering, H. G.; Grin, Y., *Z. Anorg. Allg. Chem.* 2008, *634* (10), 1651.

59. Busmann, E., *Z. Anorg. Allg. Chem.* 1961, *313* (1-2), 90.

60. Witte, J.; Schnering, H. G.; Klemm, W., *Z. Anorg. Allg. Chem.* 1964, *327* (3-4), 260.

61. von Schnering, H. G.; Llanos, J.; Chang, J. H.; Peters, K.; Peters, E. M.; Nesper, R., *Z. Kristallogr. – New Cryst. Struct.* 2005, *220*, 324.

62. von Schnering, H. G.; Schwarz, M.; Chang, J. H.; Peters, K.; Peters, E. M.; Nesper, R., *Z. Kristallogr. – New Cryst. Struct.* 2005, *220* (4), 525.

63. Stearns, L. A.; Gryko, J.; Diefenbacher, J.; Ramachandran, G. K.; McMillan, P. F., *J. Solid State Chem.* 2003, *173* (1), 251.

64. Nesper, R.; Curda, J.; von Schnering, H. G., *J. Solid State Chem.* 1986, *62* (2), 199.

65. Wang, L.; Tang, Z.; Lorenz, B.; Guloy, A. M., *J. Am. Chem. Soc.* 2008, *130* (34), 11258.

66. Gil, R. C.; Carrillo-Cabrera, W.; Schultheiss, M.; Peters, K.; von Schnering, H. G.; Grin, Y., *Z. Anorg. Allg. Chem.* 1999, *625* (2), 285.

67. von Schnering, H. G.; Bolle, U.; Curda, J.; Peters, K.; Carrillo-Cabrera, W.; Somer, M.; Schultheiss, M.; Wedig, U., *Angew. Chem. Int. Ed.* 1996, *35* (9), 984.

68. von Schnering, H. G.; Baitinger, M.; Bolle, U.; Carrillo-Cabrera, W.; Curda, J.; Grin, Y.; Heinemann, F.; Llanos, J.; Peters, K.; Schmeding, A.; Somer, M., *Z. Anorg. Allg. Chem.* 1997, *623* (7), 1037.

69. Queneau, V.; Sevov, S. C., *Angew. Chem. Int. Ed.* 1997, *36* (16), 1754.

70. Queneau, V.; Todorov, E.; Sevov, S. C., *J. Am. Chem. Soc.* 1998, *120* (13), 3263.

71. von Schnering, H. G.; Somer, M.; Kaupp, M.; Carrillo-Cabrera, W.; Baitinger, M.; Schmeding, A.; Grin, Y., *Angew. Chem. Int. Ed.* 1998, *37* (17), 2359.

72. Hoch, C.; Wendorff, M.; Röhr, C., *J. Alloys Compd.* 2003, *361* (1), 206.

73. Ponou, S.; Fässler, T. F., *Z. Anorg. Allg. Chem.* 2007, *633* (3), 393.

74. Queneau, V.; Sevov, S. C., *Angew. Chem. Int. Ed.* 1997, *36* (16), 1754.

75. Nesper, R.; Currao, A.; Wengert, S., *Chem. Eur. J.* 1998, *4* (11), 2251.

76. Klemm, W.; Busmann, E., *Z. Anorg. Allg. Chem.* 1963, *319* (5-6), 297.

77. Bentlohner, M. M.; Fischer, C.; Fässler, T. F., *Chem. Commun.* 2016, *52*, 9841.

78. Goicoechea, J. M.; Sevov, S. C., *J. Am. Chem. Soc.* 2004, *126* (22), 6860.

79. Joseph, C.; Suchentrunk, N.; Korber, N., *Z. Naturforsch. B* 2010, *65*, 1059

80. Hastreiter, F.; Lorenz, C.; Hioe, J.; Gärtner, S.; Lokesh, N.; Korber, N.; Gschwind, R. M., *Angew. Chem. Int. Ed.* 2019, *58* (10), 3133.

81. Goicoechea, J. M.; Sevov, S. C., *Inorg. Chem.* 2005, *44* (8), 2654.

82. Wade, K., *Chem. Commun.* 1971, (15), 792.

83. Wade, K., *Inorg. Nucl. Chem. Lett.* 1972, *8* (6), 559.

84. Wade, K., *Adv. Inorg. Chem. Radiochem.*, 1976, *18*, 1.

85. Downie, C.; Tang, Z.; Guloy, A. M., *Angew. Chem. Int. Ed.* 2000, *39* (2), 337.

86. Waibel, M.; Kraus, F.; Scharfe, S.; Wahl, B.; Fässler, T. F., *Angew. Chem. Int. Ed.* 2010, *49* (37), 6611.

87. Goicoechea, J. M.; Sevov, S. C., *Organometallics* 2006, *25* (19), 4530.

88. Joseph, S.; Hamberger, M.; Mutzbauer, F.; Härtl, O.; Meier, M.; Korber, N., *Angew. Chem. Int. Ed.* 2009, *48* (46), 8770.

89. Geitner, F. S.; Fässler, T. F., *Chem. Commun.* 2017, *53* (96), 12974.

90. Joseph, S.; Suchentrunk, C.; Kraus, F.; Korber, N., *Eur. J. Inorg. Chem.* 2009, *2009* (31), 4641.

91. Benda, C. B.; Henneberger, T.; Klein, W.; Fässler, T. F., *Z. Anorg. Allg. Chem.* 2017, *643* (2), 146.

92. Lorenz, C.; Gärtner, S.; Korber, N., *Z. Anorg. Allg. Chem.* 2017, *643* (2), 141.

93. Henneberger, T.; Klein, W.; Fässler, T. F., *Z. Anorg. Allg. Chem.* 2018, *644* (17), 1018.

94. Scharfe, S.; Fässler, T. F., *Eur. J. Inorg. Chem.* 2010, *2010* (8), 1207.

95. Bentlohner, M. M.; Jantke, L.-A.; Henneberger, T.; Fischer, C.; Mayer, K.; Klein, W.; Fässler, T. F., *Chem. Eur. J.* 2016, *22* (39), 13946.

96. Wang, L.; Wang, Y.; Li, Z.; Ruan, H.; Xu, L., *Dalton Trans.* 2017, *46* (21), 6839.

97. Spiekermann, A.; Hoffmann, S. D.; Fässler, T. F.; Krossing, I.; Preiss, U., *Angew. Chem. Int. Ed.* 2007, *46* (28), 5310.

98. Hauptmann, R.; Fässler, T. F., *Z. Anorg. Allg. Chem.* 2003, *629* (12-13), 2266.

99. Xu, L.; Sevov, S. C., *J. Am. Chem. Soc.* 1999, *121* (39), 9245.

100. Nienhaus, A.; Hoffmann, S. D.; Fässler, T. F., *Z. Anorg. Allg. Chem.* 2006, *632* (10-11), 1752.

101. Scharfe, S.; Fässler, T. F., *Z. Anorg. Allg. Chem.* 2011, *637* (7-8), 901.

102. Ugrinov, A.; Sevov, S. C., *J. Am. Chem. Soc.* 2002, *124* (37), 10990.

103. Yong, L.; Hoffmann, S. D.; Fässler, T. F., *Z. Anorg. Allg. Chem.* 2005, *631* (6-7), 1149.

104. Ugrinov, A.; Sevov, S. C., *Inorg. Chem.* 2003, *42* (19), 5789.

105. Yong, L.; Hoffmann, S. D.; Fässler, T. F., *Z. Anorg. Allg. Chem.* 2004, *630* (12), 1977.

106. Denning, M. S.; Goicoechea, J. M., *Dalton Trans.* 2008, (43), 5882.

107. Mayer, K.; Jantke, L.-A.; Schulz, S.; Fässler, T. F., *Angew. Chem. Int. Ed.* 2017, *56* (9), 2350.

108. Goicoechea, J. M.; Sevov, S. C., *J. Am. Chem. Soc.* 2006, *128* (12), 4155.

109. Sun, Z.-M.; Zhao, Y.-F.; Li, J.; Wang, L.-S., *J. Clust. Sci.* 2009, *20* (3), 601.

110. Goicoechea, J. M.; Sevov, S. C., *Angew. Chem. Int. Ed.* 2005, *44* (26), 4026.

111. Goicoechea, J. M.; Sevov, S. C., *J. Am. Chem. Soc.* 2005, *127* (21), 7676.

112. Trindade, T.; O'Brien, P.; Zhang, X.-m., *Chem. Mater.* 1997, *9* (2), 523.

113. Peng, X.; Wickham, J.; Alivisatos, A. P., *J. Am. Chem. Soc.* 1998, *120* (21), 5343.

114. Murray, C. B.; Norris, D. J.; Bawendi, M. G., *J. Am. Chem. Soc.* 1993, *115* (19), 8706.

115. Katari, J. E. B.; Colvin, V. L.; Alivisatos, A. P., *J. Chem. Phys.* 1994, *98* (15), 4109.

116. Douglas, T.; Theopold, K. H., *Inorg. Chem.* 1991, *30* (4), 594.

117. Guzelian, A. A.; Katari, J. E. B.; Kadavanich, A. V.; Banin, U.; Hamad, K.; Juban, E.; Alivisatos, A. P.; Wolters, R. H.; Arnold, C. C.; Heath, J. R., *J. Phys. Chem.* 1996, *100* (17), 7212.

118. Guzelian, A. A.; Banin, U.; Kadavanich, A. V.; Peng, X.; Alivisatos, A. P., *Appl. Phys. Lett.* 1996, *69* (10), 1432.

119. Micic, O. I.; Curtis, C. J.; Jones, K. M.; Sprague, J. R.; Nozik, A. J., *J. Phys. Chem.* 1994, *98* (19), 4966.

120. Micic, O. I.; Nozik, A. J., *J. Lumin.* 1996, *70* (1), 95.

121. Micic, O. I.; Sprague, J. R.; Curtis, C. J.; Jones, K. M.; Machol, J. L.; Nozik, A. J.; Giessen, H.; Fluegel, B.; Mohs, G.; Peyghambarian, N., *J. Phys. Chem.* 1995, *99* (19), 7754.

122. Vossmeyer, T.; Katsikas, L.; Giersig, M.; Popovic, I. G.; Diesner, K.; Chemseddine, A.; Eychmueller, A.; Weller, H., *J. Phys. Chem.* 1994, *98* (31), 7665.

123. Peng, X., *Adv. Mater.* 2003, *15* (5), 459.

124. Peng, X.; Manna, L.; Yang, W.; Wickham, J.; Scher, E.; Kadavanich, A.; Alivisatos, A. P., *Nature* 2000, *404* (6773), 59.

125. Chen, C.-C.; Herhold, A. B.; Johnson, C. S.; Alivisatos, A. P., *Science* 1997, *276* (5311), 398.

126. Alivisatos, A. P., *Science* 1996, *271* (5251), 933.

127. Nirmal, M.; Brus, L., *Acc. Chem. Res.* 1999, *32* (5), 407.

128. Brus, L., *Appl. Phys. A* 1991, *53* (6), 465.

129. Derfus, A. M.; Chan, W. C. W.; Bhatia, S. N., *Nano Lett.* 2004, *4* (1), 11.

130. Ding, Z.; Quinn, B. M.; Haram, S. K.; Pell, L. E.; Korgel, B. A.; Bard, A. J., *Science* 2002, *296* (5571), 1293.

131. Li, Z. F.; Ruckenstein, E., *Nano Lett.* 2004, *4* (8), 1463.

132. Wang, L.; Reipa, V.; Blasic, J., *Bioconjugate Chem.* 2004, *15* (2), 409.

133. Buriak Jillian, M., *Phil. Trans. R. Soc. A* 2006, *364* (1838), 217.

134. Cullis, A. G.; Canham, L. T.; Calcott, P. D. J., *J. Appl. Phys.* 1997, *82* (3), 909.

135. Zou, J.; Sanelle, P.; Pettigrew, K. A.; Kauzlarich, S. M., *J. Clust. Sci.* 2006, *17* (4), 565.

136. Veinot, J. G. C., *Chem. Commun.* 2006, (40), 4160.

137. Heath, J. R., *Science* 1992, *258* (5085), 1131.

138. Arul Dhas, N.; Raj, C. P.; Gedanken, A., *Chem. Mater.* 1998, *10* (11), 3278.

139. Bley, R. A.; Kauzlarich, S. M., *J. Am. Chem. Soc.* 1996, *118* (49), 12461.

140. Mayeri, D.; Phillips, B. L.; Augustine, M. P.; Kauzlarich, S. M., *Chem. Mater.* 2001, *13* (3), 765.

141. Yang, C.-S.; Bley, R. A.; Kauzlarich, S. M.; Lee, H. W. H.; Delgado, G. R., *J. Am. Chem. Soc.* 1999, *121* (22), 5191.

142. Nolan, B. M.; Henneberger, T.; Waibel, M.; Fässler, T. F.; Kauzlarich, S. M., *Inorg. Chem.* 2015, *54* (1), 396.

143. Liu, Q.; Kauzlarich, S. M., *Mater. Sci. Eng. B* 2002, *96* (2), 72.

144. Pettigrew, K. A.; Liu, Q.; Power, P. P.; Kauzlarich, S. M., *Chem. Mater.* 2003, *15* (21), 4005.

145. Lee, S.; Cho, W. J.; Han, I. K.; Choi, W. J.; Lee, J. I., *Phys. Stat. Sol. (b)* 2004, *241* (12), 2767.

146. Lee, S.; Cho, W. J.; Chin, C. S.; Han, I. K.; Choi, W. J.; Park, Y. J.; Song, J. D.; Lee, J. I., *Jpn. J. Appl. Phys.* 2004, *43* (No. 6B), L784.

147. Buriak, J. M., *Chem. Rev.* 2002, *102* (5), 1271.

148. Zhang, X.; Brynda, M.; Britt, R. D.; Carroll, E. C.; Larsen, D. S.; Louie, A. Y.; Kauzlarich, S. M., *J. Am. Chem. Soc.* 2007, *129* (35), 10668.

149. West, R.; Fink, M. J.; Michl, J., *Science* 1981, *214* (4527), 1343.

150. Roark, D. N.; Peddle, G. J. D., *J. Am. Chem. Soc.* 1972, *94* (16), 5837.

151. Masamune, S.; Hanzawa, Y.; Williams, D. J., *J. Am. Chem. Soc.* 1982, *104* (22), 6136.

152. Tsumuraya, T.; Batcheller, S. A.; Masamune, S., *Angew. Chem. Int. Ed.* 1991, *30* (8), 902.

153. Brook, A. G.; Abdesaken, F.; Gutekunst, B.; Gutekunst, G.; Kallury, R. K., *Chem. Commun.* 1981, (4), 191.

154. Brook, A. G.; Nyburg, S. C.; Abdesaken, F.; Gutekunst, B.; Gutekunst, G.; Krishna, R.; Kallury, M. R.; Poon, Y. C.; Chang, Y. M.; Winnie, W. N., *J. Am. Chem. Soc.* 1982, *104* (21), 5667.

155. Meyer, H.; Baum, G.; Massa, W.; Berndt, A., *Angew. Chem. Int. Ed.* 1987, *26* (8), 798.

156. Sekiguchi, A.; Kinjo, R.; Ichinohe, M., *Science* 2004, *305* (5691), 1755.

157. Denk, M.; Lennon, R.; Hayashi, R.; West, R.; Belyakov, A. V.; Verne, H. P.; Haaland, A.; Wagner, M.; Metzler, N., *J. Am. Chem. Soc.* 1994, *116* (6), 2691.

158. Ossig, G.; Meller, A.; Brönneke, C.; Müller, O.; Schäfer, M.; Herbst-Irmer, R., *Organometallics* 1997, *16* (10), 2116.

159. Abersfelder, K.; White, A. J. P.; Rzepa, H. S.; Scheschkewitz, D., *Science* 2010, *327* (5965), 564.

160. Mondal, K. C.; Roy, S.; Dittrich, B.; Andrada, D. M.; Frenking, G.; Roesky, H. W., *Angew. Chem. Int. Ed.* 2016, *55* (9), 3158.

161. Wiberg, N.; Finger, C. M. M.; Polborn, K., *Angew. Chem. Int. Ed.* 1993, *32* (7), 1054.

162. Wiberg, N.; Hochmuth, W.; Nöth, H.; Appel, A.; Schmidt-Amelunxen, M., *Angew. Chem. Int. Ed.* 1996, *35* (12), 1333.

163. Ichinohe, M.; Toyoshima, M.; Kinjo, R.; Sekiguchi, A., *J. Am. Chem. Soc.* 2003, *125* (44), 13328.

164. Scheschkewitz, D., *Angew. Chem. Int. Ed.* 2005, *44* (19), 2954.

165. Abersfelder, K.; White, A. J. P.; Berger, R. J. F.; Rzepa, H. S.; Scheschkewitz, D., *Angew. Chem. Int. Ed.* 2011, *50* (34), 7936.

166. Nied, D.; Oña-Burgos, P.; Klopper, W.; Breher, F., *Organometallics* 2011, *30* (6), 1419.

167. Willmes, P.; Leszczyńska, K.; Heider, Y.; Abersfelder, K.; Zimmer, M.; Huch, V.; Scheschkewitz, D., *Angew. Chem. Int. Ed.* 2016, *55* (8), 2907.

168. Leszczyńska, K. I.; Huch, V.; Präsang, C.; Schwabedissen, J.; Berger, R. J. F.; Scheschkewitz, D., *Angew. Chem. Int. Ed.* 2019, *58* (15), 5124.

169. Klapötke, T. M.; Vasisht, S. K.; Mayer, P., *Eur. J. Inorg. Chem.* 2010, *2010* (21), 3256.

170. Ito, Y.; Lee, V. Y.; Gornitzka, H.; Goedecke, C.; Frenking, G.; Sekiguchi, A., *J. Am. Chem. Soc.* 2013, *135* (18), 6770.

171. Abersfelder, K.; Russell, A.; Rzepa, H. S.; White, A. J. P.; Haycock, P. R.; Scheschkewitz, D., *J. Am. Chem. Soc.* 2012, *134* (38), 16008.

172. Kysliak, O.; Schrenk, C.; Schnepf, A., *Angew. Chem. Int. Ed.* 2016, *55* (9), 3216.

173. Heider, Y.; Scheschkewitz, D., *Dalton Trans.* 2018, *47* (21), 7104.

174. Ugrinov, A.; Sevov, S. C., *Chem. Eur. J.* 2004, *10* (15), 3727.

175. Ugrinov, A.; Sevov, S. C., *J. Am. Chem. Soc.* 2002, *124* (11), 2442.

176. Ugrinov, A.; Sevov, S. C., *J. Am. Chem. Soc.* 2003, *125* (46), 14059.

177. Li, F.; Sevov, S. C., *Inorg. Chem.* 2012, *51* (4), 2706.

178. Geitner, F. S.; Klein, W.; Fässler, T. F., *Angew. Chem. Int. Ed.* 2018, *57* (44), 14509.

179. Perla, L. G.; Muñoz-Castro, A.; Sevov, S. C., *J. Am. Chem. Soc.* 2017, *139* (42), 15176.

180. Perla, L. G.; Sevov, S. C., *J. Am. Chem. Soc.* 2016, *138* (31), 9795.

181. Hull, M. W.; Ugrinov, A.; Petrov, I.; Sevov, S. C., *Inorg. Chem.* 2007, *46* (7), 2704.

182. Hull, M. W.; Sevov, S. C., *Inorg. Chem.* 2007, *46* (26), 10953.

183. Hull, M. W.; Sevov, S. C., *J. Am. Chem. Soc.* 2009, *131* (25), 9026.

184. Benda, C. B.; Wang, J.-Q.; Wahl, B.; Fässler, T. F., *Eur. J. Inorg. Chem.* 2011, *2011* (27), 4262.

185. Bentlohner, M. M.; Klein, W.; Fard, Z. H.; Jantke, L.-A.; Fässler, T. F., *Angew. Chem. Int. Ed.* 2015, *54* (12), 3748.

186. Benda, C. B.; He, H.; Klein, W.; Somer, M.; Fässler, T. F., *Z. Anorg. Allg. Chem.* 2015, *641* (6), 1080.

187. Hull, M. W.; Sevov, S. C., *Angew. Chem. Int. Ed.* 2007, *46* (35), 6695.

188. Frischhut, S.; Bentlohner, M. M.; Klein, W.; Fässler, T. F., *Inorg. Chem.* 2017, *56* (17), 10691.

189. Hull, M. W.; Sevov, S. C., *J. Organomet. Chem.* 2012, *721-722*, 85.

190. Hull, M. W.; Sevov, S. C., *Chem. Commun.* 2012, *48* (62), 7720.

191. Schnepf, A., *Angew. Chem. Int. Ed.* 2003, *42* (23), 2624.

192. Kysliak, O.; Schnepf, A., *Dalton Trans.* 2016, *45* (6), 2404.

193. Kysliak, O.; Schrenk, C.; Schnepf, A., *Inorg. Chem.* 2017, *56* (16), 9693.

194. Henke, F.; Schenk, C.; Schnepf, A., *Dalton Trans.* 2009, (42), 9141.

195. Kysliak, O.; Schrenk, C.; Schnepf, A., *Chem. Eur. J.* 2016, *22* (52), 18787.

196. Schenk, C.; Schnepf, A., *Angew. Chem. Int. Ed.* 2007, *46* (28), 5314.

197. Schenk, C.; Henke, F.; Santiso-Quiñones, G.; Krossing, I.; Schnepf, A., *Dalton Trans.* 2008, (33), 4436.

198. Li, F.; Sevov, S. C., *Inorg. Chem.* 2015, *54* (16), 8121.

199. Kysliak, O.; Nguyen, D. D.; Clayborne, A. Z.; Schnepf, A., *Inorg. Chem.* 2018, *57* (20), 12603.

200. Geitner, F. S.; Fässler, T. F., *Eur. J. Inorg. Chem.* 2016, *2016* (17), 2688.

201. Geitner, F. S.; Dums, J. V.; Fässler, T. F., *J. Am. Chem. Soc.* 2017, *139* (34), 11933.

202. Li, F.; Sevov, S. C., *J. Am. Chem. Soc.* 2014, *136* (34), 12056.

203. Li, F.; Muñoz-Castro, A.; Sevov, S. C., *Angew. Chem. Int. Ed.* 2012, *51* (34), 8581.

204. Frischhut, S.; Fässler, T. F., *Dalton Trans.* 2018, *47* (10), 3223.

205. Li, F.; Muñoz-Castro, A.; Sevov, S. C., *Angew. Chem. Int. Ed.* 2016, *55* (30), 8630.

206. Frischhut, S.; Kaiser, F.; Klein, W.; Drees, M.; Kühn, F. E.; Fässler, T. F., *Organometallics* 2018, *37* (24), 4560.

207. Schenk, C.; Schnepf, A., *Chem. Commun.* 2009, (22), 3208.

208. Kysliak, O.; Schrenk, C.; Schnepf, A., *Inorg. Chem.* 2015, *54* (14), 7083.

209. Kysliak, O.; Kunz, T.; Schnepf, A., *Eur. J. Inorg. Chem.* 2017, *2017* (4), 805.

210. Kysliak, O.; Schnepf, A., *Z. Anorg. Allg. Chem.* 2018, *645* (3), 335.

211. Hochberg, M.; Baehr-Jones, T., *Nature Photonics* 2010, *4*, 492.

212. Rojas, J. P.; Torres Sevilla, G. A.; Ghoneim, M. T.; Inayat, S. B.; Ahmed, S. M.; Hussain, A. M.; Hussain, M. M., *ACS Nano* 2014, *8* (2), 1468.

213. Eun-Chel, C.; Sangwook, P.; Xiaojing, H.; Dengyuan, S.; Gavin, C.; Sang-Cheol, P.; Martin, A. G., *Nanotechnology* 2008, *19* (24), 245201.

214. Rath, J. K.; Stannowski, B.; van Veenendaal, P. A. T. T.; van Veen, M. K.; Schropp, R. E. I., *Thin Solid Films* 2001, *395* (1), 320.

215. Ashuri, M.; He, Q.; Shaw, L. L., *Nanoscale* 2016, *8* (1), 74.

216. Kanatzidis, M. G., *Adv. Mater.* 2007, *19* (9), 1165.

217. Canham, L. T., *Appl. Phys. Lett.* 1990, *57* (10), 1046.

218. Snedaker, M. L.; Zhang, Y.; Birkel, C. S.; Wang, H.; Day, T.; Shi, Y.; Ji, X.; Kraemer, S.; Mills, C. E.; Moosazadeh, A.; Moskovits, M.; Snyder, G. J.; Stucky, G. D., *Chem. Mater.* 2013, *25* (24), 4867.

219. Frey, J.; Schottland, E.; Rappoport, Z.; Bravo-Zhivotovskii, D.; Nakash, M.; Botoshansky, M.; Kaftory, M.; Apeloig, Y., *J. Chem. Soc., Perkin Trans. 2* 1994, (12), 2555.

220. Hwu, J. R.; Wang, N., *Chem. Rev.* 1989, *89* (7), 1599.

221. Hwu, J. R.; King, K. Y.; Wu, I. F.; Hakimelahi, G. H., *Tetrahedron Lett.* 1998, *39* (22), 3721.

222. Reichardt, C., *Solvents and Solvent Effects in Organic Chemistry (3rd Updated and Enlarged Edition)*. Wiley: 2003.

223. Mayer, K.; Schiegerl, L. J.; Kratky, T.; Günther, S.; Fässler, T. F., *Chem. Commun.* 2017, *53* (86), 11798.

224. Melaimi, M.; Soleilhavoup, M.; Bertrand, G., *Angew. Chem. Int. Ed.* 2010, *49* (47), 8810.

225. Weber, S. G.; Loos, C.; Rominger, F.; Straub, B. F., *Arkivoc* 2011, *2012* (3), 226.

226. Berthon-Gelloz, G.; Siegler, M. A.; Spek, A. L.; Tinant, B.; Reek, J. N. H.; Markó, I. E., *Dalton Trans.* 2010, *39* (6), 1444.

227. Lavallo, V.; Canac, Y.; Präsang, C.; Donnadieu, B.; Bertrand, G., *Angew. Chem. Int. Ed.* 2005, *44* (35), 5705.

228. Lavallo, V.; Canac, Y.; Donnadieu, B.; Schoeller, W. W.; Bertrand, G., *Angew. Chem. Int. Ed.* 2006, *45* (21), 3488.

229. Guisado-Barrios, G.; Bouffard, J.; Donnadieu, B.; Bertrand, G., *Angew. Chem. Int. Ed.* 2010, *49* (28), 4759.

230. Guisado-Barrios, G.; Bouffard, J.; Donnadieu, B.; Bertrand, G., *Organometallics* 2011, *30* (21), 6017.

231. Geitner, F. S.; Giebel, M. A.; Pöthig, A.; Fässler, T. F., *Molecules* 2017, *22* (7), 1204.

232. Bidal, Y. D.; Lesieur, M.; Melaimi, M.; Nahra, F.; Cordes, D. B.; Athukorala Arachchige, K. S.; Slawin, A. M. Z.; Bertrand, G.; Cazin, C. S. J., *Adv. Synth. Catal.* 2015, *357* (14-15), 3155.

233. Marciniec, B., *Comprehensive Handbook on Hydrosilylation (1st Edition)*. Pergamon: 1992

234. Marciniec, B., *Hydrosilylation: A Comprehensive Review on Recent Advances*. Springer: 2008.

235. Adam, W.; Mello, R.; Curci, R., *Angew. Chem. Int. Ed.* 1990, *29* (8), 890.

236. Landais, Y.; Planchenault, D., *Tetrahedron Lett.* 1994, *35* (26), 4565.

237. Liu, Z.; Huo, J.; Fu, T.; Tan, H.; Ye, F.; Hossain, M. L.; Wang, J., *Chem. Commun.* 2018, *54* (81), 11419.

238. Venema, L., *Nature* 2011, *479*, 309.

239. Neumeier, M.; Fendt, F.; Gärtner, S.; Koch, C.; Gärtner, T.; Korber, N.; Gschwind, R. M., *Angew. Chem. Int. Ed.* 2013, *52* (16), 4483.

240. Jantke, L.-A.; Fässler, T., *Inorganics* 2018, *6* (1), 31.

241. Goebel, T.; Ormeci, A.; Pecher, O.; Haarmann, F., *Z. Anorg. Allg. Chem.* 2012, *638* (10), 1437.

242. Beall, H.; Bushweller, C. H., *Chem. Rev.* 1973, *73* (5), 465.

243. Lorenz, C.; Hastreiter, F.; Hioe, J.; Nanjundappa, L.; Gärtner, S.; Korber, N.; Gschwind, R. M., *Angew. Chem. Int. Ed.* 2018, *57* (39), 12956.

244. Duffy, I. R.; Leigh, W. J., *Organometallics* 2019, *38* (4), 933.

245. Boudjouk, P.; Samaraweera, U.; Sooriyakumaran, R.; Chrusciel, J.; Anderson, K. R., *Angew. Chem. Int. Ed.* 1988, *27* (10), 1355.

246. Boudjouk, P.; Black, E.; Kumarathasan, R., *Organometallics* 1991, *10* (7), 2095.

247. Schiegerl, L. J.; Karttunen, A. J.; Klein, W.; Fässler, T. F., *Chem. Eur. J.* 2018, *24* (72), 19171.

248. Driver, T. G.; Woerpel, K. A., *J. Am. Chem. Soc.* 2003, *125* (35), 10659.

249. Abersfelder, K.; Nguyen, T.-l.; Scheschkewitz, D., *Z. Anorg. Allg. Chem.* 2009, *635* (13-14), 2093.

250. Ugrinov, A.; Sevov, S. C., *Chem. Eur. J.* 2004, *10* (15), 3727.

251. Kocak, F. S.; Downing, D. O.; Zavalij, P.; Lam, Y.-F.; Vedernikov, A. N.; Eichhorn, B., *J. Am. Chem. Soc.* 2012, *134* (23), 9733.

252. Akasaka, N.; Ishida, S.; Iwamoto, T., *Inorganics* 2018, *6* (4), 107.

253. Fischer, G.; Huch, V.; Mayer, P.; Vasisht, S. K.; Veith, M.; Wiberg, N., *Angew. Chem. Int. Ed.* 2005, *44* (48), 7884.

254. David, S., *Chem. Lett.* 2011, *40* (1), 2.

255. Ohmori, Y.; Ichinohe, M.; Sekiguchi, A.; Cowley, M. J.; Huch, V.; Scheschkewitz, D., *Organometallics* 2013, *32* (6), 1591.

256. Iwamoto, T.; Akasaka, N.; Ishida, S., *Nat. Commun.* 2014, *5*, 5353.

257. Takeuchi, K.; Ichinohe, M.; Sekiguchi, A., *J. Am. Chem. Soc.* 2008, *130* (50), 16848.

258. MestReNova v9.1.0, *Mestrelab Research S.L.* 2014.

259. WinXPOW v3.0.2.1, *STOE & Cie GmbH* 2011.

260. Hübschle, C. B.; Sheldrick, G. M.; Dittrich, B., *J. Appl. Crystallogr.* 2011, *44* (6), 1281.

261. Lubben, J.; Volkmann, C.; Grabowsky, S.; Edwards, A.; Morgenroth, W.; Fabbiani, F. P. A.; Sheldrick, G. M.; Dittrich, B., *Acta Cryst.* 2014, *A70* (4), 309.

262. Spek, A. L., *Acta Cryst.* 2009, *D65* (2), 148.

263. Crystal Impact GbR, *Diamond Version 3.2k*: 1997-2014.

264. TURBOMOLE GmbH, *TURBOMOLE V7.3 2018, a development of University of Karlsruhe and Forschungszentrum Karlsruhe GmbH*, 1989-2007, *TURBOMOLE GmbH*, since 2007.

265. Ahlrichs, R.; Bär, M.; Häser, M.; Horn, H.; Kölmel, C., *Chem. Phys. Lett.* 1989, *162* (3), 165.

266. Perdew, J. P.; Burke, K.; Ernzerhof, M., *Phys. Rev. Lett.* 1996, *77* (18), 3865.

267. Adamo, C.; Barone, V. J., *J. Chem. Phys.* 1999, *110* (13), 6158.

268. Weigend, F.; Ahlrichs, R., *Phys. Chem. Chem. Phys.* 2005, *7* (18), 3297.

269. Dovesi, R.; Erba, A.; Orlando, R.; Zicovich-Wilson, C. M.; Civalleri, B.; Maschio, L.; Rérat, M.; Casassa, S.; Baima, J.; Salustro, S.; Kirtman, B., *Wiley Interdiscip. Rev. Comput. Mol. Sci.* 2018, *8* (4), 1360.

270. CFOUR, Coupled-Cluster techniques for Computational Chemistry, a quantum-chemical program package by Stanton, J. F.; Gauss, J.; Cheng, L.; Harding, M. E.; Matthews, D. A.; Szalay, P. G. with contributions from Auer, A. A.; Bartlett, R. J.; Benedikt, U.; Berger, C.; Bernholdt, D. E.; Bomble, Y. J.; Christiansen, O.; Engel, F.; Faber, R.; Heckert, M.; Heun, O.; Hilgenberg, M.; Huber, C.; Jagau, T.-C.; Jonsson, D.; Jusélius, J.; Kirsch, T.; Klein, K.; Lauderdale, W. J.; Lipparini, F.; Metzroth, T.; Mück, L. A.; O'Neill, D. P.; Price, D. R.; Prochnow, E.; Puzzarini, C.; Ruud, K.; Schiffmann, F.; Schwalbach, W.; Simmons, C.; Stopkowicz, S.; Tajti, A.; Vázquez, J.; Wang, F.; Watts, J. D. and the integral packages MOLECULE (Almlöf, J.; Taylor, P. R.), PROPS (Taylor, P. R.), ABACUS (Helgaker, T.; Jensen, H. J. Aa.; Jørgensen, P.; Olsen, J.), and EC Proutines by Mitin, A. V.; van Wüllen, C. For the current version, see www.cfour.de.

271. Harding, M. E.; Metzroth, T.; Gauss, J.; Auer, A. A., *J. Chem. Theory Comput.* 2008, *4* (1), 64.

272. Clark Stewart, J.; Segall Matthew, D.; Pickard Chris, J.; Hasnip Phil, J.; Probert Matt, I. J.; Refson, K.; Payne Mike, C., *Z. Kristallogr. – Cryst. Mater.* 2005, *220* (5/6) , 567.

273. Pickard, C. J.; Mauri, F., *Phys. Rev. B* 2001, *63* (24), 245101.

274. Yates, J. R.; Pickard, C. J.; Mauri, F., *Phys. Rev. B* 2007, *76* (2), 024401.

275. Waibel, M., *Dissertation - Technischen Universität München* 2012.

6 PUBLICATIONS AND MANUSCRIPTS

This thesis is written publication based (see Declaration). This chapter provides the incorporated *Manuscripts* including the belonging *Supporting Informations*. Ambition and content of the works, as well as contributions of the authors are declared.

Full list of publications:

i) chapter 6.1: Schiegerl, L. J.; Geitner, F. S.; Fischer, C.; Klein, W.; Fässler, T. F., Functionalization of $[Ge_9]$ with Small Silanes:$[Ge_9(SiR_3)_3]^-$ (R = *i*Bu, *i*Pr, Et) and the Structures of $(CuNHC^{Dipp})[Ge_9\{Si(iBu)_3\}_3]$, (K-18c6)Au$[Ge_9\{Si(iBu)_3\}_3]_2$, and $(K\text{-}18c6)_2[Ge_9\{Si(iBu)_3\}_2]$. *Z. Anorg. Allg. Chem*. 2016, *642* (24), 1419-1426.

ii) chapter 6.2: Mayer, K.; Schiegerl, L. J.; Fässler, T. F., On the Reactivity of Silylated Ge_9 Clusters: Synthesis and Characterization of $[ZnCp^*(Ge_9\{Si(SiMe_3)_3\}_3)]$, $[CuPiPr_3(Ge_9\{Si(SiMe_3)_3\}_3)]$, and $[(CuPiPr_3)_4\{Ge_9(SiPh_3)_2\}_2]$. *Chem. Eur. J.* 2016, *22* (52), 18794-18800.

iii) chapter 6.3: Schiegerl, L. J.; Klein, W.; Fässler, T. F., Utilization of Si_9 Clusters from $K_{12}Si_{17}$ Precursor Material for Subsequent Reactions. *Manuscript for Publication.* 2019.

iv) chapter 6.4: Schiegerl, L. J.; Melaimi, M.; Tolentino, D. R.; Klein, W.; Bertrand, G.; Fässler, T. F., Silylated Ge_9 Clusters as New Ligands for Cyclic (Alkyl)amino and Mesoionic Carbene Copper Complexes. *Inorg. Chem*. 2019, *58* (5), 3256-3264.

v) chapter 6.5: Schiegerl, L. J.; Karttunen, A. J.; Tillmann, J.; Geier, S.; Raudaschl-Sieber, G.; Waibel, M.; Fässler, T. F., Charged Si_9 Clusters in Neat Solids and the Detection of $[H_2Si_9]^{2-}$ in Solution: A Combined NMR, Raman, Mass Spectrometric, and Quantum Chemical Investigation. *Angew. Chem. Int. Ed*. 2018, *57* (39), 12950-12955.

vi) chapter 6.6: Schiegerl, L. J.; Karttunen, A. J.; Klein, W.; Fässler, T. F., Anionic Siliconoids from Zintl Phases: $R_3Si_9^-$ with Six and $R_2Si_9^{2-}$ with Seven Unsubstituted Exposed Silicon Cluster Atoms $(R=Si(tBu)_2H)$. *Chem. Eur. J.* 2018, *24* (72), 19171-19174.

vii) chapter 6.7: Schiegerl, L. J.; Karttunen, A. J.; Klein, W.; Fässler, T. F., Silicon slusters with six and seven unsubstituted vertices *via* a two-step reaction from elemental silicon. *Chem. Sci.* 2019 (DOI: 10.1039/C9SC03324F).

6.1 Functionalization of [Ge_9] with Small Silanes:[$Ge_9(SiR_3)_3]^-$ (R = *i*Bu, *i*Pr, Et) and the Structures of (CuNHC^{Dipp})[Ge_9{Si(*i*Bu)$_3$}$_3$], (K-18c6)Au[Ge_9{Si(*i*Bu)$_3$}$_3$]$_2$, and (K-18c6)$_2$[Ge_9{Si(*i*Bu)$_3$}$_2$]

Lorenz J. Schiegerl,[‡] Felix S. Geitner,[‡] Christina Fischer, Wilhem Klein, and Thomas F. Fässler[*]

published in

Z. Anorg. Allg. Chem. 2016, *642* (24), 1419-1426.

[‡] authors contributed equally to this work

Access online *via*: https://onlinelibrary.wiley.com/doi/full/10.1002/zaac.201600295

Content and contributions:

Ambition of this work was the attachment of versatile silyl groups at Ge_9 cluster cores. The manuscript was authored by me within the course of this PhD Thesis and reviewed by *Dr. Wilhelm Klein*, *Dr. Felix Geitner* and *Prof. Thomas Fässler* before its submission. Submission of the manuscript was done by *Dr. Wilhelm Klein*. Recording, evaluation and submission of the single crystal diffraction data were assisted by *Dr. Wilhelm Klein*. The work was published within the framework of the WACKER INSTITUTE FOR SILICON CHEMISTRY (TECHNICAL UNIVERSITY OF MUNICH). An ESI-MS spectrum to [(Si^{i}Bu$_3$)$_3$Ge$_9$]$^-$ was previously reported in my Master's Thesis under supervision of *Dr. Kerstin Mayer* (principal instructor: *Prof. Thomas Fässler*). The EDX spectra were measured by Maria Müller (TECHNICAL UNIVERSITY OF MUNICH). Elemental analyses were carried out in the microanalytical laboratory at the CATALYTIC RESEARCH CENTER of the TECHNICAL UNIVERSITY OF MUNICH.

The tri-silylated cluster species [(SiR$_3$)$_3$Ge$_9$]$^-$ (R = ^{i}Bu, ^{i}Pr, Et) were obtained and characterized by ESI-MS in all cases and by NMR in the case of R = ^{i}Bu. Synthesis were carried out by *Christina Fischer* in the case of R = ^{i}Pr, Et, and by me in the case of R = ^{i}Bu. [(Si^{i}Bu$_3$)$_3$Ge$_9$]$^-$ was crystallized as the compound [K-18c6]$_2$[(Si^{i}Bu$_3$)$_2$Ge$_9$]. The compound was characterized (SC-XRD, ESI-MS, NMR, EDX) by me. Metal complexations of [(Si^{i}Bu$_3$)$_3$Ge$_9$]$^-$ yielded cluster metal compounds. Reaction with Cu(NHC^{Dipp})Cl led to the formation of [Cu(NHC^{Dipp}][(Si^{i}Bu$_3$)$_3$Ge$_9$]. Synthesis, characterization (NMR, elemental analysis, SC-XRD) and discussion of the results of this compound were done by *Dr. Felix Geitner*. The acquisition of the ESI-MS spectrum was assisted by *M. Sc. Christina Fischer*. Reaction of [(Si^{i}Bu$_3$)$_3$Ge$_9$]$^-$ with Au(PPh$_3$)Cl yielded the cluster metal complex [K-18c6][Au{(Si^{i}Bu$_3$)$_3$Ge$_9$}$_2$]. The compound was synthesized and characterized (SC-XRD, ESI-MS, EDX analysis) by me.

Journal of Inorganic and General Chemistry
ZAAC
Zeitschrift für anorganische und allgemeine Chemie
www.zaac.wiley-vch.de
ARTICLE

DOI: 10.1002/zaac.201600295

Functionalization of $[Ge_9]$ with Small Silanes: $[Ge_9(SiR_3)_3]^-$ (R = *i*Bu, *i*Pr, Et) and the Structures of $(CuNHC^{Dipp})[Ge_9\{Si(iBu)_3\}_3]$, $(K\text{-}18c6)Au[Ge_9\{Si(iBu)_3\}_3]_2$, and $(K\text{-}18c6)_2[Ge_9\{Si(iBu)_3\}_2]$

Lorenz J. Schiegerl,[a][‡] Felix S. Geitner,[b][‡] Christina Fischer,[a] Wilhelm Klein,[a] and Thomas F. Fässler*[a]

Keywords: Germanium; Silanes; Functionalization; Coinage Metals; *Zintl* clusters

Abstract. Novel silylation reactions at $[Ge_9]$ *Zintl* clusters starting from the chlorosilanes SiR_3Cl (R = *i*Bu, *i*Pr, Et) and the *Zintl* phase K_4Ge_9 are reported. The formation of the tris-silylated anions $[Ge_9(SiR_3)_3]^-$ [R = *i*Bu (**1a**), *i*Pr (**1b**), Et (**1c**)] by heterogeneous reactions in acetonitrile was monitored by ESI-MS measurements. For R = *i*Bu ^1H, ^{13}C and ^{29}Si NMR experiments confirmed the exclusive formation of **1a**. Subsequent reactions of **1a** with $CuNHC^{Dipp}Cl$ and $Au(PPh_3)Cl$ result in formation of the neutral metal complex $(CuNHC^{Dipp})[Ge_9\{Si(iBu)_3\}_3]$·0.5 tol (**2**·0.5 tol) and the metal bridged dimeric unit $\{Au[Ge_9\{Si(iBu)_3\}_3]_2\}^-$ (**3a**), isolated as a $(K\text{-}18c6)^+$ salt in $(K\text{-}18c6)Au[Ge_9\{Si(iBu)_3\}_3]_2$·tol (**3**·tol), respectively. Finally, from a toluene/hexane solution of **1a** in presence of 18-crown-6, crystals of the compound $(K\text{-}18c6)_2[Ge_9\{Si(iBu)_3\}_2]$·tol (**4**·tol), containing the bis-silylated cluster anion $[Ge_9(Si(iBu)_3)_2]^{2-}$ (**4a**), were obtained. The compounds **2**·0.5 tol, **3**·tol and **4**·tol were characterized by single-crystal structure determination.

Introduction

Within the last decades the research field of soluble *Zintl* clusters has grown rapidly, yielding a broad range of novel compounds. Reacting *Zintl* clusters with organometallics and organic substances in solution, new compounds which are not accessible by pure solution or solid state chemistry, were obtained. In this context *Zintl* phases of the form A_4E_9 (A: alkali metal; E: tetrel element) containing nine-atomic clusters $[E_9]^{4-}$ (E: Ge – Pb) are often applied as soluble *Zintl* cluster precursors.[1] Reactions of *Zintl* clusters in highly polar, protic solvents such as ethylenediamine or liquid ammonia with transition metal compounds yielded numerous intermetalloid clusters with $[Sn_9Cr(CO)_3]^{4-}$[2] being the first one and $[Au_3Ge_{45}]^{9-}$[3] the largest one obtained by this route so far. Further, numerous $[Ge_9]$ clusters with one or two *exo*-bonded main-group fragments[4] as well as the phenyl-substituted $[Ph\text{-}Ge_9\text{-}SbPh_2]^{2-}$[4a] and alkyl-substituted $[t\text{Bu-}Ge_9\text{-}Ge_9\text{-}t\text{Bu}]^{4-}$[5] clusters were obtained.

Recently, functionalization of *Zintl* clusters with organic substituents[6] was put in the research focus by the explorations of $[Ge_9(CH{=}CH_2)_2]^{2-}$ and $[Ge_9\{Si(SiMe_3)_3\}_3]^-$. The bis-vinylated anion $[Ge_9(CH{=}CH_2)_2]^{2-}$ [7] is obtained by reacting K_4Ge_9 with bistrimethylsilylacetylene (btmsa) in ethylenediamine. In a similar reaction procedure the linkage of two $[Ge_9]$ clusters was achieved to obtain the *Zintl* triad $[RGe_9\text{-}CH{=}CH\text{-}CH{=}CH\text{-}Ge_9R]^{4-}$.[8] In contrast, $[Ge_9\{Si(SiMe_3)_3\}_3]^-$ was at first synthesized in small amounts starting from GeBr by the group of *Schnepf*,[9] a reasonable synthesis procedure allowing the large scale synthesis of $[Ge_9\{Si(SiMe_3)_3\}_3]^-$ by heterogeneous reaction of acetonitrile solutions of $Si(SiMe_3)_3Cl$ with solid K_4Ge_9 was reported subsequently by the group of *Sevov*.[10]

Because of its low charge and the steric shielding of the $[Ge_9]$ core by the bulky $[Si(SiMe_3)_3]$ groups, tris-silylated cluster anion $[Ge_9\{Si(SiMe_3)_3\}_3]^-$ and its compounds are comparably stable and reveal solubility in standard solvents such as acetonitrile, tetrahydrofuran or toluene. Recently, a broad range of subsequent reactions of $[Ge_9\{Si(SiMe_3)_3\}_3]^-$ with organic substances and organometallic complexes has been reported in literature, such as dimeric $M[Ge_9\{Si(SiMe_3)_3\}_3]_2$ compounds (M = Zn, Cd, Hg),[11] obtained by reactions with the respective MCl_2 salts, and the coinage metal bridged dimeric anions $\{M[Ge_9\{Si(SiMe_3)_3\}_3]_2\}^-$ (M = Cu, Ag, Au).[12] Furthermore, the neutral dimeric compound $Cu_2(PPh_3)[Ge_9\{Si(SiMe_3)_3\}_3]_2$ was obtained by reaction with $Cu(PPh_3)_3Br$ and conversion with $Pd(PPh_3)_4$ yielded the Pd^0 bridged dimeric anion $\{Pd[Ge_9\{Si(SiMe_3)_3\}_3]_2\}^{2-}$.[13] Lately, the first penta-functionalized deltahedral cluster

* Prof. Dr. T. F. Fässler
E-Mail: thomas.faessler@lrz.tum.de
[a] Department of Chemistry
Technische Universität München
Lichtenbergstraße 4
85747 Garching, Germany
[b] WACKER Institute for Silicon Chemistry and Department of Chemistry
Technische Universität München
Lichtenbergstraße 4
85748 Garching, Germany
[‡] authors contributed equally to this work.
Supporting information for this article is available on the WWW under http://dx.doi.org/10.1002/zaac.201600295 or from the author.

$[Ge_9\{Si(SiMe_3)_3\}_3]Pd(PPh_3)Et$, in which a Pd atom is incorporated into the $[Ge_9]$ cluster yielding a $[Ge_9Pd]$ cluster core, was reported.[14] Additionally, neutral *Zintl* cluster coinage metal NHC compounds (*M*–NHC)$[Ge_9\{Si(SiMe_3)_3\}_3]$[15] were obtained reacting $[Ge_9\{Si(SiMe_3)_3\}_3]^-$ and *M*NHC^{Dipp}Cl[16] (NHC: N-heterocyclic carbene; *M*: Cu, Ag, Au), being the first compounds combining *Zintl* cluster- and NHC chemistry. Furthermore, the introduction of a Cu-phosphine residue in $(CuPiPr_3)[Ge_9\{Si(SiMe_3)_3\}_3]$ and a Zn-Cp* moiety in $(ZnCp^*)[Ge_9\{Si(SiMe_3)_3\}_3]$ reveal the ability of $[Ge_9\{Si(SiMe_3)_3\}_3]^-$ to act as ligand in versatile metalorganic compounds.[17]

Further examinations focusing on the variation of the number of silyl groups at the $[Ge_9]$ cluster revealed that the bis-silylated species $[Ge_9\{Si(SiMe_3)_3\}_2]^{2-}$, characterized as $(K–2.2.2–crypt)_2[Ge_9\{Si(SiMe_3)_3\}_2]$, is easily accessible by addition of solid K_4Ge_9 to acetonitrile solutions of $[Ge_9\{Si(SiMe_3)_3\}_3]^-$.[18] Moreover, novel silyl groups with varying steric demand were introduced at $[Ge_9]$ clusters, yielding $[Ge_9\{Si(SiMe_3)_2(SiPh_3)\}_3]^-$ [19] and $[Ge_9(SiPh_3)_3]^-$ [17]. The reactivity of $[Ge_9\{Si(SiMe_3)_2(SiPh_3)\}_3]^-$ is quite similar to that of $[Ge_9\{Si(SiMe_3)_3\}_3]^-$ which can be derived from formation of the dimeric Hg compounds of both tris-silylated clusters.[12] In contrast, $[Ge_9(SiPh_3)_3]^-$ shows a significantly different behavior. Therefore, reaction with $Cu(PiPr_3)Cl$ does not yield a neutral compound bearing a Cu-phosphine moiety, as it was observed for $[Ge_9\{Si(SiMe_3)_3\}_3]^-$, but $(CuPiPr_3)_4[Ge_9(SiPh_3)_2]_2$ is formed, where two bis-silylated $[Ge_9(SiPh_3)_2]^{2-}$ cluster units are bridged by two $[CuPiPr_3]^+$ groups.[17] These observations of different reactivity of the tris-silylated clusters induced by different silyl groups with varying steric demand triggered us to investigate the introduction of further sterically less bulky organo-silanes at $[Ge_9]$ and the reactivity of the resulting clusters in subsequent reactions.

Results and Discussion

Reacting K_4Ge_9 with $Si(iBu)_3Cl$ (3 equiv.) in a heterogeneous reaction according to the *Zintl* route yields, after stirring at room temperature overnight and subsequent filtration, a red solution. ESI-MS examination of the obtained solution revealed the formation of the novel tris-silylated tetrel cluster anion $[Ge_9\{Si(iBu)_3\}_3]^-$ (**1a**) (*m*/*z* = 1253; Figure 1, a). After removal of the solvent in vacuo the residual brownish solid was analyzed by ^1H, ^{13}C and ^{29}Si NMR spectroscopy. In all NMR spectra (^1H, ^{13}C, ^{29}Si) the observed signals can be assigned to one single species (further NMR discussion in the Supporting Information). Evaluation of both, NMR and ESI-MS data, manifests that exclusively the tris-silylated species **1a** is formed. Thus, functionalization of $[Ge_9]^{4-}$ clusters with sterically less demanding $[Si(iBu)_3]^+$ groups than $[Si(SiMe_3)_3]^+$ yields stable, tris-silylated clusters.

Analogously, the reactivity of K_4Ge_9 towards the chlorosilanes SiR_3Cl (R = *i*Pr, Et) was examined. ESI-MS examinations of the resulting red solutions in acetonitrile indicate the formation of the respective tris-silylated anions **1b** (Figure 1, b; *m*/*z* = 1126) and **1c** (Figure 1, c; *m*/*z* = 999). These observations manifest that silylation of $[Ge_9]$ is possible with a broad range of alkylsilanes SiR_3Cl (R = *i*Bu, *i*Pr and Et) bearing less bulky organic groups, besides the recently reported silylation reaction with $SiPh_3Cl$.[17] Thus, the introduction of silyl groups of varying steric demand is possible and probably opens up a path for a plethora of novel compounds such as recently reported $(CuPiPr_3)_4[Ge_9(SiPh_3)_2]_2$, which was obtained by reaction of $[Ge_9(SiPh_3)_3]^-$ with $Cu(PiPr_3)Cl$ with substitution of silyl groups by cationic metalorganic Cu-phosphine fragments, revealing different reactivity of the clusters induced by variation of the silyl groups.

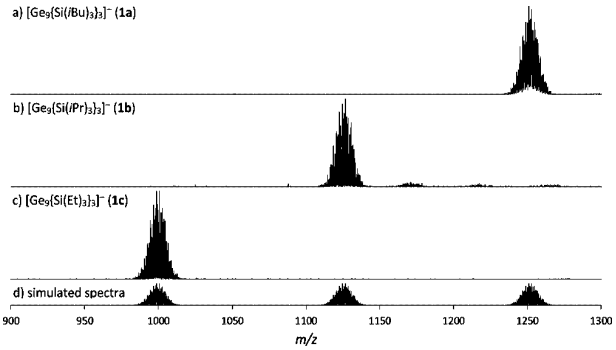

Figure 1. ESI-MS spectra of the tris-silylated species in acetonitrile. a) $[Ge_9\{Si(iBu)_3\}_3]^-$ (**1a**) (*m*/*z* = 1253); b) $[Ge_9\{Si(iPr)_3\}_3]^-$ (**1b**) (*m*/*z* = 1126); c) $[Ge_9\{Si(Et)_3\}_3]^-$ (**1c**) (*m*/*z* = 999); d) simulated spectra of the anions (an overview and a detailed view on the spectra are shown in the Supporting Information).

We examined the reactivity of **1a** towards the organometallic compound CuNHC^{Dipp}Cl, which, as recently reported by our group, forms stable neutral tetrel cluster copper NHC compounds of the form $(CuNHC^{Dipp})[Ge_9\{Si(SiMe_3)_3\}_3]$[15] upon reaction with $[Ge_9\{Si(SiMe_3)_3\}_3]^-$. Following a similar synthesis procedure, an acetonitrile solution of **1a** was added dropwise to a solution of CuNHC^{Dipp}Cl in acetonitrile yielding an orange-brownish precipitate. Subsequent isolation and purification by recrystallization from toluene at –40 °C yielded analytically pure red crystals in good yield, which were characterized by NMR spectroscopy (^1H, ^{13}C, ^{29}Si), ESI-MS, elemental analysis and single-crystal X-ray diffraction. The ^1H NMR spectrum reveals the ratio of the signals caused by the silyl substituents and the NHC^{Dipp} group to be 1:1, which was also confirmed by elemental analysis for the elements C, H and N (further NMR discussion in Supporting Information). The molecular structure of $(CuNHC^{Dipp})[Ge_9\{Si(iBu)_3\}_3]$ (**2**), which crystallizes with 0.5 toluene molecules per formula unit, is represented in Figure 2. In **2**, the $[Ge_9]$ cluster adapts the shape of a distorted tricapped trigonal prism with two elongated prism heights (C_{2v} symmetry) and the capping Ge atoms bearing the $[Si(iBu_3)_3]^+$ groups. As observed in other *M*-NHC complexes (*M* = Cu, Ag, Au), the Cu atom coordinates to a deltahedral face of the $[Ge_9]$ core. The Ge-Cu distances of 2.4911(6)–2.5594(6) Å are in the range of the known Cu-NHC complex $(CuNHC^{Dipp})[Ge_9\{Si(SiMe_3)_3\}_3]$ (average 2.53 Å).[15] The NHC ligand is staggered with respect to the three silyl ligands as expected from the steric demands of the

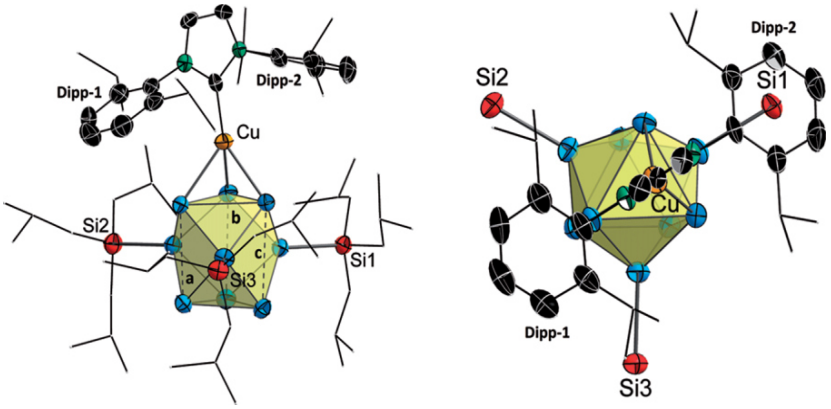

Figure 2. Molecular structure of monomeric compound (CuNHC^{Dipp})[Ge$_9${Si(*i*Bu)$_3$}$_3$)] (**2**) (left) and a detail view from the ligand side (right) on the arrangement of the groups at the [Ge$_9$] cluster. The lengths of the prismatic heights **a**, **b** and **c** are shown in Table 1. Atoms are shown as ellipsoids with 70% probability (Ge atoms blue; Si atoms red, Cu atoms orange, N atoms green and C atoms black or shown as wire/sticks for the *i*Bu (not shown on the right) and *i*Pr (NHC^{Dipp}) groups; H atoms are omitted for reasons of clarity).

ligands. A similar arrangement was found for the respective compound (CuNHC^{Dipp})[Ge$_9${Si(SiMe$_3$)$_3$}$_3$].

The distortion of the [Ge$_9$] cluster from D_{3h} towards C_{2v} symmetry is best described by the three heights of the underlying trigonal prism (Table 1). Whereas two of the heights are rather similar (3.4235(5) Å and 3.3918(5) Å given as *c* and *b* in Figure 2, respectively), the third height *a* is remarkably shorter (3.1947(5) Å), as has been found to be a frequent motif of distortion in [Ge$_9${Si(SiMe$_3$)$_3$}$_3$]$^-$ cluster anions.[20] Coordination of the [CuNHC^{Dipp}]$^+$ fragment at the tris-silylated [Ge$_9$] cluster occurs via one of the trigonal faces of the cluster with formation of a η^3-coordination. Thereby, the longest Ge–Cu distance (2.5596(7) Å) is observed towards the Ge atom in the shortest prismatic height. The two remaining Ge–Cu bonds are clearly shorter with lengths of 2.4907(7) Å and 2.4930(7) Å and located at the side of the cluster where the Dipp-2 group overlaps with a silyl group (Figure 2). In contrast, the Dipp-1 group is positioned between the two remaining silyl groups in a sterically more favorable environment. The stronger repulsion is further supported by the tilt (C–Cu–Ge angle) of the NHC^{Dipp} group towards the side of Dipp-1 (with the shorter prismatic height *a*) with 131.20(1)°. This C–Cu–Ge angle is significantly smaller than at the side of Dipp-2 (with the longer prismatic heights *b* and *c*) (143.42(1)° and 141.69(1)°).

Table 1. Selected interatomic Ge–Ge distances in Å within the tris-silylated [Ge$_9$] clusters.

compound	within prismatic base 1	within prismatic base 2	prismatic heights
2	2.6304(6)	2.7771(5) *(η^3-Cu$^+$)*	3.4235(5) *(c,* Figure 2*)*
	2.6748(6)	2.8914(6) *(η^3-Cu$^+$)*	3.3918(5) *(b,* Figure 2*)*
	2.6771(5)	2.9143(5) *(η^3-Cu$^+$)*	3.1947(5) *(a,* Figure 2*)*
3	2.6407(13) *(η^3-K$^+$)*	2.9572(12) *(η^3-Au$^+$)*	3.3651(13)
	2.6711(13) *(η^3-K$^+$)*	2.9842(13) *(η^3-Au$^+$)*	3.4238(13)
	2.6459(14) *(η^3-K$^+$)*	2.9214(13) *(η^3-Au$^+$)*	3.2870(13)

In ESI-MS experiments, carried out with a tetrahydrofuran solution of the isolated red crystals, mainly the two species {(CuNHC^{Dipp})$_2$[Ge$_9${Si(*i*Bu)$_3$}$_3$]}$^+$ (*m*/*z* = 2155) (**2a**) and {(CuNHC^{Dipp})[Ge$_9${Si(*i*Bu)$_3$}$_2$]·3thf}$^+$ (*m*/*z* = 1719) (**2b**) were detected (spectra are shown in Supporting Information). Since the presence of both observed species can be excluded in the isolated crystals (elemental analysis, single X-ray diffraction) and in solution (NMR), their formation occurs unambiguously during the ionization process. Thereby, **2a** is formed upon coordination of a second Cu-NHC fragment to the free trigonal face of **2**, while species **2b** results from cleavage of a [Si(*i*Bu$_3$)$_3$]$^+$ group. The observation of **2a** is a further hint that it is possible to add more than one metalorganic fragment to tris-silylated clusters, which is also observed for the recently reported compound (CuP*i*Pr$_3$)[Ge$_9${Si(SiMe$_3$)$_3$}$_3$],[17] whereby [(CuP*i*Pr$_3$)$_2$[Ge$_9${Si(SiMe$_3$)$_3$}$_3$]$^+$ was detected in ESI-MS measurements. The appearance of **2b** indicates the lability of one [Si(*i*Bu$_3$)$_3$]$^+$ group at [Ge$_9$] with formation of the bis-silylated species.

Moreover, the reactivity of **1a** towards gold(I) phosphine complex Au(PPh$_3$)Cl was investigated. We have successfully used this ligand before for reactions with bare [Ge$_9$]$^{4-}$ clusters.[21] Addition of 1 equiv. of Au(PPh$_3$)Cl to a red acetonitrile solution of **1a** immediately led to a color change with formation of a brownish precipitate. After stirring the reaction solution overnight and purification of the precipitate, the solvent was removed in vacuo. Subsequently, the brownish residue was dissolved in toluene and filtered in order to remove potassium chloride, yielding a brown solution. After removal of toluene in vacuo, NMR experiments (^{1}H, ^{13}C, ^{29}Si, ^{31}P), indicating the formation of a dominating signal group of one silylated [Ge$_9$] species and a second silylated species in decisively smaller amount (further NMR discussion in the Supporting Information). Furthermore, the presence of free PPh$_3$ indicates the cleavage of the Au-PPh$_3$. In order to obtain closer information about the observed species, the residue was dissolved

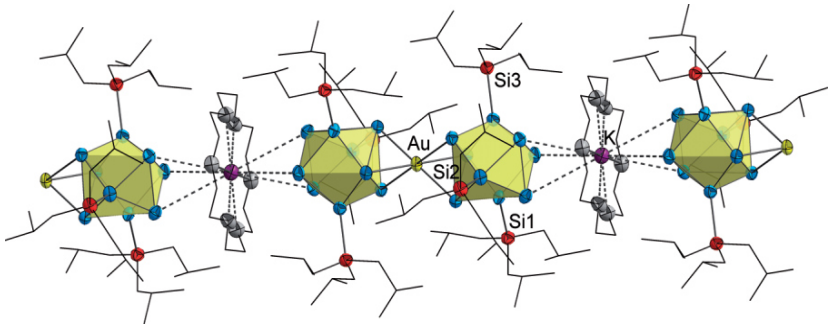

Figure 3. Molecular structure of (K-18c6)Au[Ge_9{Si(*i*Bu)$_3$}$_3$]$_2$ (**3**) showing the linear polymeric arrangement of the clusters. Atoms are shown as ellipsoids with 70 % probability (Ge atoms blue; Si atoms red, Au atoms yellow, O atoms gray and K atoms purple; C atoms are shown as wire/sticks; H atoms are omitted for reasons of clarity).

in toluene and layered with 18-crown-6 in hexane yielding red, block shaped single crystals after 5 days. Single crystal X-ray diffraction revealed the red crystals to consist of coinage metal bridged dimeric complex (K-18c6)Au[Ge_9{Si(*i*Bu)$_3$}$_3$]$_2$·tol (**3**·tol) (Figure 3).

In the molecular structure of **3**, shown in Figure 3, the central Au^+ cation coordinates to two tris-silylated [Ge_9{Si(*i*Bu)$_3$}$_3$]$^-$ (**1a**) anions, via one of their triangular faces formed by Ge atoms that are not connected to ligands. The two η^3–coordinated cluster faces have a staggered arrangement around the Au atom. The overall negative charge of the Au^+ bridged dimer is compensated by an 18-crown-6 sequestered potassium cation, which coordinates itself to two of the opposing triangular faces of the tris-silylated clusters, resulting in a linear polymeric arrangement (Figure 3). The Ge–Ge distances within the trigonal prism bases coordinating Au^+ are significantly elongated due to the metal coordination (2.9214(13)–2.9842(13) Å) (an overview to the Ge-Ge distances within the prismatic bases is shown in Table 1). This observation is in accordance with the literature-known anion {Au[Ge_9{Si(SiMe$_3$)$_3$}$_3$]$_2$}$^-$,[22] for which an average Ge–Ge distance of 2.96 Å is reported. In contrast, the Ge–Ge distances of the trigonal face, that coordinates to the cation of the [K-18c6]$^+$ unit, are remarkably shorter [2.6407(13)–2.6711(13) Å], confirming a weaker interaction of the potassium cation. The Ge–Au distances are in a range of 2.6485(10)–2.6651(9) Å and comparable to those in {Au[Ge_9{Si(SiMe$_3$)$_3$}$_3$]$_2$}$^-$ (average 2.69 Å). This observation shows that there is no decisively influence on the η^3-coordination of Au^+ by the lower steric demand of the silyl groups in **3**. However, the Ge–Au bonding distances in **3** are significantly longer if compared to the η^1-coordination of Au^+ with bare [Ge_9] clusters in [$Ge_9Au_3Ge_9$]$^{5-}$ (average value of 2.45 Å).[21]

In **3**, the [Ge_9] cluster shape is best described by a tricapped trigonal prism (D_{3h} symmetry) with the capping Ge atoms bearing the [Si(*i*Bu)$_3$]$^+$ groups. In contrast to **2**, the prismatic heights in **3** are in a closer range [3.2870(13)–3.4238(13) Å] resulting in a clearly lower deviation of the [Ge_9] cores from D_{3h} towards C_{2v} symmetry compared to **2** (Table 1). Thus, the steric demands of the ligands and the coordinated transition metal fragments might be the origin of the weaker distortion of the [Ge_9] clusters (Figure 4).

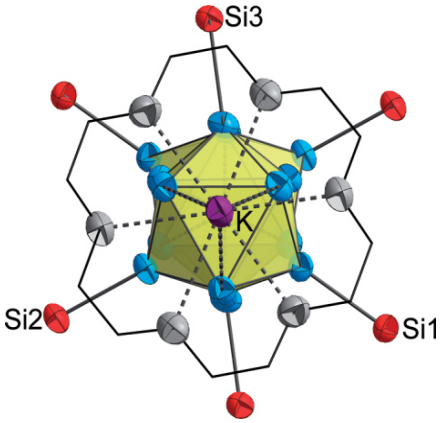

Figure 4. Detail view from the [K-18c6]$^+$ side on the arrangement of the groups at the [Ge_9] cluster in **3**. Atoms are shown as ellipsoids with 70 % probability (Ge atoms blue; Si atoms red, O atoms gray, K atoms purple and C atoms as wire/sticks; the *i*Bu groups and H atoms are omitted for reasons of clarity).

ESI-MS examinations, carried out with aliquots from the reaction solution diluted in tetrahydrofuran, revealed the presence of Au^+ bridged dimeric species {Au[Ge_9{Si(*i*Bu)$_3$}$_3$]$_2$}$^-$ (**3a**) (*m*/*z* = 2701) besides free tris-silylated cluster [Ge_9{Si(*i*Bu)$_3$}$_3$]$^-$; (**1a**) (*m*/*z* = 1053). The spectra are shown in the Supporting Information. This observation shows the presence of the dimer **3a** in the reaction solution as well as its stability in the gas phase.

Further, dissolution of the potassium salt of **1a** in toluene and subsequent layering with 18-crown-6 in hexane yielded yellow needle-shaped crystals, which were identified as (K-18c6)$_2$[Ge_9{Si(*i*Bu)$_3$}$_2$]·tol (**4**·tol) by single crystal X-ray diffraction. In **4**, the [Ge_9] cluster is covalently linked to two [Si(*i*Bu$_3$)$_3$]$^+$ groups and its twofold negative charge is compensated by two 18-crown-6 sequestered potassium atoms (Figure 5). Regarding the molecular structure of **4**, the [Ge_9] cluster possesses crystallographic C_{2v} symmetry with the C_2 axis aligned through the capping Ge5 atom and the center of the four atoms Ge, Ge', Ge2, and Ge2'. The shape is described as

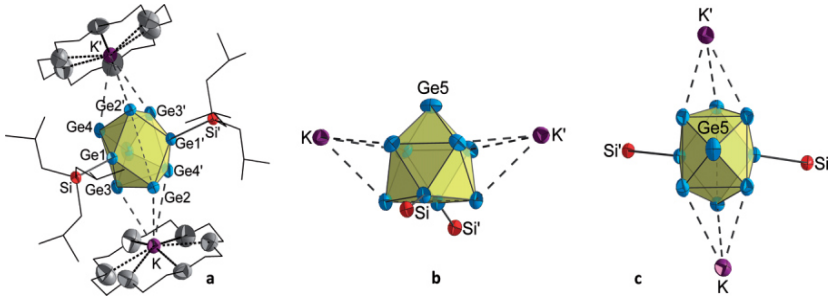

Figure 5. Molecular structure of the bis-silylated compound **4**. a) Complete molecular structure view on the square open face of the mono-capped square-antiprism [Ge_9] cluster with C_{2v} symmetry; b) Detailed side view on the square faces; c) Detailed top view on the Ge5-capped square face. Atoms are shown as ellipsoids with 70 % probability (Ge atoms blue; Si atoms red, K atoms purple and O atoms gray; C atoms are shown as wire/sticks; *i*Bu and 18-crown-6 groups are not shown in the detail views; H atoms are omitted for reasons of clarity; symmetry operation: (') $-x+1, y, -z+1.5$).

distorted mono-capped square antiprism with the two ligands connected to opposing vertex atoms of the open rectangle. This observation is in accordance to known bis-functionalized clusters such as $[Ge_9(CHCH_2)_2]^{2-}$,[7] $[RGe_9\text{-}CH{=}CH\text{-}CH{=}CH\text{-}Ge_9R]^{4-}$,[8] and $[Ge_9\{Si(SiMe_3)_3\}_2]^{2-}$ [18] as well as in the bis-silylated compound $(CuPiPr_3)_4[Ge_9(SiPh_3)_2]_2$.[17] However, the symmetry is significantly different to the tris-silylated anion $[Ge_9\{Si(SiMe_3)_3\}_3]^-$, where the [$Ge_9$] core reveals D_{3h} symmetry and can hence be described as tricapped trigonal prism with the three capping Ge atoms bearing the silyl groups. In compound **4**, the lengths of the diagonals of the rectangular open face significantly differ (d_2/d_1 = 1.23) with a distance between the two silyl bonding Ge atoms of 3.1844(8) Å and the distance between the ligand-free Ge atoms of 3.9326(6) Å. However, the Ge–Ge bond lengths within the non-capped rectangle are in the narrow range of 2.5228(6)–2.5403(6) Å, whereas the Ge-Ge distances in the Ge-capped square are significantly longer [2.7396(6)–2.8659(7) Å] forming a nearly perfect square [Ge-Ge-Ge angles are 89.411(2)° and 90.589(2)°]. The $[Si(iBu_3)_3]^+$ groups coordinate at the cluster with Ge–Si bond lengths of 2.3806(1) Å, which are slightly shorter than those reported for the bis-silylated species $[Ge_9(SiPh_3)_2]_2(CuPiPr_3)_4$ and $[Ge_9\{Si(SiMe_3)_3\}_2]^{2-}$ (average 2.41 Å each).

In **4**, two K cations coordinate to two opposing deltahedral faces of the cluster with K-Ge distances in the range of 3.475(1) Å to 3.825(1) Å (Figure 5). The two symmetry dependent K cations additionally coordinate to an 18-crown-6 molecule.

For ^{1}H NMR and ESI-MS investigations the crystals were dissolved in CD_3CN and acetonitrile, respectively, resulting in yellow solutions. In ESI-MS examinations, the pristine bis-silylated anion $[Ge_9\{Si(iBu)_3\}_2]^-$ (*m/z* = 1053) as well as $\{(K\text{-}18c6)[Ge_9\{Si(iBu)_3\}_3]\}^-$ (*m/z* = 1354) bearing one $[K\text{-}18c6]^+$ group were monitored. The latter species is also detected in ^{1}H NMR measurements according to the observed signal ratio. Further ^{1}H NMR examinations of the same sample revealed that the bis-silylated species is not stable in the more polar solvent CD_3CN for several days (further discussion and information in Supporting Information). It can be concluded that **4** is formed from the tris-silylated species **1** in the solvent mixture of toluene and hexane in presence of 18-crown-6 as sequestering agent. One $[Si(iBu_3)_3]^+$ group splits from the [Ge_9] core and the more polar bis-silylated cluster arises, which crystallizes in the non-polar solvent mixture.

Conclusion

The influence on the reactivity of silylated cluster compounds by decreasing the steric demand of the silyl groups at $[Ge_9(SiR_3)]^-$ clusters has been investigated for the organic ligands R = *i*Bu, *i*Pr and Et. ESI-MS investigations confirm the existence of the respective tris-silylated clusters in solution. Reaction of $[Ge_9\{Si(iBu)_3\}_3]^-$ (**1a**) with $CuNHC^{Dipp}Cl$ yielded the tris-silylated cluster in compound $(CuNHC^{Dipp})[Ge_9\{Si(iBu)_3\}_3]$ (**2**), which is similar to recently reported *Zintl* cluster copper NHC compound $(CuNHC^{Dipp})[Ge_9\{Si(SiMe_3)_3\}_3]$.[15] However, ESI-MS measurements indicate the lability of the $[Si(iBu)_3]^+$ group by detection of the bis-silylated species $\{(CuNHC^{Dipp})[Ge_9\{Si(iBu)_3\}_2)]\cdot 3thf\}^+$ as one of the main signals. Dimeric compound **3**, which is obtained by conversion of **1** with $Au(PPh_3)Cl$, consists of two Au^+ bridged tris-silylated [Ge_9] clusters. The different distortions of the underlying trigonal prisms in the [Ge_9] clusters cores correspond to the steric demands of the ligands and those of the coordinated transition metal fragments. The cleavage of a $[Si(iBu)_3]^+$ group from $[Ge_9\{Si(iBu)_3\}_3]^-$ (**1a**) in non-polar solution, yielding the respective bis-silylated cluster in compound **4**, reveals an increased lability of the $Si(iBu)_3$ ligand compared to $Si(SiMe_3)_3$ groups. This observation is in good accordance to recently reported isolation of bis-silylated species $(CuPiPr_3)_4[Ge_9(SiPh_3)_2]_2$, resulting from the substitution of $[SiPh_3]^+$ groups by Cu^+-phosphine fragments.[17]

The isolation of bis-silylated as well as tris-silylated compounds within this work proves that on the one hand $[Si(iBu)_3]^+$ seems to be more labile than respective $[Si(SiMe_3)_3]^+$ groups, however on the other hand the isolation of two coinage metal complexes of tris-silylated cluster **1a** indicate higher stability of $[Si(iBu)_3]^+$ compared to $[SiPh_3]^+$. Further investigations on the reactivity of the herein reported tris-silylated clusters bearing sterically less bulky $[Si(iPr)_3]^+$

and $[Si(Et)_3]^+$ groups can provide deeper insights into the relation between steric shielding of the clusters and their reactivity.

Experimental Section

General. All reactions and manipulations were performed under a purified argon atmosphere using standard Schlenk and glove box techniques. The *Zintl* compound of the nominal composition K_4Ge_9 was synthesized by heating (2 K min^{-1}) of a stoichiometric mixture of both elements K and Ge (99.999 % Chempur) at 650 °C in a stainless steel autoclave for 46 h and slow cooling (1 K min^{-1}) to room temperature. Dry solvents were obtained from solvent purifiers (MBraun) and subsequently stored over dried molecular sieves. 18-crown-6 was purified by sublimation in vacuo at 80 °C. $Au(PPh_3)Cl$ was synthesized according to known procedures[23] from $HAuCl_4$ and PPh_3 and dried in vacuo for 8 h. $CuNHC^{Dipp}Cl$ was synthesized according to a description in literature.[24] All other chemicals were purchased commercially and used as received.

Single Crystal Structure Determination. The air and moisture sensitive single crystals of **2** and **4** were transferred from the mother liquor into a perfluoropolyalkyl ether oil at 213 K under a cold N_2 stream and subsequently fixed on a glass capillary and positioned in a 120 K cold N_2 gas stream using the crystal cap system. Single crystals of **3** were prepared analogously without crystal cooling in a glove box. The single-crystal X-ray diffraction data were collected using an Oxford Diffraction Xcalibur3 diffractometer (Mo K_α radiation). The structures were solved by Direct Methods and refined by full-matrix least-squares calculations against F^2 using SHELX-2014.[25] Non-hydrogen atoms were treated with anisotropic displacement parameters. Positions of the hydrogen atoms were calculated and refined using a riding model. In $(CuNHC^{Dipp})[Ge_9\{Si(i\text{Bu})_3\}_3]\cdot 0.5$ tol (**2**·0.5 tol) one *i*Bu group attached to Si1 is disordered and has been refined at two split positions, for presentation the carbon atoms with the lower occupation (C12A, C13A, C14A and C15A) are deleted. The amount of solvent molecules was determined by using the squeeze function. The toluene molecules in $(K\text{-}18c6)Au[Ge_9\{Si(i\text{Bu})_3\}_3]_2\cdot$tol (**3**·tol) and $(K\text{-}18c6)_2[Ge_9\{Si(i\text{Bu})_3\}_2]\cdot$tol (**4**·tol) are found in two superposing orientations, respectively, therefore the respective atoms have been refined at split positions with half occupation. Crystallographic details are given in Table 2. Further information about the crystal structure investigations may be obtained from the Cambridge Crystallographic Data Centre via www.ccdc.cam.ac.uk/data_request/cif, on quoting the depository numbers CCDC-1499454 (**2**), CCDC -1499455 (**3**), CCDC-1499456 (**4**). The crystal structures have been visualized with Diamond.[26]

Electron Dispersive X-ray (EDX) Analysis: Single crystals of all compounds were analyzed with a scanning electron microscope (JEOL 5900LV) equipped with an energy dispersive X-ray analyzer (Oxford Instruments).

NMR Spectroscopy. The ^1H, ^{13}C and ^{29}Si NMR spectra were recorded on a Bruker AvanceIII400 FT system or on a Bruker AV 500c (*Bruker Corp.*) at 300 K. The signals of the ^1H and ^{13}C spectra were calibrated on the rest proton signal of the used deuterated solvents C_6D_6, CD_3CN or C_4D_8O. Chemical shifts are given in δ values by parts per million (ppm). The coupling constants J are stated in Hz. Signal multiplicities are abbreviated as follows: s - singlet, d - doublet, t - triplet, h - heptet and m - multiplet. The spectra were evaluated with MestReNova.[27]

Electrospray Ionization Mass Spectrometry (ESI-MS). The preparation of the samples was performed in a glovebox. The measurements were performed on a HCT (*Bruker Corp.*). Analysis of the data was evaluated using the program Bruker Compass Data Analysis 4.0 SP 5 (*Bruker Corp.*). The dry gas temperature was adjusted to 125 or 300 °C and the injection speed to 240 µL s^{-1}. Visualization of the spectra was done with the programs OriginPro 2016G (*Origin Lab Corp.*) and Excel 2016 (*Microsoft Corp.*).

Elemental Analysis. Elemental analyses were performed by the microanalytical laboratory at the Department of Chemistry of the Technische Universität München. The elements C, H and N were determined with a combustion analyzer (elementar vario EL, *Bruker Corp.*).

Table 2. Selected crystallographic data of the crystal structures of **2**, **3** and **4**.

Compound	**2**·0.5 tol	**3**·tol	**4**·tol
formula	$C_{63}H_{117}CuGe_9N_2Si_3$	$C_{91}H_{194}Au_1Ge_{18}K_1O_6Si_6$	$C_{55}H_{110}Ge_9K_2O_{12}Si_2$
fw /g·mol^{-1}	1703.70	3095.68	1751.11
space group (no)	$P2_1/n$ (14)	$P\bar{1}$ (2)	$C2/c$ (15)
a /Å	13.2540(4)	13.4037(4)	16.3651(4)
b /Å	46.196(13)	15.7894(5)	28.4911(7)
c /Å	13.5183(4)	18.1041(6)	17.1371(4)
α /°	90	69.111(3)	90
β /°	102.286(3)	71.815(3)	105.108(3)
γ /°	90	65.983(3)	90
V /Å^3	8087.5(4)	3206.6(2)	7714.2(3)
Z	4	1	4
T /K	120(2)	120(2)	120(2)
ρ_{calc} /g·cm^{-3}	1.399	1.603	1.508
μ /mm^{-1}	3.629	5.414	3.642
measured reflections	197984	166666	128438
independent reflections	15005	12609	7574
R_{int} / R_σ	0.0589 / 0.0660	0.2070 / 0.0980	0.0627 / 0.0446
reflections $> 2\sigma$	9888	8323	5176
parameters / restraints	756 / 18	561 / 8	382 / 0
R_1 [$I > 2\ \sigma(I)$ / all data]	0.0307 / 0.0559	0.0549 / 0.0815	0.0385 / 0.0597
wR_2 [$I > 2\ \sigma(I)$ / all data]	0.0688 / 0.0743	0.1627 / 0.1677	0.1019 / 0.1066
goodness of fit	0.913	1.050	0.985
largest difference peak/hole /e Å^{-3}	0.757 / –0.738	5.663 / –2.059	1.401 / –0.451
CCDC number	1499454	1499455	1499456

$[Ge_9\{Si(iBu)_3\}_3]^-$ (1a) and $(K\text{-}18c6)_2[Ge_9\{Si(iBu)_3\}_2]\cdot tol$ (4·tol). K_4Ge_9 (162 mg, 0.20 mmol, 1 equiv.) was added to a solution of $Si(iBu)_3Cl$ (141 mg, 0.60 mmol, 3 equiv.) in acetonitrile (4 mL). The reaction mixture was stirred overnight and filtered. Removal of the solvent in vacuo yielded a brownish solid revealing the formation of **1a** (40 %; based on the assumption of the potassium salt). For crystallization the brownish solid was dissolved in toluene (4 mL) and filtered obtaining a brown solution. Subsequent layering of this solution with hexane containing 18-crown-6 (79.3 mg, 0.30 mmol, 3 equiv.) in hexane yielded yellow, needle-shaped crystals (19 %) after storing at –32 °C for 5 months.

$[Ge_9\{Si(iBu)_3\}_3]^-$ (1a). ^{1}H NMR (400 MHz, CD_3CN, 25 °C): δ = 2.05 (m, 3 H, CH_{iBu}), 0.93 (d, J = 6.6 Hz, 18 H, $CH_{3(iBu)}$), 0.79 (d, J = 6.7 Hz, 6 H, $CH_{2(iBu)}$). **^{13}C NMR** (101 MHz, CD_3CN, 25 °C): δ = 32.05 (CH_{iBu}), 27.36 ($CH_{3(iBu)}$), 27.24 ($CH_{2(iBu)}$). **^{29}Si NMR** (99 MHz, CD_3CN, 25 °C): δ = 22.09. **ESI-MS** (negative mode, 4000 V, 125 °C): m/z = 1253 $[Ge_9\{Si(iBu)_3\}_3]^-$.

$(K\text{-}18c6)_2[Ge_9\{Si(iBu)_3\}_2]\cdot tol$ (4·tol). ^{1}H NMR (400 MHz, CD_3CN, 25 °C): δ = 3.56 (s, 24 H, $C_{12}H_{24}O_6$), 0.94 (m, 2 H, CH_{iBu}), 0.85 (d, J = 6.6 Hz, 12 H, $CH_{3(iBu)}$), 0.50 (d, J = 6.6 Hz, 4 H, $CH_{2(iBu)}$). **ESI-MS** (negative mode, 4000 V, 125 °C): m/z = 1053 $[Ge_9\{Si(iBu)_3\}_2]^-$. **ESI-MS** (negative mode, 4000 V, 125 °C): m/z = 1354 $\{[Ge_9\{Si(iBu)_3\}_3]K\text{-}18c6\}^-$; qualitative EDX analysis of crystals of **4**·tol revealed the presence of Si, Ge and K: Si 17.51 (calcd. 15.4); Ge 61.57 (calcd. 69.2); K 20.92 (calcd. 15.4) %.

$[Ge_9\{Si(Et)_3\}_3]^-$ (1b) and $[Ge_9\{Si(iPr)_3\}_3]^-$ (1c). To a solution of SiR_3Cl (R = *i*Pr: 116 mg, 0.60 mmol, 3 equiv.; R = Et: 90.4 mg, 0.60 mmol, 3 equiv.) in acetonitrile (4 mL) K_4Ge_9 (162 mg, 0.20 mmol, 1 equiv.) was added. The reaction mixture was stirred overnight and filtered yielding brownish solutions. For ESI-MS examinations the reaction solutions were diluted with acetonitrile until a suitable concentration was obtained. ESI-MS measurements revealed the formation of the tris-silylated species **1b** (34 %; based on the assumption of the potassium salt) and **1c** (37 %; based on the assumption of the potassium salt). **ESI-MS** (negative mode, 4500 V, 125 °C): m/z 1126 (**1b**). **ESI-MS** (negative mode, 4500 V, 125 °C): m/z = 999 (**1c**).

$(CuNHC^{Dipp})[Ge_9\{Si(iBu)_3\}_3]\cdot 0.5\ tol$ (2·0.5 tol). An acetonitrile solution (2 mL) of $Si(iBu)_3Cl$ (70.0 mg, 0.30 mmol, 3 equiv.) was added to K_4Ge_9 (81.0 mg, 0.10 mmol, 1 equiv.). The reaction mixture was stirred overnight and subsequently filtered to obtain a red solution. Dropwise addition of this solution to an acetonitrile solution (2 mL) of $CuNHC^{Dipp}Cl$ (48.0 mg, 0.10 mmol, 1 equiv.) instantly led to formation of an orange-brownish precipitate. After stirring the reaction mixture for 30 min, the precipitate was allowed so settle down and the colorless supernatant solution was filtered off. The precipitate was washed with acetonitrile (1 mL) and dried in vacuo yielding a brownish solid. Purification by recrystallization from toluene at –40 °C yielded red block-shaped crystals (41 %) after two weeks. **^{1}H NMR** (400 MHz, C_6D_6, 25 °C): δ = 7.42 (t, J = 7.8 Hz, 2 H, $CH_{Ph(p)}$), 7.29 (d, J = 7.8 Hz, 4 H, $CH_{Ph(m)}$), 6.29 (s, 2 H, CH_{Im}), 2.75 (h, J = 6.8 Hz, 4 H, CH_{iPr}), 2.18 (m, 9 H, CH_{iBu}), 1.66 (d, J = 6.8 Hz, 12 H, $CH_{3(iPr)}$), 1.12 (m, 66 H, $CH_{3(iPr)} + CH_{3(iBu)}$), 1.03 (d, 18 H, J = 6.8 Hz, $CH_{2(iBu)}$). **^{1}H NMR** (400 MHz, C_4D_8O, 25 °C): δ = 7.49 (t, J = 7.8 Hz, 2 H, $CH_{Ph(p)}$), 7.43 (s, 2 H, CH_{Im}), 7.37 (d, J = 7.8 Hz, 4 H, $CH_{Ph(m)}$), 2.78 (h, J = 6.8 Hz, 4 H, CH_{iPr}), 1.96 (m, 9 H, CH_{iBu}), 1.55 (d, J = 6.8 Hz, 12 H, $CH_{3(iPr)}$), 1.22 (d, J = 6.8 Hz, 12 H, $CH_{3(iPr)}$), 0.94 (d, J = 6.6 Hz, 54 H, $CH_{3(iBu)}$), 0.81 (d, 18 H, J = 6.8 Hz, $CH_{2(iBu)}$). **^{13}C NMR** (101 MHz, C_6D_6, 25 °C): δ = 145.89 ($C_{Ph(iPr)}$), 135.16 ($C_{Ph}N$), 130.81 ($CH_{Ph(p)}$), 124.45 ($CH_{Ph(m)}$), 121.60 (CH_{Im}), 30.94 (CH_{iBu}), 29.14 (CH_{iPr}), 27.33 ($CH_{3(iBu)}$), 26.99 ($CH_{2(iBu)}$), 25.78 ($CH_{3(iPr)}$), 24.77 ($CH_{3(iPr)}$). **^{29}Si NMR** (79 MHz, C_6D_6, 25 °C): δ = 22.17. **ESI-MS** (positive mode, 3500 V, 300 °C): m/z = 2155 $\{(CuNHC^{Dipp})_2\ [Ge_9\{Si(iBu)_3\}_3]\}^+$. **ESI-MS** (positive mode, 4000 V, 300 °C): m/z = 1719 $\{(CuNHC^{Dipp})[Ge_9\{Si(iBu)_3\}_2]\cdot 3thf\}^+$; Elemental analysis of **2**: C 44.6 (calcd. 44.4); H 7.1 (calcd. 6.9); N 1.7 (calcd. 1.6) %

$(K\text{-}18c6)Au[Ge_9\{Si(iBu)_3\}_3]_2\cdot tol$ (3·tol). K_4Ge_9 (162 mg, 0.20 mmol, 1 equiv.) was added to a solution of $Si(iBu)_3Cl$ (141 mg, 0.60 mmol, 3 equiv.) in acetonitrile (4 mL). After stirring overnight, the reaction mixture was filtered, yielding a red solution. Addition of $Au(PPh_3)Cl$ (98.9 mg, 0.20 mmol, 1 equiv.) immediately led to the formation of a brown precipitate. The reaction mixture was stirred at r. t. overnight. Subsequent filtration, washing with acetonitrile and removal of the solvent in in vacuo yielded a brown solid, which was extracted with toluene (2 mL). Layering with a hexane solution of 18-crown-6 (106 mg, 0.40 mmol, 2 equiv.) after filtration yielded red, block-shaped crystals (26 %) after 5 days. Single crystal X-ray diffraction confirmed formation of **3** and EDX measurements the presence of the elements Si, Ge, K and Au in the single crystals. **^{1}H NMR** (400 MHz, C_6D_6, 25 °C): δ = 1.97 (m, 3 H, CH_{iBu}), 1.07 (d, J = 6.6 Hz, 18 H, $CH_{3(iBu)}$), 0.76 (d, J = 6.8 Hz, 6 H, $CH_{2(iBu)}$). **^{13}C NMR** (101 MHz, C_6D_6, 25 °C): δ = 28.47 (CH_{iBu}), 26.91($CH_{3(iBu)}$), 24.63 ($CH_{2(iBu)}$). **^{29}Si NMR** (79 MHz, C_6D_6, 25 °C): δ = 4.67 ppm. **ESI-MS** (negative mode, 4000 V, 300 °C): m/z = 2701 $\{Au[Ge_9\{Si(iBu)_3\}_3]_2\}^-$; qualitative EDX analysis of crystals of **3**·tol revealed the presence of Si, Ge, K and Au with approximate atomic ratios: Si 25.47 (calcd. 23.1); Ge 64.42 (calcd. 69.2); K 4.2 (calcd. 3.85); Au 5.92 (calcd. 3.85) %.

Supporting Information (see footnote on the first page of this article): ^{1}H, ^{13}C, and ^{29}Si NMR spectra as well as ESI-MS spectra of compounds **1**–**4**, additional details of the crystal structures.

Acknowledgments

This work was supported by the research network "Solar Technologies go Hybrid" (State of Bavaria), the Deutsche Forschungsgemeinschaft (DFG) (FA 198/14-1) and Wacker Chemie AG. Furthermore, the authors thank Kerstin Mayer and TUM Graduate School.

References

[1] a) S. Scharfe, F. Kraus, S. Stegmaier, A. Schier, T. F. Fässler, *Angew. Chem.* **2011**, *123*, 3712; *Angew. Chem. Int. Ed.* **2011**, *50*, 3630; b) T. F. Fässler, *Coord. Chem. Rev.* **2001**, *215*, 347; c) J. D. Corbett, *Chem. Rev.* **1985**, *85*, 383; d) S. C. Sevov, J. M. Goicoechea, *Organometallics* **2006**, *25*, 5678.
[2] B. W. Eichhorn, R. C. Haushalter, W. T. Pennington, *J. Am. Chem. Soc.* **1988**, *110*, 8704.
[3] A. Spiekermann, S. D. Hoffmann, T. F. Fässler, I. Krossing, U. Preiss, *Angew. Chem.* **2007**, *119*, 5404; *Angew. Chem. Int. Ed.* **2007**, *46*, 5310.
[4] a) A. Ugrinov, S. C. Sevov, *J. Am. Chem. Soc.* **2003**, *125*, 14059; b) A. Ugrinov, S. C. Sevov, *Chem. Eur. J.* **2004**, *10*, 3727.
[5] M. W. Hull, A. Ugrinov, I. Petrov, S. C. Sevov, *Inorg. Chem.* **2007**, *46*, 2704.
[6] a) C. B. Benda, H. He, W. Klein, M. Somer, T. F. Fässler, *Z. Anorg. Allg. Chem.* **2015**, *641*, 1080; b) M. W. Hull, S. C. Sevov, *J. Am. Chem. Soc.* **2009**, *131*, 9026.
[7] a) M. W. Hull, S. C. Sevov, *Inorg. Chem.* **2007**, *46*, 10953; b) C. B. Benda, J.-Q. Wang, B. Wahl, T. F. Fässler, *Eur. J. Inorg. Chem.* **2011**, 4262.
[8] M. M. Bentlohner, W. Klein, Z. H. Fard, L.-A. Jantke, T. F. Fässler, *Angew. Chem.* **2015**, *127*, 3819; *Angew. Chem. Int. Ed.* **2015**, *54*, 3748.

[9] A. Schnepf, *Angew. Chem.* **2003**, *115*, 2728; *Angew. Chem. Int. Ed.* **2003**, *42*, 2624.
[10] F. Li, S. C. Sevov, *Inorg. Chem.* **2012**, *51*, 2706.
[11] F. Henke, C. Schenk, A. Schnepf, *Dalton Trans.* **2009**, 9141.
[12] C. Schenk, F. Henke, G. Santiso-Quinones, I. Krossing, A. Schnepf, *Dalton Trans.* **2008**, 4436.
[13] F. Li, S. C. Sevov, *Inorg. Chem.* **2015**, *54*, 8121.
[14] F. Li, A. Muñoz-Castro, S. C. Sevov, *Angew. Chem.* **2016**, *128*, 8772–8775; *Angew. Chem. Int. Ed.* **2016**, *55*, 8630.
[15] F. S. Geitner, T. F. Fässler, *Eur. J. Inorg. Chem.* **2016**, 2688.
[16] Dipp = 1,3-bis(2,6-diisopropylphenyl-)imidazol-2-ylidene.
[17] K. Mayer, L. J. Schiegerl, T. F. Fässler, *Chem. Eur. J.* **2016**, published online, DOI: 10.1002/chem.201603475.
[18] O. Kysliak, A. Schnepf, *Dalton Trans.* **2016**, *45*, 2404.
[19] O. Kysliak, C. Schrenk, A. Schnepf, *Inorg. Chem.* **2015**, *54*, 7083.
[20] C. Fischer, W. Klein, L.-A. Jantke, L. J. Schiegerl, T. F. Fässler, *Z. Anorg. Allg. Chem.* **2016**, published online, DOI: 10.1002/zaac.201600296.
[21] A. Spiekermann, S. D. Hoffmann, F. Kraus, T. F. Fässler, *Angew. Chem.* **2007**, *119*, 1663; *Angew. Chem. Int. Ed.* **2007**, *46*, 1638.
[22] C. Schenk, A. Schnepf, *Angew. Chem.* **2007**, *119*, 5408; *Angew. Chem. Int. Ed.* **2007**, *46*, 5314.
[23] S. Ahrland, K. Dreisch, B. Norén, Å. Oskarsson, *Mater. Chem. Phys.* **1993**, *35*, 281.
[24] H. Kaur, F. K. Zinn, E. D. Stevens, S. P. Nolan, *Organometallics* **2004**, *23*, 1157.
[25] C. B. Hübschle, G. M. Sheldrick, B. Dittrich, *J. Appl. Crystallogr.* **2011**, *44*, 1281.
[26] H. Putz, K. Brandenburg, *DIAMOND - Crystal and Molecular Structure Visualization*, Version 3.2k **2014**, Bonn, Germany.
[27] MestrelabResearch, *MestReNova v9.1.0–14011*, **2014**.

Received: August 19, 2016
Published Online: November 15, 2016

Z. Anorg. Allg. Chem. **2016** · ISSN 0044–2313

SUPPORTING INFORMATION

Title: Functionalization of $[Ge_9]$ with Small Silanes: $[Ge_9(SiR_3)_3]^-$ (R = *i*Bu, *i*Pr, Et) and the Structures of $(CuNHC^{Dipp})[Ge_9\{Si(iBu)_3\}_3]$, (K-18c6)Au$[Ge_9\{Si(iBu)_3\}_3]_2$, and (K-18c6)$_2[Ge_9\{Si(iBu)_3\}_2]$
Author(s): L. J. Schiegerl, F. S. Geitner, C. Fischer, W. Klein, T. F. Fässler*
Ref. No.: z201600295

Supporting Information

for

Functionalization of [Ge_9] with Small Silanes: [$Ge_9(SiR_3)_3]^-$ (R = *i*Bu, *i*Pr, Et) and the Structures of ($CuNHC^{Dipp}$)[Ge_9{$Si(iBu)_3$}$_3$], (K-18c6)Au[Ge_9{$Si(iBu)_3$}$_3$]$_2$, and (K-18c6)$_2$[Ge_9{$Si(iBu)_3$}$_2$]

Lorenz J. Schiegerl,[‡[a]] Felix S. Geitner,[‡ [b]] Christina Fischer,[[a]] Wilhelm Klein,[[a]]

and Thomas F. Fässler*[[a]]

[a] Department of Chemistry, Technische Universität München

Lichtenbergstraße 4, 85747 Garching, Germany

E-Mail: thomas.faessler@lrz.tum.de

[b] WACKER Institute for Silicon Chemistry and Department of Chemistry, Technische Universität München

Lichtenbergstraße 4, 85748 Garching, Germany

[‡]authors contributed equally to this work

Content

1 NMR data of **1a** and the compounds **2 – 4**

[Ge_9{Si(*i*Bu)$_3$}$_3$]$^-$ (**1a**):

The ^{1}H NMR spectrum shows three proton signals (2.05, 0.93, and 0.79 ppm) of the *i*Bu groups in [Ge_9{Si(*i*Bu)$_3$}$_3$]$^-$ (**1a**) with the expected signal ratio of 1:6:2 (reactant Si(*i*Bu)$_3$Cl in CD_3CN: 1.91, 0.98, and 0.88 ppm). The ^{13}C NMR spectrum also shows three signals for the three different carbon atoms in **1a** (Si(*i*Bu)$_3$Cl in CD_3CN: 28.41, 26.40, and 25.24 ppm). In the ^{29}Si NMR spectrum one signal is observed at 22.09 ppm (Si(*i*Bu)$_3$Cl in CD_3CN: 31.08 ppm).

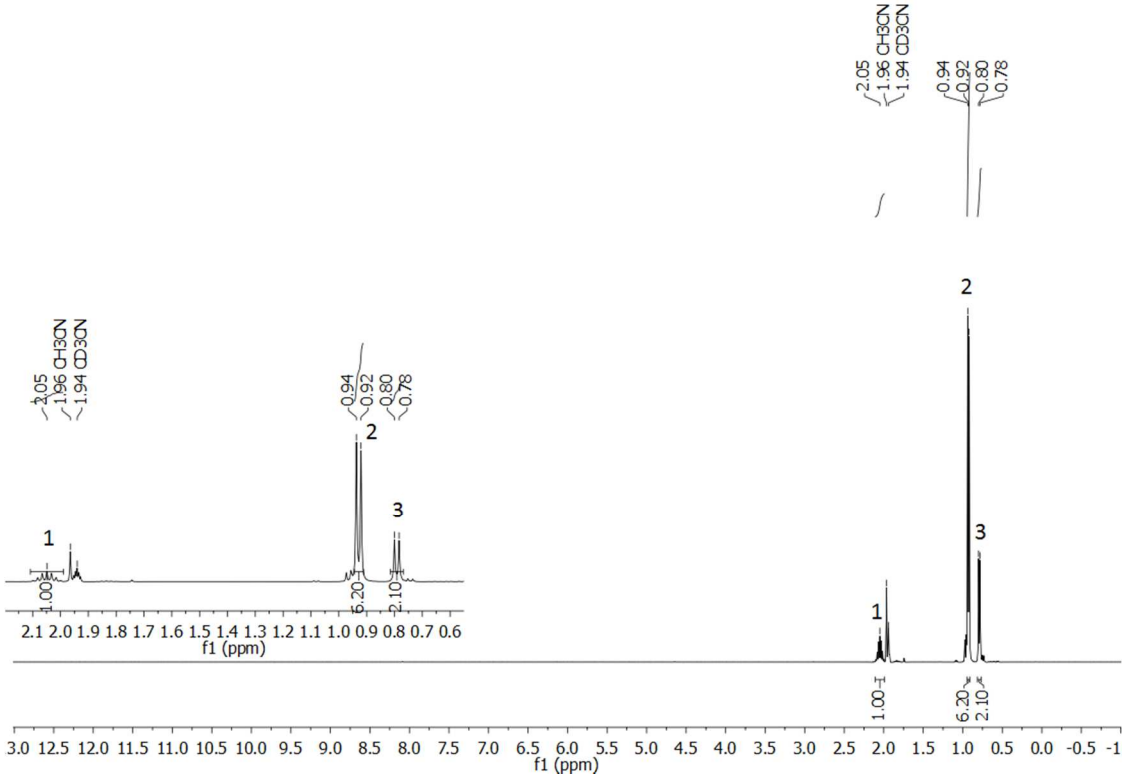

Figure SI 1: ^{1}H NMR spectrum of [Ge_9{Si(*i*Bu)$_3$}$_3$]$^-$ (**1a**) in CD_3CN.

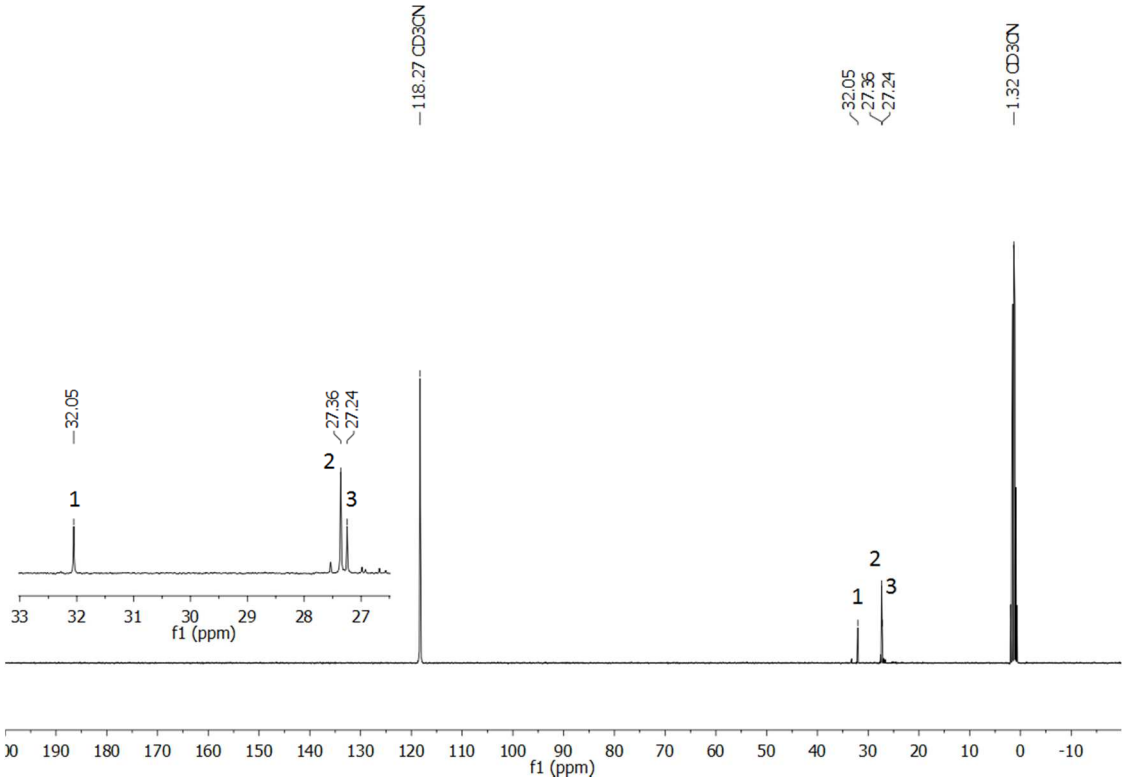

Figure SI 2: ^{13}C NMR spectrum of $[Ge_9\{Si(iBu)_3\}_3]^-$ (**1a**) in CD_3CN.

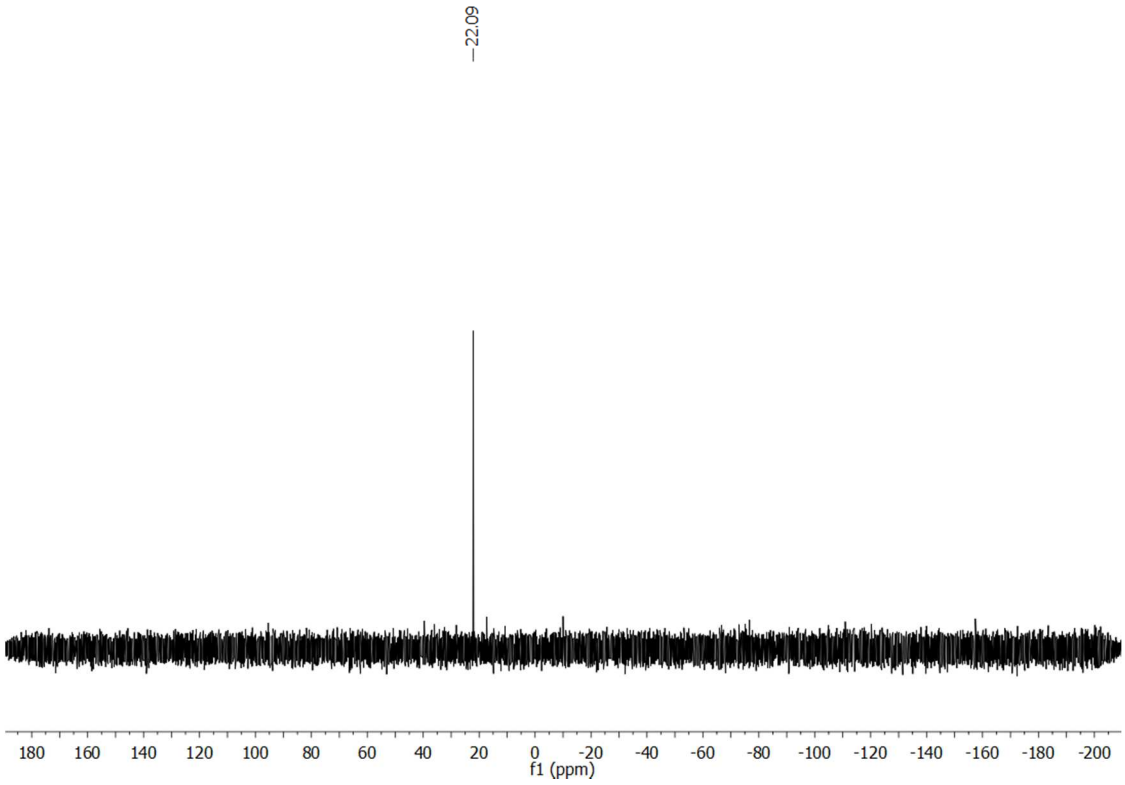

Figure SI 3: ^{29}Si NMR spectrum of $[Ge_9\{Si(iBu)_3\}_3]^-$ (**1a**) in CD_3CN.

(CuNHC^{Dipp})[Ge$_9${Si(*i*Bu)$_3$}$_3$] (**2**):

The ^{1}H NMR spectrum measured in C_6D_6 consists of eight proton signals with a ratio of 2:4:2:4:9:12:66:18. Since the signals caused by the methyl groups of the silyl residues (54 H) overlap with those of two Dipp groups (12 H) of the NHC (d at 1.12 ppm), a second ^{1}H NMR spectrum in C_4D_8O is provided, where no signal overlapping occurs. The ^{13}C NMR spectrum consists of eleven signals, in the ^{29}Si NMR spectrum one signal is observed at 22.17 ppm.

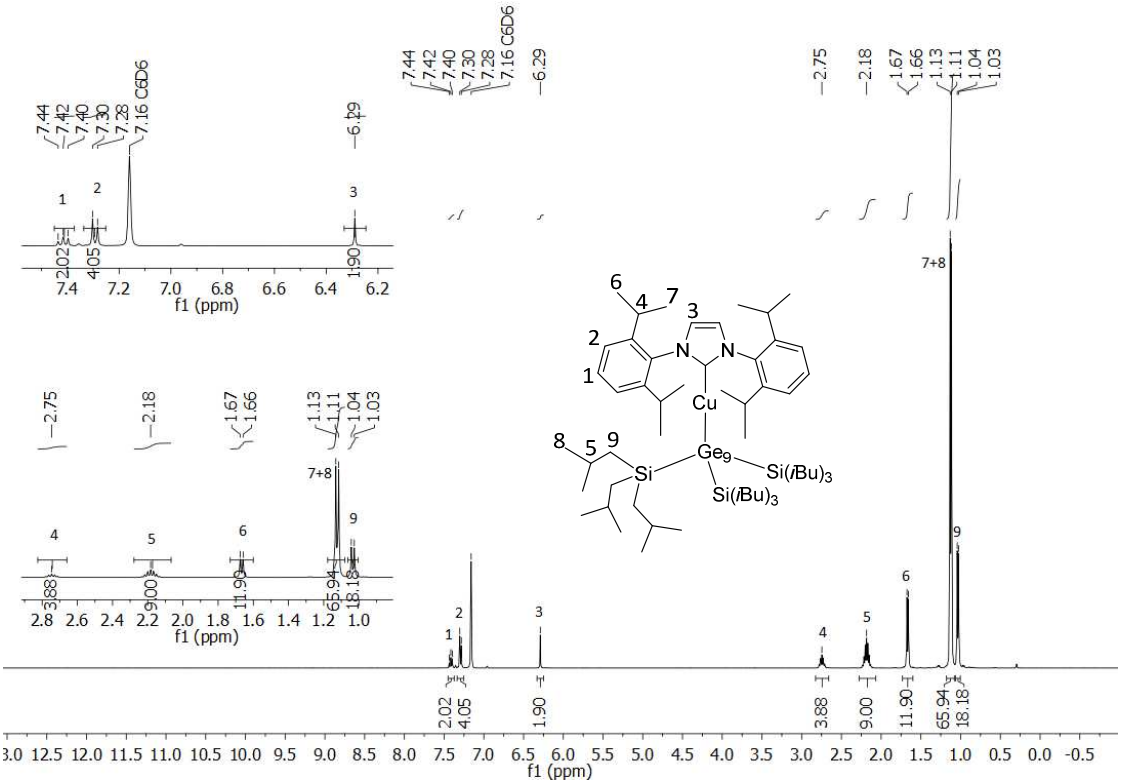

Figure SI 4: ^{1}H NMR spectrum of (CuNHC^{Dipp})[Ge$_9${Si(*i*Bu)$_3$}$_3$] (**2**) in C_6D_6.

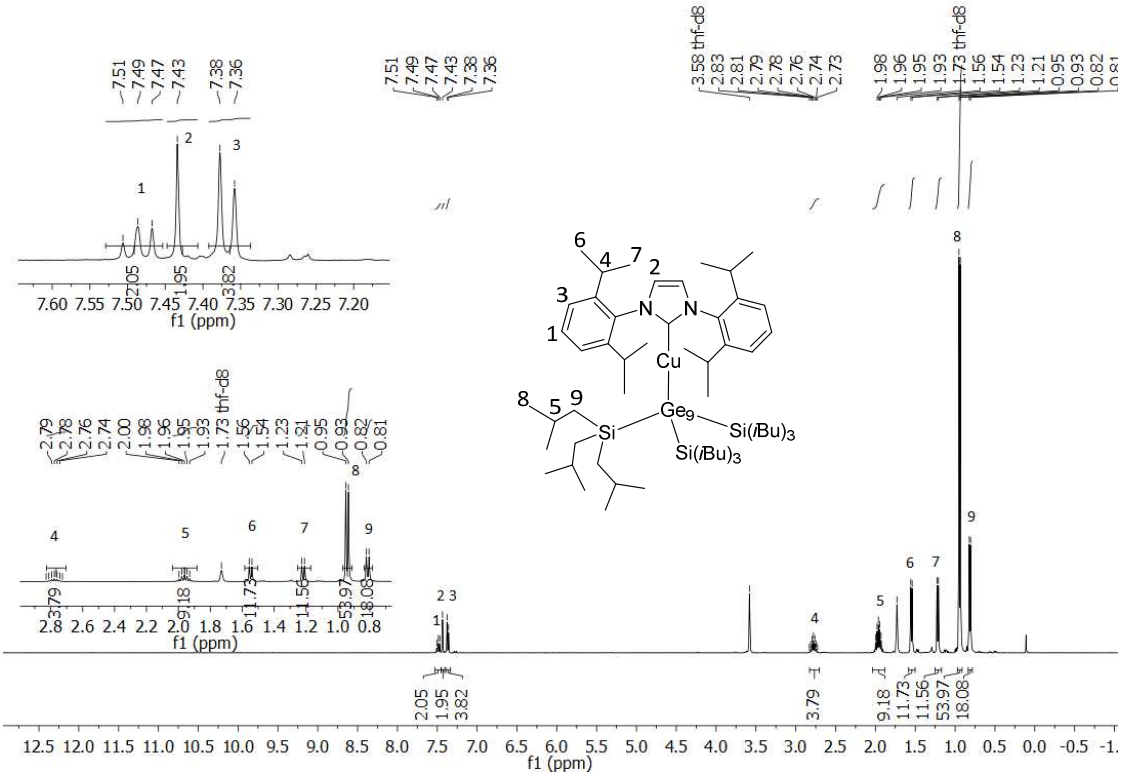

Figure SI 5: ^{1}H NMR spectrum of (CuNHC^{Dipp})[Ge$_9${Si(*i*Bu)$_3$}$_3$] (**2**) in C_4D_8O.

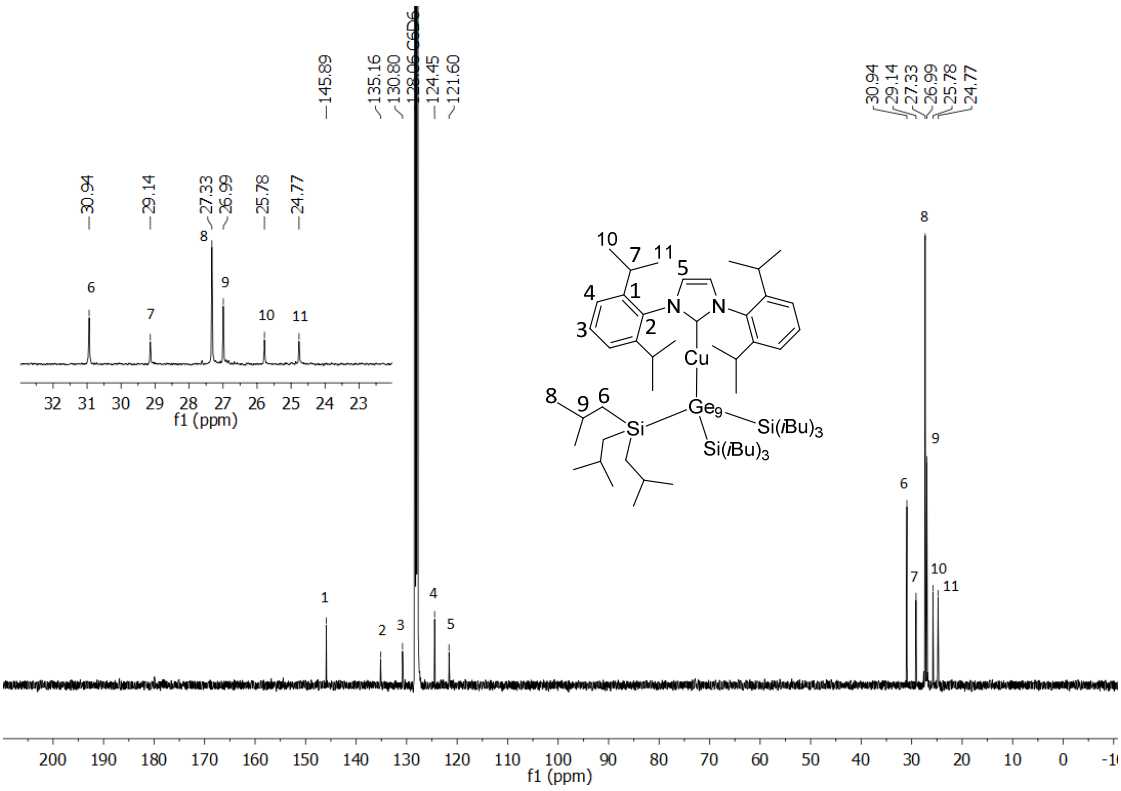

Figure SI 6: ^{13}C NMR spectrum of (CuNHC^{Dipp})[Ge$_9${Si(*i*Bu)$_3$}$_3$] (**2**) in C_6D_6.

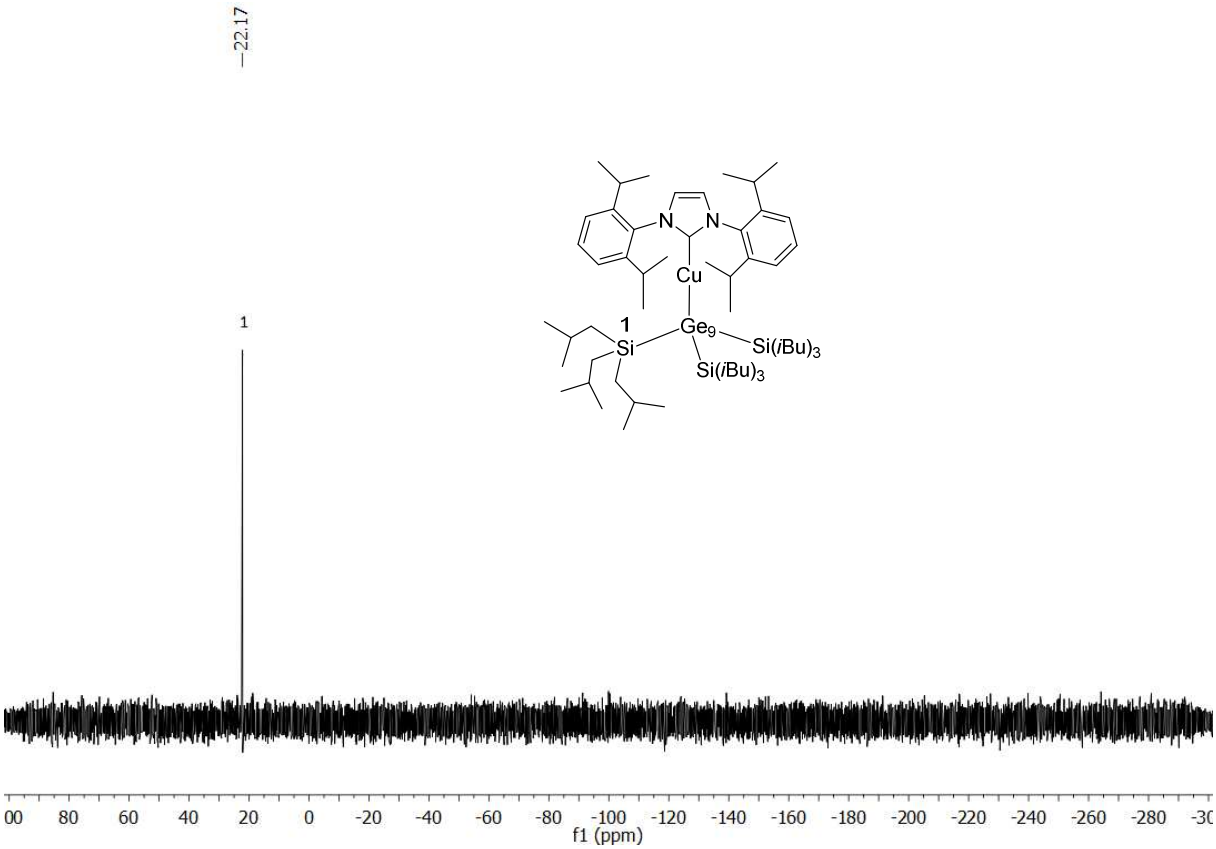

Figure SI 7: ^{29}Si NMR spectrum of (CuNHC^{Dipp})[Ge$_9${Si(*i*Bu)$_3$}$_3$] (**2**)in C_6D_6.

(K-18c6)Au[Ge$_9${Si(*i*Bu)$_3$}$_3$]$_2$ (**3**):

In the ^{1}H NMR spectrum the main signals (1.97 (C*H*$_{i\text{Bu}}$), 1.07 (C*H*$_{3(i\text{Bu})}$), and 0.76 ppm (C*H*$_{2(i\text{Bu})}$)) originate from the [Si(*i*Bu)$_3$]$^+$ groups of one silylated species with the expected signal ratio of 1:6:2. Another silylated species can be assigned in clearly smaller amount to the signals 1.64, 0.86, and 0.54 ppm with the same expected signal ratio. Verification of the existence of the two signal groups further derives from 2D COSY experiments. The signals between 7.0 and 7.5 ppm can be assigned to free PPh_3. The ^{13}C NMR spectrum confirms the presence of the three species by showing mainly three signal groups (28.47 (*C*H$_{i\text{Bu}}$), 26.91 (*C*H$_{3(i\text{Bu})}$), and 24.63 ppm (*C*H$_{2(i\text{Bu})}$)) for the three different carbon atoms of the [Si(*i*Bu)$_3$]$^+$ groups of the silylated species, the smaller amount of a second silylated species is confirmed by the smaller signals at 26.49, 24.74, and 23.99 ppm. The carbon signals for PPh_3 appear between 128 and 138 ppm, doublet splitting originates from phosphorous coupling. Further evidence for the presence of two silylated species in different amounts provides the ^{29}Si NMR spectrum. A dominating signal appears at 4.67 ppm and a decisively smaller signal at 2.04 ppm. The ^{31}P NMR spectrum exclusively shows the signal of free PPh_3 at 5.33 ppm. The corresponding ESI-MS spectra are shown in Figure SI 19 and 20 and show the presence of [Ge$_9${Si(*i*Bu)$_3$}$_3$]$^-$ (**1a**) and {Au[Ge$_9${Si(*i*Bu)$_3$}$_3$]$_2$}$^-$ (**3a**) under measurement conditions.

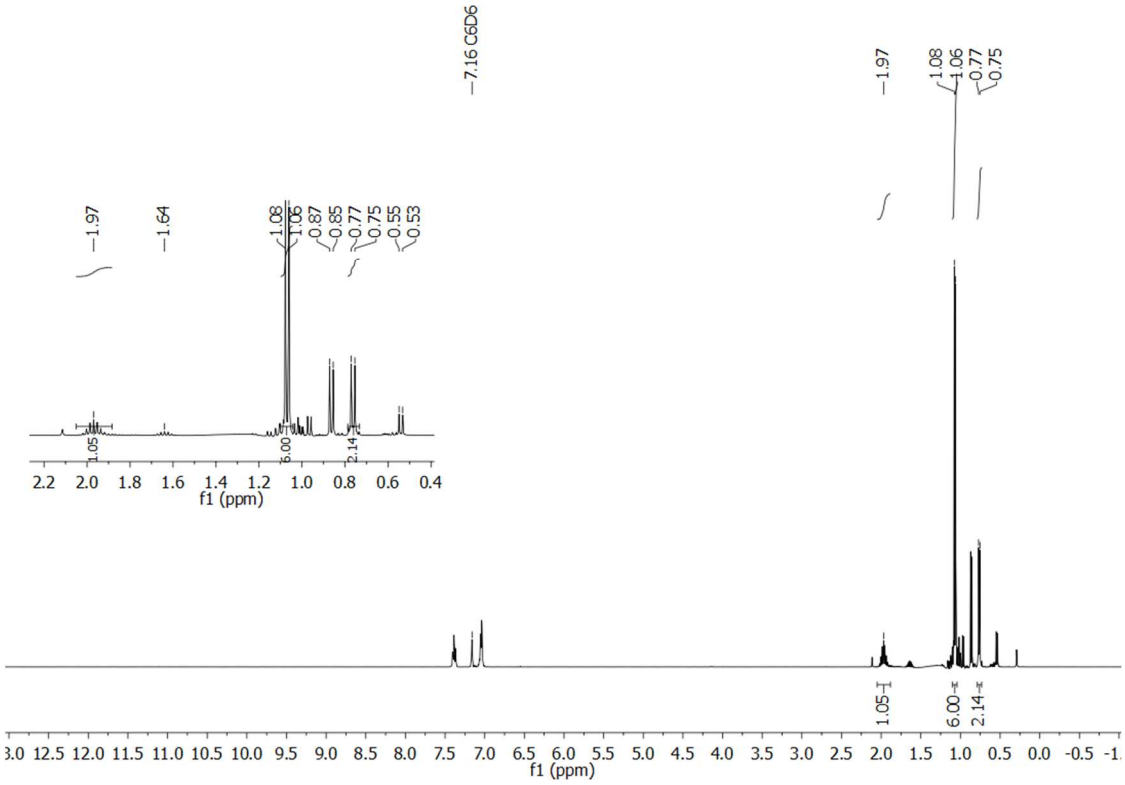

Figure SI 8: ^{1}H NMR spectrum of $\{Au[Ge_9\{Si(iBu)_3\}_3]_2\}^-$ (**3a**) in C_6D_6.

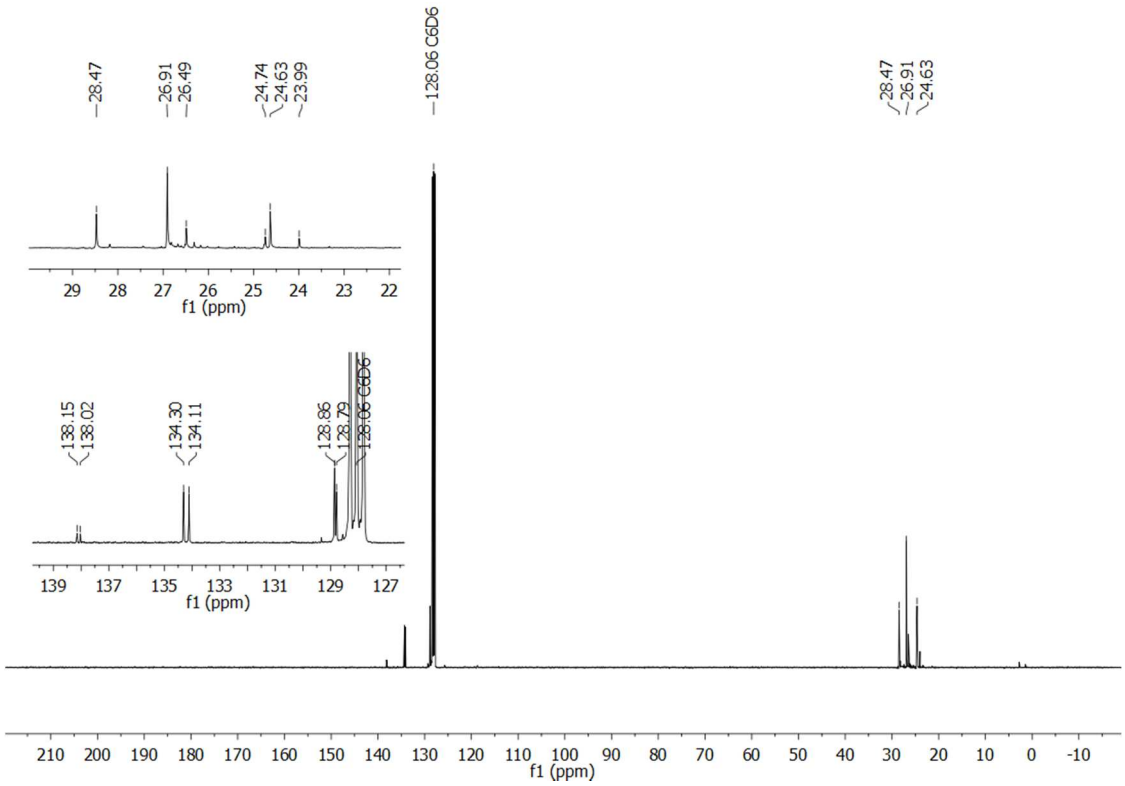

Figure SI 9: ^{13}C NMR spectrum of $\{Au[Ge_9\{Si(iBu)_3\}_3]_2\}^-$ (**3a**) in C_6D_6.

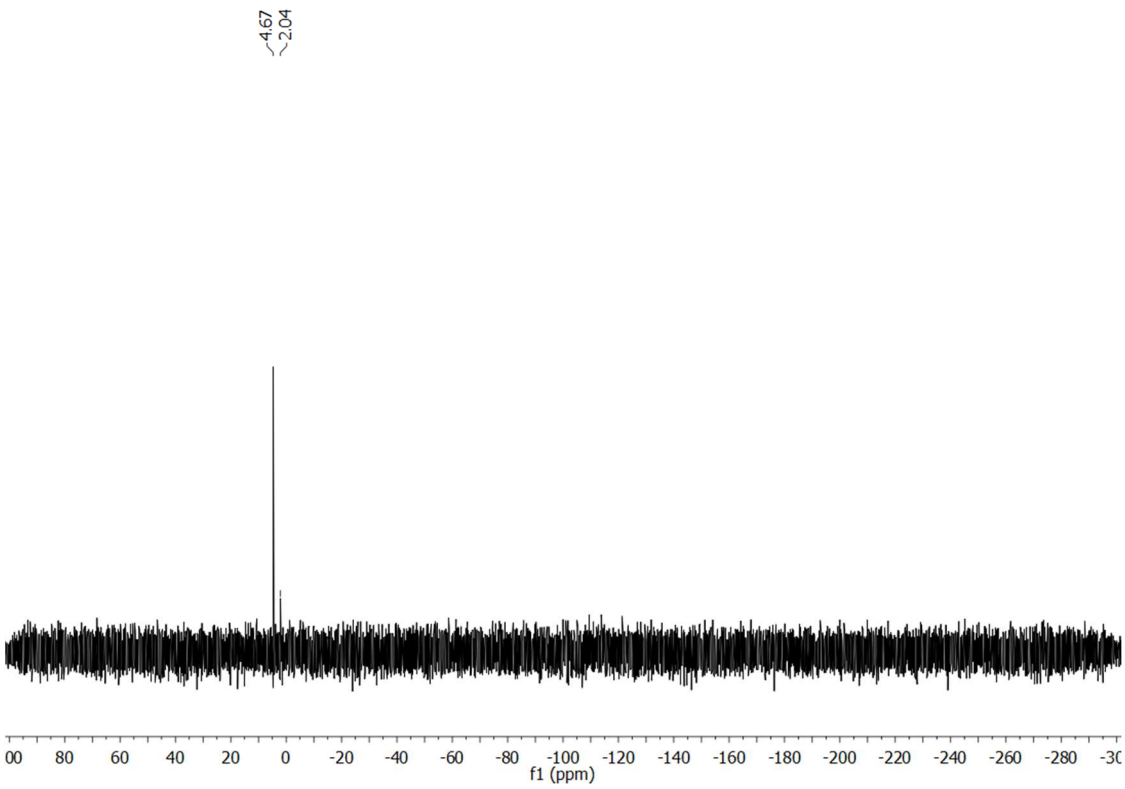

Figure SI 10: ^{29}Si NMR spectrum of $\{Au[Ge_9\{Si(i\text{Bu})_3\}_3]_2\}^-$ (**3a**) in C_6D_6.

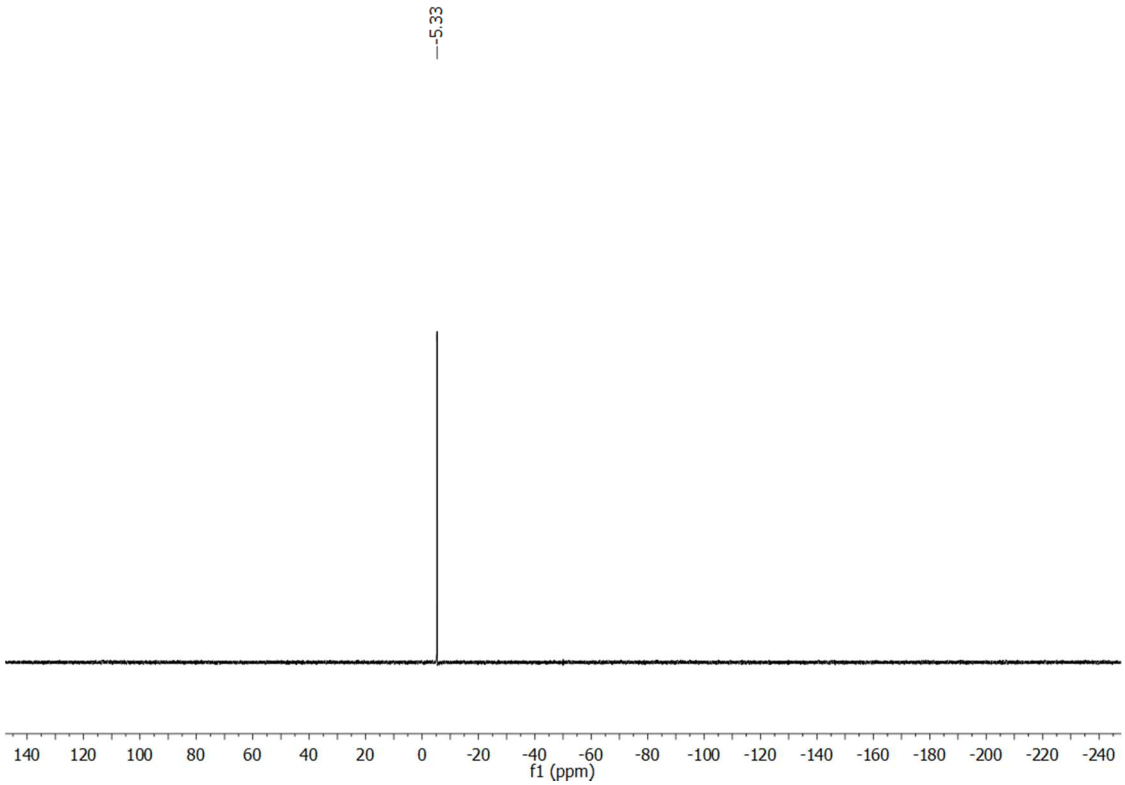

Figure SI 11: ^{31}P NMR spectrum of $\{Au[Ge_9\{Si(i\text{Bu})_3\}_3]_2\}^-$ (**3a**) in C_6D_6.

$(K\text{-}18c6)_2[Ge_9\{Si(i\text{Bu})_3\}_2]$ (**4**):

The ^{1}H NMR spectrum consists of four signals with an integral ratio of 24:2:12:4 for the bis-silylated compound. The bis-silylated anion $[Ge_9\{Si(i\text{Bu})_3\}_2]^{2-}$ (**4a**), obtained from hexane/toluene solution, is observed to be unstable in the more polar solvent CD_3CN over several days and its decomposition can be monitored by time dependent ^{1}H NMR investigation (Figure SI 12b).

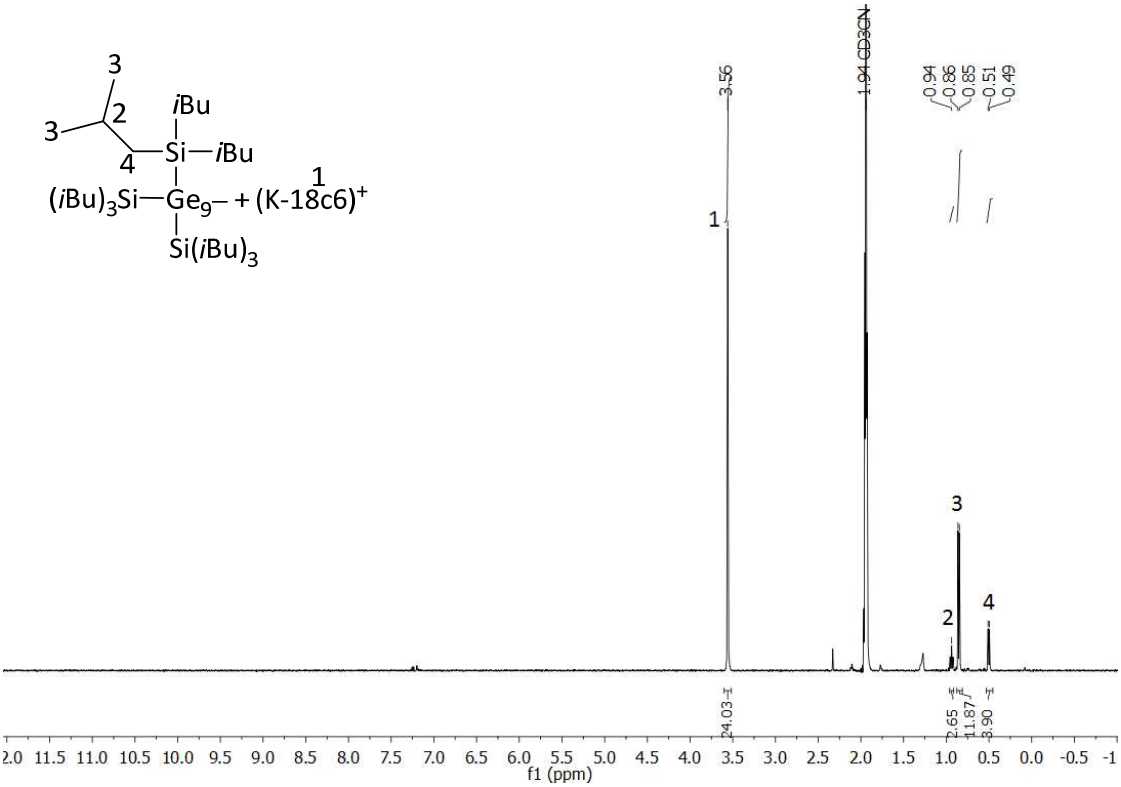

Figure SI 12a: ^{1}H NMR spectrum of $(K\text{-}18c6)_2[Ge_9\{Si(i\text{Bu})_3\}_2]$ (**4**) in CD_3CN.

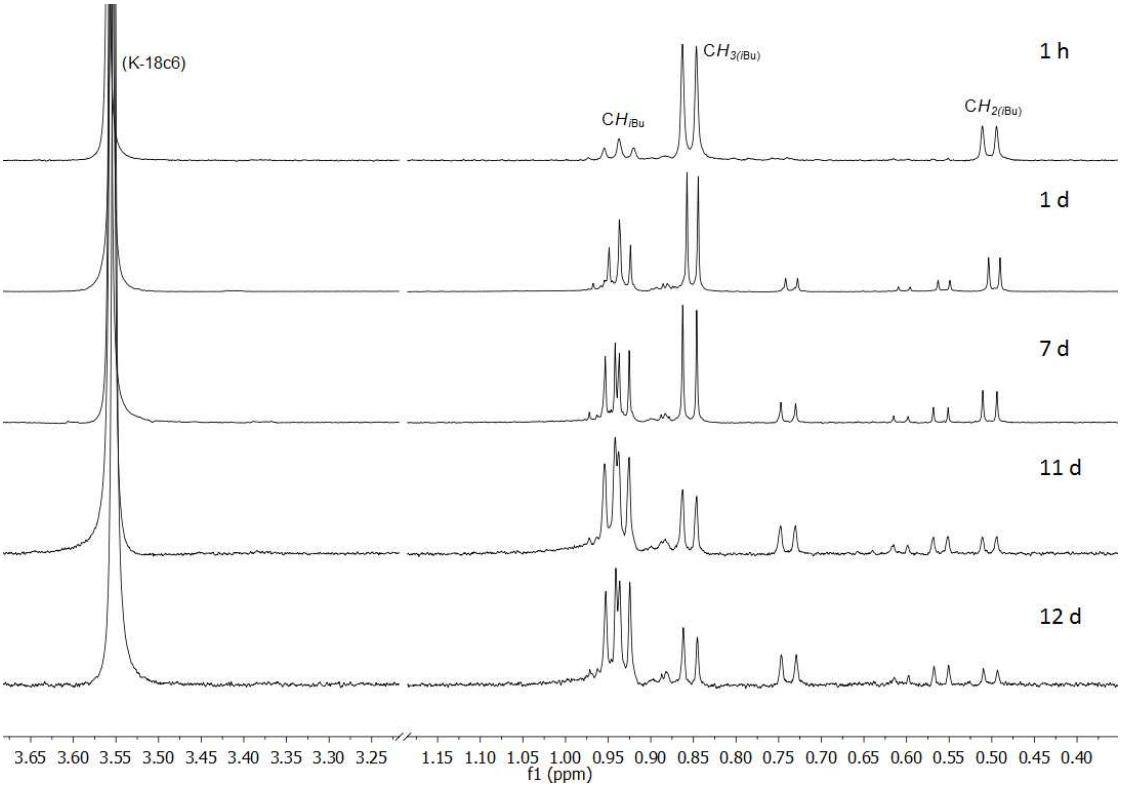

Figure SI 12b: Time-depending ^{1}H NMR spectra of (K-18c6)$_2$[Ge$_9${Si(*i*Bu)$_3$}$_2$] (**4**) in CD_3CN.

2 ESI-MS data of **1a**, **1b**, **1c** and the compounds **2 – 4**

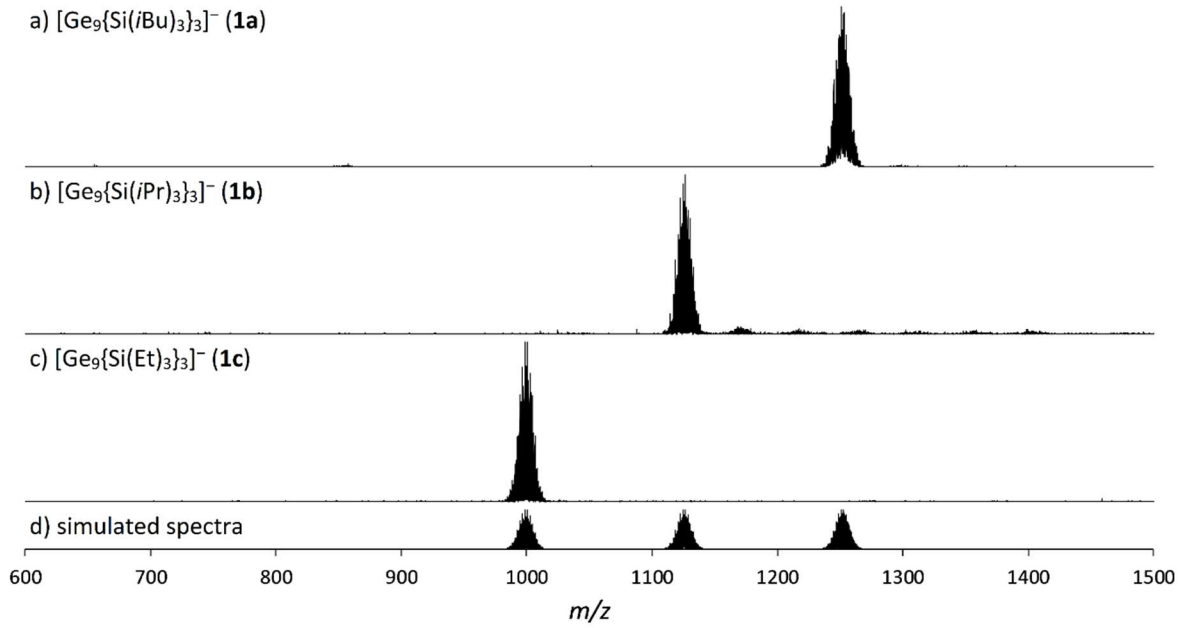

Figure SI 13. Overview on the ESI-MS spectra of the tris-silylated species in acetonitrile. a) $[Ge_9\{Si(i\text{Bu})_3\}_3]^-$ (**1a**) (*m/z* = 1253); b) $[Ge_9\{Si(i\text{Pr})_3\}_3]^-$ (**1b**) (*m/z* = 1126); c) $[Ge_9\{Si(\text{Et})_3\}_3]^-$ (**1c**) (*m/z* = 999); d) simulated spectra of the anions.

<u>$[Ge_9\{Si(i\text{Bu})_3\}_3]^-$ (**1a**):</u>

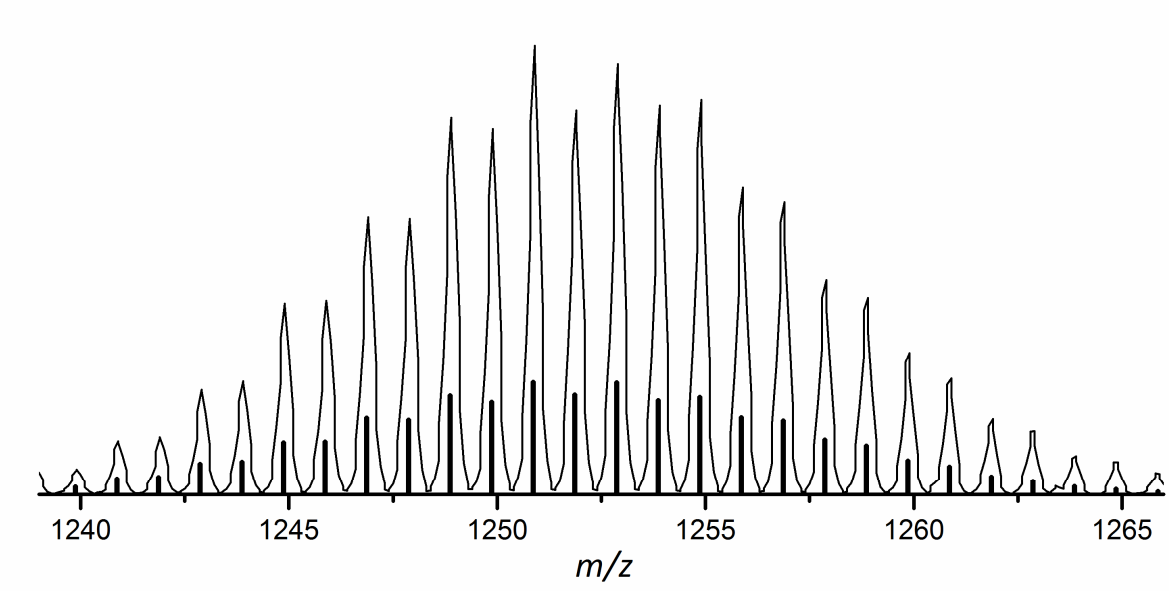

Figure SI 14. ESI-MS spectrum of $[Ge_9\{Si(i\text{Bu})_3\}_3]^-$ (**1a**) (*m/z* = 1253); line: simulated mass spectrum, bars: calculated mass spectrum.

$[Ge_9\{Si(iPr)_3\}_3]^-$ (**1b**):

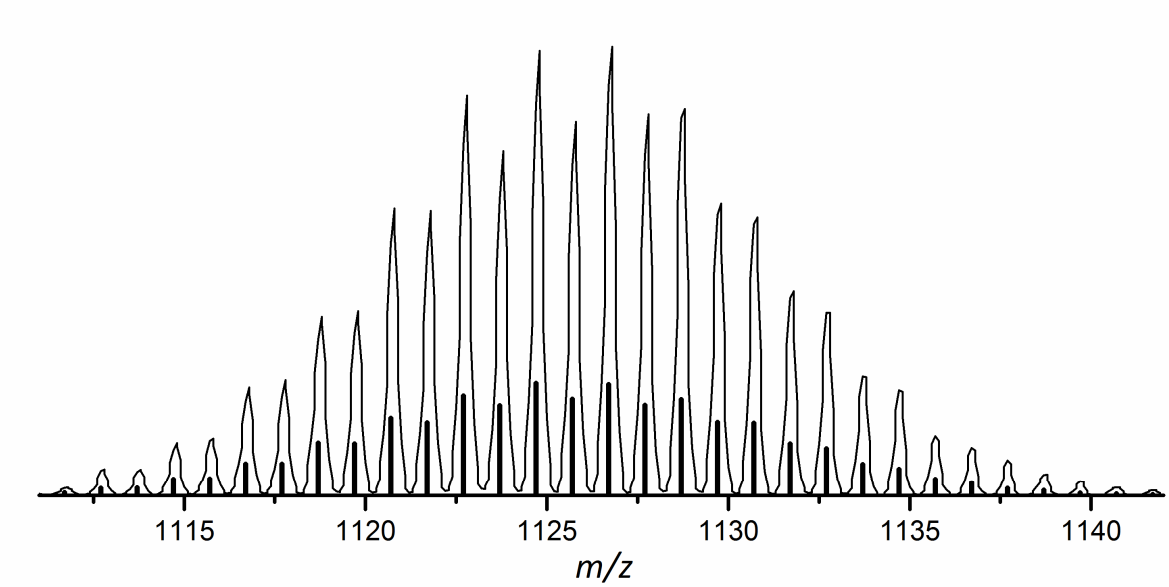

Figure SI 15. ESI-MS spectrum of $[Ge_9\{Si(iPr)_3\}_3]^-$ (**1b**) (*m/z* = 1126) line: measured mass spectrum, bars: simulated mass spectrum.

$[Ge_9\{Si(Et)_3\}_3]^-$ (**1c**):

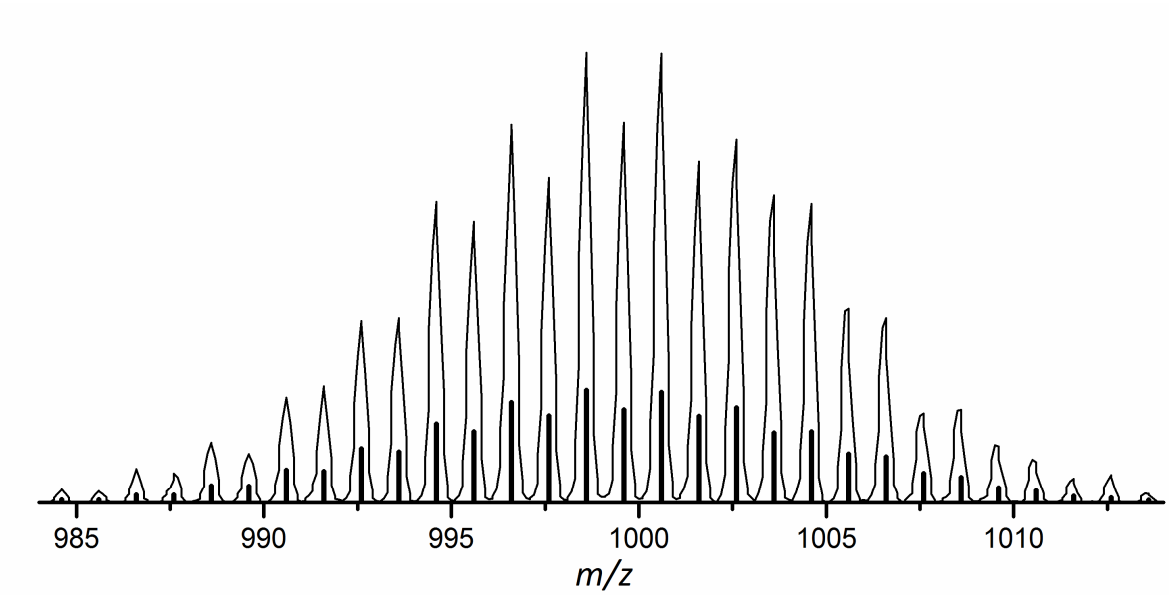

Figure SI 16. ESI-MS spectrum of $[Ge_9\{Si(Et)_3\}_3]^-$ (**1c**) (*m/z* = 999) line: measured mass spectrum, bars: simulated mass spectrum.

(CuNHC^{Dipp})[Ge$_9${Si(*i*Bu)$_3$}$_3$] (**2**):

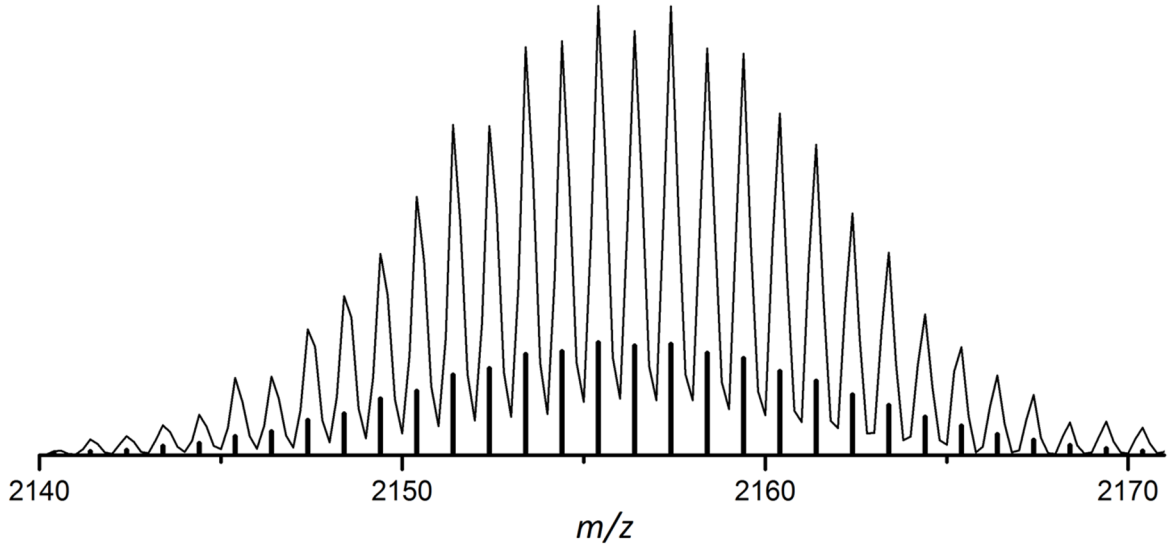

Figure SI 17. ESI-MS spectrum of {(CuNHC^{Dipp})$_2$[Ge$_9${Si(*i*Bu)$_3$}$_3$]}$^+$ (*m/z* = 2155); line: measured mass spectrum, bars: simulated mass spectrum.

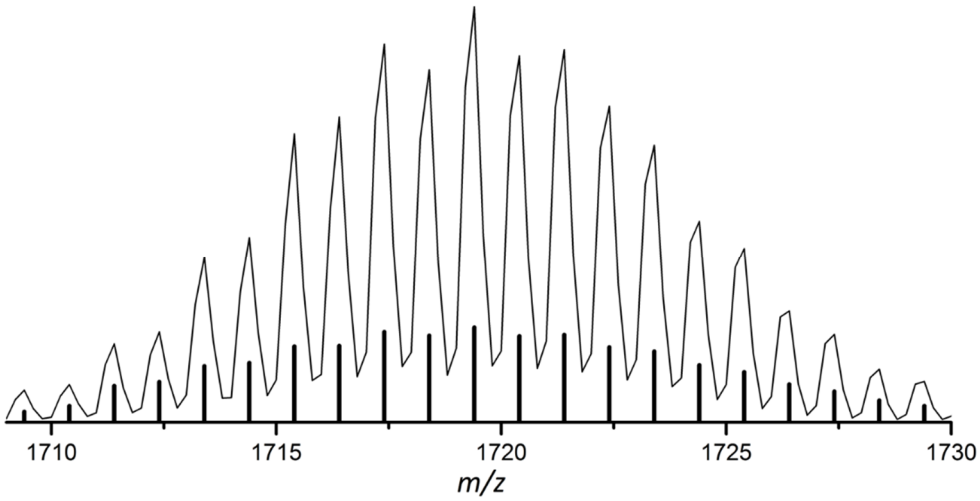

Figure SI 18. ESI-MS spectrum of {(CuNHC^{Dipp})[Ge$_9${Si(*i*Bu)$_3$}$_2$]·3thf}$^+$ (*m/z* = 1719); line: measured mass spectrum, bars: simulated mass spectrum.

(K-18c6)Au[Ge_9{Si(*i*Bu)$_3$}$_3$]$_2$ (**3**):

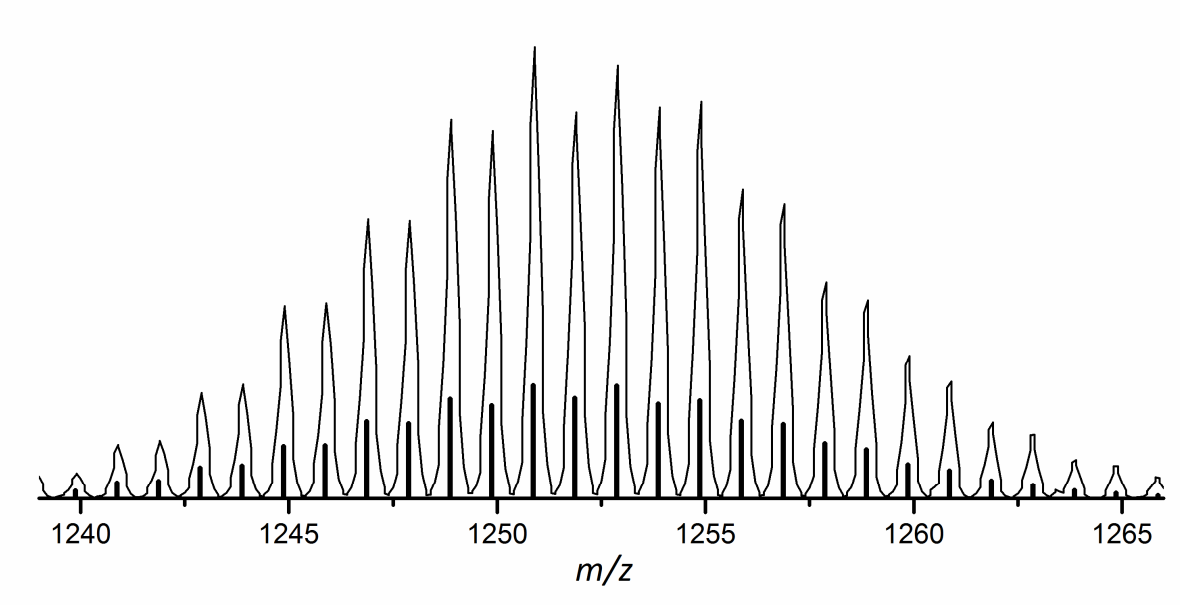

Figure SI 19. ESI-MS spectrum of [Ge_9{Si(*i*Bu)$_3$}$_3$]$^-$ (**1a**) (*m/z* = 1252); line: measured mass spectrum, bars: simulated mass spectrum.

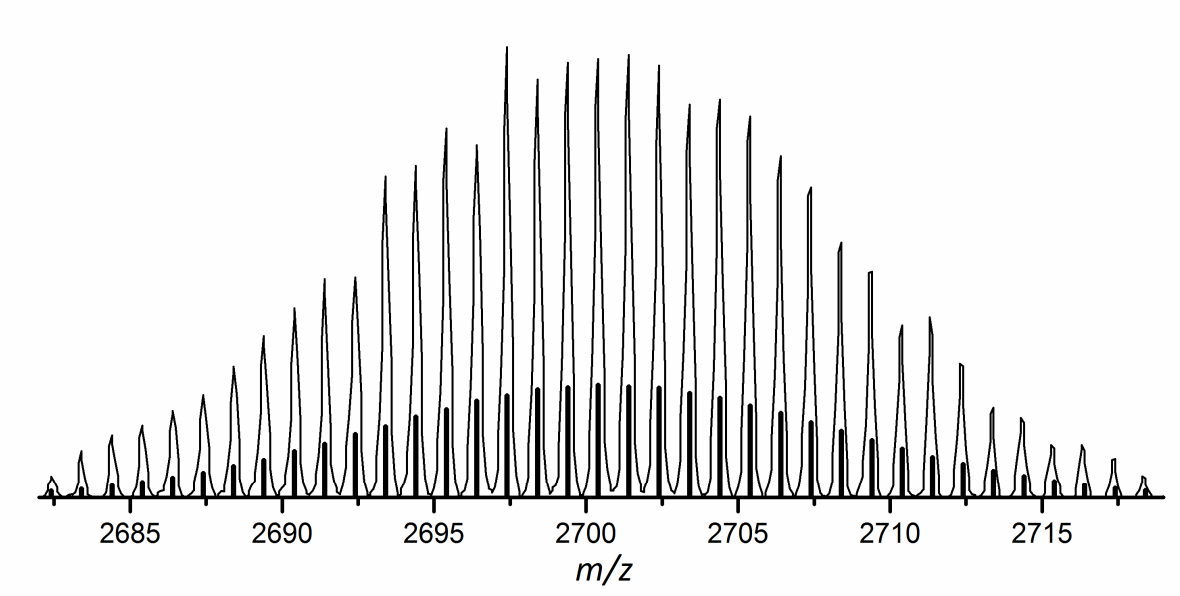

Figure SI 20. ESI-MS spectrum of {Au[Ge_9{Si(*i*Bu)$_3$}$_3$]$_2$}$^-$ (**3a**) (*m/z* = 2701) line: measured mass spectrum, bars: simulated mass spectrum.

(K-18c6)$_2$[Ge$_9${Si(*i*Bu)$_3$}$_2$] (**4**):

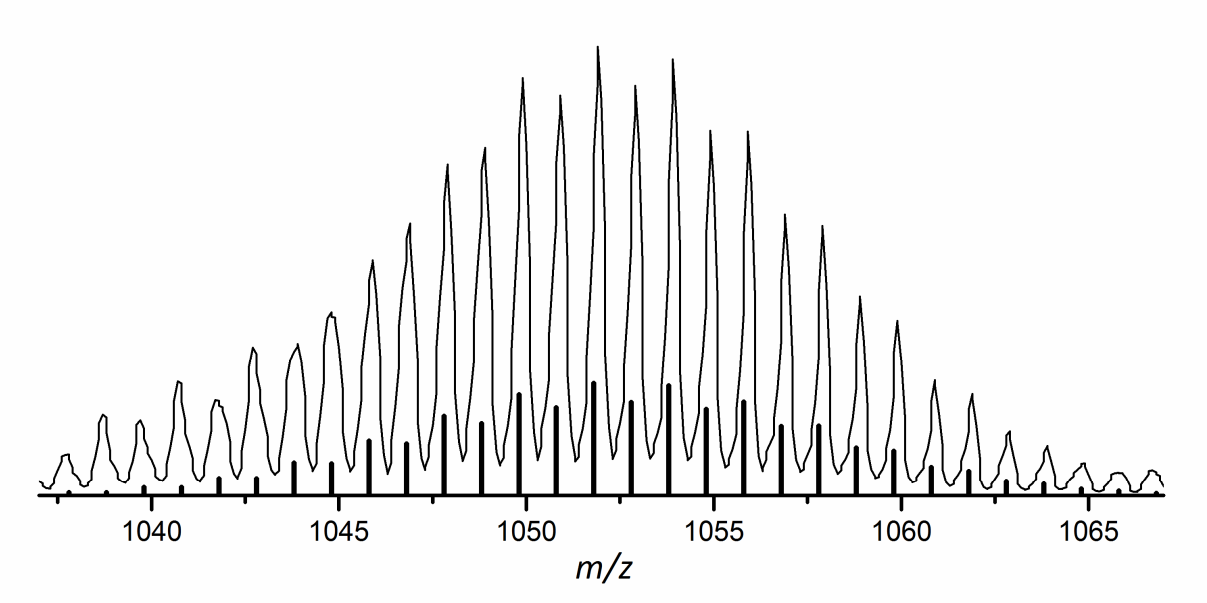

Figure SI 21. ESI-MS spectrum of [Ge$_9${Si(*i*Bu)$_3$}$_2$]$^-$ (**4a**) (*m/z* = 1053; negative mode, 4000 V, 125 °C); line: measured mass spectrum, bars: simulated mass spectrum.

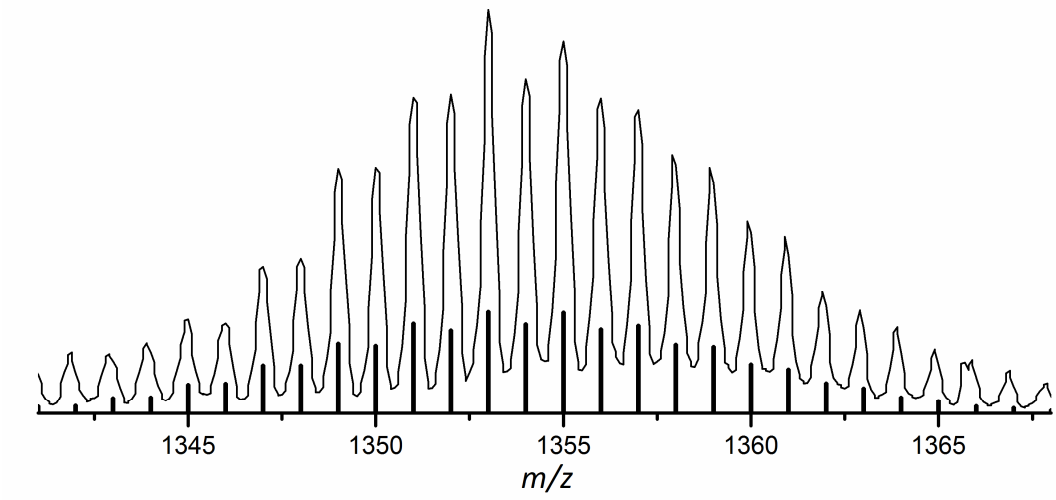

Figure SI 22. ESI-MS spectrum of {(K-18c6)[Ge$_9${Si(*i*Bu)$_3$}$_2$]}$^-$ (*m/z* = 1354); line: measured mass spectrum, bars: simulated mass spectrum.

3 Crystallographic details of the compounds **2 – 4**

Unit cells:

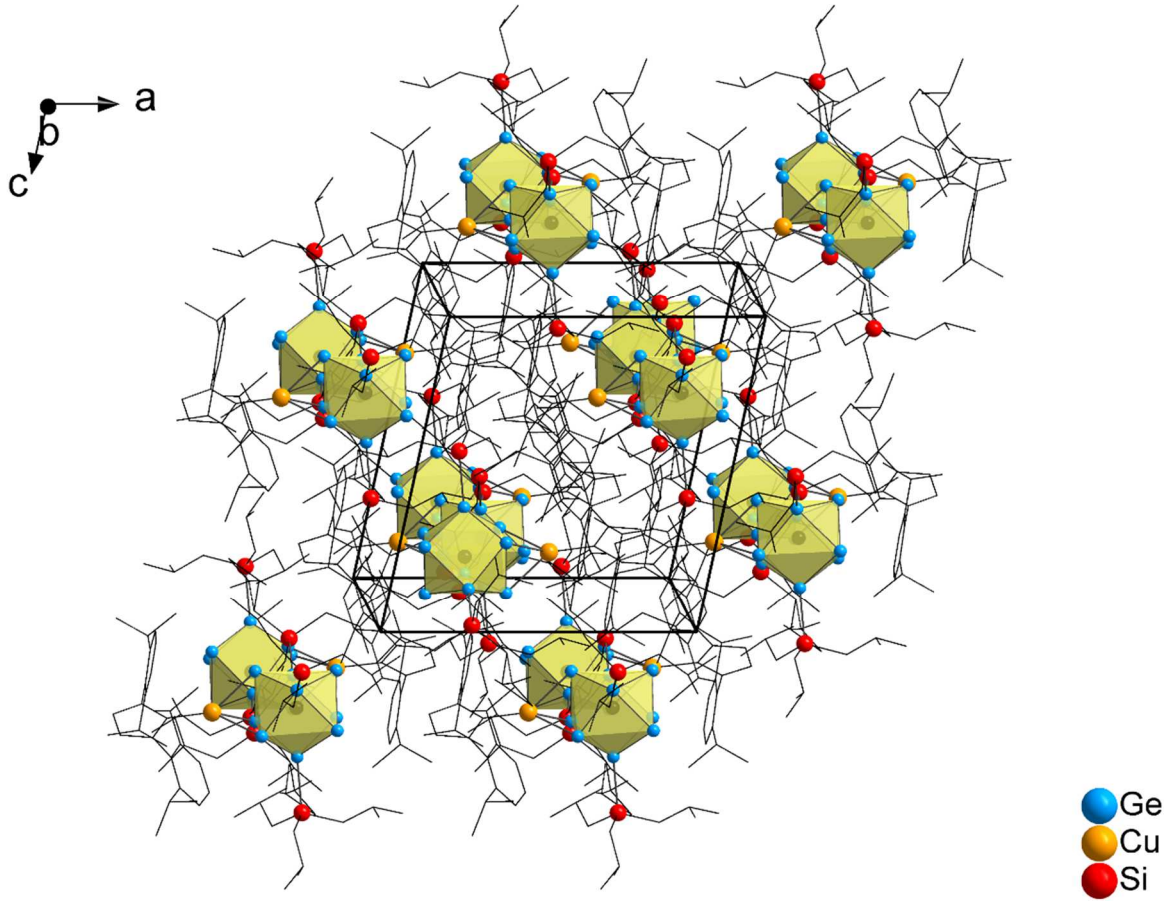

Figure SI 23: Unit cell of compound **2**. Ge atoms are blue, Si atoms red, and Cu atoms orange. The clusters are shown as polyhedra, whereas for reasons of clarity C and N atoms are represented as wire/sticks and H atoms are omitted.

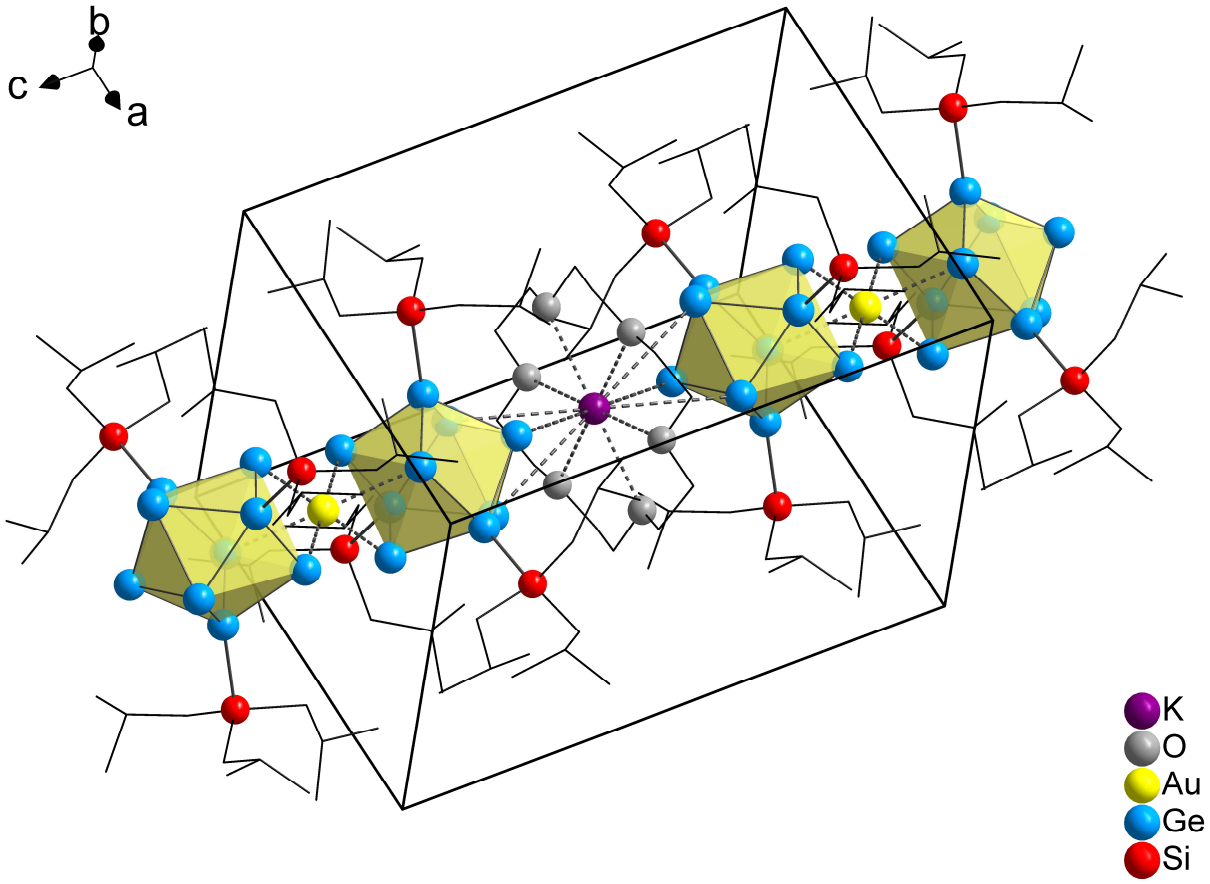

Figure SI 24: Unit cell of compound **3**. Ge atoms are blue, Si atoms red, Au atoms yellow, and K atoms purple. The clusters are shown as polyhedra, whereas for reasons of clarity C atoms are represented as wire/sticks and H atoms are omitted.

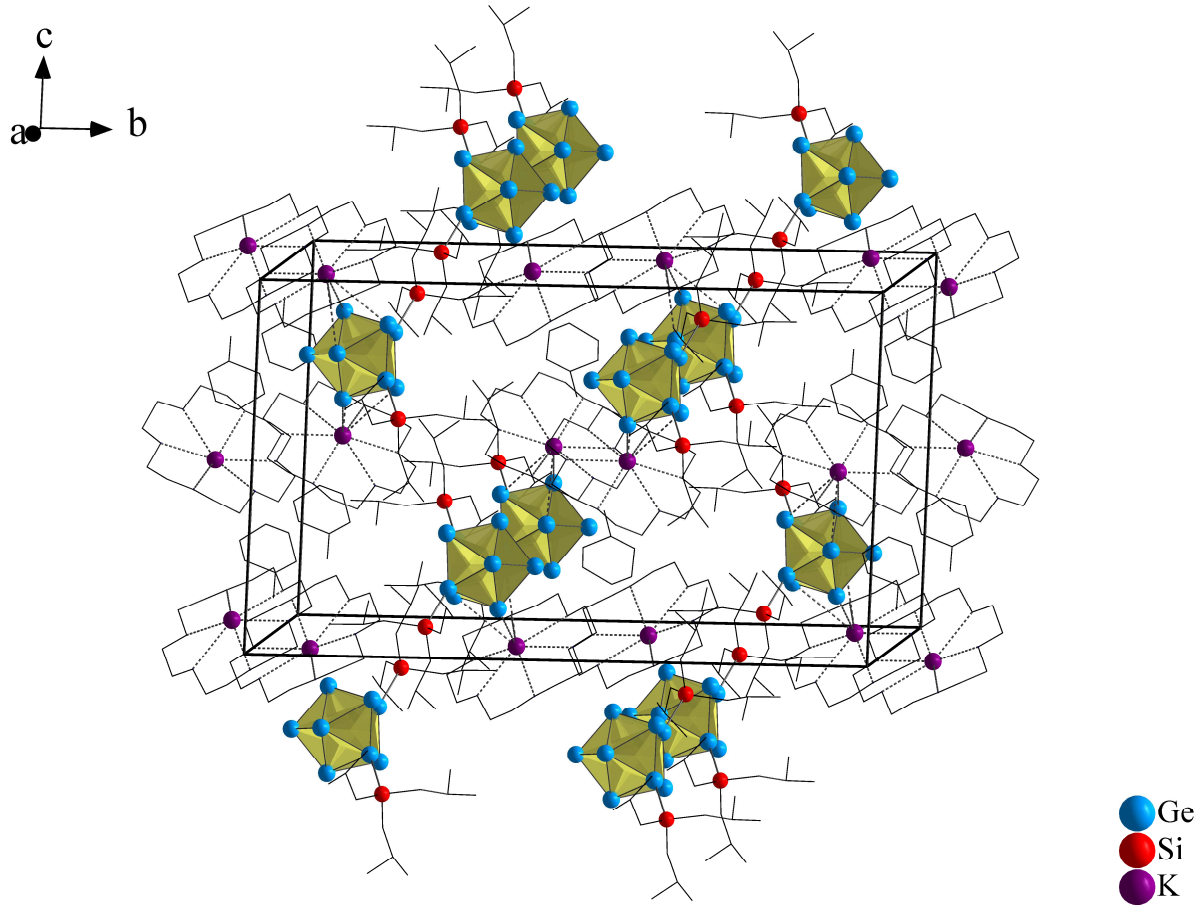

Figure SI 25: Unit cell of compound **4**. Ge atoms are blue, Si atoms red, and K atoms purple. The clusters are shown as polyhedra, whereas for reasons of clarity C and O atoms are represented as wire/sticks and H atoms are omitted.

Selected bond lengths of the compounds **2 – 4**: The molecular structures, including selected atom names, are shown for further clarification.

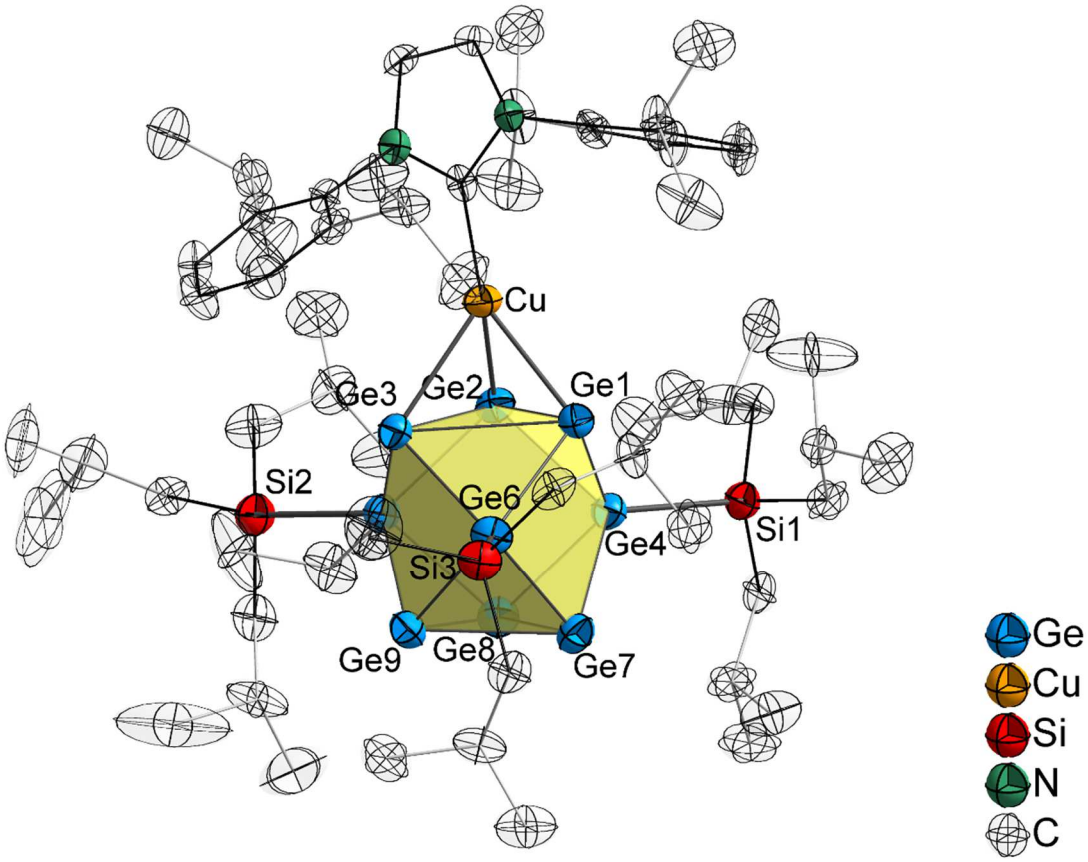

Figure SI 26. Molecular structure **2**. Atoms are shown as ellipsoids with 70 %, H atoms are omitted.

Table SI 1. Selected bond lengths (Å) in **2**.

atom 1	atom 2	distance	atom 1	atom 2	distance
Ge4	Si1	2.3849(11)	Ge1	Ge4	2.5118(5)
Ge5	Si2	2.3826(12)	Ge1	Ge6	2.5023(5)
Ge6	Si3	2.3854(10)	Ge2	Ge4	2.5080(6)
Ge1	Cu1	2.4911(6)	Ge2	Ge5	2.5016(6)
Ge2	Cu1	2.4933(6)	Ge3	Ge5	2.5112(5)
Ge3	Cu1	2.5594(6)	Ge3	Ge6	2.5163(6)
Cu1	C1	1.943(3)	Ge4	Ge7	2.5577(5)
Ge1	Ge2	2.7771(5)	Ge4	Ge8	2.5554(6)
Ge1	Ge3	2.8914(6)	Ge5	Ge8	2.5533(6)
Ge2	Ge3	2.9143(5)	Ge5	Ge9	2.5520(5)
Ge7	Ge8	2.6304(6)	Ge6	Ge7	2.5493(5)
Ge7	Ge9	2.6748(6)	Ge6	Ge9	2.5482(5)
Ge8	Ge9	2.6771(5)			

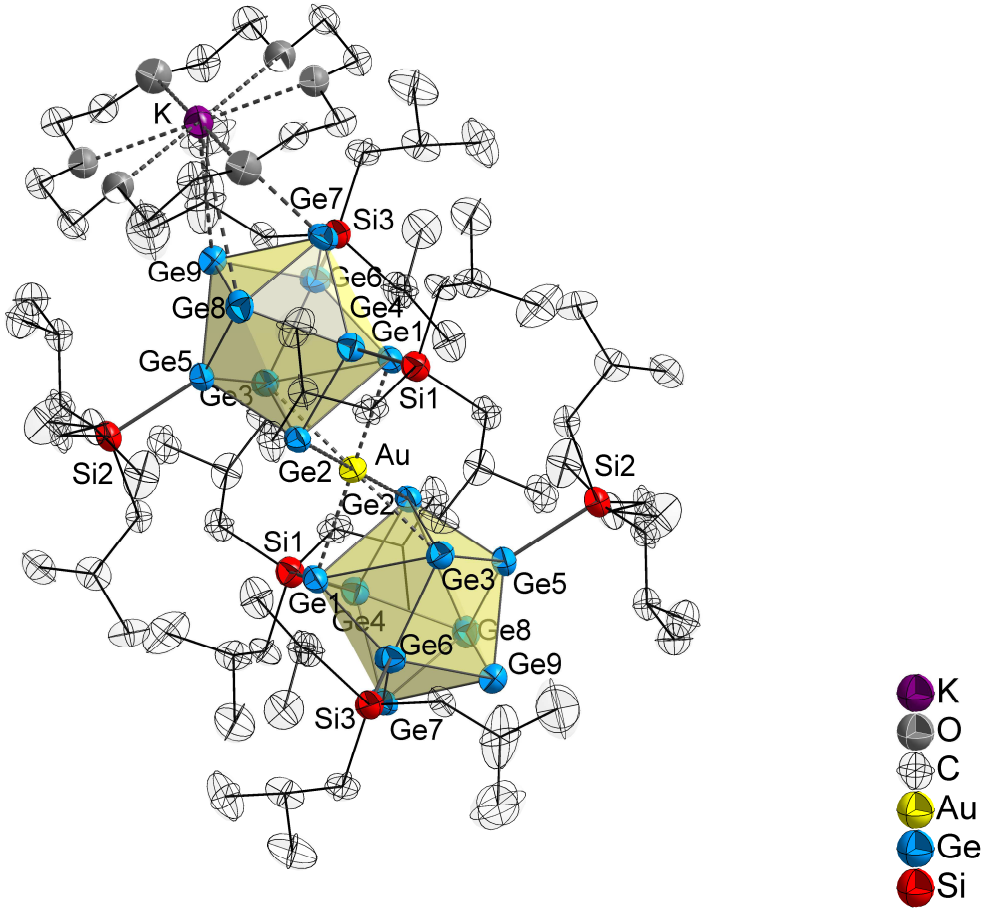

Figure SI 27. Molecular structure **3**. Atoms are shown as ellipsoids with 70 %, H atoms are omitted.

Table SI 2. Selected bond lengths (Å) in **3**.

atom 1	atom 2	distance	atom 1	atom 2	distance
Ge4	Si1	2.391(3)	Ge1	Ge4	2.5110(14)
Ge5	Si2	2.381(2)	Ge1	Ge6	2.5036(12)
Ge6	Si3	2.377(3)	Ge2	Ge4	2.4986(12)
Ge1	Au	2.6651(9)	Ge2	Ge5	2.4981(13)
Ge2	Au	2.6592(9)	Ge3	Ge5	2.4965(12)
Ge3	Au	2.6485(10)	Ge3	Ge6	2.4991(13)
Ge1	Ge2	2.9572(12)	Ge4	Ge7	2.5781(14)
Ge1	Ge3	2.9842(13)	Ge4	Ge8	2.5742(13)
Ge2	Ge3	2.9214(13)	Ge5	Ge8	2.5589(13)
Ge7	Ge8	2.6407(13)	Ge5	Ge9	2.5657(13)
Ge7	Ge9	2.6711(13)	Ge6	Ge7	2.5563(13)
Ge8	Ge9	2.6459(14)	Ge6	Ge9	2.5592(13)

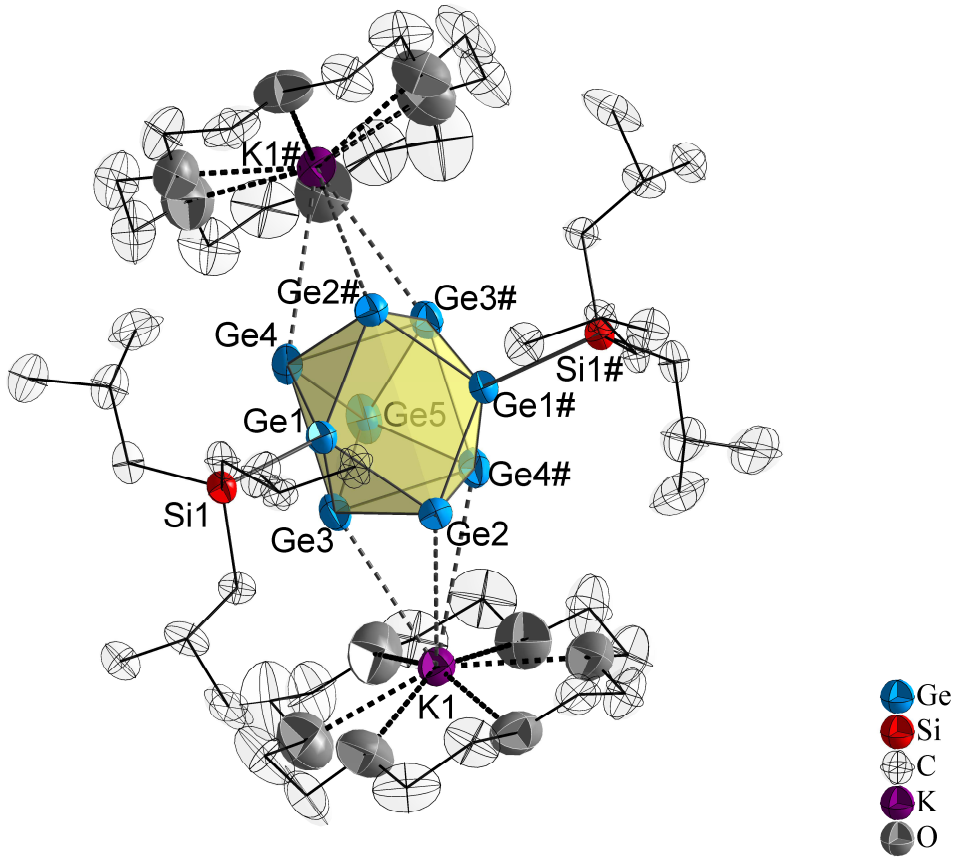

Figure SI 28. Molecular structure **4**. Atoms are shown as ellipsoids with 70 % probability, H atoms are omitted. Symmetry operation: (#) −x+1, y, −z+1.5).

Table SI 3. Selected bond lengths (Å) in **4**.

atom 1	atom 2	distance
Ge1	Si1	2.3807(12)
Ge2	K1	3.8253(11)
Ge3	K1	3.4750(11)
Ge4	K1	3.7259(11)
Ge1	Ge2	2.5228(6)
Ge1#	Ge2#	2.5403(6)
Ge1	Ge3	2.5762(6)
Ge1	Ge4	2.5748(6)
Ge2	Ge3	2.6511(6)
Ge2	Ge4	2.6656(6)
Ge3	Ge4#	2.7396(6)
Ge3	Ge4	2.8659(7)
Ge3	Ge5	2.5745(6)
Ge4	Ge5	2.5847(6)

6.2 On the Reactivity of Silylated Ge_9 Clusters: Synthesis and Characterization of $[ZnCp^*(Ge_9\{Si(SiMe_3)_3\}_3)]$, $[CuPiPr_3(Ge_9\{Si(SiMe_3)_3\}_3)]$, and $[(CuPiPr_3)_4\{Ge_9(SiPh_3)_2\}_2]$

Kerstin Mayer,[‡] Lorenz J. Schiegerl,[‡] and Thomas F. Fässler[*]

published in

Chem. Eur. J. **2016**, *22* (52), 18794-18800.

Access online *via*: https://onlinelibrary.wiley.com/doi/full/10.1002/chem.201603475

[‡] authors contributed equally to this work

Content and contributions:

Ambition of this work was the exploration of clusters metal complexation with silylated Ge_9. The manuscript was authored within the course of my PhD Thesis by me and *Dr. Kerstin Mayer*, and was reviewed by *Prof. Thomas Fässler* before its submission. Evaluation and submission of the single crystal diffraction data were assisted by *Dr. Wilhelm Klein*. Submission of the manuscript was done by *Prof. Thomas Fässler*. The acquisition of the ESI-MS spectra was assisted by *M. Sc. Christina Fischer*. Single crystals of the compounds $[Cu(P^iPr_3)][\{Si(TMS)_3\}_3Ge_9]$ and $[Cu(P^iPr_3)]_4[(SiPh_3)_2Ge_9]_2$ (insufficient X-ray diffraction data sets for publication) and an ESI-MS spectrum of $[(SiPh_3)_3Ge_9]^-$ were initially obtained during my Master's Thesis under supervision of *Dr. Kerstin Mayer* (principal instructor: *Prof. Thomas Fässler*). The EDX spectra were measured by Maria Müller (TECHNICAL UNIVERSITY OF MUNICH). Elemental analyses were carried out in the microanalytical laboratory at the CATALYTIC RESEARCH CENTER of the TECHNICAL UNIVERSITY OF MUNICH

Reaction of the tri-silylated cluster $[\{Si(TMS)_3\}_3Ge_9]^-$ with $Zn(Cp^*)_2$ and $Cu(P^iPr_3)Cl$ yielded the cluster metal compounds $[Zn(Cp^*)][\{Si(TMS)_3\}_3Ge_9]$ and $[Cu(P^iPr_3)][\{Si(TMS)_3\}_3Ge_9]$. Synthesis and characterization (NMR, ESI-MS, EDX analysis, elemental analysis) of $[Cu(P^iPr_3)][\{Si(TMS)_3\}_3Ge_9]$ were done by me. Synthesis and characterization (NMR, SC-XRD, ESI-MS, EDX) of $[Zn(Cp^*)][\{Si(TMS)_3\}_3Ge_9]$ were done by *Dr. Kerstin Mayer*. Reaction of K_4Ge_9 with $SiPh_3Cl$ yielded $[(SiPh_3)_3Ge_9]^-$ and $[(SiPh_3)_2Ge_9]^{2-}$. Syntheses and characterization (NMR and ESI-MS) were done by me. Complexation of $[(SiPh_3)_3Ge_9]^-$ with $Cu(P^iPr_3)Cl$ yielded single crystals of $[Cu(P^iPr_3)]_4[(SiPh_3)_2Ge_9]_2$. The compound was characterized (NMR and EDX) by me, SC-XRD was carried out in cooperation with *Dr. Kerstin Mayer*.

ChemPubSoc Europe

DOI: 10.1002/chem.201603475

CHEMISTRY A European Journal Full Paper

Zintl Clusters

On the Reactivity of Silylated Ge_9 Clusters: Synthesis and Characterization of $[ZnCp^*(Ge_9\{Si(SiMe_3)_3\}_3)]$, $[CuPiPr_3(Ge_9\{Si(SiMe_3)_3\}_3)]$, and $[(CuPiPr_3)_4\{Ge_9(SiPh_3)_2\}_2]$

Kerstin Mayer[+], Lorenz J. Schiegerl[+], and Thomas F. Fässler*[a]

Abstract: We report on the synthesis of new derivatives of silylated clusters of the type $[Ge_9(SiR_3)_3]^-$ (R = $SiMe_3$, Me = CH_3; R = Ph, Ph = C_6H_5) as well as on their reactivity towards copper and zinc compounds. The silylated cluster compounds were synthesized by heterogeneous reactions starting from the Zintl phase K_4Ge_9. Reaction of $K[Ge_9\{Si(SiMe_3)_3\}_3]$ with $ZnCl_2$ leads to the already known dimeric compound $[Zn(Ge_9\{Si(SiMe_3)_3\}_3)_2]$ (**1**), whereas upon the reaction with $[ZnCp^*_2]$ the coordination of $[ZnCp^*]^+$ to the cluster takes place (Cp* = 1,2,3,4,5-pentamethylcyclopentadienyl) under the formation of $[ZnCp^*(Ge_9\{Si(SiMe_3)_3\}_3)]$ (**2**). A similar reaction leads to $[CuPiPr_3(Ge_9\{Si(SiMe_3)_3\}_3)]$ (**3**) from $[CuPiPr_3Cl]$ (*i*Pr = isopropyl). Further we investigated the novel silylated cluster units $[Ge_9(SiPh_3)_3]^-$ (**4**) and $[Ge_9(SiPh_3)_2]^-$ (**5**), which could be identified by mass spectroscopy. Bis- and tris-silylated species can be synthesized by the respective stoichiometric reactions, and the products were characterized by ESI-MS and NMR experiments. These clusters show rather different reactivity. The reaction of the tris-silylated anion **4** with $[CuPiPr_3Cl]$ leads to $[(CuPiPr_3)_3Ge_9(SiPh_3)_2]^+$ as shown from NMR experiments and to $[(CuPiPr_3)_4\{Ge_9(SiPh_3)_2\}_2]$ (**6**), which was characterized by single-crystal X-ray diffraction. Compound **6** shows a new type of coordination of the Cu atoms to the silylated Zintl clusters.

Introduction

Although being in the focus of interest for decades, fundamental parts of the reactivity of Zintl phases are still barely understood. The soluble Zintl phases of the tetrel elements provide a direct source for homoatomic cluster compounds. In particular the nine-atom Zintl cluster anions $[E_9]^{n-}$ (E = Si–Pb, n = 2, 3, 4) represent a fascinating class of molecular ions. They exist with different charges, adopt various shapes, and promise outstanding physical and chemical properties. Several review articles have been published that provide an overview of the rich Zintl chemistry.[1]

The reaction potential of Zintl clusters is versatile. It comprises oxidative coupling reactions under formation of dimers,[2] oligomers,[3] or polymers;[4] the insertion of metal ions into cluster compounds leading to endohedrally filled clusters like $[(Pd_2)@Ge_{18}]^{4-}$,[5] $[Pt@Pb_{12}]^{2-}$[6] or $[Cu@E_9]^{3-}$ (E = Sn, Pb);[7] or fragmentation of clusters thereby creating new polymetallic structures, such as $[(Sn_{15})Ti(Cp_2Ti)_2(CpTi)]^+$[8] as a recent example among many others.[1] Another huge field comprises the formation of intermetalloid cluster compounds, in which the nine-atom tetrel clusters often act as a ligand for metal–organic complexes, as in $[Sn_9Cr(CO)_3]^{4-}$,[9] $[Ge_9CuPiPr_3]^{3-}$,[10] or $[E_9\text{-}ZnPh]^{3-}$ (E = Si–Pb).[11] A diminution of the relatively high charge of the Zintl anions by the addition of organic groups gives access to an even more versatile chemistry. The first organo-Zintl cluster was obtained by the reaction of K_4Ge_9 with bis(trimethylsilyl)acetylene (btmsa) in ethylenediamine resulting in the bis-vinylated Ge_9 cluster species $[Ge_9(CH{=}CH_2)_2]^{2-}$.[12] In this reaction the ethylenediamine solvent plays a key role by providing the protons for the formation of the vinyl group from the alkyne.[12a] By this route several vinylated Ge_9 clusters with different chain lengths and organic ligands have been synthesized,[13] and also the linkage of two cluster units has been realized, as shown by the synthesis of the compound $[RGe_9{-}CH{=}CH{-}CH{=}CH{-}Ge_9R]^{4-}$ (R = (2*Z*,4*E*)-7-amino-5-azahepta-2,4-dien-2-yl) obtained from the reaction of K_4Ge_9 with 1,4-bis(trimethylsilyl)butadiyne.[14] Furthermore, the functionalization of Ge_9 clusters increases their solubility in more common organic solvents, so that the vinylated Ge_9 clusters are soluble in acetonitrile (ACN), and functionalization with SiR_3Cl organosilane reagents leads to products that are soluble even in tetrahydrofuran (THF), hexane, or toluene. The first silylated Ge_9 cluster compound $[Ge_9\{Si(SiMe_3)_3\}_3]^-$ was obtained in small amounts starting from GeBr.[15] The synthesis from the Zintl ion $[Ge_9]^{4-}$ was achieved by the heterogeneous reaction of K_4Ge_9 and $Si(SiMe_3)_3Cl$ in ACN.[16] Such silylated cluster compounds are able to undergo further reactions. The dimeric compounds $[M(Ge_9\{Si(SiMe_3)_3\}_3)_2]$ (M = Zn, Cd, Hg) were obtained by reaction with the corresponding MCl_2 salts in THF,[17] and reactions of coinage metal compounds lead to anionic dimeric com-

[a] K. Mayer,[+] L. J. Schiegerl,[+] Prof. Dr. T. F. Fässler
Department Chemie, Technische Universität München
Lichtenbergstraße 4, 85747 Garching (Germany)
E-mail: thomas.faessler@lrz.tum.de

[+] These authors contributed equally to this work.

Supporting information and ORCID(s) from the author(s) for this article are available on the WWW under http://dx.doi.org/10.1002/chem.201603475.

plexes $[M(Ge_9\{Si(SiMe_3)_3\}_3)_2]^-$ (M = Cu, Ag, and Au),[18] but also monomeric cluster units like $[(Ge_9\{Si(SiMe_3)_3\}_3)Cr(CO)_5]^-$ and $[(Ge_9\{Si(SiMe_3)_3\}_3)Cr(CO)_3]^-$ are accessible by this route.[19]

Starting from the precursor phase K_4Ge_9 it is also possible to introduce other silyl groups to the cluster and recently the introduction of R = *i*Bu, *i*Pr, and Et was realized in $[Ge_9(SiR_3)_3]^-$,[20] whereas $[Ge_9\{Si(SiMe_3)_2(SiPh_3)\}_3]^-$ was found in a dimeric Hg^+ complex.[21] Aside from the tris-silylated cluster compounds analogous mono- and bis-silylated derivatives can also be synthesized. The addition of K_4Ge_9 to a solution of tris-silylated Ge_9 clusters leads to the formation of the bis-silylated analogues, which suggests an equilibrium between the different silylated clusters in solution that can be adjusted by the ratio of silylation reactant and Zintl phase.[22] More recent investigations also showed the existence of the anion $[Pd(Ge_9\{Si(SiMe_3)_3\}_3)_2]^{2-}$ formed in the reaction of $[Ge_9\{Si(SiMe_3)_3\}_3]^-$ with $[Pd(PPh_3)_4]$, and the neutral dimeric compound $[Cu_2(PPh_3)(Ge_9\{Si(SiMe_3)_3\}_3)_2]$ was obtained by reaction with $[Cu(PPh_3)_3Br]$.[23] The latter compound consists of the known dimeric unit $[Cu(Ge_9\{Si(SiMe_3)_3\}_3)_2]^-$ with an additional η^3-coordination to $[Cu(PPh_3)]^+$. Additionally, neutral Zintl cluster coinage metal NHC compounds $[M(NHC)(Ge_9\{Si(SiMe_3)_3\}_3)]$[24] were obtained by reaction of $[Ge_9\{Si(SiMe_3)_3\}_3]^-$ and M(NHC)Cl (NHC = *N*-heterocyclic carbene; M = Cu, Ag, Au), being the first compounds combining Zintl-cluster and NHC chemistry.[25] Until recently[20] only clusters with $[Si(SiMe_3)_3]^+$ and $[Si(SiMe_3)_2(SiPh_3)]^+$ groups have been reported.[15,16,21] We expected that less bulky ligands and ligands with different electronic properties might lead to an enhanced and different reactivity, respectively. In order to get a better understanding of the reactions and to improve the reactivity of these species, we studied the reactions of the tris-silylated cluster $[Ge_9\{Si(SiMe_3)_3\}_3]^-$ with organometallic compounds and the influence on the reactivity of the cluster core also by introducing different silyl groups.

Results and Discussion

For the synthesis of the silylated species we followed the Zintl route.[16] The tris-silylated Ge_9 cluster $K[Ge_9\{Si(SiMe_3)_3\}_3]$ is conveniently available in high yields from K_4Ge_9 by means of a heterogeneous reaction in ACN. The crude product can be directly used for further reactions. The reaction with $ZnCl_2$ in ACN leads to the known neutral dimeric compound $[Zn(Ge_9\{Si(SiMe_3)_3\}_3)_2]$ (**1**),[17] first synthesized by Schnepf et al. who used the $[Li(THF)_4]^+$ salt as a starting material. The formation of compound **1** is thus independent from the choice of the cation and solvent (THF or ACN). The crude product (26% yield) was recrystallized from toluene/Et_2O leading to a small amount of bright orange block-like crystals of the new solvate **1**·Et_2O.

^1H, ^{13}C, and ^{29}Si NMR spectroscopy in $[D_6]$benzene confirms the composition of the product. A single-crystal structure determination of the solvate **1**·Et_2O shows that the Zn atom is bridging two $[Ge_9\{Si(SiMe_3)_3\}_3]^-$ cluster units (Figure 1a).

However, when $[ZnCp^*_2]$ is used instead of $ZnCl_2$ a new monomeric compound is formed. Neutral

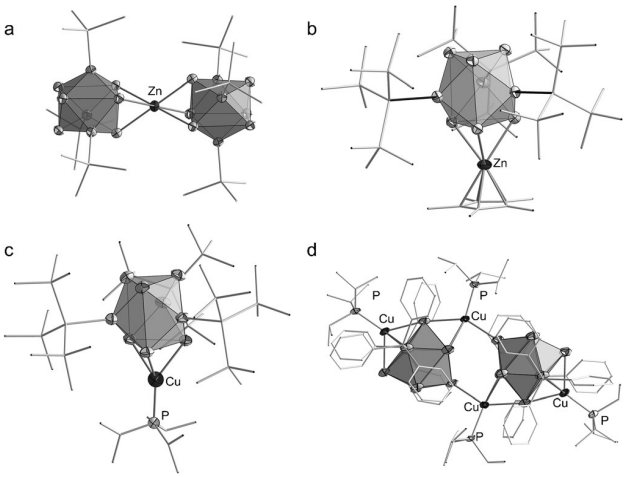

Figure 1. Molecular structures of **1**–**3** and **6** (ellipsoids with 70% probability, $[Ge_9]$ is shown as polyhedron, for reasons of clarity C and Si atoms are drawn as wire-sticks, and H atoms are omitted): a) $[Zn(Ge_9\{Si(SiMe_3)_3\}_3)_2]$ (**1**); b) $[ZnCp^*(Ge_9\{Si(SiMe_3)_3\}_3)]$ (**2**); c) $[CuPiPr_3(Ge_9\{Si(SiMe_3)_3\}_3)]$ (**3**); d) $[(CuPiPr_3)_4\{Ge_9(SiPh_3)_2\}_2]$ (**6**).

$[ZnCp^*(Ge_9\{Si(SiMe_3)_3\}_3)]$ (**2**) (Figure 1b) crystallizes as the toluene solvate **2**·Tol. In this molecule one of the Cp* ligands of $[ZnCp^*_2]$ is substituted by one $[Ge_9\{Si(SiMe_3)_3\}_3]^-$ cluster unit, and KCp* precipitates from the toluene solution. The slightly distorted D_{3h} symmetrical cluster is η^3- and the Cp* ligand η^5-connected to the Zn ion. This is remarkable, since the Cp* ligands in $[ZnCp^*_2]$ are bonded asymmetrically in η^5- and η^1-modes in order to fulfill the "18 electron rule".[26] However, a fluxional behavior of $[ZnCp^*_2]$ is observed in solution.[27] The Zn–Cp* distances in **2**·Tol are, with an average value of 2.28 Å, equal to those in $[ZnCp^*_2]$.[28] The distances of the metal atom to the cluster (2.6380(5)–2.6622(6) Å) are shorter than in the dimeric compound **1**. The Ge–Ge distances of the coordinating triangular polyhedral face of 2.9566(5)–2.9702(5) Å are slightly elongated compared to those in the dimeric compound **1**. The Zn atom in **2** is almost perfectly linearly coordinated with an angle of 177° between the centers of the cluster core and the Cp* ligand. Compound **2** was further characterized by ^1H, ^{13}C, and ^{29}Si NMR spectroscopy in $[D_6]$benzene (Supporting Information).

Similar monomeric compounds have been described in the literature, as for example $[M(NHC)(Ge_9\{Si(SiMe_3)_3\}_3)]$ (M = Cu, Ag, Au),[24] in which the coinage metal is coordinated to one NHC ligand and a tris-silylated Ge_9 cluster. For the coinage metals also dimeric monoanionic complexes $[M(Ge_9\{Si(SiMe_3)_3\}_3)_2]^-$ (M = Cu, Ag, Au) are known.[18] NMR investigations have shown that at elevated temperatures the monomeric $[Ag(NHC)(Ge_9\{Si(SiMe_3)_3\}_3)]$ complexes transform into dimers in which two cluster units coordinate to the Ag atom;[24] this is not the case for the Zn compound **2**.

Phosphines, that compared to NHCs from weaker M-ligand bonds, might lead to an enhanced reactivity of complexes of the tris-silylated cluster. It has been shown that the reaction of $[Cu(PPh_3)_3Br]$ with such a unit resulted in the formation of

[({Ge_9{$Si(SiMe_3)_3$}$_3$-Cu-{$Cu(PPh_3)Ge_9${$Si(SiMe_3)_3$}$_3$}$_3$)].[23] We found that in analogy to **2** also [Cu(P*i*Pr$_3$)Cl] can be added. Reaction of [CuP*i*Pr$_3$]$^+$ with [Ge_9{$Si(SiMe_3)_3$}$_3$]$^-$ in ACN leads to the formation of a brownish precipitate, which could be recrystallized from toluene. The product was identified as [Cu(-P*i*Pr$_3$)(Ge_9{$Si(SiMe_3)_3$}$_3$)$_3$]·0.5 Tol (**3**·0.5 Tol). Purification of the crude product resulted in a red solid (59% yield). Investigation of the bulk product by ^{1}H, ^{13}C, ^{29}Si, and ^{31}P NMR spectroscopy in [D$_6$]benzene as well as elemental analysis showed the high purity of this product (see Supporting Information).

The molecular structure of the neutral monomeric compound **3** is shown in Figure 1 c. The shape of the Ge_9 cluster core corresponds to a slightly distorted D_{3h} symmetric tricapped trigonal prism. As in compounds **1** and **2** the η^3-coordination of the [CuP*i*Pr$_3$]$^+$ fragment causes an elongation of all three prism edges. The Ge–Ge distances in the trigonal prismatic bases without contact to the [CuP*i*Pr$_3$]$^+$ group are in the range of 2.627(1)–2.696(1) Å and thus in accordance with those in the tris-silylated anion. The respective bond lengths within the coordinated fragment are in the range of 2.837(1)–2.918(1) Å. The Ge–Cu distances (2.461(1)–2.519(1) Å) are slightly longer than those in the known complex [$Cu_2(PPh_3)Ge_9${$Si(SiMe_3)_3$}$_3$)$_2$] with an average distance of 2.40 Å.[23] The Ge–Cu distances in **3** compare well with those in [η^4-Ge_9-Cu(P*i*Pr$_3$)]$^{3-}$, with an average value of 2.50 Å,[10] even though in the latter case the more negatively charged [Ge_9]$^{4-}$ cluster coordinates with its open square to the copper ion. This can be attributed to the electronic influence of the different phosphine ligands. Whereas phenyl groups act as electron-withdrawing groups, thereby causing a more positively charged copper ion and a stronger interaction with the singly charged silylated clusters, the *i*Pr groups are much less electron-withdrawing. This may also explain the formation of the dimeric [$Cu_2(PPh_3)$(Ge_9{$Si(SiMe_3)_3$}$_3$)$_2$][23] instead of the monomeric compound **3**, since the ligand PPh_3 is more easily eliminated than P*i*Pr$_3$. The monomeric compound [Cu(NHC)-(Ge_9{$Si(SiMe_3)_3$}$_3$)][24] shows slightly longer Ge–Cu distances (average 2.53 Å), probably due to the bulkier carbene ligand.

The known silylated Ge_9 clusters [Ge_9{$Si(SiMe_3)_3$}$_3$]$^-$[15] and [Ge_9{$Si(SiMe_3)_2(SiPh_3)$}$_3$]$^-$[21] carry both very bulky substituents. Therefore, we attempted to synthesize silylated species with sterically less demanding silyl groups.[20] The reaction of K_4Ge_9 with three equivalents of $SiPh_3Cl$ in ACN leads to a spontaneous coloring of the solution, similar to other known reactions.[16,21] Investigation of the resulting red solution by ESI-MS and NMR spectroscopy shows the formation of the tris-silylated species [$Ge_9(SiPh_3)_3$]$^-$ (**4**). In contrast, the reaction with two equivalents of $SiPh_3Cl$ under identical conditions leads to the formation of the bis-silylated species [$Ge_9(SiPh_3)_2$]$^-$ (**5**), indicating that both species are available by the stoichiometric control of the reaction. The ESI-MS investigations (Figure 2) of the reaction solutions show exclusively the tris-silylated species **4** (negative mode: [$Ge_9(SiPh_3)_3$]$^-$ m/z = 1432; positive mode: K_2[$Ge_9(SiPh_3)_3$]$^+$ m/z = 1510) with three equivalents of $SiPh_3Cl$, whereas with two equivalents of $SiPh_3Cl$ mainly bis-silylated species **5** (negative mode: K[$Ge_9(SiPh_3)_2$]$^-$ m/z = 1212; positive mode: K_3[$Ge_9(SiPh_3)_2$]$^+$ m/z = 1290) together with small amounts of mono-silylated (m/z = 913) and "naked" Ge_9 (m/z = 654) clusters are observed. It should be mentioned that polyanionic Zintl ions often appear as mono-anions in the ESI-MS experiments, apparently due to their partial oxidation by the attracting positive electrode in the mass spectrometer.[23]

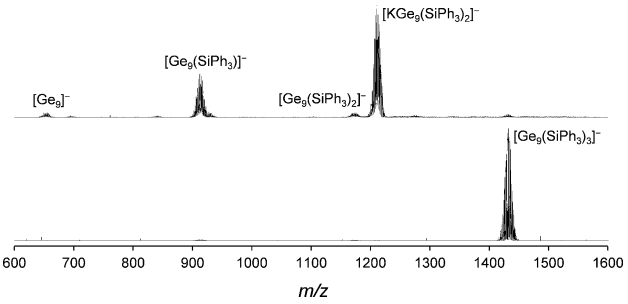

Figure 2. ESI-MS spectra of the anions **4** and **5**. Reaction with three equivalents of the silyl reactant (bottom) results in the almost selective formation of the tris-silylated product **4**. By addition of two equivalents (top) the bis-(**5**) and the mono-silylated products as well as the "naked" [Ge_9]$^{4-}$ cluster can be observed.

Evidently, the stability of the tris-silylated compound is higher under ionization conditions, but a fragmentation of the unit [$Ge_9(SiPh_3)_3$]$^-$ (**4**) into [$Ge_9(SiPh_3)_2$]$^-$ (**5**), [$Ge_9(SiPh_3)$]$^-$ and [Ge_9]$^{4-}$ can take place depending on the choice of the measurement conditions. The same behavior has been observed for [Ge_9{$Si(SiMe_3)_3$}$_3$]$^-$ in further experiments.

^{1}H NMR investigations of solutions of the potassium salts of **4** and **5** in [D$_3$]ACN reveal different shifts of the signals of the phenyl groups. For the bis- and tris-silylated species, the signals are shifted with respect to the signals of $SiPh_3Cl$ (7.71–7.65 ppm and 7.15–7.06 ppm). For K_2[$Ge_9(SiPh_3)_2$] we found resonances between 7.52–7.48 ppm and 7.21–7.14 ppm, and signals between 7.63–7.56 ppm and 7.37–7.25 ppm for K[$Ge_9(SiPh_3)_3$]. All signals show an integral ratio of 2:3 and both spectra reveal the presence of traces of the respective other compound. The ^{13}C NMR spectra reveal four carbon signals each for the four different aromatic carbon atoms of the respective species (K_2[$Ge_9(SiPh_3)_2$]: 143.17, 137.18, 128.61, and 127.59 ppm; K[$Ge_9(SiPh_3)_3$]: 139.74, 137.17, 129.97, and 128.42 ppm), which can be clearly distinguished from the resonances of the reactant $SiPh_3Cl$ (135.66, 133.41, 130.93, and 128.45 ppm). In the ^{29}Si NMR experiments the bis- and tris-silylated species show one signal (K_2[$Ge_9(SiPh_3)_2$]: 6.36 ppm; K[$Ge_9(SiPh_3)_3$]: 8.00 ppm; $SiPh_3Cl$: 1.21 ppm). Thus, it has been confirmed that, depending on the applied stoichiometry, the Ge_9 clusters can be gradually silylated by $SiPh_3Cl$.

Up to now the crystallization of compounds with the silylated cluster anions **4** and **5** was not successful, but NMR and ESI-MS experiments clearly reveal the progress of the silylation reactions and the existence of these silylated species. The reaction of **4** with [CuP*i*Pr$_3$Cl] in ACN results in a brown precipitate. Layering a solution of this solid in toluene with hexane leads to orange block-shaped crystals of the composition [(Cu-P*i*Pr$_3$)$_4${$Ge_9(SiPh_3)_2$}$_2$]·3.4 Tol (**6**·3.4 Tol). The molecular structure of **6** (shown in Figure 1 d) contains two doubly bridged bis-silylat-

ed $[Ge_9(SiPh_3)_2]^{2-}$ (**5**) units. The Ge—Si distances in a range of 2.401(4)–2.416(4) Å are longer than those in $[Ge_9\{Si(SiMe_3)_3\}_3]^-$ (2.37 Å). Since the cone angle of $SiPh_3$ is smaller than that of $Si(SiMe_3)_3$, the distance elongation may not be caused by a steric but an electronic effect resulting in weaker Ge—Si bonds.[30] However, the most striking structural feature in compound **6** is that the tris-silylated clusters are bridged by two $[CuPiPr_3]^+$ units in a coordination mode that has not been observed before. The copper ions are η^3-coordinated to three Ge atoms of a triangular face of one cluster and bind to only one Ge atom of the other. A third and fourth $[CuPiPr_3]^+$ group is attached to a square of each of the two bis-silylated clusters under formation of an uncharged complex. An even larger number of bridging metal atoms has been observed before in $[Ge_9Au_3Ge_9]^{5-}$,[31] in which three Au atoms in a triangular arrangement each bridge two Ge atoms of two different bare $[Ge_9]^{4-}$ clusters leading to three coplanar triangles $[Ge_9Au_3Ge_9]^{5-}$. The bis-silylated cluster $[Ge_9(SiPh_3)_2]^{2-}$ (**5**) as a fragment of **6** adopts the shape of a strongly distorted C_{4v} symmetric mono-capped square antiprism with a strong distortion towards C_{2v} symmetry. The undistorted variant is usually observed for the bare $[Ge_9]^{4-}$ cluster. The open rectangular faces with two ligands attached to two opposed Ge atoms of the open square deviate from planarity (ideal 0°) by a torsion angle of 14.1° and 14.6° and are each capped by a $[CuPiPr_3]^+$ fragment. The capping Ge atom of the square antiprism of this cluster is connected to the Cu atom of the second $[CuPiPr_3]^+$ fragment. A third Cu atom is η^3-coordinated to an open triangular face of the cluster (Figure 3 b). Comparable

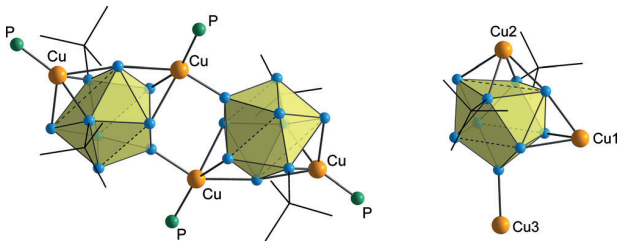

Figure 3. Details of the molecular structure of $[(CuPiPr_3)_4\{Ge_9(SiPh_3)_2\}_2]$ (**6**). Left: the dimeric structure of the two clusters. Right: The coordination modes of the Cu atoms to one $[Ge_9]^{4-}$ cluster unit. The four silyl-groups are η^1-bonded, the two terminal $[CuPiPr_3]^+$ fragments are η^4-connected. The two bridging $[CuPiPr_3]^+$ fragments show a η^1-bonding mode to one cluster and a η^3-coordination to the other. Ge atoms are blue, Cu atoms orange and P atoms green. The silyl groups are shown schematically.

cluster shapes are described for other clusters carrying two ligands such as the bis-vinylated species,[12a] $[Ge_9(GePh_3)_2]^{2-}$ and $[Ge_9(SnPh_3)_2]^{2-}$[32] and the recently reported $[Ge_9\{Si(SiMe_3)_3\}_2]^{2-}$.[22a] The coordination of the open square of a bis-functionalized cluster has not been reported before, but it resembles the η^4-coordination of $[CuPR_3]^+$ to a $[Ge_9]^{4-}$ cluster.[10] The Cu—Ge bond lengths of the η^4 coordination with an average value of 2.51 Å compare well to the distances in $[\eta^4\text{-}Ge_9\text{-}CuPiPr_3]^{3-}$ (2.50 Å) and are slightly shorter than in $[(\eta^4\text{-}Ge_9)\text{-}Cu\text{-}(\eta^1\text{-}Ge_9)]^{7-}$ (2.57 Å).[10] The bond lengths of the η^3-coordinated copper atoms (average of 2.59 Å) are longer than those in **3**; this might be attributed to the higher coordination number of Cu. An η^1-coordination to a second cluster is also observed in $[(\eta^4\text{-}Ge_9)\text{-}Cu\text{-}(\eta^1\text{-}Ge_9)]^{7-}$, which, however, shows a significantly shorter Cu—Ge distance of 2.42 Å as the one observed in **6** (2.57 Å), probably due to the much higher charge of the former unit.

A comparison of the arrangement of the units in compound **6** with the structure of the tris-silylated unit $[Ge_9\{Si(SiMe_3)_3\}_3]^-$, in which all capping atoms are attached to the silyl group, reveals that the η^1-connection to the bridging $[CuPiPr_3]^+$ in **6** can be regarded as the third ligand that occupies the position of the third silyl group leading to a C_{2v}-distortion of the C_{4v} symmetry. Thus, three different coordination modes of the $[CuPiPr_3]^+$ unit are present in compound **6**, which is shown in more detail in Figure 3 a.

NMR investigations of the dried crude product of the reaction performed in [D$_6$]benzene give clear hints for an initial formation of the species $[(CuPiPr_3)_3Ge_9(SiPh_3)_2]^+$ (Figure 4) in solution. The ^{1}H NMR spectrum (Figure 4) shows the signals of

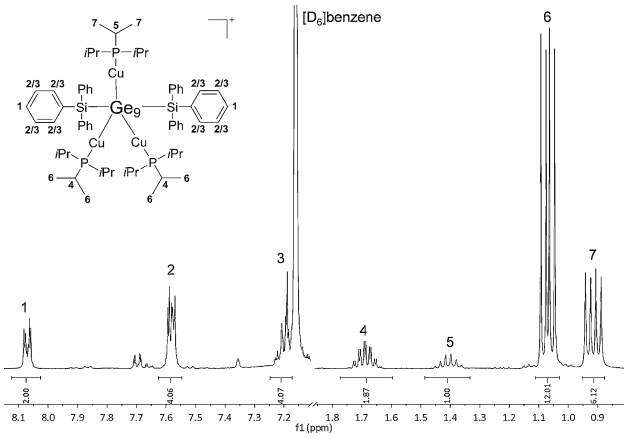

Figure 4. ^{1}H NMR spectrum of the crude product of $[(CuPiPr_3)_4\{Ge_9(SiPh_3)_2\}_2]$ (**6**), suggesting the formation of the monomeric compound $[Ge_9(SiPh_3)_2(CuPiPr_3)_3]^+$ in solution. Dimerization and abstraction of $[CuPiPr_3Cl]$ then lead to the formation of the dimeric compound **6**.

a bis-silylated species with an integral ratio of 1:2:2 for the phenyl protons and the presence of two different *i*Pr groups with integral ratios of 1:6 and 2:12. The affiliation of the different signals has been determined by 2D NMR experiments, and the signals could easily be distinguished from those of the reactant $[CuPiPr_3Cl]$ at 1.87 ppm ($CH(CH_3)_2$) and 1.18 ppm ($CH(CH_3)_2$). Thus, the integration of the proton signals reveals the presence of two identical (1.69 ppm ($CH(CH_3)_2$) and 1.07 ppm ($CH(CH_3)_2$) and one different *i*Pr group (1.40 ppm ($CH(CH_3)_2$) and 0.92 ppm ($CH(CH_3)_2$)) per bis-silylated species $[Ge_9(SiPh_3)_2]^{2-}$ (**4**). The two distinct groups of signals indicate that the $[CuPiPr_3]^+$ units bind to Ge_9 within two different coordination modes: a $[\eta^1\text{-}CuPiPr_3]^+$ unit substitutes the $[SiPh_3]^+$ group, and the two remaining identical $[CuPiPr_3]^+$ groups are η^3- or η^4-coordinated to the cluster core.

The ^{29}Si NMR spectrum shows exclusively one signal for the silylated cluster species (4.21 ppm) that is clearly different from that of the bis- and tris-silylated Ge_9 clusters $K[Ge_9(SiPh_3)_3]$ and $K_2[Ge_9(SiPh_3)_2]$ (6.36 ppm and 8.00 ppm, respectively). Conclusively, the ^{31}P NMR spectrum shows only two signals (36.50 and 19.49 ppm) which are different from that of $[CuPiPr_3Cl]$ (24.19 ppm), originating from the two not identical $[CuPiPr_3]^+$ groups. In the ^{13}C NMR spectrum the signals of two different $[CuPiPr_3]^+$ groups (doublet splitting due to the coupling to phosphorus) together with the four new aromatic $[SiPh_3]^+$ signals are detected.

Conclusion

The reactivity of the tris-silyated cluster $[Ge_9\{Si(SiMe_3)_3\}_3]^-$ and its derivatives $[Ge_9(SiPh_3)_3]^-$ has been investigated. The silylated clusters act as a η^3-ligand in organometallic complexes, but also cluster expansion reactions have been reported.[33] The monomeric $[\eta^3\text{-}Ge_9R_3]^-$ cluster units react with $[ZnCp^*]^+$ and $[Cu(PPh_3)]^+$ fragments to give $[ZnCp^*(Ge_9\{Si(SiMe_3)_3\}_3)]$ (**2**) and $[CuPiPr_3(Ge_9\{Si(SiMe_3)_3\}_3)]$ (**3**), and the existence of silylated Ge_9 units with a less bulky ligand $[Ge_9R_2]^{2-}$ and $[Ge_9R_3]^-$ ($R = SiPh_3$) has been shown by ESI-MS and ^{1}H NMR investigations. It has been demonstrated that the formation of the bis- and tris-silylated species can be influenced by the stoichiometry of the reaction partners K_4Ge_9 and $SiPh_3Cl$. The formation of $[(Cu(PiPr_3))_3\{Ge_9(SiPh_3)_2\}]^+$ upon the addition of $[CuPiPr_3Cl]$ has been shown by NMR experiments, and the copper phosphine complex **6** has been isolated in good yields. The product $[\{Cu(PiPr_3)_4\}\{Ge_9(SiPh_3)_2\}_2]$ (**6**) represents the first metal complex of a cluster carrying two ligands. It shows a η^4-coordination of the Cu atom to four Ge atoms, which can be regarded as an intermediate step for cluster expansion reactions observed for tris-silylated species, and it contains relatively long Ge–Si bonds as compared to those in the more common $[Si(SiMe_3)_3]^+$ group; the latter may indicate a higher reactivity of the Ge–Si bond.

Experimental Section

General: All reactions and manipulations were performed under a purified argon atmosphere using standard Schlenk and glove box techniques. The Zintl compound of nominal composition K_4Ge_9 was synthesized by heating (2 K min^{-1}) of a stoichiometric mixture of both elements K and Ge (99.999% Chempur) at 650 °C in a stainless steel autoclave for 46 h and slow cooling (1 K min^{-1}) to room temperature. The solvents ACN, hexane, Et_2O, and toluene were dried over molecular sieves (3 Å, 4 Å) and THF over a special drying material in a solvent purificator (MBraun MB-SPS). $[ZnCp^*_2]$[28] and $[CuPiPr_3Cl]$[34] were synthesized according to the literature. All other chemicals were received commercially and used without further purification.

Single-crystal structure determination: Single crystals were fixed on a glass fiber with perfluorinated ether and positioned in a 120 K cold N_2 stream. For single-crystal X-ray diffraction data collection an Oxford-Diffraction Xcalibur3 diffractometer (Mo-K_α radiation) was used. The structures were solved by direct methods and refined by full-matrix least-squares calculations against F^2 using SHELX-2014.[35] Non-hydrogen atoms were treated with anisotropic displacement parameters (compound **3** shows a disorder at several isopropyl groups, which required an isotropic treatment of some of the atoms; also compound **6** contains several carbon atoms that could not be refined anisotropically). Positions of the hydrogen atoms were calculated and refined using a riding model. For compound **6** the amount of solvent molecules was determined by using the squeeze function. CCDC 1494960 (**1**), CCDC 1494959 (**2**), CCDC 1494958 (**3**), and 1494961 (**6**) contain the supplementary crystallographic data. These data can be obtained free of charge by The Cambridge Crystallographic Data Centre. Selected crystallographic data are given in Table 1. The crystal structures have been visualized with Diamond.[29]

Electron-dispersive X-ray (EDX) analysis: Single crystals of all compounds were analyzed with a scanning electron microscope (JEOL 5900LV) equipped with an energy dispersive X-ray analyzer (Oxford Instruments).

NMR spectroscopy: The ^{1}H, ^{13}C, ^{31}P, and ^{29}Si NMR spectra were recorded on a Bruker AvanceIII400 FT system or on a Bruker AV 500c (Bruker Corp.) at 300 K. The signals of the ^{1}H and ^{13}C spectra were calibrated on the rest proton signal of the used deuterated solvents $[D_6]$benzene or $[D_3]$ACN. Chemical shifts are given in δ values by parts per million (ppm). The coupling constants J are stated in Hz. Signal multiplicities are abbreviated as follows: s singlet, d doublet, t triplet and m multiplet. The spectra were evaluated with MestReNova.[36]

ESI-MS: The preparation of the samples was performed in a glovebox. The measurements were carried out on a HCT (Bruker Corp.). Analysis of the data was evaluated using the program Bruker Compass Data Analysis 4.0 SP 5 (Bruker Corp.). The dry gas temperature was adjusted to 125 °C and the injection speed to 240 μL s^{-1}. Visualization of the spectra was done with the programs OriginPro 2015G (Origin Lab Corp.) and Excel 2015 (Microsoft Corp.).

Elemental analysis: Elemental analyses were performed by the microanalytically laboratory at the Department Chemie of the Technische Universität München. The elements C and H were determined with a combustion analyzer (elementar vario EL, Bruker Corp.). Phosphorus was measured photometrically as phosphorus molybdenium blue at 820 nm with a PhotoXF 500 photometer (Bruker Corp.) The determination of Cu was carried out by atom absorption spectroscopy at a Varian AA 280 FS (Agilent Technologies Ltd.).

Synthesis of $K[Ge_9\{Si(SiMe_3)_3\}_3]$: The compound was prepared according to the literature: K_4Ge_9 (2.00 g, 2.47 mmol, 1.0 equiv) and chlorotris(trimethylsilyl)silane (2.18 g, 7.70 mmol, 3.1 equiv) were suspended in ACN (30 mL). After stirring overnight, the solution was filtered and the solvent removed in vacuo. The raw product was obtained as a reddish brown solid (yield 85%). ^{1}H NMR (400 MHz, $[D_6]$benzene, 25 °C): $\delta = 0.52$ ppm (s, 81 H, CH_3); ^{13}C NMR (101 MHz, $[D_6]$benzene, 25 °C): $\delta = 3.1$ ppm (CH_3); ^{29}Si NMR (79 MHz, $[D_6]$benzene, 25 °C): $\delta = -106.2$ (Si(SiMe)$_3$), -9.1 ppm (Si(SiMe)$_3$).

Synthesis of $[Zn(Ge_9\{Si(SiMe_3)_3\}_3)_2]$ (**1**): $ZnCl_2$ (13.6 mg, 0.10 mmol, 0.5 equiv) was added to a solution of $K[Ge_9\{Si(SiMe_3)_3\}_3]$ (287 mg, 0.20 mmol, 1 equiv) in ACN (6 mL). A light brown precipitate was formed immediately. After filtration and extraction of the solid the residue was dried under vacuum and redissolved in THF (5 mL). The red brownish solution was filtered and dried under vacuum. ^{1}H and ^{29}Si NMR experiments showed the presence of compound **1** with a yield of about 26%. Compound **1** was crystallized by slow diffusion of Et_2O into a solution of **1** in toluene. The solution was stored at -32 °C for crystallization. Orange block-shaped crystals of

Table 1. Selected crystallographic data of the crystal structures of **1**, **2**, **3**, and **6**.

	1	**2**	**3**	**6**
formula	$C_{62}H_{182}Ge_{18}O_2Si_{24}Zn$	$C_{44}H_{104}Ge_9Si_{12}Zn$	$C_{79}H_{212}Cu_2Ge_{18}P_2Si_{24}$	$C_{108}H_{144}Cu_4Ge_{18}P_4Si_4$
M_r [g mol^{-1}]	3006.21	1689.02	3332.27	3239.24
space group (no)	$P2_1/n$ (14)	$P\bar{1}$ (2)	$P\bar{1}$ (2)	$P2_1/n$ (14)
a [Å]	14.8627(13)	14.8394(3)	20.4027(6)	20.2978(14)
b [Å]	18.9493(17)	15.4172(3)	21.1404(8)	22.4054(12)
c [Å]	23.594(2)	19.0621(3)	22.5412(7)	30.0399(16)
α [°]	90	92.1590(10)	97.329(3)	90
β [°]	92.415(8)	98.671(2)	109.572(3)	92.922(6)
γ [°]	90	115.659(2)	118.183(4)	90
V [Å^3]	6639.2(10)	3860.05(14)	7581.6(5)	13643.8(14)
Z	2	2	2	4
T [K]	120(2)	120(2)	120(2)	120(2)
λ [Å]	0.71073	0.71073	0.71073	0.71073
ρ_{calcd} [g cm^{-3}]	1.50	1.45	1.46	1.58
μ [mm^{-1}]	4.429	3.967	4.023	4.625
collected reflections	12915	14708	29772	26542
independent reflections	5727	9318	13175	9366
R_{int}	0.0974	0.0513	0.1121	0.1204
parameters/restraints	513/0	628/0	1225/78	1268/42
R_1 [all data/$I > 2\sigma(I)$]	0.1080/0.0378	0.0567/0.0309	0.1267/0.0566	0.1446/0.0626
wR_2 [all data/$I > 2\sigma(I)$]	0.0553/0.0483	0.0686/0.0615	0.1375/0.1257	0.1876/0.1698
goodness of fit	0.680	0.862	0.850	0.842
max/min diff. el. density [e Å^{-3}]	0.635/−0.640	0.692/−0.589	1.749/−0.930	1.470/−1.060

the composition **1**·Et_2O were obtained after four months, suitable for single-crystal X-ray diffraction. EDX measurements confirmed the presence of the elements Zn, Ge, and Si in the single crystals. ^{1}H NMR (400 MHz, [D_6]benzene, 25 °C): $\delta = 0.54$ ppm (s, 162 H, CH_3); ^{13}C NMR (101 MHz, [D_6]benzene, 25 °C): $\delta = 3.27$ ppm (CH_3); ^{29}Si NMR (79 MHz, [D_6]benzene, 25 °C): $\delta = -8.94$ (Si($SiMe_3$)$_3$, −97.30 ppm (Si($SiMe_3$)$_3$).

Synthesis of [ZnCp*(Ge_9{Si($SiMe_3$)$_3$}$_3$)] (**2**): K[Ge_9{Si($SiMe_3$)$_3$}$_3$] (85.7 mg, 0.06 mmol, 1 equiv) and [ZnCp*$_2$] (40.3 mg, 0.12 mmol, 2 equiv) were dissolved in toluene (3 mL). After stirring overnight, the red solution was filtered and concentrated. Storing at −32 °C for four days resulted in the formation of orange block-like crystals of the composition 2·Tol, suitable for single-crystal determination. EDX measurements confirmed the presence of the elements Zn, Ge, and Si in the single crystals. ^{1}H NMR (400 MHz, [D_6]benzene, 25 °C): $\delta = 2.29$ (s, 15 H, ZnCp*), 0.39 ppm (s, 81 H, CH_3); ^{13}C NMR (101 MHz, [D_6]benzene, 25 °C): $\delta = 10.9$ (ZnCp*), 2.4 ppm (CH_3); ^{29}Si NMR (79 MHz, [D_6]benzene, 25 °C): $\delta = -8.8$ (Si($SiMe_3$)$_3$), −101.0 ppm (Si($SiMe_3$)$_3$); EDX analysis calcd (%) for **2**: Ge 40.9, Si 54.6, Zn 3.3; found: Ge 37.6, Si 59.4, Zn 3.0; ESI-MS (negative mode, 4000 V, 300 °C): *m/z*: 1397 [Ge_9{Si($SiMe_3$)$_3$}$_3$]$^-$; ESI-MS (positive mode, −6000 V, 300 °C): *m/z*: 1639 [Ge_9{Si($SiMe_3$)$_3$}$_3$ZnCp*(ACN)]$^+$.

Synthesis of [CuP*i*Pr_3(Ge_9{Si($SiMe_3$)$_3$}$_3$)] (**3**): A solution of [CuP*i*Pr_3Cl] (51.8 mg, 0.20 mmol, 1 equiv) in ACN (4 mL) was added to a solution of K[Ge_9{Si($SiMe_3$)$_3$}$_3$] (287 mg, 0.20 mmol, 1 equiv) in ACN (6 mL). A brown precipitate was formed immediately, and the reaction mixture was stirred overnight. After filtration and washing of the solid with ACN the residue was dried under vacuum and redissolved in toluene (2 mL). The red solution was filtered and dried under vacuum. Compound **3** was obtained as a red solid with high purity (yield 59%). For crystallization, the product was redissolved in toluene (2 mL) and stored at room temperature. Orange-brown needle-shaped crystals of the composition **3**·(tol)$_{0.5}$ were obtained after one month, suitable for single-crystal X-ray diffraction. EDX measurements confirmed the presence of the elements Cu, Ge, Si, and P in the single crystals. ^{1}H NMR (400 MHz, [D_6]benzene, 25 °C): $\delta = 1.85$ (m, 3 H, CH(CH_3)$_2$), 1.19 (dd, $J = 14.5$, 7.1 Hz, 18 H, CH(CH_3)$_2$), 0.49 ppm (s, 81 H, CH_3); ^{13}C NMR (101 MHz, [D_6]benzene, 25 °C): $\delta =$ 22.36 (d, $J = 15.3$ Hz, CH(CH_3)$_2$), 20.57 (d, $J = 3.7$ Hz, CH(CH_3)$_2$), 2.92 ppm (s, CH_3); ^{31}P NMR (162 MHz, [D_6]benzene, 25 °C): δ [ppm] = 6.68 ppm; ^{29}Si NMR (79 MHz, [D_6]benzene, 25 °C, TMS): $\delta =$ −9.20 (Si($SiMe_3$)$_3$), −104.27 ppm (Si($SiMe_3$)$_3$); elemental analysis calcd (%) for **3**: C 26.68, H 6.35, Cu 3.92; found: C 27.39, H 6.29, Cu 3.59; EDX analysis calcd (%) for **3**: Ge 39.1, Si 52.2, Cu 4.35, P 4.35; found: Ge 45.9, Si 45.8, Cu 3.18, P 5.13; ESI-MS (negative mode, 4000 V, 300 °C): *m/z*: 1496 [Ge_9{Si($SiMe_3$)$_3$}$_3$CuCl]$^-$; ESI-MS (positive mode, −4000 V, 300 °C): *m/z*: 1848 [Ge_9{Si($SiMe_3$)$_3$}$_3$(CuP*i*Pr_3)$_2$]$^+$.

Synthesis of [Ge_9($SiPh_3$)$_3$]$^-$ (4) and [Ge_9($SiPh_3$)$_2$]$^{2-}$ (5) as potassium salts: K_4Ge_9 (162 mg, 0.20 mmol 1 equiv) was added to a solution of $SiPh_3$Cl (for K[Ge_9($SiPh_3$)$_3$]: 177 mg, 0.60 mmol, 3 equiv; for K[Ge_9($SiPh_3$)$_2$]: 118 mg, 0.40 mmol, 2 equiv) in ACN (4 mL). The reaction mixtures turned immediately red and were filtered after stirring overnight. ESI-MS and NMR investigations revealed the formation of the respective bis- and tris-silylated species **5** and **4**.

*K_2[Ge_9($SiPh_3$)$_2$] (K_2-**5**)*: ^{1}H NMR (400 MHz, [D_3]ACN, 25 °C): $\delta = 7.52$–7.48 (m, 2 H, ($SiPh_3$)$_2$), 7.21–7.14 ppm (m, 3 H, ($SiPh_3$); ^{13}C NMR (101 MHz, [D_3]ACN, 25 °C): $\delta = 143.17$ ($SiPh_3$), 137.18 (Ge_9($SiPh_3$), 128.61 ($SiPh_3$), 127.59 ppm ($SiPh_3$); ^{29}Si NMR (79 MHz, [D_3]ACN, 25 °C): $\delta = 6.36$ ppm; ESI-MS (negative mode, 4000 V, 300 °C): *m/z*: 1212 [K{Ge_9($SiPh_3$)$_2$}]$^-$, 1172 [Ge_9($SiPh_3$)$_2$]$^-$, 913 [Ge_9($SiPh_3$)]$^-$, 654 [Ge_9]$^-$; ESI-MS (positive mode, −6000 V, 300 °C): *m/z* 1290 [K_3{Ge_9($SiPh_3$)$_2$}]$^+$.

*K[Ge_9($SiPh_3$)$_3$] (K-**4**)*: ^{1}H NMR (400 MHz, [D_3]ACN, 25 °C): $\delta = 7.63$–7.56 (m, 2 H, ($SiPh_3$), 7.37–7.25 ppm (m, 3 H, ($SiPh_3$); ^{13}C NMR (101 MHz, [D_3]ACN, 25 °C): $\delta = 139.74$ ($SiPh_3$), 137.17 ($SiPh_3$), 129.97 ($SiPh_3$), 128.42 ppm ($SiPh_3$); ^{29}Si NMR (79 MHz, [D_3]ACN, 25 °C): $\delta =$ 8.00 ppm. ESI-MS (negative mode, 3500 V, 300 °C): *m/z*: 1432 [Ge_9($SiPh_3$)$_3$]$^-$; ESI-MS (positive mode, −3700 V, 300 °C): *m/z* 1510 [K_2{Ge_9($SiPh_3$)$_3$}]$^+$.

Synthesis of [Ge_9($SiPh_3$)$_2$]$_2$(CuP*i*Pr_3)$_4$ (**6**): A solution of [CuP*i*Pr_3Cl] (25.9 mg, 0.10 mmol, 1 equiv) in ACN (2 mL) was added to a solu-

tion of $K[Ge_9(SiPh_3)_3]$ (147 mg, 0.10 mmol, 1 equiv) in ACN (3 mL). A brown precipitate was formed immediately. The reaction mixture was stirred overnight and dried under vacuum, resulting in a brown residue. After filtration and washing of the solid with ACN the residue was extracted with toluene (2 mL). The brown filtrate was carefully layered with hexane and stored at −32 °C for crystallization. Orange brown block-shaped crystals of the composition **5**·$(tol)_{3.4}$ were obtained after two weeks, suitable for single crystal X-ray diffraction. EDX measurements confirmed the presence of the elements Cu, Ge, Si and P in the single crystals. ^{1}H NMR (400 MHz, [D_6]benzene, 25 °C): δ = 8.11–8.04 (m, 2H, Si*Ph*$_3$), 7.61–7.54 (m, 4H, Si*Ph*$_3$), 7.24–7.18 (m, 4H, Si*Ph*$_3$), 1.69 (m, 2H, C*H*$(CH_3)_2$), 1.41 (m, 1H, C*H*$(CH_3)_2$), 1.07 (dd, J = 11.7, 7.1 Hz, 12H, CH(C*H*$_3$)$_2$), 0.92 ppm (dd, J = 14.2, 7.1 Hz, 6H, CH(C*H*$_3$)$_2$); ^{13}C NMR (101 MHz, [D_6]benzene, 25 °C): δ = 138.61 (Si*Ph*$_3$), 137.40 (Si*Ph*$_3$), 136.73 (Si*Ph*$_3$), 130.04 (Si*Ph*$_3$), 22.55 (d, J = 16.1 Hz, CH$(CH_3)_2$), 22.02 (d, J = 18.4 Hz, CH$(CH_3)_2$), 21.02 (d, J = 13.4 Hz, CH$(CH_3)_2$), 20.43 ppm (d, J = 2.7 Hz, CH$(CH_3)_2$); ^{29}Si NMR (79 MHz, [D_6]benzene, 25 °C): δ = 4.21 ppm; ^{31}P NMR (162 MHz, [D_6]benzene, 25 °C): δ = 36.50 (Cu*P*iPr_3), 19.49 ppm (Cu*P*iPr_3).

Acknowledgements

This work was supported by Deutsche Forschungsgemeinschaft (DFG) within International Research Training Group 2022 (ATUMS), and through the TUM International Graduate School of Science and Engineering (IGSSE) and by the research network "Solar Technologies go Hybrid" (State of Bavaria). The authors thank Christina Fischer for the support by ESI-MS measurements and Dr. Wilhelm Klein for the assistance performing the structure refinements.

Keywords: copper · germanium · silanes · zinc · Zintl clusters

[1] a) S. Scharfe, F. Kraus, S. Stegmaier, A. Schier, T. F. Fässler, *Angew. Chem. Int. Ed.* **2011**, *50*, 3630–3670; *Angew. Chem.* **2011**, *123*, 3712–3754; b) T. F. Fässler, S. D. Hoffmann, *Angew. Chem. Int. Ed.* **2004**, *43*, 6242–6247; *Angew. Chem.* **2004**, *116*, 6400–6406; c) S. C. Sevov, J. M. Goicoechea, *Organometallics* **2006**, *25*, 5678–5692; d) J. D. Corbett, *Chem. Rev.* **1985**, *85*, 383–397.

[2] a) L. Xu, S. C. Sevov, *J. Am. Chem. Soc.* **1999**, *121*, 9245–9246; b) A. Nienhaus, S. D. Hoffmann, T. F. Fässler, *Z. Anorg. Allg. Chem.* **2006**, *632*, 1752–1758.

[3] a) A. Ugrinov, S. C. Sevov, *J. Am. Chem. Soc.* **2002**, *124*, 10990–10991; b) A. Ugrinov, S. C. Sevov, *Inorg. Chem.* **2003**, *42*, 5789; c) L. Yong, S. D. Hoffmann, T. F. Fässler, *Z. Anorg. Allg. Chem.* **2005**, *631*, 1149–1153.

[4] C. Downie, Z. Tang, A. M. Guloy, *Angew. Chem. Int. Ed.* **2000**, *39*, 337–340; *Angew. Chem.* **2000**, *112*, 346–348.

[5] J. M. Goicoechea, S. C. Sevov, *J. Am. Chem. Soc.* **2005**, *127*, 7676–7677.

[6] E. N. Esenturk, J. Fettinger, Y.-F. Lam, B. Eichhorn, *Angew. Chem. Int. Ed.* **2004**, *43*, 2132–2134; *Angew. Chem.* **2004**, *116*, 2184–2186.

[7] S. Scharfe, T. F. Fässler, S. Stegmaier, S. D. Hoffmann, K. Ruhland, *Chem. Eur. J.* **2008**, *14*, 4479–4483.

[8] C. B. Benda, M. Waibel, T. F. Fässler, *Angew. Chem. Int. Ed.* **2015**, *54*, 522–526; *Angew. Chem.* **2015**, *127*, 532–536.

[9] B. W. Eichhorn, R. C. Haushalter, W. T. Pennington, *J. Am. Chem. Soc.* **1988**, *110*, 8704–8706.

[10] S. Scharfe, T. F. Fässler, *Eur. J. Inorg. Chem.* **2010**, 1207–1213.

[11] J. M. Goicoechea, S. C. Sevov, *Organometallics* **2006**, *25*, 4530–4536.

[12] a) M. W. Hull, S. C. Sevov, *Inorg. Chem.* **2007**, *46*, 10953–10955; b) C. B. Benda, J.-Q. Wang, B. Wahl, T. F. Fässler, *Eur. J. Inorg. Chem.* **2011**, 4262–4269.

[13] M. W. Hull, S. C. Sevov, *J. Am. Chem. Soc.* **2009**, *131*, 9026–9037.

[14] M. M. Bentlohner, W. Klein, Z. H. Fard, L.-A. Jantke, T. F. Fässler, *Angew. Chem. Int. Ed.* **2015**, *54*, 3748–3753; *Angew. Chem.* **2015**, *127*, 3819–3824.

[15] A. Schnepf, *Angew. Chem. Int. Ed.* **2003**, *42*, 2624–2625; *Angew. Chem.* **2003**, *115*, 2728–2729.

[16] F. Li, S. C. Sevov, *Inorg. Chem.* **2012**, *51*, 2706–2708.

[17] F. Henke, C. Schenk, A. Schnepf, *Dalton Trans.* **2009**, 9141–9145.

[18] C. Schenk, F. Henke, G. Santiso-Quinones, I. Krossing, A. Schnepf, *Dalton Trans.* **2008**, 4436–4441.

[19] C. Schenk, A. Schnepf, *Chem. Commun.* **2009**, 3208–3210.

[20] L. J. Schiegerl, F. S. Geitner, C. Fischer, W. Klein, T. F. Fässler, *Z. Anorg. Allg. Chem.* DOI: 10.1002/zaac.201600295.

[21] O. Kysliak, C. Schrenk, A. Schnepf, *Inorg. Chem.* **2015**, *54*, 7083–7088.

[22] a) O. Kysliak, A. Schnepf, *Dalton Trans.* **2016**, *45*, 2404–2408; b) F. Li, S. C. Sevov, *J. Am. Chem. Soc.* **2014**, *136*, 12056–12063.

[23] F. Li, S. C. Sevov, *Inorg. Chem.* **2015**, *54*, 8121–8125.

[24] F. S. Geitner, T. F. Fässler, *Eur. J. Inorg. Chem.* **2016**, 2688–2691.

[25] C. Fischer, W. Klein, L.-A. Jantke, L. J. Schiegerl, T. F. Fässler, *Z. Anorg. Allg. Chem.* accepted, DOI: 10.1002/zaac.201600296.

[26] B. Fischer, P. Wijkens, J. Boersma, G. van Koten, W. J. J. Smeets, A. L. Spek, P. H. M. Budzelaar, *J. Organomet. Chem.* **1989**, *376*, 223–233.

[27] J. M. Lopez del Amo, G. Buntkowsky, H.-H. Limbach, I. Resa, R. Fernández, E. Carmona, *J. Phys. Chem. A* **2008**, *112*, 3557–3565.

[28] R. Blom, J. Boersma, P. H. M. Budzelaar, B. Fischer, A. Haaland, H. V. Volden, J. Weidlein, *Acta Chem. Scand. A* **1986**, *40*, 113.

[29] H. Putz, K. Brandenburg, DIAMOND—Crystal and Molecular Structure Visualization, Version 3.2k, **2014**, Bonn (Germany).

[30] a) A. Schulz, *Z. Anorg. Allg. Chem.* **2014**, *640*, 2183–2192; b) M. R. Wilson, D. C. Woska, A. Prock, W. P. Giering, *Organometallics* **1993**, *12*, 1742–1752.

[31] A. Spiekermann, S. D. Hoffmann, F. Kraus, T. F. Fässler, *Angew. Chem. Int. Ed.* **2007**, *46*, 1638–1640; *Angew. Chem.* **2007**, *119*, 1663–1666.

[32] A. Ugrinov, S. C. Sevov, *Chem. Eur. J.* **2004**, *10*, 3727–3733.

[33] O. Kysliak, C. Schrenk, A. Schnepf, *Angew. Chem. Int. Ed.* **2016**, *55*, 3216–3219; *Angew. Chem.* **2016**, *128*, 3270–3274.

[34] S. Scharfe, T. F. Fässler, *Z. Naturforsch. Sect. B* **2012**, *67*, 564.

[35] G. M. Sheldrick, *Acta Crystallogr. Sect. C* **2015**, *71*, 3–8.

[36] MestreNova, Mestrelab Research, Version 10.0, **2015**.

Manuscript received: July 22, 2016

Accepted Article published: November 8, 2016

Final Article published: November 25, 2016

CHEMISTRY
A European Journal

Supporting Information

On the Reactivity of Silylated Ge_9 Clusters: Synthesis and Characterization of $[ZnCp^*(Ge_9\{Si(SiMe_3)_3\}_3)]$, $[CuP\textit{i}Pr_3(Ge_9\{Si(SiMe_3)_3\}_3)]$, and $[(CuP\textit{i}Pr_3)_4\{Ge_9(SiPh_3)_2\}_2]$

Kerstin Mayer[+], Lorenz J. Schiegerl[+], and Thomas F. Fässler*[a]

chem_201603475_sm_miscellaneous_information.pdf

Supporting Information

Contents

1 NMR data of compounds **1** – **6**

Inpurities in ^{1}H NMR ([D_6]benzene 0.29 ppm) and ^{29}Si NMR (between −21 and −22 ppm solvent independent) spectra are caused by silicon grease.

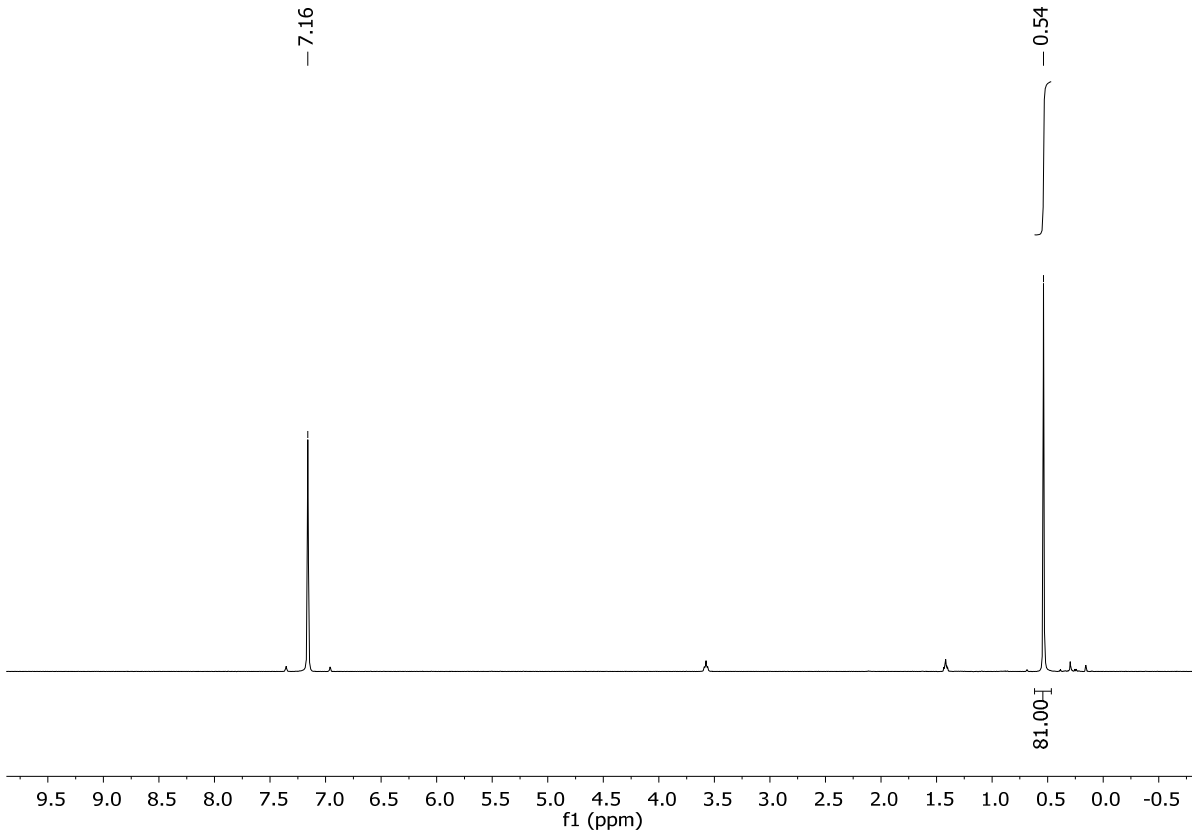

Figure SI 1: ^{1}H NMR spectrum of compound $[Ge_9(Si(SiMe_3)_3)_3]_2Zn$ (**1**) in [D_6]benzene.

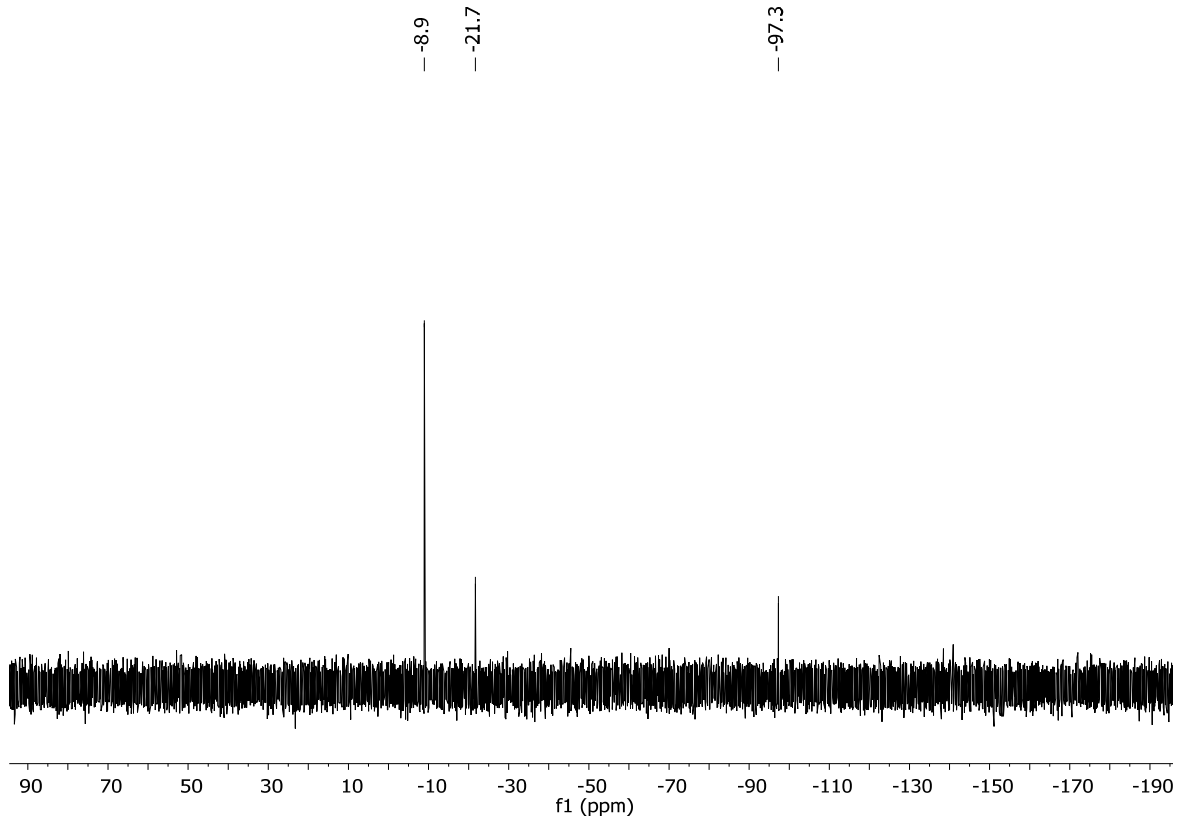

Figure SI 2: ^{29}Si NMR spectrum of compound $[Ge_9(Si(SiMe_3)_3)_3]_2Zn$ (**1**) in $[D_6]$benzene.

<u>^{1}H, ^{13}C and ^{29}Si NMR spectra of compound **2** in $[D_6]$Benzene.</u>

The ^{1}H NMR signal of the cluster protons at 0.39 ppm is significantly upfield shifted, whereas the Cp* protons at 2.28 ppm are downfield shifted ($ZnCp^*_2$ 1.88 ppm). In the ^{29}Si NMR spectrum a downfield shift is observed for both groups: −8.80 ppm (SiMe$_3$) and −101.0 ppm (Si(SiMe$_3$)$_3$). Further NMR investigations show that, independent of the concentration ratio $K[Ge_9[Si(SiMe_3)_3]_3]$ / $ZnCp^*_2$, only one of the two Cp* ligands is abstracted, and neither heating nor addition of a protonating additive leads to the substitution of the second ligand. The formation of product **2** does not take place in THF, and according to NMR and ESI-MS experiments, dissolving of compound **2** in THF immediately leads to a splitting into $[ZnCp^*]^+$ and $[Ge_9(Si(SiMe_3)_3)_3]^-$. Measurements of the toluene solution diluted in ACN exclusively show the free tris-silylated cluster (*m/z* = 1396) in the negative spectrum, and in the positive mode the signal of the ACN adduct of $[Ge_9(Si(SiMe_3)_3)_3]ZnCp^*$ can be identified (m/z = 1640).

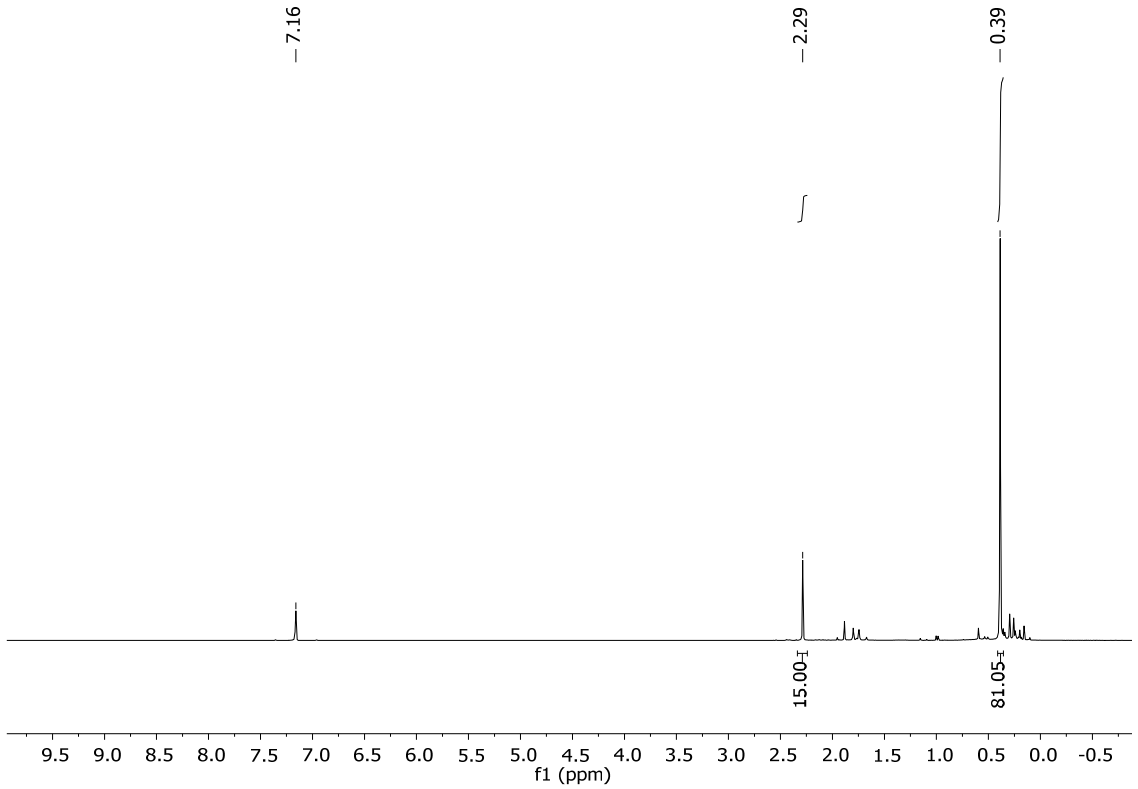

Figure SI 3: ^{1}H NMR spectrum of compound $[Ge_9(Si(SiMe_3)_3)_3]ZnCp^*$ (**2**) in $[D_6]$benzene.

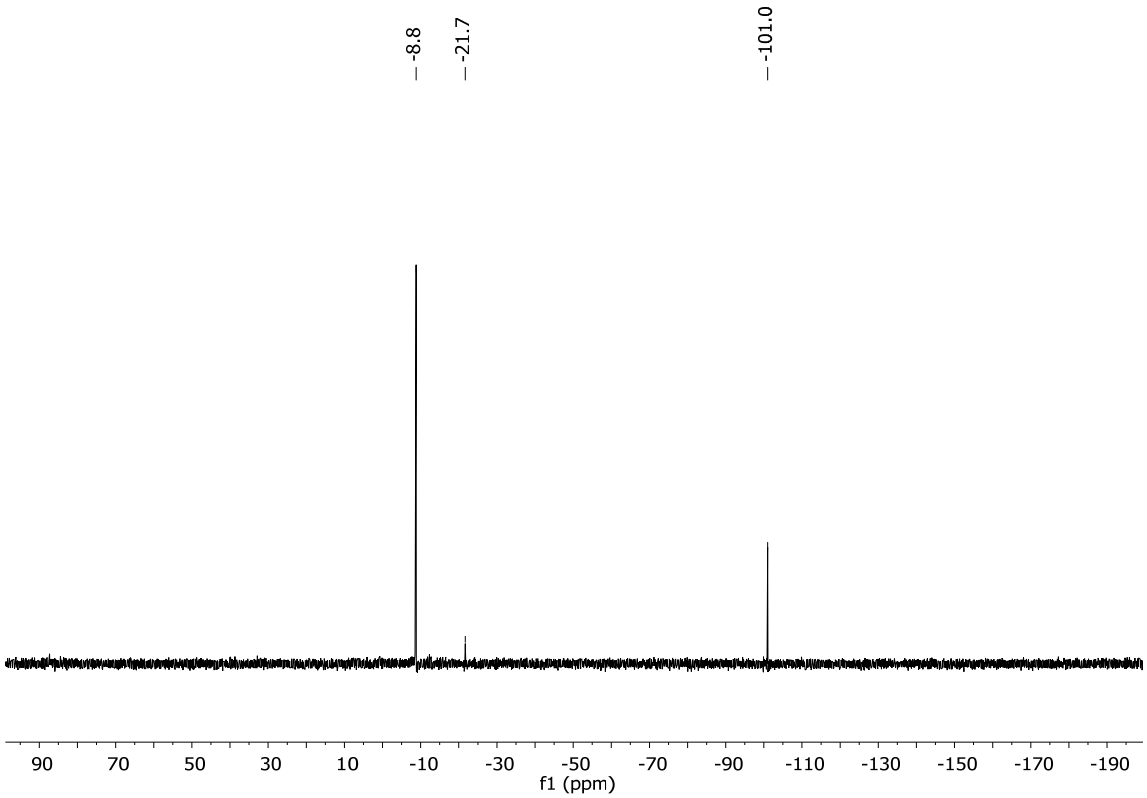

Figure SI 4: ^{29}Si NMR spectrum of compound $[Ge_9(Si(SiMe_3)_3)_3]ZnCp^*$ (**2**) in $[D_6]$benzene.

^{1}H and ^{29}Si NMR spectra of compound **3** in [D_6]benzene.

The singlet signal of the TMS protons of **3** is slightly upfield shifted (0.49 ppm) compared to that of the reactant K[Ge_9[Si($SiMe_3$)$_3$]$_3$] (0.52 ppm). The two proton signals of the *i*Pr groups are observed at 1.13 ppm (CH(C*H*$_3$)$_2$) and 1.85 ppm (C*H*(CH_3)$_2$) (CuP*i*Pr_3Cl: 1.18 and 1.87 ppm). The signal splitting of the *i*Pr protons is caused by proton and phosphorus coupling, and the integral ratio of 27:6:1 (TMS:CH(C*H*$_3$)$_2$:C*H*(CH_3)$_2$) is in accordance with a pure monomeric product. An upfield shift of the TMS carbon signal is also observed in the ^{13}C NMR spectrum from 3.09 ppm (K[Ge_9[Si($SiMe_3$)$_3$]$_3$]) to 2.92 ppm. The two doublets (phosphorus coupling) for the *i*Pr carbon atoms appear at 20.57 ppm (*C*H(CH_3)$_2$) and 22.36 ppm (CH(*C*H_3)$_2$) and are slightly different from those of the reactant CuP*i*Pr_3Cl (20.95 and 22.55 ppm). The ^{29}Si NMR spectrum of **3** shows a downfield shift from −106.26 ppm (K[Ge_9[Si($SiMe_3$)$_3$]$_3$]) to −104.27 ppm of the signal of the *Si*($SiMe_3$)$_3$ silicon atoms, whereas the signal of the *Si*Me_3 silicon atoms is not affected by the coordination. The signal of the phosphorus atom in the ^{31}P NMR spectrum is upfield shifted from 24.17 ppm (CuP*i*Pr_3Cl) to 6.68 ppm upon complexation. ESI-MS measurements reveal the species [{Ge_9[Si($SiMe_3$)$_3$]$_3$}CuCl]$^-$ (m/z = 1496) in negative mode, whereby an *i*Pr group is obviously substituted by a chloride under measurement conditions. In contrast, the species [{Ge_9[Si($SiMe_3$)$_3$]$_3$}(CuP*i*Pr_3)$_2$]$^+$ (m/z = 1848) is observed in positive mode in which two copper phosphine groups are bonded to the tris-silylated cluster.

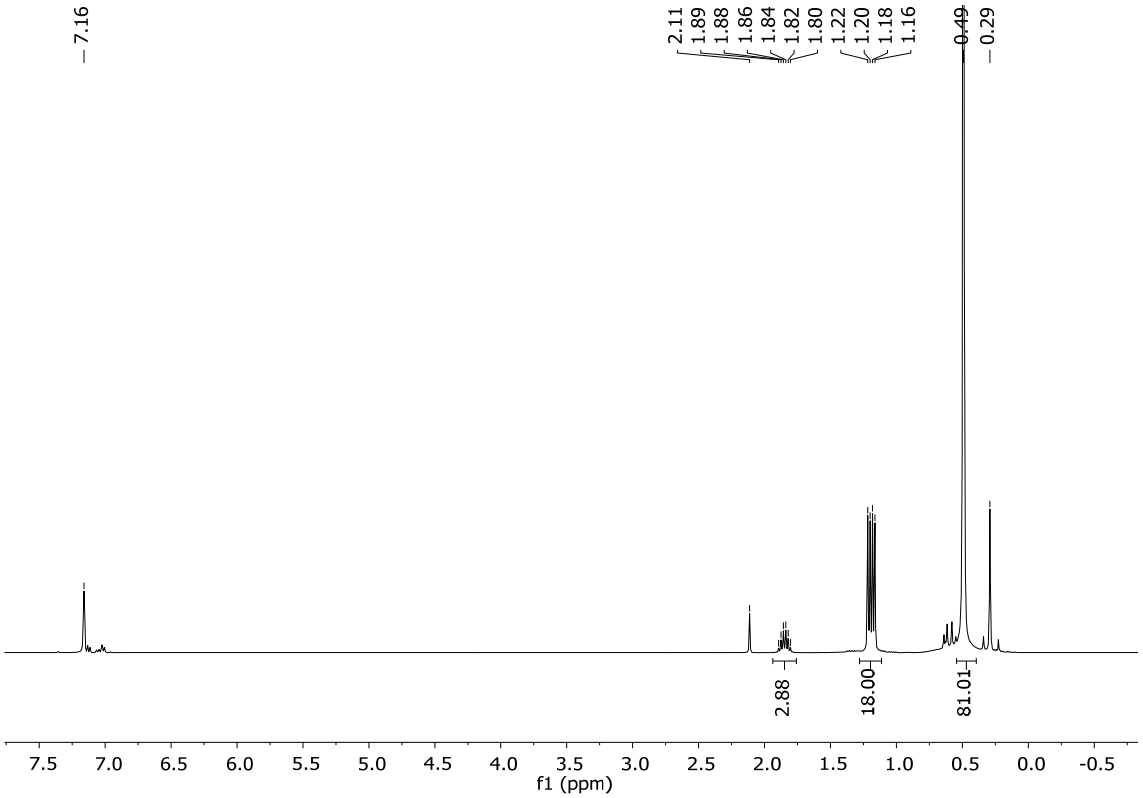

Figure SI 5: ^{1}H NMR spectrum of compound [$Ge_9(Si(SiMe_3)_3)_3$]CuP*i*Pr_3 (**3**) in [D_6]benzene.

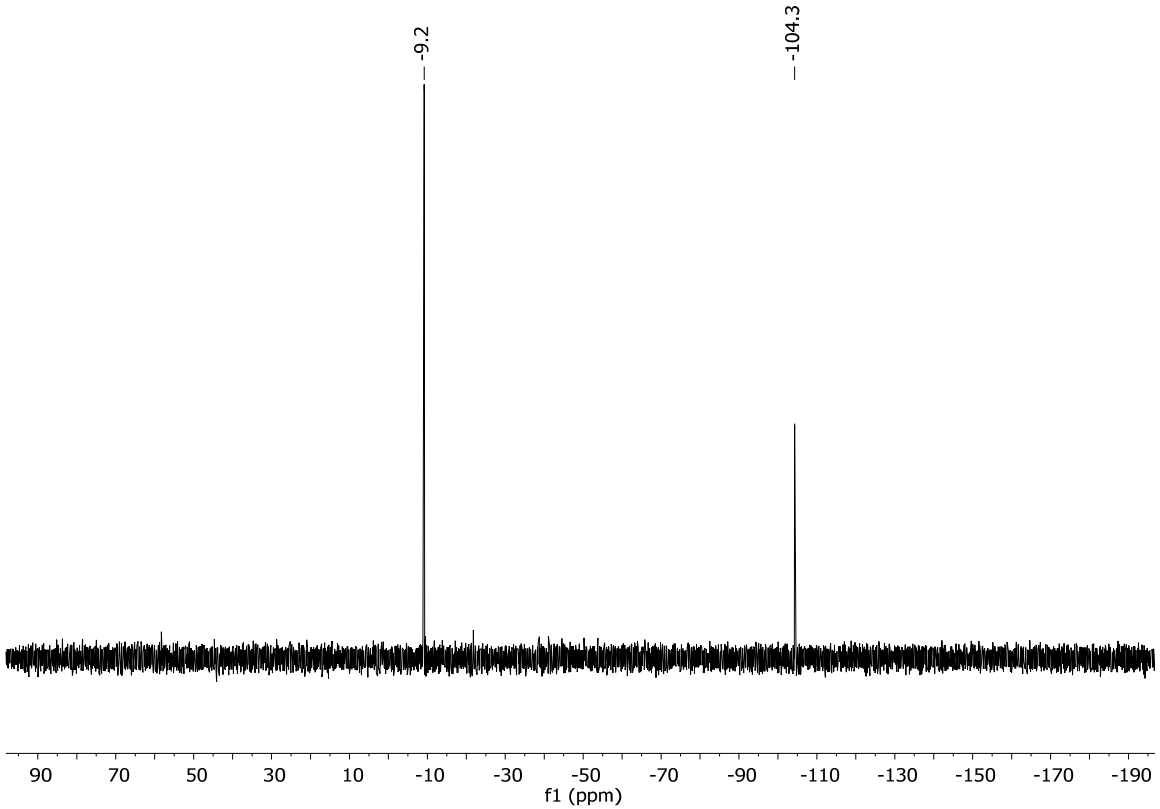

Figure SI 6: ^{29}Si NMR spectrum of compound [$Ge_9(Si(SiMe_3)_3)_3$]CuP*i*Pr_3 (**3**) in [D_6]benzene.

^{1}H and ^{29}Si NMR spectra of compound **4** in $[D_3]ACN$.

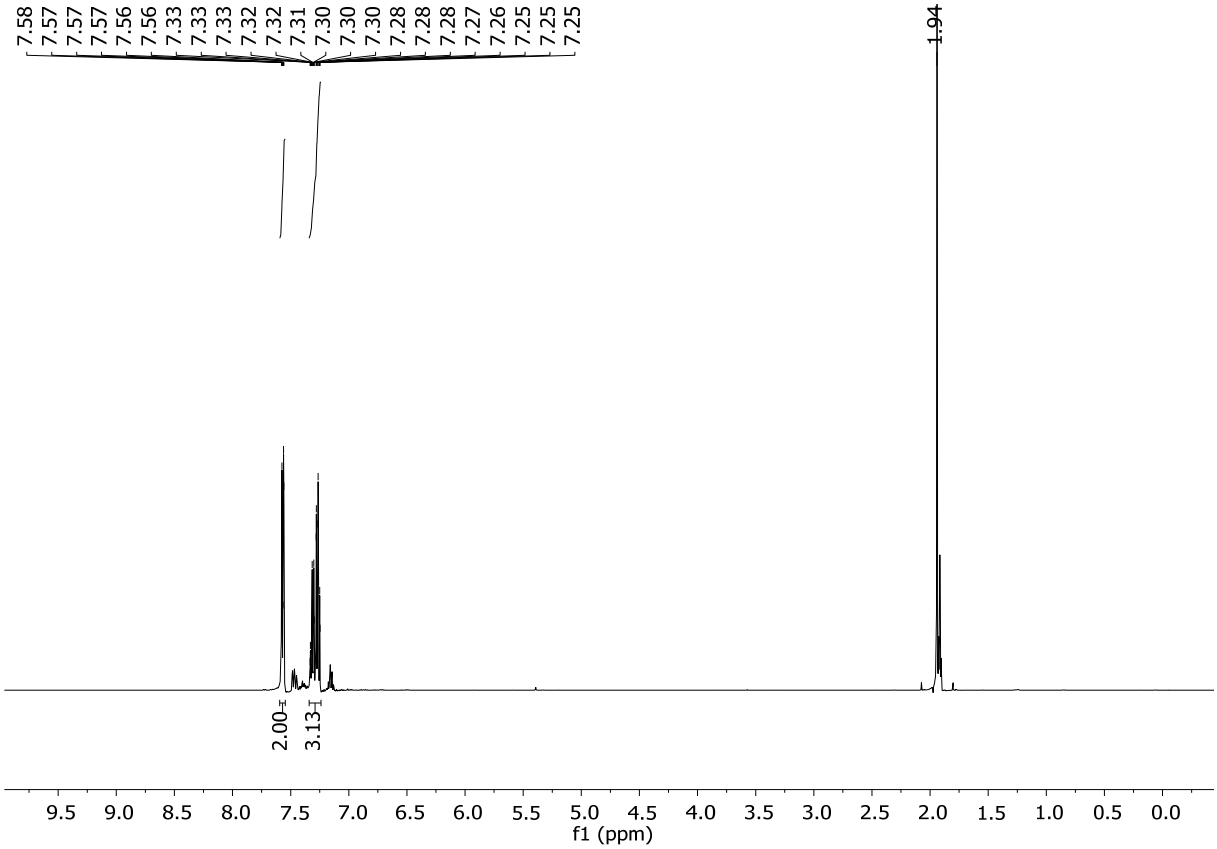

Figure SI 7: ^{1}H NMR spectrum of compound $K[Ge_9(SiPh_3)_3]$ (**4**) in $[D_3]ACN$.

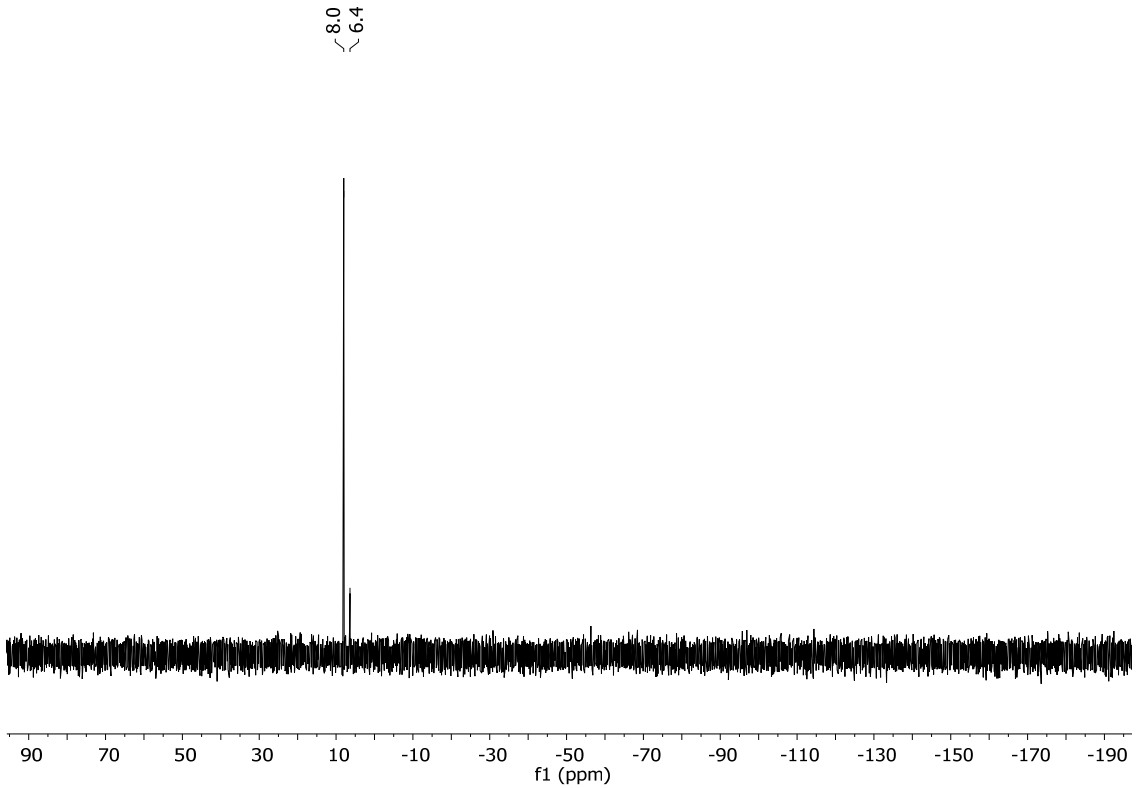

Figure SI 8: ^{29}Si NMR spectrum of compound $K[Ge_9(SiPh_3)_3]$ (**4**) in $[D_3]ACN$.

[1]H NMR spectrum of compound **5** in [D3]ACN.

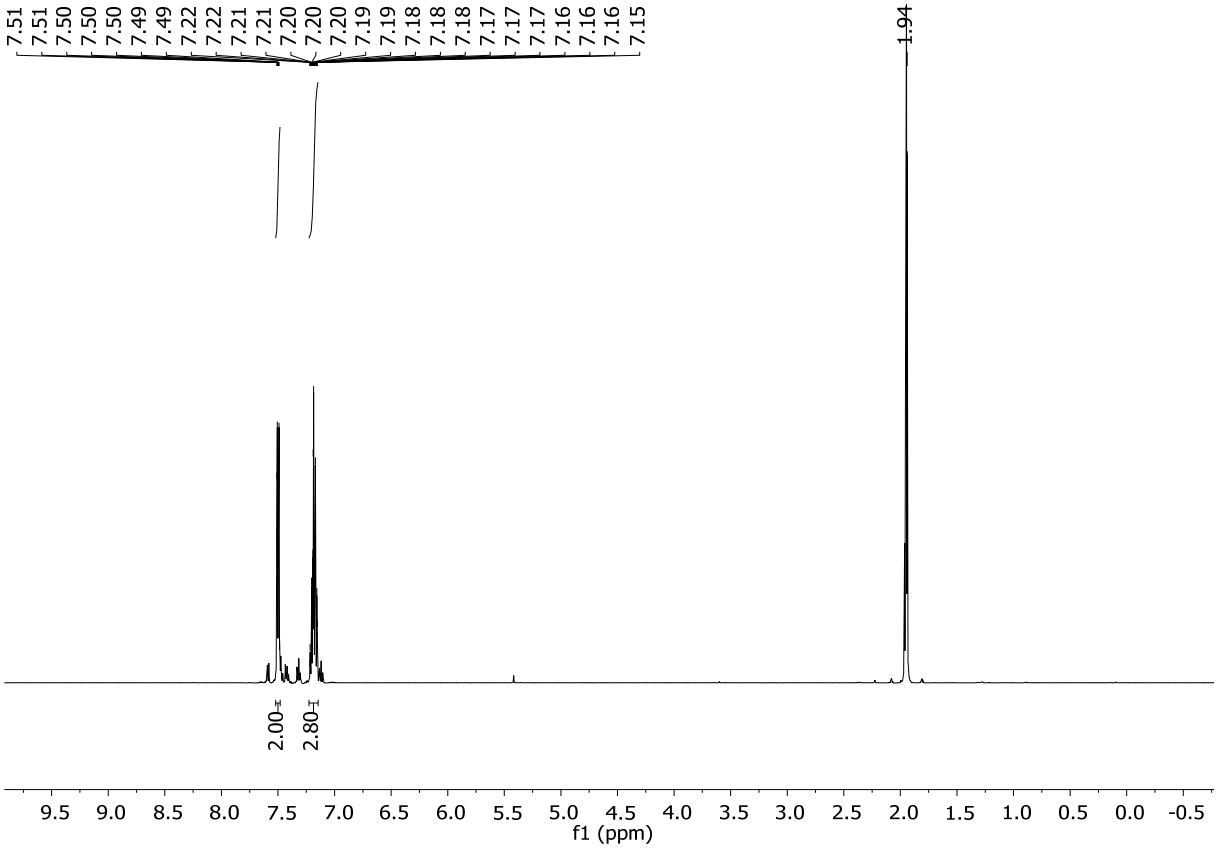

Figure SI 9: [1]H NMR spectrum of compound $K_2[Ge_9(SiPh_3)_2]$ (**5**) in [D3]ACN.

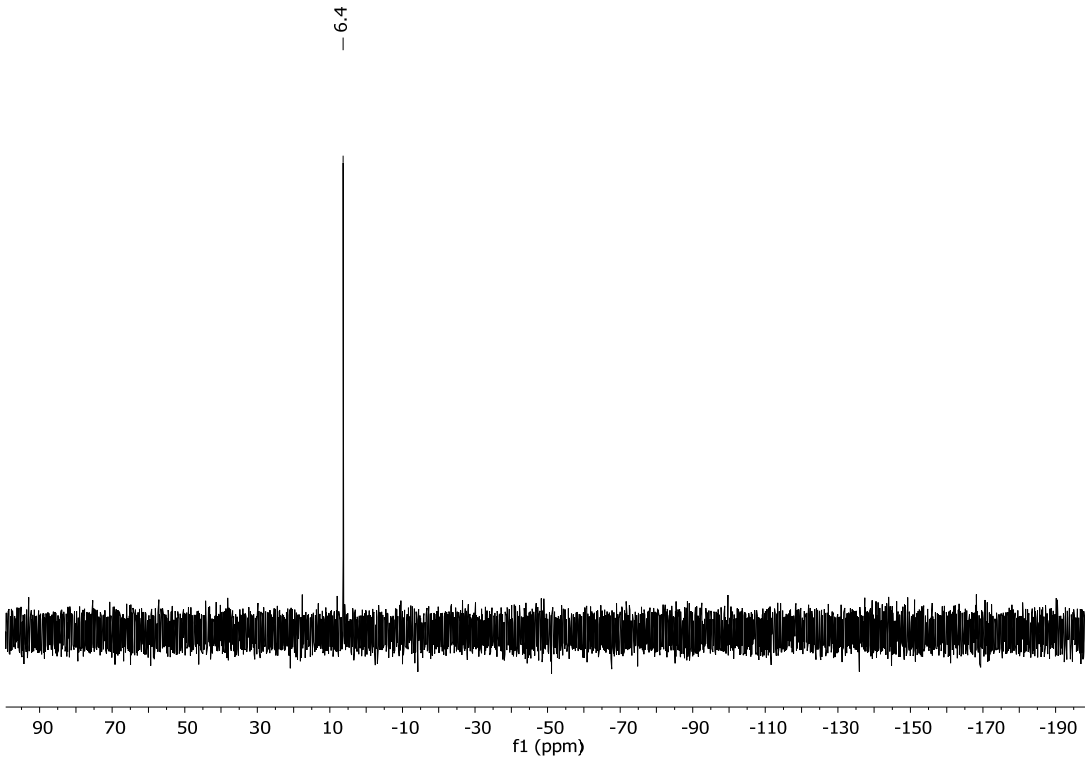

Figure SI 10: [29]Si NMR spectrum of compound $K_2[Ge_9(SiPh_3)_2]$ (**5**) in [D3]ACN.

Comparison of the ^{1}H and ^{29}Si NMR spectra of compounds **4** ($K[Ge_9(SiPh_3)_3]$; top) and **5** ($K_2[Ge_9(SiPh_3)_2]$; bottom).

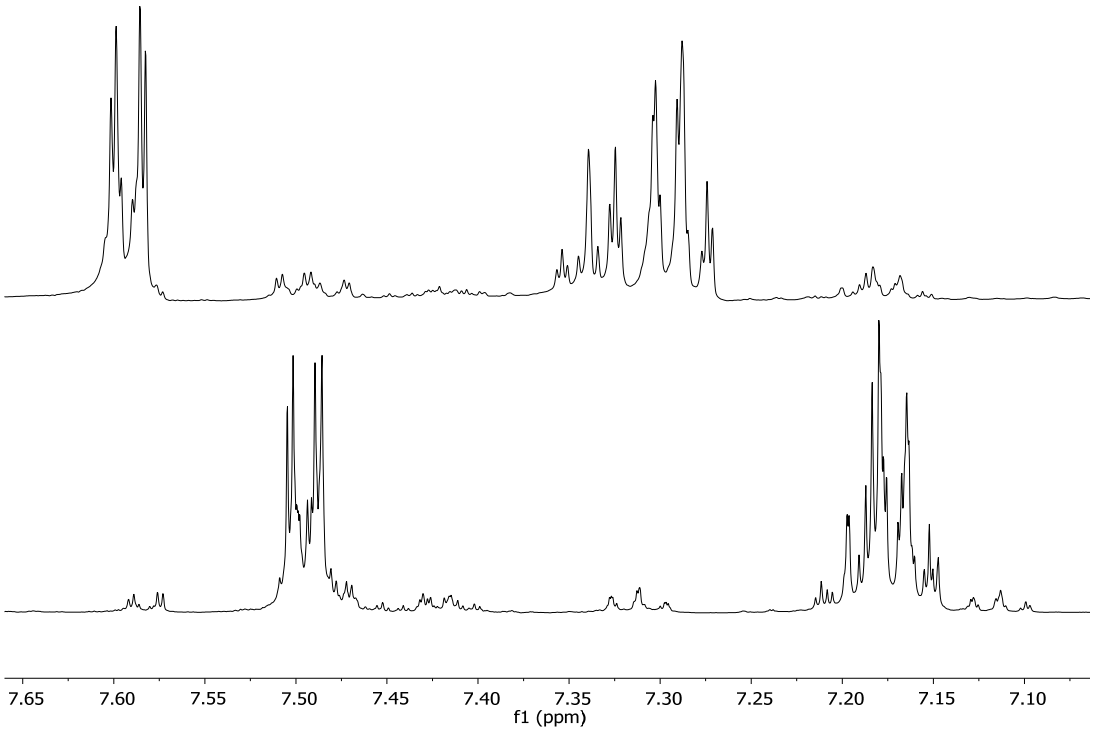

Figure SI 11: ^{1}H NMR spectra of compounds **4** (top) and **5** (bottom) in $[D_3]ACN$.

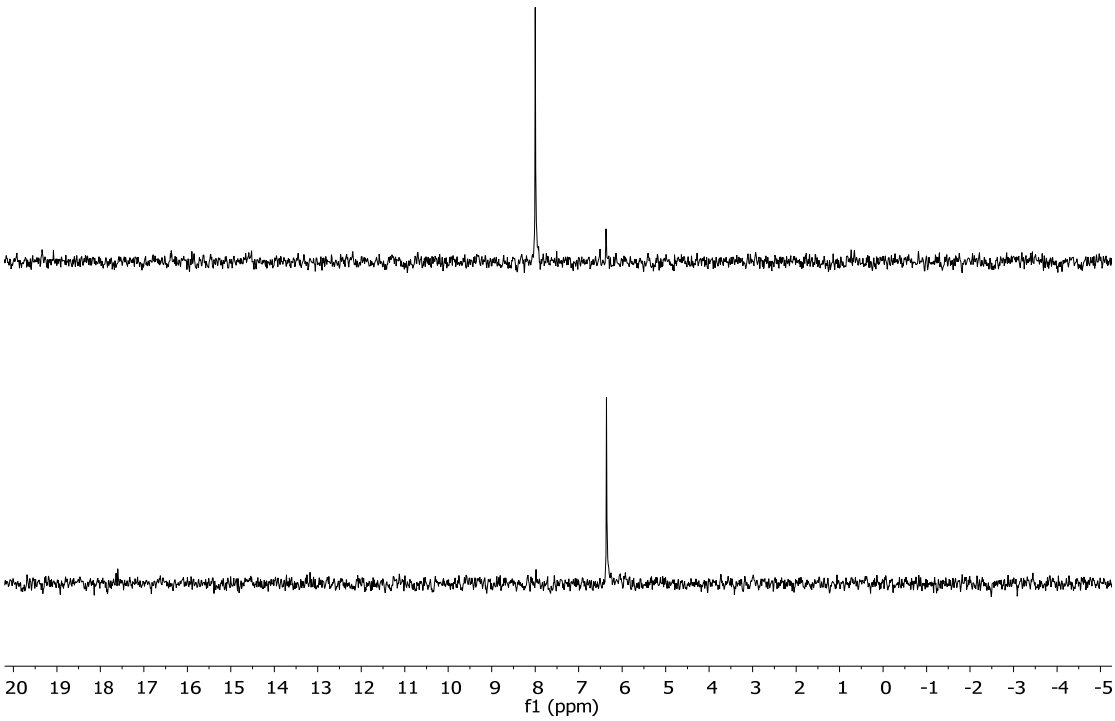

Figure SI 12: ^{29}Si NMR spectra of compounds **4** (top) and **5** (bottom) in $[D_3]ACN$.

^{1}H and ^{29}Si NMR spectra of compound **6** in [D_6]benzene.

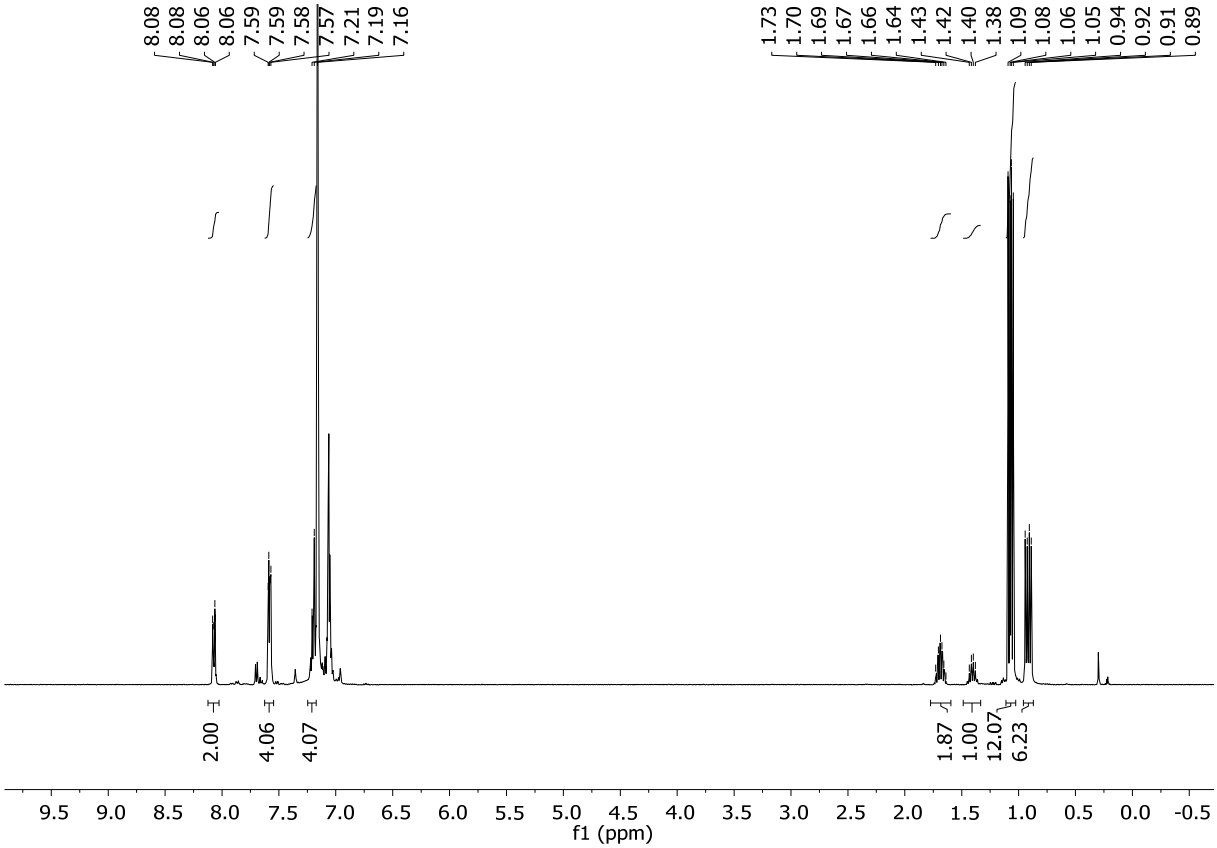

Figure SI 13: ^{1}H NMR spectrum of compound [$Ge_9(SiPh_3)_2]_2(Cu^iPr_3)_4$ (**6**) in [D_6]Benzene.

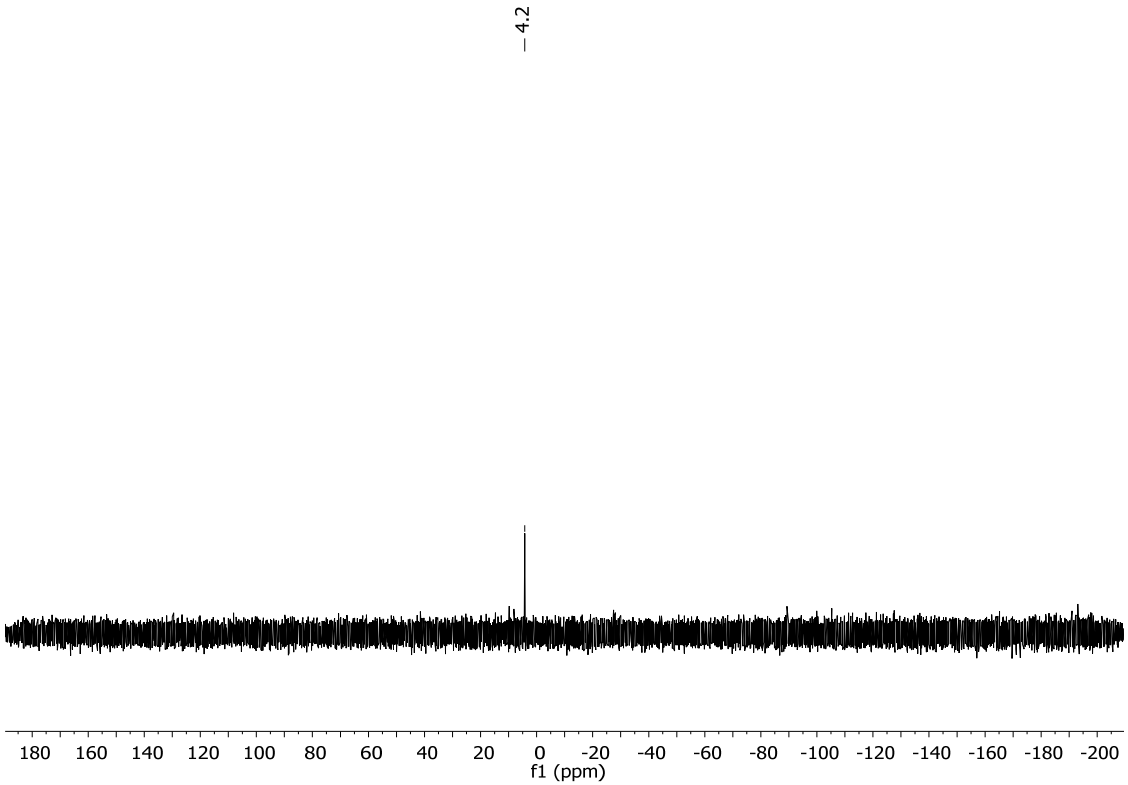

Figure SI 14: ^{29}Si NMR spectrum of compound [$Ge_9(SiPh_3)_2]_2(Cu^iPr_3)_4$ (**6**) in [D_6]Benzene.

2 ESI-MS data of compounds **2** – **6**.

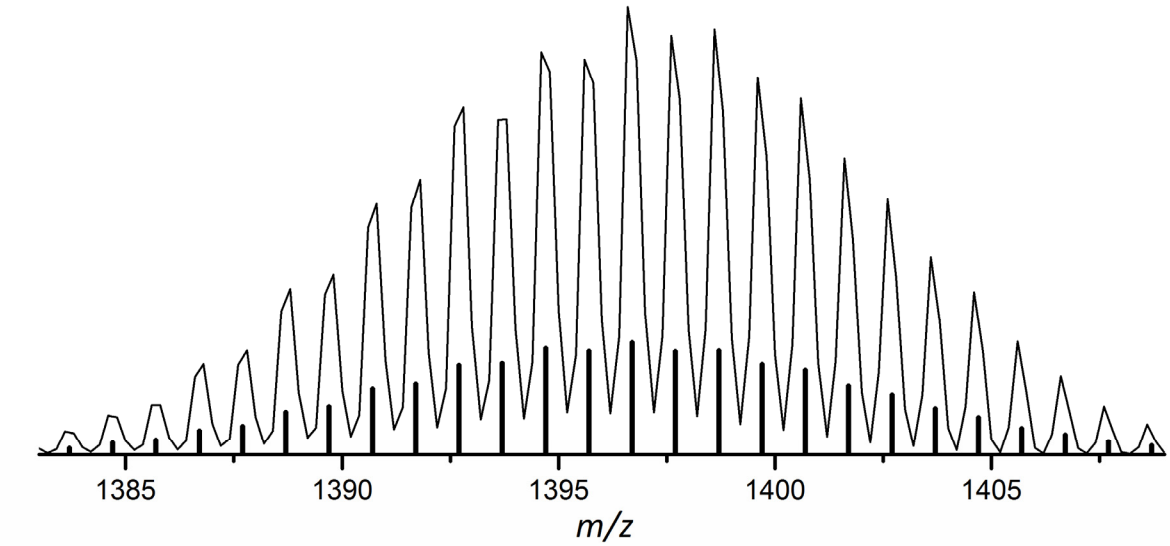

Figure SI 15: ESI-MS spectrum of compound **2**: $[Ge_9(SiPh_3)_3]^-$ (negative mode, 4000 V, 300 °C).

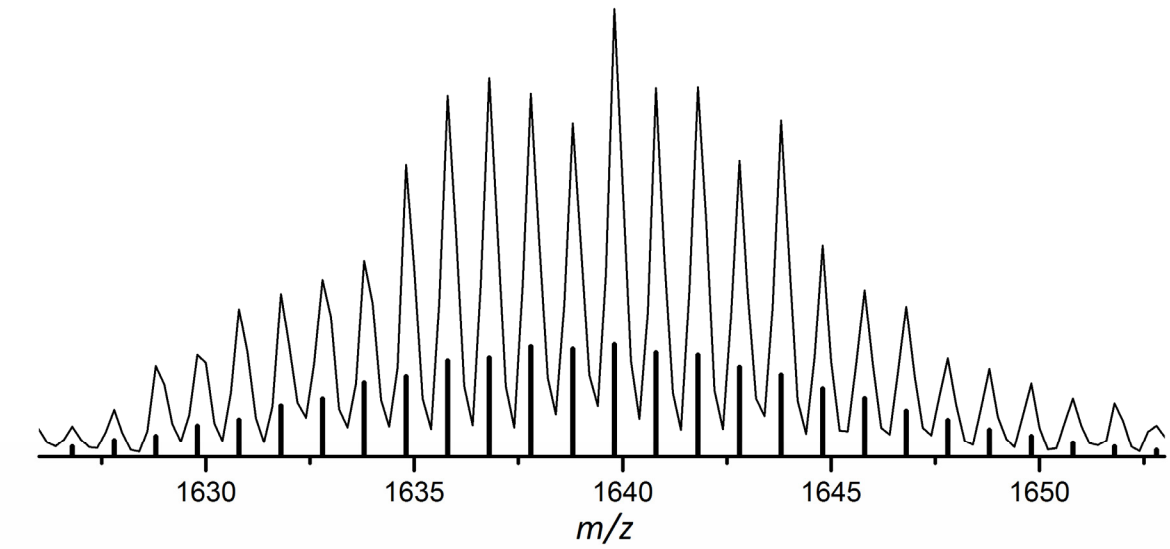

Figure SI 16: ESI-MS spectrum of compound **2**: $[Ge_9(Si(SiMe_3)_3)_3ZnCp^*(ACN)]^+$ (positive mode, −6000 V, 300 °C).

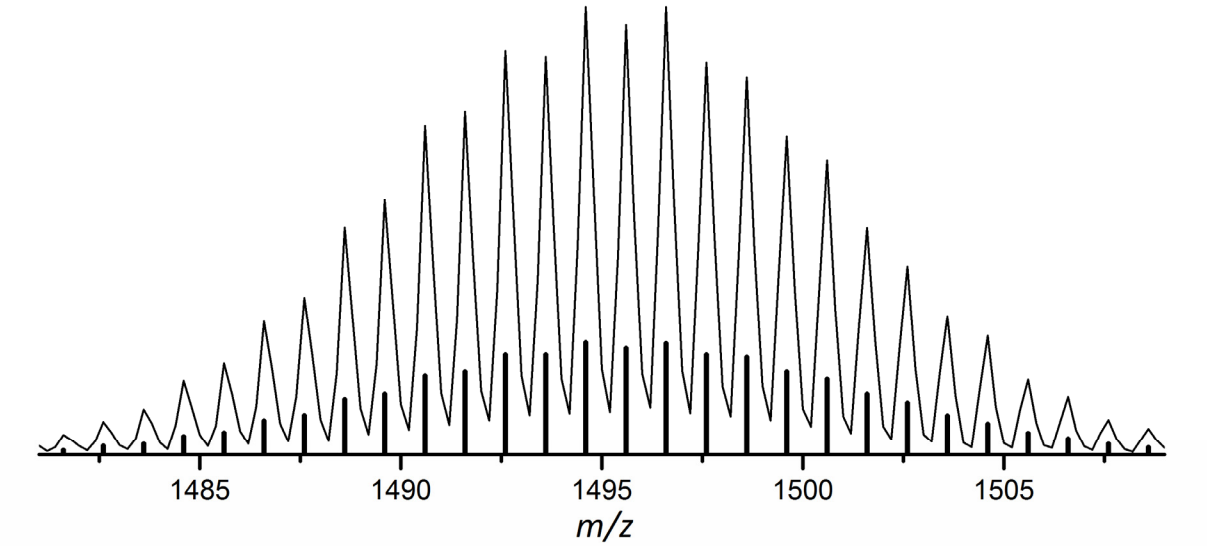

Figure SI 17: ESI-MS spectrum of compound **3**: $[Ge_9(Si(SiMe_3)_3)_3CuCl]^-$ (negative mode, 4000 V, 300 °C).

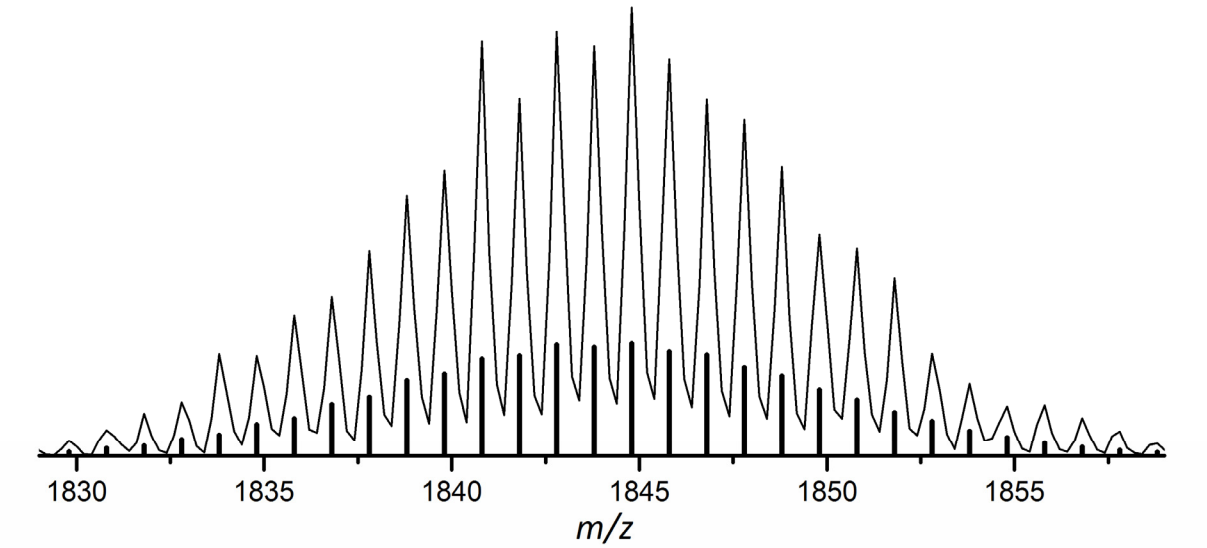

Figure SI 18: ESI-MS spectrum of compound **3**: $[Ge_9(Si(SiMe_3)_3)_3(CuP\textit{i}Pr_3)_2]^+$ (positive mode, −4000 V, 300 °C).

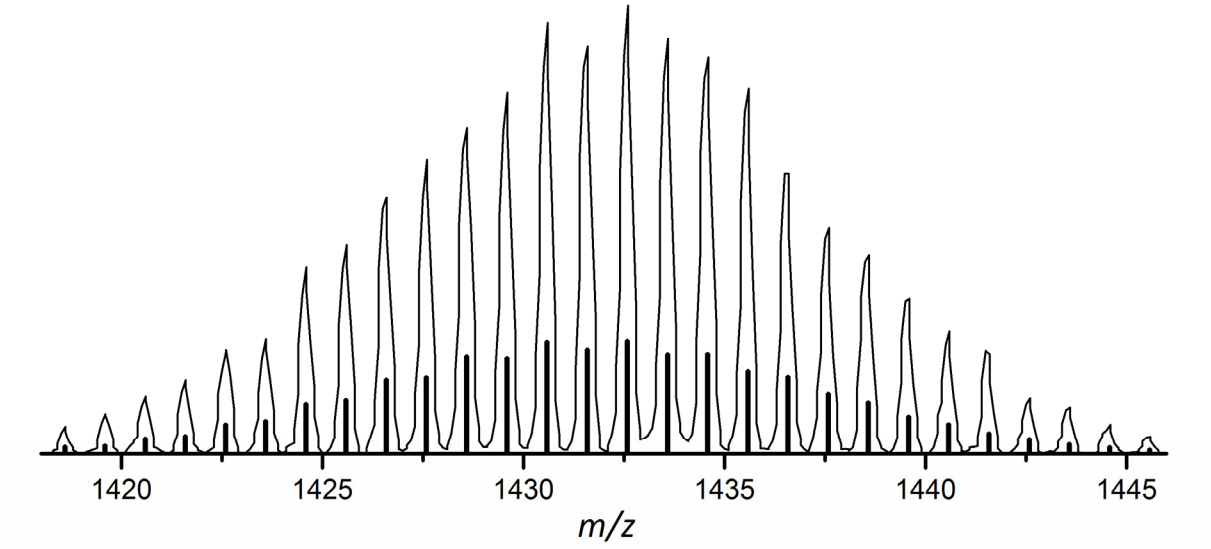

Figure SI 19: ESI-MS spectrum of compound **4**: $[Ge_9(SiPh_3)_3]^-$ (negative mode, 3500 V, 300 °C).

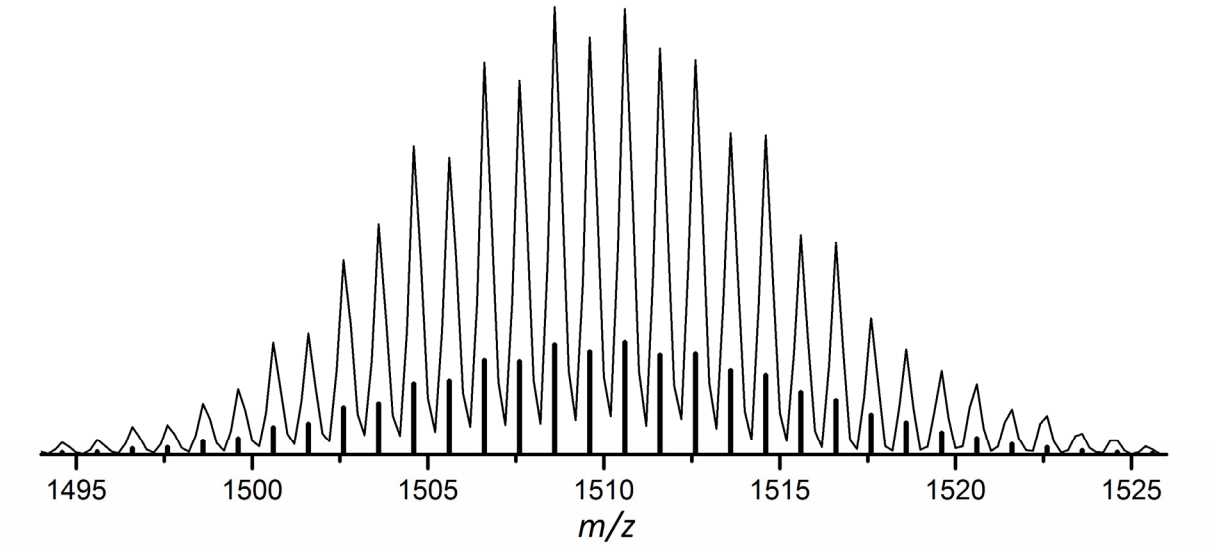

Figure SI 20: ESI-MS spectrum of compound **4**: $[K_2Ge_9(SiPh_3)_3]^+$ (positive mode, −3700 V, 300 °C).

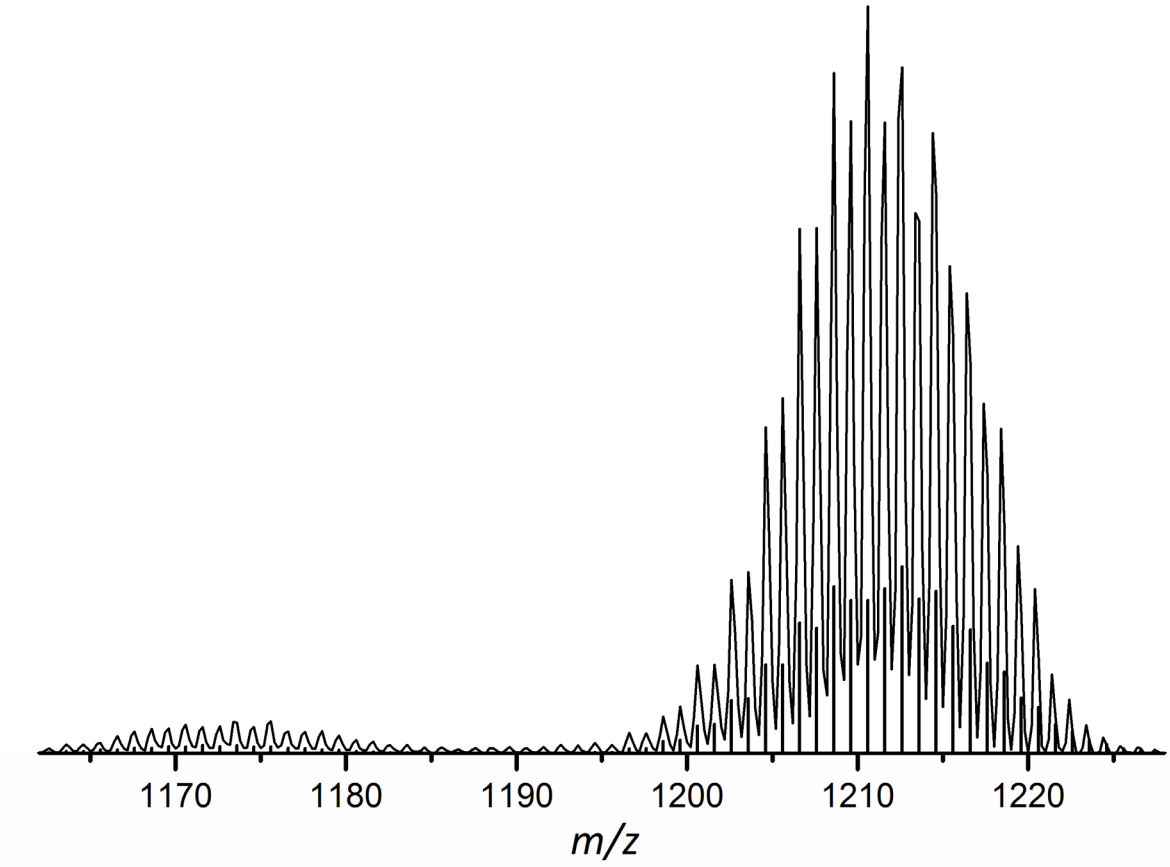

Figure SI 21: ESI-MS spectrum of compound **4**: $[KGe_9(SiPh_3)_2]^-$ (*m/z* = 1212) and $[Ge_9(SiPh_3)_2]^-$ (*m/z* = 1172) (negative mode, 4000 V, 300 °C).

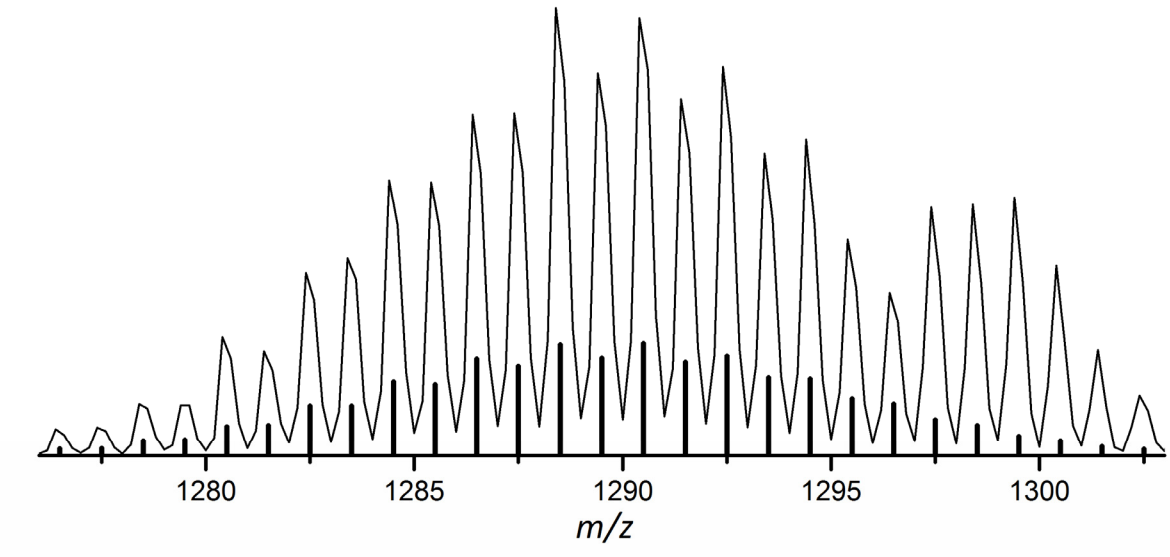

Figure SI 22: ESI-MS spectrum of compound **4**: $[K_3Ge_9(SiPh_3)_2]^+$ (positive mode, −6000 V, 300 °C).

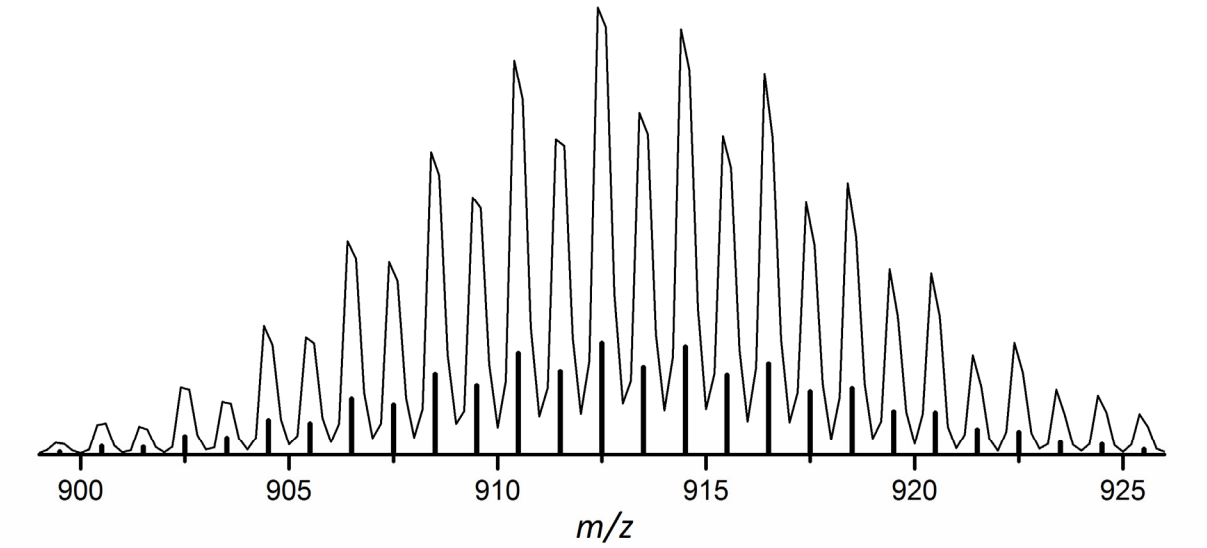

Figure SI 23: ESI-MS spectrum of compound **4**: $[Ge_9(SiPh_3)]^-$ (negative mode, 4000 V, 300 °C).

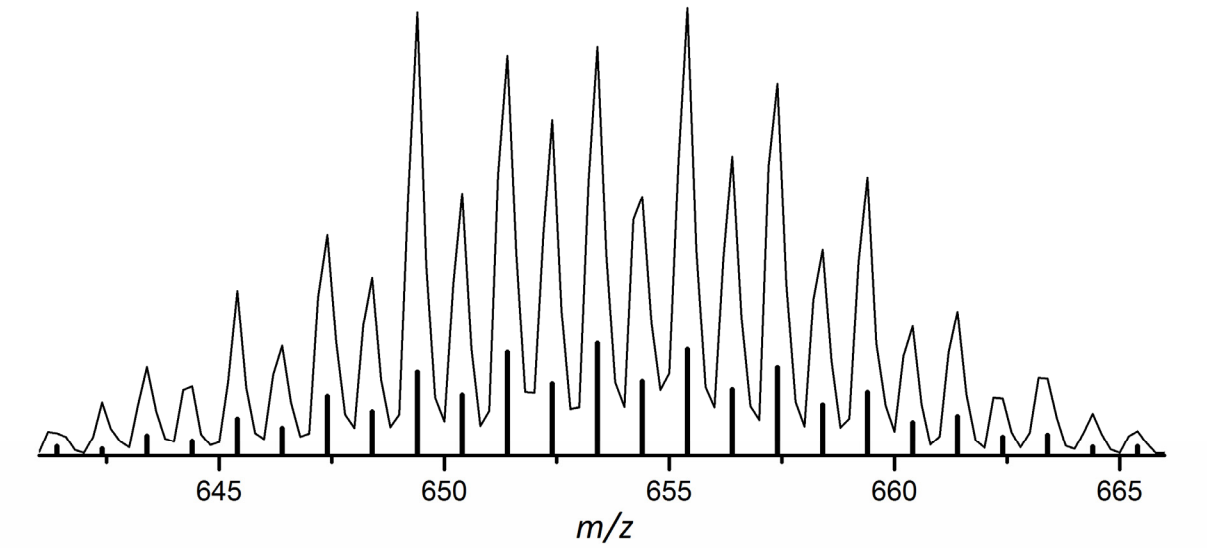

Figure SI 24: ESI-MS spectrum of compound **4**: $[Ge_9]^-$ (negative mode, 4000 V, 300 °C).

3 Crystallographic details

Unit cells of compound **1** – **3** and **6**

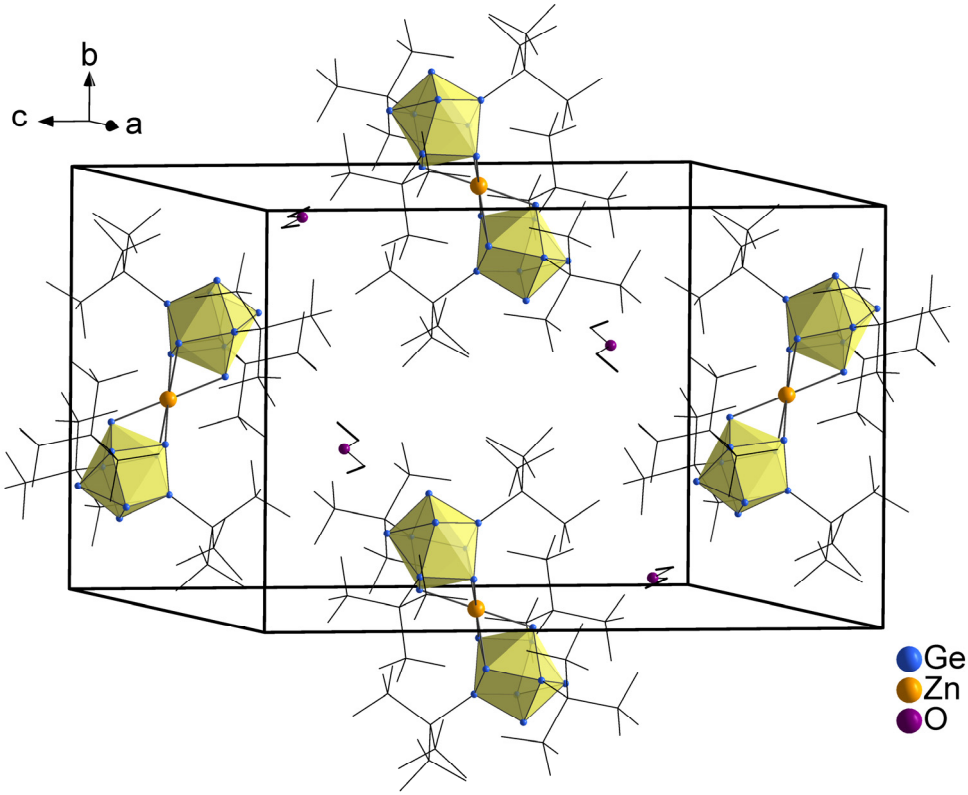

Figure SI 25: Unit cell of compound **1**. Ge atoms are blue, Zn atoms orange and oxygen atoms purple. The clusters are shown as polyhedra, whereas for reasons of clarity Si and C atoms are represented as wire/sticks, and H atoms are not shown.

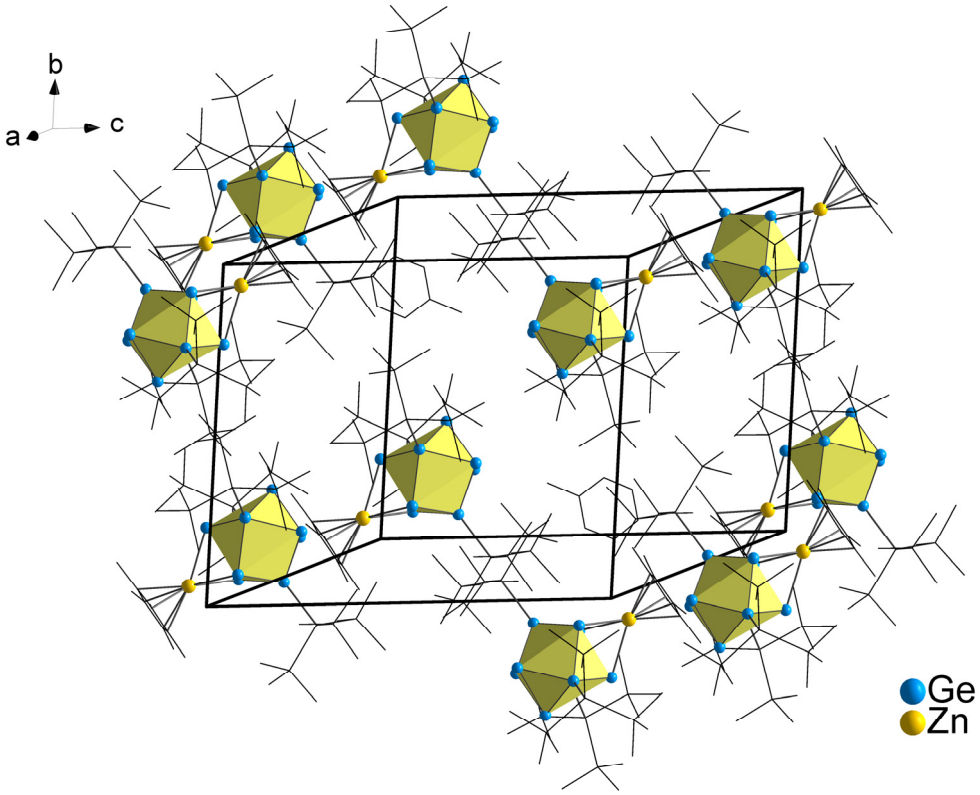

Figure SI 26: Unit cell of compound **2**. Ge atoms are blue and Zn atoms orange. The clusters are shown as polyhedra, whereas for reasons of clarity Si and C atoms are represented as wire/sticks, and H atoms are not shown.

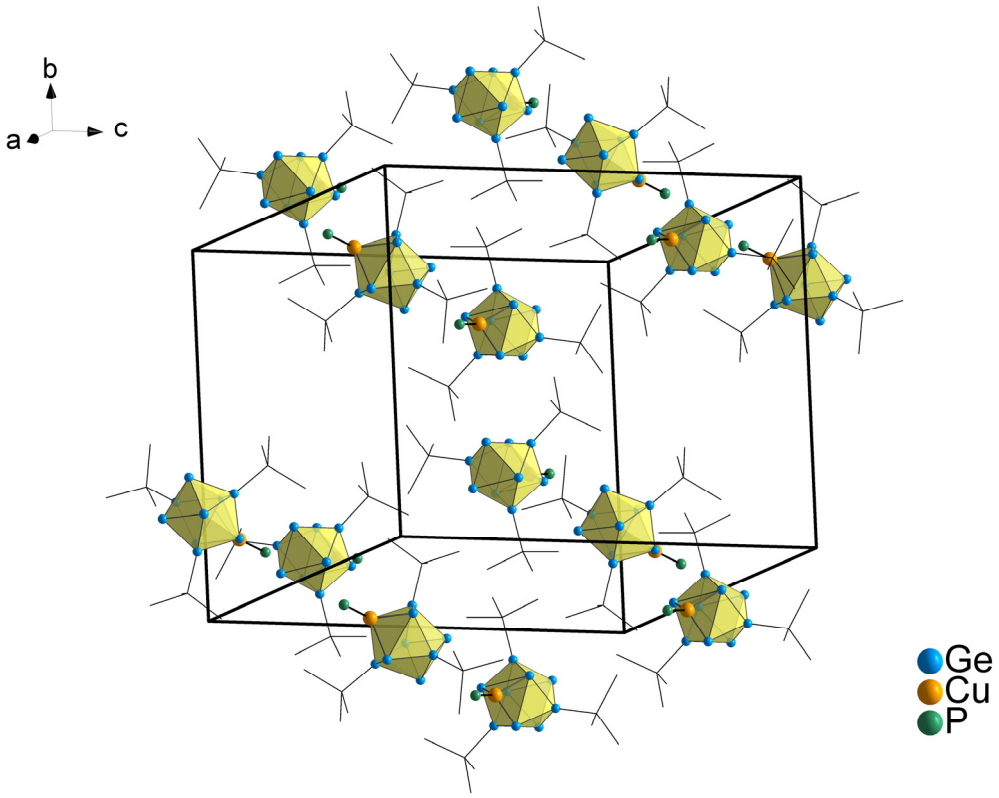

Figure SI 27: Unit cell of compound **3**. Ge atoms are blue, Cu atoms orange and P atoms green. The clusters are shown as polyhedra, whereas for reasons of clarity Si atoms are represented as wire/sticks, and H and C atoms are not shown.

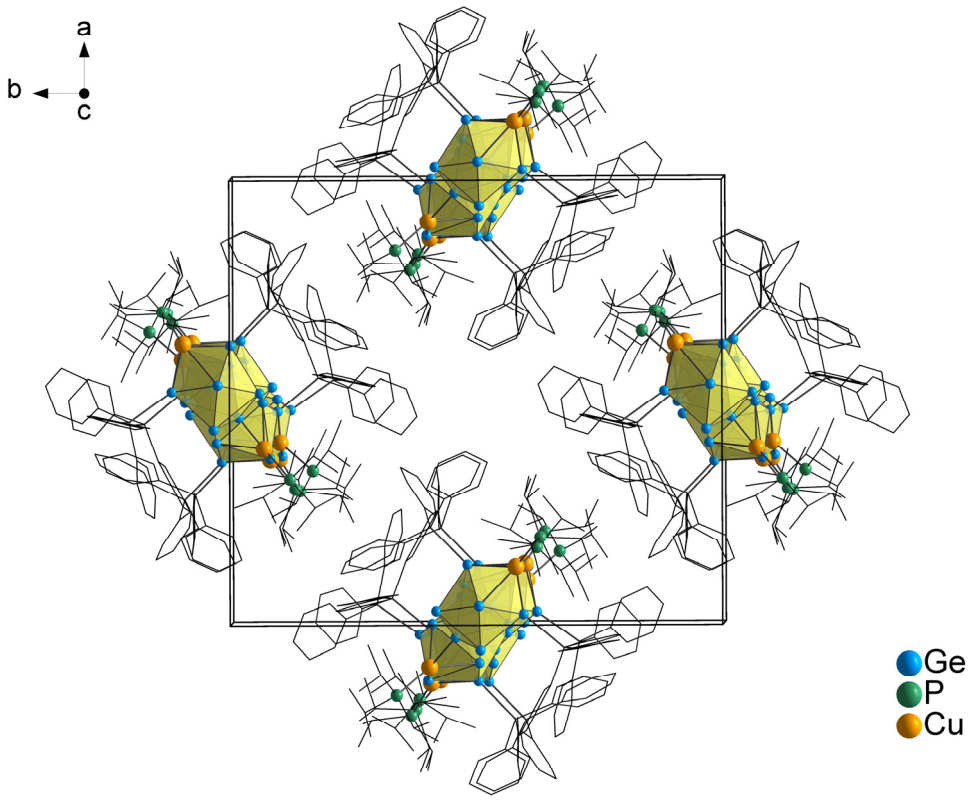

Figure SI 28: Unit cell of compound **6**. Ge atoms are blue, Cu atoms orange and P atoms green. The clusters are shown as polyhedra, whereas for reasons of clarity Si and C atoms are represented as wire/sticks, and H atoms are not shown.

Anisptropic view on molecular structures of compound **1** – **3** and **6**

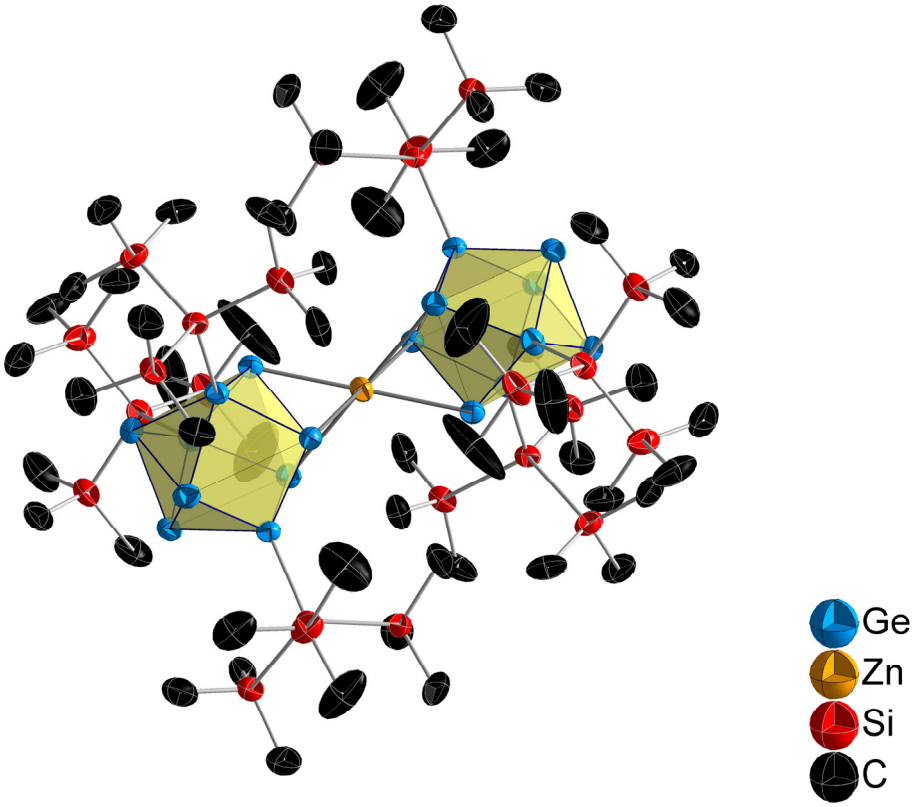

Figure SI 29: Molecular structure of **1**. Ge atoms are blue, Zn atoms orange, Si atoms red and C atom black. H atoms are not shown. The clusters are shown as polyhedral and all atoms are shown as ellipsoids with 70% probability.

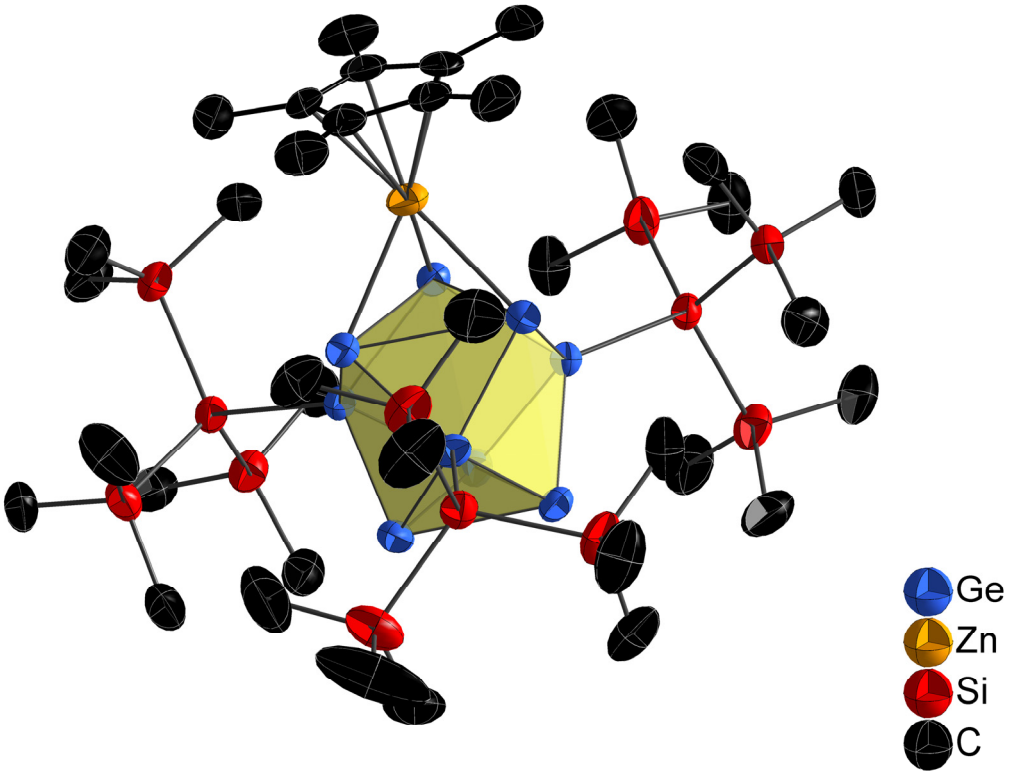

Figure SI 30: Molecular structure of **2**. Ge atoms are blue, Zn atoms orange, Si atoms red and C atom black. H atoms are not shown. The clusters are shown as polyhedral and all atoms are shown as ellipsoids with 70% probability.

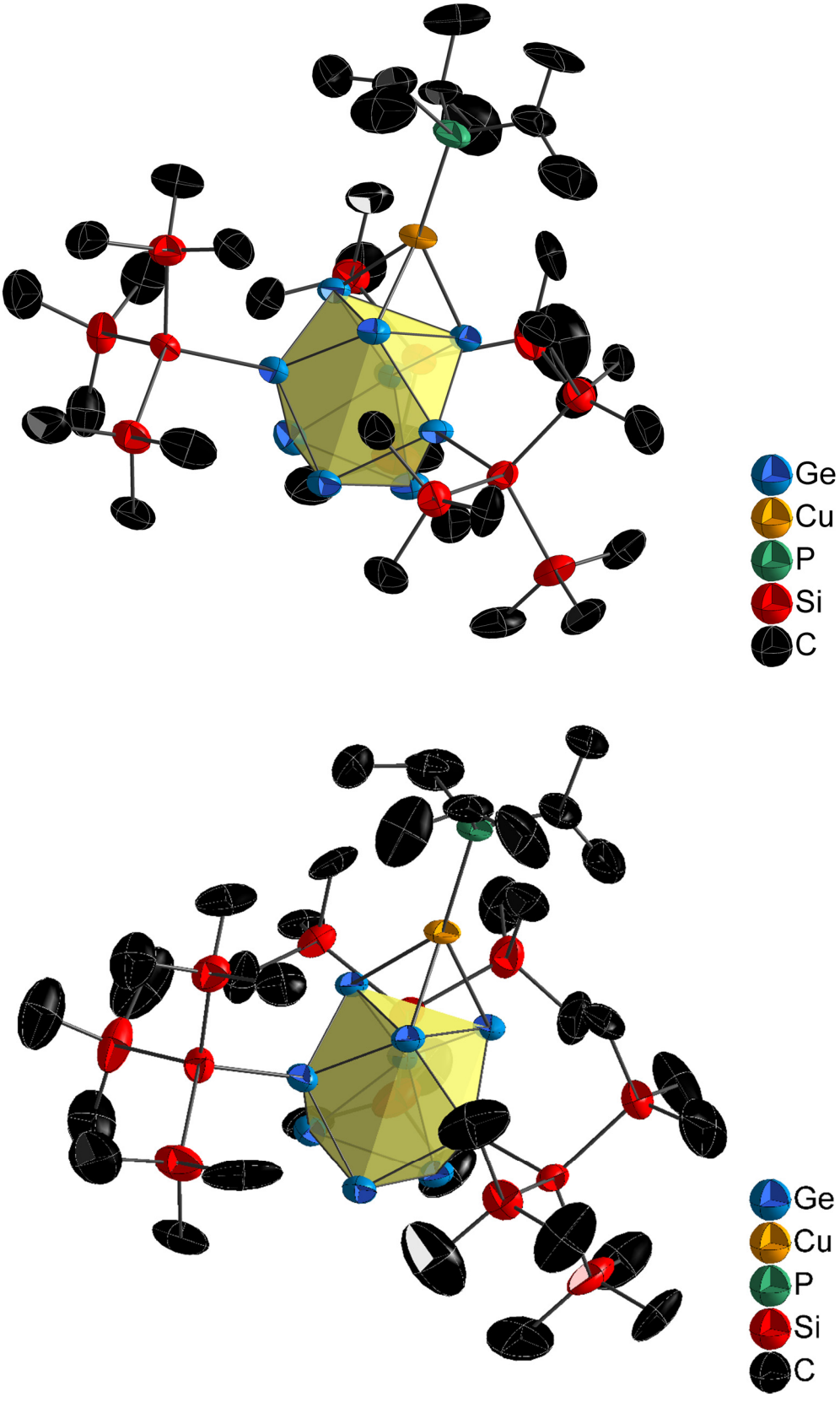

Figure SI 31: Molecular structure of the two crystallographic independent clusters of **3**. Only one position of the disorded *i*Pr groups is shown in the top picture. Ge atoms are blue, Cu atoms orange, Si atoms red, P atoms green and C atoms black. H atoms are not shown. The clusters are shown as polyhedral and all atoms are shown as ellipsoids with 70% probability.

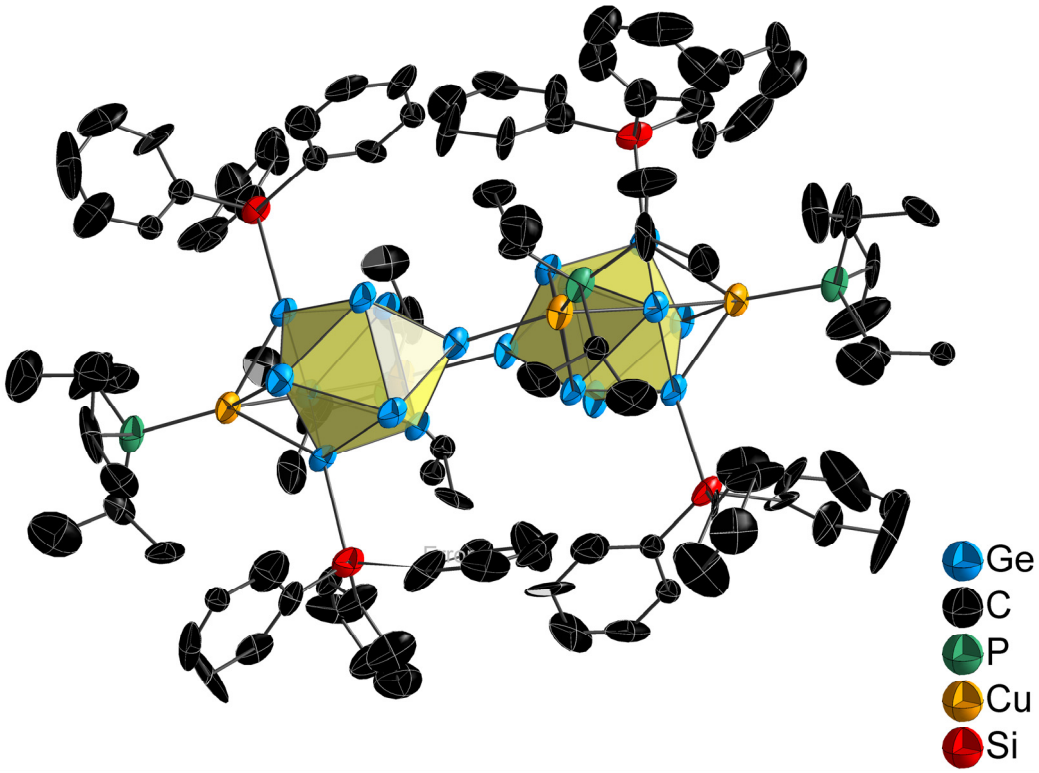

Figure SI 31: Molecular structure of **6**. Ge atoms are blue, Cu atoms orange, Si atoms red, P atoms green and C atoms black. H atoms are not shown. The clusters are shown as polyhedral and all atoms are shown as ellipsoids with 70% probability.

Selected bond lengths of compounds **1** – **3** and **6**.

Table SI 1: Selected bond lengths (Å) in **1**.

$[Ge_9(Si(SiMe_3)_3)_3]_2Zn(Et_2O)$ (**1**)			
Ge1-Ge2	2.9292(8)	Ge4-Ge7	2.5654(8)
Ge1-Ge3	2.8909(9)	Ge4-Ge8	2.5635(8)
Ge1-Ge4	2.5145(8)	Ge5-Ge8	2.5671(9)
Ge1-Ge6	2.5098(8)	Ge5-Ge9	2.5661(8)
Ge2-Ge4	2.5050(9)	Ge6-Ge7	2.5635(8)
Ge2-Ge3	2.8660(8)	Ge6-Ge9	2.5633(8)
Ge2-Ge5	2.5088(8)	Ge7-Ge8	2.6572(8)
Ge3-Ge5	2.5116(8)	Ge7-Ge9	2.6403(9)
Ge3-Ge6	2.5025(9)	Ge8-Ge9	2.6156(8)
Ge1-Zn1	2.7409(6)	Ge4-Si1	2.391(2)
Ge2-Zn1	2.7253(6)	Ge5-Si5	2.382(2)
Ge3-Zn1	2.6985(6)	Ge6-Si9	2.390(1)

Table SI 2: Selected bond lengths (Å) in **2**.

$[Ge_9(Si(SiMe_3)_3)_3]ZnCp^*(tol)$ (**2**)			
Ge1-Ge2	2.9676(6)	Ge4-Ge7	2.5796(6)
Ge1-Ge3	2.9564(6)	Ge4-Ge9	2.5633(6)
Ge1-Ge4	2.4889(6)	Ge5-Ge7	2.5550(6)
Ge1-Ge6	2.4927(6)	Ge4-Ge8	2.5594(6)
Ge2-Ge4	2.4934(6)	Ge6-Ge8	2.5630(6)
Ge2-Ge3	2.9707(6)	Ge6-Ge9	2.5709(6)
Ge2-Ge5	2.4958(5)	Ge7-Ge8	2.6593(6)
Ge3-Ge5	2.5001(6)	Ge7-Ge9	2.6356(6)
Ge3-Ge6	2.4930(6)	Ge8-Ge9	2.6314(6)
Ge1-Zn1	2.6427(6)	Ge4-Si1	2.383(1)
Ge2-Zn1	2.6383(6)	Ge5-Si5	2.379(1)
Ge3-Zn1	2.6619(6)	Ge6-Si9	2.378(1)

Table SI 3: Selected bond lengths (Å) in **3**.

$[Ge_9(Si(SiMe_3)_3)_3]CuP\textit{i}Pr_3(tol)_{0.5}$ (**3**)			
Ge1-Ge2	2.918(1)	Ge10-Ge11	2.837(1)
Ge1-Ge3	2.870(1)	Ge10-Ge12	2.835(1)
Ge1-Ge4	2.507(1)	Ge10-Ge13	2.501(1)
Ge1-Ge5	2.514(1)	Ge10-Ge15	2.501(1)
Ge2-Ge3	2.845(1)	Ge11-Ge12	2.908(1)
Ge2-Ge5	2.497(1)	Ge11-Ge14	2.508(1)
Ge2-Ge6	2.504(1)	Ge11-Ge15	2.506(1)
Ge3-Ge4	2.450(1)	Ge12-Ge13	2.507(1)
Ge3-Ge6	2.507(1)	Ge12-Ge14	2.521(1)
Ge4-Ge7	2.563(1)	Ge13-Ge16	2.563(1)
Ge4-Ge9	2.566(1)	Ge13-Ge18	2.557(1)
Ge5-Ge7	2.558(1)	Ge14-Ge16	2.566(1)
Ge5-Ge8	2.554(1)	Ge14-Ge17	2.558(1)
Ge6-Ge8	2.559(1)	Ge15-Ge17	2.574(1)
Ge6-Ge9	2.559(1)	Ge16-Ge18	2.564(1)
Ge7-Ge8	2.687(1)	Ge16-Ge17	2.696(1)
Ge7-Ge9	2.651(1)	Ge16-Ge18	2.645(1)
Ge8-Ge9	2.627(1)	Ge17-Ge18	2.635(1)

Ge1-Cu1	2.503(1)	Ge10-Cu2	2.470(1)
Ge2-Cu1	2.488(1)	Ge11-Cu2	2.515(1)
Ge3-Cu1	2.461(1)	Ge12-Cu2	2.519(1)
Ge4-Si1	2.381(3)	Ge13-Si21	2.381(2)
Ge5-Si5	2.380(3)	Ge14-Si17	2.394(3)
Ge6-Si9	2.379(2)	Ge15-Si13	2.384(3)

Table SI 4: Selected bond lengths (Å) in **6**.

$[Ge_9(SiPh_3)_2]_2(Cu\textit{i}Pr_3)_4\,(tol)_{3.4}$(**6**)			
Ge1-Ge2	2.728(2)	Ge10-Ge11	2.792(2)
Ge1-Ge3	2.793(2)	Ge10-Ge12	2.724(2)
Ge1-Ge4	2.542(2)	Ge10-Ge14	2.554(2)
Ge1-Ge5	2.556(2)	Ge10-Ge15	2.559(2)
Ge2-Ge3	2.692(2)	Ge11-Ge12	2.727(2)
Ge2-Ge5	2.655(2)	Ge11-Ge13	2.554(2)
Ge2-Ge6	2.653(2)	Ge11-Ge14	2.541(2)
Ge3-Ge4	2.538(2)	Ge12-Ge13	2.655(2)
Ge3-Ge6	2.559(2)	Ge12-Ge15	2.635(2)
Ge4-Ge7	2.565(2)	Ge13-Ge16	2.681(2)
Ge4-Ge8	2.589(2)	Ge13-Ge17	2.571(2)
Ge5-Ge8	2.578(2)	Ge14-Ge17	2.581(2)
Ge5-Ge9	2.678(2)	Ge14-Ge18	2.581(2)
Ge6-Ge7	2.559(2)	Ge15-Ge16	2.688(2)
Ge6-Ge9	2.677(2)	Ge15-Ge18	2.571(2)
Ge7-Ge8	2.683(2)	Ge16-Ge17	2.613(2)
Ge7-Ge9	2.629(2)	Ge16-Ge18	2.642(2)
Ge8-Ge9	2.631(2)	Ge17-Ge18	2.688(2)
Ge1-Cu1	2.569(2)	Ge10-Cu3	2.621(2)
Ge2-Cu1	2.553(2)	Ge11-Cu3	2.615(2)
Ge3-Cu1	2.667(2)	Ge12-Cu3	2.514(2)
Ge2-Cu2	2.533(2)	Ge12-Cu4	2.544(2)
Ge5-Cu2	2.449(2)	Ge13-Cu4	2.426(2)
Ge6-Cu2	2.452(2)	Ge15-Cu4	2.473(2)
Ge9-Cu2	2.570(2)	Ge16-Cu4	2.576(2)
Ge4-Cu3	2.424(2)	Ge14-Cu1	2.421(2)
Ge5-Si1	2.416(4)	Ge13-Si3	2.413(4)
Ge6-Si2	2.401(4)	Ge15-Si4	2.408(4)

6.3 Utilization of Si_9 Clusters from $K_{12}Si_{17}$ Precursor Material for Subsequent Reactions

Lorenz J. Schiegerl, Wilhelm Klein and Thomas F. Fässler*

Manuscript for Publication. 2019.

Content and contributions:

Ambition of this work was the exploration of Si–H functionalization *via* silylation for Ge_9 clusters and the utilization of Si_9 clusters in ethylenediamine solution as well as *via* silylation including reactivity studies. The manuscript was authored by me within the course of this PhD Thesis and reviewed by *Prof. Thomas Fässler* and *Dr. Wilhelm Klein.* Synthesis of the silirane compound (2-butene)Si^{t}Bu$_2$ was done by *Fabian Herz* (TECHNICAL UNIVERSITY OF MUNICH) who also supported data evaluation to the reactivity experiments. The work was done within the framework of the WACKER INSTITUTE FOR SILICON CHEMISTRY (TECHNICAL UNIVERSITY OF MUNICH).

Solubility experiments of $K_{12}Si_{17}$ in ethylenediamine yielded $[H_2Si_9]^{2-}$ cluster species. The species was synthesized and characterized by me (NMR, ESI-MS). A reactivity experiment with TMS-C≡C-TMS in ethylenediamine indicated the formation of a $[(CH_2CH)_xSi_9]^{(4-x)-}$ species in NMR (synthesis and characterization by me). Si–H-functionalized $[(SiHR_2)_3Ge_9]^-$ and $[\{Si(TMS)_3\}_2(SiHR_2)Ge_9]^-$ (R = ^{i}Pr, Ph) clusters were obtained from reactions of K_4Ge_9 and $[\{Si(TMS)_3\}_2Ge_9]^{2-}$ with $SiHR_2Cl$ (R = ^{i}Pr, Ph) chlorosilanes, respectively. All cluster species were synthesized and characterized (ESI-MS) by me. Reaction of $K_{12}Si_{17}$ with Si^{i}Pr$_3$Cl showed the formation of $[(Si^iPr_3)_3Si_9]^-$ (ESI-MS) and yielded single crystals of $[(Si^iPr_3)_2Si_9]^{2-}$ (SC-XRD). Synthesis and characterization of $[(Si^iPr_3)_3Si_9]^-$ and $[(Si^iPr_3)_2Si_9]^{2-}$ were supported by *Hussayn Ahmed* (TECHNICAL UNIVERSITY OF MUNICH) during a research laboratory course, which was supervised by me. A reactivity experiment of $[(SiH^tBu_2)_3Si_9]^-$ with (2-butene)Si^{t}Bu$_2$ silirane indicated the formation of $[(SiH^tBu_2)_7Si_9]^-$ in ESI-MS and NMR experiments. The reactivity experiment and its characterization were carried out by me.

Utilization of Si_9 Clusters from $K_{12}Si_{17}$ Precursor Material for Subsequent Reactions

Lorenz J. Schiegerl,[ab] Wilhelm Klein[a] and Thomas F. Fässler*[ab]

[a] Department of Chemistry, Technische Universität München; [b] WACKER Institute of Silicon Chemistry; Technische Universität München, Lichtenbergstraße 4, 85748 Garching (Germany);

E-mail: thomas.faessler@lrz.tum.de

Abstract

The transfer of vinylation and silylation reactions from Ge_9 to Si_9 clusters was investigated to develop the utilization of silicon clusters in the $K_{12}Si_{17}$ *Zintl* precursor for material building blocks. In analogy to previously reported investigations in pyridine, a transfer of $K_{12}Si_{17}$ solid material to ethylenediamine solution yielded soluble $[H_2Si_9]^{2-}$ (**1**) clusters which were detected by NMR (^{1}H, ^{29}Si) and ESI-MS measurements. Thereby, precursor "*activation*" with 222crypt/liquid ammonia was manifested to play a key-role for the precursor utilization. The utilization of ethylenediamine as cluster solvents paves the way for Si_9 cluster vinylations by reaction with TMS-C≡C-TMS, as already established for Ge_9 clusters, and the formation of a $[(CH_2CH)_xSi_9]^{n-}$ (x = 1, 2, 3; n = 4–x) species was indicated by NMR (^{1}H, ^{29}Si) measurements. Furthermore, reaction of "$K_{12}Si_{17}$ (*activated*)" with Si^iPr_3Cl in thf yielded the ligand-stabilized cluster $[(Si^iPr_3)_2Si_9]^{2-}$ (**2**) in single crystals. The molecular structure of **2** was determined by X-ray diffraction and promotes the transfer of a wide range of known silylation reaction from Ge_9 to Si_9 clusters. Thereto, Ge_9 cluster silylations with the $SiHR_2Cl$ (R = ^{i}Pr, Ph) chlorosilanes were studied in ESI-MS experiments and revealed mass peaks for triple and mono Si–H-functionalized $[(SiHR_2)_3Ge_9]^-$ {R = ^{i}Pr (**3**), Ph (**4**)} and $[\{Si(TMS)_3\}_2(SiHR_2)Ge_9]^-$ {R = ^{i}Pr (**5**), Ph (**6**)} clusters, respectively. The reactivity of Si–H bonds at functionalized *Zintl* cluster cores was tested by reaction of the Si_9 cluster species $[(SiH^tBu_2)_3Si_9]^-$ with (2-butene)Si^tBu_2 silirane. A detected mass peak for $[(SiH^tBu_2)_7Si_9]^-$ (**7**) in ESI-MS indicated an extension of the cluster reactant by four SiH^tBu_2 groups, and thus, offers a first perspective for further cluster modification.

Introduction

Silicon is a non-toxic semi-conductor, and its abundancy and low costs promote its application for numerous industrial products on larger scale as *e.g.* polysiloxanes (silicones).[1-4] Regarding nowadays high-tech products, fabricated silicon-based materials are key-components and find *inter alia* application in electronics,[5-7] photovoltaics[8-10] and batteries.[11-13] Due to the high demand on novel silicon materials, synthetic access to preformed silicon structures as contained in $A_{12}Si_{17}$ silicon *Zintl* precursors (readily containing 1x Si_9^{4-} and 2x Si_4^{4-} clusters, *A* = K–Cs)[14-16] is of central interest with focus on cluster species with tunable properties and accessibility for future material fabrications.[5, 17-21]

The chemistry of soluble tetrel clusters, which are obtained by extrusion of clusters that are performed in binary solids, is well established for Ge_9 units.[22-25] Thereby, the utilization of K_4Ge_9 precursor material (readily containing Ge_9^{4-}) was constantly promoted by its solubility in ethylenediamine.

Cluster solutions of this solvent yielded oxidative clusters couplings under formation of larger cluster structures as *e.g.* Ge_9 tetramers[26] and polymers.[27] Moreover, olefin groups were attached at Ge_9 cluster cores in reactions with alkyne reactants in ethylenediamine and allowed tetrel cluster functionalization for the first time. It was shown that the solvent plays a key-role for the mechanistic hydrogenation of the triple bond to a double bond.[28-30] Among many other examples, vinyl-functionalized $[(CH_2CH)_xGe_9]^{n-}$ (x = 1, 2, 3; n = 4–x) species (Figure 1c and d)[29-31] were obtained by reaction of K_4Ge_9 with bis(trimethylsilyl)acetylene (TMS-C≡C-TMS). Moreover, reactions of K_4Ge_9 with 1,4-bis-(trimethylsilyl)butadiyne (TMS-C≡C-C≡C-TMS) revealed an application potential of vinylation reactions for the formation of *Zintl* triads by linking Ge_9 clusters to $[R\text{-}Ge_9\text{-}CH{=}CH\text{-}CH{=}CH\text{-}Ge_9\text{-}R]^{4-}$ {R = H or (2Z,4E)-7-amino-5-aza-hepta-2,4-dien-2-yl}.[32-33]

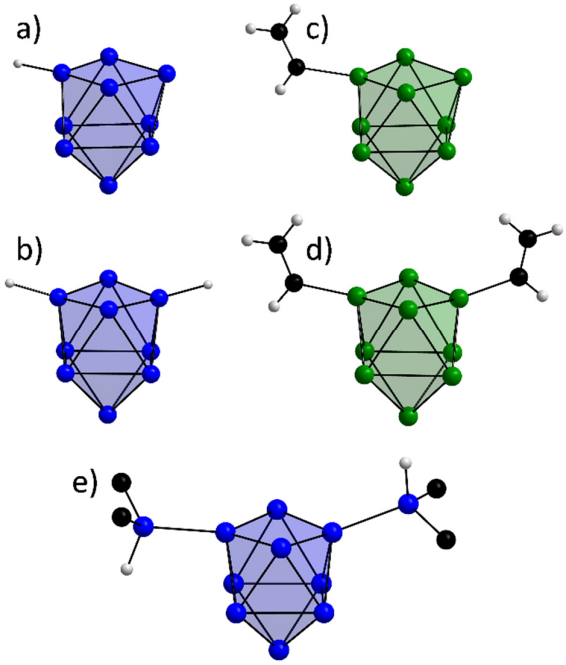

Figure 1. Functionalized Si_9 and Ge_9 cluster species in literature: a) the mono-protonated Si_9 cluster $[HSi_9]^{3-}$;[34] b) the di-protonated Si_9 cluster $[H_2Si_9]^{2-}$;[35] c) the mono-vinylated Ge_9 cluster $[(CH_2CH)Ge_9]^{3-}$;[31] d) the di-vinylated Ge_9 cluster $[(CH_2CH)_2Ge_9]^{2-}$;[31] e) the di-silylated Si_9 cluster $[(SiH^tBu_2)_2Si_9]^{2-}$.[36] Si and Ge atoms in blue and green, respectively; Si_9 and Ge_9 clusters as blue and green polyhedra, respectively; C atoms in black; H atoms in gray; Me_{tBu} groups are not shown.

Even though also homologues Si_9 clusters are known in $A_{12}Si_{17}$ [14-15] (*A* = K–Cs; readily containing 1x Si_9^{4-} and 2x Si_4^{4-} clusters) binary phases, the chemistry with this cluster precursor is less developed due to solubility limitations (liquid ammonia).[34, 37-39] Only four metal complexes have been reported from further reactions of this precursor in liquid ammonia up to date: $(CuMes)_2Si_4^{4-}$ (Mes = 1,3,5-trimethylbenzene),[40] $(PhZn)Si_9^{3-}$,[41] $(\{Ni(CO)_2\}_2Si_9)_2^{8-}$,[42] and $(NHC^{Dipp}Cu)Si_9^{3-}$ [NHC^{Dipp} = 1,3-bis-(2,6-di-*iso*-propylphenyl)imidazole-2-ylidene].[43]

In contrast, the utilization of Ge_9 clusters was further promoted by cluster silylations that succeeded by modification of the synthetic protocol of Ge_9 clusters. Thereby, attachment of silyl groups at Ge_9 cores proceeds by reaction of K_4Ge_9 with chlorosilanes, along with charge reduction of the polyanionic cluster cores, triggering rapid synthetic progress in this field. The first reported silyated Ge_9 species is

the tri-silylated cluster anion $[\{Si(TMS)_3\}_3Ge_9]^-$ [44] in 2012, and subsequent reports constantly extended the synthetic achievements as *e.g.* by isolation of the di-silyated derivative $[\{Si(TMS)_3\}_2Ge_9]^{2-}$,[45] and by attachment of versatile silyl groups in $[(SiR_3)_3Ge_9]^-$ (R = Ph, *i*Bu, *i*Pr, Et).[46-47] Straight-forward synthetic progress also initiated Ge_9 cluster functionalization *via* silylation as reported by olefin-functionalized $[\{SiPh_2(olefin)\}_3Ge_9]^-$ and $[\{Si(TMS)_3\}_2\{SiPh_2(olefin)\}Ge_9]^-$ (olefin = vinyl, pentenyl) species,[48] and by a Si–H-functionalized $[(SiH^tBu_2)_3Ge_9]^-$ cluster.[49] Silylated Ge_9 cluster species are finely soluble in organic solvents, what gives access to a wide range of practicable synthetic modifications.

The idea to transform anionic silicon structures in *Zintl* precursors to ligand-stabilized silicon clusters was already mentioned in *Wiberg's* report on the tetra-substituted $(Si^tBu_3)_4Si_4$[50] species in 1993. For a long time, synthetic effort towards silicon *Zintl* precursor utilization was repeatedly discarded due to the high reducing properties of contained polyanionic silicon structures,[50-51] but recently, crucial synthetic progress regarding the utilization of $A_{12}Si_{17}$ (*A* = K, Rb) precursor material was achieved. Investigations of precursor solutions in liquid ammonia revealed the formation of protonated $[HSi_9]^{3-}$ clusters (Figure 1a)[34, 52] that undergo a further protonation to $[H_2Si_9]^{2-}$ (Figure 1b) by subsequent transfer to pyridine.[35] Such protonated clusters were not reported for Ge_9 before, and their detection could finally clarify the transfer of $A_{12}Si_{17}$ precursor material to cluster-rich solutions. Therewith, the ground was prepared for further reactivity studies in solution as already established for the related Ge_9 clusters from K_4Ge_9 precursor material.

Synthetic progress to Ge_9 cluster vinylations and silylations demonstrates the synthetic potential of *Zintl* precursor utilization for the fabrication of nanostructures materials as *e.g.* by coupling or surface grafting of obtained cluster species. Regarding Si_9 cluster utilization, the previously reported detection of $[H_2Si_9]^{2-}$ clusters[35] could pave the way for solution-based conversions by introducing the "*activation*" of $K_{12}Si_{17}$ precursor material by 222crypt addition and liquid ammonia treatment as key-step. This led to the first successful silylation of Si_9 clusters, in analogy to reported reactions with K_4Ge_9, by reaction of "$K_{12}Si_{17}$ (*activated*)" with SiH^tBu_2Cl in thf.[49] This crucial synthetic success triggered us to further study the transfer of cluster functionalization *via* vinylation and silylation from Ge_9 to Si_9 clusters with the ambition to generate soluble silicon cluster species which are suitable for further material fabrication from a precursor.

Results and Discussion

The "*activation*" of $K_{12}Si_{17}$ by prior 222crypt/NH_3 treatment improves the solubility of the precursor as confirmed by detection of $[H_2Si_9]^{2-}$ (**1**) clusters in pyridine solution.[35] Herein, the solubility of $K_{12}Si_{17}$ was tested in ethylenediamine by direct addition of the solvent to "*activated*" precursor material and subsequent filtration. An orange filtrate was obtained and investigated in ESI-MS and NMR experiments. ESI-MS revealed the same $\{[K\text{-}222crypt]_3[H_2Si_9]\}^+$ (*m/z* = 1501; Figure 2a, b) mass peak in positive mode as previously obtained from pyridine solution of "$K_{12}Si_{17}$ (*activated*)" (**1**, Figure 1b). The presence of **1** in ethylenediamine was manifested by an ^1H NMR measurement that reveals an indicative signal at −1.51 ppm with a small $<J_{HSi}>$ of 20.4 Hz, which splitting and shift is in agreement with the reported formation of **1** in pyridine {**1** in pyridine: −0.71 ppm, $<J_{HSi}>$ = 19.7 Hz, see Figure 2c}.

The ^{29}Si NMR spectrum shows two peaks at −95.0 and −324 ppm which are consistent with partially substituted Si_9 cluster cores if compared to $[HSi_9]^{3-}$ [52] (substituted atoms Si_H:−159 ppm, ligand-free atoms Si_{Si}: −358 ppm) and corresponding calculated averaged shift for $[H_2Si_9]^{2-}$ at −185 (Si_H) and −395 (Si_{Si}) ppm (NMR spectra in Supporting Information).[35]

The presence of **1** in ethylenediamine solution points towards the testing of cluster vinylations using the TMS-C≡C-TMS reactant, because for the formation of $[(CH_2CH)_xGe_9]^{n-}$ (x = 1, 2, 3; n = 4–x) (Scheme 1a, Figure 1) from K_4Ge_9 the solvent ethylenediamine plays a key-role for the cluster vinylation mechanism including the splitting of the TMS groups and providing vinyl protons in the product.[29-31] TMS-C≡C-TMS (4 eq.) was added to an ethylenediamine solution of "$K_{12}Si_{17}$ (*activated*)" in a sealed NMR tube and NMR spectra (^1H, ^{29}Si) were recorded (NMR spectra in Supporting Information).

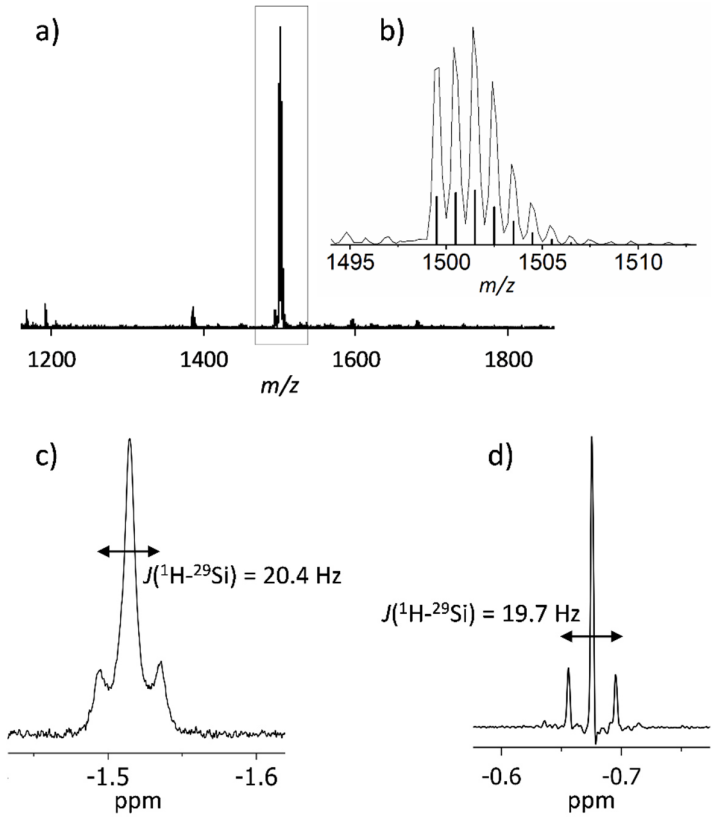

Figure 2. a) ESI-MS mass peak of $\{[K\text{-}222crypt]_3[H_2Si_9]\}^+$ in positive ion mode (*m/z* = 1501); b) Detail view on the mass peak (line: measurement, bars: simulated pattern); c) ^1H NMR signal of $[H_2Si_9]^{2-}$ (**1**) in ethylenediamine (500 MHz); d) ^1H NMR signal of **1** in pyridine.[35] NMR spectra in the Supporting Information.

The ^1H NMR spectrum (spectrum in Supporting Information) of the reaction solution shows three signals each revealing a "doublet of doublet" splitting at 7.57 ppm (J_{HH} = 4.7, 12.8 Hz), 6.68 ppm (J_{HH} = 13.1, 19.5 Hz) and 5.86 ppm (J_{HH} = 5.1, 19.4 Hz). Signal shifts and coupling constants are in good agreement with reported literature values for $[(CH_2CH)Ge_9]^{3-}$ (7.93 ppm, J_{HH} = 12.4, 19.2 Hz; 6.55 ppm, J_{HH} = 4.8, 19.2 Hz; 6.02 ppm, J_{HH} = 4.8, 12.4 Hz) and $[(CH_2CH)_2Ge_9]^{2-}$ (7.35 ppm, J_{HH} = 12.2, 19.3 Hz; 6.44 ppm, J_{HH} = 3.9, 19.3 Hz; 5.94, J_{HH} = 3.9, 12.2 Hz).[31] Thus, the three signals in the ^1H NMR spectrum are consistent with one set of vinyl protons of a corresponding $[(CH_2CH)_xSi_9]^{n-}$ cluster species with equivalent vinyl groups.

The number of attached vinyl groups at the Si_9 core in the molecule cannot be determined by literature comparison because ^1H NMR investigations of reaction solutions containing vinylated Ge_9 species

revealed that mono-, di- and also tri-vinylated cluster species are simultaneously present.[31] Si_9 cluster vinylation was also indicated by a ^{29}Si NMR measurement (spectrum in Supporting Information) of the reaction solution showing two new signals, which are plausible for partially substituted Si_9 cluster cores (substituted atoms Si_{Vinyl}: −38.9 ppm, ligand-free atoms Si_{Si}: −342 ppm). Besides, signals for **1** were found in the ^{1}H and ^{29}Si NMR spectra of the reaction solution. As mentioned, the solvent ethylenediamine plays a key-role the mechanistic hydrogenation of the triple bond to a double bond in Ge_9 cluster vinylation.[28-30] Due to the observation of protonated Si_9 clusters **1** in ethylenediamine, another more simple mechanism might be determining for Si_9 cluster vinylation as *e.g.* alkyne insertion into the Si_9–H bonds.

As mentioned, cluster silylation was recently transferred from Ge_9 to Si_9 by reaction of "$K_{12}Si_{17}$ (*activated*)" with SiH^tBu_2Cl under formation of $[(SiH^tBu_2)_3Si_9]^-$ in bulk material and $[(SiH^tBu_2)_2Si_9]^{2-}$ in single crystals (Figure 1e).[36] To further explore the synthesis of ligand-stabilized silicon clusters with the $K_{12}Si_{17}$ precursor, the reactivity of "$K_{12}Si_{17}$ (*activated*)" was tested with the chlorosilane Si^iPr_3Cl in thf. The reaction yielded a brownish solid after purification. An ESI-MS measurement in thf showed a mass peak corresponding to the simulated isotope pattern of $[(Si^iPr_2)_3Si_9]^-$ (*m/z* = 725, spectrum in Supporting Information), and conclusive for the formation of a tri-silylated Si_9 species in analogy to $[(SiH^tBu_2)_3Si_9]^-$. However, ^{1}H and ^{13}C NMR investigations showed the presence of multiple ^{i}Pr signals and remained inconclusive. A ^{29}Si NMR measurement indicated the formation of silylated Si_9 cluster species within a comparable signal shift range to $[(SiH^tBu_2)_3Si_9]^-$ along with unknown side-products. Crystallization of the bulk material in a fluorobenzene/hexane solvent mixture yielded yellow single crystals, which revealed the molecular structure of $[(Si^iPr_3)_2Si_9]^{2-}$ (**2**, Figure 3) as new derivative to $[(SiH^tBu_2)_2Si_9]^{2-}$ in X-ray diffraction and could prove the silylation of Si_9 clusters in the reaction.

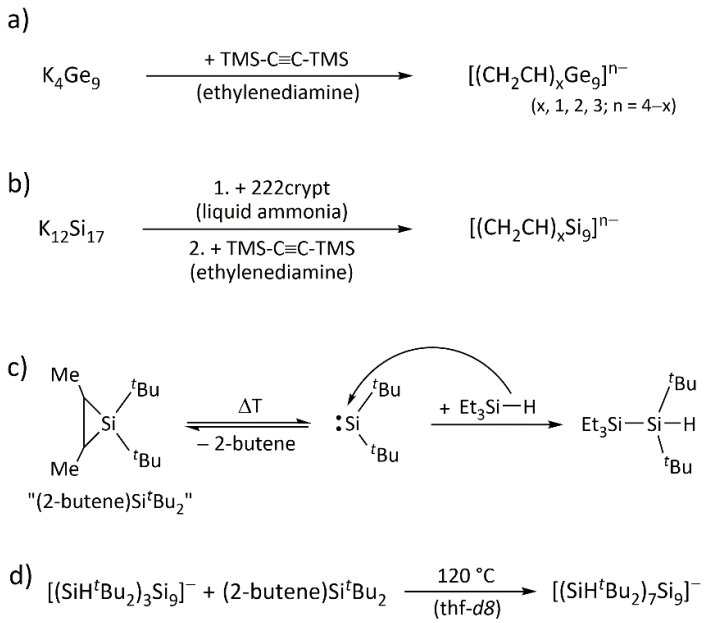

Scheme 1. a) Literature: vinyl-functionalization of Ge_9 clusters from K_4Ge_9 under formation of $[(CH_2CH)_xGe_9]^{n-}$;[29-31] b) This work: vinyl-functionalization of Si_9 clusters from $K_{12}Si_{17}$ under formation of $[(CH_2CH)_xSi_9]^{n-}$; c) Literature: thermic formation of the (tBu)$_2$Si: silylene and Si–H insertion reaction with Et_3SiH; [53-55] d) This work: formation of $[(SiH^tBu_2)_7Si_9]^-$ (**7**) from reaction of $[(SiH^tBu_2)_3Si_9]^-$ with (2-butene)Si^tBu_2 silirane as indicated by ESI-MS.

The structural arrangement in the molecular structure of **2** is comparable with its Si_9 derivative $[(SiHtBu_2)_2Si_9]^{2-}$,[36] as well as the di-silylated Ge_9 derivative $[(SiTMS_3)_2Ge_9]^{2-}$.[45] The structures bear C_{2v} symmetric cluster cores deriving from a mono-capped square antiprism. The silyl groups form covalent *exo*-bonds with the two opposing vertex atoms of the open face of the cluster polyhedron (Si1, Si2, Si3, Si4). Within the Si_9 core, the Si–Si bonds that are formed with the silyl-substituted Si1 and Si3 atoms {range: 2.3515(9) to 2.4395(9) Å} are shortened if compared to Si–Si distances between exposed Si atoms {range: 2.4398(9) to 2.7680(9) Å}. In analogy to $[(SiHtBu_2)_2Si_9]^{2-}$, the longest Si–Si cluster edges are found for Si5–Si6 {2.7680(9) Å} and Si7–Si8 {2.7311(9) Å}, which bond vector lies perpendicular to the external Si–Si bond (corresponding bond length in $[(SiHtBu_2)_2Si_9]^{2-}$: 2.782(2) and 2.764(2) Å). Elongated Si–Si bonds including solely unsubstituted silicon cluster atoms are also found in literature reports to $(Tip)_6Si_6$ {2.7076(8) Å}[56] and $(Mes)_6Si_6$ {2.636(1) Å}[57] as well as in the protonated Si_9 cluster $[HSi_9]^{3-}$ {2.643(2) Å}.[34]

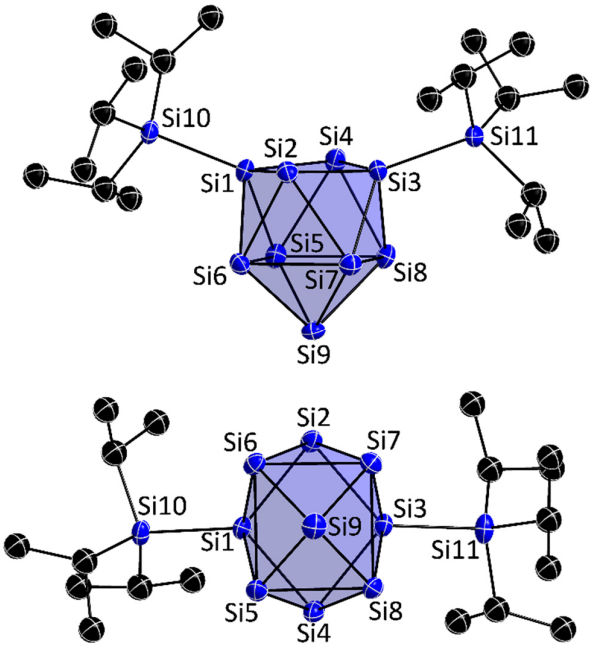

Figure 3. Molecular structure of $[(Si^iPr_3)_2Si_9]^{2-}$ (**2**) [Si atoms (blue) and C atoms (gray) are shown as ellipsoids with 50% probability; H atoms are omitted; Si_9 clusters are shown as blue polyhedra]. Selected Si–Si distances [Å]: Si1–Si10: 2.3638(9), Si3–Si4: 2.4135(9), Si1–Si6: 2.4395(9), Si2–Si6: 2.4731(9), Si5–Si6: 2.7680(9), Si5–Si8: 2.5426(9), Si6–Si7: 2.5449(9), Si6–Si9: 2.4439(9), Si7–Si8: 2.7311(9), Si7–Si9: 2.4398(9). Crystallographic detail in the Supporting Information.

Triggered by the successful silylation of Si_9 clusters *via* transfer of known Ge_9 reactions, the possibility for Si–H functionalization *via* silylation was further studied for Ge_9 clusters because reports were limited to attached -SiH^tBu_2 groups before this work.[36, 49] Thereto, $SiHR_2Cl$ (R = Ph, *i*Pr) chloro-silanes were added to solutions of K_4Ge_9 or the di-silylated Ge_9 cluster $[\{Si(TMS)_3\}_2Ge_9]^{2-}$ [45] in acetonitrile, and obtained reaction products were investigated in ESI-MS (Figure 4). Red filtrates were obtained after filtration in all cases and ESI-MS measurements revealed mass peaks for Si–H functionalized Ge_9 clusters. Triple Si–H functionalized $[(SiHR_2)_3Ge_9]^-$ {R = ^{i}Pr (**3**), Ph (**4**); Figure 4a} clusters were detected from reactions with K_4Ge_9, and mass peaks of mono Si–H functionalized $[\{Si(TMS)_3\}_2(SiHR_2)Ge_9]^-$ {R = ^{i}Pr (**5**), Ph (**6**); Figure 4b} clusters from reactions with $[\{Si(TMS)_3\}_2Ge_9]^{2-}$. The results indicate the

formation of tri-silylated Ge_9 cluster species in analogy to reported olefin-functionalized $[\{SiPh_2(olefin)\}_3Ge_9]^-$ and $[\{Si(TMS)_3\}_2\{SiPh_2(olefin)\}Ge_9]^-$ (olefin = vinyl, pentenyl) clusters.[48] If compared to previously reported "bulky" ^{t}Bu groups in -SiH^tBu_2 silyl ligands, the ^{i}Pr and Ph groups in the -$SiHR_2$ silyl ligands bear a more favorable steric environment for accessible Si–H bonds, what can be favorable for further reactions as *e.g.* hydrosilylation or insertion reactions with a view on further cluster modification.[58-62]

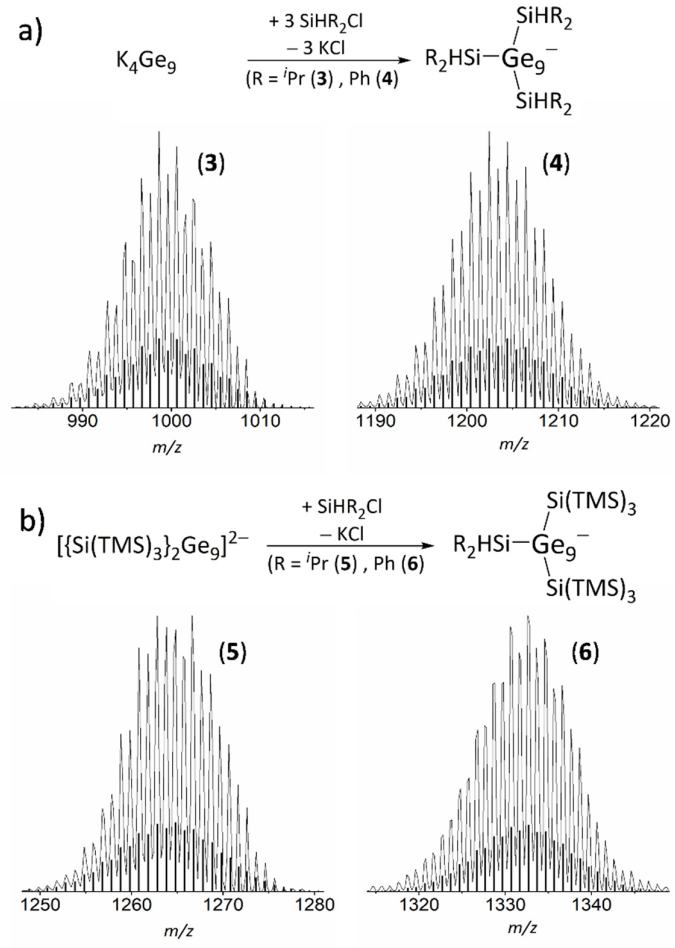

Figure 4. Syntheses and ESI-MS spectra to silylated Ge_9 species with Si–H functionalization: a) the tri-functionalized species $[(SiH^iPr_2)_3Ge_9]^-$ (**3**, *m/z* = 999) and $[(SiHPh_2)_3Ge_9]^-$ (**4**, *m/z* = 1204); b) the mono-functionalized species $[\{Si(TMS)_3\}_2(SiH^iPr_2)Ge_9]^-$ (**5**, *m/z* = 1264) and $[\{Si(TMS)_3\}_2(SiHPh_2)Ge_9]^-$ (**6**, *m/z* = 1332). Synthesis details and ESI-MS spectra in Supporting Information; Lines: measured mass spectrum, bars: simulated isotope pattern.

To fathom the reactivity of Si–H functionalized Si_9 clusters, the reactivity of the Si–H bonds in $[(SiH^tBu_2)_3Si_9]^-$ [36] was tested in a reactivity experiment with (2-butene)Si^{t}Bu$_2$ silirane.[53-54] This silirane forms the ^{t}Bu$_2$Si: silylene by thermic treatment in solution, which is *e.g.* feasible for Si–H σ-bond insertion reactions as demonstrated with Et_3SiH silanes (Scheme 1c).[55, 63] Moreover, the high synthetic potential the silylene was pointed out as *e.g.* by methanol insertion and cycloaddition with substituted alkenes.[53] For the experiment, the silirane reactant (4 eq.) was added to a thf-*d8* solution of $[(SiH^tBu_2)_3Si_9]^-$ in a sealed NMR tube. Initial NMR monitoring at room temperature showed no reaction

of the reactants (NMR spectra in Supporting Information). The reaction mixture was heated to 120 °C, and subsequently recorded NMR (^{1}H, ^{29}Si) spectra revealed signal changes along with the disappearance of the $[(SiH^{t}Bu_2)_3Si_9]^-$ reactant signals. An ESI-MS measurement of the obtained reaction solution showed a mass peak for $[(SiH^{t}Bu_2)_7Si_9]^-$ (**7**) as main signal (Scheme 1d, ESI-MS spectra in the Supporting Information). An ESI-MS fragmentation experiment of **7** showed the cleavage of four $SiH^{t}Bu_2$ (*m/z* = 143) units under reformation of the $[(SiH^{t}Bu_2)_3Si_9]^-$ reactant, and thus, suggests an extension of the reactant by four of these units. Although the molecular structure of such a species could not be determined within this work, an insertion mechanism is assumed.

Conclusions

Si_9 clusters from the $K_{12}Si_{17}$ precursor were transferred to ethylenediamine solutions as $[H_2Si_9]^{2-}$ (**1**) clusters, what paved the way cluster vinylations of Si_9 clusters with TMS-C≡C-TMS. Thereby, the formation of vinylated $[(CH_2CH)_xSi_9]^{n-}$ (x = 1, 2, 3; n = 4–x) cluster species was indicated by NMR experiments. The transfer of cluster silylations from Ge_9 to Si_9 was further promoted by single crystals containing $[(Si^{i}Pr_3)_2Si_9]^{2-}$ (**2**) as second representative for a silylated Si_9 cluster. An ESI-MS study to accessible Si–H functionalized Ge_9 clusters showed that versatile silyl groups are suitable for cluster functionalization *via* silylation by the detection of $[(SiHR_2)_3Ge_9]^-$ {R = ^{i}Pr (**3**), Ph (**4**)} and $[\{Si(TMS)_3\}_2(SiHR_2)Ge_9]^-$ {R = ^{i}Pr (**5**), Ph (**6**)} mass peaks. To fathom the reactivity of Si–H bonds at silylated Si_9 cluster cores, a reactivity experiment of $[(SiH^{t}Bu_2)_3Si_9]^-$ with (2-butene)$Si^{t}Bu_2$ silirane indicated the formation of an extended $[(SiH^{t}Bu_2)_7Si_9]^-$ (**7**) species and offers a first perspective for the utilization of the $K_{12}Si_{17}$ precursor in further fabrication steps.

Acknowledgements

The authors are thankful for the financial support by WACKER Chemie AG and Deutsche Forschungsgemeinschaft. Moreover, they thank Fabian Herz, Matthias Nobis, Hussayn Ahmed and Brigita Bratic for their assisting the synthesis.

Experimental Section

General: All reactions and manipulations were performed under a purified argon atmosphere using standard Schlenk and glove box techniques. Thf was dried over a special drying material in a solvent purificator (MBraun MB-SPS). 222Crypt was dried *in vacuo* prior to usage. Liquid ammonia was dried and stored over sodium metal prior to usage, all other solvents (including deuterated solvents) were stored over molecular sieves (3 Å). $[\{Si(TMS)_3\}_2Ge_9]^{2-}$,[45] "$K_{12}Si_{17}$ (*activated*)",[36] $[(SiH^{t}Bu)_2)_3Si_9]^-$ [36] and (2-butene)$Si^{t}Bu_2$ [54] were synthesized according to literature procedures. All other chemicals were received commercially and used without further purification.

Synthesis of $[H_2Si_9]^{2-}$ (1): Ethylenediamine (1 ml) was added to "$K_{12}Si_{17}$ (*activated*)" (50.0 mg) in a glovebox. An orange solution was obtained after filtration (stable for several hours at room temperature) and investigated by NMR and ESI-MS experiments. For ESI-MS measurements, the filtrate was diluted in a 1:1 ratio with thf. For NMR (^{1}H, ^{29}Si) experiments, the filtrate was filled into a sealed NMR tube (J-Young) containing a capillary filled with CD_2Cl_2 for signal locking. ^{1}H NMR (500 MHz, ethylenediamine) δ 3.73 (s, O-CH_2-CH_2-$O_{222crypt}$), 3.68 (t, *J* = 4.79 Hz, O-CH_2-CH_2-$N_{222crypt}$), −1.51 (t, H_{Si9}, *J* = 20.4 Hz); ^{29}Si NMR (99 MHz, ethylenediamine) δ −95.00 (Si_H), −323.53 (Si_{Si}); ESI-MS (positive mode, − 4000 V, 300 °C): *m/z* = 1501 $\{[K\text{-}222crypt]_3\mathbf{1}\}^+$.

Reactivity Study of "$K_{12}Si_{17}$ (*activated*)" with TMS-C≡C-TMS: Ethylenediamine (1 ml) was added to "$K_{12}Si_{17}$ (*activated*)" (40.0 mg) in a glovebox and an orange solution was obtained after filtration. TMS-C≡C-TMS {bis(trimethylsilyl)acetylene} (0.064 mmol, 4 eq.) was added. For NMR (^{1}H, ^{29}Si) experiments, the reaction solution was filled into a sealed NMR tube (J-Young) containing a capillary filled with CD_2Cl_2 for signal locking. ^{1}H NMR (400 MHz, ethylenediamine) δ 7.57 (dd, J = 12.8, 4.7 Hz, C*H*CH_2), 6.68 (dd, J = 19.5, 13.1 Hz, CHC*H*$_2$), 5.86 (dd, J = 19.4, 5.1 Hz, C*H*CH_2), 3.72 (s, O-C*H*$_2$-C*H*$_2$-$O_{222crypt}$), 3.67 (t, J = 4.79 Hz, O-C*H*$_2$-CH_2-$N_{222crypt}$), −1.50 (t, H_{Si}, J = 20.4 Hz, **1**); ^{29}Si NMR (99 MHz, ethylenediamine) δ −38.85 (*Si*$_{CHCH2}$), −324.00 (**1**, *Si*$_{Si}$), −342.12 (*Si*$_{Si}$).

Synthesis of $[(Si^{i}Pr_3)_2Si_9]^{2-}$ (2): "$K_{12}Si_{17}$ (*activated*)" (batch with 200 mg $K_{12}Si_{17}$) was cooled to 0 °C (ice bath) and suspended in thf (12 ml). $Si^{i}Pr_3Cl$ (1.26 mmol, 6 eq.) was added under continuous stirring as pre-cooled thf solution (3 ml). The reaction mixture was stirred overnight and allowed to warm to room temperature. A brownish colored filtrate was obtained after filtration and the volatile parts were removed *in vacuo*. The residue was washed with hexane and extracted with fluorobenzene (2 mL) yielding a red filtrate. For crystallization, the filtrate was overlayered with hexane (4 ml). Yellow, block-shaped crystals, suitable for single crystal X-ray diffraction, were obtained after 5 days and revealed the molecular structure of [K-222crypt]$_2$**2**.

Synthesis of $[(SiHR_2)_3Ge_9]^-$ [R = *i*Pr (3), Ph (4)]: K_4Ge_9 (0.12 mmol, 1 eq.) was weighed into a *Schlenk* tube and $SiHR_2Cl$ (0.43 mmol, 3.5 eq.; R = *i*Pr or Ph) was added as acetonitrile solution (3 ml). The reaction mixture was stirred for 1 d at ambient temperature and subsequently filtrated. Red filtrates were obtained and investigated by ESI-MS. The mass spectra revealed mass peaks of the tri-silylated clusters $[(SiHR_2)_3Ge_9]^-$ [R = *i*Pr (**3**), Ph (**4**)]. ESI-MS (negative mode, 300 °C): *m/z* = 999 (**3**, 4500 V), *m/z* = 1204 (**4**, 4000 V).

Synthesis of $[\{Si(TMS)_3\}_2(SiHR_2)Ge_9]^-$ [R = *i*Pr (5), Ph (6)]: $K_2(Si(TMS)_3)_2Ge_9$ (0.05 mmol, 1 eq.) was weighed into a *Schlenk* tube and $SiHR_2Cl$ (0.07 mmol, 1.5 eq.; R = *i*Pr or Ph) was added as acetonitrile solution (3 ml). The reaction mixture was stirred for 1 d at ambient temperature and subsequently filtrated. Red filtrates were obtained and investigated by ESI-MS. The mass spectra revealed mass peaks of the tri-silylated clusters $[\{Si(TMS)_3\}_2(SiHR_2)Ge_9]^-$ [R = *i*Pr (**5**), Ph (**6**)]. ESI-MS (negative mode, 300 °C): *m/z* = 1264 (**5**, 4500 V), *m/z* = 1332 (**6**, 4500 V).

Reactivity Study of $[(SiH^{t}Bu_2)_3Si_9]^-$ with (2-butene)$Si^{t}Bu_2$ Silirane: [K-222crypt][$(SiH^{t}Bu_2)_3Si_9$] (13.6 µmol, 1 eq.) was weighed into a sealed NMR tube (J-Young) and (2-butene)$Si^{t}Bu_2$ (54.6 µmol, 4 eq.) was added as thf-*d8* solution (0.5 ml). The reaction mixture was heated to 120 °C for 1 d (oil bath) and investigated by ESI-MS and NMR (^{1}H, ^{13}C, ^{29}Si). ESI-MS (negative mode, 300 °C, 3500 V): *m/z* = 1256 $[(SiH^{t}Bu_2)_7Si_9]^-$ (**7**); ^{1}H NMR (400 MHz, thf-*d8*) δ 3.64 (s, 4H, O-C*H*$_2$-C*H*$_2$-$O_{222crypt}$), 3.60 (m, 4H, O-C*H*$_2$-CH_2-$N_{222crypt}$), 2.60 (m, 4H, O-CH_2-C*H*$_2$-$N_{222crypt}$), 1.29 (m, CH*Me*), 1.21 (s, ^{t}Bu), 1.17 (s, C*H*Me), 1.13 (s, ^{t}Bu), 1.06 (s, C*H*Me), 1.03 (s, ^{t}Bu); ^{13}C NMR (101 MHz, thf-*d8*) δ 71.47 (O-*C*H$_2$-*C*H_2-$O_{222crypt}$), 68.64 (O-*C*H_2-CH_2-$N_{222crypt}$), 54.98 (O-CH_2-*C*H_2-$N_{222crypt}$), 35.11 (*C*Me_3), 31.82 (C*Me*$_3$), 30.17 (C*Me*$_3$), 21.44 (SiCH*Me*), 19.13 (SiCH*Me*), 17.91 (SiCH*Me*), 16.76 (SiCH*Me*), 14.42 (Si*C*HMe), 10.36 (Si*C*HMe), 10.27 (Si*C*HMe); ^{29}Si NMR (79 MHz, thf-*d8*) δ −43.63 (*trans-Si*^{t}Bu$_2$), −53.25 (*cis-Si*^{t}Bu$_2$).

Nuclear Magnetic Resonance Spectroscopy (NMR): ^{1}H, ^{13}C and ^{29}Si NMR spectra were recorded on a *Bruker AVIII* Ultrashield 400 MHz or a *Bruker AVIII* 500 MHz Cryo system (BRUKER INC). The signals of the ^{1}H and ^{13}C spectra were calibrated on the rest proton signal of the used deuterated solvent thf-*d8*. Chemical shifts are given in δ values by parts per million [ppm]. The coupling constants J are stated in Hz. Signal multiplicities are abbreviated as follows: s – singlet, d – doublet, t – triplet, m – multiplet. The spectra were evaluated with MestReNova.[64]

Electrospray Ionization Mass Spectrometry (ESI-MS): The preparation of the samples was done in a glove box. The spectra were measured on an *HCT* instrument (BRUKER INC). The data was analyzed using the program *Bruker Compass Data Analysis 4.0 SP 5* (BRUKER INC). The dry gas temperature was adjusted to 300 °C and the injection speed to 240 $\mu L \cdot s^{-1}$.

Single-crystal Structure Determination: For single crystal data collection, the crystals were fixed on a glass capillary and positioned in a cold stream of N_2 gas. Single crystal data collection was carried out on a STOE StadiVari (Mo *Kα* radiation) diffractometer equipped with a DECTRIS PILATUS 300K detector**.** Structures were solved by Direct Methods (SHELXS 97)[65] and refined by full-matrix least-squares calculations against F^2 (SHELXL-2014).[66] The positions of the hydrogen atoms were calculated and refined using a riding model. All non-hydrogen atoms were treated with anisotropic displacement parameters. The crystallographic data has been deposited with the Cambridge Structural Database and is available free of charge via www.ccdc.cam.ac.uk/ data_request/cif on quoting the depository numbers CCDC 1921145. The crystal structure has been plotted with Diamond.[67]

References

1. Wiberg, N., *Holleman Wiberg — Lehrbuch der Anorganischen Chemie (102. Auflage)*. Walter de Gruyter, Berlin: 2007.
2. Mitra, A.; Atwood, D. A., *Polysiloxanes & Polysilanes in Encyclopedia of Inorganic Chemistry*. John Wiley & Sons, Ltd.: 2006.
3. Ackermann, J.; Damrath, V., *Chem. Unserer Zeit* **1989,** *23* (3), 86.
4. Schliebs, R.; Ackermann, J., *Chem. Unserer Zeit* **1987,** *21* (4), 121.
5. Claeys, C.; Simoen, E., *Germanium-Based Technologies: From Materials to Devices*. Elsevier Science: 2007.
6. Hochberg, M.; Baehr-Jones, T., *Nature Photonics* **2010,** *4*, 492.
7. Rojas, J. P.; Torres Sevilla, G. A.; Ghoneim, M. T.; Inayat, S. B.; Ahmed, S. M.; Hussain, A. M.; Hussain, M. M., *ACS Nano* **2014,** *8* (2), 1468.
8. Eun-Chel, C.; Sangwook, P.; Xiaojing, H.; Dengyuan, S.; Gavin, C.; Sang-Cheol, P.; Martin, A. G., *Nanotechnology* **2008,** *19* (24), 245201.
9. Rath, J. K.; Stannowski, B.; van Veenendaal, P. A. T. T.; van Veen, M. K.; Schropp, R. E. I., *Thin Solid Films* **2001,** *395* (1), 320.
10. Müller-Buschbaum, P.; Thelakkat, M.; Fässler, T. F.; Stutzmann, M., *Adv. Energy Mater.* **2017,** *7* (16), 1700248.
11. Ashuri, M.; He, Q.; Shaw, L. L., *Nanoscale* **2016,** *8* (1), 74.
12. Eickhoff, H.; Strangmüller, S.; Klein, W.; Kirchhain, H.; Dietrich, C.; Zeier, W. G.; van Wüllen, L.; Fässler, T. F., *Chem. Mater.* **2018,** *30* (18), 6440.
13. Su, X.; Wu, Q.; Li, J.; Xiao, X.; Lott, A.; Lu, W.; Sheldon, B. W.; Wu, J., *Adv. Energy Mater.* **2014,** *4* (1), 1300882.
14. Hoch, C.; Wendorff, M.; Röhr, C., *J. Alloys Compd.* **2003,** *361* (1), 206.
15. Quéneau, V.; Todorov, E.; Sevov, S. C., *J. Am. Chem. Soc.* **1998,** *120* (13), 3263.
16. von Schnering, H. G.; Somer, M.; Kaupp, M.; Carrillo-Cabrera, W.; Baitinger, M.; Schmeding, A.; Grin, Y., *Angew. Chem. Int. Ed.* **1998,** *37* (17), 2359.
17. Kanatzidis, M. G., *Adv. Mater.* **2007,** *19* (9), 1165.
18. Bley, R. A.; Kauzlarich, S. M., *J. Am. Chem. Soc.* **1996,** *118* (49), 12461.
19. Canham, L. T., *Appl. Phys. Lett.* **1990,** *57* (10), 1046.
20. Snedaker, M. L.; Zhang, Y.; Birkel, C. S.; Wang, H.; Day, T.; Shi, Y.; Ji, X.; Kraemer, S.; Mills, C. E.; Moosazadeh, A.; Moskovits, M.; Snyder, G. J.; Stucky, G. D., *Chem. Mater.* **2013,** *25* (24), 4867.
21. Stein, A., *Nature* **2006,** *441*, 1055.

22. von Schnering, H. G.; Baitinger, M.; Bolle, U.; Carrillo-Cabrera, W.; Curda, J.; Grin, Y.; Heinemann, F.; Llanos, J.; Peters, K.; Schmeding, A.; Somer, M., *Z. Anorg. Allg. Chem.* **1997,** *623* (7), 1037.
23. Queneau, V.; Sevov, S. C., *Angew. Chem. Int. Ed.* **1997,** *36* (16), 1754.
24. Ponou, S.; Fässler, T. F., *Z. Anorg. Allg. Chem.* **2007,** *633* (3), 393.
25. Queneau, V.; Sevov, S. C., *Angew. Chem. Int. Ed.* **1997,** *36* (16), 1754.
26. Ugrinov, A.; Sevov, S. C., *Inorg. Chem.* **2003,** *42* (19), 5789.
27. Downie, C.; Tang, Z.; Guloy, A. M., *Angew. Chem. Int. Ed.* **2000,** *39* (2), 337.
28. Hull, M. W.; Sevov, S. C., *Angew. Chem. Int. Ed.* **2007,** *46* (35), 6695.
29. Hull, M. W.; Sevov, S. C., *J. Am. Chem. Soc.* **2009,** *131* (25), 9026.
30. Hull, M. W.; Sevov, S. C., *Inorg. Chem.* **2007,** *46* (26), 10953.
31. Benda, C. B.; Wang, J.-Q.; Wahl, B.; Fässler, T. F., *Eur. J. Inorg. Chem.* **2011,** *2011* (27), 4262.
32. Frischhut, S.; Bentlohner, M. M.; Klein, W.; Fässler, T. F., *Inorg. Chem.* **2017,** *56* (17), 10691.
33. Bentlohner, M. M.; Klein, W.; Fard, Z. H.; Jantke, L.-A.; Fässler, T. F., *Angew. Chem. Int. Ed.* **2015,** *54* (12), 3748.
34. Henneberger, T.; Klein, W.; Fässler, T. F., *Z. Anorg. Allg. Chem.* **2018,** *644* (17), 1018.
35. Schiegerl, L. J.; Karttunen, A. J.; Tillmann, J.; Geier, S.; Raudaschl-Sieber, G.; Waibel, M.; Fässler, T. F., *Angew. Chem. Int. Ed.* **2018,** *57* (39), 12950.
36. Schiegerl, L. J.; Karttunen, A. J.; Klein, W.; Fässler, T. F., *Chem. Eur. J.* **2018,** *24* (72), 19171.
37. Lorenz, C.; Gärtner, S.; Korber, N., *Z. Anorg. Allg. Chem.* **2017,** *643* (2), 141.
38. Benda, C. B.; Henneberger, T.; Klein, W.; Fässler, T. F., *Z. Anorg. Allg. Chem.* **2017,** *643* (2), 146.
39. Joseph, S.; Suchentrunk, C.; Kraus, F.; Korber, N., *Eur. J. Inorg. Chem.* **2009,** *2009* (31), 4641.
40. Waibel, M.; Kraus, F.; Scharfe, S.; Wahl, B.; Fässler, T. F., *Angew. Chem. Int. Ed.* **2010,** *49* (37), 6611.
41. Goicoechea, J. M.; Sevov, S. C., *Organometallics* **2006,** *25* (19), 4530.
42. Joseph, S.; Hamberger, M.; Mutzbauer, F.; Härtl, O.; Meier, M.; Korber, N., *Angew. Chem. Int. Ed.* **2009,** *48* (46), 8770.
43. Geitner, F. S.; Fässler, T. F., *Chem. Commun.* **2017,** *53* (96), 12974.
44. Schnepf, A., *Angew. Chem. Int. Ed.* **2003,** *42* (23), 2624.
45. Kysliak, O.; Schnepf, A., *Dalton Trans.* **2016,** *45* (6), 2404.
46. Schiegerl, L. J.; Geitner, F. S.; Fischer, C.; Klein, W.; Fässler, T. F., *Z. Anorg. Allg. Chem.* **2016,** *642* (24), 1419.
47. Mayer, K.; Schiegerl, L. J.; Fässler, T. F., *Chem. Eur. J.* **2016,** *22* (52), 18794.
48. Mayer, K.; Schiegerl, L. J.; Kratky, T.; Günther, S.; Fässler, T. F., *Chem. Commun.* **2017,** *53* (86), 11798.
49. Kysliak, O.; Kunz, T.; Schnepf, A., *Eur. J. Inorg. Chem.* **2017,** *2017* (4), 805.
50. Wiberg, N.; Finger, C. M. M.; Polborn, K., *Angew. Chem. Int. Ed.* **1993,** *32* (7), 1054.
51. Heider, Y.; Scheschkewitz, D., *Dalton Trans.* **2018,** *47* (21), 7104.
52. Lorenz, C.; Hastreiter, F.; Hioe, J.; Nanjundappa, L.; Gärtner, S.; Korber, N.; Gschwind, R. M., *Angew. Chem. Int. Ed.* **2018,** *57* (39), 12956.
53. Duffy, I. R.; Leigh, W. J., *Organometallics* **2019,** *38* (4), 933.
54. Boudjouk, P.; Samaraweera, U.; Sooriyakumaran, R.; Chrusciel, J.; Anderson, K. R., *Angew. Chem. Int. Ed.* **1988,** *27* (10), 1355.
55. Boudjouk, P.; Black, E.; Kumarathasan, R., *Organometallics* **1991,** *10* (7), 2095.
56. Abersfelder, K.; White, A. J. P.; Berger, R. J. F.; Rzepa, H. S.; Scheschkewitz, D., *Angew. Chem. Int. Ed.* **2011,** *50* (34), 7936.
57. Nied, D.; Köppe, R.; Klopper, W.; Schnöckel, H.; Breher, F., *J. Am. Chem. Soc.* **2010,** *132* (30), 10264.
58. Marciniec, B., *Comprehensive Handbook on Hydrosilylation (1st Edition)*. Pergamon: 1992
59. Marciniec, B., *Hydrosilylation: A Comprehensive Review on Recent Advances*. Springer: 2008.
60. Adam, W.; Mello, R.; Curci, R., *Angew. Chem. Int. Ed.* **1990,** *29* (8), 890.
61. Landais, Y.; Planchenault, D., *Tetrahedron Lett.* **1994,** *35* (26), 4565.
62. Liu, Z.; Huo, J.; Fu, T.; Tan, H.; Ye, F.; Hossain, M. L.; Wang, J., *Chem. Commun.* **2018,** *54* (81), 11419.
63. Driver, T. G.; Woerpel, K. A., *J. Am. Chem. Soc.* **2003,** *125* (35), 10659.

64. MestReNova v9.1.0, *Mestrelab Research S.L.* **2014**.
65. Sheldrick, G., *Acta Crystallogr. A.* **2008,** *64* (1), 112.
66. Sheldrick, G., *Acta Crystallogr. C* **2015,** *71* (1), 3.
67. Diamond Version 3.2k, Crystal Impact GbR **1997-2014**.

TOC

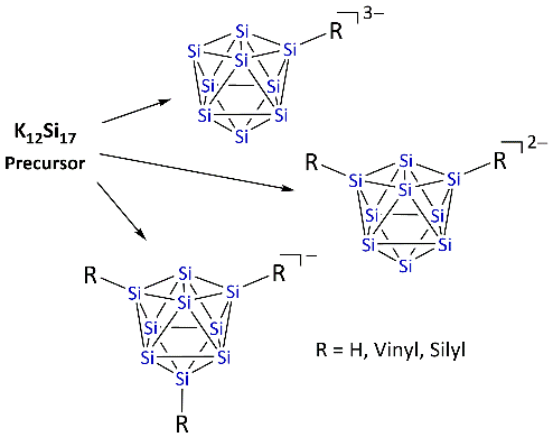

Utilization of Si_9 Clusters from $K_{12}Si_{17}$ Precursor Material for Subsequent Reactions

Supporting Information

1. ESI-MS Studies
2. NMR Studies
3. Crystallographic Details

1. ESI-MS Studies

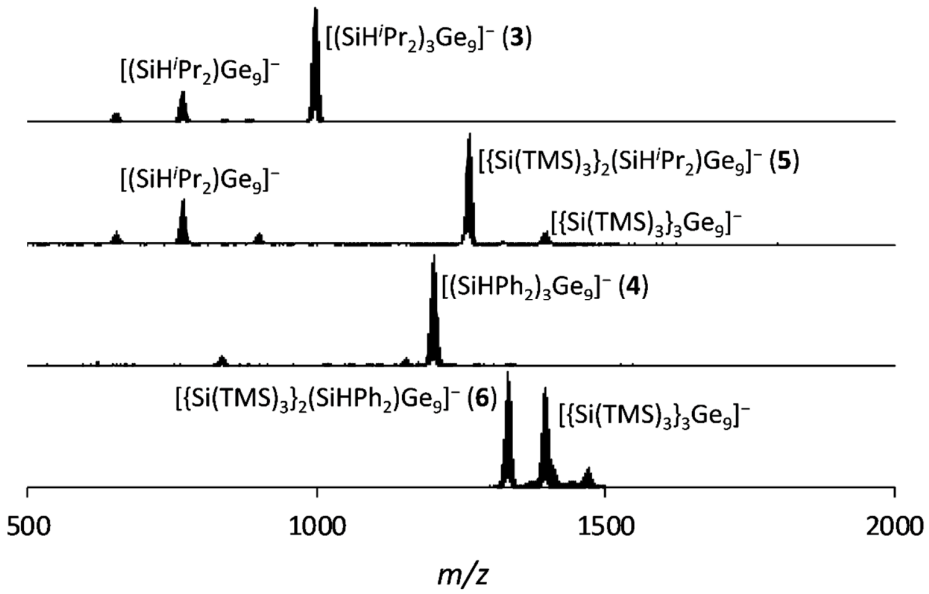

Figure SI 1. ESI-MS measurements of **3**–**6** in negative mode.

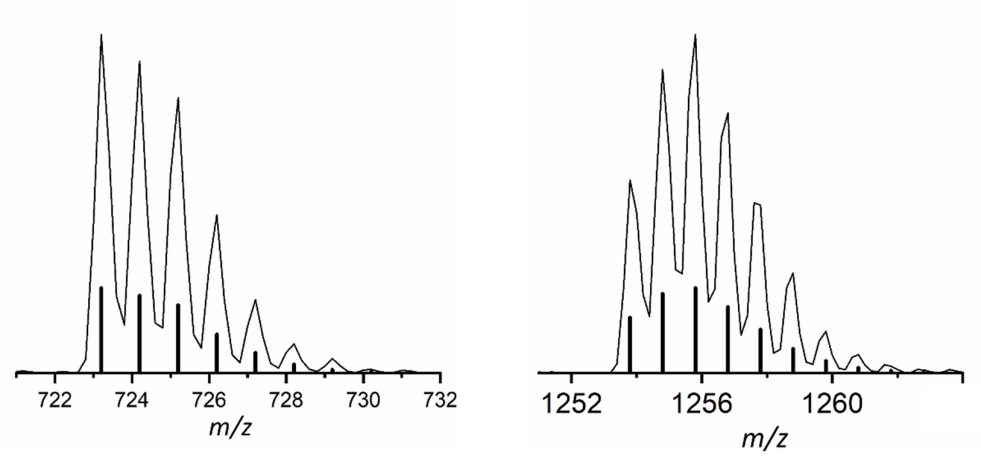

Figure SI 2. ESI-MS spectra: left) [(Si^{i}Pr$_3$)$_3$Si$_9$]$^-$ in negative mode; right) [(SiH^{t}Bu$_2$)$_7$Si$_9$]$^-$ (**7**) in negative mode; line: measured mass spectrum, bars: simulated isotope pattern.

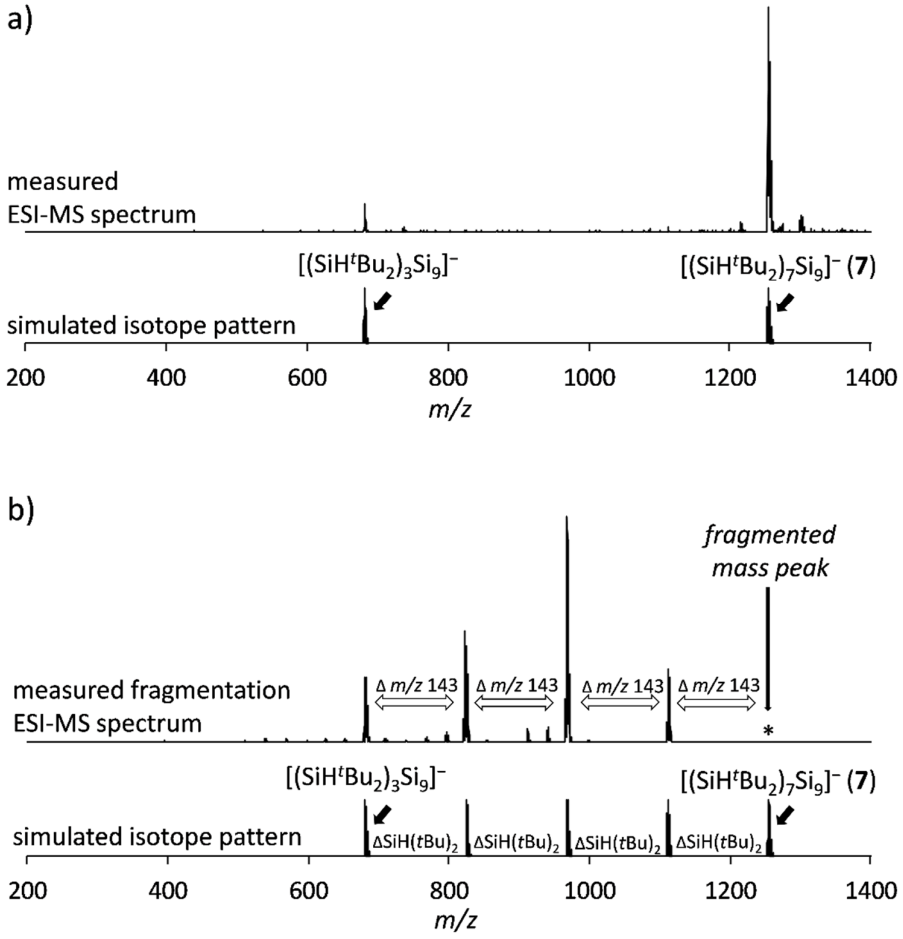

Figure SI 3. ESI-MS measurement of reaction of [(SiH^{t}Bu$_2$)$_3$Si$_9$]$^-$ with (2-butene)Si^{t}Bu$_2$ in thf-*d8*: a) ESI-MS spectrum (negative mode) in comparison to simulated isotope pattern; b) ESI-MS fragmentation spectrum (negative mode) in comparison to simulated isotope pattern.

2. NMR Studies

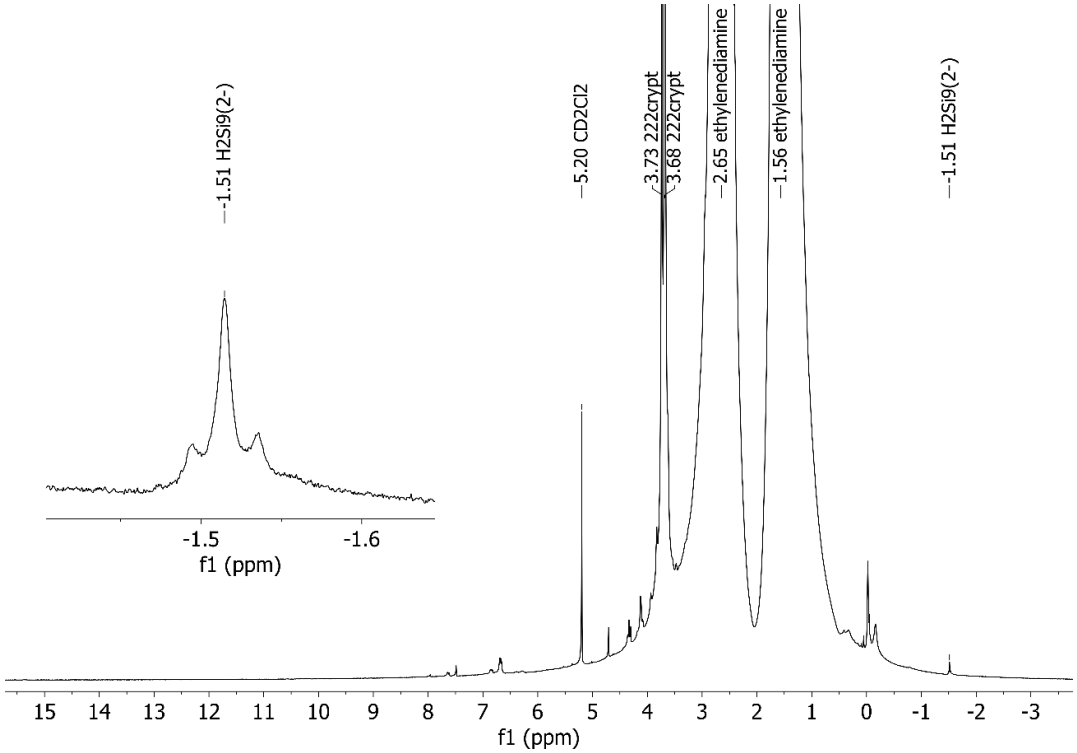

Figure SI 4. ^{1}H NMR measurement of "$K_{12}Si_{17}$ (*activated*)" in ethylenediamine (capillary with CD_2Cl_2 for signal locking).

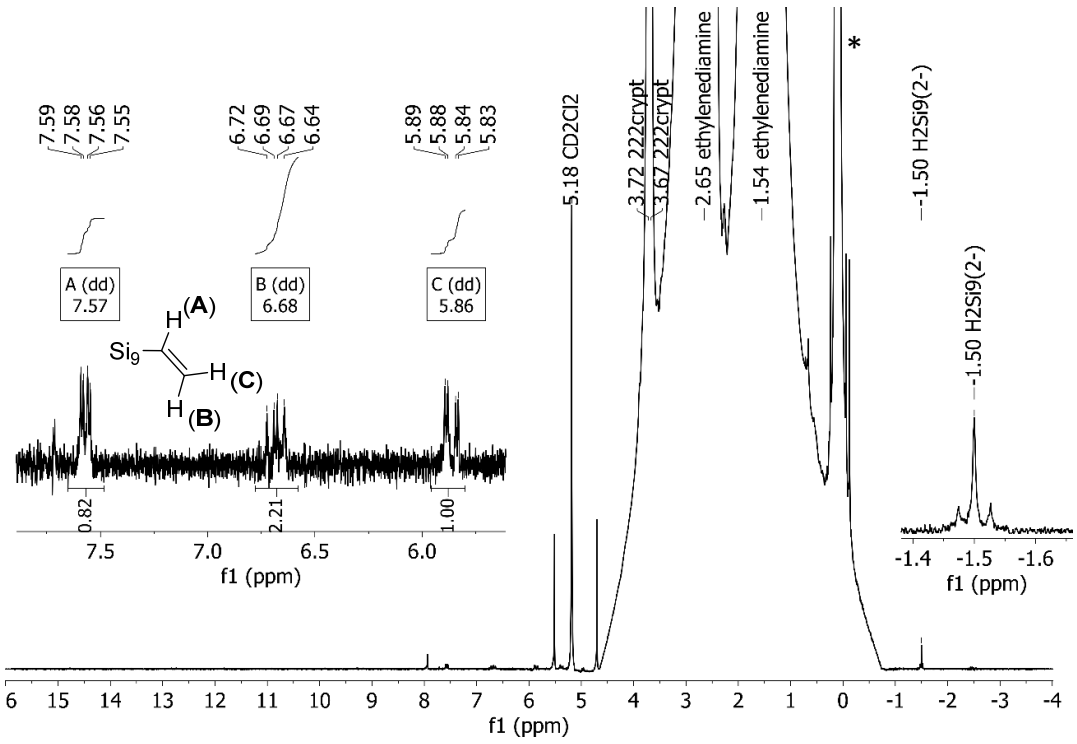

Figure SI 5. ^{1}H NMR measurement of reaction of "$K_{12}Si_{17}$ (*activated*)" in ethylenediamine with TMS-C≡C-TMS (capillary with CD_2Cl_2 for signal locking; *: reactant TMS-C≡C-TMS).

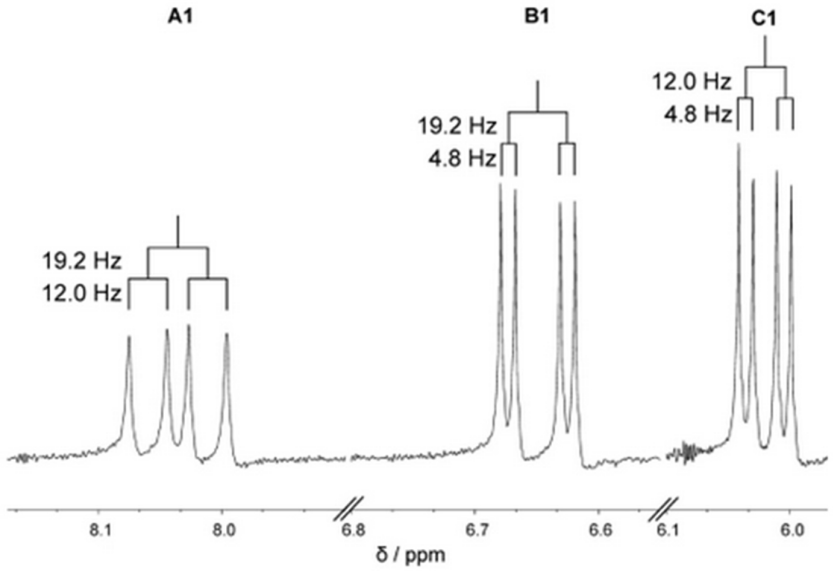

Figure SI 6. Detail view on the ^{1}H NMR spectrum of the mono-vinylated $[(CHCH_2)_3Ge_9]^-$ with corresponding coupling constants [Benda, C. B.; Wang, J.-Q.; Wahl, B.; Fässler, T. F., *Eur. J. Inorg. Chem.* **2011,** *2011* (27), 4262].

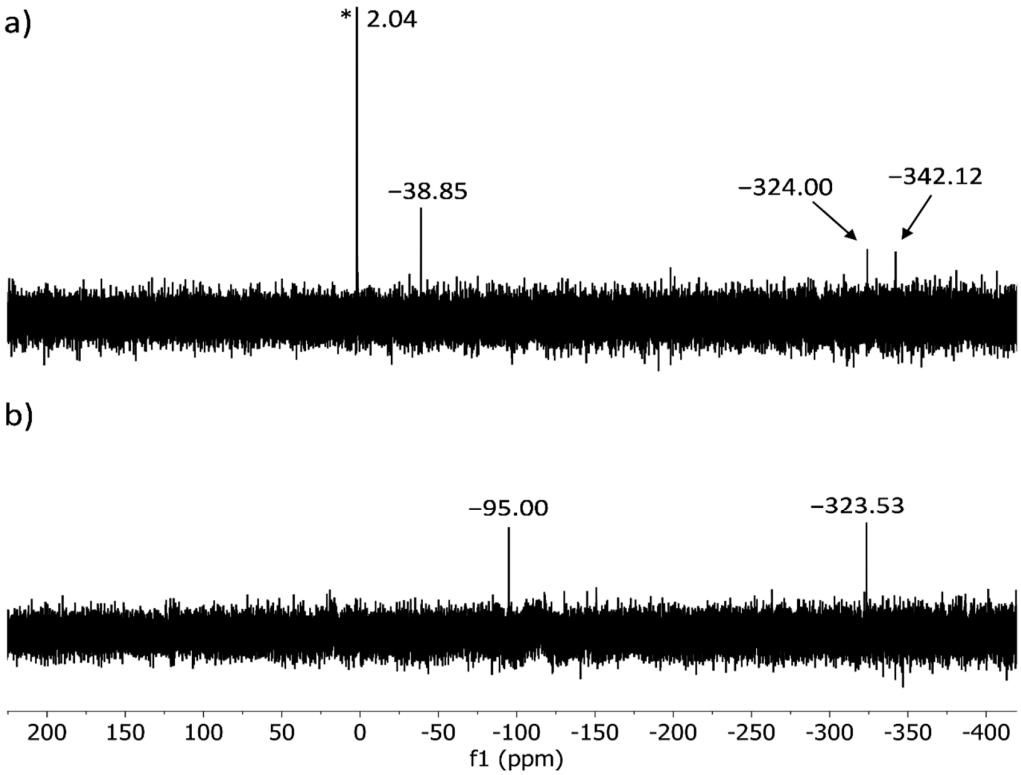

Figure SI 7. ^{29}Si NMR measurements in ethylenediamine (capillary with CD_2Cl_2 for signal locking): a): "$K_{12}Si_{17}$ (*activated*)" with TMS-C≡C-TMS (*: TMS-C≡C-TMS reactant); b) "$K_{12}Si_{17}$ (*activated*)".

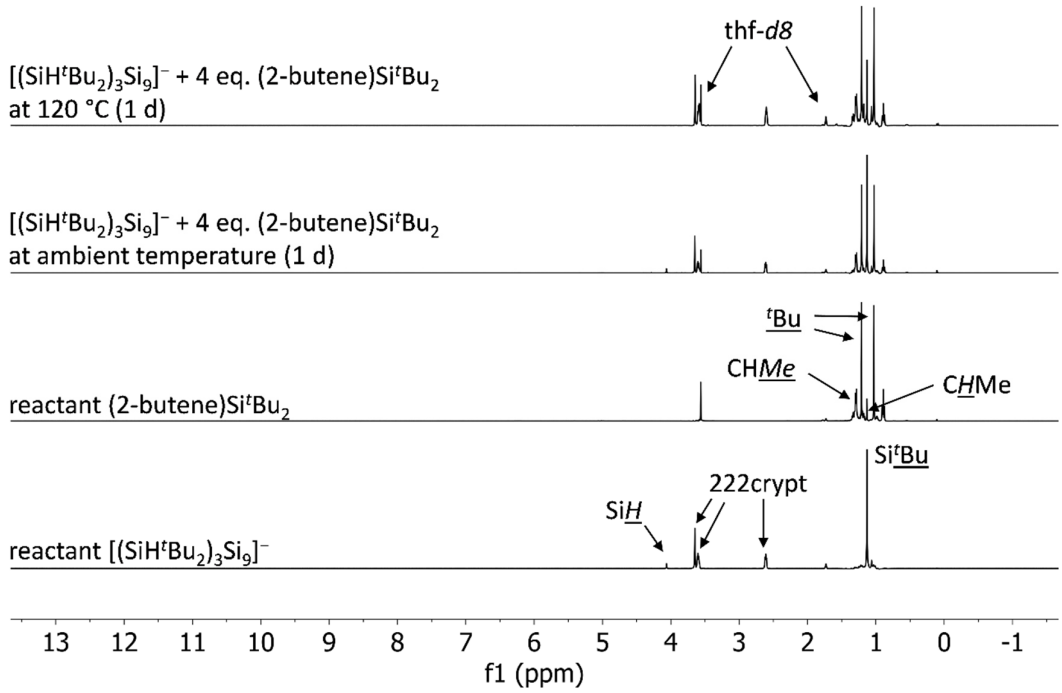

Figure SI 8. ^{1}H NMR study of the reaction solution of [(SiH^{t}Bu$_2$)$_3$Si$_9$]$^-$ with (2-butene)Si^{t}Bu$_2$ in thf-*d8*.

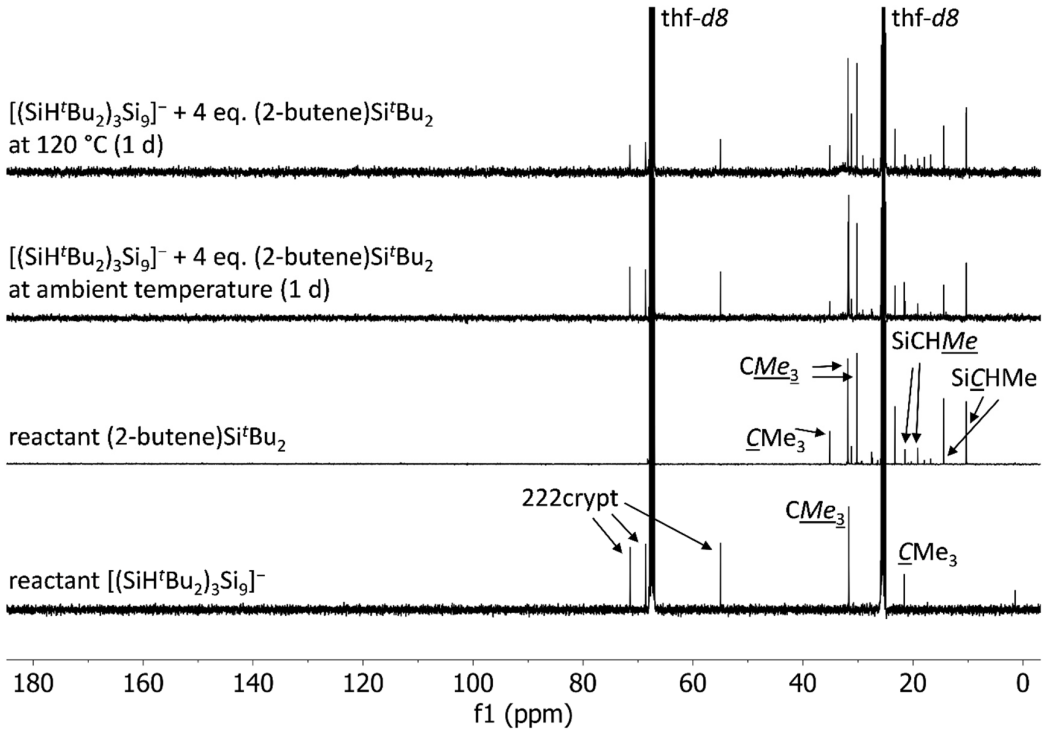

Figure SI 9. ^{13}C NMR study of the reaction solution of [(SiH^{t}Bu$_2$)$_3$Si$_9$]$^-$ with (2-butene)Si^{t}Bu$_2$ in thf-*d8*.

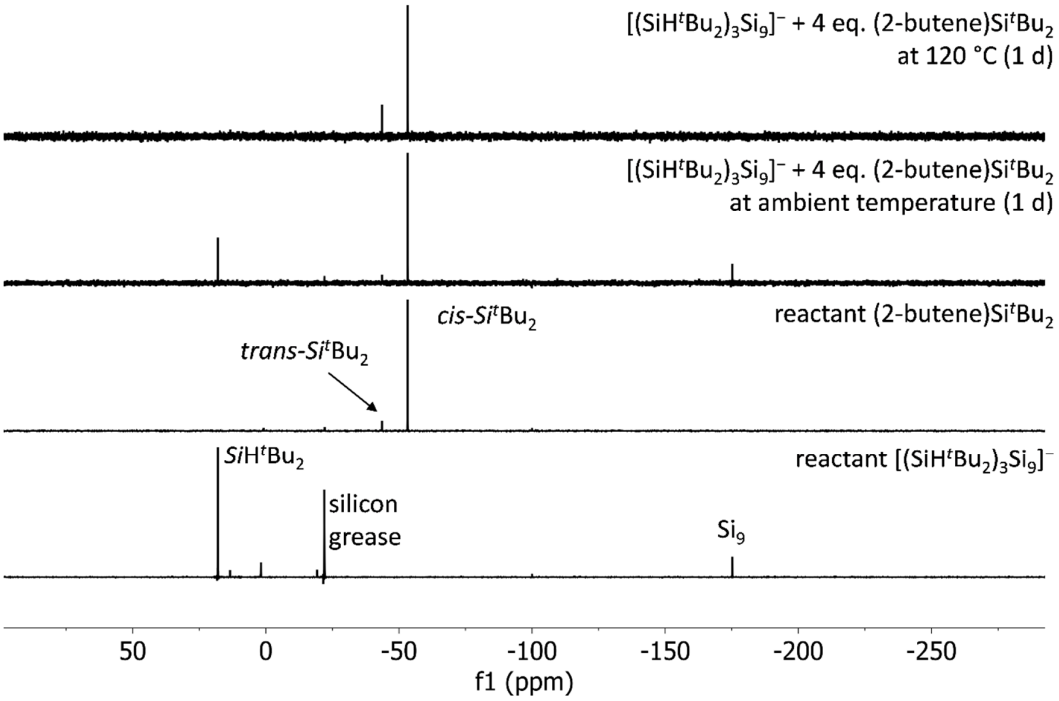

Figure SI 10. ^{29}Si NMR study of the reaction solution of [(SiH^{t}Bu$_2$)$_3$Si$_9$]$^-$ with (2-butene)Si^{t}Bu$_2$ in thf-*d8*.

3. Crystallographic Details

Table SI 1. Selected crystallographic data for the molecular structure of **2**.

Compound	**[K-222crypt]$_2$[(Si^{i}Pr$_3$)$_2$Si$_9$]**
formula	$C_{54}H_{114}K_2N_4O_{12}Si_{11}$
fw (g·mol^{-1})	1398.68
space group (no)	$P\bar{1}$ (2)
a (Å)	11.5307(9)
b (Å)	14.320(1)
c (Å)	24.476(2)
α (deg)	89.654(6)
β (deg)	83.446(6)
γ (deg)	73.418(6)
V (Å^3)	3846.7(5)
Z	2
T (K)	150(2)

ρ_{calc} (g·cm^{-3})	1.208
μ (mm^{-1})	0.347
measured reflections	78575
R_{int} / R_{δ}	0.0562/ 0.0420
	−14 < *h* < 14
hkl range	−17 < *k* < 17
	−30 < *l* < 30
2 θ range	2.688 – 25.999
independent reflections	15090
reflections [$I > 2\,\sigma(I)$]	11160
parameters / restraints	760 / 0
R_1 [$I > 2\,\sigma(I)$ / all data]	0.0391/ 0.0646
wR_2 [$I > 2\,\sigma(I)$ / all data]	0.0876 / 0.0974
goodness of fit	1.015
largest difference peak/hole [e Å^{-3}]	1.008 / −0.688
CCDC	1921145

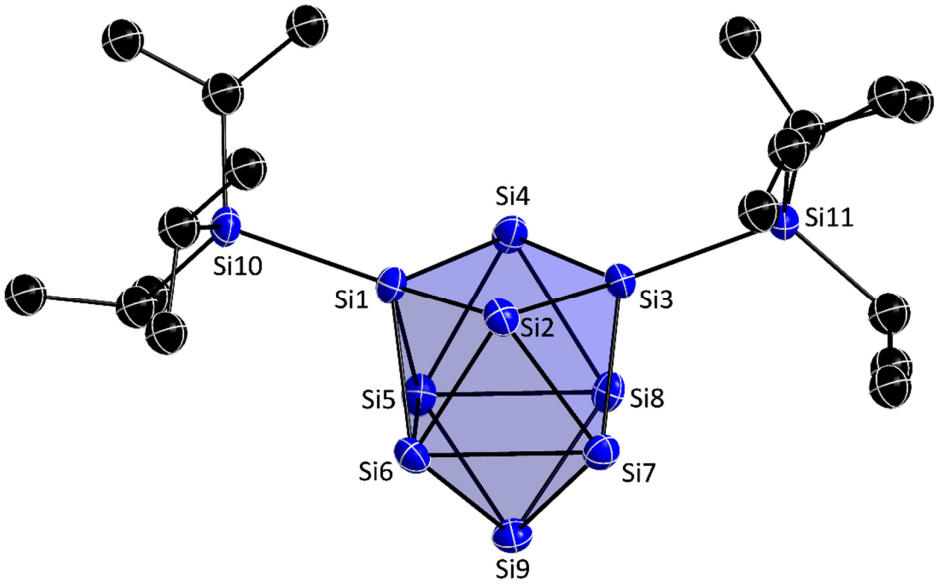

Figure SI 11. Molecular structure of **2** [Si atoms (blue) and C atoms (gray) are shown as ellipsoids with 50% probability; H atoms are omitted; Si_9 cluster is shown as blue polyhedron]. Atom labeling according to Table SI 2.

Table SI 2. Si–Si distances in **2** (atom labeling according to Figure SI 11).

Atom 1	Atom 2	Si–Si Distance [Å]	Atom 1	Atom 2	Si–Si Distance [Å]
Si1	Si2	2.4214(9)	Si3	Si8	2.4205(9)
Si1	Si3	2.3515(9)	Si4	Si5	2.494(1)
Si1	Si4	2.4102(9)	Si4	Si8	2.5002(9)
Si1	Si6	2.4395(9)	Si5	Si9	2.444(1)
Si1	Si5	2.4317(9)	Si5	Si6	2.7680(9)
Si1	Si10	2.3638(9)	Si5	Si8	2.5426(9)
Si2	Si3	2.4167(8)	Si6	Si7	2.5449(9)
Si2	Si6	2.4731(9)	Si6	Si9	2.4439(9)
Si2	Si7	2.4834(9)	Si7	Si8	2.7311(9)
Si3	Si4	2.4135(9)	Si7	Si9	2.4398(9)
Si3	Si7	2.4281(9)	Si8	Si9	2.452(1)

6.4 Silylated Ge_9 Clusters as New Ligands for Cyclic (Alkyl)amino and Mesoionic Carbene Copper Complexes

Lorenz J. Schiegerl, Mohand Melaimi, Daniel R. Tolentino, Wilhelm Klein, Guy Bertrand, and Thomas F. Fässler*

published in

Inorg. Chem. 2019, *58* (5), 3256-3264.

Access online *via*: https://pubs.acs.org/doi/10.1021/acs.inorgchem.8b03338

Content and contributions:

Ambition of this work was the synthesis of Ge_9 copper complexes with cyclic alkyl(amino) and mesoionic copper carbenes. The work was initiated by a research stay of mine at the laboratories of *Prof. Guy Bertrand* (UNIVERSITY OF CALIFORNIA SAN DIEGO) in the course of this PhD Thesis in 2016. The manuscript was authored by me in the course of this PhD Thesis and reviewed by *Dr. Mohand Melaimi*, *Daniel Tolentino*, and *Prof. Thomas Fässler* before its submission. Submission of the manuscript was done by *Prof. Thomas Fässler*. Recording, evaluation and submission of the single crystal diffraction data were assisted by *Dr. Wilhelm Klein*. The IR spectra were measured by *David Mayer* (TECHNICAL UNIVERSITY OF MUNICH), Raman spectra by *Dr. Sebastian Geier* (TECHNICAL UNIVERSITY OF MUNICH). The EDX spectra were measured by Maria Müller (TECHNICAL UNIVERSITY OF MUNICH). Elemental analyses were carried out in the microanalytical laboratory at the CATALYTIC RESEARCH CENTER of the TECHNICAL UNIVERSITY OF MUNICH

The Ge_9 copper carbene compounds [Cu(CAAC)][{Si(TMS)$_3$}$_3$Ge$_9$] and [Cu(MIC)][{Si(TMS)$_3$}$_3$Ge$_9$] were synthesized by reaction of [{Si(TMS)$_3$}$_3$Ge$_9$]$^-$ with Cu(CAAC)Cl and Cu(MIC)Cl, respectively. Syntheses and characterization (NMR, ESI-MS, SC-XRD, elemental analysis, EDX) were done by me. NMR investigation were supported by *Dr. Mohand Melaimi* (for CAAC compounds) and *Daniel Tolentino* (for MIC compounds). The co-authors also assisted in the synthesis of the respective carbene reactants Cu(CAAC)Cl and Cu(MIC)Cl in the laboratories of *Prof. Guy Bertrand*. Furthermore, reaction of [{Si(TMS)$_3$}$_2$Ge$_9$]$^{2-}$ with Cu(CAAC)Cl yielded the compound [Cu(CAAC)]$_2$[{Si(TMS)$_3$}$_2$Ge$_9$]. Synthesis and characterization (NMR, ESI-MS, SC-XRD, elemental analysis, EDX) of this compound were done by me.

Inorganic Chemistry
Article
Cite This: Inorg. Chem. 2019, 58, 3256−3264
pubs.acs.org/IC

Silylated Ge_9 Clusters as New Ligands for Cyclic (Alkyl)amino and Mesoionic Carbene Copper Complexes

Lorenz J. Schiegerl,[†] Mohand Melaimi,[‡] Daniel R. Tolentino,[‡] Wilhelm Klein,[†] Guy Bertrand,[‡] and Thomas F. Fässler*[,†]

[†]Department of Chemistry, Technische Universität München (TUM), Lichtenbergstraße 4, 85748 Garching, Germany
[‡]UCSD−CNRS Joint Research Chemistry Laboratory (UMI 3555), University of California—San Diego, La Jolla, California 92093-0353, United States

Supporting Information

ABSTRACT: The coordination of Ge_9 Zintl clusters at (carbene)Cu^I moieties is explored, and the complexes $[(CAAC)Cu]_2[\eta^3\text{-}Ge_9\{Si(TMS)_3\}_2]$ (**1**), $(CAAC)Cu[\eta^3\text{-}Ge_9\{Si(TMS)_3\}_3]$ (**2**), and $(MIC)Cu[\eta^3\text{-}Ge_9\{Si(TMS)_3\}_3]$ (**3**) are compared with their known N-heterocyclic carbene (NHC) derivatives (**A** and **B**), where CAAC = cyclic (alkyl)amino carbene, MIC = mesoionic carbene, and TMS = trimethylsilane. In analogy to the NHC derivatives, the synthesis of **1**−**3** proceeds by single-step reactions of (CAAC)CuCl or (MIC)CuCl with the $[Ge_9R_2]^{2-}$ and $[Ge_9R_3]^-$ [R = $Si(TMS)_3$] cluster ligands, respectively, and yields complexes of (carbene)Cu^I (carbene = CAAC, MIC) moieties exhibiting η^3-coordination modes of the Ge_9 deltahedron to the Cu atom. In **1**, $[Ge_9R_2]^{2-}$ acts as a η^3-bridging unit for two (CAAC)Cu^I moieties, and **2** and **3** feature single (carbene)Cu^I (CAAC and MIC) fragments η^3-connected to $[Ge_9R_3]^-$ units. Analysis of the bond lengths in comparison with known examples shows a bond expansion within the coordinated Ge_3 triangular faces for all (carbene)Cu^IGe_9 complexes (carbene = NHC, MIC, CAAC). All compounds are characterized by single-crystal X-ray diffractometry, NMR spectroscopy [^1H, $^{13}C\{^1H\}$, and $^{29}Si\{^1H\}$], electrospray ionization mass spectometry, elemental analysis (C, H, and N), and for the first time also by IR and Raman investigations (for **2** and **3**). The new complexes add to the known NHC derivatives and extend the exploration of Ge_9 clusters with carbene ligands at Cu^I atoms.

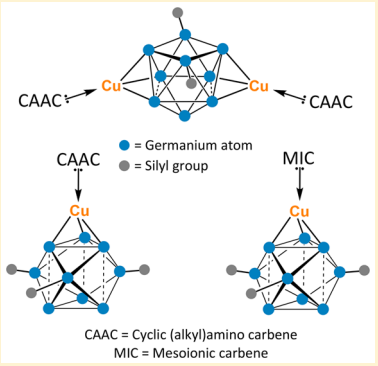

INTRODUCTION

Recently, we introduced Ge_9 Zintl clusters as ligands to carbene complexes, and although the direct attachment of Ge_9 to an N-heterocyclic carbene (NHC) unit has been unsuccessful so far,[1] NHC-supported coinage metal complexes offered versatile possibilities for the coordination. This approach was successful in the case of the tris-silylated Ge_9 species $[Ge_9R_3]^-$ [R = $Si(TMS)_3$; TMS = tetramethylsilane],[2] which exhibits excellent solubility and can be readily obtained by a single-step reaction of K_4Ge_9 with $Si(TMS)_3Cl$ in high yield. The clusters were attached to $(NHC^{Dipp})M^+$ moieties [M = Cu, Ag, Au; NHC^{Dipp} = 1,3-bis(2,6-diisopropylphenyl)-imidazol-2-ylidene] to give the first (carbene)M^I-Ge_9 species $(NHC)M[\eta^3\text{-}Ge_9\{Si(TMS)_3\}_3]$ (**B**; M = Cu; Scheme 1).[3] Further investigations revealed that the formation of metal carbene complexes carrying Ge_9 clusters is not dependent on the presence of the bulky hypersilyl groups at Ge_9, and the synthesis of $(NHC)Cu[\eta^3\text{-}Ge_9\{Si(i\text{Bu})_3\}_3]$[4] and $(NHC)Cu[\eta^3\text{-}Ge_9\{Si(i\text{Pr})_3\}_3]$[5] with sterically less demanding $Si(i\text{Bu})_3$ and $Si(i\text{Pr})_3$ silane substituents was also successful. In all cases, the NHC−Cu^I bonds are retained, and the NHC ligands are not displaced by a cluster unit as it was frequently observed for phosphine and halide ligands at transition-metal atoms.[4,6] Moreover, recent reports revealed that the coordination of nine-atomic Zintl cluster ligands to coinage metal carbene complexes is not limited to Ge_9 units because $(NHC)M^+$ moieties have also been combined with Sn_9 clusters in the anions $[(NHC)M(\eta^4\text{-}Sn_9)]^{3-}$[7] (M = Cu, Ag, Au) and with Si_9 clusters in the anions $[(NHC)Cu(\eta^4\text{-}Si_9)]^{3-}$.[8]

Regarding carbene ligands, the development of a variety has been accompanied by a flurry of new applications[9] since the first isolation of stable carbenes 3 decades ago.[10] First, in the field of organometallic chemistry and catalysis, the introduction of NHCs has surpassed the use of phosphines. More recently, considerable interest has been devoted to the development of carbenes with different steric and electronic properties.[11] Most notable is the cyclic (alkyl)amino carbene (CAAC)[12] in which one of the electronegative and π-donor amino substituents of NHCs is replaced by a σ-donor quaternary C atom. As a result, CAACs simultaneously exhibit an increase of their nucleophilicity [higher highest occupied molecular orbital (HOMO) energy] and electrophilicity [lower lowest unoccupied molecular orbital (LUMO) energy] with respect to NHCs and therefore feature a smaller singlet−triplet gap.[13] Moreover, the presence of a quaternary C atom next to the carbene atoms provides a different steric situation and amplifies the flexible steric bulk effect.[12] Owing to their unique

Received: November 30, 2018
Published: February 11, 2019

DOI: 10.1021/acs.inorgchem.8b03338
Inorg. Chem. 2019, 58, 3256−3264

Scheme 1. Syntheses of Compounds 1−3 and Their NHC Derivatives (A and B) via the Reaction of the Respective Silylated Ge_9 Clusters $[Ge_9R_2]^{2-}$ (a) and $[Ge_9R_3]^-$ (b) [R = $Si(TMS)_3$] with Carbene Copper Chlorides (NHC, left; MIC, middle; CAAC, right)

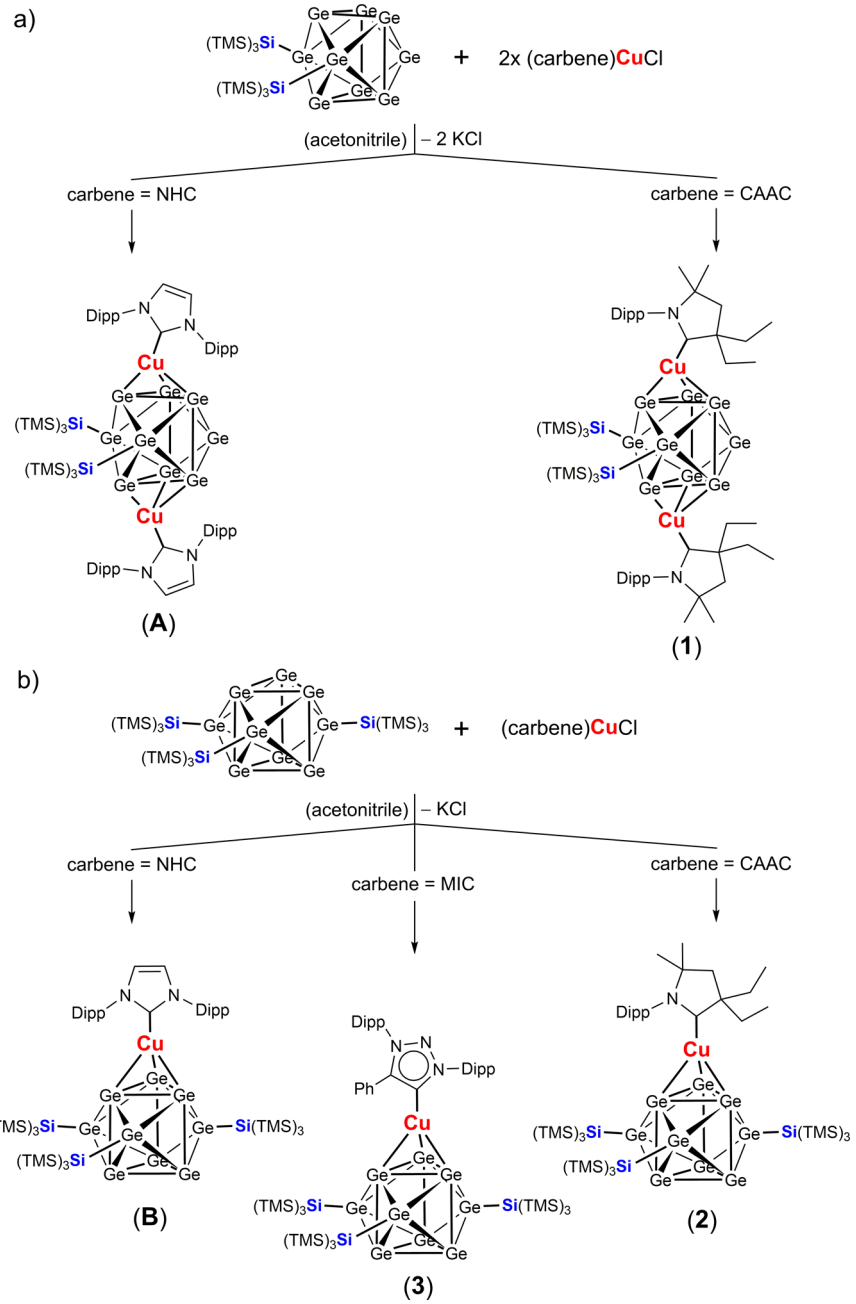

electronic properties, CAACs have been successfully used in the activation of small molecules[13,14] and for the stabilization of a variety of organic radicals[15] as well as of dia- and paramagnetic main-group and transition-metal species.[16] Moreover, 1,2,3-triazol-5-ylidenes, the so-called mesoionic carbenes (MICs),[17] have emerged as a new type of carbene having an electron donation strength between that of NHCs and CAACs, and they have found applications in the stabilization of various late-transition-metal complexes.[18]

Regarding complexation with coinage metals, CAACs have proven to be excellent ligands,[19] and catalytically active[20] and light-emitting[21] species have been reported. Moreover, the existence of neutral dimeric homoleptic complexes $M(CAAC)_2$ (M = Cu, Au),[16c,22] dinuclear species[16c] $[Au_2(CAAC)_2]$, and the mixed-valent $Au_3^{0/I+}$ clusters[23] $[Au_3(CAAC)_3]^+$, in which the metal is at a formal oxidation state below I+, demonstrates their versatile potential as stabilizing ligands. Similarly, with Ge_9 cluster ligands, dimeric homoleptic $[M(Ge_9R_3)_2]^-$ [M = Cu, Au; R = $Si(TMS)_3$] complexes[24] as well as trinuclear Au_3 units $[Au_3Ge_{18}]^{5-}$[25] and $[Au_3Ge_{45}]^{9-}$ have also been obtained.[26]

These results demonstrate a fruitful synthetic approach for the coordination of carbene as well as Zintl cluster ligands to carbene coinage metal complexes. Here, the continually increasing variety of carbene transition-metal complexes will only further advance the synthetic possibilities. In the case of Zintl clusters, the large variety of known $(NHC)Cu^I$ complexes shows high potential for the syntheses of $(carbene)Cu^IGe_9$

DOI: 10.1021/acs.inorgchem.8b03338
Inorg. Chem. 2019, 58, 3256−3264

systems featuring η^3-coordination of the cluster ligand. Computational studies on D_{3h}-$[Ge_9]^{4-}$ clusters show that the η^3-coordinated triangular germanium face of the cluster serves as an electron donor, and thus the clusters can be understood as electron-donating ligands.[27] In the case of the reactions of Ni^0, Pd^0, and Pt^0 phosphine complexes with $[Ge_9R_3]^-$ [R = $Si(TMS)_3$], the insertion of the transition metal into the cluster framework has been observed.[6d,28] Herein, we investigate the formation of (carbene)$Cu^I$$Ge_9$ compounds with different electronic properties using CAAC ($CAAC^{Dipp,Et}$; [:C(N-Dipp)(CMe_2)(CH_2)(CEt_2)]) and MIC ($MIC^{Dipp,Ph}$; [:C(C-Ph)(N-Dipp)(N)(N-Dipp)]) to extend the reported results with NHC and Ge_9 ligands at Cu^I atoms by further characterizations.

RESULTS AND DISCUSSION

$[(CAAC)Cu]_2[\eta^3$-$Ge_9\{Si(TMS)_3\}_2]$ (1). The dianion $[Ge_9R]^{2-}$ [R = $Si(TMS)_3$][29] was recently introduced as a ligand for two (NHC)Cu^I moieties by the reaction of (NHC)CuCl and $K_2[Ge_9\{Si(TMS)_3\}_2]$ in acetonitrile and the formation of $[(NHC^{Dipp})Cu]_2[\eta^3$-$Ge_9\{Si(TMS)_3\}_2]$ (**A**; Scheme 1).[5] An analogous reaction of $K_2[Ge_9\{Si(TMS)_3\}_2]$ with (CAAC)CuCl in acetonitrile leads to the immediate formation of a large amount of a brown solid, which was characterized by NMR spectroscopy (^1H, $^{13}C\{^1H\}$, and $^{29}Si\{^1H\}$), elemental analysis, and electrospray ionization mass spectrometry (ESI-MS). Single crystals obtained by recrystallization from a toluene solution are characterized by X-ray diffraction structure determination. By contrast, the reaction of (MIC)CuCl with $K_2[Ge_9\{Si(TMS)_3\}_2]$ in acetonitrile only yields a small amount of a dark-brown solid, which could not be characterized (Scheme 1).

The NMR spectra (^1H, $^{13}C\{^1H\}$, and $^{29}Si\{^1H\}$) of the product from the reaction of $K_2[Ge_9\{Si(TMS)_3\}_2]$ with (CAAC)CuCl in benzene-d_6 indicate the formation of a single species. The ^1H NMR spectrum exclusively shows one signal set for a (CAAC)Cu^I moiety together with a signal for the TMS protons (δ = 0.45 ppm). An atomic ratio of 2:1 (CAAC)Cu/(Ge_9R_2) [R = $Si(TMS)_3$] indicates the presence of one bis-silylated Ge_9 cluster ligand with two (carbene)Cu^I moieties. The $^{13}C\{^1H\}$ NMR spectrum contains a single signal for the carbene C atom ($C_{carbene}$; δ = 248.1 ppm) and reveals the presence of only one type of (carbene)Cu^I species. The $^{29}Si\{^1H\}$ NMR spectrum shows two signals, one for TMS (δ = −9.9 ppm) and one for $Si(TMS)_3$ (δ = −105.0 ppm), in accordance with the presence of one type of silylated Ge_9 ligand. Thus, the results of the NMR investigations indicate the complexation of two (CAAC)Cu^I moieties with one $[Ge_9\{Si(TMS)_3\}_2]^{2-}$ cluster ligand as an analytically pure solid.

The ESI-MS measurement of the product (the spectrum is shown in the Supporting Information) shows a signal corresponding to $\{[(CAAC)Cu]_3[Ge_9\{Si(TMS)_3\}_2]\}^+$ (m/z 2281) in the positive-ion mode. Similar mass peaks were detected for the uncharged compounds (NHC)Cu[η^3-$Ge_9\{Si(i\text{Bu})_3\}_3$][4] and (NHC)Cu[$\eta^3$-$Ge_9\{Si(i\text{Pr})_3\}_3$],[5] which form $\{[(NHC)Cu]_2[Ge_9\{Si(i\text{Bu})_3\}_3]\}^+$ and $\{[(NHC)Cu]_2[Ge_9\{Si(i\text{Pr})_3\}_3]\}^+$ during the ESI-MS measurements, respectively. For $[(NHC)Cu]_2[\eta^3$-$Ge_9\{Si(TMS)_3\}_2]$, the attachment of a K^+ cation was detected in the species $[(NHC)Cu]_2[\{Ge_9(Si\{TMS\}_3\}_2\}K]^+$.[5]

The single-crystal X-ray diffraction study (crystallographic details are given in the Supporting Information) shows that two (CAAC)Cu^I fragments coordinate two opposing triangular faces of a $[Ge_9R]^{2-}$ [R = $Si(TMS)_3$] unit to give **1** (Figure 1a). Molecules with one silylated Ge_9 cluster that coordinates to

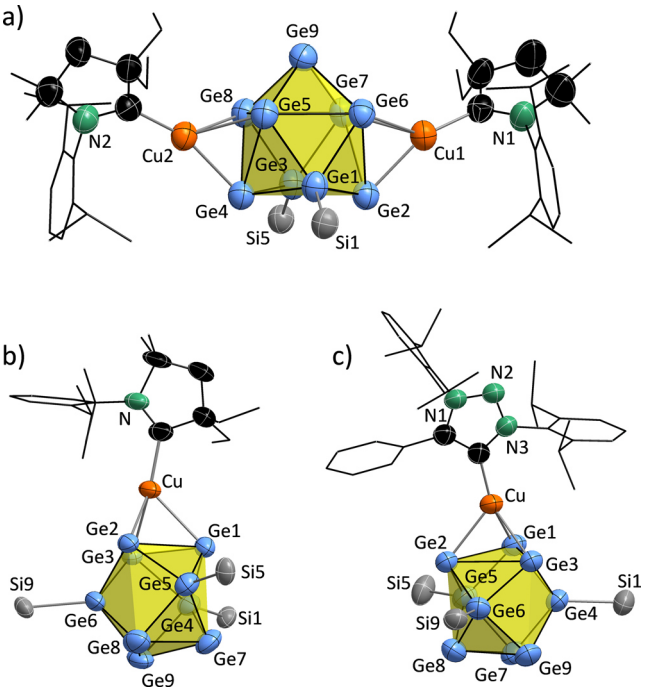

Figure 1. Molecular structures of (a) **1**, (b) **2**, (c) **3**. The Ge, Cu, C, Si, and N atoms are shown as light blue, orange, black, gray, and green ellipsoids, respectively, at a 70% probability level; the Ge_9 cluster is drawn as a yellow polyhedron; C atoms of the organic substituents Dipp, Ph, Et, and Me at the carbene units are displayed in a wire-stick model; H atoms and TMS groups are omitted.

two transition-metal atoms are rare, and only one further example has been characterized crystallographically to date besides **1** and **A**, Ni(dppe)$_2$[η^3-$Ge_9\{Si(TMS)_3\}_3$]$^+$ [dppe = 1,2-bis(diphenylphosphino)ethane].[30]

The structural arrangement in **1** is analogous to that of the NHC derivative **A** (Figure 2b),[5] and the η^1-bonded carbene ligands remain at the Cu^I atoms and are tilted toward the atoms Ge5−Ge9 of the cluster that carry no further ligands (Figure 2a). The bond angles of 158.7(3)° (C23−Cu2−Ge4) and 155.9(3)° (C1−Cu1−Ge2) in **1** are larger compared to the corresponding angles in the NHC derivative with respective angles of 152.7(2)° (C4−Cu2−Ge7) and 152.9(2)° (C1−Cu1−Ge9). The NMR investigations show only one set of carbene units for the CAAC and NHC species, indicating in both cases rotational freedom of the homoleptic carbene ligands at Cu^I atoms in solution, and thus the twist of the two carbene ligands at the two the Cu^I atoms differs with respect to each other in the solid-state structures, most probably due to packing effects.

Both Cu−$C_{carbene}$ distances in **1** are equal [1.95(1) Å; Figure 2a], whereas in the NHC derivative (Figure 2b), one of the two Cu−$C_{carbene}$ distances is significantly shorter [1.913(5) Å for C4−Cu2] compared to the other one [1.941(5) Å for C1−Cu1]. The Ge−Ge distances within the η^3-Cu-coordinated prismatic faces of the Ge_9 unit in **1** and **A** are in the same range but slightly shorter in **1** compared to the NHC derivative **A** with (averaged) values of 2.79(4) Å (CAAC) and 2.81(2) Å (NHC), respectively.

DOI: 10.1021/acs.inorgchem.8b03338
Inorg. Chem. 2019, 58, 3256−3264

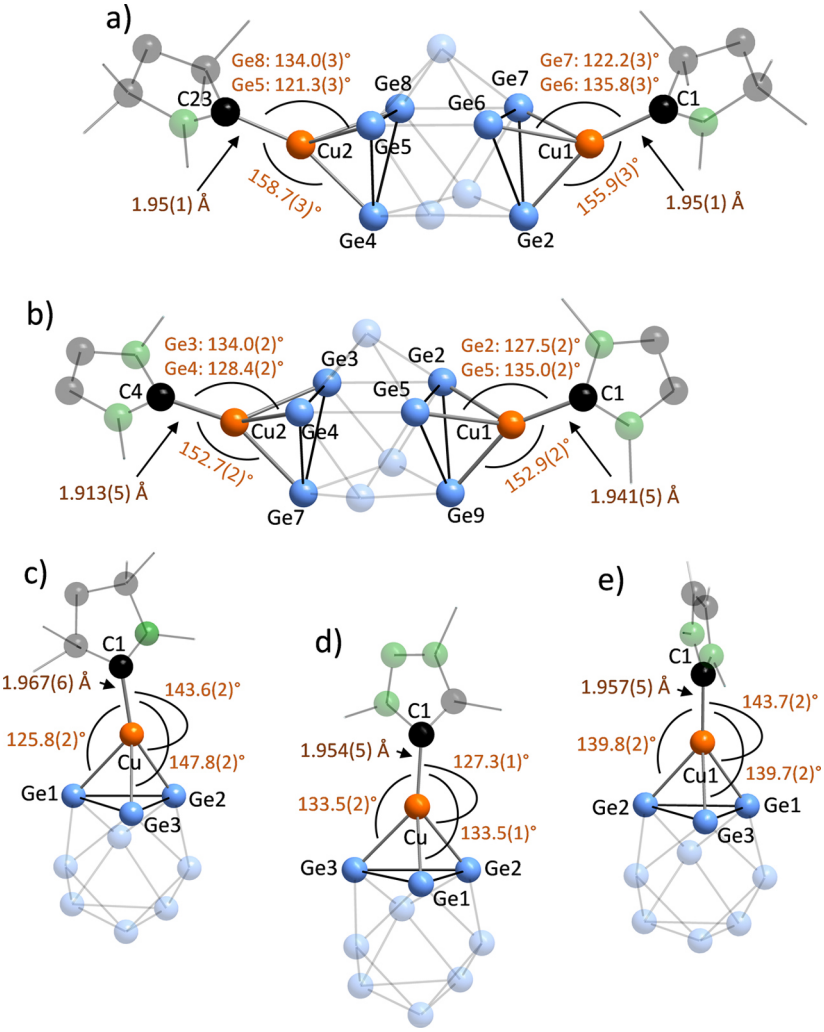

Figure 2. View of the (η^1-carbene)Cu^I(η^3-Ge$_9$) (carbene = CAAC, NHC, MIC) units in the single-crystal X-ray structures of the compounds (Scheme 1): (a) **1**; (b) **A**; (c) **2**; (d) **3**; (e) **B**. The Ge, Cu, C, and N atoms are shown as light blue, orange, black, and green, respectively; the organic groups Dipp, Ph, Et, and Me at the five-membered rings of the carbene units are drawn as black sticks; H atoms and hypersilyl groups are omitted.

The symmetry of the Ge$_9$ core for **1** and **A** is close to point group C_{2v} and can be derived from a tricapped trigonal prism with one elongated prism height between the Ge atoms bearing the silyl groups. Among the Ge−Cu bonds, the ones to the Ge atoms of the noncapped square of the Ge$_9$ cluster (Ge2 and Ge4) are clearly shortened in **1** [bond range in **1**: 2.425(2)−2.432(2) Å] compared to the bonds to the atoms (Ge5, Ge6, Ge7, and Ge8) of the capped square (bond range in **1**: 2.574(2)−2.661(2) Å]. This structural arrangement is in agreement with that of the NHC derivative **A**.

(CAAC)Cu[η^3-Ge$_9${Si(TMS)$_3$}$_3$] (**2**) and (MIC)Cu[η^3-Ge$_9${Si(TMS)$_3$}$_3$] (**3**) are formed in good yield in acetonitrile upon the reaction of K[Ge$_9${Si(TMS)$_3$}$_3$] with (CAAC)CuCl as an orange solid material and (MIC)CuCl as a brown solid material, respectively (Figure 1). In both cases, ^{1}H NMR spectra in benzene-d_6 indicate the formation of a single product that consists of one (carbene)Cu^I unit per [Ge$_9$R$_3$]$^-$ cluster species. The ^{13}C{^{1}H} NMR spectra substantiate attachment of the [Ge$_9$R$_3$]$^-$ unit at the Cu^I atoms by the presence of new carbene carbon signals [$C_{carbene}$ from the reaction with (CAAC)CuCl, δ = 244.2 ppm; $C_{carbene}$ from the reaction with (MIC)CuCl, δ = 167.6 ppm]. In the ^{29}Si{^{1}H} NMR spectra, signals in the specific region of the hypersilyl groups at Ge$_9$ clusters are detected with slightly different chemical shift values compared to those of the reactant K[Ge$_9${Si(TMS)$_3$}$_3$] [carbene = CAAC, δ = −9.3 ppm (TMS), −104.0 ppm (Si(TMS)$_3$); carbene = MIC, δ = −9.3 ppm (TMS), −104.7 ppm (Si(TMS)$_3$)]. Thus, the presence of a new set of carbene and TMS signals in the ^{1}H and ^{13}C{^{1}H} NMR spectra and of new hypersilyl resonances in ^{29}Si{^{1}H} NMR experiments indicates attachment of the corresponding (carbene)Cu^I moieties at the tris-silylated Ge$_9$ cores. ESI-MS investigations (spectra are given in the Supporting Information) show m/z 2151 {[(CAAC)Cu)]$_2$[Ge$_9${Si(TMS)$_3$}$_3$]}$^+$ and m/z 2455 {[(MIC)Cu)]$_2$[Ge$_9${Si(TMS)$_3$}$_3$)]}$^+$ corresponding to [Ge$_9$R$_3$]$^-$ connected with two [(carbene)Cu)]$^+$ units, as has also been reported for (NHC)Cu[Ge$_9${Si(iBu)$_3$}$_3$] and (NHC)Cu[Ge$_9${Si(iPr)$_3$}$_3$] in the positive-ion mode and discussed for **1** before.[4,5] The $C_xH_yN_z$ ratios of the elemental analyses (C, H, and N) of the purified solids suggest compositions of (CAAC)Cu[Ge$_9${Si(TMS)$_3$}$_3$] and (MIC)-Cu[Ge$_9${Si(TMS)$_3$}$_3$] for the respective products.

Single crystals of the products suitable for single-crystal X-ray diffraction (crystallographic details are given in the

DOI: 10.1021/acs.inorgchem.8b03338
Inorg. Chem. 2019, 58, 3256−3264

Supporting Information) were obtained from toluene solutions at −40 °C. The molecular structures of **2** (Figure 1b) and **3** (Figure 1c) show the same coordination environment as that found in the NHC derivative **B** (Figure 2c−e), with the Ge_9 clusters being η^3-coordinated to the Cu^I atoms under retention of the carbene−Cu bonds.

The $Cu-C_{carbene}$ distances (Figures 2c−e) are 1.967(6) Å (in **2**, CAAC), 1.954(5) Å (in **3**, MIC), and 1.957(5) Å (**B**). The longest $Cu-C_{carbene}$ distance is observed for the CAAC ligand, which is the strongest σ donor. In accordance, the $Cu-C_{carbene}$ distances are also elongated in **1** with CAAC compared to its NHC derivative **A**.

A further comparison of the structures of **2**, **3**, and **B** shows that the carbene ligands are tilted with different angles with respect to the Ge_9 clusters [Ge1−Cu−C1 = 125.8(2)° with CAAC in **2** (Figure 2c); Ge3−Cu−C1 = 133.5(2)° with MIC in **3** (Figure 2d); Ge2−Cu1−C1 = 139.8(2)° with NHC in **B** (Figure 2e)]. Again, one set of carbene signals is observed in the NMR spectra of **2**, **3**, and **B**, indicative of rotational freedom of the different carbene ligands around the Cu^I atoms in solution. The different carbene types are arranged with different angles at Cu^I with respect to the Ge_9 clusters. The Ge−Cu distances are in a narrow range with values between 2.512(1) and 2.6586(10) Å [carbene = CAAC (**2**)], 2.4576(8) and 2.5277(8) Å [carbene = MIC (**3**)], and 2.4943(9) and 2.5660(9) Å [carbene = NHC (**B**)].

IR spectra of **1** and **2** (Figure 3, top) reveal typical vibration modes of the organic carbene ligands and hypersilyl groups

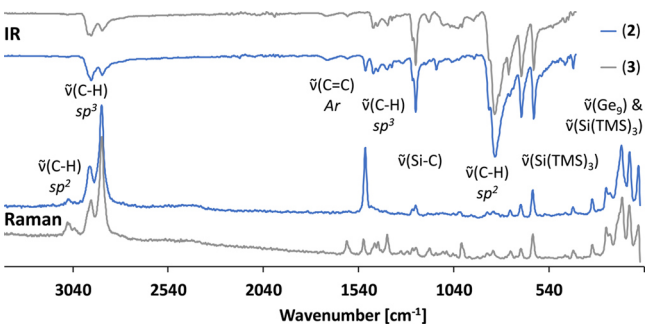

Figure 3. IR and Raman spectra of compounds **2** (blue; IR, bottom line; Raman, top line) and **3** (gray; IR, top line, Raman, bottom line).

such as sp^3 C−H vibrations (2940 and 2886 cm^{-1}), aromatic C=C vibrations (1697 and 1597 cm^{-1}), and Si−C vibrations (1240 cm^{-1}). In the fingerprint region (1500−400 cm^{-1}), both spectra show similarities but differ with respect to the CH_2/CH_3 deformation vibrations of the alkanes (1462−1385 cm^{-1}) and the aromatic units (825 cm^{-1}). Specific vibrations of the hypersilyl groups are further observed at 685 cm^{-1} (Si−C stretching and Si−C−H bending), 620 cm^{-1} (Si−C stretching), and 452 cm^{-1} (Si−Si stretching).[31] The Raman spectra (Figure 3, bottom) show Ge−Ge vibrations of the Ge_9 cluster cores in the range of 40−300 cm^{-1}.[32] The vibrations of the hypersilyl groups at Ge_9 compare well to those of the characteristic vibrations of the tris-silylated cluster species in $[K(222\text{-crypt})][Ge_9\{Si(TMS)_3\}_3]$ from a previous report[1] and prove the detection of specific vibrations for the moieties of the (carbene)$Cu(\eta^3\text{-}Ge_9R_3)$ [R = $Si(TMS)_3$] structures of **2** and **3**.

The structure of the Ge_9 cluster in **2**, **3**, and **B** is best described by point group symmetry D_{3h} derived from a trigonal prism with the three capping Ge atoms that bear the silyl groups. Further analysis of the bond parameters reveals different Ge−Ge distances within the η^3-Cu^i-coordinated triangular faces of the compounds (Ge1−Ge2−Ge3 triangles in Figure 2c−e). Average values are 2.83(4) Å for **2** with the CAAC ligand, 2.92(23) Å for **3** with the MIC ligand, and 2.85(2) Å for the NHC ligand **B**. Interestingly, the sequence of increasing Ge−Ge bond lengths within the η^3-coordinated germanium triangles by the respective (carbene)Cu^I species (MIC > NHC > CAAC) correlates with the reported catalytic activities of these species in "click chemistry",[33] even though no obvious connection between the properties can be found. A similar correlation is observed when **1** is compared with **B** (NHC > CAAC), where expansion of the Ge_3 triangle is comparable to $Ni(dppe)_2[\eta^3\text{-}Ge_9\{Si(TMS)_3\}_3]^+$ with an average Ge−Ge distance of 2.76(19) Å.[30] For **2**, **3**, and **B**, the comparison of the Ge−Ge distances within the opposing, noncoordinated Ge_3 faces (Figure 1; Ge7−Ge8−Ge9) manifests a strong Ge−Ge bond expansion induced by the η^3-Cu coordination of the unit. The average values of 2.66(5) Å (in **2** with the CAAC ligand), 2.64(8) Å (in **3** with the MIC ligand), and 2.64(1) Å (in the NHC derivative) are significantly shorter within the noncoordinated faces.

CONCLUSIONS

A comprehensive study of the compounds $[(carbene)Cu]_2[\eta^3\text{-}Ge_9\{Si(TMS)_3\}_2]$ and $(carbene)Cu[\eta^3\text{-}Ge_9\{Si(TMS)_3\}_3]$ (carbene = CAAC, MIC, NHC) is presented. The herein reported results on CAAC and MIC (carbene)Cu complexes of Ge_9 clusters extend the reports on their NHC derivatives. All compounds feature $(\eta^1\text{-carbene})Cu^I(\eta^3\text{-}Ge_9)$ units, and the study compiles the structural differences of the compounds caused by different electronic and steric properties of the carbene ligands. Bond expansion within the η^3-Cu-coordinated triangles of the Ge_3 units is detected for all (carbene)$CuGe_9$ compounds, and the longest $Cu-C_{carbene}$ and Cu−Ge distances are detected for the CAAC ligands with the strongest σ-donor capacity.

EXPERIMENTAL DETAILS

General Procedures. All reactions and manipulations were performed under a purified argon atmosphere using standard Schlenk and glovebox techniques. K_4Ge_9 was synthesized by heating (2 K min^{-1}) a stoichiometric mixture of both elements K and Ge at 650 °C in a stainless steel autoclave for 46 h and slow cooling (1 K min^{-1}) it to room temperature. All solvents were dried over molecular sieves (3 Å) and THF over a special drying material in a solvent purificator (MBraun MB-SPS). $K[Ge_9\{Si(TMS)_3\}_2]$,[2b] $K_2[Ge_9\{Si(TMS)_3\}_2]$,[29] $(CAAC^{Dipp,Et})CuCl$,[20] and $(MIC^{Dipp,Ph})CuCl$[20] were synthesized according to modified literature procedures. All other chemicals were received commercially and used without further purification.

Single-Crystal Structure Determination. The air- and moisture-sensitive crystals of **1**−**3** were transferred from the mother liquor into cooled perfluoroalkyl ether oil under a cold stream of N_2 gas. For data collection, the crystals were fixed on a glass capillary and positioned in a 150 K cold stream of N_2 gas using the crystal cap system. Single-crystal data collection was performed at a STOE StadiVari (Mo Kα radiation) diffractometer equipped with a DECTRIS PILATUS 300 K detector. Structures were solved by direct methods (*SHELXS-2014*) and refined by full-matrix least-squares calculations against F^2 (*SHELXL-2014*).[34] The positions of the H atoms were calculated and refined using a riding model.

Unless otherwise stated, all non-H atoms were treated with anisotropic displacement parameters. For **2**, all crystals were found to be weakly diffracting, and the R(int) statistics are affected by these low intensities. The supplementary crystallographic data for CCDC

DOI: 10.1021/acs.inorgchem.8b03338
Inorg. Chem. 2019, 58, 3256−3264

1570249 (**1**), 1570247 (**2**), and 1570248 (**3**) have been deposited with the Cambridge Structural Database. The crystal structures have been plotted with *Diamond*.[35] One of the hypersilyl groups in **2** and two of the hypersilyl groups in **3** show orientational disorder, which is omitted in the presentation of the structures.

Electron-Dispersive X-ray (EDX) Analysis. Single crystals of all compounds were analyzed with SWIFT-ED-TM (Oxford Instruments) and Hitachi TM-1000 Tabletop (Hitachi High-Technologies) microscopes with the *INCA* system software.

NMR Spectroscopy. ^{1}H, ^{13}C{^{1}H}, and ^{29}Si{^{1}H} NMR spectra were recorded on a Bruker AVIII Ultrashield 400 MHz or a Bruker AVIII 500 MHz Cryo system. The signals of the ^{1}H and ^{13}C{^{1}H} spectra were calibrated on the rest proton signal of the used deuterated solvent benzene-d_6. Chemical shifts are given in δ values by parts per million (ppm). The coupling constants J are stated in hertz. Signal multiplicities are abbreviated as follows: s, singlet; d, doublet; t, triplet; m, multiplet. The spectra were evaluated with *MestReNova*.[36]

ESI-MS. The measurements were performed on an HCT instrument (Bruker Corp.). Analysis of the data was carried out using the program *Bruker Compass Data Analysis 4.0 SP 5* (Bruker Corp.). The dry gas temperature was adjusted to 300 °C and the injection speed to 240 μL s^{-1}. Visualization of the spectra was done with the programs *OriginPro 2016G* (Origin Lab Corp.) and *Excel 2016* (Microsoft Corp.).

Elemental Analysis. Elemental analyses were performed by the Microanalytical Laboratory at the Catalytic Research Center of TUM. The elements C, H, and N were determined with a Euro EA CHNS elemental analyzer (HEKAtech Ltd.).

IR Spectroscopy. Fourier transform infrared (FT-IR) spectra were recorded on a Bruker Alpha FT-IR spectrometer with an attenuated-total-reflectance (ATR) geometry using a diamond ATR unit under an argon atmosphere.

Raman Spectroscopy. Raman spectra were recorded with a Renishaw RE04 inVia Raman microscope with a charge-coupled detector and 500 mW maximum power (software *WiRE 4.2 build 5037*, Renishaw 2002) at λ = 532 nm. For the measurements, single crystals of the compounds were sealed in glass capillaries.

Compound **1**. A solution of (CAAC)CuCl (0.12 mmol, 2 equiv) in acetonitrile is added to a solution of $K_2[Ge_9\{Si(TMS)_3\}_2]$ (0.06 mmol, 1 equiv) in acetonitrile. A brown solid starts to precipitate immediately, and the reaction mixture is stirred overnight. The precipitate is allowed to settle, separated by filtration, and washed with acetonitrile. After drying in vacuo, the residue is redissolved in toluene (5 mL) and filtered, yielding a red solution. After removal of the volatiles, NMR (^{1}H, ^{13}C{^{1}H}, and ^{29}Si{^{1}H}) investigations in benzene-d_6 reveal the formation of a pure product (brown solid; yield 41.1 mg/36%). ESI-MS measurement in toluene/THF shows the peak of the species $\{[(CAAC^{Dipp,Et})Cu]_3[Ge_9\{Si(TMS)_3\}_2]\}^+$ in the positive-ion mode. Red single crystals are obtained from a concentrated toluene solution at −40 °C and investigated by single-crystal X-ray diffraction. EDX measurements show the presence of the elements Si, Ge, and Cu in the single crystals. ^{1}H NMR (400 MHz, benzene-d_6): δ 7.16−7.10 (d, J = 6.9 Hz, 2H, C$H_{Ph(p)}$), 7.09−7.00 (d, J = 7.4 Hz, 4H C$H_{Ph(m)}$), 2.90−2.71 (p, J = 6.6 Hz, 4H CH_{iPr}), 2.4−2.06 (m, 8H C$H_{2(Et)}$), 1.86−1.71 (d, J = 6.6 Hz, 12H C$H_{3(iPr)}$), 1.45−1.36 (s, 4H, C$H_{2(Pyr)}$), 1.21−1.09 (d, J = 6.7 Hz, 12H, C$H_{3(iPr)}$), 1.06−0.96 (t, J = 7.4 Hz, 12H, C$H_{3(Et)}$), 0.92−0.83 (s, 12H, C$H_{3(Me)}$), 0.54−0.40 (s, 54H, C$H_{3(TMS)}$). ^{13}C{^{1}H} NMR (101 MHz, benzene-d_6): δ 248.14 ($C_{carbene}$), 145.54 ($C_{Ph(N)}$), 135.20 ($C_{Ph(iPr)}$), 129.58 (CH_{Ph}), 125.13 (CH_{Ph}), 79.65 (C$Me_{2(Pyr)}$), 64.16 (C$H_{2(Pyr)}$), 41.66 (C$Et_{2(Pyr)}$), 32.08 (C$H_{2(Et)}$), 30.29 (CH_{iPr}), 29.25 (C$H_{3(Me)}$), 23.58 (C$H_{3(iPr)}$), 10.15 (C$H_{3(Et)}$), 3.15 (C$H_{3(TMS)}$). ^{29}Si{^{1}H} NMR (79 MHz, benzene-d_6): δ −9.88 (TMS), − 104.95 (Si(TMS)$_3$). ESI-MS (positive mode, −6000 V, 300 °C): m/z 2281 ($\{[(CAAC^{Dipp,Et})Cu]_3[Ge_9\{Si(TMS)_3\}_2]\}^+$). Elem anal. Found (calcd): C, 40.56 (39.13); H, 6.70 (6.57); N, 1.52 (1.47). Semiquantitative EDX anal. Found (calcd): Si, 34.6 (42.1); Ge, 57.0 (47.4); Cu, 8.1 (10.5).

Compounds **2** *and* **3**. A solution of (carbene)CuCl (carbene = CAAC, MIC; 0.06 mmol, 1.5 equiv) in acetonitrile is added to a solution of $K[Ge_9\{Si(TMS)_3\}_3]$ (0.04 mmol, 1 equiv) in acetonitrile. Precipitation of the products starts immediately, and the reaction mixtures are stirred overnight. The precipitates are allowed to settle, separated by filtration, and washed with acetonitrile. After drying in vacuo, the solids are redissolved in toluene (5 mL) and filtered, yielding red solutions. After removal of the volatiles, NMR (^{1}H, ^{13}C{^{1}H}, and ^{29}Si{^{1}H}) investigations in benzene-d_6 reveal the formation of pure products [CAAC (orange solid), yield 72.4 mg/68%; MIC (brown solid), yield 56.6 mg/49%]. ESI-MS measurements show the peaks of the respective $\{[(carbene)Cu]_2[Ge_9\{Si(TMS)_3\}_3]\}^+$ species in the positive-ion mode. Red single crystals of the solids are obtained from a concentrated toluene solution at −40 °C and investigated by single-crystal X-ray diffraction. EDX measurements show the presence of the elements Si, Ge, and Cu in the single crystals.

2. ^{1}H NMR (500 MHz, benzene-d_6): δ 7.14−7.09 (dd, J = 8.6 and 6.8 Hz, 1H, C$H_{Ph(p)}$), 7.08−7.01 (d, J = 7.2 Hz, 2H C$H_{Ph(m)}$), 3.00−2.81 (m, 2H, CH_{iPr}), 2.40−2.25 (q, 4H, J = 7.2 Hz, C$H_{2(Et)}$), 1.94−1.79 (d, J = 6.7 Hz, 6H, C$H_{3(iPr)}$), 1.56−1.45 (s, 2H, C$H_{2(Pyr)}$), 1.28−1.18 (d, J = 6.7 Hz, 6H, C$H_{3(iPr)}$), 1.17−1.06 (t, J = 7.4 Hz, 6H, C$H_{3(Et)}$), 0.98−0.87 (s, 6H, C$H_{3(Me)}$), 0.54−0.36 (s, 81H, C$H_{3(TMS)}$). ^{13}C{^{1}H} NMR (101 MHz, benzene-d_6): δ 244.27 ($C_{carbene}$), 145.37 ($C_{Ph(N)}$), 134.70 ($C_{Ph(iPr)}$), 130.01 (CH_{Ph}), 125.31 (CH_{Ph}), 80.22 (C$Me_{2(Pyr)}$), 64.52 (C$H_{2(Pyr)}$), 41.66 (C$Et_{2(Pyr)}$), 32.11 (C$H_{2(Et)}$), 30.25 (CH_{iPr}), 29.44 (C$H_{3(Me)}$), 23.52 (C$H_{3(iPr)}$), 10.52 (C$H_{3(Et)}$), 3.00 (C$H_{3(TMS)}$). ^{29}Si{^{1}H} NMR (60 MHz, benzene-d_6): δ −9.31 (TMS), −103.96 (Si(TMS)$_3$). ESI-MS (positive mode, −6000 V, 300 °C): m/z 2151 ($\{[(CAAC^{Dipp,Et})Cu]_2[Ge_9\{Si(TMS)_3\}_3]\}^+$). Elem anal. Found (calcd): C, 33.17 (33.18); H, 6.61 (6.59); N, 0.80 (0.79). Semiquantitative EDX anal. Found (calcd): Si, 50.2 (54.5); Ge, 45.5 (40.9); Cu, 4.0 (4.54).

3. ^{1}H NMR (500 MHz, benzene-d_6): δ 7.88−7.79 (d, J = 7.3 Hz, 2H, CH_{Arom}), 7.30−7.20 (m, 5H, CH_{Arom}), 7.13−6.99 (m, 2H, CH_{Arom}), 6.91−6.82 (d, J = 7.8 Hz, 2H, CH_{Arom}), 2.96−2.78 (m, 2H, CH_{iPr}), 2.55−2.39 (m, 2H, CH_{iPr}), 1.90−1.77 (d, J = 6.8 Hz, 6H, C$H_{3(iPr)}$), 1.27−1.14 (d, J = 6.9 Hz, 6H, C$H_{3(iPr)}$), 1.09−0.98 (d, J = 6.8 Hz, 6H, C$H_{3(iPr)}$), 0.95−0.84 (d, J = 6.8 Hz, 6H, C$H_{3(iPr)}$), 0.53−0.35 (s, 81H, C$H_{3(TMS)}$). ^{13}C{^{1}H} NMR (126 MHz, benzene-d_6): δ 167.57 ($C_{carbene}$), 149.82 ($C_{triazole}$), 145.61 ($C_{Ph(N)}$), 144.93 ($C_{Ph(N)}$), 136.10 ($C_{Ph(iPr)}$), 132.01 ($C_{Ph(iPr)}$), 131.95 (CH_{Ph}), 131.30 (CH_{Ph}), 130.99 (CH_{Ph}), 130.26 (CH_{Ph}), 128.82 (CH_{Ph}), 126.43 (CH_{Ph}), 124.96(CH_{Ph}), 124.64(CH_{Ph}), 29.28 (C$H_{3(iPr)}$), 29.24 (C$H_{3(iPr)}$), 25.67 (CH_{iPr}), 25.31 (C$H_{3(iPr)}$), 25.27 (C$H_{3(iPr)}$), 22.46 (CH_{iPr}), 3.02 (C$H_{3(TMS)}$). ^{29}Si{^{1}H} NMR (79 MHz, benzene-d_6): δ −9.34 (TMS), −104.70 (Si(TMS)$_3$). ESI-MS (positive mode, −6000 V, 300 °C): m/z 2455 ($\{[(MIC^{Dipp,Ph})Cu)]_2[Ge_9\{Si(TMS)_3\}_3]\}^+$). Elem anal. Found (calcd): C, 34.98 (36.80); H, 6.10 (6.28); N, 2.16 (2.18). Semiquantitative EDX anal. Found (calcd): Si, 57.0 (54.5); Ge, 39.4 (40.9); Cu, 3.5 (4.54).

■ ASSOCIATED CONTENT

Supporting Information

The Supporting Information is available free of charge on the ACS Publications website at DOI: 10.1021/acs.inorgchem.8b03338.

Crystallographic details and NMR and ESI-MS spectra (PDF)

Accession Codes

CCDC 1570247−1570249 contain the supplementary crystallographic data for this paper. These data can be obtained free of charge via www.ccdc.cam.ac.uk/data_request/cif, or by emailing data_request@ccdc.cam.ac.uk, or by contacting The Cambridge Crystallographic Data Centre, 12 Union Road, Cambridge CB2 1EZ, UK; fax: +44 1223 336033.

DOI: 10.1021/acs.inorgchem.8b03338
Inorg. Chem. 2019, 58, 3256−3264

AUTHOR INFORMATION

Corresponding Author

*E-mail: thomas.faessler@lrz.tum.de. Phone: +49-89-289-13131.

ORCID

Mohand Melaimi: 0000-0003-3553-1381

Wilhelm Klein: 0000-0002-6351-9921

Thomas F. Fässler: 0000-0001-9460-8882

Author Contributions

The manuscript was written through contributions of all authors.

Notes

The authors declare no competing financial interest.

ACKNOWLEDGMENTS

We are grateful for support by Wacker Chemie AG, the Bavaria California Technology Center (BaCaTeC), and the TUM Graduate School. Furthermore, the authors thank Tassilo Restle for help with single-crystal X-ray measurements, Michael Huber for supporting the syntheses, Maria Müller for EDX measurements, Sebastian Geier for Raman measurements, David Mayer for IR measurements, and Ulrike Ammari for elemental analyses.

REFERENCES

(1) Fischer, C.; Klein, W.; Jantke, L.-A.; Schiegerl, L. J.; Fässler, T. F. Reaction of $SiCl_2$·dipp with $K[Ge_9\{Si(SiMe_3)_3\}_3]$ − Synthesis and Characterization of $[K(dipp)_2][Ge_9\{Si(SiMe_3)_3\}_3]$·tol and [dipp-H]$[Ge_9\{Si(SiMe_3)_3\}_3]$·2acn [dipp = 1,3-Bis(2,6-Diisopropylphenyl)-imidazol-2-ylidene]. *Z. Anorg. Allg. Chem.* **2016**, *642* (22), 1314−1319.

(2) (a) Schnepf, A. $[Ge_9\{Si(SiMe_3)_3\}_3]^-$: A Soluble Polyhedral Ge_9 Cluster Stabilized by Only Three Silyl Ligands. *Angew. Chem., Int. Ed.* **2003**, *42* (23), 2624−2625. (b) Li, F.; Sevov, S. C. Rational Synthesis of $[Ge_9\{Si(SiMe_3)_3\}_3]^-$ from Its Parent Zintl Ion Ge_9^{4-}. *Inorg. Chem.* **2012**, *51* (4), 2706−2708.

(3) Geitner, F. S.; Fässler, T. F. Introducing Tetrel Zintl Ions to N-Heterocyclic Carbenes − Synthesis of Coinage Metal NHC Complexes of $[Ge_9\{Si(SiMe_3)_3\}_3]^-$. *Eur. J. Inorg. Chem.* **2016**, *2016* (17), 2688−2691.

(4) Schiegerl, L. J.; Geitner, F. S.; Fischer, C.; Klein, W.; Fässler, T. F. Functionalization of $[Ge_9]$ with Small Silanes:$[Ge_9(SiR_3)_3]^-$ (R = *i*Bu, *i*Pr, Et) and the Structures of (CuNHCDipp)$[Ge_9\{Si(iBu)_3\}_3]$, (K-18c6)Au$[Ge_9\{Si(iBu)_3\}_3]_2$, and $(K\text{-}18c6)_2[Ge_9\{Si(iBu)_3\}_2]$. *Z. Anorg. Allg. Chem.* **2016**, *642* (24), 1419−1426.

(5) Geitner, F. S.; Giebel, M. A.; Pöthig, A.; Fässler, T. F. N-Heterocyclic Carbene Coinage Metal Complexes of the Germanium-Rich Metalloid Clusters $[Ge_9R_3]^-$ and $[Ge_9R^I_2]^{2-}$ with R = $Si(iPr)_3$ and R^I = $Si(TMS)_3$. *Molecules* **2017**, *22* (7), 1204.

(6) (a) Geitner, F. S.; Dums, J. V.; Fässler, T. F. Derivatization of Phosphine Ligands with Bulky Deltahedral Zintl Clusters—Synthesis of Charge Neutral Zwitterionic Tetrel Cluster Compounds $[(Ge_9\{Si(TMS)_3\}_2)tBu_2P]M(NHCDipp)$ (*M*: Cu, Ag, Au). *J. Am. Chem. Soc.* **2017**, *139* (34), 11933−11940. (b) Mayer, K.; Schiegerl, L. J.; Fässler, T. F. On the Reactivity of Silylated Ge_9 Clusters: Synthesis and Characterization of $[ZnCp^*(Ge_9\{Si(SiMe_3)_3\}_3)]$, $[CuPiPr_3(Ge_9\{Si(SiMe_3)_3\}_3)]$, and $[(CuPiPr_3)_4\{Ge_9(SiPh_3)_2\}_2]$. *Chem. - Eur. J.* **2016**, *22* (52), 18794−18800. (c) Geitner, F. S.; Wallach, C.; Fässler, T. F. On the Variable Reactivity of Phosphine-Functionalized $[Ge_9]$ Clusters: Zintl Cluster-Substituted Phosphines or Phosphine-Substituted Zintl Clusters. *Chem. - Eur. J.* **2018**, *24* (16), 4103−4110. (d) Li, F.; Muñoz-Castro, A.; Sevov, S. C. $[(Me_3Si)Si]_3EtGe_9Pd(PPh_3)$, a Pentafunctionalized Deltahedral Zintl Cluster: Synthesis, Structure, and Solution Dynamics. *Angew. Chem., Int. Ed.* **2016**, *55* (30), 8630−8633. (e) Henke, F.; Schenk, C.; Schnepf, A. $[Si(SiMe_3)_3]_6Ge_{18}M$ (*M* = Zn, Cd, Hg): neutral metalloid cluster compounds of germanium as highly soluble building blocks for supramolecular chemistry. *Dalton Trans.* **2009**, No. 42, 9141−9145. (f) Schenk, C.; Schnepf, A. $[AuGe_{18}\{Si(SiMe_3)_3\}_6]^-$: A Soluble Au−Ge Cluster on the Way to a Molecular Cable? *Angew. Chem., Int. Ed.* **2007**, *46* (28), 5314−5316. (g) Mayer, K.; Jantke, L.-A.; Schulz, S.; Fässler, T. F. Retention of the Zn−Zn bond in $[Ge_9Zn{-}ZnGe_9]^{6-}$ and Formation of $[(Ge_9Zn){-}(Ge_9){-}(ZnGe_9)]^{8-}$ and Polymeric $[{-}(Ge_9Zn)^{2-}{-}]$. *Angew. Chem., Int. Ed.* **2017**, *56* (9), 2350−2355. (h) Li, F.; Sevov, S. C. Coordination of Tri-Substituted Nona−Germanium Clusters to Cu(I) and Pd(0). *Inorg. Chem.* **2015**, *54* (16), 8121−8125. (i) Perla, L. G.; Sevov, S. C. A Stannyl-Decorated Zintl Ion $[Ge_{18}Pd_3(SniPr_3)_6]^{2-}$: Twinned Icosahedron with a Common Pd_3-Face or 18-Vertex Hypho-Deltahedron with a Pd_3-Triangle Inside. *J. Am. Chem. Soc.* **2016**, *138* (31), 9795−9798. (j) Perla, L. G.; Muñoz-Castro, A.; Sevov, S. C. Eclipsed- and Staggered-$[Ge_{18}Pd_3\{EiPr_3\}_6]2-$ (*E* = Si, Sn): Positional Isomerism in Deltahedral Zintl Clusters. *J. Am. Chem. Soc.* **2017**, *139* (42), 15176−15181.

(7) Geitner, F. S.; Klein, W.; Fässler, T. F. Formation of the intermetalloid cluster $[AgSn_{18}]^{7-}$ − the reactivity of coinage metal NHC compounds towards $[Sn_9]^{4-}$. *Dalton Trans.* **2017**, *46* (18), 5796−5800.

(8) Geitner, F. S.; Fässler, T. F. Low oxidation state silicon clusters − synthesis and structure of $[NHC^{Dipp}Cu(\eta^4\text{-}Si_9)]^{3-}$. *Chem. Commun.* **2017**, *53* (96), 12974−12977.

(9) (a) Rovis, T.; Nolan, S. P. Stable Carbenes: From 'Laboratory Curiosities' to Catalysis Mainstays. *Synlett* **2013**, *24* (10), 1188−1189. (b) Arduengo, A. J.; Bertrand, G. Carbenes Introduction. *Chem. Rev.* **2009**, *109* (8), 3209−3210. (c) Nesterov, V.; Reiter, D.; Bag, P.; Frisch, P.; Holzner, R.; Porzelt, A.; Inoue, S. NHCs in Main Group Chemistry. *Chem. Rev.* **2018**, *118* (19), 9678−9842.

(10) (a) Igau, A.; Grutzmacher, H.; Baceiredo, A.; Bertrand, G. Analogous.alpha.,.alpha.'-bis-carbenoid, triply bonded species: synthesis of a stable.lambda.3-phosphino carbene-.lambda.5-phosphaacetylene. *J. Am. Chem. Soc.* **1988**, *110* (19), 6463−6466. (b) Igau, A.; Baceiredo, A.; Trinquier, G.; Bertrand, G. [Bis(diisopropylamino)-phosphino]trimethylsilylcarbene: A Stable Nucleophilic Carbene. *Angew. Chem., Int. Ed. Engl.* **1989**, *28* (5), 621−622. (c) Bourissou, D.; Guerret, O.; Gabbaï, F. P.; Bertrand, G. Stable Carbenes. *Chem. Rev.* **2000**, *100* (1), 39−92. (d) Arduengo, A. J.; Harlow, R. L.; Kline, M. A stable crystalline carbene. *J. Am. Chem. Soc.* **1991**, *113* (1), 361−363.

(11) (a) Melaimi, M.; Soleilhavoup, M.; Bertrand, G. Stable Cyclic Carbenes and Related Species beyond Diaminocarbenes. *Angew. Chem., Int. Ed.* **2010**, *49* (47), 8810−8849. (b) Weber, S. G.; Loos, C.; Rominger, F.; Straub, B. F. Synthesis of an extremely sterically shielding N-heterocyclic carbene ligand. *Arkivoc* **2011**, *2012* (3), 226−242. (c) Berthon-Gelloz, G.; Siegler, M. A.; Spek, A. L.; Tinant, B.; Reek, J. N. H.; Markó, I. E. IPr* an easily accessible highly hindered N-heterocyclic carbene. *Dalton Trans.* **2010**, *39* (6), 1444−1446. (d) Dierick, S.; Dewez, D. F.; Markó, I. E. IPr*(2-Np)—An Exceedingly Bulky N-Heterocyclic Carbene. *Organometallics* **2014**, *33* (3), 677−683. (e) Weinstein, C. M.; Junor, G. P.; Tolentino, D. R.; Jazzar, R.; Melaimi, M.; Bertrand, G. Highly Ambiphilic Room Temperature Stable Six-Membered Cyclic (Alkyl)(amino)carbenes. *J. Am. Chem. Soc.* **2018**, *140* (29), 9255−9260.

(12) Lavallo, V.; Canac, Y.; Präsang, C.; Donnadieu, B.; Bertrand, G. Stable Cyclic (Alkyl)(Amino)Carbenes as Rigid or Flexible, Bulky, Electron-Rich Ligands for Transition-Metal Catalysts: A Quaternary Carbon Atom Makes the Difference. *Angew. Chem., Int. Ed.* **2005**, *44* (35), 5705−5709.

(13) Lavallo, V.; Canac, Y.; Donnadieu, B.; Schoeller, W. W.; Bertrand, G. CO Fixation to Stable Acyclic and Cyclic Alkyl Amino Carbenes: Stable Amino Ketenes with a Small HOMO−LUMO Gap. *Angew. Chem., Int. Ed.* **2006**, *45* (21), 3488−3491.

(14) (a) Frey, G. D.; Lavallo, V.; Donnadieu, B.; Schoeller, W. W.; Bertrand, G. Facile Splitting of Hydrogen and Ammonia by Nucleophilic Activation at a Single Carbon Center. *Science* **2007**,

DOI: 10.1021/acs.inorgchem.8b03338
Inorg. Chem. 2019, 58, 3256−3264

316 (5823), 439−441. (b) Masuda, J. D.; Schoeller, W. W.; Donnadieu, B.; Bertrand, G. Carbene Activation of P_4 and Subsequent Derivatization. *Angew. Chem., Int. Ed.* **2007**, *46* (37), 7052−7055.
(15) (a) Mahoney, J. K.; Martin, D.; Moore, C. E.; Rheingold, A. L.; Bertrand, G. Bottleable (Amino)(Carboxy) Radicals Derived from Cyclic (Alkyl)(Amino) Carbenes. *J. Am. Chem. Soc.* **2013**, *135* (50), 18766−18769. (b) Jin, L.; Melaimi, M.; Liu, L.; Bertrand, G. Singlet carbenes as mimics for transition metals: synthesis of an air stable organic mixed valence compound $[M_2(C_2)^{+}$; M = cyclic(alkyl)-(amino)carbene]. *Org. Chem. Front.* **2014**, *1* (4), 351−354. (c) Li, Y.; Mondal, K. C.; Samuel, P. P.; Zhu, H.; Orben, C. M.; Panneerselvam, S.; Dittrich, B.; Schwederski, B.; Kaim, W.; Mondal, T.; Koley, D.; Roesky, H. W. C_4 Cumulene and the Corresponding Air-Stable Radical Cation and Dication. *Angew. Chem., Int. Ed.* **2014**, *53* (16), 4168−4172. (d) Styra, S.; Melaimi, M.; Moore, C. E.; Rheingold, A. L.; Augenstein, T.; Breher, F.; Bertrand, G. Crystalline Cyclic (Alkyl)(amino)carbene-tetrafluoropyridyl Radical. *Chem. - Eur. J.* **2015**, *21* (23), 8441−8446. (e) Hansmann, M. M.; Melaimi, M.; Bertrand, G. Crystalline Monomeric Allenyl/Propargyl Radical. *J. Am. Chem. Soc.* **2017**, *139* (44), 15620−15623. (f) Hansmann, M. M.; Melaimi, M.; Bertrand, G. Organic Mixed Valence Compounds Derived from Cyclic (Alkyl)(amino)carbenes. *J. Am. Chem. Soc.* **2018**, *140* (6), 2206−2213.
(16) (a) Martin, C. D.; Soleilhavoup, M.; Bertrand, G. Carbene-stabilized main group radicals and radical ions. *Chem. Sci.* **2013**, *4* (8), 3020−3030. (b) Chandra Mondal, K.; Roy, S.; Roesky, H. W. Silicon based radicals, radical ions, diradicals and diradicaloids. *Chem. Soc. Rev.* **2016**, *45* (4), 1080−1111. (c) Weinberger, D. S.; Melaimi, M.; Moore, C. E.; Rheingold, A. L.; Frenking, G.; Jerabek, P.; Bertrand, G. Isolation of Neutral Mono- and Dinuclear Gold Complexes of Cyclic (Alkyl)(amino)carbenes. *Angew. Chem., Int. Ed.* **2013**, *52* (34), 8964−8967. (d) Singh, A. P.; Samuel, P. P.; Roesky, H. W.; Schwarzer, M. C.; Frenking, G.; Sidhu, N. S.; Dittrich, B. A Singlet Biradicaloid Zinc Compound and Its Nonradical Counterpart. *J. Am. Chem. Soc.* **2013**, *135* (19), 7324−7329. (e) Ung, G.; Rittle, J.; Soleilhavoup, M.; Bertrand, G.; Peters, J. C. Two-Coordinate Fe^0 and Co^0 Complexes Supported by Cyclic (alkyl)(amino)carbenes. *Angew. Chem., Int. Ed.* **2014**, *53* (32), 8427−8431. (f) Kinjo, R.; Donnadieu, B.; Bertrand, G. Isolation of a Carbene-Stabilized Phosphorus Mononitride and Its Radical Cation ($PN^{+\cdot}$). *Angew. Chem., Int. Ed.* **2010**, *49* (34), 5930−5933. (g) Kinjo, R.; Donnadieu, B.; Celik, M. A.; Frenking, G.; Bertrand, G. Synthesis and Characterization of a Neutral Tricoordinate Organoboron Isoelectronic with Amines. *Science* **2011**, *333* (6042), 610−613. (h) Mondal, K. C.; Roy, S.; Dittrich, B.; Andrada, D. M.; Frenking, G.; Roesky, H. W. A Triatomic Silicon(0) Cluster Stabilized by a Cyclic Alkyl(amino) Carbene. *Angew. Chem., Int. Ed.* **2016**, *55* (9), 3158−3161.
(17) (a) Guisado-Barrios, G.; Bouffard, J.; Donnadieu, B.; Bertrand, G. Crystalline 1H-1,2,3-Triazol-5-ylidenes: New Stable Mesoionic Carbenes (MICs). *Angew. Chem., Int. Ed.* **2010**, *49* (28), 4759−4762. (b) Guisado-Barrios, G.; Bouffard, J.; Donnadieu, B.; Bertrand, G. Bis(1,2,3-triazol-5-ylidenes) (i-bitz) as Stable 1,4-Bidentate Ligands Based on Mesoionic Carbenes (MICs). *Organometallics* **2011**, *30* (21), 6017−6021.
(18) (a) Donnelly, K. F.; Petronilho, A.; Albrecht, M. Application of 1,2,3-triazolylidenes as versatile NHC-type ligands: synthesis, properties, and application in catalysis and beyond. *Chem. Commun.* **2013**, *49* (12), 1145−1159. (b) Crabtree, R. H. Abnormal, mesoionic and remote N-heterocyclic carbene complexes. *Coord. Chem. Rev.* **2013**, *257* (3), 755−766. (c) Krüger, A.; Albrecht, M. Abnormal N-heterocyclic Carbenes: More than Just Exceptionally Strong Donor Ligands. *Aust. J. Chem.* **2011**, *64* (8), 1113−1117. (d) Schuster, O.; Yang, L.; Raubenheimer, H. G.; Albrecht, M. Beyond Conventional N-Heterocyclic Carbenes: Abnormal, Remote, and Other Classes of NHC Ligands with Reduced Heteroatom Stabilization. *Chem. Rev.* **2009**, *109* (8), 3445−3478. (e) Arnold, P. L.; Pearson, S. Abnormal N-heterocyclic carbenes. *Coord. Chem. Rev.* **2007**, *251* (5), 596−609. (f) Keitz, B. K.; Bouffard, J.; Bertrand, G.; Grubbs, R. H. Protonolysis of a Ruthenium−Carbene Bond and Applications in Olefin Metathesis. *J. Am. Chem. Soc.* **2011**, *133* (22), 8498−8501. (g) Bezuidenhout, D. I.; Kleinhans, G.; Guisado-Barrios, G.; Liles, D. C.; Ung, G.; Bertrand, G. Isolation of a potassium bis(1,2,3-triazol-5-ylidene)-carbazolide: a stabilizing pincer ligand for reactive late transition metal complexes. *Chem. Commun.* **2014**, *50* (19), 2431−2433. (h) Kleinhans, G.; Guisado-Barrios, G.; Liles, D. C.; Bertrand, G.; Bezuidenhout, D. I. A rhodium(i)−oxygen adduct as a selective catalyst for one-pot sequential alkyne dimerization-hydrothiolation tandem reactions. *Chem. Commun.* **2016**, *52* (17), 3504−3507. (i) Kleinhans, G.; Hansmann, M. M.; Guisado-Barrios, G.; Liles, D. C.; Bertrand, G.; Bezuidenhout, D. I. Nucleophilic T-Shaped (LXL)Au(I)-Pincer Complexes: Protonation and Alkylation. *J. Am. Chem. Soc.* **2016**, *138* (49), 15873−15876.
(19) (a) Melaimi, M.; Jazzar, R.; Soleilhavoup, M.; Bertrand, G. Cyclic (Alkyl)(amino)carbenes (CAACs): Recent Developments. *Angew. Chem., Int. Ed.* **2017**, *56* (34), 10046−10068. (b) Paul, U. S. D.; Radius, U. What Wanzlick Did Not Dare To Dream: Cyclic (Alkyl)(amino)carbenes (cAACs) as New Key Players in Transition-Metal Chemistry. *Eur. J. Inorg. Chem.* **2017**, *2017* (28), 3362−3375. (c) Soleilhavoup, M.; Bertrand, G. Cyclic (Alkyl)(Amino)Carbenes (CAACs): Stable Carbenes on the Rise. *Acc. Chem. Res.* **2015**, *48* (2), 256−266. (d) Martin, D.; Melaimi, M.; Soleilhavoup, M.; Bertrand, G. A Brief Survey of Our Contribution to Stable Carbene Chemistry. *Organometallics* **2011**, *30* (20), 5304−5313. (e) Hahn, F. E.; Jahnke, M. C. Heterocyclic Carbenes: Synthesis and Coordination Chemistry. *Angew. Chem., Int. Ed.* **2008**, *47* (17), 3122−3172.
(20) Hu, X.; Soleilhavoup, M.; Melaimi, M.; Chu, J.; Bertrand, G. Air-Stable (CAAC)CuCl and (CAAC)$CuBH_4$ Complexes as Catalysts for the Hydrolytic Dehydrogenation of BH_3NH_3. *Angew. Chem., Int. Ed.* **2015**, *54* (20), 6008−6011.
(21) (a) Di, D.; Romanov, A. S.; Yang, L.; Richter, J. M.; Rivett, J. P. H.; Jones, S.; Thomas, T. H.; Abdi Jalebi, M.; Friend, R. H.; Linnolahti, M.; Bochmann, M.; Credgington, D. High-performance light-emitting diodes based on carbene-metal-amides. *Science* **2017**, *356*, 159. (b) Gernert, M.; Müller, U.; Haehnel, M.; Pflaum, J.; Steffen, A. A Cyclic Alkyl(amino)carbene as Two-Atom π-Chromophore Leading to the First Phosphorescent Linear Cu^{I} Complexes. *Chem. - Eur. J.* **2017**, *23* (9), 2206−2216.
(22) (a) Weinberger, D. S.; Amin SK, N.; Mondal, K. C.; Melaimi, M.; Bertrand, G.; Stückl, A. C.; Roesky, H. W.; Dittrich, B.; Demeshko, S.; Schwederski, B.; Kaim, W.; Jerabek, P.; Frenking, G. Isolation of Neutral Mononuclear Copper Complexes Stabilized by Two Cyclic (Alkyl)(amino)carbenes. *J. Am. Chem. Soc.* **2014**, *136* (17), 6235−6238. (b) Jerabek, P.; Roesky, H. W.; Bertrand, G.; Frenking, G. Coinage Metals Binding as Main Group Elements: Structure and Bonding of the Carbene Complexes $[TM(cAAC)_2]$ and $[TM(cAAC)_2]^+$ (TM = Cu, Ag, Au). *J. Am. Chem. Soc.* **2014**, *136* (49), 17123−17135.
(23) Jin, L.; Weinberger, D. S.; Melaimi, M.; Moore, C. E.; Rheingold, A. L.; Bertrand, G. Trinuclear Gold Clusters Supported by Cyclic (alkyl)(amino)carbene Ligands: Mimics for Gold Heterogeneous Catalysts. *Angew. Chem., Int. Ed.* **2014**, *53* (34), 9059−9063.
(24) Schenk, C.; Henke, F.; Santiso-Quiñones, G.; Krossing, I.; Schnepf, A. $[Si(SiMe_3)_3]_6Ge_{18}M$ (*M* = Cu, Ag, Au): metalloid cluster compounds as unusual building blocks for a supramolecular chemistry. *Dalton Trans.* **2008**, No. 33, 4436−4441.
(25) Spiekermann, A.; Hoffmann, S. D.; Kraus, F.; Fässler, T. F. $[Au_3Ge_{18}]^{5-}$—A Gold−Germanium Cluster with Remarkable Au−Au Interactions. *Angew. Chem., Int. Ed.* **2007**, *46* (10), 1638−1640.
(26) Spiekermann, A.; Hoffmann, S. D.; Fässler, T. F.; Krossing, I.; Preiss, U. $[Au_3Ge_{45}]^{9-}$—A Binary Anion Containing a $\{Ge_{45}\}$ Cluster. *Angew. Chem., Int. Ed.* **2007**, *46* (28), 5310−5313.
(27) Bentlohner, M. M.; Jantke, L.-A.; Henneberger, T.; Fischer, C.; Mayer, K.; Klein, W.; Fässler, T. F. On the Nature of Bridging Metal Atoms in Intermetalloid Clusters: Synthesis and Structure of the Metal-Atom-Bridged Zintl Clusters $[Sn(Ge_9)_2]^{4-}$ and $[Zn(Ge_9)_2)]^{6-}$. *Chem. - Eur. J.* **2016**, *22* (39), 13946−13952.
(28) Frischhut, S.; Kaiser, F.; Klein, W.; Drees, M.; Kühn, F. E.; Fässler, T. F. Capping *nido*-Nonagermanide Clusters with *M*-PPh_3

DOI: 10.1021/acs.inorgchem.8b03338
Inorg. Chem. 2019, 58, 3256−3264

and Dynamics in Solution: Synthesis and Structure of *closo*-$[(Me_3Si)_3Si]_3Et[Ge_9M](PPh_3)$ (M = Ni, Pt). *Organometallics* **2018**, *37* (24), 4560−4567.
(29) Kysliak, O.; Schnepf, A. $\{Ge_9[Si(SiMe_3)_3]_2\}^{2-}$: a starting point for mixed substituted metalloid germanium clusters. *Dalton Trans.* **2016**, *45* (6), 2404−2408.
(30) Kysliak, O.; Schrenk, C.; Schnepf, A. Reactivity of $[Ge_9\{Si(SiMe_3)_3\}_3]^-$ Towards Transition-Metal M^{2+} Cations: Coordination and Redox Chemistry. *Chem. - Eur. J.* **2016**, *22* (52), 18787−18793.
(31) Boo, B. H. Infrared and Raman spectroscopic studies of tris(trimethylsilyl)silane derivatives of $(CH3)_3Si)_3Si$-X [X = H, Cl, OH, CH_3, OCH_3, $Si(CH_3)_3$]: vibrational assignments by Hartree-Fock and density-functional theory calculations. *J. Korean Phys. Soc.* **2011**, *59* (51), 3192−3200.
(32) Von Schnering, H. G.; Baitinger, M.; Bolle, U.; Carrillo-Cabrera, W.; Curda, J.; Grin, Y.; Heinemann, F.; Llanos, J.; Peters, K.; Schmeding, A.; Somer, M. Binary alkali metal compounds with the zintl anions $[Ge_9]^{4-}$ and $[Sn_9]^{4-}$. *Z. Anorg. Allg. Chem.* **1997**, *623* (7), 1037−1039.
(33) Bidal, Y. D.; Lesieur, M.; Melaimi, M.; Nahra, F.; Cordes, D. B.; Athukorala Arachchige, K. S.; Slawin, A. M. Z.; Bertrand, G.; Cazin, C. S. J. Copper(I) Complexes Bearing Carbenes Beyond Classical N-Heterocyclic Carbenes: Synthesis and Catalytic Activity in "Click Chemistry. *Adv. Synth. Catal.* **2015**, *357* (14−15), 3155−3161.
(34) Hübschle, C. B.; Sheldrick, G. M.; Dittrich, B. ShelXle: a Qt graphical user interface for SHELXL. *J. Appl. Crystallogr.* **2011**, *44* (6), 1281−1284.
(35) *Diamond*, version 3.2k; Crystal Impact GbR, 1997−2014.
(36) *MestReNova v9.1.0*; Mestrelab Research SL, 2014.

DOI: 10.1021/acs.inorgchem.8b03338
Inorg. Chem. 2019, 58, 3256−3264

Supporting Information

for

Silylated Ge_9 Clusters as New Ligands for Cyclic (Alkyl)amino and Mesoionic Carbene Copper Complexes

Content

1. Crystallographic Details

Table SI 1. Selected crystallographic data of the crystal structures of **1**, **2** and **3**.

Compound	**1**·1.5*toluene*	**2**·*toluene*	**3**·2.5*toluene*
formula	$C_{72.5}H_{136}Cu_2Ge_9N_2Si_8$	$C_{56}H_{124}CuGe_9NSi_{12}$	$C_{76.50}H_{140}CuGe_9N_3Si_{12}$
fw (g·mol^{-1})	2040.93	1865.48	2155.84
space group (no)	$P\bar{1}$ (2)	$P2_1/n$ (14)	$P2_1/n$ (14)
***a* (Å)**	15.9773(5)	15.5851(7)	15.9666(3)
***b* (Å)**	19.0077(6)	24.8121(8)	29.4018(6)
***c* (Å)**	31.8685(10)	23.5914(10)	22.8305(5)
α (deg)	88.743(3)	90	90
β (deg)	89.469(3)	101.422(3)	90.440(2)
γ (deg)	81.787(3)	90	90
***V* (Å^3)**	9576.4(5)	8942.1(6)	10717.4(4)
Z	4	4	4
***T* (K)**	150(2)	150(2)	150(2)
ρ_{calc} (g·cm^{-3})	1.416	1.386	1.336
μ (mm^{-1})	3.351	3.402	2.849
measured reflections	94412	136060	179558
R_{int}* / *R_δ	0.0795 / 0.1110	0.1183 / 0.0646	0.0841 / 0.0397
***hkl* range**	-19 < *h* < 19 -20 < *k* < 23 -37 < *l* < 38	-19 < *h* < 19 -27 < *k* < 30 -29 < *l* < 28	-19 < *h* < 19 -36 < *k* < 36 -28 < *l* < 28
2 θ range	3.804 - 51.0	3.726 - 52.0	4.160 - 52.0
independent reflections	35469	17559	21048
reflections [*I* > 2 σ(*I*)]	17725	11612	14514
parameters / restraints	1756 / 30	860 / 189	1194 / 480
***R_1* [*I* > 2 σ(*I*) / all data]**	0.0676 / 0.1360	0.0694 / 0.1081	0.0534 / 0.0859
w*R_2* [*I* > 2 σ(*I*) / all data]	0.1675 / 0.2158	0.1656 / 0.1934	0.1250 / 0.1439
goodness of fit	0.957	0.995	1.012
largest difference peak/hole [e·Å^{-3}]	0.818 / −1.168	1.709 / −1.500	0.711 / −0.581
CCDC number	1570249	1570247	1570248

1.1 Compound **1**

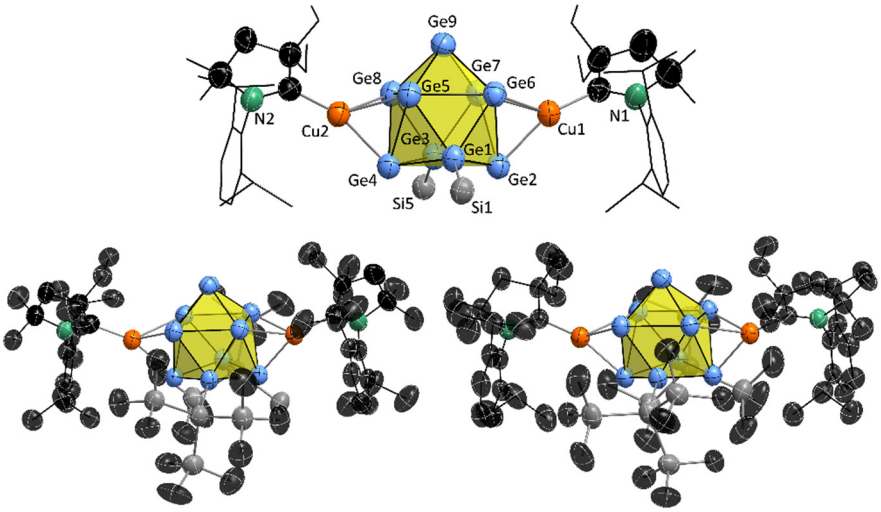

Figure SI 1. Top: Molecular structure of **1** with atom labelling according to manuscript and Table SI 2 (Ge_9 cluster is shown as yellow polyhedron; Ge, Cu, C, Si, and N atoms are shown as light blue, orange, black, gray and green ellipsoids, respectively, at 70% probability level; C atoms of the organic substituents Dipp, Ph, Et, and Me at the carbene units are drawn as wire-stick model; H atoms and TMS groups are omitted); bottom: molecular structures of the two independent cluster units in the unit cell of **1** (Ge_9 clusters is shown as yellow polyhedron; Ge, Cu, C, Si, and N atoms are shown as light blue, orange, black, gray, and green ellipsoids, respectively, at a 70% probability level; H atoms are omitted).

Table SI 2. Selected bond lengths (Å) in **1**.

Cu1	C1	1.95(1)
Cu2	C23	1.95(1)
Ge2	Cu1	2.432(2)
Ge6	Cu1	2.577(2)
Ge7	Cu1	2.637(2)
Ge4	Cu2	2.425(2)
Ge5	Cu2	2.604(2)
Ge8	Cu2	2.600(2)
Ge1	Ge2	2.495(2)
Ge2	Ge3	2.514(2)
Ge3	Ge4	2.503(2)
Ge1	Ge4	2.52(3)
Ge1	Ge3	3.343(2)
Ge2	Ge4	3.692(2)
Ge1	Ge5	2.564(2)
Ge1	Ge6	2.577(2)
Ge2	Ge6	2.799(2)
Ge2	Ge7	2.802(2)

Ge3	Ge7	2.553(2)
Ge3	Ge8	2.560(2)
Ge4	Ge8	2.774(2)
Ge4	Ge5	2.796(2)
Ge5	Ge6	2.883(2)
Ge6	Ge7	2.794(2)
Ge7	Ge8	2.913(2)
Ge5	Ge8	2.791(2)
Ge5	Ge9	2.579(2)
Ge6	Ge9	2.595(2)
Ge7	Ge9	2.585(2)
Ge8	Ge9	2.599(2)
Ge1	Si1	2.391(3)
Ge3	Si5	2.389(3)

1.2 Compound **2**

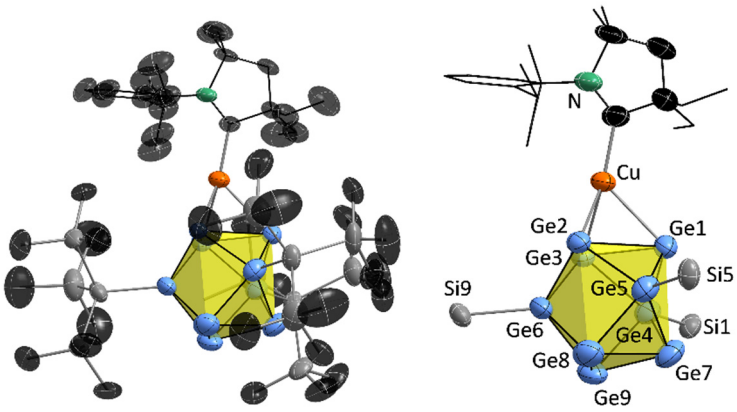

Figure SI 2. Left: molecular structure of **2** (Ge_9 clusters is shown as yellow polyhedron; Ge, Cu, C, Si, and N atoms are shown as light blue, orange, black, gray, and green ellipsoids, respectively, at a 70% probability level; H atoms are omitted); right: molecular structure of **2** with atom labelling according to manuscript and Table SI 3 (Ge_9 clusters is shown as yellow polyhedron; Ge, Cu, C, Si, and N atoms are shown as light blue, orange, black, gray and green ellipsoids, respectively, at a 70% probability level; C atoms of the organic substituents Dipp, Ph, Et, and Me at the carbene units are drawn as wire-stick model; H atoms and TMS groups are omitted).

Table SI 3. Selected bond lengths (Å) in **2**.

Cu	C1	1.967(6)
Ge1	Cu	2.659(1)
Ge2	Cu	2.512(1)
Ge3	Cu	2.525(1)
Ge1	Ge2	2.8710(9)
Ge1	Ge3	2.823(1)

Ge2	Ge3	2.785(1)
Ge1	Ge4	2.517(1)
Ge3	Ge4	2.522(1)
Ge1	Ge5	2.514(1)
Ge2	Ge5	2.506(1)
Ge4	Ge5	3.720(1)
Ge2	Ge6	2.511(1)
Ge3	Ge6	2.513(1)
Ge4	Ge6	3.545(1)
Ge5	Ge6	3.665(1)
Ge1	Ge7	3.204(1)
Ge4	Ge7	2.553(1)
Ge5	Ge7	2.541(1)
Ge2	Ge8	3.326(1)
Ge5	Ge8	2.549(1)
Ge6	Ge8	2.570(1)
Ge7	Ge8	2.699(1)
Ge3	Ge9	3.522(1)
Ge4	Ge9	2.549(1)
Ge6	Ge9	2.560(1)
Ge7	Ge9	2.669(1)
Ge8	Ge9	2.623(1)
Ge4	Si1	2.380(2)
Ge5	Si5	2.378(2)
Ge6	Si9A	2.383(2)
Ge6	Si9B	2.383(2)

1.3 Compound **3**

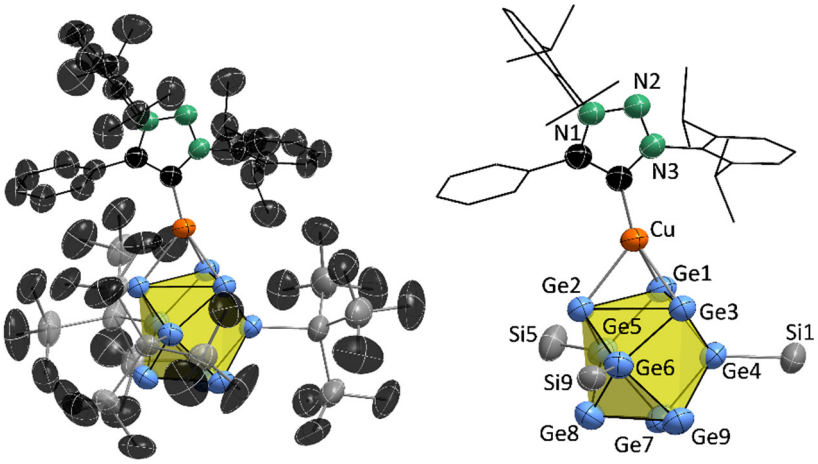

Figure SI 3. Left: molecular structure of **3** (Ge_9 clusters is shown as yellow polyhedron; Ge, Cu, C, Si, and N atoms are shown as light blue, orange, black, gray and green ellipsoids, respectively, at a 70% probability level; H atoms are omitted); right: molecular structure of **3** with atom labelling according to manuscript and Table SI 4 (Ge_9 clusters is shown as yellow polyhedron; Ge, Cu, C, Si, and N atoms are shown as light blue, orange, black, gray and green ellipsoids, respectively, at a 70% probability level; C atoms of the organic substituents Dipp, Ph, Et, and Me at the carbene units are drawn as wire-stick model; H atoms and TMS groups are omitted).

Table SI 4. Selected bond lengths (Å) in **3**.

Cu	C1	1.954(5)
Ge1	Cu	2.4576(8)
Ge2	Cu	2.5226(8)
Ge3	Cu	2.5277(8)
Ge1	Ge2	2.8730(8)
Ge1	Ge3	2.7818(8)
Ge2	Ge3	3.0924(8)
Ge1	Ge4	2.5183(8)
Ge3	Ge4	2.5131(8)
Ge1	Ge5	2.5071(8)
Ge2	Ge5	2.5165(8)
Ge4	Ge5	3.4061(9)
Ge2	Ge6	2.5081(8)
Ge3	Ge6	2.4952(8)
Ge4	Ge6	3.6711(8)
Ge5	Ge6	3.7633(9)
Ge1	Ge7	3.7094(8)
Ge4	Ge7	2.5727(9)
Ge5	Ge7	2.5505(8)
Ge2	Ge8	3.0667(8)
Ge5	Ge8	2.5691(9)

Ge6	Ge8	2.5599(9)
Ge7	Ge8	2.620(1)
Ge3	Ge9	3.2609(8)
Ge4	Ge9	2.5702(9)
Ge6	Ge9	2.5543(9)
Ge7	Ge9	2.597(1)
Ge8	Ge9	2.7101(9)
Ge4	Si1	2.381(2)
Ge5	Si5A	2.377(4)
Ge5	Si5B	2.44(2)

2. NMR Data

2.1 Compound **1**

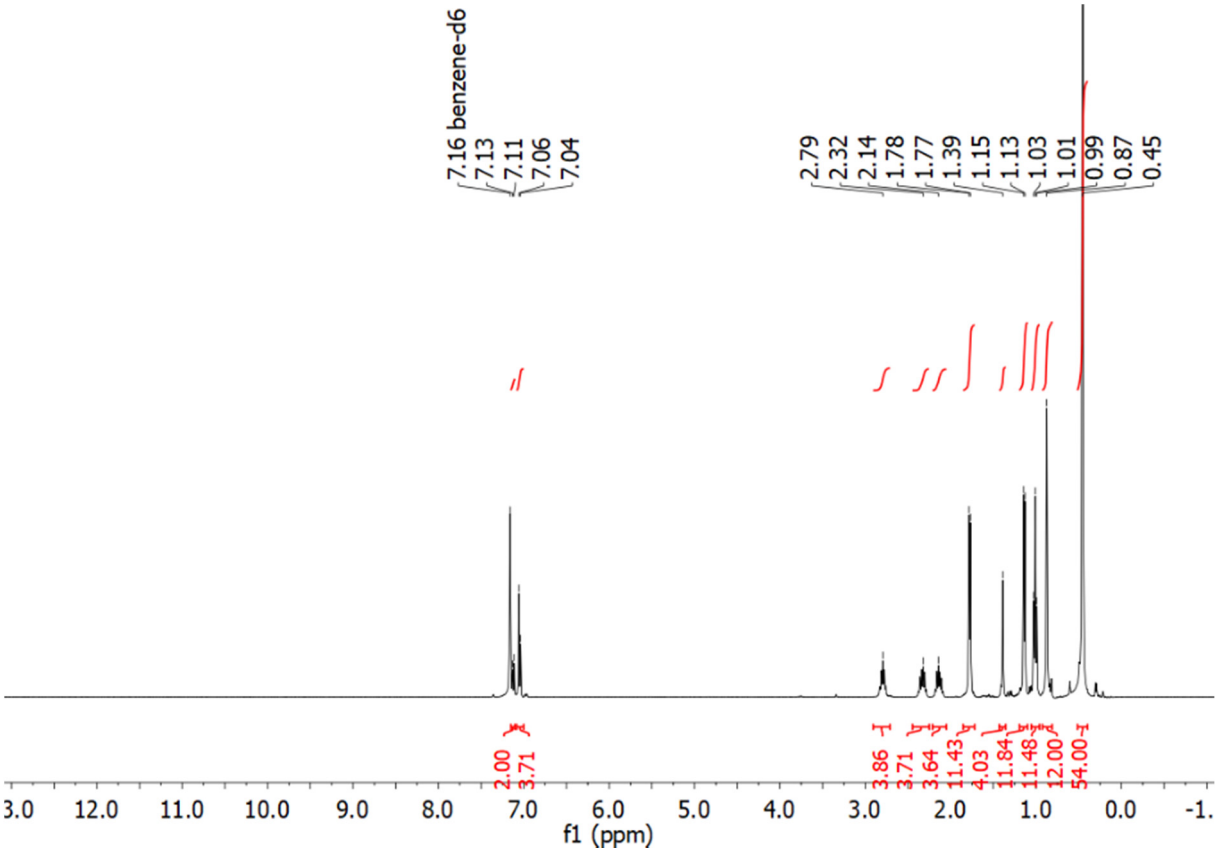

Figure SI 4. ^{1}H NMR spectrum of **1** in benzene-*d6*.

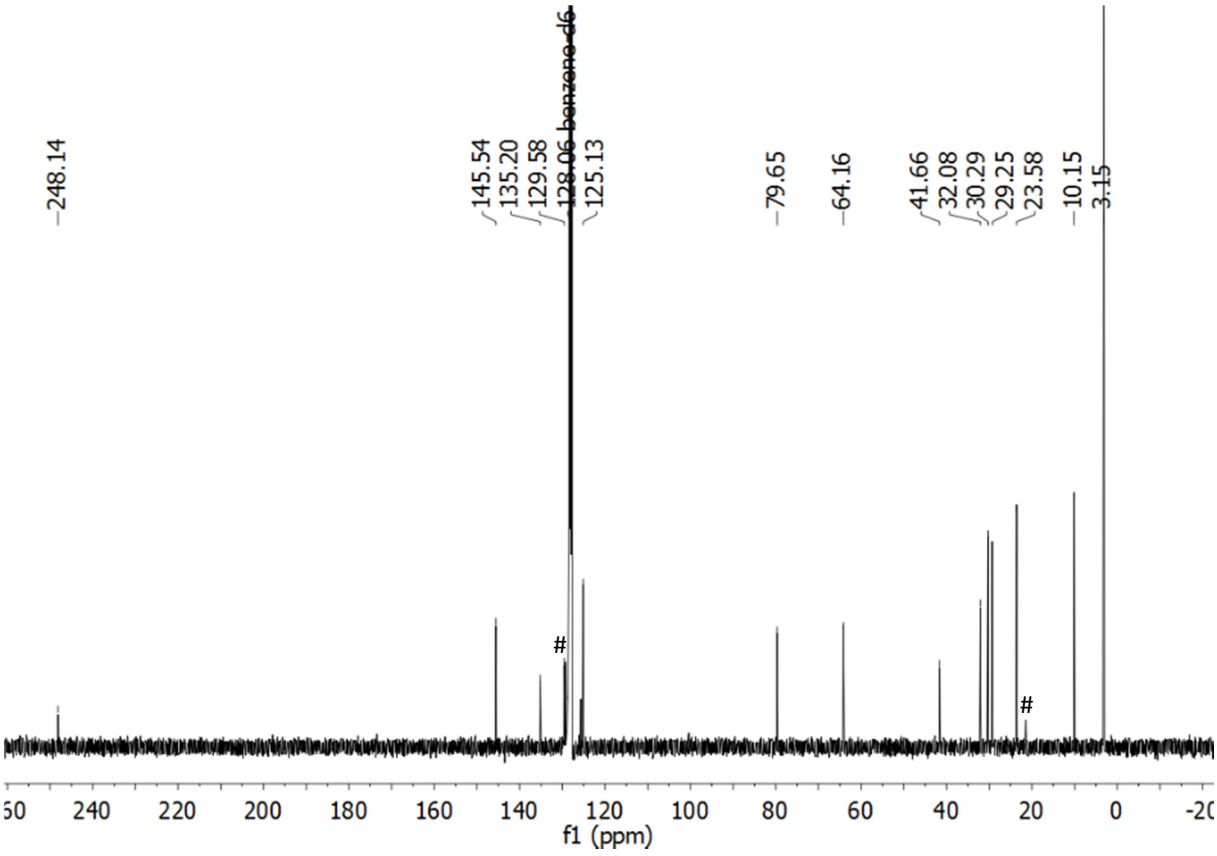

Figure SI 5. $^{13}C\{^{1}H\}$ NMR spectrum of **1** in benzene-*d6* (#: toluene).

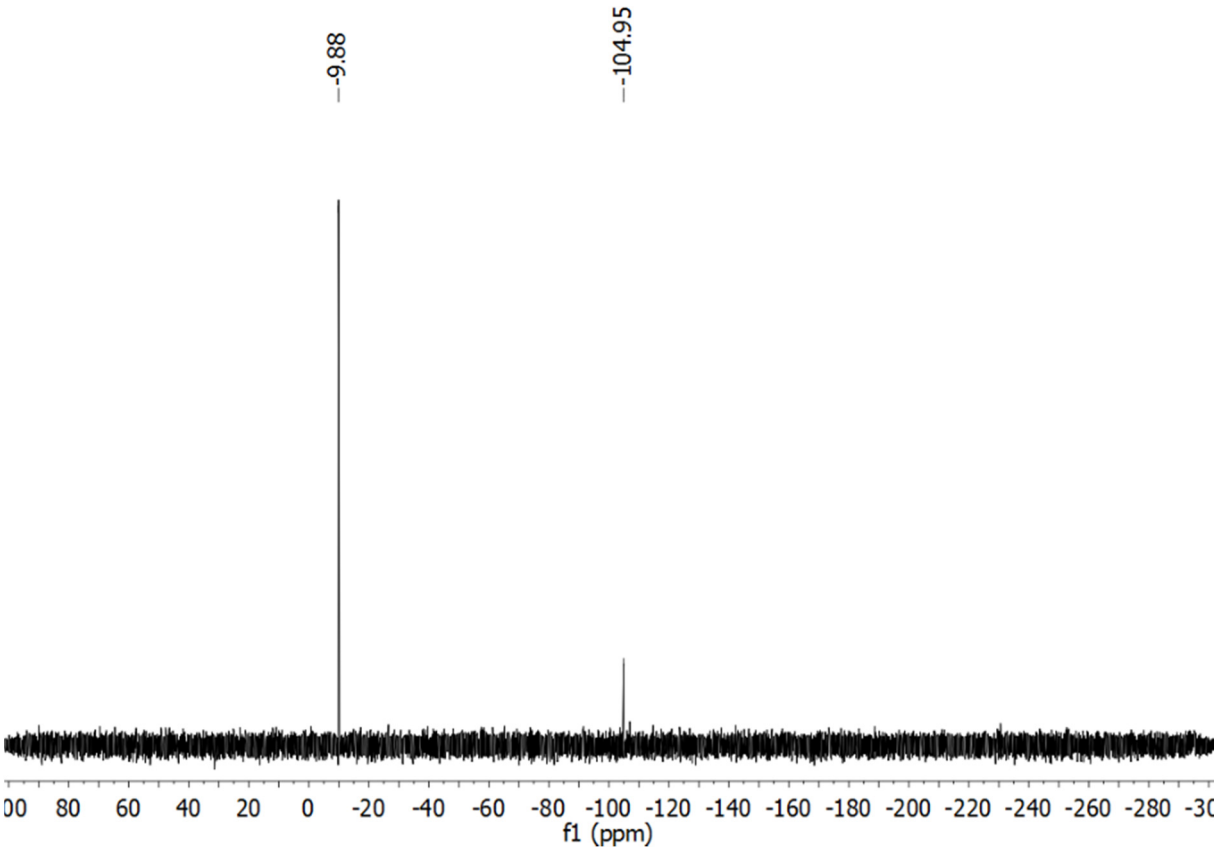

Figure SI 6. $^{29}Si\{^{1}H\}$ NMR spectrum of **1** in benzene-*d6*.

2.2 Compound **2**

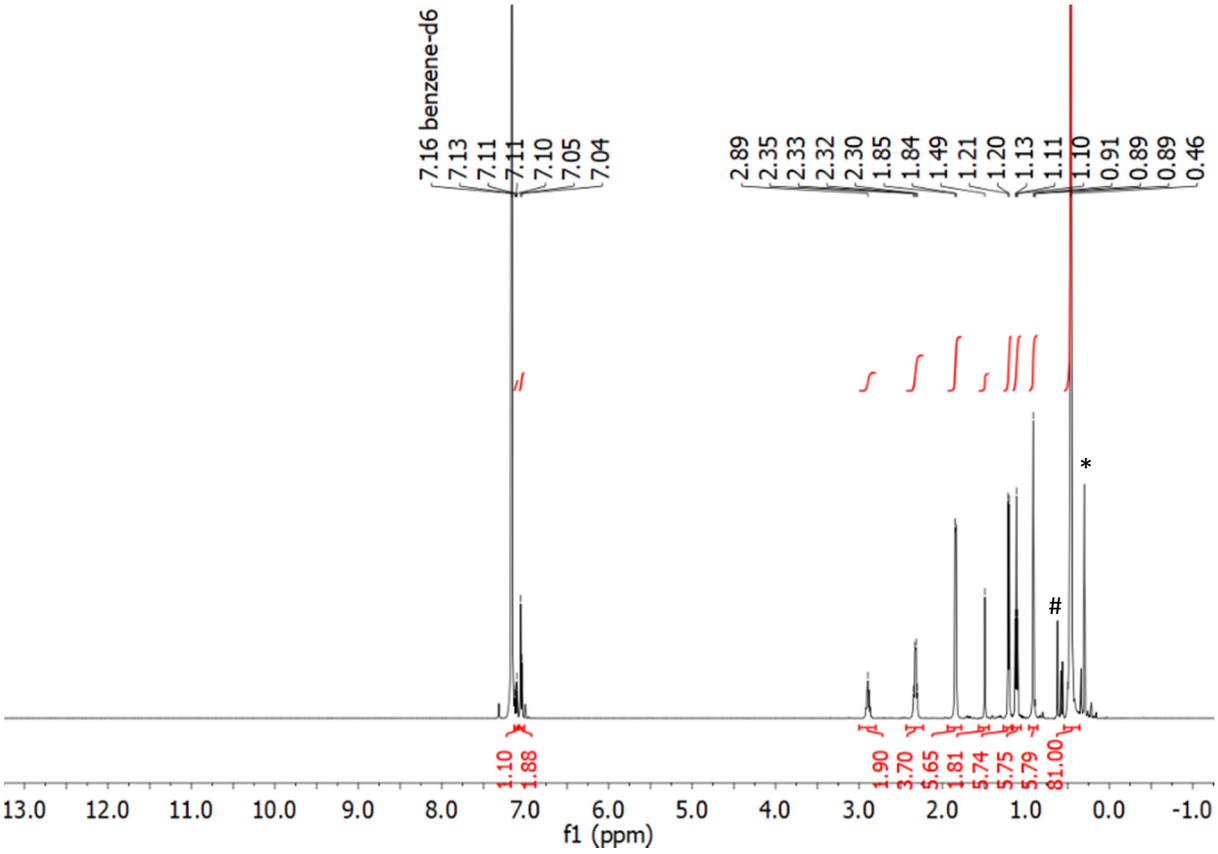

Figure SI 7. ^{1}H NMR spectrum of **2** in benzene-*d6* (*: silicon grease; #: impurity).

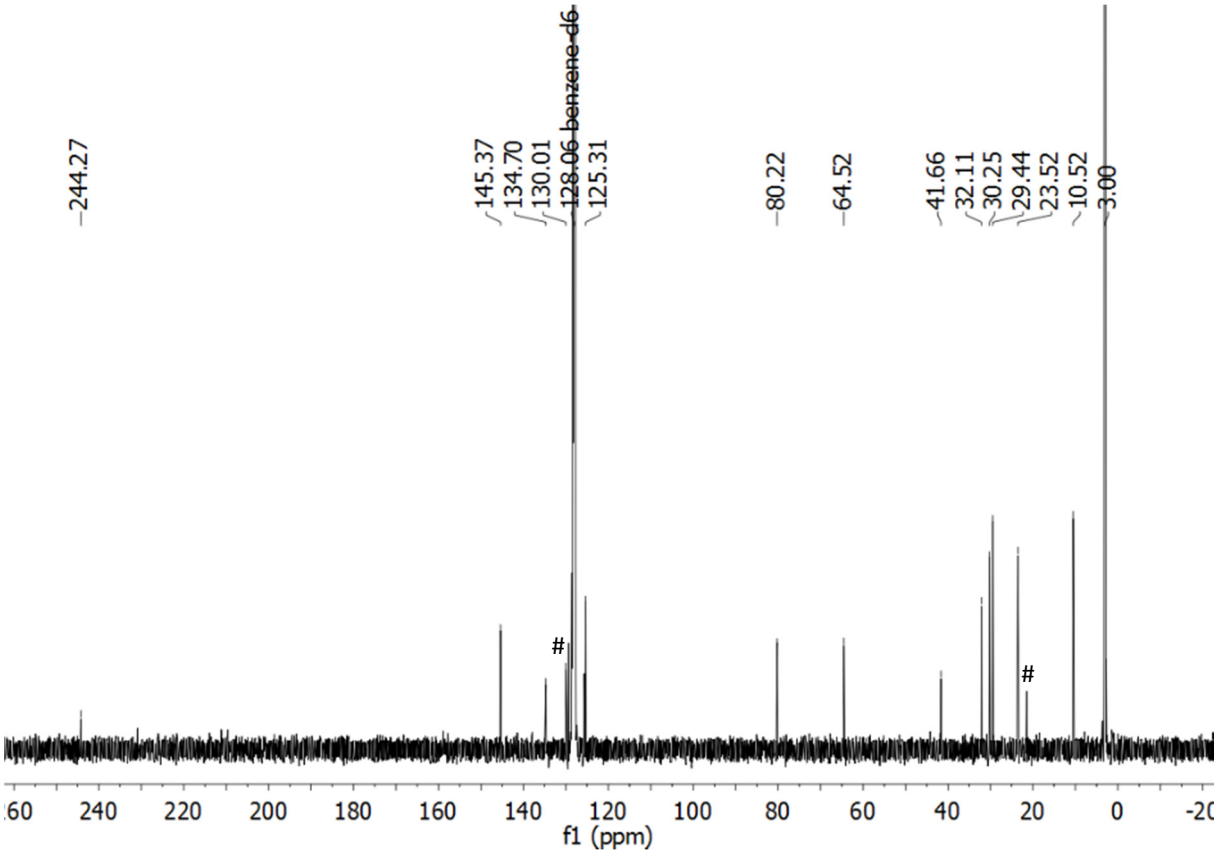

Figure SI 8. ^{13}C{^{1}H} NMR spectrum of **2** in benzene-*d6* (#: toluene).

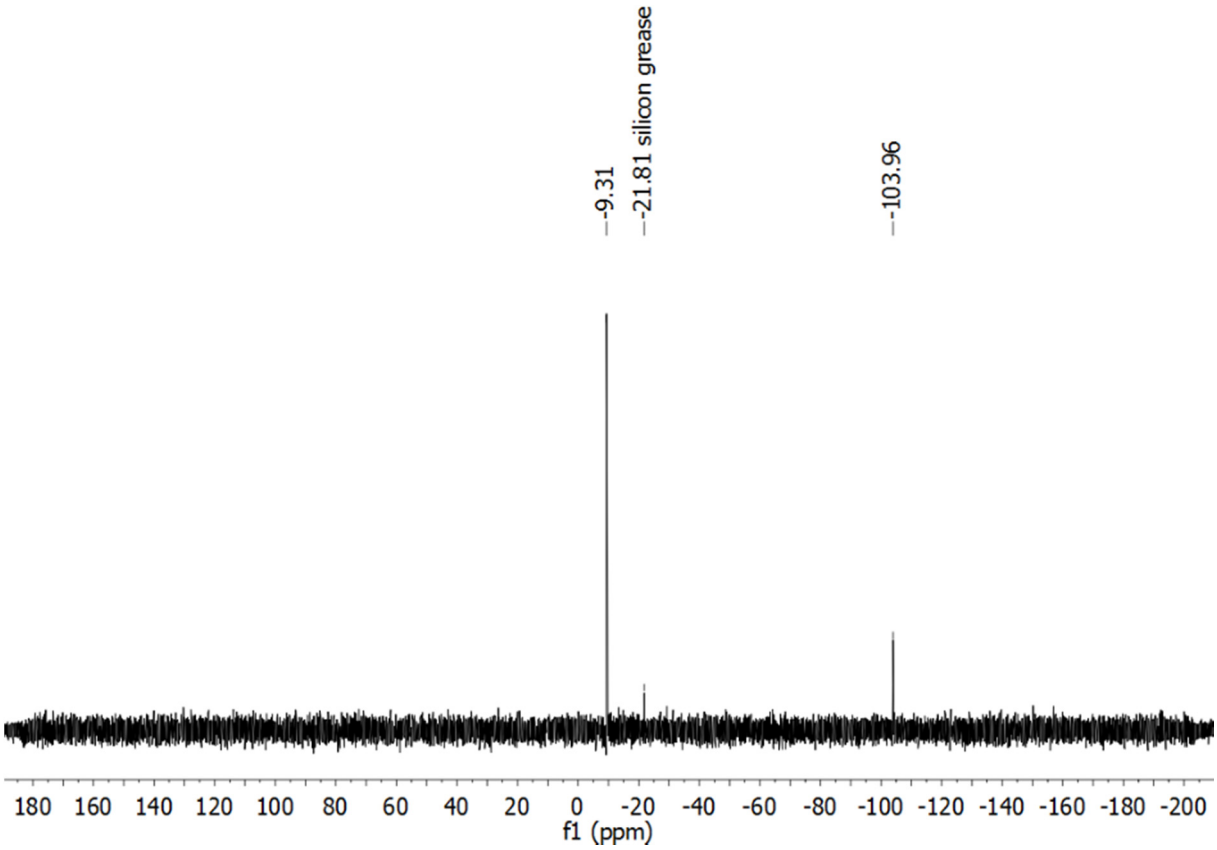

Figure SI 9. $^{29}Si\{^{1}H\}$ NMR spectrum of **2** in benzene-*d6*.

2.3 Compound **3**

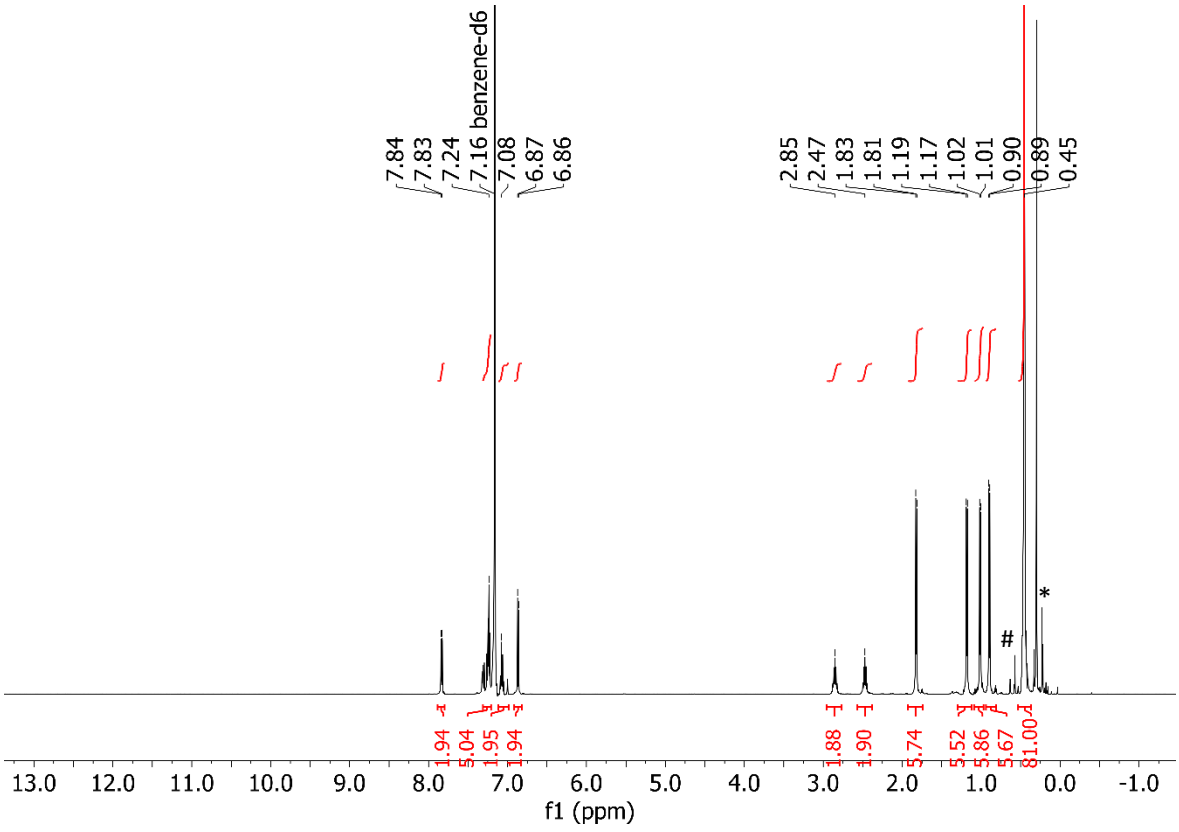

Figure SI 10. ^{1}H NMR spectrum of **3** in benzene-*d6* (*: silicon grease; #: impurity).

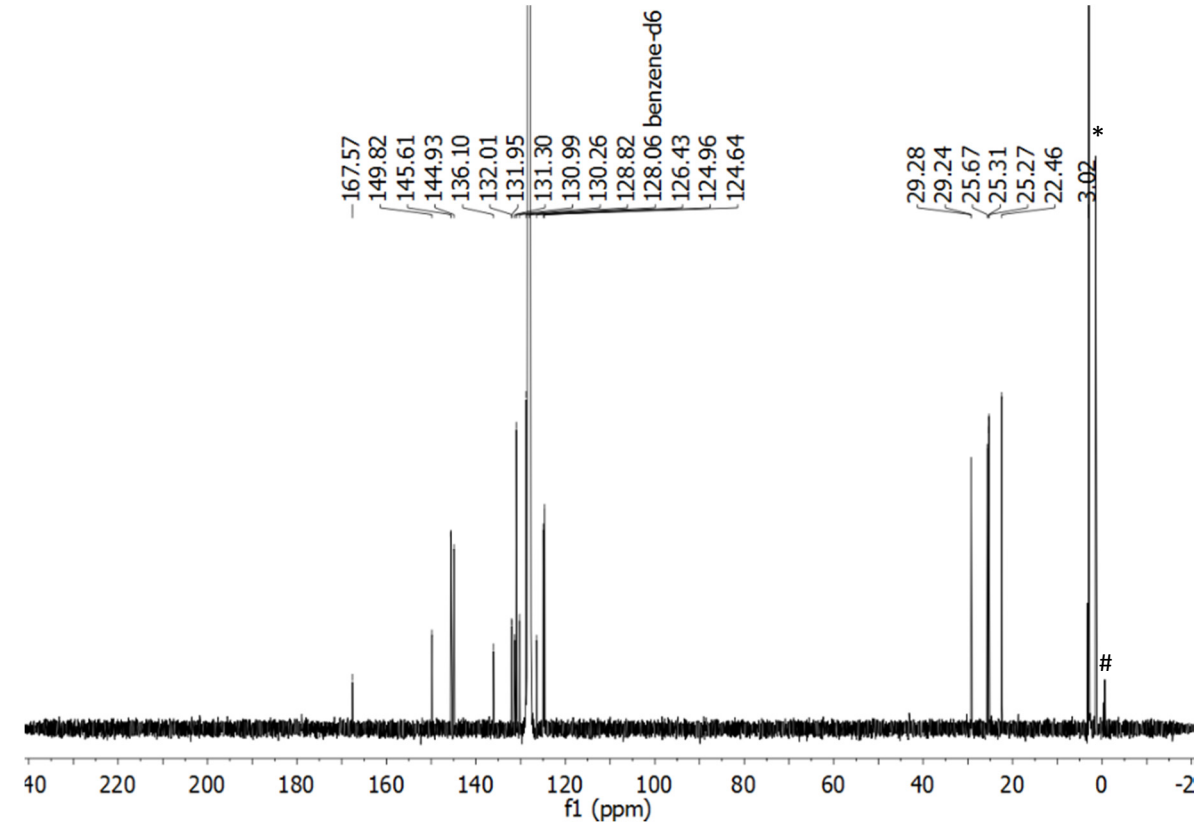

Figure SI 11. $^{13}C\{^{1}H\}$ NMR spectrum of **3** in benzene-*d6* (*: silicon grease; #: impurity).

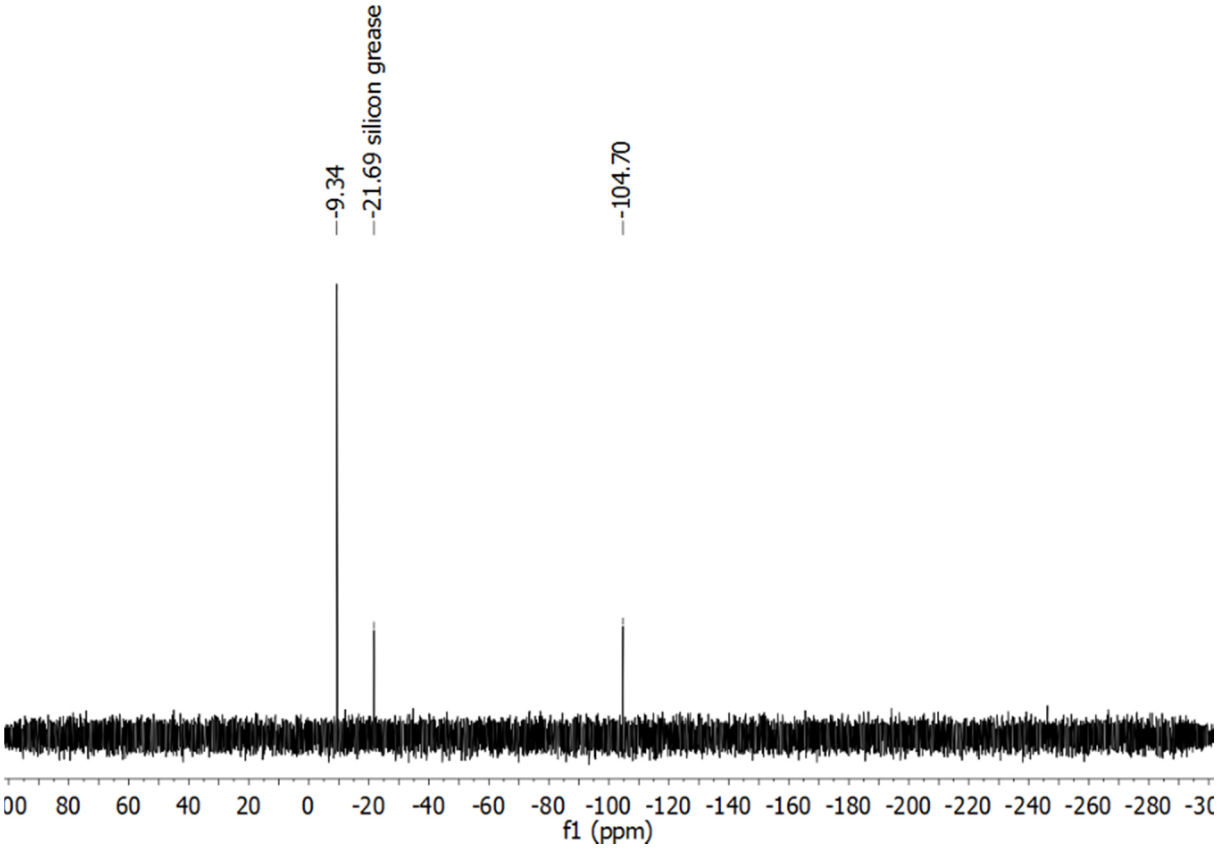

Figure SI 12. $^{29}Si\{^{1}H\}$ NMR spectrum of **3** in benzene-*d6*.

3. ESI-MS Data

3.1 Compound **1**

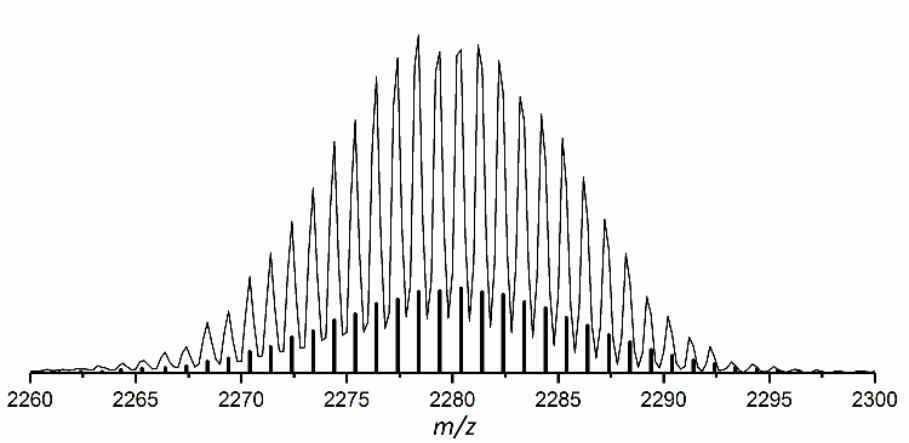

Figure SI 13. ESI-MS spectrum of $\{[(CAAC)Cu]_3[Ge_9\{Si(TMS)_3\}_2]\}^+$ (*m/z* = 2281); line: measured mass spectrum, bars: simulated mass spectrum (positive mode, −6000 V, 300 °C).

3.2 Compound **2**

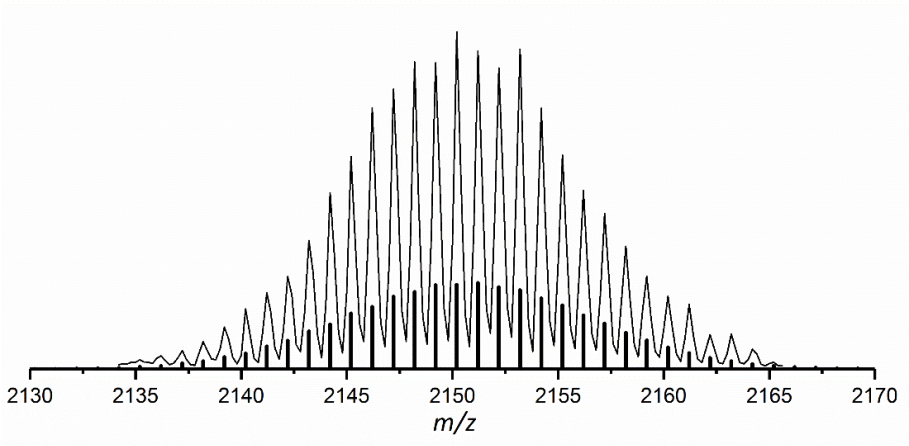

Figure SI 14. ESI-MS spectrum of $\{[(CAAC)Cu)]_2[Ge_9\{Si(TMS)_3\}_3]\}^+$ (*m/z* = 2151); line: measured mass spectrum, bars: simulated mass spectrum (positive mode, −6000 V, 300 °C).

3.3 Compound **3**

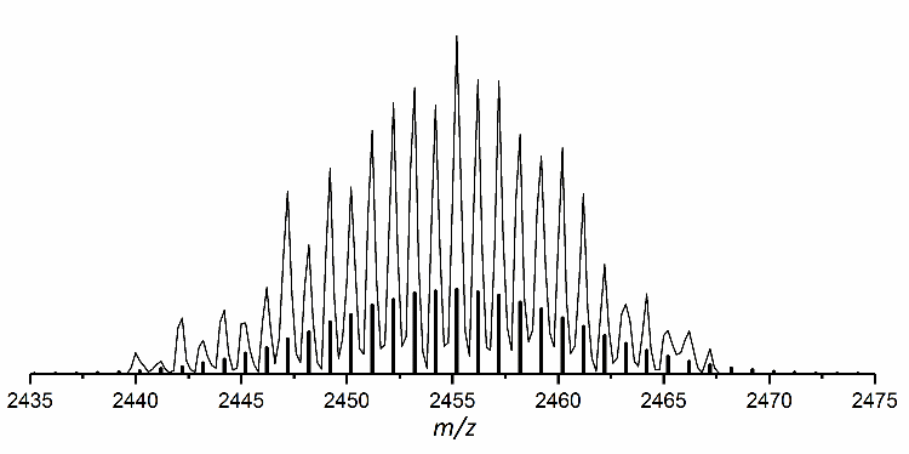

Figure SI 15. ESI-MS spectrum of $\{[(MIC)Cu)]_2[Ge_9\{Si(TMS)_3\}_3]\}^+$ (*m/z* = 2455); line: measured mass spectrum, bars: simulated mass spectrum (positive mode, −6000 V, 300 °C).

6.5 Charged Si_9 Clusters in Neat Solids and the Detection of $[H_2Si_9]^{2-}$ in Solution: A Combined NMR, Raman, Mass Spectrometric, and Quantum Chemical Investigation

Lorenz J. Schiegerl, Antti J. Karttunen, Jan Tillmann, Sebastian Geier, Gabriele Raudaschl-Sieber, Markus Waibel, and Thomas F. Fässler*

published in

Angew. Chem. Int. Ed. 2018, *57* (39), 12950-12955 and

Angew. Chem. 2018, *130* (39), 13132-13137.

Access online *via*: https://onlinelibrary.wiley.com/doi/full/10.1002/anie.201804756

Content and contributions:

Ambition of this work was the characterization of contained silicon clusters in intermetallic $K_{12}Si_{17}$ material in solid-state and solution. The manuscript was authored by me within the course of this PhD Thesis and reviewed by *Prof. Antti Karttunen*, *Dr. Jan Tillmann*, *Dr. Gabriele Raudaschl-Sieber* and *Prof. Thomas Fässler* before its submission. Submission of the manuscript was done by *Prof. Thomas Fässler*. *Prof. Antti Karttunen* did the computational studies and contributed concerning text passages. Raman spectra were measured by *Dr. Sebastian Geier*, ^{29}Si MAS NMR spectra by *Dr. Gabriele Raudaschl-Sieber*, and temperature-dependent NMR measurements in solution as well as their interpretation were assisted by *Dr. Jan Tillmann* at the CONSORTIUM FÜR ELEKTROCHEMISCHE INDUSTRIE of the WACKER CHEMIE AG. *Prof. Wolfgang Eisenreich* assisted the ^{29}Si–^{1}H decoupling NMR experiments. The EDX spectra were measured by Maria Müller (TECHNICAL UNIVERSITY OF MUNICH). Elemental analyses were carried out in the microanalytical laboratory at the CATALYTIC RESEARCH CENTER of the TECHNICAL UNIVERSITY OF MUNICH. The work was published within the framework of the WACKER INSTITUTE FOR SILICON CHEMISTRY (TECHNICAL UNIVERSITY OF MUNICH).

The *Zintl* compounds $K_{12}Si_{17}$ and K_4Si_4 were synthesized in solid-state reactions by me. The compounds were investigated by Raman spectroscopy, ^{29}Si MAS NMR spectroscopy, PXRD and computational studies (co-author contributions see above). Thereto, a previous ^{29}Si MAS NMR spectrum of $Rb_{12}Si_{17}$ was reported before in the PhD Thesis of *Dr. Markus Waibel* without signal assignment.[275] $[H_2Si_9]^{2-}$ was synthesized by me *via* dissolving $K_{12}Si_{17}$ (prior "*activation*" with 222crypt/NH_3) in pyridine and isolated as bulk material. Synthesis and characterization (NMR, Raman spectroscopy, ESI-MS, EDX) of the bulk material were done by me (co-author contributions see above). Results were discussed by comparison with calculations including NMR and Raman shifts in cooperation with *Prof. Antti Karttunen*.

Cluster Compounds

International Edition: DOI: 10.1002/anie.201804756
German Edition: DOI: 10.1002/ange.201804756

Charged Si_9 Clusters in Neat Solids and the Detection of $[H_2Si_9]^{2-}$ in Solution: A Combined NMR, Raman, Mass Spectrometric, and Quantum Chemical Investigation

*Lorenz J. Schiegerl, Antti J. Karttunen, Jan Tillmann, Sebastian Geier, Gabriele Raudaschl-Sieber, Markus Waibel, and Thomas F. Fässler**

Abstract: *Polyanionic silicon clusters are provided by the Zintl phases K_4Si_4, comprising $[Si_4]^{4-}$ units, and $K_{12}Si_{17}$, consisting of $[Si_4]^{4-}$ and $[Si_9]^{4-}$ clusters. A combination of solid-state MAS-NMR, solution NMR, and Raman spectroscopy, electrospray ionization mass spectrometry, and quantum-chemical investigations was used to investigate four- and nine-atomic silicon Zintl clusters in neat solids and solution. The results were compared to ^{29}Si isotope-enriched samples. ^{29}Si-MAS NMR and Raman shifts of the phase-pure solids K_4Si_4 and $K_{12}Si_{17}$ were interpreted by quantum-chemical calculations. Extraction of $[Si_9]^{4-}$ clusters from $K_{12}Si_{17}$ with liquid ammonia/222crypt and their transfer to pyridine yields in a red solid containing Si_9 clusters. This compound was characterized by elemental and EDX analyses and ^{29}Si-MAS NMR and Raman spectroscopy. Charged Si_9 clusters were detected by ^{29}Si NMR in solution. ^{29}Si and ^{1}H NMR spectra reveal the presence of the $[H_2Si_9]^{2-}$ cluster anion in solution.*

As silicon is an abundant, inexpensive, and nontoxic semiconducting material, research on this element is of particular interest. Silicon compounds already play an important role in daily-life products such as electronic devices, solar cells, anode materials, and micro- and optoelectronics.[1] Nowadays, the field of silicon-based applications is constantly growing and of increasing importance. Low-valent nanoscale silicon compounds can play a key role by providing tailor-made building blocks for the design of well-defined materials. Promising candidates are so-called siliconoids,[2] best described as neutral silicon clusters with unsaturated silicon atoms.[2,3] Further research also brought up a [20]silafullerane with a Si_{20} core[4] as well as a neutral triatomic silicon(0) cluster stabilized by three cyclic (alkyl)amino carbenes.[5] However, the synthesis of silicon cluster compounds often requires multi-step reactions[6] which still hamper technical applications. In this context, Zintl phases consisting of silicon and alkali metals, which already contain polyatomic silicon clusters, can be employed as precursors. Such silicon-rich phases can be directly obtained in quantitative yield from high-temperature reactions of the respective elements.[7] Via these reactions, binary phases of the compositions A_4Si_4 (A = Li–Cs) and $A_{12}Si_{17}$ (A = K–Cs), containing either solely $[Si_4]^{4-}$ or $[Si_4]^{4-}$ beside $[Si_9]^{4-}$ clusters in a 2:1 ratio, respectively, are easily accessible (Figure 1).

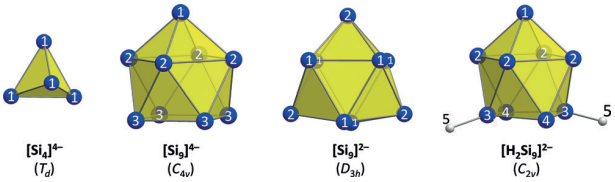

Figure 1. Silicon polyanions and point groups of the computational studies (atom labels according to point group symmetry used for computational studies for cluster species in solution). In neat solids the symmetry differs.

For further conversions, solutions of well-defined silicon clusters are of fundamental interest. However, A_4E_9 phases (E = Si–Pb) that contain exclusively nine-atomic clusters, and which are soluble in aprotic solvents, are only known for the heavier Group 14 homologues Ge–Pb, but not for Si. Since the A_4Si_4 phases are rather insoluble in any solvent, the focus lies on the $A_{12}Si_{17}$ phases that are sufficiently soluble in liquid ammonia. Here, solvate crystals containing $[Si_4]^{4-}$ and $[Si_9]^{4-}$ units could be obtained[8] and the $[Si_9]^{4-}$ cluster units can further react to $[PhZn(Si_9)]^{3-}$,[9] $[\{Ni(CO)_2\}_2(Si_9)_2]^{8-}$,[10] and $[NHC^{Dipp}Cu(Si_9)]^{3-}$ [11] from liquid ammonia solutions. For the $[Si_4]^{4-}$ unit only the $[(MesCu)_2(Si_4)]^{4-}$ complex could be obtained.[12]

However, in solutions of $A_{12}Si_{17}$ not only $[Si_4]^{4-}$ and $[Si_9]^{4-}$, but also $[Si_9]^{3-}$,[13] $[Si_9]^{2-}$,[14] and $[Si_5]^{2-}$ [8d,13] clusters have been detected. Thus, the question as to which species readily appear in solution and what their charges are remained unclear for many years. This triggered us to investigate $K_{12}Si_{17}$ and K_4Si_4 in the solid-state as well as solutions of $K_{12}Si_{17}$ by several spectroscopic methods combined with theoretical studies[15] (see details in the Supporting Information) with the

[*] L. J. Schiegerl, S. Geier, G. Raudaschl-Sieber, M. Waibel, T. F. Fässler
Department of Chemistry, Technische Universität München
Lichtenbergstraße 4, 85748 Garching (Germany)
E-mail: thomas.faessler@lrz.tum.de
L. J. Schiegerl, T. F. Fässler
Wacker Institute of Silicon Chemistry
Technische Universität München
Lichtenbergstraße 4, 85748 Garching (Germany)
A. J. Karttunen
Department of Chemistry and Materials Science, Aalto University
00076 Aalto (Finland)
J. Tillmann
Wacker Chemie AG, Consortium für elektrochemische Industrie
Zielstattstraße 20, 81379 Munich (Germany)
Supporting information and the ORCID identification number(s) for the author(s) of this article can be found under: https://doi.org/10.1002/anie.201804756.

prerequisite of using well defined single-phase intermetallic compounds. Of special interest was the NMR-spectroscopic detection of a nine-atomic cluster species, as so far only ^{29}Si NMR signals for $[Si_4]^{4-}$ clusters in A_4Si_4[16] solid phases and in liquid ammonia solution[17] arising from a solid phase of nominal composition $Rb_6K_6Si_{17}$ have been reported.

The syntheses of K_4Si_4 and $K_{12}Si_{17}$ (including ^{29}Si enrichment for $K_{12}Si_{17}$) were optimized to obtain single-phase materials (for details see the Supporting Information) of which the high purity and crystallinity could be shown by powder X-ray diffraction.[18] The Raman spectra of the phases (Figure 2 e,f) reveal the characteristic vibrations indicative for the polyanionic four- and nine-atomic silicon clusters. For K_4Si_4 four specific vibrations (measd.: 287, 337, 364, and 481 cm^{-1}) are observed. The calculated Raman vibrations (calcd: 286, 344, 366, and 483 cm^{-1}; Figure 2 g) are in accordance with the measurement, and thus underline the accuracy of the applied synthesis and characterization methods. The Raman spectrum of $K_{12}Si_{17}$ reveals four vibrations, of which three (at 281, 354, and 482 cm^{-1}) are assigned to the $[Si_4]^{4-}$ cluster, whereas the fourth signal at 390 cm^{-1} is allocated to the $[Si_9]^{4-}$ unit by comparison with literature data of $A_{12}Si_{17}$ comprising different alkali metals.[17,18b,19] Quantum-chemical calculations on vibrations of solid $K_{12}Si_{17}$ were not feasible owing to the large unit cell, and thus the signal is compared to the calculated spectrum of an isolated $[Si_9]^{4-}$ cluster (calcd: 395 cm^{-1}; Figure 2 c), which is in reasonable agreement with the experiment but differs from the results of an earlier calculation (calcd: 367 cm^{-1}).[19]

The recorded spectra and the calculated ^{29}Si-MAS NMR shifts of K_4Si_4 and $K_{12}Si_{17}$ are given in Figure 3 a,b and Table 1. The spectrum of K_4Si_4 shows two signals (1a and 2a) with chemical shifts which agree well with previously reported values.[16a] The calculated shifts (DFT-PBE) at −326 and −353 ppm are in accordance with the signals 1a (−323 ppm) and 1b (−346 ppm), respectively, and are in agreement with two crystallographically different Si atoms building the $[Si_4]^{4-}$ clusters in K_4Si_4 (two Wyckoff positions). The ^{29}Si-MAS NMR spectrum of ^{29}Si-enriched $K_{12}Si_{17}$ reveals several signals within a similar shift range as those of K_4Si_4. Four main signals (1b–4b) are detected besides three broader signals with smaller intensities (5b–7b). Calculations on the ^{29}Si NMR shifts of the primitive unit cell result in 144 atom shifts for the $[Si_9]^{4-}$, and 128 atom shifts for the $[Si_4]^{4-}$ cluster anions according to the 272 Si atoms in the unit cell of $K_{12}Si_{17}$.[18b] This large number of signals (68 independent Si atoms are present if crystallographic symmetry is taken into account) enforces the application of an averaging method and a histogram plot of the calculated shifts of the respective cluster types allows a reliable comparison of the data sets.[20] Thereby, we combined signal groups within 18 ppm resulting in 10 bins in a range from −281 to −398 ppm. The match with the measured intensities and the arrangement of the measured signals is satisfactory (for details see the Supporting Information), whereas the distribution range differs. The broader calculated distribution (measd. range: −316 to −344 ppm) is traced back to the circumstance that the calculations were carried out for 0 K, and the atoms were kept at the experimental X-ray positions without any thermal averaging. Finally, a qualitative comparison of the computational bins and the experimental data results in an assignment of three signals for the $[Si_4]^{4-}$, and four signals for the $[Si_9]^{4-}$ cluster units (Table 1).

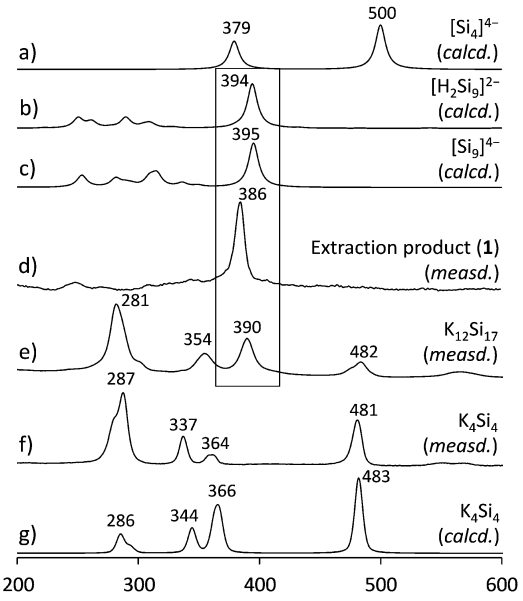

Figure 2. Measured and calculated (DFT-PBE0) Raman spectra of nine- and four-atomic silicon clusters. The vibrations of the Si_9 cluster anions are framed.

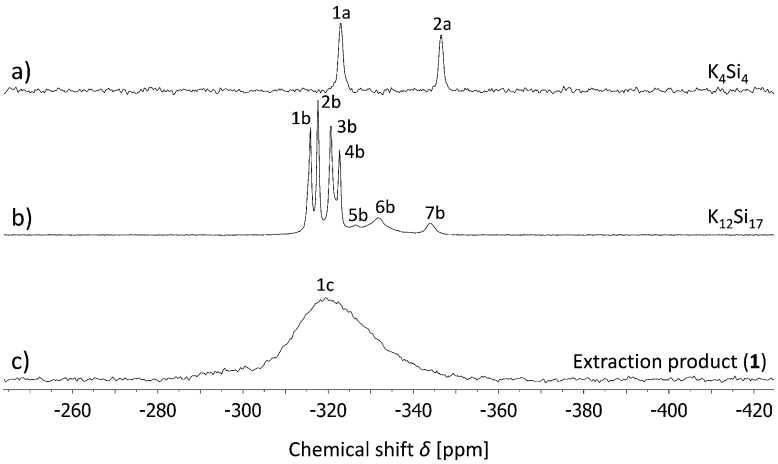

Figure 3. ^{29}Si MAS NMR spectra: a) K_4Si_4; b) $K_{12}Si_{17}$ (^{29}Si-enriched); c) extraction product (**1**; ^{29}Si-enriched). Chemical shift values [ppm]: −323 (1a), −346 (2a), −316 (1b), −317 (2b), −320 (3b), −322 (4b), −326 (5b), −331 (6b), −344 (7b), −319 (1c). Full spectra are given in the Supporting Information.

Table 1: Calculated ^{29}Si NMR shifts [ppm] of nine- and four-atomic silicon clusters.

Cluster system	Calculated: Atoms/ Clusters	Shift for each atom	Weighted average shifts	Details	Measured: Atoms/ Clusters	Shifts
$[Si_4]^{4-}$ (T_d)	1[a]	−484	−484	–	–	–
$[Si_9]^{4-}$ (C_{4v})	1[a]	−405	−403	–	–	–
	2[a]	−374				
	3[a]	−431				
$[H_2Si_9]^{2-}$ (C_{2v})	1[a]	−395	−348 (^{29}Si)	py-d_5/ thf-d_8	^{29}Si	−346
	2[a]	−361	−1.3 (^{1}H)		^{1}H	−0.71
	3[a]	−185				
	4[a]	−462				
	5[a]	−1.3 (^{1}H)				
$[Si_9]^{2-}$ (D_{3h})	1[a]	−342	−308	py-d_5/ thf-d_8	^{29}Si	−309
	2[a]	−239				
K_4Si_4 (solid)	24*i*[b]	−326	–	solid state	$[Si_4]^{4-}$	−323
	8*e*[b]	−353			$[Si_4]^{4-}$	−346
$K_{12}Si_{17}$ (solid)	$[Si_4]^{4-}$	Supporting	−281[c]	solid	$[Si_4]^{4-}$	−316
	$[Si_4]^{4-}$	Information	−300[c]	state	$[Si_4]^{4-}$	−317
	$[Si_9]^{4-}$		−308[c]		$[Si_9]^{4-}$	−320
	$[Si_4]^{4-}$		−318[c]		–	–
	$[Si_9]^{4-}$		−326[c]		$[Si_9]^{4-}$	−322
	$[Si_4]^{4-}$		−337[c]		$[Si_4]^{4-}$	−326
	$[Si_9]^{4-}$		−344[c]		$[Si_9]^{4-}$	−331
	$[Si_9]^{4-}$		−362[c]		$[Si_9]^{4-}$	−344
	$[Si_9]^{4-}$		−380[c]		–	–
	$[Si_9]^{4-}$		−398[c]		–	–

[a] Labeling according to the point groups in Figure 1. [b] Wyckoff position in the K_4Si_4 solid phase. [c] Signals within a range of 18 ppm are collected in bins. Shifts of $[Si_9]^{4-}$, $[H_2Si_9]^{2-}$, $[Si_9]^{2-}$, and $[Si_4]^{4-}$ are calculated with CCSD(T)/cc-pVTZ, shifts of solid-state K_4Si_4 and $K_{12}Si_{17}$ with DFT-PBE (details in the Supporting Information).

Concerning the solubility of the silicon clusters obtained from $K_{12}Si_{17}$ in liquid ammonia, the number of known solvate structures and reaction products indicates a better solubility of the nine-atomic versus four-atomic clusters. Moreover, the nine-atomic clusters could be initially transferred to the organic solvents pyridine (py) and dimethylformamide (dmf).[13,14] Herein, this transfer was optimized by dissolving single-phase $K_{12}Si_{17}$ in a Schlenk tube in liquid ammonia at −78 °C in the presence of 222crypt. After two hours of stirring, the liquid ammonia was evaporated, and a brown solid ($K_{12}Si_{17}$ pre-extracted) remained. Subsequent extraction with py and filtration lead to a red-brown filtrate which yielded a brown–blueish solid after removal of the volatiles. In previous investigations we found[21] that the blue color originates from the 4,4′-bipyridinyl radical mono-anion $[C_{10}H_8N_2]^{\bullet-}$, which is formed from py by reduction through the cluster anions. The radical unit could be removed by washing with fluorobenzene, and a red solid (**1**) was obtained. Regarding the extraction of nine-atomic clusters in $K_{12}Si_{17}$ and $K_{12}Si_8Ge_9$ with liquid ammonia or py after subsequent transfer from liquid NH_3 solution, a recent report establishes the presence of protonated $[HSi_9]^{3-}$ and $[H_2Si_{9-x}Ge_x]^{2-}$ (x = 4.1) species by the single-crystal X-ray structure determination of $[(K\text{-}18crown6)_3(HSi_9)]\cdot 2\,NH_3\cdot 2\,thf$ and $[(K\text{-}18crown6)_2[H_2Si_{4.9}Ge_{4.1}]\cdot py$.[22] As the mono-protonated species crystallizes from liquid ammonia solution and the di-protonated species after the subsequent transfer to py, $[H_2Si_9]^{2-}$ is assumed to be present in the extraction product here. The Raman spectrum of **1** (Figure 2d) reveals one dominating vibration at 386 cm^{-1}, which is indicative for $[Si_9]^{4-}$ and $[H_2Si_9]^{2-}$ clusters as this value compares well to the calculated value of $[Si_9]^{4-}$ and $[H_2Si_9]^{2-}$ at 395 cm^{-1} and 394 cm^{-1}, respectively (Figure 2). ^{29}Si-MAS NMR investigation of solid **1** (Figure 3c) reveals a broad signal 1c (signal range: 65 ppm) within the range of the Si_9 clusters in the $K_{12}Si_{17}$ solid phase, indicative of a strong disorder or a glass-like behavior of the sample.

The ESI-MS spectra of **1** in py reveal the presence of the di-protonated cluster species $[H_2Si_9]^{2-}$ by detection of $\{(K\text{-}222crypt)[H_2Si_9]\}^-$ (m/z = 670) in the negative ion mode, and of $\{(K\text{-}222crypt)_3\text{-}[H_2Si_9]\}^+$ (m/z = 1501) in the positive ion mode (Figure 5b). The corresponding ESI-MS spectrum of a ^{29}Si-enriched sample shows the typical isotope distribution of a sample with approximately 15% enrichment (Figure 5a) and confirms also the presence of the doubly protonated species. An addition of two protons at the $[Si_9]^{4-}$ cluster units was also observed for $[Cu(NHC^{Dipp})Si_9]^{3-}$ after its transfer from liquid ammonia to py, resulting in the mass peak of $\{(NHC^{Dipp}Cu)[H_2Si_9]\}^-$.[11]

The ^{29}Si NMR measurement of a ^{29}Si-enriched sample of **1** in solution at ambient temperature shows a broad signal around −305 to −310 ppm (Figure 4). Upon cooling to −20 °C the pattern changes to a broad main signal at −346 ppm and a smaller broad resonance at −309 ppm. Quantum-chemical calculations on the NMR shifts of $[Si_4]^{4-}$, $[Si_9]^{4-}$, $[H_2Si_9]^{2-}$, and $[Si_9]^{2-}$ (Figure 1/Table 1) show a good match with the weighted average signal shifts of $[H_2Si_9]^{2-}$ (calcd: −348 ppm; measd.: −346 ppm) and $[Si_9]^{2-}$ (calcd: −308 ppm; measd.: −309 ppm), respectively.[23] Thus, these signals are the first ever detected ^{29}Si NMR resonances for a nine-atomic silicon cage in solution. Conclusively, the di-protonated majority species $[H_2Si_9]^{2-}$ is also observed in the ESI-MS measurements of **1**. Small amounts of $[Si_9]^{2-}$ are probably formed in py solution through an oxidation of the clusters under formation of the 4,4′-bipyridinyl radical mono-anion. Besides the discussed signals, all spectra show rather sharp signals between −327 and −330 ppm of lower intensity (Supporting Information), which could not be assigned to a known species yet. At −40 °C the intensity of the main signal at −346 ppm increases under sharping to smaller line width. The coalescence of this ^{29}Si NMR signal indicates dynamic processes: the Si atoms of the cage very likely undergo a fast exchange, and the H atoms are assumed to scramble over the cluster surface. The dynamic behavior of the Si cluster cores is

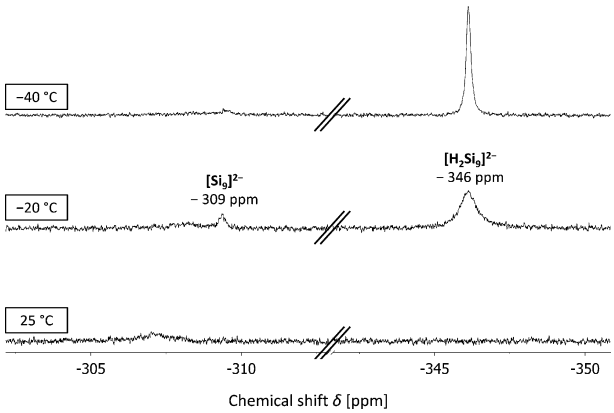

Figure 4. The ^{29}Si NMR spectra of **1** (^{29}Si-enriched) in solution at different temperatures with 99 MHz. py-d_5/thf-d_8 (1:1) solvent mixture for measurements at lower temperatures; the corresponding ^{1}H NMR spectrum at 25 °C is shown in Figure 5e; full ^{29}Si NMR spectra and temperature-dependent ^{1}H NMR spectra are shown in the Supporting Information.

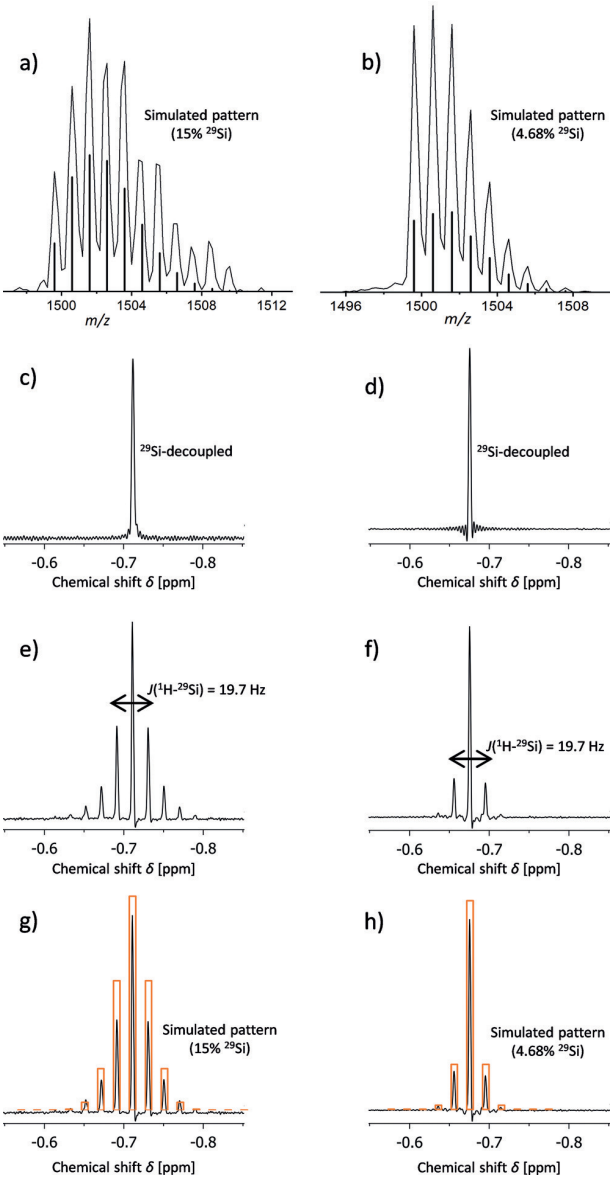

Figure 5. a) ESI-MS spectrum of **1** without ^{29}Si enrichment (line: measurement, bars: simulated pattern); b) ESI-MS spectrum of **1** with ^{29}Si enrichment (line: measurement, bars: simulated pattern); c) ^{29}Si inverse gated decoupled ^{1}H NMR spectrum of **1** with ^{29}Si enrichment at 25 °C/500 MHz; d) ^{29}Si inverse gated decoupled ^{1}H NMR spectrum of **1** without ^{29}Si enrichment at 25 °C/500 MHz; e) coupled ^{1}H NMR spectrum of **1** with ^{29}Si enrichment at 25 °C/500 MHz; f) coupled ^{1}H NMR spectrum of **1** without ^{29}Si enrichment at 25 °C/500 MHz; g) ^{1}H NMR in Figure 5e with simulated ^{1}H-^{29}Si splitting pattern for 15% ^{29}Si (orange bars); h) ^{1}H NMR in Figure 5f with simulated ^{1}H–^{29}Si splitting pattern for 4.68% ^{29}Si (orange bars). Full spectra are shown in the Supporting Information.

supported by calculations on their rigidity which have shown that the energy surface of such clusters is indeed rather flat with an energy difference of less than 2 kJ mol^{-1} between C_{4v}- and D_{3h}-symmetric $[Si_9]^{4-}$ anions at 0 K (Figure 1). Thus, a rigid cluster framework, which has to result in a NMR spectrum with discrete signals in dependence of the symmetry, cannot be expected (Figure 1/Table 1). Further, the dynamic behavior of nine-atomic Group 14 clusters is well known for the heavier homologue $[Sn_9]^{4-}$, for which also a single averaged ^{119}Sn-NMR signal is observed.[17,24] Investigations of the endohedrally filled cluster $[Cu@Sn_9]^{3-}$ also show a single ^{119}Sn resonance and a typical splitting in the ^{63}Cu NMR experiment due to $^{117/119}$Sn coupling is reported.[25]

Further proof of the presence of a protonated species provide the ^{1}H NMR spectra. The spectrum of a ^{29}Si-enriched sample shows a multiplet in the range of −0.6 to −0.8 ppm (Figure 5e) beside signals for the potassium-complexed 222crypt units. This shift is in reasonable agreement with the calculated ^{1}H NMR shift of the $[H_2Si_9]^{2-}$ cluster species at −1.3 ppm (Table 1), and also here signal coalescence is observed upon lowering of the temperature (for the full spectra see the Supporting Information). The respective spectrum of a sample with natural-abundant ^{29}Si content (4.68%) shows the same chemical shifts, but with a different splitting pattern (Figure 5f).

The occurrence of the detected multiplets indicates that the protons are in contact with more than one Si atom. The signal patterns in Figure 5e,f arise from different $[H_2{}^{29}Si_n/Si_{9-n}]^{2-}$ isotopomers in which a variable amount of ^{29}Si atoms (^{29}Si: I = 1/2; ^{28}Si/^{30}Si: I = 0) couples with the H atoms. The intensity distributions of the observed peaks are consistent with the simulated patterns (bars in Figure 5g,h) for Si_9 cluster cores with a ^{29}Si isotope abundance of 15% (enriched) and 4.68% (natural abundance), respectively. As presented above, the amount of ^{29}Si in the samples matches also the corresponding isotope ratio obtained from the ESI-MS experiment of **1**. Even though a higher amount of ^{29}Si enrichment was used for the solid-state synthesis of $K_{12}Si_{17}$ (see the Supporting Information), the intensity distribution of our experiments shows an enrichment of 15%. This discrepancy most probably arises from a lower ^{29}Si content in the enriched starting material and from an unknown amount of contained carbon impurity therein.

In the ^{1}H NMR splitting pattern of $[H_2Si_9]^{2-}$ we find a remarkably small $J(^{29}Si–^1H)$ coupling constant of 19.7 Hz, verified by ^{29}Si inverse-gated decoupling ^{1}H NMR experiments, which result in the corresponding singlets (Figure 5c and d, respectively). Shielded cluster protons are present with a stronger upfield shift and a smaller coupling constant than in common organosilane compounds (TMS_3SiH: $J(^{29}Si–^1H) = 154$ Hz, $\delta = 2.55$ ppm; $ClfBu_2SiH$: $J(^{29}Si–^1H) = 212$ Hz $\delta = 4.34$ ppm; C_6D_6). The delocalized nature of the protons in $[H_2Si_9]^{2-}$ is further comparable to the situation in borane compounds which also undergo hydrogen scrambling and show negative resonances in the ^{1}H NMR spectra.[26] Moreover, also the ^{1}H NMR coupling pattern of the protonated cluster species $[HSn_9]^{3-}$ displays a very small ^{1}H–^{119}Sn coupling constant of 21 Hz, and also here a scrambling of the attached proton is observed supporting a comparable dynamic behavior in $[H_2Si_9]^{2-}$.[27]

The investigations here identify the stepwise transformation of the Zintl phase $K_{12}Si_{17}$, comprising two different anions, to solutions that contain solely nine-atom silicon clusters. For the first time deltahedral Si_9 clusters are detected in solution by ^{29}Si NMR establishing also the double protonation of these clusters. Temperature-dependent NMR measurements confirm their dynamic behavior at ambient temperatures and a coalescence by lowering of the temperature. Thereto, details on the dynamic process such as the correlation of proton scrambling and the Si atom rearrangement in the framework will be investigated in forthcoming studies.

Acknowledgements

The authors are thankful for the financial support by Wacker Chemie AG, by Deutsche Forschungsgemeinschaft (DFG, FA 198/14-1) and TUM.solar in the context of the Bavarian Collaborative Research Project "Solar Technologies Go Hybrid" (SolTech). A.J.K. thanks the Academy of Finland for funding (grant 308089) and the Finnish IT Center for Science (CSC) for computational resources. L.J.S. thanks Kerstin Mayer, Michael Giebel and Benedikt Witzel for supporting the syntheses as well as the Raman investigations. Further, the authors thank Maria Weindl for supporting the ^{29}Si NMR measurements in solution, Prof. Dr. Wolfgang Eisenreich for the ^{29}Si inverse gated decoupled ^{1}H NMR measurements, Prof. Dr. Klaus Ruhland (University of Augsburg) for simulating the ^{1}H NMR coupling pattern, and Maria Müller for the EDX measurements.

Conflict of interest

The authors declare no conflict of interest.

Keywords: cluster compounds · isotope enrichment · NMR spectroscopy · quantum chemical calculations · silicon

How to cite: *Angew. Chem. Int. Ed.* **2018**, *57*, 12950–12955
Angew. Chem. **2018**, *130*, 13132–13137

[1] a) M. Ashuri, Q. He, L. L. Shaw, *Nanoscale* **2016**, *8*, 74–103; b) M. G. Kanatzidis, *Adv. Mater.* **2007**, *19*, 1165–1181; c) R. A. Bley, S. M. Kauzlarich, *J. Am. Chem. Soc.* **1996**, *118*, 12461–12462; d) C. Eun-Chel, P. Sangwook, H. Xiaojing, S. Dengyuan, C. Gavin, P. Sang-Cheol, A. G. Martin, *Nanotechnology* **2008**, *19*, 245201; e) L. T. Canham, *Appl. Phys. Lett.* **1990**, *57*, 1046–1048.

[2] P. Willmes, K. Leszczyńska, Y. Heider, K. Abersfelder, M. Zimmer, V. Huch, D. Scheschkewitz, *Angew. Chem. Int. Ed.* **2016**, *55*, 2907–2910; *Angew. Chem.* **2016**, *128*, 2959–2963.

[3] a) D. Scheschkewitz, *Angew. Chem. Int. Ed.* **2005**, *44*, 2954–2956; *Angew. Chem.* **2005**, *117*, 3014–3016; b) K. Abersfelder, A. J. P. White, H. S. Rzepa, D. Scheschkewitz, *Science* **2010**, *327*, 564–566; c) K. Abersfelder, A. J. P. White, R. J. F. Berger, H. S. Rzepa, D. Scheschkewitz, *Angew. Chem. Int. Ed.* **2011**, *50*, 7936–7939; *Angew. Chem.* **2011**, *123*, 8082–8086; d) K. Abersfelder, A. Russell, H. S. Rzepa, A. J. P. White, P. R. Haycock, D. Scheschkewitz, *J. Am. Chem. Soc.* **2012**, *134*, 16008–16016; e) J. Jeck, I. Bejan, A. J. P. White, D. Nied, F. Breher, D. Scheschkewitz, *J. Am. Chem. Soc.* **2010**, *132*, 17306–17315; f) G. Fischer, V. Huch, P. Mayer, S. K. Vasisht, M. Veith, N. Wiberg, *Angew. Chem. Int. Ed.* **2005**, *44*, 7884–7887; *Angew. Chem.* **2005**, *117*, 8096–8099; g) A. Tsurusaki, C. Iizuka, K. Otsuka, S. Kyushin, *J. Am. Chem. Soc.* **2013**, *135*, 16340–16343; h) A. Tsurusaki, J. Kamiyama, S. Kyushin, *J. Am. Chem. Soc.* **2014**, *136*, 12896–12898.

[4] J. Tillmann, J. H. Wender, U. Bahr, M. Bolte, H.-W. Lerner, M. C. Holthausen, M. Wagner, *Angew. Chem. Int. Ed.* **2015**, *54*, 5429–5433; *Angew. Chem.* **2015**, *127*, 5519–5523.

[5] K. C. Mondal, S. Roy, B. Dittrich, D. M. Andrada, G. Frenking, H. W. Roesky, *Angew. Chem. Int. Ed.* **2016**, *55*, 3158–3161; *Angew. Chem.* **2016**, *128*, 3210–3213.

[6] "Functional Molecular Silicon Compounds II": D. S. Carsten Präsang, D. Scheschkewitz, *Struct. Bonding (Berlin)* **2014**, *156*, 1–48.

[7] a) T. F. Fässler, *Coord. Chem. Rev.* **2001**, *215*, 347–377; b) S. Scharfe, F. Kraus, S. Stegmaier, A. Schier, T. F. Fässler, *Angew. Chem. Int. Ed.* **2011**, *50*, 3630–3670; *Angew. Chem.* **2011**, *123*, 3712–3754.

[8] a) S. Joseph, C. Suchentrunk, F. Kraus, N. Korber, *Eur. J. Inorg. Chem.* **2009**, 4641–4647; b) C. B. Benda, T. Henneberger, W. Klein, T. F. Fässler, *Z. Anorg. Allg. Chem.* **2017**, *643*, 146–148; c) C. Lorenz, S. Gärtner, N. Korber, *Z. Anorg. Allg. Chem.* **2017**, *643*, 141–145; d) S. Joseph, C. Suchentrunk, N. Korber, *Z. Naturforsch.* **2010**, *65*, 1059–1065.

[9] J. M. Goicoechea, S. C. Sevov, *Organometallics* **2006**, *25*, 4530–4536.

[10] a) S. Joseph, M. Hamberger, F. Mutzbauer, O. Härtl, M. Meier, N. Korber, *Angew. Chem. Int. Ed.* **2009**, *48*, 8770–8772; *Angew. Chem.* **2009**, *121*, 8926–8929; b) S. Gärtner, M. Hamberger, N. Korber, *Crystals* **2015**, *5*, 275–282.

[11] F. S. Geitner, T. F. Fässler, *Chem. Commun.* **2017**, *53*, 12974–12977.

[12] M. Waibel, F. Kraus, S. Scharfe, B. Wahl, T. F. Fässler, *Angew. Chem. Int. Ed.* **2010**, *49*, 6611–6615; *Angew. Chem.* **2010**, *122*, 6761–6765.

[13] J. M. Goicoechea, S. C. Sevov, *J. Am. Chem. Soc.* **2004**, *126*, 6860–6861.

[14] J. M. Goicoechea, S. C. Sevov, *Inorg. Chem.* **2005**, *44*, 2654–2658.

[15] a) R. Dovesi, R. Orlando, A. Erba, C. M. Zicovich-Wilson, B. Civalleri, S. Casassa, L. Maschio, M. Ferrabone, M. De La Pierre, P. D'Arco, Y. Noël, M. Causà, M. Rérat, B. Kirtman, *Int. J. Quantum Chem.* **2014**, *114*, 1287–1317; b) TURBOMOLE V7.2 2017—a development of University of Karlsruhe and Forschungszentrum Karlsruhe GmbH, 1989–2007, TURBOMOLE GmbH, since 2007, available from http://www.

turbomole.com; c) CFOUR—Coupled-Cluster techniques for Computational Chemistry, a quantum-chemical program package by J. F. Stanton et al., see http://www.cfour.de; d) J. C. Stewart, D. S. Matthew, J. P. Chris, J. H. Phil, I. J. P. Matt, K. Refson, C. P. Mike, *Z. Kristallogr. Cryst. Mater.* **2005**, *220*, 567; e) J. R. Yates, C. J. Pickard, F. Mauri, *Phys. Rev. B* **2007**, *76*, 024401.

[16] a) T. Goebel, A. Ormeci, O. Pecher, F. Haarmann, *Z. Anorg. Allg. Chem.* **2012**, *638*, 1437 – 1445; b) L. A. Stearns, J. Gryko, J. Diefenbacher, G. K. Ramachandran, P. F. McMillan, *J. Solid State Chem.* **2003**, *173*, 251 – 258; c) D. Mayeri, B. L. Phillips, M. P. Augustine, S. M. Kauzlarich, *Chem. Mater.* **2001**, *13*, 765 – 770; d) J. He, D. D. Klug, K. Uehara, K. F. Preston, C. I. Ratcliffe, J. S. Tse, *J. Phys. Chem. B* **2001**, *105*, 3475 – 3485.

[17] M. Neumeier, F. Fendt, S. Gärtner, C. Koch, T. Gärtner, N. Korber, R. M. Gschwind, *Angew. Chem. Int. Ed.* **2013**, *52*, 4483 – 4486; *Angew. Chem.* **2013**, *125*, 4579 – 4582.

[18] a) H. G. von Schnering, M. Schwarz, J. H. Chang, K. Peters, E. M. Peters, R. Nesper, *Z. Kristallogr. New Cryst. Struct.* **2005**, *220*, 525; b) C. Hoch, M. Wendorff, C. Röhr, *J. Alloys Compd.* **2003**, *361*, 206 – 221; c) V. Quéneau, E. Todorov, S. C. Sevov, *J. Am. Chem. Soc.* **1998**, *120*, 3263 – 3264.

[19] H. G. von Schnering, M. Somer, M. Kaupp, W. Carrillo-Cabrera, M. Baitinger, A. Schmeding, Y. Grin, *Angew. Chem. Int. Ed.* **1998**, *37*, 2359 – 2361; *Angew. Chem.* **1998**, *110*, 2507 – 2509.

[20] E. Zurek, C. J. Pickard, J. Autschbach, *J. Am. Chem. Soc.* **2007**, *129*, 4430 – 4439.

[21] C. B. Benda, T. F. Fässler, *Z. Naturforsch. B* **2014**, *69*, 1119 – 1123.

[22] T. Henneberger, W. Klein, T. F. Fässler, *Z. Anorg. Allg. Chem.* **2018**, https://doi.org/10.1002/zaac.201800227.

[23] We also calculated the the CCSD(T) shifts of $[Si_5]^{2-}$ and found them at +225 and −455 ppm.

[24] R. W. Rudolph, W. L. Wilson, F. Parker, R. C. Taylor, D. C. Young, *J. Am. Chem. Soc.* **1978**, *100*, 4629 – 4630.

[25] S. Scharfe, T. F. Fässler, S. Stegmaier, S. D. Hoffmann, K. Ruhland, *Chem. Eur. J.* **2008**, *14*, 4479 – 4483.

[26] a) H. Beall, C. H. Bushweller, *Chem. Rev.* **1973**, *73*, 465 – 486; b) E. W. Corcoran, L. G. Sneddon, *J. Am. Chem. Soc.* **1985**, *107*, 7446 – 7450.

[27] F. S. Kocak, D. O. Downing, P. Zavalij, Y.-F. Lam, A. N. Vedernikov, B. Eichhorn, *J. Am. Chem. Soc.* **2012**, *134*, 9733 – 9740.

Manuscript received: April 24, 2018
Revised manuscript received: July 11, 2018
Accepted manuscript online: July 16, 2018
Version of record online: August 6, 2018

Angewandte Chemie
Eine Zeitschrift der Gesellschaft Deutscher Chemiker

Supporting Information

Charged Si_9 Clusters in Neat Solids and the Detection of $[H_2Si_9]^{2-}$ in Solution: A Combined NMR, Raman, Mass Spectrometric, and Quantum Chemical Investigation

*Lorenz J. Schiegerl, Antti J. Karttunen, Jan Tillmann, Sebastian Geier, Gabriele Raudaschl-Sieber, Markus Waibel, and Thomas F. Fässler**

anie_201804756_sm_miscellaneous_information.pdf

Supporting Information

1. Experimental Section

1.1 Syntheses

Syntheses of $K_{12}Si_{17}$ and $K_{12}Si_{17}$ (^{29}Si-enriched). *^{29}Si-enriched $K_{12}Si_{17}$ is obtained by mixing of 249 mg Si (99% ^{29}Si) and 750 mg Si (natural-abundant) and direct usage of the mixture for the following synthesis procedure:* The Zintl compound $K_{12}Si_{17}$ is synthesized by heating (heating rate: 2 °C/min) a stochiometric mixture of 9.78 mmol (1 eq.) K and 13.9 mmol (1.42 eq.) Si to 800 °C in a sealed tantalum ampoule for 15 h and subsequent cooling (cooling rate: 0.5 °C/min) to room temperature. The ampoule is opened in a glove box, and the product is finely ground yielding $K_{12}Si_{17}$ in 94% and $K_{12}Si_{17}$ (^{29}Si-enriched) in 96% yield as black solids. The products are characterized by powder X-ray diffraction and Raman spectroscopy and $K_{12}Si_{17}$ additionally by ^{29}Si-MAS NMR spectroscopy. Raman vibrations: 281 ($[Si_4]^{4-}$), 354 ($[Si_4]^{4-}$), 390 ($[Si_9]^{4-}$), 482 ($[Si_4]^{4-}$) cm^{-1}; ^{29}Si-MAS NMR (^{29}Si-enriched) (60 MHz, 12 kHz) δ = −315.63 ($[Si_4]^{4-}$), −317.40 ($[Si_4]^{4-}$), −320.43 ($[Si_9]^{4-}$), −322.49 ($[Si_9]^{4-}$), −326.29 ($[Si_4]^{4-}$), −331.47 ($[Si_9]^{4-}$), −343.85 ($[Si_9]^{4-}$).

Synthesis of K_4Si_4. The Zintl compound K_4Si_4 is synthesized by heating (heating rate: 5 °C/min) a mixture of 30.4 mmol (1.02 eq.) K and 29.8 mmol (1 eq.) Si to 500 °C in a sealed tantalum ampoule for 1 h, subsequent heating (heating rate: 5 °C/min) to 600 °C for 30 h and subsequent cooling (cooling rate: 5 °C/min) to room temperature. The ampoule is opened in a glove box, and the product is finely ground yielding K_4Si_4 in 92% as a black solid. The product is characterized by powder X-ray diffraction and Raman spectroscopy as well as ^{29}Si-MAS NMR spectroscopy. Raman vibrations: 287 ($[Si_4]^{4-}$), 337 ($[Si_4]^{4-}$), 364 ($[Si_4]^{4-}$), 481 ($[Si_4]^{4-}$) cm^{-1}; ^{29}Si-MAS NMR (60 MHz, 12 kHz) δ = −322.75 ($[Si_4]^{4-}$), −346.29 ($[Si_4]^{4-}$).

Synthesis of extraction product 1. 0.32 mmol, (1 eq.) $K_{12}Si_{17}$ and 0.57 mmol (1.8 eq.) 222crypt {4,7,13,16,21,24-hexaoxa-1,10-diazabicyclo[8.8.8]hexacosan} are weight into a Schlenk tube, and liquid ammonia is added at −78 °C (*i*PrOH/CO_2) resulting in a dark red solution. The mixture is stirred at−78 °C for 2 h, and a brown solid ($K_{12}Si_{17}$ *pre-extracted*) is yielded after removal of the liquid ammonia. For the extraction of the $[Si_9]^{4-}$ clusters py (30 mL) is added to the solid, and the red-brown suspension is filtered. The dark-red solution is dried under vacuum, and the obtained brown-blueish solid is washed with fluorobenzene (30 mL). The residue is dried *in vacuo* yielding **1** as a red solid [154 mg]. The solid is characterized by ESI-MS in py, NMR (^{1}H, ^{13}C, ^{29}Si) spectroscopy in a 1:1 mixture of py-*d5* and thf-*d8* for measurements at lower temperature, Raman spectroscopy, ^{29}Si-MAS NMR spectroscopy as well as EDX and elemental analyses. The amount of silicon and potassium are further detected by EDX analysis. **^{1}H NMR** (500 MHz, py-d_5) δ = 3.46 (s, 24H, O-C*H*2-C*H*2-$O_{222crypt}$), 3.38 (s, 24H, O-C*H*2-CH2-$N_{222crypt}$), 2.37 (s, 24H, O-CH2-C*H*2-$N_{222crypt}$), −0.32 (m, *J* = 19.7 Hz, 0.36H, H_2Si_9); **^{1}H NMR (^{29}Si-enriched)** (500 MHz, py-d_5) δ = 3.70 (s, 24H, O-C*H*2-C*H*2-$O_{222crypt}$), 3.58 (t, *J* = 4.25 Hz, 24H, O-C*H*2-CH2-$N_{222crypt}$), 2.54 (m, 24H, *J* = 4.33 Hz, O-CH2-C*H*2-$N_{222crypt}$), −0.71 (m, *J* = 19.7 Hz, 0.32H, H_2Si_9); **^{13}C NMR (^{29}Si-enriched)** (101 MHz, py-d_5) δ = 71.42 (O-*C*H2-*C*H2-$O_{222crypt}$), 68.58 (O-*C*H2-CH2-$N_{222crypt}$), 54.92 (O-CH2-*C*H2-$N_{222crypt}$); **^{29}Si NMR (−20 °C, ^{29}Si-enriched)** (99 MHz, py-d_5) δ = −309.37 ($[Si_9]^{2-}$), −346.12 ($[H_2Si_9]^{2-}$); **ESI-MS** (negative mode, 4000 V, 300 °C): *m/z* = 670 {(K-222crypt)$[H_2Si_9]$}$^-$, (positive mode, −4000 V, 300 °C): *m/z* = 1501 {$(K\text{-}222crypt)_3[H_2Si_9]$}$^+$; **ESI-MS (^{29}Si-enriched)** (positive mode,

−4000 V, 300 °C): *m/z* = 1501 {(K-222crypt)$_3$[H_2Si_9]}$^+$; Raman vibrations: 386 cm^{-1} ([Si_9]$^{4-}$); ^{29}Si-MAS NMR (60 MHz, 8 kHz) δ = −319.20 ([Si_9]$^{4-}$); **EDX analysis:** Si 62.3%, K 37.7%; **Elemental analysis:** C 35.22%, H 5.32, N 4.56%, Si 21.12%, K 13.0%.

1.2 General

General. All reactions and manipulations were performed under a purified argon atmosphere using standard Schlenk and glove box techniques. Deuterated solvents were dried over molecular sieves (3 Å). Thf was dried over a special drying material in a solvent purificator (MBraun MB-SPS). Py was received anhydrously (VWR). Fluorobenzene was dried over CaH_2 prior to usage. 222Crypt was dried *in vacuo* overnight prior to usage. Liquid ammonia was dried and stored over sodium metal prior to usage, all other solvents were stored over molecular sieves (3 Å) prior to usage. All other chemicals were received commercially and used without further purification.

1.3 Characterization Methods

Electron Dispersive X-ray (EDX) Analysis. Single crystals of all compounds were analyzed with a SWIFT-ED-TM (Oxford Instruments) and a Hitachi TM-1000 Tabletop microscope (Hitachi High-Technologies) with an INCA system software.

NMR Spectroscopy. ^{1}H, ^{13}C and ^{29}Si NMR spectra were recorded on a Bruker AVIII Ultrashield 400 MHz, a Bruker AVIII HD Ultrashield 500 MHz or a Bruker AVIII Cryo 500 MHz spectrometer. The signals of the ^{1}H and ^{13}C spectra were calibrated on the rest proton signal of the used deuterated solvent py-*d5*. A relaxation-time of 20 s was chosen for the ^{29}Si NMR measurements. Chemical shifts are given in δ values by parts per million (ppm). The coupling constants *J* are stated in Hz. Signal multiplicities are abbreviated as follows: s – singlet, t – triplet and m – multiplet. The spectra were visualized with *MestReNova 9.1*[1].

Electrospray Ionization Mass Spectrometry (ESI-MS). The preparation of the samples was performed in a glove box. The measurements were performed on a HCT instrument (Bruker Corp.). Analysis of the data was evaluated using the program Bruker Compass Data Analysis 4.0 SP 5 (Bruker Corp.) [for the simulation of the isotopic pattern of **1** (^{29}Si-enriched) the corresponding isotopic pattern of the respective [$H_2{}^{29}Si_n/Si_{9-n}$]$^{2-}$ isotopomers (n = 1–4) were combined weighted]. The dry gas temperature was adjusted to 300 °C and the injection speed to 240 µLs^{-1}. *OriginPro 2017*[2] and *Excel 2016*[3] was used for the visualization of the spectra.

Elemental Analysis. Elemental analyses were performed by the microanalytical laboratory at the Catalytic Research Center of the Technische Universität München. The elements C, H and N were determined with an Euro EA CHNS Elemental Analysator (*HEKAtech Ltd.*), Si was detected photometrically on a Shimadzu UV 160 at 810 nm, and K was detected on a Agilent AAS 280 FS.

Raman spectroscopy. Raman spectra were recorded with a Renishaw inVia Raman Microscope RE04 with a CCD Detector and 500 mW max. power (Software WiRE 4.2 build 5037, Renishaw 2002) at λ =

785 nm in a sealed glass capillary (Ø = 0.5 mm). *Excel 2016*[3] was used for the visualization of the spectra.

Solid-State ^{29}Si-MAS NMR Spectroscopy. Magic-angle spinning (MAS) ^{29}Si NMR spectra were recorded on a Bruker Avance 300 spectrometer operating at 7.04 T at ambient temperature with single pulse technique. Samples were packed in 4 mm ZrO_2 MAS NMR probes and rotated with frequencies of 8 and 12 kHz. *MestReNova 9.1*[1] was used for the visualization of the spectra. $Si(Si(CH_3)_3)_4$ was used as extern (secondary) standard for referencing.

Powder X-ray Diffraction (PXRD). The data was collected at room temperature on a STOE Stadi P diffractometer (Ge(111) monochromator, Cu Kα_1 radiation, λ = 1.54056 Å) with a Dectris MYTHEN 1K detector in Debye-Scherrer geometry. Samples were sealed in glass capillaries (Ø 0.5 mm) for the measurement. The raw data was processed with *WinX-POW*[4], *OriginPro 2017*[2] was used for the visualization.

2. Computational Details

2.1 Structural Optimizations and Raman Spectra for the Molecular Cluster Anions

Quantum-chemical structural optimizations and Raman spectrum calculations on the molecular silicon cluster anions were carried out using the TURBOMOLE program package.[5] We used PBE0 hybrid density functional methods and a triple-zeta-valence quality basis set with polarization functions (def2-TZVP).[6] Resolution-of-the-identity technique was used to speed up the calculations.[7] The structures of the silicon cluster anions were fully optimized within their respective point group symmetries, and they were confirmed to be true local minima by means of harmonic frequency calculations. The energy landscape of the silicon cluster anions is rather flat, and they are expected to be highly fluxional in solution. For example, the energy difference between the C_{4v}- and D_{3h}-symmetric $[Si_9]^{4-}$ anions is less than 2 kJ/mol at 0 K. The optimized structures of the studied systems are reported in Section 4 below. The COSMO continuum solvation model was used to counter the negative charge of the anions.[8] In the Raman spectrum calculations (λ = 785 nm; T = 298.15 K, unpolarized radiation, scattering angle of 90°),[9,10] the COSMO solvent model was applied only for the ground state of the highly charged $[Si_4]^{4-}$ cluster and not used in the dynamic polarizability derivatives calculation. The Raman intensities are given relative to the most intensive peak. The final Raman spectra were convoluted using Lorenzian peak profiles with FWHM of 10 cm^{-1}.

2.2 Raman Spectrum of K_4Si_4 in Solid State

The solid-state Raman spectrum of K_4Si_4 was calculated using the CRYSTAL14 program package. [11] We carried out periodic quantum-chemical calculations with the PBE0 hybrid density functional method and a polarized split-valence level basis set (SVP).[7] The basis sets for Si and K were derived from the Karlsruhe def2 basis sets.[8] The Si basis set has been used in previous studies,[12] while the K basis set is listed in Section 4 below. The reciprocal space was sampled using a 2x2x2 Monkhorst-Pack-type *k*-point grid.[13] For the evaluation of the Coulomb and exchange integrals (TOLINTEG), tight tolerance factors of 8, 8, 8, 8, and 16 were used. Both the atomic positions and lattice constants were fully optimized within the constraints imposed by the space group symmetry. Default optimization convergence thresholds and an extra-large integration grid (XLGRID) for the DFT part were applied in all calculations. The harmonic vibrational frequencies and Raman intensities were obtained by using the computational schemes implemented in CRYSTAL.[14] The predicted spectrum is based on the harmonic approximation, and the wavenumbers have been scaled by a factor of 0.95 to account for the overestimation typical for predicted harmonic frequencies.[15] The Raman intensities have been calculated for a polycrystalline powder sample (total isotropic intensity in arbitrary units). The Raman final spectrum was obtained by using pseudo-Voigt peak profile (50:50 Lorenzian:Gaussian) and FWHM of 8 cm^{-1}. When simulating the Raman spectrum, the temperature and laser wavelength were set to values corresponding to the experimental setup (T = 298.15 K, λ = 785.8 nm).

2.3 NMR Calculations for the Molecular Cluster Anions

Quantum-chemical NMR calculations on the molecular silicon cluster anions were carried out using the CFOUR program package.[16] We used the *ab initio* CCSD(T) coupled-cluster method together with a polarized correlation-consistent triple-zeta-valence quality cc-pVTZ basis set to calculate the NMR shielding tensors.[17] The CCSD(T) calculations were carried at DFT-PBE0/def2-TZVP geometries. The ^{29}Si and ^{1}H NMR chemical shifts are reported with respect to tetramethylsilane ($SiMe_4$). An important point in the comparison of experimental solution-state ^{29}Si NMR shifts and the calculated CCSD(T) chemical shifts is the temperature: the calculated values are for fixed gas-phase geometries at 0 K, while the experimental ^{29}Si spectra showing includes averaging of the signals due to finite measurement temperature and solvent effects. Due to the high computational cost of the CCSD(T) NMR calculations, it was not yet feasible to carry out molecular dynamics (MD) simulations that could be sampled to obtain thermally averaged spectroscopic parameters with solvent effects (see refs. [18] for the application of MD simulations in the calculation of finite-temperature solution-state NMR spectra). In the present case we calculated the average NMR chemical shift for a silicon cluster anion by taking the weighted average of all atomic chemical shifts (the weights are determined by the symmetry-multiplicity of each atom).

2.4 NMR Calculations for K_4Si_4 and $K_{12}Si_{17}$ in Solid State

The solid-state NMR shielding tensors were calculated using the DFT-PBE method[6] using the CASTEP program package and the GIPAW formalism as implemented in CASTEP-NMR. [19] The CASTEP-NMR calculations were carried out at the experimental geometries of K_4Si_4 (structure ICSD-409852, *P*-43*, a* = 12.62 Å, primitive cell $K_{32}Si_{32}$), $K_{12}Si_{17}$ (structure ICSD-97395, $P2_1/c$, *a* = 23.689 Å, *b* = 13.572 Å, *c* = 44.509 Å, primitive cell $K_{192}Si_{272}$), and α-Si (ICSD-76268, *Fd*-3*m*, *a* = 5.431 Å). Ultrasoft pseudopotentials generated with the on-the-fly scheme[20] and a plane-wave basis set cut-off of 300 eV were applied. 3x3x3 (K_4Si_4), Gamma-point ($K_{12}Si_{17}$), and 8x8x8 (α-Si) Monkhorst-Pack sampling were used for integrations in the reciprocal space.[MP] The NMR calculations for the molecular $SiMe_4$ reference system were carried out in a primitive cubic cell (a = 15 Å) using a plane-wave basis set cut-off of 300 eV and Gamma *k*-point. The structure of the $SiMe_4$ molecule was relaxed within the T_d point group.

In the case of K_4Si_4 there are only two symmetry-independent Si atoms in the primitive unit cell, and the interpretation of the calculated NMR shifts is straightforward. However, in the case of $K_{12}Si_{17}$, there are 272 Si atoms Si atoms in the primitive unit cell, making the interpretation of the calculated NMR shifts more complicated (all calculated ^{29}Si chemical shifts are listed below in Section 5). The DFT-PBE chemical shifts are calculated for 0 K, while the experimental ^{29}Si-MAS NMR spectrum showing less than 10 signals includes some averaging of the signals due to finite measurement temperature. To enable comparison between the computational and experimental data, we created a histogram of the calculated shifts (Figure SI 1). In the histogram, all atom signals appearing within a chemical shift range of about 18 ppm are collected into a bin. Bins then provide averaging that enables a comparison with the experimental signals. The total number of atoms in each bin should reflect at least qualitatively the intensity of the NMR signal. It is possible to make separate histograms for $[Si_9]^{4-}$ and $[Si_4]^{4-}$, which

facilitates the interpretation of the experimentally observed NMR spectrum (^{29}Si-MAS NMR signals of $K_{12}Si_{17}$, Table SI 1 and Figure SI 1 below). In the calculated NMR histogram, a few Si atoms show chemical shifts of almost –400 ppm, while the most negative experimental value is –343.95 ppm. In addition, the calculated shift of –281 ppm at the other extreme also shows a larger difference in comparison to the experiment. These discrepancies most likely arise because the calculations have been carried out at 0 K, and the atoms are kept at the experimental X-ray positions without any thermal averaging. Unfortunately, it is not yet computationally feasible to carry out a finite-temperature molecular dynamics simulation for $K_{12}Si_{17}$, which could then be used for the sampling of temperature-averaged structures.

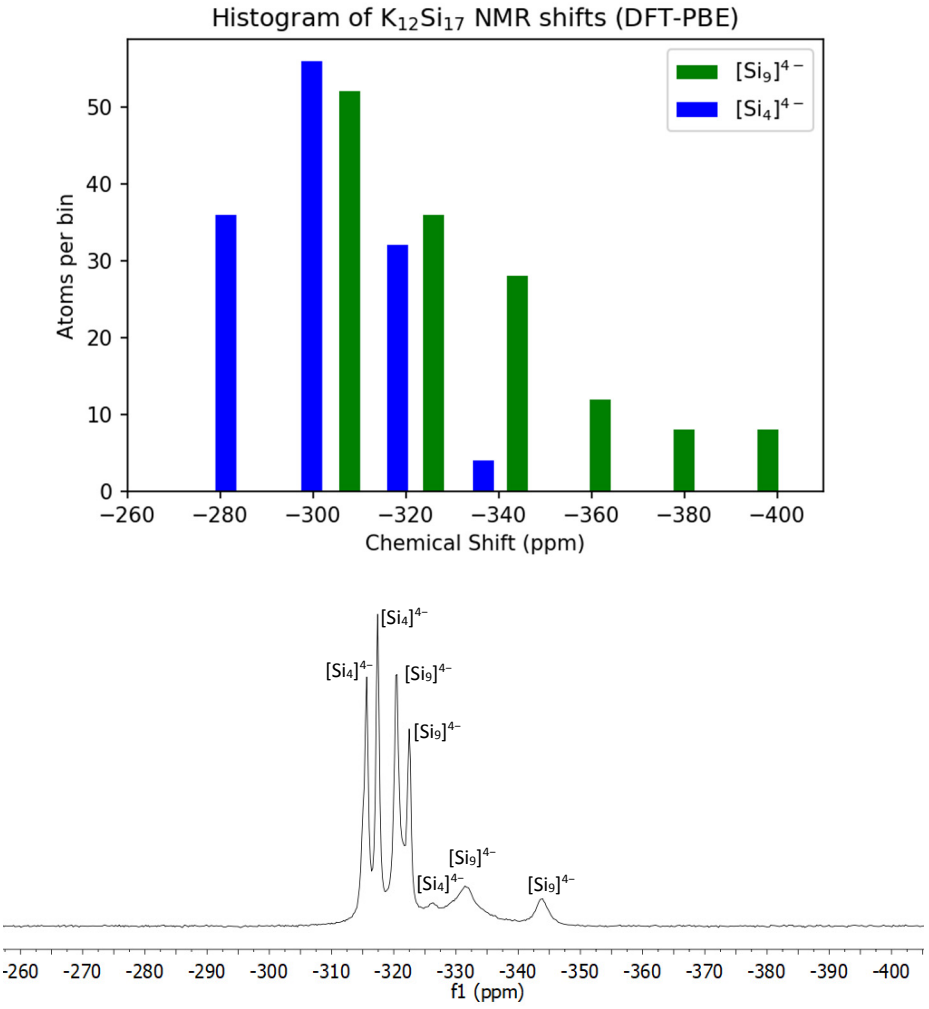

Figure SI 1. Top: Histogram of $K_{12}Si_{17}$ NMR shifts calculated with DFT-PBE (CASTEP-NMR) (atom signals appearing of the respective cluster types within a chemical shift range of 18 ppm are collected into bins); bottom: ^{29}Si-MAS NMR spectrum of $K_{12}Si_{17}$ (^{29}Si-enriched) with cluster assignments for comparison (full spectrum in Figure SI 14).

3. Characterization Details

3.1 PXRD

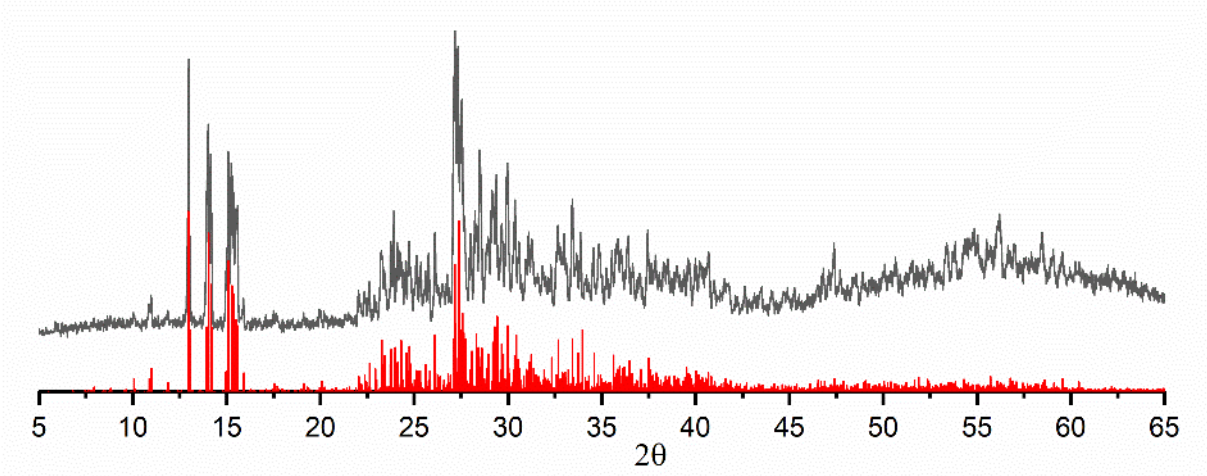

Figure SI 2. Powder X-ray diffractogram of the Zintl phase $K_{12}Si_{17}$ (gray: measured diffractogram; red: theoretical diffractogram).

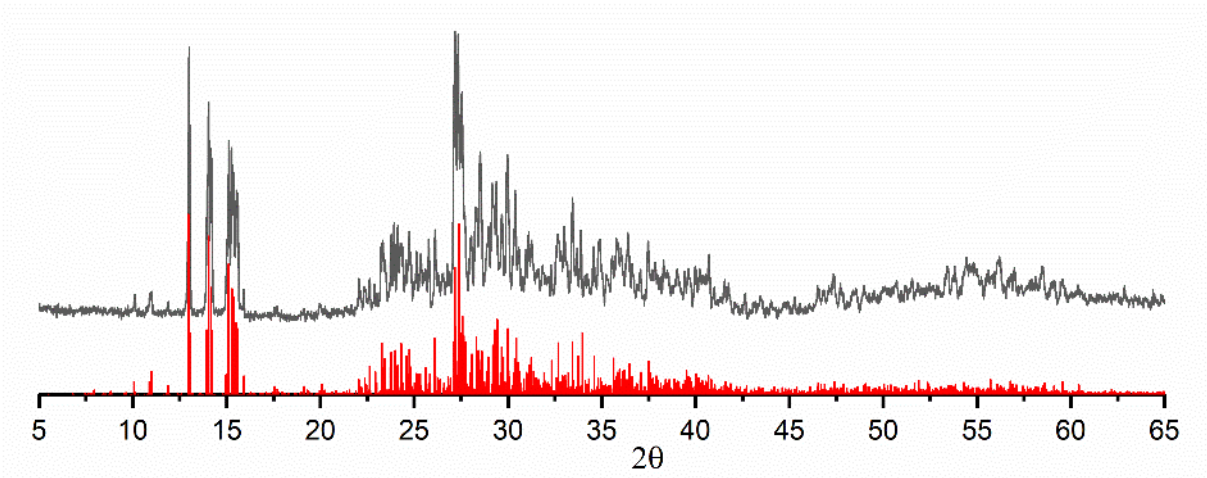

Figure SI 3. Powder X-ray diffractogram of the Zintl phase $K_{12}Si_{17}$ (^{29}Si-enriched) (gray: measured diffractogram; red: theoretical diffractogram).

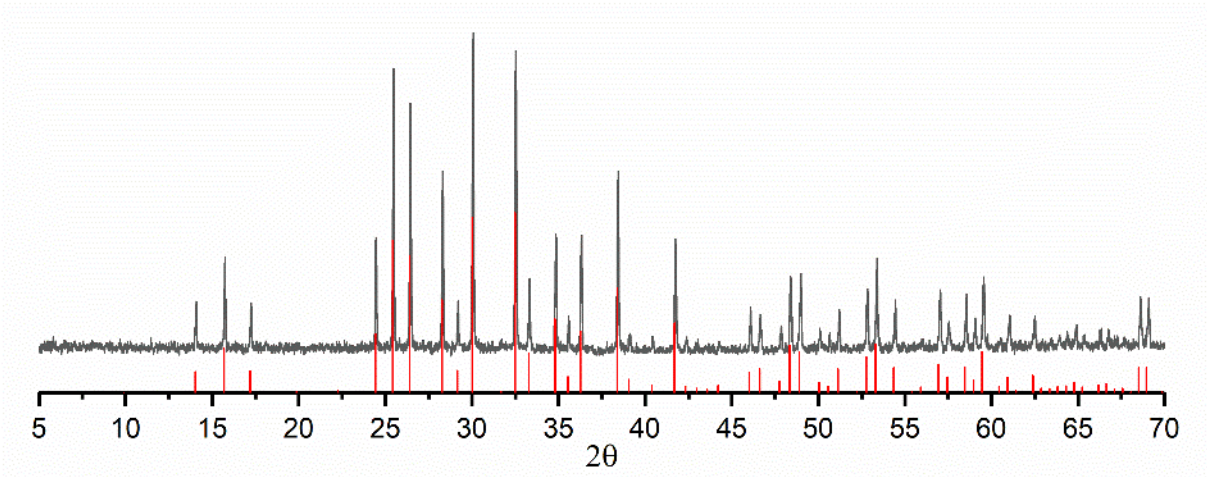

Figure SI 4. Powder X-ray diffractogram of the Zintl phase K_4Si_4 (gray: measured diffractogram; red: theoretical diffractogram).

3.2 ESI-MS

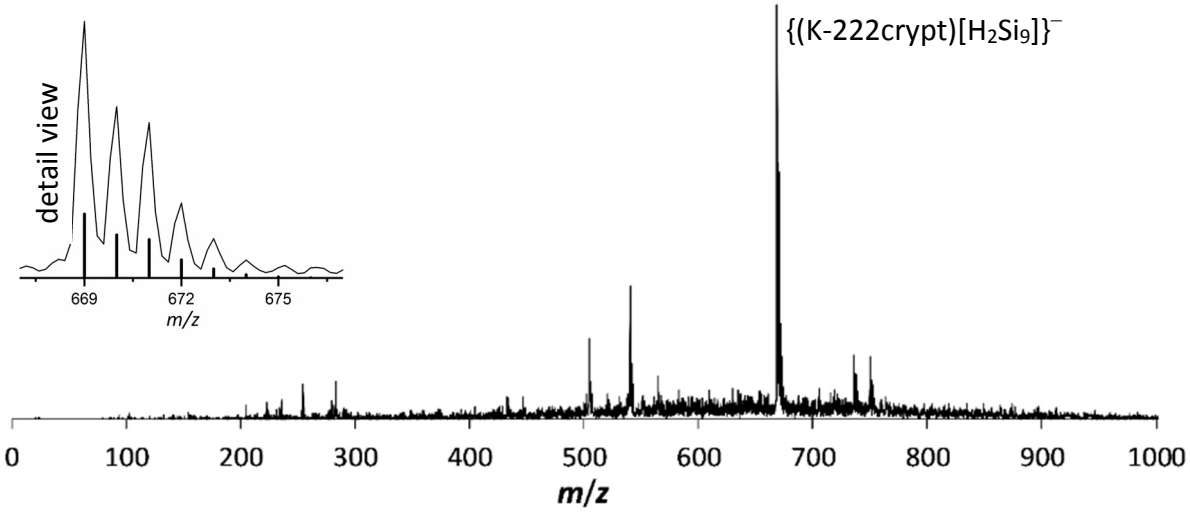

Figure SI 5. ESI-MS spectrum (full and detail view) of **1** in negative ion mode (detail view: line: measured spectrum, bars: simulated spectrum).

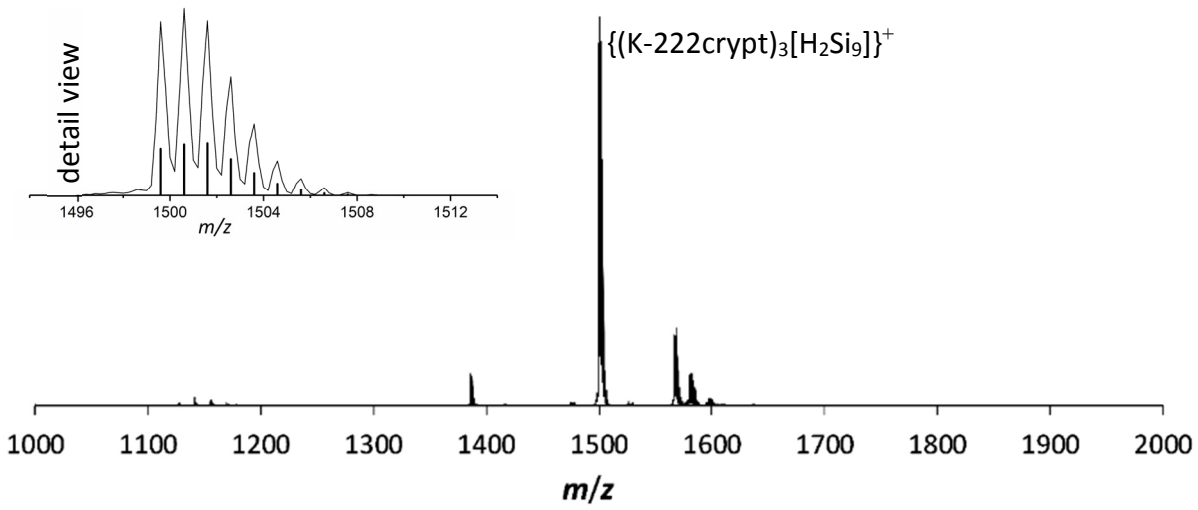

Figure SI 6. ESI-MS spectrum (full and detail view) of **1** in positive ion mode (detail view: line: measured spectrum, bars: simulated spectrum).

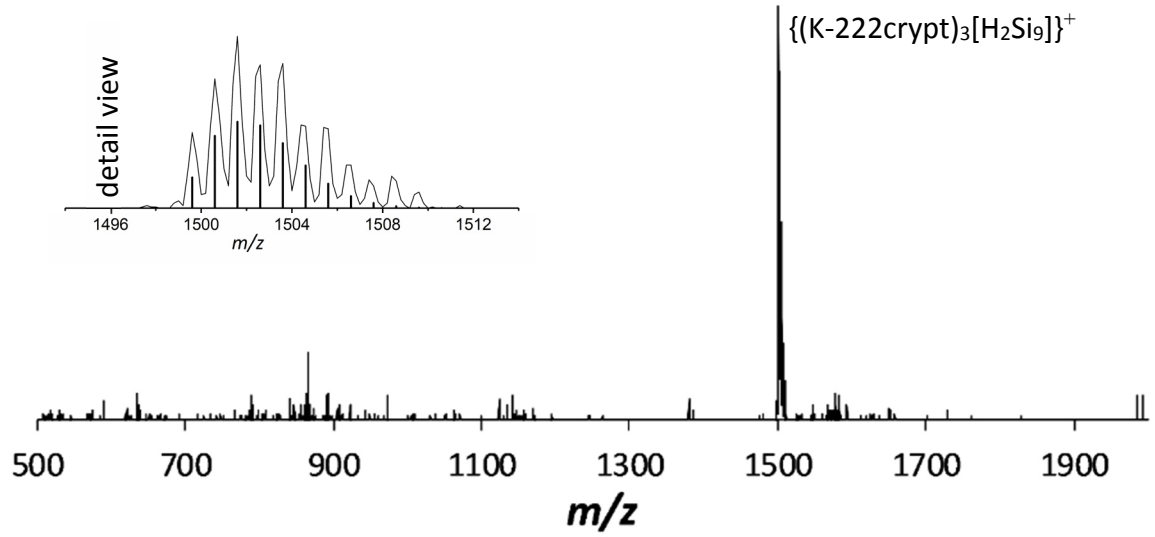

Figure SI 7. ESI-MS spectrum (full and detail view) of **1** (^{29}Si-enriched) in positive ion mode (detail view: line: measured spectrum, bars: simulated spectrum for 15% ^{29}Si content).

3.3 NMR

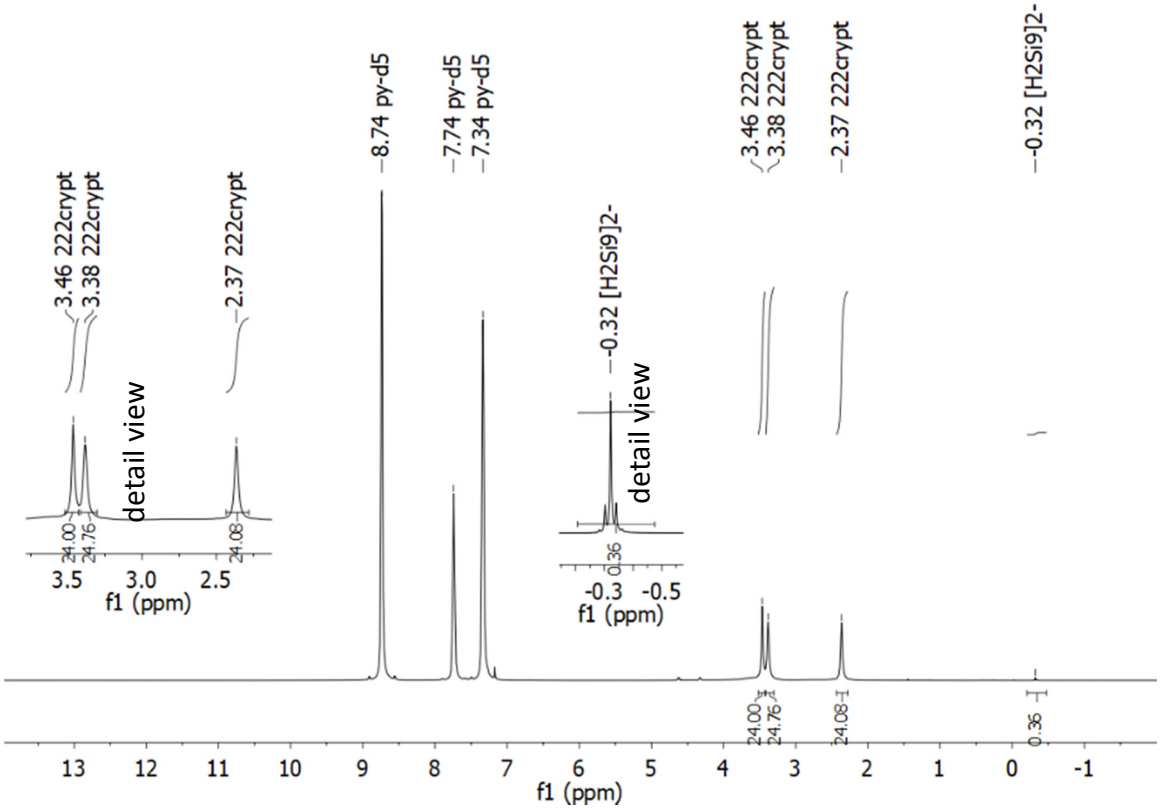

Figure SI 8. ^{1}H NMR spectrum of **1** in py-*d5*/thf-*d8* (1:1) at 25 °C without ^{29}Si enrichment (referring to Figure 5f in the manuscript).

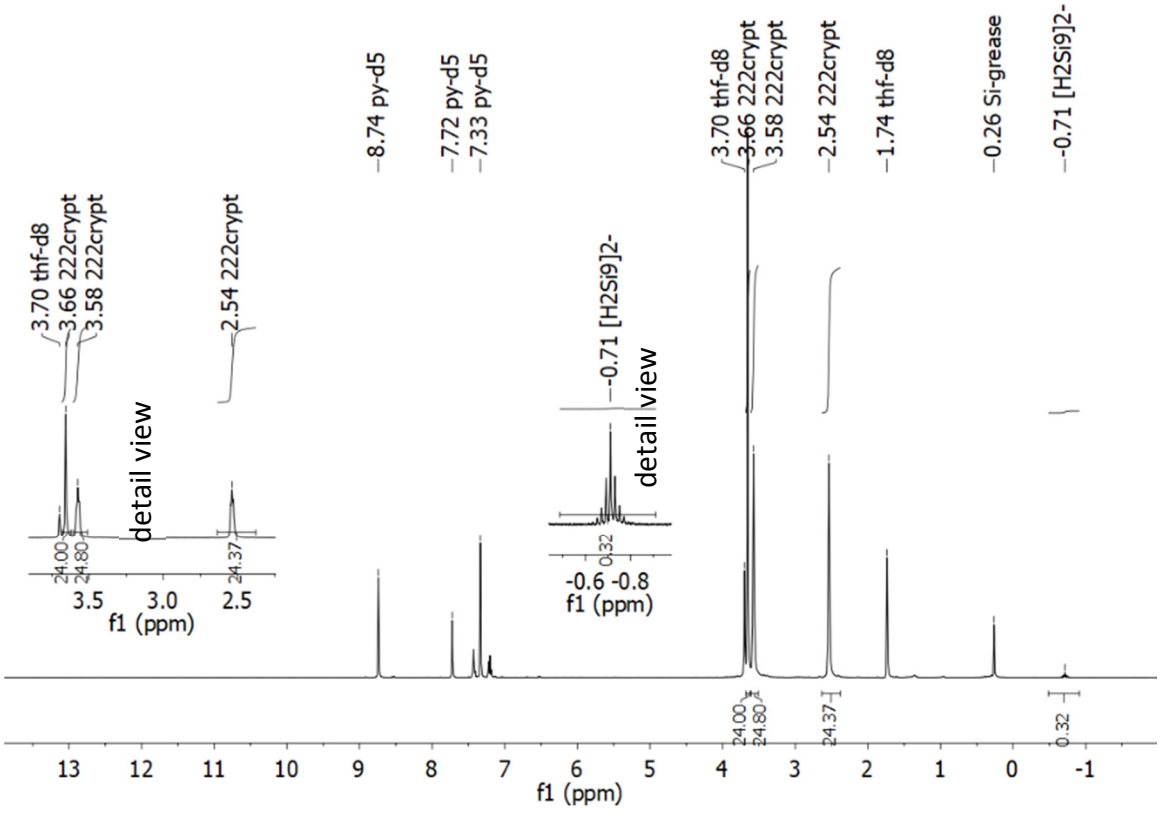

Figure SI 9 ^{1}H NMR spectrum of **1** (^{29}Si-enriched) in py-*d5*/thf-*d8* (1:1) at 25 °C with ^{29}Si enrichment (referring to Figure 5e in the manuscript).

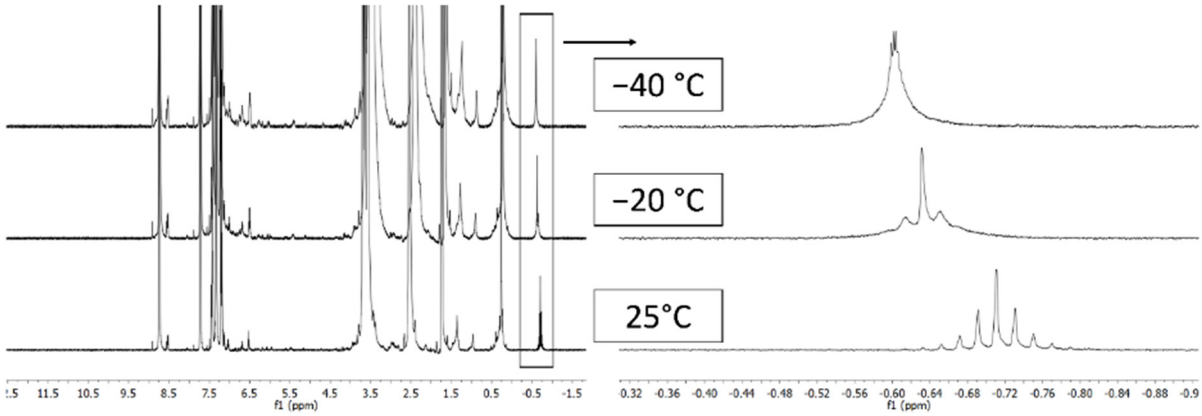

Figure SI 10. Detail view on the ^{1}H NMR spectra of **1** (with ^{29}Si enrichment) in py-*d5*/thf-*d8* (1:1) at varied temperatures (the corresponding ^{29}Si NMR spectra at varied temperatures are shown in the manuscript in Figure 4; bottom spectrum at 25 °C is also shown in Figure SI 9).

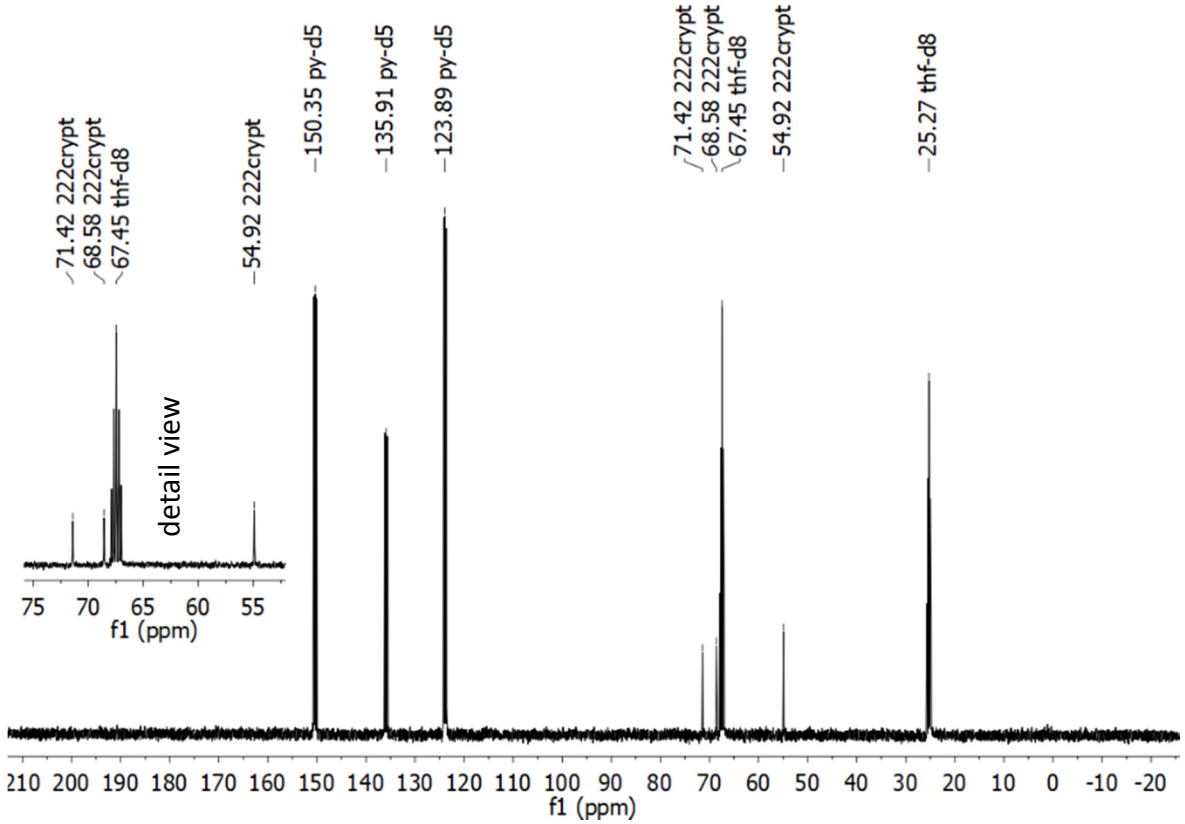

Figure SI 11. ^{13}C NMR spectrum of **1** (^{29}Si-enriched) in py-*d5*/thf-*d8* (1:1) at 25 °C.

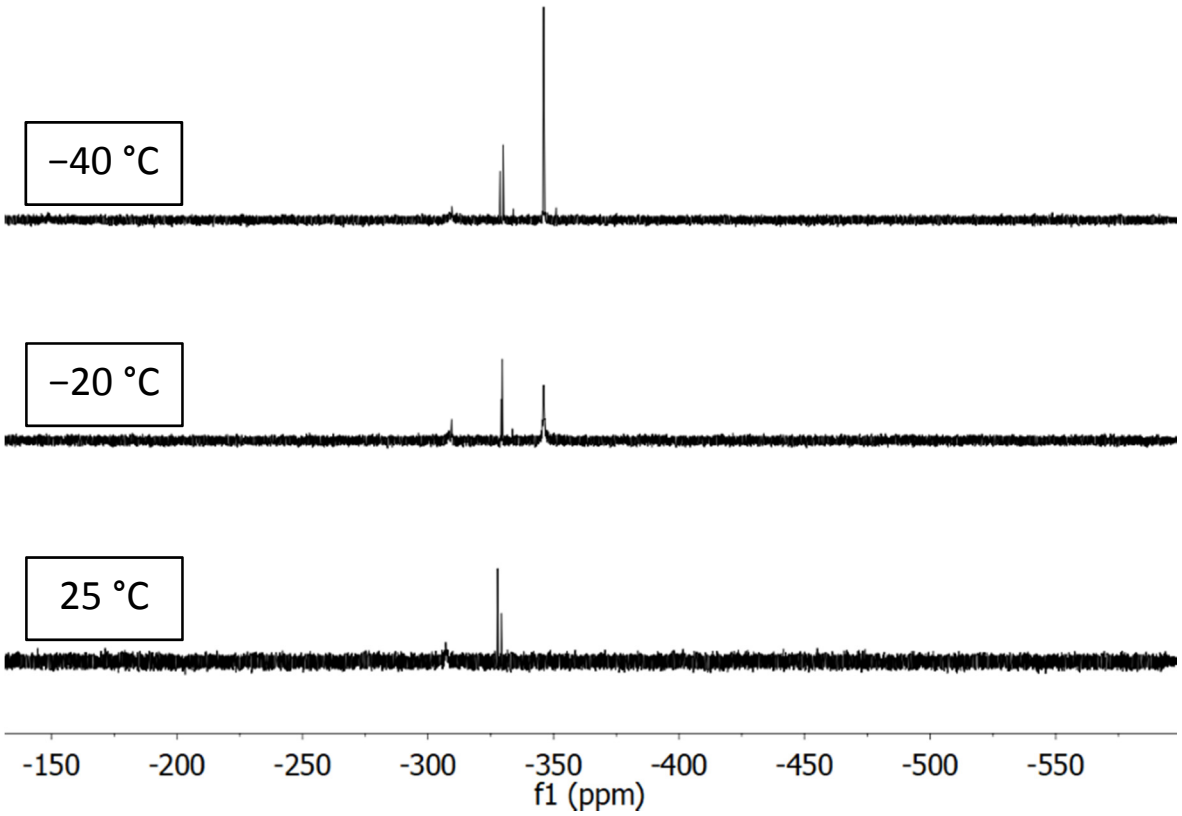

Figure SI 12. ^{29}Si NMR spectra of **1** (^{29}Si-enriched) in py-*d5*/thf-*d8* (1:1) at varied temperatures (referring to Figure 4 in the manuscript).

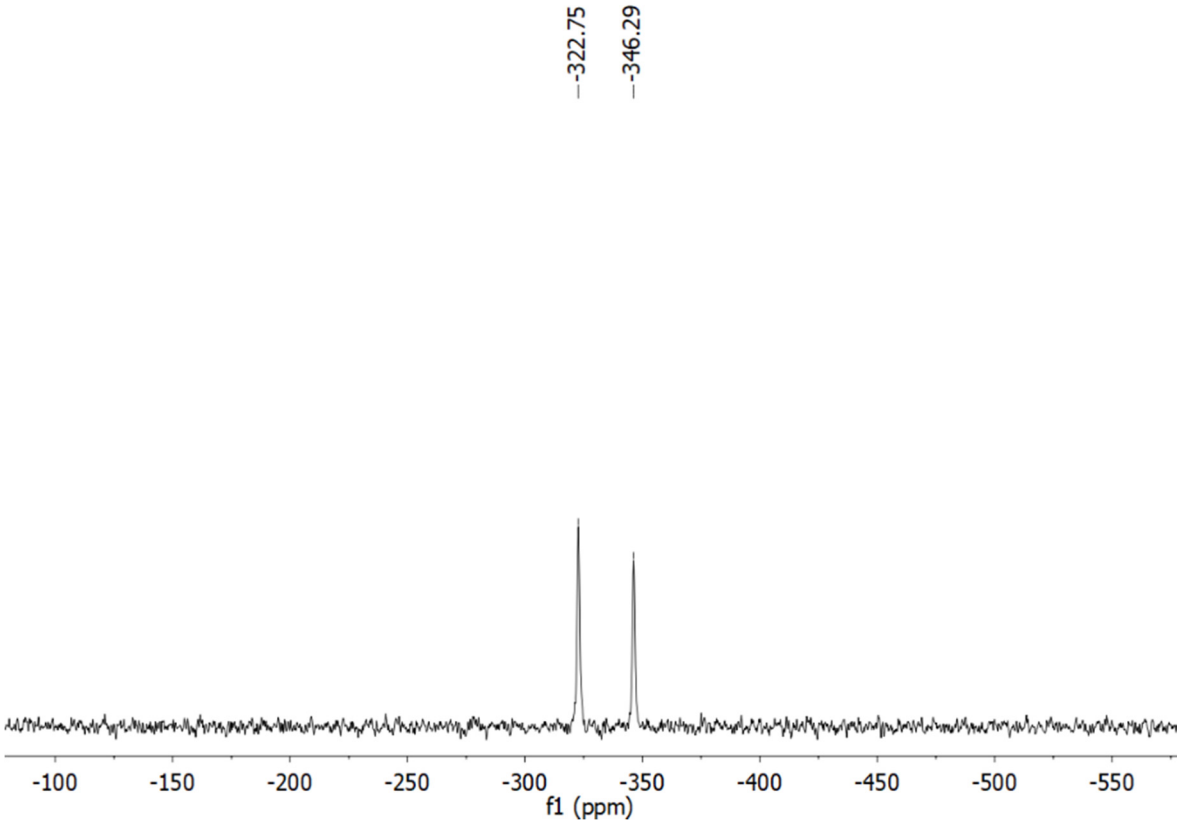

Figure SI 13. ^{29}Si MAS NMR spectrum of K_4Si_4.

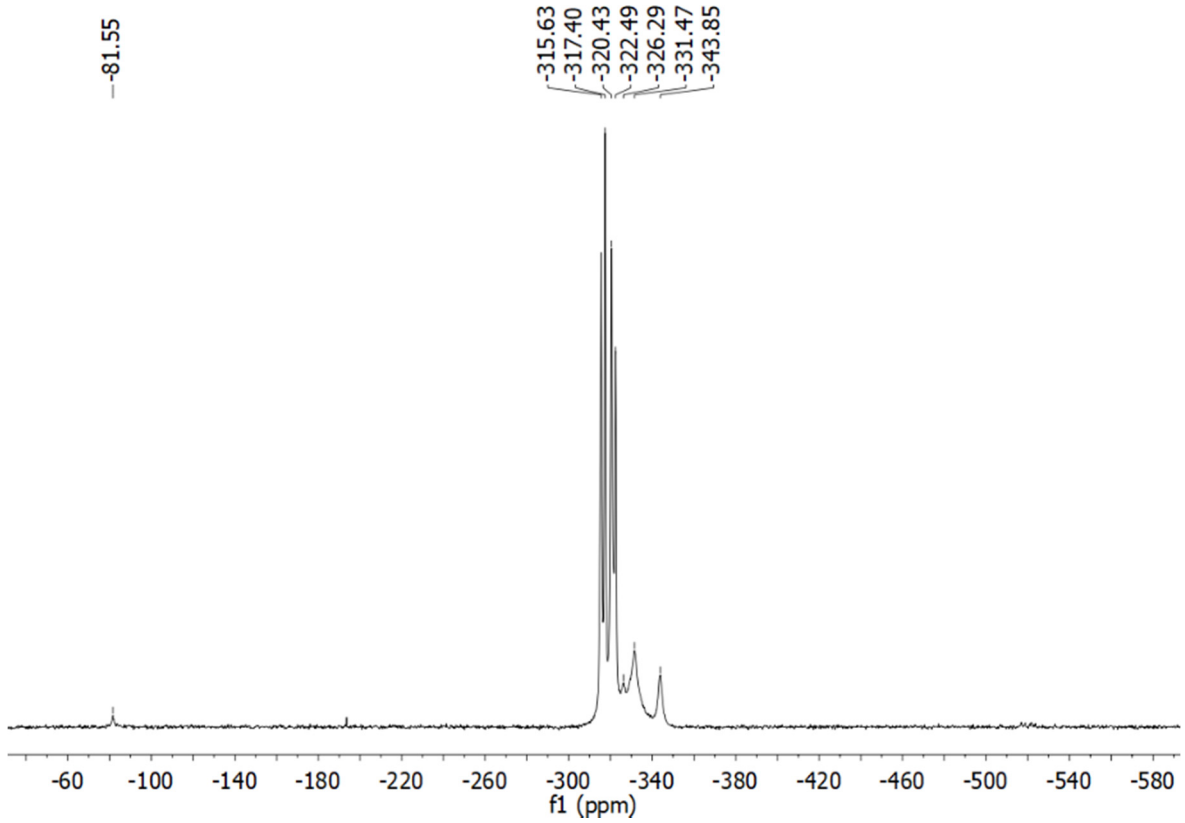

Figure SI 14. ^{29}Si MAS NMR spectrum of $K_{12}Si_{17}$ (^{29}Si-enriched). The signal at −81.55 ppm originates from α-Si (*calcd.* DFT-PBE −83 ppm).

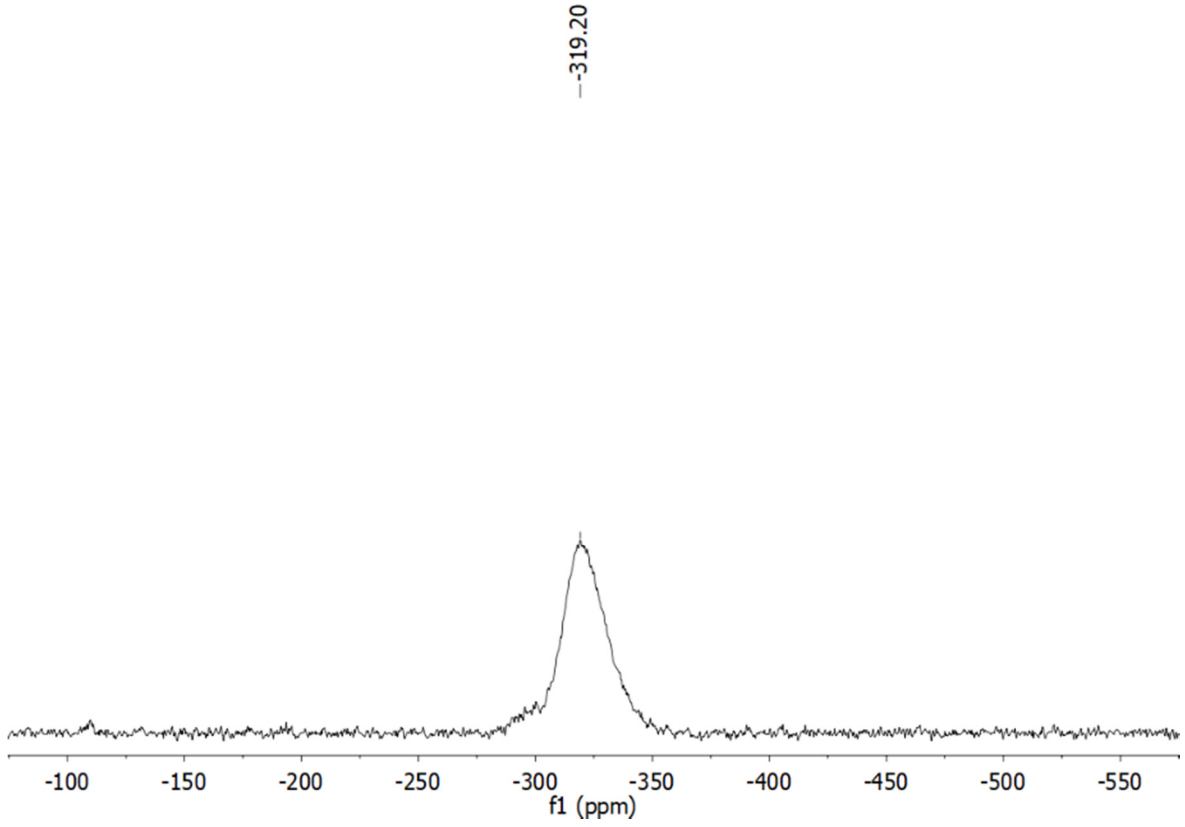

Figure SI 15. ^{29}Si-MAS NMR spectrum of **1** (^{29}Si-enriched).

4. Coordinates and Basis Sets

Molecular calculations with TURBOMOLE (DFT-PBE0/def2-TZVP). XYZ coordinates [Å].

$[Si_4]^{4-}$ (T_d)

4

Td

Si 0.8489078 -0.8489078 0.8489078
Si -0.8489078 0.8489078 0.8489078
Si 0.8489078 0.8489078 -0.8489078
Si -0.8489078 -0.8489078 -0.8489078

$[Si_9]^{4-}$ (C_{4v})

9

C4v

Si 0.0000000 0.0000000 2.3784365
Si -1.2880655 1.2880655 0.7460300
Si -1.7254289 -0.0000000 -1.3406391
Si -1.2880655 -1.2880655 0.7460300
Si 0.0000000 -1.7254289 -1.3406391
Si 1.7254289 0.0000000 -1.3406391
Si -0.0000000 1.7254289 -1.3406391
Si 1.2880655 1.2880655 0.7460300
Si 1.2880655 -1.2880655 0.7460300

$[Si_9]^{2-}$ (D_{3h})

9

D_{3h}

Si 1.4894724 0.0000000 1.2717394
Si 1.4894724 0.0000000 -1.2717394
Si -0.7447362 1.2899210 1.2717394
Si -0.7447362 1.2899210 -1.2717394
Si -0.7447362 -1.2899210 1.2717394
Si 1.1870620 -2.0560517 -0.0000000
Si -2.3741240 0.0000000 -0.0000000
Si -0.7447362 -1.2899210 -1.2717394
Si 1.1870620 2.0560517 -0.0000000

$[H_2Si_9]^{2-}$ (C_{2v})

11

C_{2v}

Si 0.0000000 0.0000000 2.6182052
Si -1.2584590 1.3676520 1.0359533
Si -1.4800858 0.0000000 -0.9520333
Si -1.2584590 -1.3676520 1.0359533
Si 0.0000000 -1.8759634 -1.0585899
Si 1.4800858 0.0000000 -0.9520333
Si 0.0000000 1.8759634 -1.0585899
Si 1.2584590 1.3676520 1.0359533
Si 1.2584590 -1.3676520 1.0359533
H -2.9167050 0.0000000 -1.3703860
H 2.9167050 0.0000000 -1.3703860

$[Si_9]^{4-}$ (D_{3h})

9

D_{3h}

Si	1.4193462	0.0000000	1.4452447
Si	1.4193462	0.0000000	-1.4452447
Si	-0.7096731	1.2291898	1.4452447
Si	-0.7096731	1.2291898	-1.4452447
Si	-0.7096731	-1.2291898	1.4452447
Si	1.1160077	-1.9329821	0.0000000
Si	-2.2320155	0.0000000	0.0000000
Si	-0.7096731	-1.2291898	-1.4452447
Si	1.1160077	1.9329821	0.0000000

Trimethylsilane (T_d)

17

T_d

Si	-0.0000000	0.0000000	0.0000000
C	1.0840983	-1.0840983	1.0840983
H	0.4798290	-1.7284789	1.7284789
H	1.7284789	-1.7284789	0.4798290
H	1.7284789	-0.4798290	1.7284789
C	-1.0840983	1.0840983	1.0840983
C	-1.0840983	-1.0840983	-1.0840983
C	1.0840983	1.0840983	-1.0840983
H	-1.7284789	1.7284789	0.4798290
H	-0.4798290	-1.7284789	-1.7284789
H	1.7284789	1.7284789	-0.4798290
H	-1.7284789	-0.4798290	-1.7284789
H	-1.7284789	0.4798290	1.7284789
H	-0.4798290	1.7284789	1.7284789
H	1.7284789	0.4798290	-1.7284789
H	-1.7284789	-1.7284789	-0.4798290
H	0.4798290	1.7284789	-1.7284789

Solid-state calculations with CRYSTAL (DFT-PBE0/SVP)

K_4Si_4

218 (space group)

12.50807027 (lattice constant in angstrom units)

4 (number of atoms in the asymmetric unit, followed by fractional coordinates of each atom)

19	3.334785087857E-01	3.334785087857E-01	3.334785087857E-01
19	3.361146857629E-01	1.426201914668E-01	6.702800332308E-02
14	6.848273523891E-02	6.848273523891E-02	6.848273523891E-02
14	6.394697390630E-02	3.177525150474E-01	4.264763226751E-01

Details for the K basis set: The Karlsruhe def2-SVP basis set was used as a starting point (for references see Computational details above). The two most diffuse s-functions were removed (exponents 0.012 and 0.029, respectively). Next, the outermost (3s)-function was decontracted to (2s1s) by taking out the s-function with an exponent of 0.28 and another s-type function with an exponent of 0.14 was added to the valence space. The most diffuse p-type function (exponent 0.042) was removed. Next, the outermost (3p)-function was decontracted to [2p1p] by taking out the p-function with an exponent

of 0.21. The exponent of the most diffuse function was increased to 0.28 and another p-type function with an exponent of 0.14 was added to the valence space. Finally, the outermost s and p functions were combined into a two sp-type functions to increase the efficiency of the CRYSTAL code and the diffuse d function (0.098) was removed.

Full basis set listing for Si and K in CRYSTAL input format

```
14 7
0 0 5 2.0 1.0
  6903.7118686     0.13373962995E-02
  1038.4346419     0.99966546241E-02
  235.87581480     0.44910165101E-01
  66.069385169     0.11463638540
  20.247945761     0.10280063858
0 0 3 2.0 1.0
  34.353481730     0.70837285010E-01
  3.6370788192    -0.43028836252
  1.4002048599    -0.41382774969
0 0 1 2.0 1.0
 0.25943211957      1.0000000000
0 1 1 0.0 1.0
 0.12000000000      1.0 1.0
0 2 5 6.0 1.0
  179.83907373     0.61916656462E-02
  41.907258846     0.43399431982E-01
  12.955294367     0.15632019351
  4.4383267393     0.29419996982
  1.5462247904     0.23536823814
0 2 1 2.0 1.0
 0.40981363585      1.0000000000
0 3 1 0.0 1.0
 0.35000000000      1.0000000000

19 8
0 0 6 2.0 1.0
  31478.746764     0.39838653994E-02
  4726.8876066     0.30501759762E-01
  1075.4345353     0.15073752622
  303.39811023     0.51912939801
  98.327112831     1.0366957005
  33.636222177     0.76398963199
0 0 3 2.0 1.0
  65.639209962    -0.28242617106
  7.3162592218     1.6914935860
  2.8902580135     1.2965331953
0 0 2 2.0 1.0
  4.5459748965    -0.76343555273E-02
  .70404124062     0.25635718960E-01
0 1 1 1.0 1.0
  0.28           1.0 1.0
0 1 1 0.0 1.0
  0.14           1.0 1.0
0 2 5 6.0 1.0
  361.22492154     0.20906479823E-01
  84.670222166     0.15043641740
```

26.469088236 0.55440061077
9.2658077615 1.0409009991
3.3423388293 0.67825341194
0 2 2 6.0 1.0
1.5100876104 0.75248191146
0.56568375163 1.3708585031
0 3 1 0.0 1.0
0.353 1.0

5. ^{29}Si NMR Chemical Shift Data for $K_{12}Si_{17}$

Table S5.1. ^{29}Si NMR chemical shift data for $K_{12}Si_{17}$ (DFT-PBE with CASTEP-NMR). Chemical shifts w.r.t. TMS. Only the shifts of the 68 symmetry-independent Si atoms are listed here (there are 272 Si atoms in total in the unit cell).

#Si	Si9/Si4	Shift (ppm)
1	Si9	-326
2	Si9	-330
3	Si9	-303
4	Si9	-344
5	Si9	-303
6	Si9	-342
7	Si9	-357
8	Si9	-376
9	Si9	-366
10	Si9	-301
11	Si9	-312
12	Si9	-316
13	Si9	-324
14	Si9	-315
15	Si9	-315
16	Si9	-336
17	Si9	-301
18	Si9	-387
19	Si9	-311
20	Si9	-333
21	Si9	-330
22	Si9	-312
23	Si9	-330
24	Si9	-316
25	Si9	-341
26	Si9	-324
27	Si9	-399
28	Si9	-348
29	Si9	-329
30	Si9	-342
31	Si9	-301
32	Si9	-299
33	Si9	-345
34	Si9	-354
35	Si9	-327
36	Si9	-407
37	Si4	-273
38	Si4	-313
39	Si4	-322
40	Si4	-272
41	Si4	-310
42	Si4	-305
43	Si4	-283
44	Si4	-287
45	Si4	-297
46	Si4	-310
47	Si4	-324
48	Si4	-291
49	Si4	-294
50	Si4	-324
51	Si4	-346

52	Si4	-311
53	Si4	-305
54	Si4	-302
55	Si4	-284
56	Si4	-283
57	Si4	-303
58	Si4	-296
59	Si4	-293
60	Si4	-303
61	Si4	-308
62	Si4	-311
63	Si4	-282
64	Si4	-288
65	Si4	-288
66	Si4	-297
67	Si4	-304
68	Si4	-295

6. References

[1] *MestReNova 9.1,* Version 9.1.0-14011; MestreLab Research S.L.*:* Santiago de Compostela, Spain, **2014**.

[2] *OriginPro 2017*, Version 9.4.1.354; OriginLab Corp.: Northampton, USA, **2017**.

[3] *Excel 2016*, Version 2016; Microsoft Corp.: Redmond, USA, **2016**.

[4] *Win XPOW*, Version 3.0.2.1; STOE & Cie GmbH: Darmstadt, Germany, **2011**.

[5] a) TURBOMOLE V7.2 2017, a development of University of Karlsruhe and Forschungszentrum Karlsruhe GmbH, 1989-2007, TURBOMOLE GmbH, since 2007; available from www.turbomole.com; b) R. Ahlrichs, M. Bär, M. Häser, H. Horn, C. Kölmel, *Chem. Phys. Lett.* **1989**, *62*, 165–169.

[6] a) J. P. Perdew, K. Burke, M. Ernzerhof, *Phys. Rev. Lett.* **1996**, *77*, 3865–3868; b) [PBE0] C. Adamo, V. *J.* Barone, *Chem. Phys.* **1999**, *110*, 6158–6170; c) F. Weigend, R. Ahlrichs, *Phys. Chem. Chem. Phys.* **2005**, *7*, 3297-3305.

[7] a) K. Eichkorn, O. Treutler, H.Öhm, M.Häser, R. Ahlrichs, *Chem. Phys. Lett.* **1995**, *240*, 283-290; b) F. Weigend, *Phys. Chem. Chem. Phys.* **2006**, *8*, 1057-1065.

[8] A. Klamt, G. Schüürmann, *J. Chem. Soc. Perkin Trans.2* **1993**, *5*, 799–805.

[9] D. Rappoport, F. Furche, *J. Chem. Phys.* **2007**, 126, 201104.

[10] F. Furche, R. Ahlrichs, *J. Chem. Phys.* **2002**, *117*, 7433.

[11] a) R. Dovesi, R. Orlando, A. Erba, C. M. Zicovich-Wilson, B. Civalleri, S. Casassa, L. Maschio, M. Ferrabone, M. De La Pierre, P. D'Arco, Y. Noel, M. Causa, M. Rerat, B. Kirtman. *Int. J. Quantum Chem.* **2014**, *114*, 1287–1317; b) R. Dovesi, V. R. Saunders, C. Roetti, R. Orlando, C. M. Zicovich-Wilson, F. Pascale, B. Civalleri, K. Doll, N. M. Harrison, I. J. Bush, P. D'Arco, M. Llunell, M. Causà, Y. Noël *CRYSTAL14 User's Manual* (University of Torino, Torino, 2014).

[12] A. J. Karttunen, T. F. Fässler, M. Linnolahti, T. A. Pakkanen, *Inorg. Chem.* **2011**, *50*, 1733–1742.

[13] H. J. Monkhorst, J. D. Pack, *Phys. Rev. B* **1976***, 13*, 5188–5192.

[14] a) F. Pascale, C. M. Zicovich-Wilson, F. Lopez, B. Civalleri, R. Orlando, R. Dovesi, *J. Comput. Chem.* **2004**, *25*, 888–897; b) C. M. Zicovich-Wilson, F.Pascale,; C.Roetti, V. R.Saunders, R.Orlando, R. *J.* Dovesi, *Comput. Chem.* **2004**, *25*, 1873–1881; c) L. Maschio, B. Kirtman, M. Rerat, R. Orlando, R. Dovesi, *J.*

Chem. Phys. **2013**, 139, 161101; d) L. Maschio, B. Kirtman, M. Rerat, R. Orlando, R. Dovesi, *J. Chem. Phys.* **2013**, 139, 161102.

[15] J.P. Merrick, D. Moran, L. Radom, *J. Phys. Chem. A*, **2007**, *111*, 11683–11700.

[16] a) CFOUR, Coupled-Cluster techniques for Computational Chemistry, a quantum-chemical program package by J. F. Stanton, J. Gauss, L. Cheng, M. E. Harding, D. A. Matthews, P. G. Szalay with contributions from A. A. Auer, R. J. Bartlett, U. Benedikt, C. Berger, D. E. Bernholdt, Y. J. Bomble, O. Christiansen, F. Engel, R. Faber, M. Heckert, O. Heun, M. Hilgenberg, C. Huber, T.-C. Jagau, D. Jonsson, J. Jusélius, T. Kirsch, K. Klein, W. J. Lauderdale, F. Lipparini, T. Metzroth, L. A. Mück, D. P. O'Neill, D. R. Price, E. Prochnow, C. Puzzarini, K. Ruud, F. Schiffmann, W. Schwalbach, C. Simmons, S. Stopkowicz, A. Tajti, J. Vázquez, F. Wang, J. D. Watts and the integral packages MOLECULE (J. Almlöf and P. R. Taylor), PROPS (P. R. Taylor), ABACUS (T. Helgaker, H. J. Aa. Jensen, P. Jørgensen, and J. Olsen), and ECP routines by A. V. Mitin and C. van Wüllen. For the current version, see www.cfour.de; b) M. E. Harding, T. Metzroth, J. Gauss, A. A. Auer, *J. Chem. Theory Comput.* **2008,** *4,* 64–74.

[17] a) K. Raghavachari, G. W. Trucks, J. A. Pople and M. Head-Gordon, *Chem. Phys. Lett.* **1989**, *157*, 479–483; b) R. J. Bartlett, J. D. Watts, S. A. Kucharski, J. Noga, *Chem. Phys. Lett.* **1990**, *165*, 513–522; c) R. J. Bartlett, M. Musial, *Rev. Mod. Phys.*, **2007**, *79*, 291–352; d) D. E. Woon, T. H. Dunning Jr., *J. Chem. Phys.* **1993**, *98*, 1358.

[18] a) T. S. Pennanen, J. Vaara, P. Lantto, A. J. Sillanpää, K. Laasonen, J. Jokisaari, *J. Am. Chem. Soc.* **2004**, *126*, 11093-11102; b) J. Mareš, H. Liimatainen, T. O. Pennanen, J. Vaara, *J. Chem. Theory Comput.* **2011**, *7*, 3248-3260.

[19] a) S. J. Clark, M. D. Segall, C. J. Pickard, P. J. Hasnip, M. I. J. Probert, K. Refson, M. C. Payne, *Z. Kristallogr.* **2005**, *220*, 567–570; b) [GIPAW] a) C. J. Pickard, F. Mauri, *Phys. Rev. B* **2001**, *63*, 245101; b) J. R. Yates, C. J. Pickard, F. Mauri, *Phys. Rev. B* **2007**, *76*, 024401.

[20] D. Vanderbilt, *Phys. Rev. B* **1990**, *41*, 7892–7895.

6.6 Anionic Siliconoids from *Zintl* Phases: $R_3Si_9^-$ with Six and $R_2Si_9^{2-}$ with Seven Unsubstituted Exposed Silicon Cluster Atoms (R = Si(*t*Bu)$_2$H)

Lorenz J. Schiegerl, Antti J. Karttunen, Wilhelm Klein, and Thomas F. Fässler*

published in

Chem. Eur. J. 2018, *24* (72), 19171-19174.

Access online *via*: https://onlinelibrary.wiley.com/doi/full/10.1002/chem.201805442

Content and contributions:

Ambition of this work was the synthesis of anionic siliconoids with Si_9 clusters from the precursor $K_{12}Si_{17}$. The manuscript was authored by me within the course of this PhD Thesis and reviewed by *Prof. Antti Karttunen* and *Prof. Thomas Fässler* before its submission. *Prof. Antti Karttunen* did the computational studies and contributed concerning text passages in the Supporting Information. *Prof. Wolfgang Eisenreich* (TECHNICAL UNIVERSITY OF MUNICH) supported the ^{29}Si HMBC measurement. Submission of the manuscript was done by *Prof. Thomas Fässler*. Recording, evaluation and submission of the single crystal diffraction data were assisted by *Dr. Wilhelm Klein*. Elemental analyses were carried out in the microanalytical laboratory at the CATALYTIC RESEARCH CENTER of the TECHNICAL UNIVERSITY OF MUNICH. The EDX spectra were measured by Maria Müller (TECHNICAL UNIVERSITY OF MUNICH). The work was published within the framework of the WACKER INSTITUTE FOR SILICON CHEMISTRY (TECHNICAL UNIVERSITY OF MUNICH).

The anionic siliconoid $[(SiH^tBu_2)_3Si_9]^-$ was obtained as bulk material by reaction of $K_{12}Si_{17}$ (prior "*activation*" with 222crypt/NH_3) with SiH^tBu_2Cl as first ligand-stabilized Si_9 cluster from a precursor. Synthesis and characterization (NMR, ESI-MS, elemental analysis) were done by me. The di-anionic siliconoid species $[(SiH^tBu_2)_2Si_9]^{2-}$ was obtained as $[K\text{-}222crypt]^+$ salt by crystallization of $[(SiH^tBu_2)_3Si_9]^-$ containing bulk material. The single crystals were synthesized and characterized (EDX, SC-XRD) by me. Results were discussed in comparison with calculations including bond length determination, NMR shifts and partial atomic cluster charges in cooperation with *Prof. Antti Karttunen*.

ChemPubSoc Europe

DOI: 10.1002/chem.201805442

CHEMISTRY
A European Journal
Communication

Silicon

Anionic Siliconoids from Zintl Phases: $R_3Si_9^-$ with Six and $R_2Si_9^{2-}$ with Seven Unsubstituted Exposed Silicon Cluster Atoms ($R = Si(tBu)_2H$)

Lorenz J. Schiegerl,[a, b] Antti J. Karttunen,[c] Wilhelm Klein,[b] and Thomas F. Fässler*[a, b]

Abstract: Neutral and anionic silicon clusters (siliconoids) are regarded as important model systems for bulk silicon surfaces. For 25 years their formation from binary alkali metal silicide phases has been proposed, but experimentally never realized. Herein the silylation of a silicide, leading to the anionic siliconoids $(Si(tBu)_2H)_3Si_9^-$ (**1a**) and $(Si(tBu)_2H)_2Si_9^{2-}$ (**2a**) with the highest known number of ligand-free silicon atoms is reported for the first time. The new anions are obtained in a one-step reaction of $K_{12}Si_{17}$/NH_3(liq.) and $Si(tBu)_2HCl$/THF. Electrospray ionization spectrometry and ^1H, ^{13}C, ^{29}Si, as well as ^{29}Si-HMBC (heteronuclear multiple bond correlation) NMR spectroscopy, confirm the attachment of three silyl groups at a $[Si_9]^{4-}$ cluster under formation of **1a**, in accordance with calculated NMR shifts. During crystal growth the siliconoid di-anion **2a** is formed. The single-crystal X-ray structure determination reveals that two silyl groups are connected to the deltahedral Si_9 cluster core, revealing seven unsubstituted exposed silicon cluster atoms with a hemispheroidal coordination. The negative charges −1 and −2 are delocalized over the six and seven siliconoid Si atoms in **1a** and **2a**, respectively.

More than two decades ago, the synthesis of polyhedral Si compounds was regarded as one of the greatest challenge in molecular silicon chemistry.[1] Shortly after, Wiberg et al. reported in 1993 the synthesis and structural characterization of tetrakis(tri-*tert*-butylsilyl)-*tetrahedro*-tetrasilane R_4Si_4 ($R = tBu_3Si$) featuring a Si_4 tetrahedron, obtained by the reaction of RBr_2Si–$SiBr_2R$ with RNa.[2] In his contribution Wiberg also suggested that such compounds should more be straightforwardly accessible through the reaction of alkylhalides with tetrahedral Si_4^{4-} polyanions. Such polyanions are present in intermetallic compounds *A*Si (*A* = Li–Cs), accessible in a one-step reaction by fusion of the respective elements in quantitative yields.[3] The idea of using so-called Zintl ions as precursors for Si-rich molecules was supported by the synthesis of Sekiguchi's anionic species $R'_3Si_4^-$[4] (R′ = -SiMeDis$_2$, Dis = $CH(SiMe_3)_2$) in 2003 and was for more than two decades frequently considered, but repeatedly discarded due to the high reducing properties of silicides.[2,5] The development in the synthesis of molecules with low-valent Si atoms,[6] as well as with unsubstituted Si atoms,[5,7] triggered again the demand for faster synthetic routes towards compounds with a considerable number of Si–Si bonds and unsubstituted Si atoms. Therefore, application of silicon Zintl phases as precursors is of particular interest for the design of well-defined molecular silicon structures with a high number of exposed silicon atoms. According to a recent definition,[5] so-called siliconoids require at least one exposed cluster atom with a hemispheroidal coordination sphere, which forms bonds solely to adjacent Si clusters atoms. Consequently, such units display only homoatomic bonds and are free of ligands ("naked"). Such neutral and anionic silicon clusters (siliconoids) are regarded as important model systems for bulk silicon surfaces.

In 2011 our group showed that Si_4^{4-} Zintl clusters are accessible to chemical transformation from solid Zintl phases, for example, by reacting it with CuMes (Mes = 1,3,5-trimethylbenzene), thereby giving $(CuMes)_2Si_4^{4-}$,[8] whereas in 2016 Scheschkewitz et al. obtained LiR''_5Si_6 (R″ = 2,4,6-triisopropylphenyl) with one anionic and two neutral unsubstituted vertex atoms[9] by a "purely molecular" approach. However, an approach from Zintl phases with covalently bonded ligands was still missing.

In contrast, during the last decade the vinylation, silylation and phosphinylation of polyhedral germanium Zintl anions Ge_9^{4-} with different substituents has been demonstrated by using mainly the Zintl phase K_4Ge_9.[10] However, similar reactions of Si_9^{4-} clusters were not yet achieved due to the absence of the corresponding 4:9 phases. To date, A_4Si_4[3] (*A* = Li–Cs) and $A_{12}Si_{17}$[11] (*A* = K–Cs) phases that contain either solely Si_4^{4-} units, or Si_4^{4-} beside Si_9^{4-} deltahedral clusters in a 2:1 ratio, are known. Si_4^{4-} and Si_9^{4-} clusters are species which have nucleophilic character, due to their highly negative charge, but are also electrophilic in character due to the electron-deficient bonding situation of the cluster skeleton.[12] Since the A_4Si_4

[a] L. J. Schiegerl, Prof. Dr. T. F. Fässler
Department of Chemistry
Technical University of Munich (TUM)
Lichtenbergstraße 4, 85748 Garching (Germany)
E-mail: Thomas.faessler@lrz.tum.de

[b] L. J. Schiegerl, Dr. W. Klein, Prof. Dr. T. F. Fässler
WACKER Institute of Silicon Chemistry
Technical University of Munich (TUM)
Lichtenbergstraße 4, 85748 Garching (Germany)

[c] Prof. Dr. A. J. Karttunen
Department of Chemistry and Materials Science
Aalto University, 00076 Aalto (Finland)

Supporting information and the ORCID identification number(s) for the author(s) of this article can be found under:
https://doi.org/10.1002/chem.201805442.

phases are rather insoluble in any solvent, the focus was put on the $A_{12}Si_{17}$ phases that are sufficiently soluble in liquid ammonia. Crystal structures of solvates containing Si_4^{4-} [13] and Si_9^{4-} [14] units have been obtained, and subsequent reactions in liquid ammonia as solvent led to the formation of $(PhZn)Si_9^{3-}$,[15] $(\{Ni(CO)_2\}_2Si_9)_2^{8-}$,[16] and $(NHC^{Dipp}Cu)Si_9^{3-}$ (Dipp = 2,6-diisopropylphenyl).[17]

Recently, the mono-protonated cluster HSi_9^{3-} [18] was obtained upon the isolation of crystals of $A_{12}Si_{17}$ (A = K, Rb) from liquid ammonia with the help of sequestering agents. A transfer of the extraction products from liquid ammonia to pyridine yielded the doubly-protonated species $H_2Si_9^{2-}$.[19] A similar procedure allowed for the structural characterization of the iso-valence-electronic cluster with mixed tetrel elements $H_2Si_{9-x}Ge_x^{2-}$ ($x = 4.1$).[18a] Both, HSi_9^{3-} [18b] and $H_2Si_9^{2-}$,[19] were fully characterized by ^{1}H and ^{29}Si NMR spectroscopy in solution. The formation of well-defined solutions that contain nine-atom silicon clusters after activation with liquid ammonia finally paved the way for further conversions of these clusters in solution with appropriate reactants. Theoretical studies support the formation of siliconoids by the attachment of sp^3-Si linkers,[20] and triggered us to investigate the reactivity of Si_9^{4-} clusters obtained from $K_{12}Si_{17}$ and chloro-silanes with the ambition to synthesize larger siliconoid units. The experimental results are supported by computational methods (DFT-PBE0/TZVP level of theory).[21]

In analogy to our recent synthesis of $H_2Si_9^{2-}$,[19] we dissolved $K_{12}Si_{17}$/222crypt (222crypt = 4,7,13,16,21,24-hexaoxa-1,10-diazabicyclo[8.8.8]hexacosane) in liquid ammonia. After removal of the solvent the brown residue was treated with THF under continuous cooling in an ice bath, and a pre-cooled solution of Si(tBu$_2$)HCl in THF was added. After several hours the initially heterogenous reaction mixture gave a red-brown solution, from which a brown solid was obtained after removal of all volatiles and washing with hexane. ESI-MS investigations of the solid in THF solution indicated the presence of $(Si(tBu)_2H)_3Si_9^-$ (**1 a**) as the only product species (Figure 1 a). ESI-MS fragmentation experiments confirmed the groups in **1 a** (full ESI-MS and the ESI-MS fragmentation spectra are shown in the Supporting Information).

^{1}H and ^{13}C NMR spectra of the brown solid dissolved in THF-d_8 exclusively show one set of signals for (K-222crypt) and the Si(tBu)$_2$H groups (Figure 1 c, full NMR spectra in the Supporting Information). The integrals of the peaks in the ^{1}H NMR spectra reveal a ratio of 1:3 as expected for the composition of (K-222crypt)$(Si(tBu)_2H)_3Si_9$ (**1**). This composition is supported by an elemental analysis (C, H, N) of the solid that forms in 36% yield.

The ^{29}Si NMR spectrum of **1 a** shows three resonances at 18.00 (α), −175.16 (β) and −358.81 ppm (γ) which are in considerably good agreement with the calculated values of 21, −184 and −385 ppm, respectively for an optimized structure of **1 a** with D_{3h} symmetric cluster core (Figure 1 c, NMR calculation details in the Supporting Information). All ^{1}H and ^{13}C NMR chemical shifts were allocated by the quantum chemical shift calculations to the atoms as labeled in Figure 1 b. The ^{29}Si NMR resonance at 18.00 ppm is attributed to the three equivalent

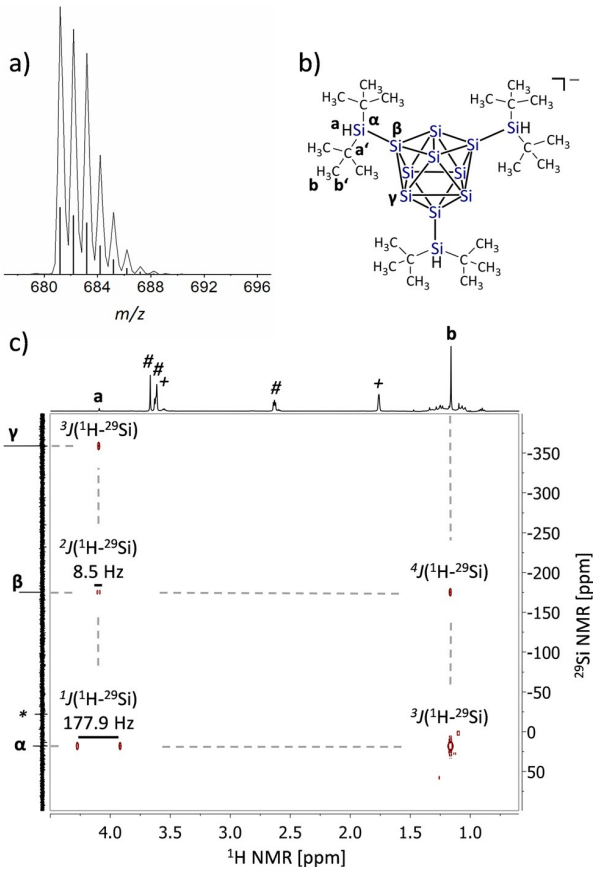

Figure 1. a) ESI-MS spectrum of $(Si(tBu)_2H)_3Si_9^-$ (**1 a**) (m/z = 683; line: measured spectra, bars: simulated isotope distribution); b) atom labelling of the anionic siliconoid **1 a**; c) ^{29}Si HMBC (Heteronuclear Multiple Bond Correlation) NMR spectrum of **1 a** in THF-d_8 (vertical axis: ^{29}Si NMR; horizontal axis: ^{1}H NMR; #: 222crypt; +: THF-d_8; *: silicon grease).

Si(tBu)$_2$H groups, whereas the strongly high-field shifted signals at −175.16 and −358.81 ppm arise from the three substituted and six unsubstituted Si vertex atoms in the Si_9 polyhedron, respectively. The experimental ^{29}Si NMR signal γ (−358.81 ppm) of the unsubstituted vertex atoms shows a stronger upfield shift, as usually observed for prominent siliconoid species,[5] and is comparable to the signals for the protonated Si_9 cluster species HSi_9^{3-} [18b] (unsubstituted vertex atoms: −359 ppm) and to the experimental and calculated ^{29}Si NMR average values for $H_2Si_9^{2-}$ [19] (exp.: −346 ppm; calcd: −348 ppm).

Since the ligand carries H atoms with different bond separations to the Si atoms of the cluster, a two-dimensional ^{29}Si heteronuclear multiple bond correlation (HMBC) NMR spectrum was used to establish the structure of **1 a** (Figure 1 c). Analysis of the cross peaks reveals a strong coupling between the ^{1}H NMR resonance a (Si*H*) and the ^{29}Si NMR resonance α (*Si*H) with a $^1J(^1H-^{29}Si) = 177.9$ Hz scalar coupling constant. A cross peak is also observed for α with the ^{29}Si NMR resonance β (silyl-substituted Si vertex atoms) with a decisively smaller scalar coupling of $^2J(^1H-^{29}Si) = 8.5$ Hz. The detected ^1J and ^2J coupling constants are comparable to the ones in $H_2Si_5(Mes)_6$ [22] with ^1J and ^2J values of 207 and 5.5 Hz, respec-

tively. No signal splitting is observed for the $^{3}J(^{1}H\text{-}^{29}Si)$ cross peak of a and γ. Cross peaks are also observed for the proton signal b with the silicon signals α and β, but again no $^{3}J(^{1}H\text{-}^{29}Si)$ and $^{4}J(^{1}H\text{-}^{29}Si)$ signal splitting is observed. Moreover, no cross peak is observed between b and γ which would correspond to a $^{5}J(^{1}H\text{-}^{29}Si)$ coupling. Ligand scrambling as observed for $R'_3Si_4^{-}$ [4] cannot be excluded for **1a**. A fast exchange of the ligands as well as the D_{3h} symmetry of **1a** will both lead to the same number of signals in the NMR spectrum. No NMR-line broadening was observed by decreasing the temperature to −20 °C.

Crystallization experiments of **1** from fluorobenzene solutions led to the formation of small amounts of orange needle-shaped crystals, suitable for single-crystal X-ray diffraction (crystallographic details are given in the Supporting Information). The structure determination, however, reveals the composition $(K\text{-}222crypt)_2(Si(tBu)_2H)_2Si_9$ (**2**) with only two silyl groups attached at the Si_9 cluster core. An Si:K ratio of 9:2 is confirmed by an EDX analysis of the single crystals. A fragmentation product in the ESI spectrum (see Supporting Information) also matches with $(Si(tBu)_2H)_2Si_9^{2-}$ (**2a**). A similar transformation of a tris- to a bis-silylated cluster upon the crystallization process has also been detected for $(Si(iBu)_3)_3Ge_9^{-}$.[23] The molecular structure of the di-anion **2a** (Figure 2) shows a C_{2v} symmetric cluster that derives from a mono-capped square antiprism. The silyl groups are bonded to two opposing vertex atoms of the open face of the polyhedron. The shortest Si–Si distance occurs between the Si atoms of the cluster atoms to the *exo*-bonded atoms [Si1–Si10: 2.349(2) Å and Si3–Si11: 2.379(2) Å]. However, all bonds between silicon framework atoms and the atoms that carry the silyl groups (Si1 and Si2) are shortened and lie in the narrow range between 2.405(2) and 2.445(2) Å. In contrast are the two bonds Si5–Si6 and Si7–Si8, of which the bond vector lies perpendicular to the external Si–Si bond, elongated [2.782(2) and 2.764(2) Å, respectively]. The remaining multicenter bonds are also elongated with respect to the localized covalent bonds and are found in the range 2.429–2.534 Å. Polyhedral edges of the unsubstituted Si_9^{4-} cluster are overall longer [2.423(4) to 2.881(4) Å].[14a] Longer Si5–Si6 and Si7–Si8 distances compares well to the distances between the unsubstituted bridgehead atoms in the siliconoids $[Li\text{-}(12crown4)_2](Tip)_5Si_5$[9] (Tip = 2,4,6-triisopropylphenyl) with 2.5506(9) Å, $(Tip)_6Si_5$[24] with 2.7076(8) Å, and $(Mes)_6Si_5$[22] with a corresponding bond length of 2.636(1) Å.

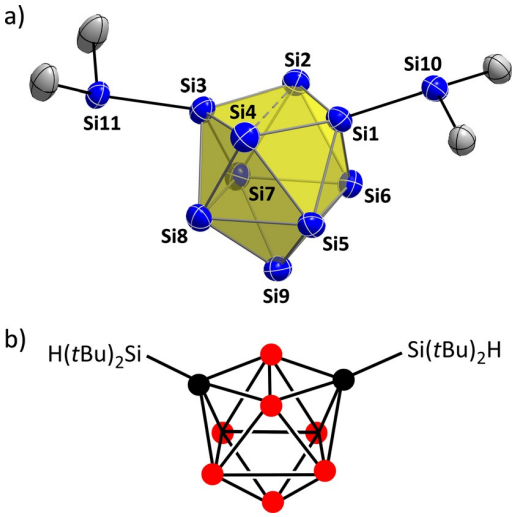

Figure 2. a) Molecular structure of the siliconoid anion $(Si(tBu)_2H)_2Si_9^{2-}$ (**2a**). Si and C atoms (blue and grey, respectively) are shown as ellipsoids at a 50% probability level; CH_3 groups and H_{Si} atoms are omitted for the reason of clarity. The disorder of one silyl group is shown in the Supporting Information; b) Schematic view of **2a** with emphasis on the seven unsubstituted exposed silicon cluster atoms with a hemispheroidal coordination shown in red.

DFT calculations and structure optimization reveal that the structures **1a** and **2a** represent minima in energy. All calculated distances of **2a** show an almost perfect match with the measured values after structure optimization (Si–Si distances and partial atom charges of **1a** and **2a** are given in the Supporting Information). Calculation of the partial atom charges reveals that in **1a** the extra negative charge is almost equally delocalized over the six siliconoid atoms (partial charge −0.13 e^- for each atom), whereas in **2a**, the two negative charges distribute over the seven siliconoid atoms Si2, Si4 (−0.33 e^- each), Si5–Si8 (−0.23 e^- each), and the square-capping atom Si9—that carries the third ligand in **1a**—having a slightly higher value (−0.37 e^-). Intrinsic bond orbital (IBO) analysis of the Si–Si bonding shows clear differences between the intracluster bonds (delocalized multicenter bonds) and *exo*-bonds (localized two-center two-electron bonds) (see Supporting Information).

Opening of a novel and relatively simple synthetic protocol to siliconoid clusters will allow for a faster development of the field. The formation of six and seven unsubstituted vertex atoms with hemispheroidal coordination, which requires a multi-step synthesis through the molecular approach, is achieved in one-step synthesis from the activated Zintl phase $K_{12}Si_{17}$. The binary phase itself is obtained by simply melting together the elements. The synthetic route is not restricted to the examples shown here, and we will report on the introduction of other ligands in a forthcoming paper. Moreover, we foresee that the manifold chemistry known for Ge_9 clusters might now be transferred to Si_9.

Acknowledgements

The authors are thankful for the financial support by Wacker Chemie AG and Deutsche Forschungsgemeinschaft (DFG, FA 198/14-1). Further, they thank Prof. Dr. Wolfgang Eisenreich for supporting the ^{29}Si NMR measurements, Maria Müller for the EDX analyses, and Ulrike Ammari for the elemental analyses. A.J.K thanks the Finnish IT Center for Science (CSC) for computational resources.

Conflict of interest

The authors declare no conflict of interest.

Keywords: cluster compounds · functionalization · quantum chemical calculations · silicon · siliconoids · synthesis

[1] T. Tsumuraya, S. A. Batcheller, S. Masamune, *Angew. Chem. Int. Ed. Engl.* **1991**, *30*, 902 – 930; *Angew. Chem.* **1991**, *103*, 916 – 944.

[2] N. Wiberg, C. M. M. Finger, K. Polborn, *Angew. Chem. Int. Ed. Engl.* **1993**, *32*, 1054 – 1056; *Angew. Chem.* **1993**, *105*, 1140 – 1142.

[3] a) T. Goebel, A. Ormeci, O. Pecher, F. Haarmann, *Z. Anorg. Allg. Chem.* **2012**, *638*, 1437 – 1445; b) H. G. von Schnering, M. Schwarz, J. H. Chang, K. Peters, E. M. Peters, R. Nesper, *Z. Kristallogr. - New Cryst. Struct.* **2005**, *220*, 525 – 527; c) L. A. Stearns, J. Gryko, J. Diefenbacher, G. K. Ramachandran, P. F. McMillan, *J. Solid State Chem.* **2003**, *173*, 251 – 258; d) J. He, D. D. Klug, K. Uehara, K. F. Preston, C. I. Ratcliffe, J. S. Tse, *J. Phys. Chem. B* **2001**, *105*, 3475 – 3485.

[4] M. Ichinohe, M. Toyoshima, R. Kinjo, A. Sekiguchi, *J. Am. Chem. Soc.* **2003**, *125*, 13328 – 13329.

[5] Y. Heider, D. Scheschkewitz, *Dalton Trans.* **2018**, *47*, 7104 – 7112.

[6] a) Y. Wang, Y. Xie, P. Wei, R. B. King, H. F. Schaefer, P. v. R. Schleyer, G. H. Robinson, *Science* **2008**, *321*, 1069 – 1071; b) Y. Wang, G. H. Robinson, *Dalton Trans.* **2012**, *41*, 337 – 345; c) C. D. Martin, M. Soleilhavoup, G. Bertrand, *Chem. Sci.* **2013**, *4*, 3020 – 3030; d) E. Rivard, *Struct. Bonding* **2014**, *156*, 203; e) K. C. Mondal, S. Roy, B. Dittrich, D. M. Andrada, G. Frenking, H. W. Roesky, *Angew. Chem. Int. Ed.* **2016**, *55*, 3158 – 3161; *Angew. Chem.* **2016**, *128*, 3210 – 3213.

[7] a) K. Abersfelder, A. J. P. White, H. S. Rzepa, D. Scheschkewitz, *Science* **2010**, *327*, 564 – 566; b) G. Fischer, V. Huch, P. Mayer, S. K. Vasisht, M. Veith, N. Wiberg, *Angew. Chem. Int. Ed.* **2005**, *44*, 7884 – 7887; *Angew. Chem.* **2005**, *117*, 8096 – 8099; c) S. Ishida, K. Otsuka, Y. Toma, S. Kyushin, *Angew. Chem. Int. Ed.* **2013**, *52*, 2507 – 2510; *Angew. Chem.* **2013**, *125*, 2567 – 2570.

[8] M. Waibel, F. Kraus, S. Scharfe, B. Wahl, T. F. Fässler, *Angew. Chem. Int. Ed.* **2010**, *49*, 6611 – 6615; *Angew. Chem.* **2010**, *122*, 6761 – 6765.

[9] P. Willmes, K. Leszczyńska, Y. Heider, K. Abersfelder, M. Zimmer, V. Huch, D. Scheschkewitz, *Angew. Chem. Int. Ed.* **2016**, *55*, 2907 – 2910; *Angew. Chem.* **2016**, *128*, 2959 – 2963.

[10] a) M. W. Hull, S. C. Sevov, *Angew. Chem. Int. Ed.* **2007**, *46*, 6695 – 6698; *Angew. Chem.* **2007**, *119*, 6815 – 6818; b) F. Li, S. C. Sevov, *Inorg. Chem.* **2012**, *51*, 2706 – 2708; c) F. S. Geitner, J. V. Dums, T. F. Fässler, *J. Am. Chem. Soc.* **2017**, *139*, 11933 – 11940; d) F. S. Geitner, W. Klein, T. F. Fässler, *Angew. Chem. Int. Ed.* **2018**, *57*, 14509 – 14513; *Angew. Chem.* **2018**, *130*, 14717 – 14721.

[11] a) V. Quéneau, E. Todorov, S. C. Sevov, *J. Am. Chem. Soc.* **1998**, *120*, 3263 – 3264; b) C. Hoch, M. Wendorff, C. Röhr, *J. Alloys Compd.* **2003**, *361*, 206 – 221.

[12] a) K. Wade, *Inorg. Nucl. Chem. Lett.* **1972**, *8*, 559 – 562; b) K. Wade, *J. Chem. Soc. D* **1971**, 792 – 793.

[13] C. Lorenz, S. Gärtner, N. Korber, *Z. Anorg. Allg. Chem.* **2017**, *643*, 141 – 145.

[14] a) S. Joseph, C. Suchentrunk, F. Kraus, N. Korber, *Eur. J. Inorg. Chem.* **2009**, 4641 – 4647; b) C. B. Benda, T. Henneberger, W. Klein, T. F. Fässler, *Z. Anorg. Allg. Chem.* **2017**, *643*, 146 – 148.

[15] J. M. Goicoechea, S. C. Sevov, *Organometallics* **2006**, *25*, 4530 – 4536.

[16] S. Joseph, M. Hamberger, F. Mutzbauer, O. Härtl, M. Meier, N. Korber, *Angew. Chem. Int. Ed.* **2009**, *48*, 8770 – 8772; *Angew. Chem.* **2009**, *121*, 8926 – 8929.

[17] F. S. Geitner, T. F. Fässler, *Chem. Commun.* **2017**, *53*, 12974 – 12977.

[18] a) T. Henneberger, W. Klein, T. F. Fässler, *Z. Anorg. Allg. Chem.* **2018**, *644*, 1018 – 1027; b) C. Lorenz, F. Hastreiter, J. Hioe, L. Nanjundappa, S. Gärtner, N. Korber, R. M. Gschwind, *Angew. Chem. Int. Ed.* **2018**, *57*, 12956 – 12960; *Angew. Chem.* **2018**, *130*, 13138 – 11314.

[19] L. J. Schiegerl, A. J. Karttunen, J. Tillmann, S. Geier, G. Raudaschl-Sieber, M. Waibel, T. F. Fässler, *Angew. Chem. Int. Ed.* **2018**, *57*, 12950 – 12955; *Angew. Chem.* **2018**, *130*, 13132 – 13137.

[20] L.-A. Jantke, T. Fässler, *Inorganics* **2018**, *6*, 31.

[21] a) TURBOMOLE V7.3 2017, a development of University of Karlsruhe and Forschungszentrum Karlsruhe GmbH, 1989 – 2007, TURBOMOLE GmbH, since **2007**; b) R. Ahlrichs, M. Bär, M. Häser, H. Horn, C. Kölmel, *Chem. Phys. Lett.* **1989**, *162*, 165 – 169; c) J. P. Perdew, K. Burke, M. Ernzerhof, *Phys. Rev. Lett.* **1996**, *77*, 3865 – 3868; d) C. Adamo, V. J. Barone, *J. Chem. Phys.* **1999**, *110*, 6158 – 6170; e) F. Weigend, R. Ahlrichs, *Phys. Chem. Chem. Phys.* **2005**, *7*, 3297 – 3305.

[22] D. Nied, R. Köppe, W. Klopper, H. Schnöckel, F. Breher, *J. Am. Chem. Soc.* **2010**, *132*, 10264 – 10265.

[23] L. J. Schiegerl, F. S. Geitner, C. Fischer, W. Klein, T. F. Fässler, *Z. Anorg. Allg. Chem.* **2016**, *642*, 1419 – 1426.

[24] K. Abersfelder, A. J. P. White, R. J. F. Berger, H. S. Rzepa, D. Scheschkewitz, *Angew. Chem. Int. Ed.* **2011**, *50*, 7936 – 7939; *Angew. Chem.* **2011**, *123*, 8082 – 8086.

Manuscript received: October 30, 2018
Accepted manuscript online: November 4, 2018
Version of record online: December 11, 2018

CHEMISTRY
A European Journal

Supporting Information

Anionic Siliconoids from Zintl Phases: $R_3Si_9^-$ with Six and $R_2Si_9^{2-}$ with Seven Unsubstituted Exposed Silicon Cluster Atoms ($R = Si(tBu)_2H$)

Lorenz J. Schiegerl,[a, b] Antti J. Karttunen,[c] Wilhelm Klein,[b] and Thomas F. Fässler*[a, b]

chem_201805442_sm_miscellaneous_information.pdf

SUPPORTING INFORMATION

Table of Contents

Experimental Section

General: All reactions and manipulations were performed under a purified argon atmosphere using standard Schlenk and glove box techniques. thf (HPLC grade) was dried over a special drying material in a solvent purificator (MBraun MB-SPS), fluorobenzene was dried over CaH_2 prior to usage. 222crypt was dried *in vacuo* prior to usage. Liquid ammonia was dried and stored over sodium metal prior to usage, all other solvents (including deuterated solvents) were stored over molecular sieves (3 Å) prior to usage. All other chemicals were received commercially and used without further purification.

Synthesis of $K_{12}Si_{17}$: The Zintl compound $K_{12}Si_{17}$ is synthesized by heating (heating rate: 2 °C/min) a stochiometric mixture of 0.55 g (14.0 mmol, 1 eq.) K and 0.59 g (21.1 mmol, 1.5 eq.) Si to 800 °C in a sealed tantalum ampoule for 15 h and subsequent cooling (cooling rate: 0.5 °C/min) to room temperature. The ampoule is opened in a glove box, and the product is finely ground yielding 1.04 g (1.10 mmol, 94%) $K_{12}Si_{17}$ as a black solid. The solid is characterized by powder X-ray diffraction showing high purity for the solid phase (see Figure SI 9).

Synthesis of $K_{12}Si_{17}$ (*activated*): 0.20 g (0.21 mol, 1 eq.) $K_{12}Si_{17}$ and 0.15 g (0.39 mol, 1.9 eq.) 222crypt {4,7,13,16,21,24-hexaoxa-1,10-diazabicyclo[8.8.8]hexacosan} are weighed into a Schlenk tube and liquid ammonia (6 ml) is added at −78 °C (*i*PrOH/CO_2) resulting in a dark red solution. The mixture is stirred at −78 °C for 2 h, and $K_{12}Si_{17}$ *activated* is obtained as a brown solid after removal of the liquid ammonia.

Synthesis of (K-222crypt)(Si(*t*Bu)$_2$H)$_3$Si$_9$ (1): $K_{12}Si_{17}$ (*activated*) (batch with 200 mg $K_{12}Si_{17}$) is cooled to 0 °C (ice bath) and thf (10 ml) is added. 0.23 g (1.26 mol, 6 eq.) Si(*t*Bu)$_2$HCl are added under continuous stirring as pre-cooled thf solution (3 ml). The reaction mixture is stirred overnight and allowed to warm to room temperature. A red solution is obtained after filtration yielding a brown solid after removal of the volatiles. After washing with hexane (20 ml) a brown solid remains (yield, calcd. for the composition of **1**: 83.4 mg, 75.9 mmol, 36%). The solid is characterized by ESI-MS in thf, NMR (^{1}H, ^{13}C, ^{29}Si, ^{29}Si HMBC) in thf-*d8*, and elemental analysis (C, H, N): ^{1}H NMR (500 MHz, thf-*d8*) *δ* 4.06 (s, 1H, Si*H*, a), 3.63 (s, 12H, O-C*H*2-C*H*2-$O_{222crypt}$), 3.59 (t, *J* = 4.79 Hz, 12H, O-C*H*2-CH2-$N_{222crypt}$), 2.60 (t, 12H, *J* = 4.61 Hz, O-CH2-C*H*2-$N_{222crypt}$), 1.13 (s, 54H, C(C*H*$_3$)3, b); ^{13}C NMR (101 MHz, thf-*d8*) *δ* 71.45 (O-*C*H2-*C*H2-$O_{222crypt}$), 68.63 (O-*C*H2-CH2-$N_{222crypt}$), 54.98 (O-CH2-*C*H2-$N_{222crypt}$), 31.67 (*C*H$_3$, a'), 25.37 (*C*(CH$_3$)$_3$, b'); ^{29}Si NMR (99 MHz, thf-*d8*) *δ* 18.00 (*Si*(*t*Bu)$_2$H, α), −175.16 (*Si*-Si(*t*Bu)$_2$H, β), −358.81 (*Si*-Si-Si(*t*Bu)$_2$H, γ); ESI-MS (negative mode, 4500 V, 300 °C): *m/z* = 683 {(Si(*t*Bu)$_2$H)$_3$Si$_9$}$^-$; Elemental analysis C 46.87% (*calcd.*: 45.93% for **1**), H 8.77 (*calcd.*: 8.54% for **1**), N 2.75% (*calcd.*: 2.55% for **1**).

Synthesis of (K-222crypt)$_2$(Si(*t*Bu)$_2$H)$_2$Si$_9$ (2): For crystallization, **1** is dissolved in fluorobenzene (2 ml) and overlayered with hexane (3 ml). A small amount of orange needle-shaped crystals, suitable for single crystal X-ray diffraction, is obtained after 7 days and reveals the compound **2**. The K:Si ratio single crystals is confirmed by EDX analysis: EDX analysis (single crystal): Si : K = 79.9% : 20.1% (*calcd.*: 79.8% : 20.2% for **2**).

Single-crystal Structure Determination: For single crystal data collection, the crystals were fixed on a glass capillary and positioned in a cold stream of N_2 gas. Single crystal data collection was performed at a STOE StadiVari (Mo *Kα* radiation) diffractometer equipped with a DECTRIS PILATUS 300K detector**.** Structures were solved by Direct Methods (SHELXS-2014) and refined by full-matrix least-squares calculations against F^2 (SHELXL-2014).[1] The positions of the hydrogen atoms were calculated and refined using a riding model. Unless

otherwise stated, all non-hydrogen atoms were treated with anisotropic displacement parameters. The crystallographic data of **2** has been deposited with the Cambridge Structural Database and is available free of charge via www.ccdc.cam.ac.uk/data_request/cif on quoting the depository numbers CCDC 1863376. The crystal structures have been plotted with Diamond.[2] In **2**, one -Si(*t*Bu)$_2$H group is d orientationally disordered, the atoms were refined with one common occupation factor.

Electron Dispersive X-ray (EDX) Analysis: Single crystals of all compounds were analyzed with a SWIFT-ED-TM (Oxford Instruments) and a Hitachi TM-1000 Tabletop microscope (Hitachi High-Technologies) with the INCA system software.

NMR Spectroscopy: ^{1}H, ^{29}Si, and ^{29}Si HMBC NMR spectra were recorded on a Bruker AVIII 500 MHz Cryo system, the ^{13}C NMR spectrum on a Bruker AVIII Ultrashield 400 MHz. The signals of the ^{1}H and ^{13}C spectra were calibrated on the rest proton signal of the used deuterated solvent thf-*d8*. Chemical shifts are given in δ values by parts per million [ppm]. The coupling constants *J* are stated in Hz. Signal multiplicities are abbreviated as follows: s – singlet, t – triplet. The spectra were evaluated with MestReNova.[3]

Electrospray Ionization Mass Spectrometry (ESI-MS): The preparation of the samples was performed in a glove box. The measurements were performed on an HCT instrument (Bruker Corp.). Analysis of the data was carried out using the program Bruker Compass Data Analysis 4.0 SP 5 (Bruker Corp.). The dry gas temperature was adjusted to 300 °C and the injection speed to 240 $\mu L \cdot s^{-1}$. Visualization of the spectra was done with the programs *OriginPro 2017* (*Origin Lab Corp.*) and Excel 2016 (*Microsoft Corp.*).

Elemental Analysis: Elemental analyses were performed by the microanalytical laboratory at the Catalytic Research Center of the Technische Universität München. The elements C, H and N were determined with an Euro EA CHNS Elemental Analysator (*HEKAtech Ltd*).

Powder X-ray Diffraction (PXRD): The data was collected at room temperature on a STOE Stadi P diffractometer (Ge(111) monochromator, Cu Kα_1 radiation, λ = 1.54056 Å) with a Dectris MYTHEN 1K detector in Debye-Scherrer geometry. Samples were sealed in glass capillaries (Ø 0.5 mm) for the measurement. The raw data was processed with *WinX-POW*[4], *OriginPro 2017* (*Origin Lab Corp.*) was used for the visualization.

Computational Details

General: Quantum-chemical calculations on **1a** and **2a** were carried out using the TURBOMOLE program package.[5] We used PBE0 hybrid density functional method and a triple-zeta-valence quality basis set with polarization functions (def2-TZVP for Si, def-TZVP for C and H).[7] Multipole-accelerated resolution-of-the-identity technique was used to speed up the calculations.[8] The COSMO continuum solvation model was used to counter the twofold negative charge of the dianion **2a**.[9] The molecular structures of **1a** and **2a** were fully optimized within C_{3v} and C_{2v} point group symmetries, respectively. In the case of **1a**, the Si-tBu$_2$ groups can rotate in a solution and the ideal point group symmetry would be D_{3h}. However, in a 0 K calculation the C_{3v} subgroup had to be used. The optimized structures of the studied systems in XYZ format are reported below. The clusters were confirmed to be true local minima by means of harmonic frequency calculations. The final **2a** structure reported here is C_1-symmetric, slightly distorted from the ideal C_{2v} point group. An orientation, where the H(tBu$_2$)Si groups are rotated by 180° is only 7 kJ/mol less stable than the lower-energy conformation used here. The ^{29}Si, ^{13}C, and ^{1}H NMR chemical shifts are reported with respect to tetramethylsilane (SiMe$_4$) optimized at the same level of theory.[10] An important point in the comparison of experimental solution-state NMR shifts and the calculated DFT-PBE0 chemical shifts is the temperature: the calculated values are reported for 0 K without any solvent effects, while the experimental NMR spectra includes both solvent effects and averaging of the signals due to finite measurement temperature. The calculated NMR chemical shifts have been averaged in cases where a freely rotating group is fixed in the 0 K calculation or the ideal D_{3h} symmetry of **1a** is broken due to the use of C_{3v} subgroup. Intrinsic Atomic Orbitals (IAOs) and Intrinsic Bond Orbitals were used to analyze the partial charges and bonding of the clusters, respectively.[11] The plotted IBO iso-surfaces enclose 80% of the total electron density of the IBO.

Computational results: The optimized structure of **2a** is in good agreement with the experimental crystal structure determined by single-crystal XRD (Table SI 2). **1a** and **2a** show rather large HOMO–LUMO gaps of 4.2 eV and 4.4 eV, respectively. The partial atomic charges of **1a** and **2a** obtained from IAO analysis are listed in Table SI 3 and selected Intrinsic Bond Orbitals in **2a** are illustrated in Figure SI 10. The ^{29}Si, ^{13}C, and ^{1}H NMR chemical shifts of **1a** are well in line with the experimental chemical shifts (Table SI 4).

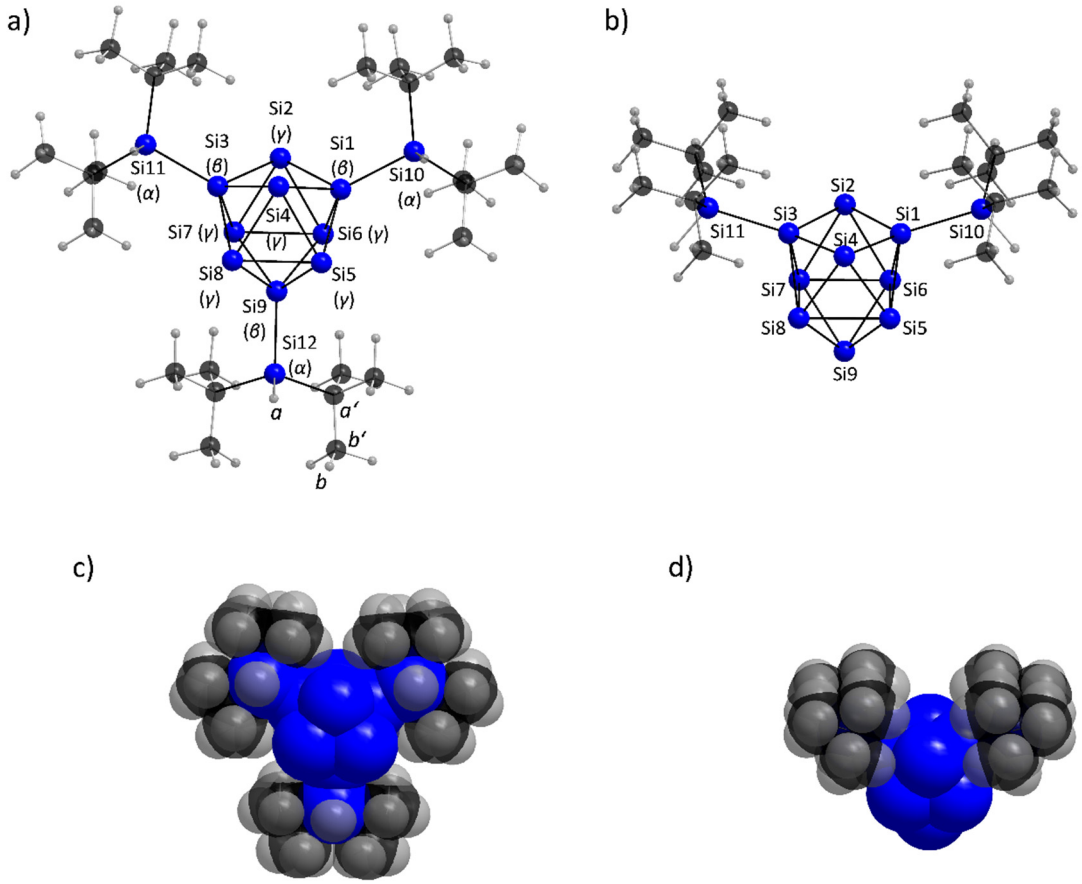

Figure SI 1. Visualization of the optimized structures from the computational studies: a) **1a**, atoms are shown as 'ball and stick model'; b) **2a**, atoms are shown as 'ball and stick model'; c) **1a**, atoms are shown as 'space-filling model'; d) **2a**, atoms are shown as 'space-filling model' (Si atoms in blue, C atoms in black, H atoms in gray; atom assignments as used within this publication).

SUPPORTING INFORMATION

Table SI 1. ^{29}Si, ^{13}C, and ^{1}H NMR chemical shifts of **1a** and **2a** at the DFT-PBE0/TZVP level of theory and the partial atomic charges of the Si atoms in **1a** and **2a** (Intrinsic Atomic Orbital charge analysis, atom labeling according to Figure SI 1).

Cluster	Atom	Partial Charge (e^-)	Calcd. [ppm]	Measd. [ppm]
1a	Si2, Si4, Si5, Si6, Si7, Si8 (γ)	–0.13	–385	−358.81
	Si1, Si3, Si9 (β)	–0.10	–184	−175.16
	Si10, Si11, Si12 (α)	+0.64	21	18.00
	Si*H* (a)	–0.13	4.7	4.06
	C(C*H*$_3$)$_3$ (b)	+0.13	1.0	1.13
	*C*H$_3$ (a')	–0.42	32.0	31.67
	C(CH$_3$)$_3$ (b')	–0.18	24.5	25.37
2a	Si1, Si3	–0.08	–228	
	Si2, Si4	–0.33	–451	
	Si5, Si6, Si7, Si8	–0.23	–339	
	Si9	–0.37	–389	
	Si10, Si11	+0.64	21	
	Si*H*	–0.15	4.2	
	C(C*H*$_3$)$_3$	+0.14	1.1	
	*C*H$_3$	–0.42	31.9	
	C(CH$_3$)$_3$	-0.18	24.4	

SUPPORTING INFORMATION

Table SI 2. Comparison of experimental X-Ray and DFT-PBE0/TZVP Si–Si distances in **1a** and **2a** (atom labeling according to Figure SI 1).

Si–Si Distance	in 1a Calcd. [Å]	in 2a Measd. [Å]	in 2a Calcd. [Å]
Si1–Si2	2.41	2.405(2)	2.41
Si1–Si4	2.41	2.423(2)	2.41
Si1–Si5	2.41	2.441(2)	2.42
Si1–Si6	2.41	2.423(2)	2.42
Si1–Si10	2.35	2.349(2)	2.37
Si2–Si3	2.41	2.418(2)	2.41
Si2–Si6	2.49	2.496(2)	2.48
Si2–Si7	2.49	2.473(2)	2.48
Si3–Si4	2.41	2.414(2)	2.41
Si3–Si7	2.41	2.427(2)	2.42
Si3–Si8	2.41	2.445(2)	2.42
Si3–Si11	2.35	2.379(2)	2.37
Si4–Si5	2.48	2.499(2)	2.48
Si4–Si8	2.48	2.498(2)	2.48
Si5–Si6	3.26	2.782(2)	2.73
Si5–Si8	2.48	2.534(2)	2.53
Si5–Si9	2.41	2.429(2)	2.44
Si6–Si7	2.49	2.534(2)	2.53
Si6–Si9	2.41	2.441(2)	2.44
Si7–Si8	3.26	2.764(2)	2.73
Si7–Si9	2.41	2.450(2)	2.44
Si8–Si9	2.41	2.447(2)	2.44
Si9–Si12	2.35		

Crystallographic details

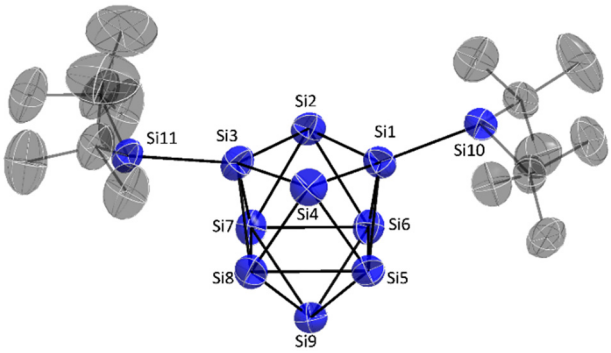

Figure SI 2. Molecular structure of **2a** in the single crystal X-ray structure of **2** [Si atoms (blue) and C atoms (gray) are shown as ellipsoids with 70% probability; H atoms are omitted; the lower occupation of the disordered silyl group is not shown].

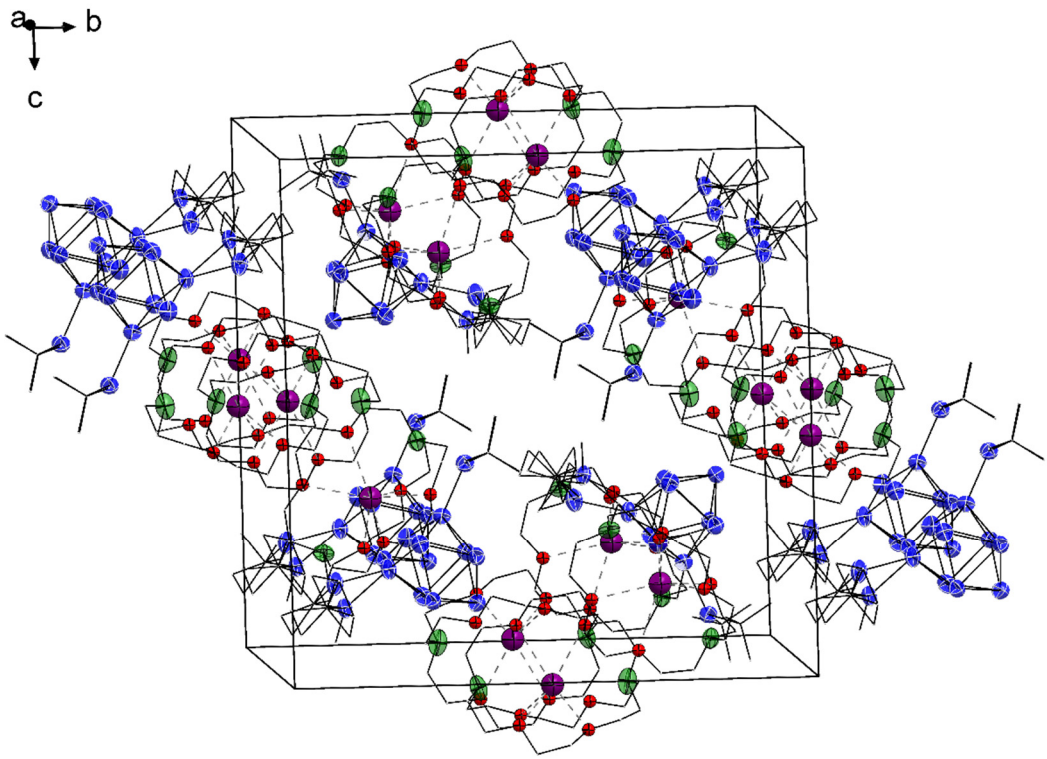

Figure SI 3. Unit cell of **2** [Si atoms (blue), K atoms (purple), O atoms (red), and N atoms (green) are shown as ellipsoids with 70% probability; C atoms are shown as wire/sticks; H atoms are omitted].

Table SI 3. Selected crystallographic data of the crystal structure of **2**.

Compound	**(K-222crypt)$_2$(Si(*t*Bu)$_2$H)$_2$Si$_9$ (2)**
formula	$C_{52}H_{110}K_2N_4O_{12}Si_{11}$
fw (g·mol^{-1})	1370.62
space group (no)	$P2_1/n$ (14)
***a* (Å)**	17.002(2)
***b* (Å)**	21.4346(18)
***c* (Å)**	21.542(3)
***α* (deg)**	90
***β* (deg)**	98.494(10)
***γ* (deg)**	90
***V* (Å^3)**	7764.6(15)
Z	4
***T* (K)**	150(2)
ρ_{calc} (g·cm^{-3})	1.172
***μ* (mm^{-1})**	0.342
measured reflections	105193
R_{int} / R_δ	0.1474 / 0.0902
***hkl* range**	$-20 < h < 20$ $-26 < k < 26$ $-26 < l < 26$
2 θ range	2.32 - 34.34
independent reflections	15244
reflections [$I > 2\,\sigma(I)$]	8260
parameters / restraints	818 / 74
R_1 [$I > 2\,\sigma(I)$ / all data]	0.0544 / 0.1233
wR_2 [$I > 2\,\sigma(I)$ / all data]	0.1186 / 0.1508
goodness of fit	0.927
largest difference peak/hole [e Å^{-3}]	0.579 / −0.376
CCDC number	1863376

NMR spectra

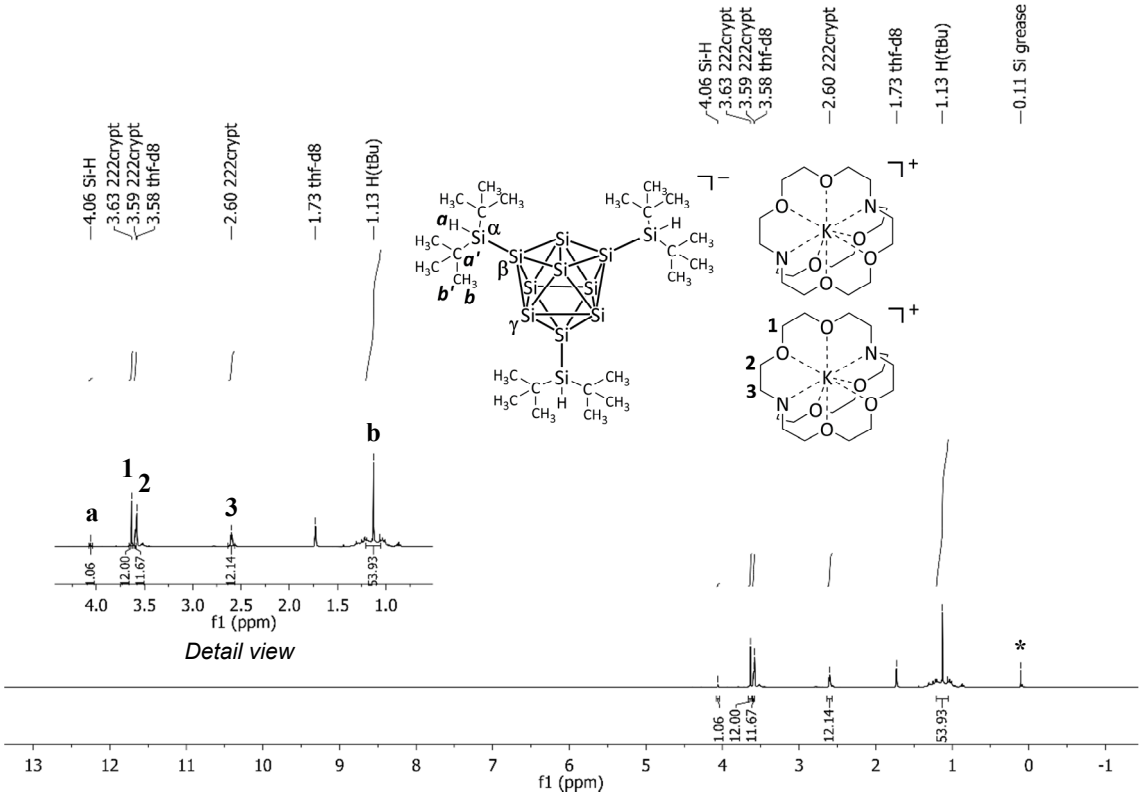

Figure SI 4. ^{1}H NMR (500 MHz, thf-*d8*) spectrum of the solid **1** (*: silicon grease).

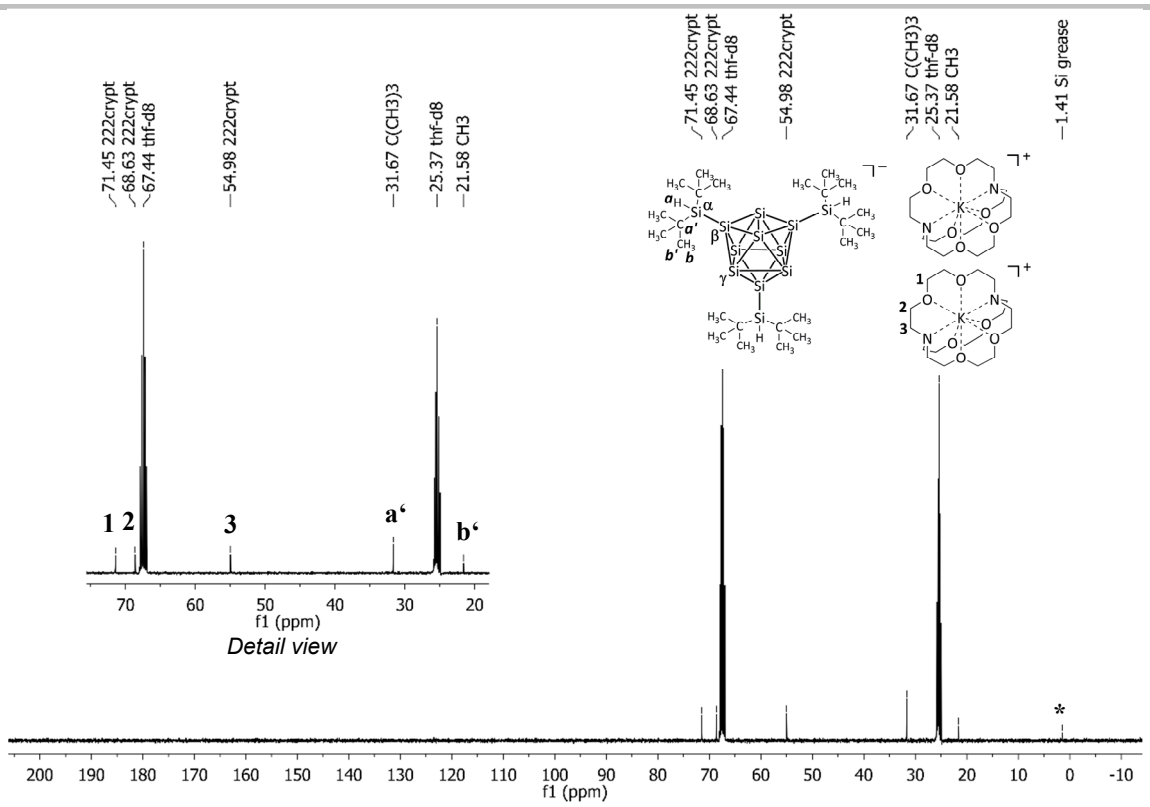

Figure SI 5. ^{13}C NMR (101 MHz, thf-*d8*) spectrum of the solid **1** (*: silicon grease).

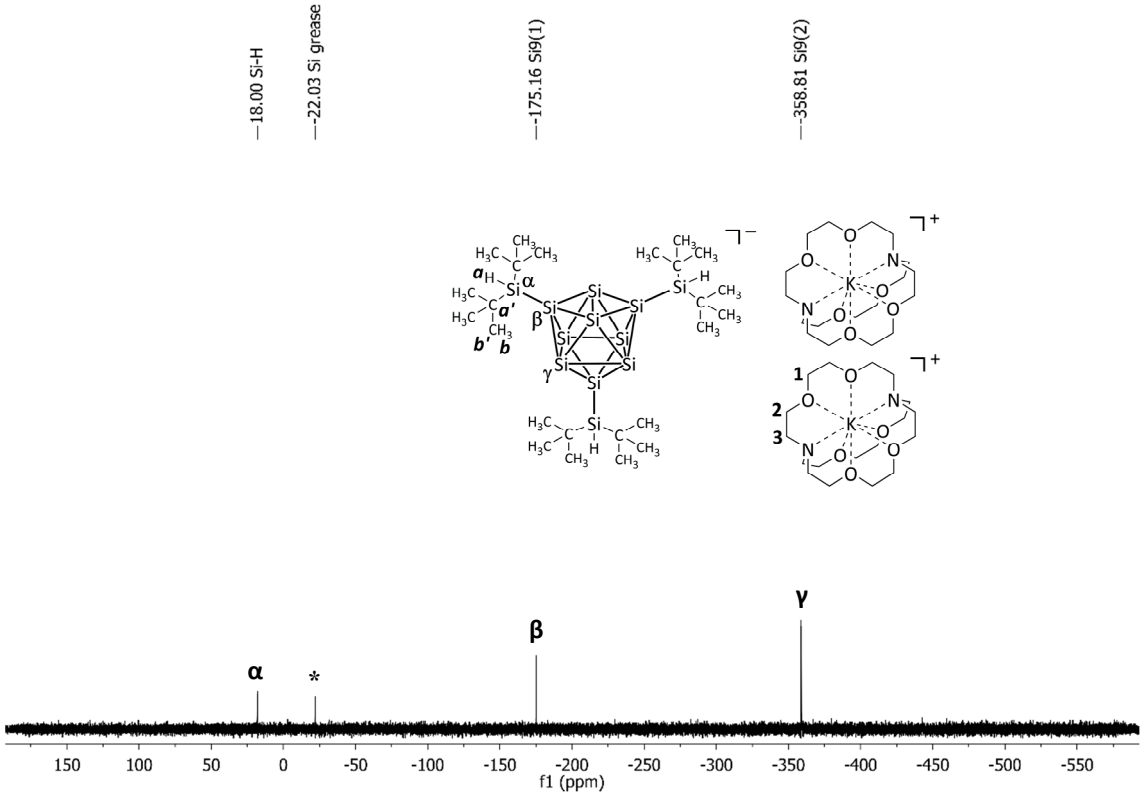

Figure SI 6. ^{29}Si NMR (99 MHz, thf-*d8*) spectrum of the solid **1** (*: silicon grease).

ESI-MS spectra

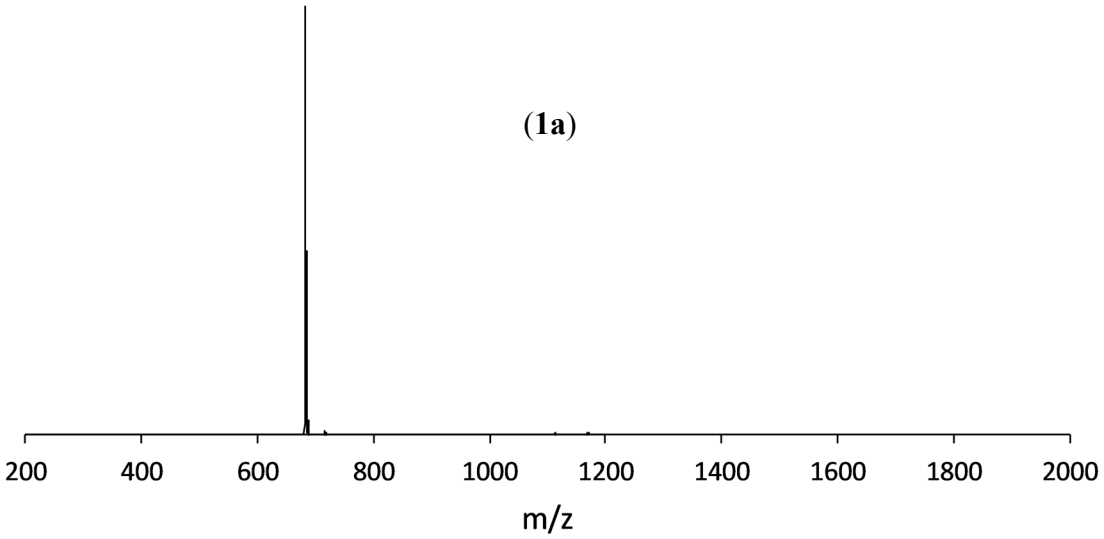

Figure SI 7. ESI-MS spectrum of **1** in thf; ESI-MS (negative mode, 4500 V, 300 °C): *m/z* = 683; $\{(Si(t\mathrm{Bu})_2H)_3Si_9\}^-$ (**1a**).

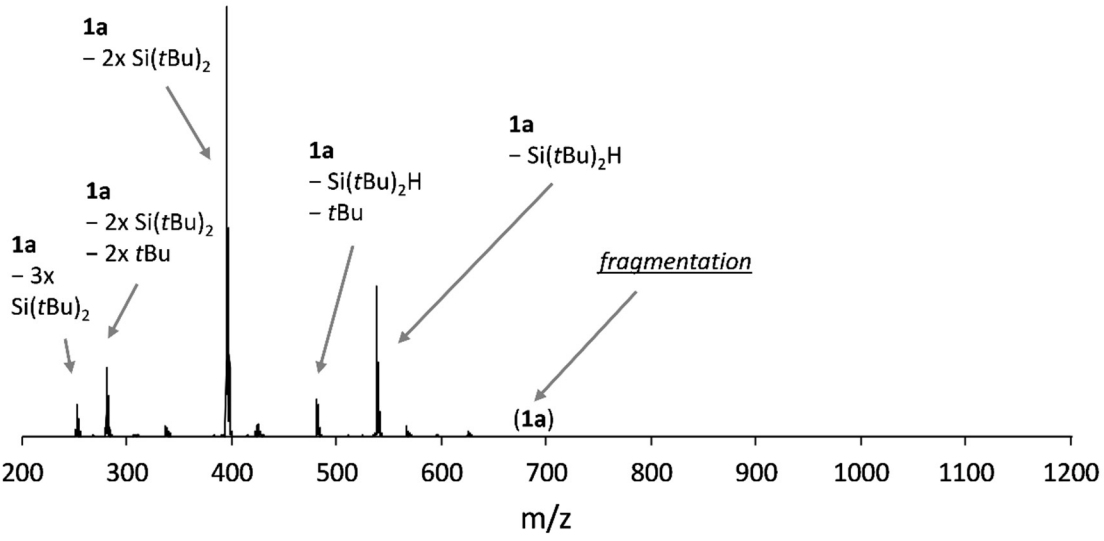

Figure SI 8. ESI-MS fragmentation spectrum of the **1a** mass peak (Figure SI 7) in thf; ESI-MS (negative mode, 4500 V, 300 °C).

PXRD of $K_{12}Si_{17}$

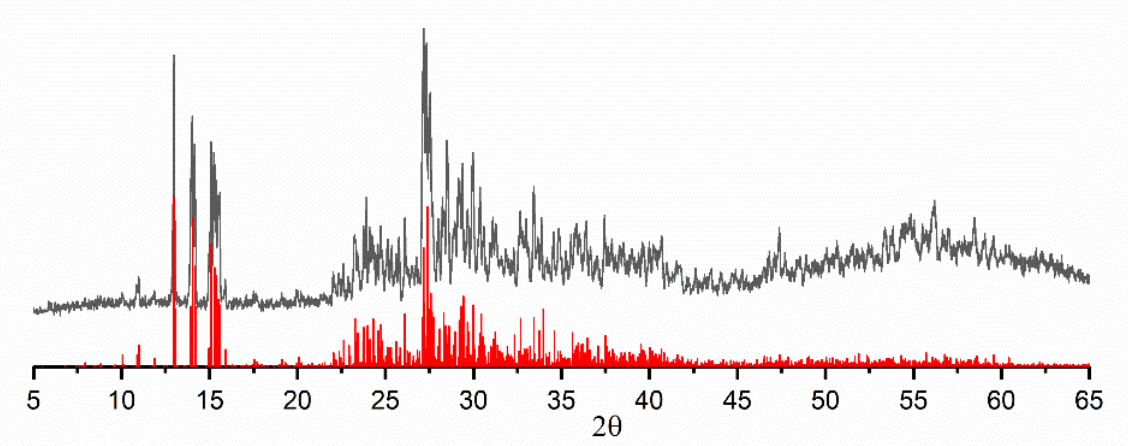

Figure SI 9. Powder X-ray diffractogram of the Zintl phase precursor $K_{12}Si_{17}$ (gray: measured diffractogram; red: theoretical diffractogram).

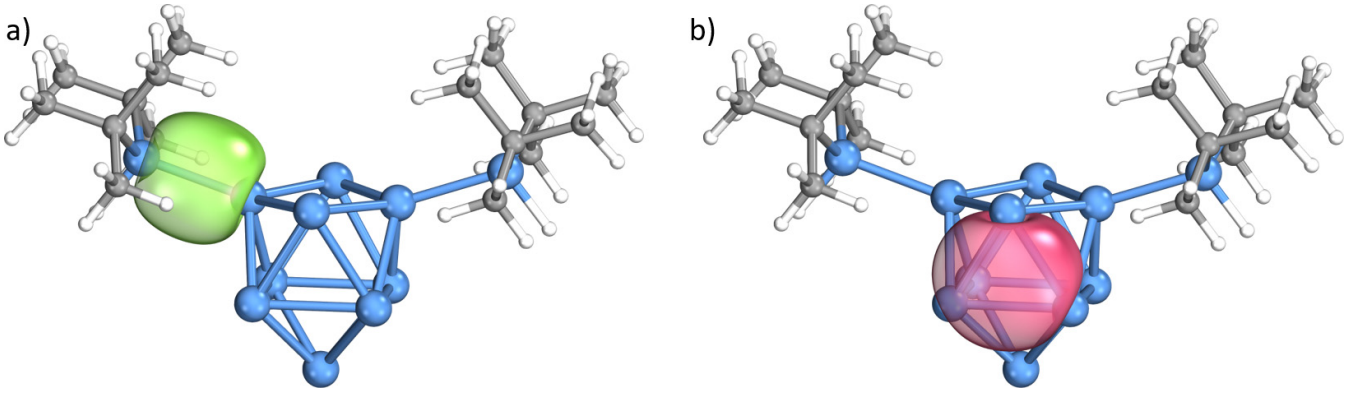

Figure SI 10. Selected Intrinsic Bond Orbitals of **2a**, illustrating the difference between exo Si–Si and intracluster Si–Si bonds. a) two-center two-electron exo-bond between Si1 and Si10. Si1 and Si10 atoms contribute 53% and 44% in the bond, respectively (other atoms contribute 3%). b) Example of an intracluster multicenter bond involving atoms Si2, Si6, and Si7, each atom contributing 32-34% to the bond. Atom labeling according to Figure SI 1

SUPPORTING INFORMATION

XYZ coordinates of 1a and 2a from the computational studies

	1a (C_{3v})				2a (C_1, close to C_{2v})		
	93				65		
Si	-0.7167945	1.2415245	2.1739998	Si	-1.2637845	1.3567618	-3.3509605
Si	-0.717407	1.2425855	-1.0848749	Si	-1.2645772	-1.3684294	-3.3446967
Si	-0.7167945	-1.2415245	2.1739998	Si	-0.000002	1.8324582	-1.2722669
Si	-0.717407	-1.2425855	-1.0848749	Si	-0.0013425	-1.835496	-1.263823
Si	1.433589	0	2.1739998	Si	1.2667394	1.3556525	-3.3487992
Si	0.9901909	1.7150609	0.5439955	Si	0.0022374	-0.009824	-4.9182976
Si	0.9901909	-1.7150609	0.5439955	Si	1.5553536	-0.0023081	-1.36102
Si	1.4348141	0	-1.0848749	Si	1.2658438	-1.3689723	-3.3426333
Si	-1.9803818	0	0.5439955	Si	-1.5565907	-0.0011383	-1.3641084
Si	2.1624652	-3.7454995	0.6622552	Si	3.8035108	0.0008824	-0.6104865
H	2.3332185	-4.041253	2.1227663	H	4.7327147	0.0111183	-1.7893866
Si	-4.3249303	0	0.6622552	Si	-3.8046305	0.0002874	-0.6135091
H	-4.666437	0	2.1227663	H	-4.7345031	-0.0053674	-1.7918967
Si	2.1624652	3.7454995	0.6622552	C	-4.1745569	-1.6490283	0.3087022
H	2.3332185	4.041253	2.1227663	C	-4.1794594	1.6556221	0.2956378
C	-5.0570331	1.6537211	-0.0046672	C	4.1848926	-1.6540711	0.296724
C	-5.0570331	-1.6537211	-0.0046672	C	4.1686253	1.6500034	0.3140226
C	1.0963521	5.2063797	-0.0046672	C	3.274202	-1.8753394	1.50514
C	3.9606811	3.5526586	-0.0046672	H	3.4723872	-2.8612317	1.9453176
C	3.9606811	-3.5526586	-0.0046672	H	3.4396522	-1.1289209	2.2864838
C	1.0963521	-5.2063797	-0.0046672	H	2.2173778	-1.8438756	1.2227396
C	4.0059443	-3.2588537	-1.5037959	C	3.2396028	1.8612501	1.5103071
H	5.0405159	-3.0590831	-1.8136727	H	3.3931567	1.1084518	2.2879205
H	3.6432036	-4.1011283	-2.0988599	H	3.430965	2.8435367	1.961431
H	3.4087179	-2.3795488	-1.7620918	H	2.1872587	1.8320595	1.2115172
C	0.819278	-5.0986763	-1.5037959	C	-3.2592705	1.8775402	1.4967344
H	1.7300794	-5.205671	-2.0988599	H	-3.4553743	2.8628125	1.9392319
H	0.1289857	-5.8947564	-1.8136727	H	-3.4170329	1.1302385	2.2788807
H	0.3563908	-4.1418107	-1.7620918	H	-2.20482	1.8478877	1.2054953
C	-4.8252222	-1.8398226	-1.5037959	C	-3.2435975	-1.8665457	1.5023325
H	-5.1695016	-2.8356733	-1.8136727	H	-3.3907021	-1.1134433	2.2809645
H	-5.3732831	-1.1045428	-2.0988599	H	-3.4394023	-2.8480786	1.9532026
H	-3.7651086	-1.7622619	-1.7620918	H	-2.1919723	-1.8431073	1.20062
C	-4.8252222	1.8398226	-1.5037959	C	-3.9571597	-2.7795617	-0.7023145
H	-5.3732831	1.1045428	-2.0988599	H	-4.6206812	-2.6816103	-1.567221
H	-5.1695016	2.8356733	-1.8136727	H	-2.9284819	-2.8044103	-1.073066
H	-3.7651086	1.7622619	-1.7620918	H	-4.1701923	-3.7452044	-0.2251517
C	0.819278	5.0986763	-1.5037959	C	-5.6295313	-1.7130757	0.781731
H	0.1289857	5.8947564	-1.8136727	H	-6.3348569	-1.4911263	-0.0251511
H	1.7300794	5.205671	-2.0988599	H	-5.8506797	-2.7255788	1.1438784
H	0.3563908	4.1418107	-1.7620918	H	-5.8279981	-1.0237745	1.6041595

C	4.0059443	3.2588537	-1.5037959
H	3.6432036	4.1011283	-2.0988599
H	5.0405159	3.0590831	-1.8136727
H	3.4087179	2.3795488	-1.7620918
C	4.79836	4.7975229	0.2973749
H	4.757012	5.0707208	1.3561706
H	5.8502229	4.6045085	0.0463381
H	4.4798064	5.6634542	-0.2869259
C	4.577318	2.369355	0.7484248
H	4.5584766	2.5201877	1.831972
H	4.0519622	1.4350343	0.5360725
H	5.6254306	2.2445123	0.4445895
C	1.7555967	6.5542631	0.2973749
H	2.6647921	6.7113532	-0.2869259
H	1.0625099	7.3686959	0.0463381
H	2.012867	6.6550537	1.3561706
C	-0.2367374	5.1487512	0.7484248
H	-0.7832049	4.2266194	0.5360725
H	-0.0966918	5.2078504	1.831972
H	-0.8689106	5.9940219	0.4445895
C	-4.3405806	2.7793962	0.7484248
H	-4.4617849	2.6876627	1.831972
H	-3.2687573	2.7915851	0.5360725
H	-4.75652	3.7495096	0.4445895
C	-6.5539567	1.7567402	0.2973749
H	-6.769879	1.5843329	1.3561706
H	-6.9127328	2.7641874	0.0463381
H	-7.1445984	1.047899	-0.2869259
C	-6.5539567	-1.7567402	0.2973749
H	-7.1445984	-1.047899	-0.2869259
H	-6.9127328	-2.7641874	0.0463381
H	-6.769879	-1.5843329	1.3561706
C	-4.3405806	-2.7793962	0.7484248
H	-3.2687573	-2.7915851	0.5360725
H	-4.4617849	-2.6876627	1.831972
H	-4.75652	-3.7495096	0.4445895
C	4.577318	-2.369355	0.7484248
H	4.0519622	-1.4350343	0.5360725
H	4.5584766	-2.5201877	1.831972
H	5.6254306	-2.2445123	0.4445895
C	4.79836	-4.7975229	0.2973749
H	5.8502229	-4.6045085	0.0463381
H	4.757012	-5.0707208	1.3561706
H	4.4798064	-5.6634542	-0.2869259
C	1.7555967	-6.5542631	0.2973749
H	2.012867	-6.6550537	1.3561706
C	-5.6389449	1.7248815	0.7539855
H	-5.8478134	1.0390604	1.5766673
H	-5.8612126	2.7392972	1.1100535
H	-6.3363761	1.5017902	-0.0594187
C	-3.9506652	2.7804819	-0.7191103
H	-2.9178127	2.8036457	-1.0780431
H	-4.6039559	2.6775404	-1.5912199
H	-4.169631	3.7486743	-0.2498354
C	3.9486082	-2.7800924	-0.7149358
H	2.9124257	-2.8054797	-1.0638065
H	4.5930903	-2.6766651	-1.5935269
H	4.1740134	-3.7474704	-0.2469986
C	5.6480684	-1.7224199	0.743439
H	5.8731514	-2.7360437	1.0999814
H	6.3386909	-1.5013152	-0.0762708
H	5.8639139	-1.0347255	1.5627574
C	5.6244534	1.718989	0.7836374
H	6.3285653	1.5036421	-0.0260738
H	5.8418256	2.7310253	1.1493711
H	5.8284033	1.0272603	1.6027181
C	3.9439808	2.7818118	-0.6939419
H	4.6047422	2.6880353	-1.561425
H	2.9138817	2.8038457	-1.0609304
H	4.155277	3.7471873	-0.2154589

H	1.0625099	-7.3686959	0.0463381
H	2.6647921	-6.7113532	-0.2869259
C	-0.2367374	-5.1487512	0.7484248
H	-0.0966918	-5.2078504	1.831972
H	-0.7832049	-4.2266194	0.5360725
H	-0.8689106	-5.9940219	0.4445895

References

[1] C. B. Hübschle, G. M. Sheldrick, B. Dittrich, *J. Appl. Crystallogr.* **2011**, *44*, 1281-1284.
[2] Diamond Version 3.2k, *Crystal Impact GbR* **1997**–**2014**.
[3] MestReNovav 9.1.0, *Mestrelab Research S.L.* **2014**.
[4] WinXPOW v3.0.2.1, *STOE & Cie GmbH* **2011**.
[5] a) TURBOMOLE V7.3 2018*, a development of University of Karlsruhe and Forschungszentrum Karlsruhe GmbH, 1989–2007, TURBOMOLE GmbH, since 2007*; b) R. Ahlrichs, M.Bär, M. Häser, H.Horn, C. Kölmel, *Chem. Phys. Lett.* **1989**, *162*, 165-169.
[7] a) J. P.Perdew, K. Burke, M. Ernzerhof, *Phys. Rev. Lett.* **1996**, *77*, 3865-3868; b) C. Adamo, V. J. Barone, *J. Chem. Phys.* **1999**, *110*, 6158-6170; c) F.Weigend, R. Ahlrichs, *Phys. Chem. Chem. Phys.* **2005**, *7*, 3297-3305.
[8] a) K. Eichkorn, O. Treutler, H. Öhm, M. Häser, R. Ahlrichs, *Chem. Phys. Lett.* **1995**, *242*, 652-660; b) F. Weigend, *Phys. Chem. Chem. Phys.* **2006**, *8*, 1057-1065; c) M. Sierka, A. Hogekamp, R. Ahlrichs, *J. Chem. Phys.* **2003**, *118*, 9136-9148.
[9] A. Klamt, G. Schüürmann, *J. Chem. Soc., Perkin Trans. 2* **1993**, 799-805.
[10] K. Reiter, F. Mack, F. Weigend, *J. Chem. Theory. Comput.* **2018**, *14*, 191-197.
[11] G. Knizia, *J. Chem. Theory. Comput.* **2013**, *9*, 4834-4843.

6.7 Silicon Clusters with six and seven unsubstituted vertices *via* a two-step reaction from elemental silicon

Lorenz J. Schiegerl, Antti J. Karttunen, Wilhelm Klein, and Thomas F. Fässler*

published in

Chem. Sci., 2019, Advance Article, DOI: 10.1039/C9SC03324F.

Access online *via*: https://pubs.rsc.org/en/content/articlelanding/2019/sc/c9sc03324f

Content and contributions:

Ambition of this work was the study of accessible Si_9 cluster siliconoids with $K_{12}Si_{17}$ precursor material. The manuscript was authored by me within the course of this PhD Thesis and reviewed by *Prof. Antti Karttunen*, *Dr. Wilhelm Klein*, *Dr. Annette Schier* and *Prof. Thomas Fässler*. *Prof. Antti Karttunen* did the computational studies and contributed concerning text passages in the Supporting Information. Recording, evaluation and submission of the single crystal diffraction data were assisted by *Dr. Wilhelm Klein*. *Dr. Sebastian Geier* (TECHNICAL UNIVERSITY OF MUNICH) measured the Raman spectra. The EDX spectra were measured by Maria Müller (TECHNICAL UNIVERSITY OF MUNICH). The work was published within the framework of the WACKER INSTITUTE FOR SILICON CHEMISTRY (TECHNICAL UNIVERSITY OF MUNICH).

In extension to the first Si_9 siliconoids $[(SiH^tBu_2)_3Si_9]^-$ / $[(SiH^tBu_2)_2Si_9]^{2-}$ (chapter 6.6), the anionic siliconoids $[\{Si(TMS)_3\}_3Si_9]^-$ and $[(SnCy_3)_3Si_9]^-$ were obtained as bulk materials by reaction of $K_{12}Si_{17}$ (prior "*activation*" with 222crypt/NH_3) with $Si(TMS)_3Cl$ and $SnCy_3Cl$, respectively. Synthesis and characterization (NMR, ESI-MS) were done by me. Single crystals containing $[K\text{-}222crypt]^+$ salts of $[\{Si(TMS)_3\}_2Si_9]^{2-}$ / $[(SnCy_3)_2Si_9]^{2-}$ were synthesized and characterized (EDX, SC-XRD, Raman) by me. Results were discussed in comparison with calculations to partial atomic cluster charges, IBOs (intrinsic atomic bond orbitals) and Raman shifts in cooperation with *Prof. Antti Karttunen*.

Chemical Science

EDGE ARTICLE

View Article Online
View Journal

Cite this: DOI: 10.1039/c9sc03324f

All publication charges for this article have been paid for by the Royal Society of Chemistry

Silicon clusters with six and seven unsubstituted vertices *via* a two-step reaction from elemental silicon†‡

Lorenz J. Schiegerl,[ab] Antti J. Karttunen,[c] Wilhelm Klein[a] and Thomas F. Fässler*[ab]

Unsaturated silicon clusters with only partial substitution, and thus, "naked" Si atoms are well studied species as they are proposed intermediates in gas-phase deposition processes. Although a remarkable number of stable molecular clusters has been reported, they are typically still obtained by multi-step syntheses. Herein we introduce a newly developed synthetic approach which led to the formation of the anionic species $\{Si(TMS)_3\}_3Si_9^-$ (**1a**) and $\{Si(TMS)_3\}_2Si_9^{2-}$ (**1b**), and an extension of this synthetic protocol resulted in the first covalent attachment of ligands through metal atoms to these clusters, $(SnCy_3)_3Si_9^-$ (**2a**) and $(SnCy_3)_2Si_9^{2-}$ (**2b**). The influence of the substituents on the electron localization in the central Si_9 unit is analyzed by means of intrinsic bond orbital (IBO) analysis and partial atomic charge distribution. The IBO analyses reveal a new type of delocalization including 5-center-6-electron besides 3-center-2-electron bonds. The Raman spectra of **1b** and **2b** allow an assignment of the Si–Si intra-cluster vibrations by comparison to calculated (DFT-PBE0) spectra. The anions are formed in a one-step synthesis from binary $K_{12}Si_{17}$ which can easily be obtained by fusing the elements K and Si. The anions are characterized by ESI mass spectrometry and comprehensive NMR studies (^{1}H, ^{13}C, ^{29}Si, ^{119}Sn). Attempts to crystallize **1a** and **2a** as their $(K–222crypt)^+$ salts yielded after the loss of one of the substituents single crystals containing **1b** and **2b**. The single crystal X-ray structure analyses reveal the presence of anionic siliconoids with surfaces of seven unsubstituted silicon atoms.

Received 4th July 2019
Accepted 14th August 2019

DOI: 10.1039/c9sc03324f

rsc.li/chemical-science

Introduction

The call for new sources of silicon-based materials is steadily increasing due to applications in numerous daily-life products as *e.g.* batteries, photovoltaics and electronic devices.[1–8] The wide range of applications is promoted by the abundancy, low costs, non-toxicity and semiconducting properties of silicon. After the first reports on Si=Si double bonds[9,10] a new field for the exploration of tailor-made low-valent silicon compounds has been established that undergoes constant expansion, mirrored *e.g.* by the synthesis of stable silaethenes $(SiMe_3)_2Si=C(OSiMe_3)R$ (R = adamantyl, CEt_3, CMe),[11,12] compounds with silicon–silicon triple bonds as in $(^iPrR'_2)Si–Si\equiv Si–Si(R'_2{}^iPr)$ (R′ = $CH(SiMe_3)_2$),[13] a stable silylene $(CH)_2(NC(CH_3)_3)_2Si$,[14] an aromatic hexasilabenzene isomer $(Tip)_6Si_6$ (Tip = 2,4,6-triisopropylphenyl),[15] the triatomic Si(0) unit $(CAAC)_3Si_3$ (CAAC = cyclic (alkyl)amino carbene),[16] and of so-called siliconoid clusters.[17–21] Siliconoids are best described as partially substituted silicon clusters with ligand-free silicon atoms (Fig. 1), and further modifications of such silicon compounds have frequently been achieved, which underlines their versatile synthetic potential for the formation of silicon-based materials.[19–27]

Their synthesis has made major progress in recent years, and just lately a step-wise, atomically precise expansion of the anionic siliconoid $(Tip)_5Si_6^-$ (Fig. 1b) was reported using $(Cp^*)_2Si$.[31] The formation of siliconoids of higher nuclearity from molecular precursors, however, generally affords several synthetic steps. In 1993, Wiberg *et al.* already suggested in their report on the synthesis of $(Si^tBu_3)_4Si_4$ that such substituted Si_4 cluster compounds should probably be accessible in a more straightforward manner through the reaction of alkyl halides with tetrahedral Si_4^{4-} polyanions that occur in binary alkali metal alloys of silicon.[32] This idea was promoted by subsequent reports on $(SiMeDis_2)_3Si_4^-$ (Dis = $CH(SiMe_3)_2$)[28] (Fig. 1a) and $(Si^tBu_3)_3Si_4^-$ (ref. 33) in which – again *via* molecular precursors – tri-substituted tetrahedral Si_4 clusters have been obtained. The idea of using *Zintl* anions as precursors for Si-rich

[a]Department of Chemistry, Technische Universität München, Lichtenbergstraße 4, 85748 Garching, Germany. E-mail: thomas.faessler@lrz.tum.de
[b]WACKER Institute of Silicon Chemistry, Technische Universität München, Lichtenbergstraße 4, 85748 Garching, Germany
[c]Department of Chemistry and Materials Science, Aalto University, 00076 Aalto, Finland

† Dedicated to Professor Reinhold Tacke on the occasion of his 70th birthday.

‡ Electronic supplementary information (ESI) available. CCDC 1896557 and 1896556. For ESI and crystallographic data in CIF or other electronic format see DOI: 10.1039/c9sc03324f

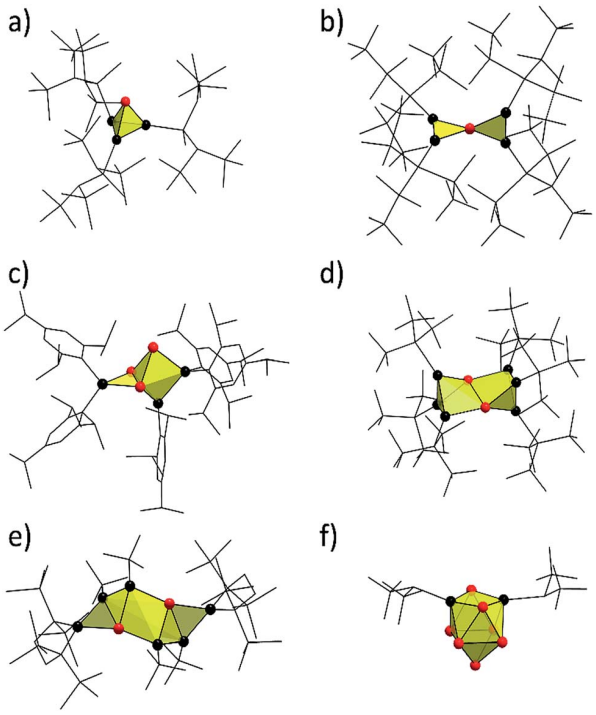

Fig. 1 Selected examples of known molecular silicon cluster species with naked cluster atoms: (a) $(SiMeDis_2)_3Si_4^-$ (Dis = $CH(SiMe_3)_2$);[28] (b) $\{Si(SiMe^tBu_2)_3\}_4Si_5$;[29] (c) the siliconoid $(Tip)_5Si_6^-$ (Tip = 2,4,6-triisopropylphenyl);[18] (d) $(Si^tBu_3)_6Si_8$;[21] (e) $(^tBu)_4\{C_4(SiMe_3)_4\}_2Si_8$;[20] (f) the siliconoid $(SiH^tBu_2)_2Si_9^{2-}$ (**3b**).[30] Silicon clusters are shown as yellow polyhedra; naked and substituted Si cluster atoms are shown as red and black spheres, respectively, and the cluster substituents are drawn in the wire-and-stick mode.

molecules has constantly been pursued for more than two decades, nevertheless, many approaches were repeatedly discarded due to the high reducing properties of such silicides.[19,32]

Examples of *Zintl* phases with deltahedral clusters are A_4Si_4 (ref. 34–37) (A = Li–Cs) and $A_{12}Si_{17}$ (ref. 38 and 39) (A = K–Cs), which contain solely Si_4^{4-} units and Si_4^{4-} alongside Si_9^{4-} in a 2 : 1 ratio, respectively. The Si_4^{4-} and Si_9^{4-} clusters are unsaturated species with interesting properties firstly due to their nucleophilic character (multiple negative charge). Secondly, they are electrophilic in character at the same time due to an electron-deficient bonding situation of the cluster skeleton.[40,41] Since the A_4Si_4 phases are rather insoluble in any solvent, the focus was set on the $A_{12}Si_{17}$ phases which are soluble in liquid ammonia, from which solvates containing Si_4^{4-} (ref. 42 and 43) and Si_9^{4-} (ref. 43–45) units could be obtained, and it has been shown that the Si_4^{4-} *Zintl* clusters from such an $A_{12}Si_{17}$ phase are receptive to chemical conversion. $(CuMes)_2Si_4^{4-}$ (ref. 46) was obtained by the reaction with CuMes (Mes = 1,3,5-trimethylbenzene). But also the Si_9^{4-} clusters could be derivatized *e.g.* by the addition of transition metal fragments yielding $(PhZn)Si_9^{3-}$,[47] $(\{Ni(CO)_2\}_2Si_9)_2^{8-}$ (ref. 48) and $(NHC^{Dipp}Cu)Si_9^{3-}$ (NHC^{Dipp} = 1,3-bis-(2,6-di-iso-propylphenyl) imidazole-2-ylidene).[49]

However, a synthetic approach including Si_4^{4-} or Si_9^{4-} units to form covalent bonds to ligands is still missing, although such reactions of the corresponding Ge_9^{4-} clusters (from the precursor *Zintl* phase K_4Ge_9)[50–53] are very well known. Investigations on the solubility of the silicon clusters in $A_{12}Si_{17}$ revealed that in liquid ammonia solution the mono-protonated species HSi_9^{3-} (ref. 45 and 54) is present, and that a subsequent transfer to pyridine yields even the doubly-protonated species $H_2Si_9^{2-}$.[55] Furthermore, theoretical studies suggest the formation of siliconoids with Si_9^{4-} units by the attachment of sp^3-Si linkers.[56] Just recently, we used Si_9 clusters from the precursor $K_{12}Si_{17}$ for the production of the anionic siliconoids $(SiH^tBu_2)_3Si_9^-$ (**3a**) and $(SiH^tBu_2)_2Si_9^{2-}$ (**3b**, Fig. 1d) *via* direct ligand attachment.[30] The silylation of Si_9 clusters by the reaction of $K_{12}Si_{17}$ with SiH^tBu_2Cl yields species with covalently bonded SiH^tBu_2 groups at the cluster vertex atoms. These siliconoids contain the so far highest number of unsubstituted silicon atoms (six in **3a** and seven in **3b**) and are more easily accessible than those siliconoids obtained *via* the established "molecular multi-step" approaches. By a recent definition of siliconoids,[19] the unsubstituted Si atoms only display homoatomic bonds with a hemispheroidal coordination sphere and are free of ligands. Herein we report on the reactivity of $K_{12}Si_{17}$ towards $SiTMS_3Cl$ and $SnCy_3Cl$ (TMS = trimethylsilane, Cy = cyclohexyl).

Results and discussion

The recently introduced synthetic route for the formation of anionic siliconoids by substitution of Si_9 clusters from $K_{12}Si_{17}$ was further explored employing $SiTMS_3Cl$ and $SnCy_3Cl$ as reagents. Reactions of Ge_9 clusters from the K_4Ge_9 precursor with such reactants led to an attachment of silyl[51,57–61] and stannyl[62,63] groups at the cluster cores, and the products were characterized as tri-substituted cluster species by ESI-MS and NMR investigations in solution as well as by X-ray analysis in solid-state. Regarding the corresponding reaction of Si_9 clusters from $K_{12}Si_{17}$ in solution, an "*activation*" of the precursor by liquid NH_3/222crypt[30,55] has been found to be a key-step. The silylation of Si_9 was accomplished by the reaction of $K_{12}Si_{17}$ after pretreatment with liquid NH_3/222crypt[30] with $Si(TMS)_3Cl$ and $SnCy_3Cl$ in thf and pyridine, respectively, and yielded deep brownish filtrates which were dried *in vacuo*. Digesting the residue with fluorobenzene, decanting of the solutions, and removal of all volatile ingredients yielded bulk materials which were further characterized by ESI-MS and NMR spectroscopy (^1H, ^{13}C, ^{119}Sn, ^{29}Si).

The ESI-MS spectrum of the reaction product with $SiTMS_3Cl$ shows the mass peak of the tri-silylated species $\{Si(TMS)_3\}_3Si_9^-$ (**1a**) as single species (Fig. 2a). Fragmentation of the isolated mass peak leads to the corresponding di- and mono-silylated cluster species (Fig. 2b) and confirms the composition of **1a**. The isotope distribution of the mass peaks comprises a unit of 21 silicon atoms in accordance with the presence of three $Si(TMS)_3$ substituents at the Si_9 cluster. In analogy, the ESI-MS spectrum of the reaction product with $SnCy_3Cl$ shows the mass peak for the tri-stannylated species $(SnCy_3)_3Si_9^-$ (**2a**) (Fig. 2c). However, the mass peak of the di-stannylated species $(SnCy_3)_2Si_9^-$ (Fig. 2d) was also present, although with lower

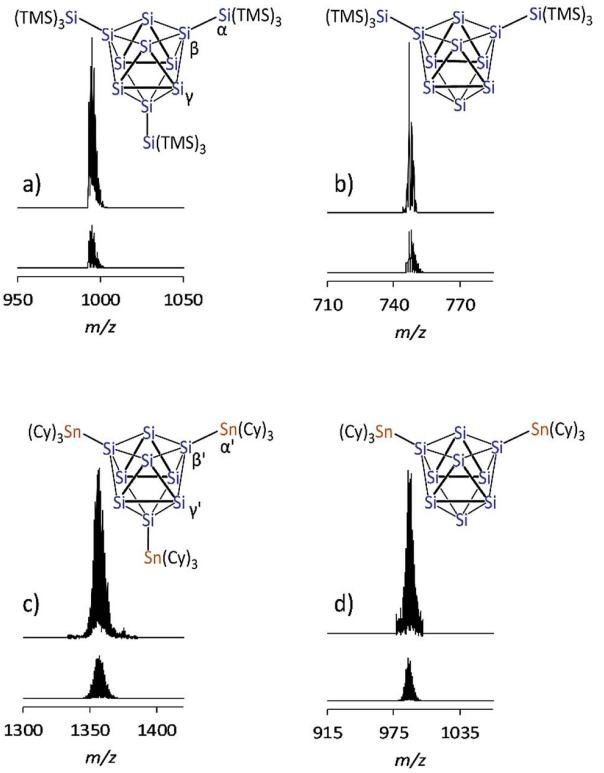

Fig. 2 ESI-MS mass peaks of the Si_9 species (top: measured spectrum, bottom: simulated isotope pattern): (a) $\{Si(TMS)_3\}_3Si_9$ (**1a**), $m/z = 996$; (b) $\{Si(TMS)_3\}_2Si_9$ from mass fragmentation (**1b**), $m/z = 748$; (c) $(SnCy_3)_3Si_9$ (**2a**), $m/z = 1357$; (d) $(SnCy_3)_2Si_9$ (**2b**), $m/z = 989$. For details of the measurement, see ESI.‡

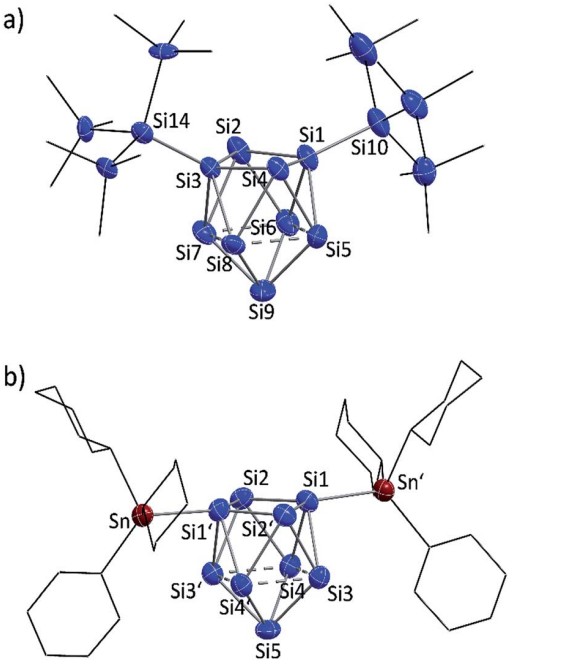

Fig. 3 Single crystal structures of di-anionic siliconoids: (a) $\{Si(TMS)_3\}_2Si_9^{2-}$ (**1b**); (b) $(SnCy_3)_2Si_9^{2-}$ (**2b**); symmetry operation: (′) = $-x, y, 0.5 - z$; Si and Sn atoms (blue and red-brown, respectively) are shown as ellipsoids at 50% probability level; C atoms are drawn in the wire-and-stick mode; H atoms are omitted.

intensity. A fragmentation mass experiment of **2a** confirmed the composition by the loss of $SnCy_3$ in analogy to **1a** and **3a**.[30]

^1H and ^{13}C NMR spectra of **1a** (NMR spectra in the ESI‡) exclusively show one type of TMS group (^1H: 0.25 ppm; ^{13}C: 3.51 ppm) and one set of signals for 222crypt (^1H: 3.64, 3.59, 2.61 ppm; ^{13}C: 71.47, 67.44, 55.01 ppm). The ^1H NMR integral ratio of TMS : 222crypt = 3 : 1 confirms the composition of a triply silylated species for **1a** (Fig. 2a). The ^1H and ^{13}C NMR spectra of **2a** show the expected signals for the cyclohexyl groups. The Cy signals appear superimposed due to their signal splitting, but the ^{13}C NMR spectrum reveals four peaks (33.96, 31.10, 25.86, 21.54 ppm) for the $SnCy_3$ groups of **2a**. A ^{119}Sn NMR measurement reveals one single peak at −70.50 ppm, indicative of one sort of $SnCy_3$ groups in the reaction product, although the integral ratio ($SnCy_3$: 222crypt) in the ^1H NMR measurement does not perfectly match a ratio of 3 : 1 of **2a**. Most likely, small amounts of side-products containing $(K\text{–}222crypt)^+$ units are responsible for this observation.

The ^{29}Si NMR spectrum of a solution of the bulk material containing **1a** reveals four signals at −8.70, −129.94, −175.29, and −360.72 ppm, indicative of a tri-silylated D_{3h} symmetric Si_9 core. The signals at −8.70 ppm (TMS) and −129.94 ppm (α, Fig. 2a) originate from the attached silyl groups and conform well to reported shifts of the corresponding Ge_9 species $\{Si(TMS)_3\}_3Ge_9^-$.[51,60] The signals at −175.29 (β, Fig. 2a) and −360.72 ppm (γ, Fig. 2a) match well with the signals reported for the Si_9 cluster atoms of $(SiH^tBu_2)_3Si_9^-$ (**3a**) (−175.16 and −358.81 ppm, which were confirmed in computational studies).[30] The ^{29}Si NMR spectrum of **2a** reveals signals at −100.01 (β′, Fig. 2c) and −335.50 ppm (γ′, Fig. 2c). The signals of the substituted cluster atoms β/β′ are shifted more downfield if compared to the one of the ligand-free cluster atoms of the prismatic faces γ/γ′, which bear the highest negative ppm values for known siliconoids.[19] The shift range of γ/γ′ is comparable to that of the protonated species $H_2Si_9^{2-}$ (−346 ppm)[55] and HSi_9^{3-} (−359 ppm).[54]

Yellow block-shaped crystals suitable for single crystal X-ray diffraction were obtained from fluorobenzene/hexane solutions of bulk materials **1a** and **2a**. However, the structure determinations show the presence of the di-anionic siliconoid species $\{Si(TMS)_3\}_2Si_9^{2-}$ (**1b**) and $(SnCy_3)_2Si_9^{2-}$ (**2b**). The occurrence of the di-substituted species in the single crystals is traced back to substituent cleave from the cluster cores during crystallization. Ligand scrambling has been observed before in anionic Si_4 clusters.[28] However, a disproportionation according to "2 $\{Si(TMS)_3\}_3Si_9^-$ → $\{Si(TMS)_3\}_2Si_9^{2-}$ + $\{Si(TMS)_3\}_4Si_9$" is excluded by to calculations due to the strongly endoenergetic nature of +92 kJ mol^{-1} (further information in ESI‡). EDX analyses confirmed the corresponding K : Si (**1b**) and K : Si : Sn (**2b**) ratios in the single crystals. The molecular structures of the siliconoid di-anions **1b** and **2b** are shown in Fig. 3a and b, respectively. The structures can be described as di-substituted Si_9 clusters with the shape of a C_{2v}-distorted mono-capped square anti-prism. The substituents are attached at two opposing silicon vertex atoms of the open square of the cluster.

Beside the Si–Si and Si–Sn exo-bonds, the nine Si atoms of the central units in **1b** and **2b** display two groups of Si–Si bond lengths, which are listed and compared to the ones in the known anion **3b** in Table 1 (type 1 and type 2). The shorter bonds (type 1) in the range between 2.40 and 2.48 Å are slightly longer than typical single bonds. Interestingly, the elongations are quite small considering that Si1/Si3 in **1a** and Si1/Si1′ in **2b** show a coordination number of 5. A comparison to the bond lengths within the non-capped square in the cluster HSi_9^{3-} shows a significant influence of the hydrogen substituent on the Si–Si distances. The bonds within the square with the substituted Si atom (coordination number 5) of 2.34 Å are clearly shorter if compared to the ones between the unsubstituted atoms (2.55 Å).[45,54] By contrast, the atoms Si9 (**1a**) and

Table 1 Selected interatomic distances [Å] in the molecular structures of the siliconoid anions **1b**, **2b** and **3b** from single crystal structure determinations (molecular structures with atom labelling in Fig. 3 and 4)

Bond type	$\{Si(TMS)_3\}_2Si_9^{2-}$ (**1b**)	$(SiH^tBu_2)_2Si_9^{2-}$ (**3b**)[30]	$(SnCy_3)_2Si_9^{2-}$ (**2b**)
Exo-bonds	Si1–Si10: 2.357(5)	Si1–Si10: 2.349(2)	Si1–Sn: 2.578(1)
	Si3–Si14: 2.339(5)	Si3–Si11: 2.379(2)	Si1′–Sn′: 2.578(1)
Type 1	Si1–Si2: 2.396(5)	Si1–Si2: 2.405(2)	Si1–Si2: 2.430(2)
	Si1–Si4: 2.427(5)	Si1–Si4: 2.423(2)	Si1–Si2′: 2.433(2)
	Si2–Si3: 2.395(4)	Si2–Si3: 2.418(2)	Si1′–Si2: 2.433(2)
	Si3–Si4: 2.398(5)	Si3–Si4: 2.414(2)	Si1′–Si2′: 2.430(2)
	Si5–Si9: 2.468(6)	Si5–Si9: 2.429(2)	Si4–Si5: 2.436(2)
	Si6–Si9: 2.470(6)	Si6–Si9: 2.441(2)	Si3–Si5: 2.432(2)
	Si7–Si9: 2.427(6)	Si7–Si9: 2.450(2)	Si4′–Si5: 2.436(2)
	Si8–Si9: 2.475(7)	Si8–Si9: 2.447(2)	Si3′–Si5: 2.432(2)
Type 2	Si5–Si6: 2.772(6)	Si5–Si6: 2.782(2)	Si3–Si4: 2.664(2)
	Si7–Si8: 2.738(5)	Si7–Si8: 2.764(2)	Si3′–Si4′: 2.664(2)
	Si6–Si7: 2.569(6)	Si6–Si7: 2.534(2)	Si3–Si4′: 2.565(2)
	Si5–Si8: 2.585(6)	Si5–Si8: 2.534(2)	Si3′–Si4: 2.565(2)

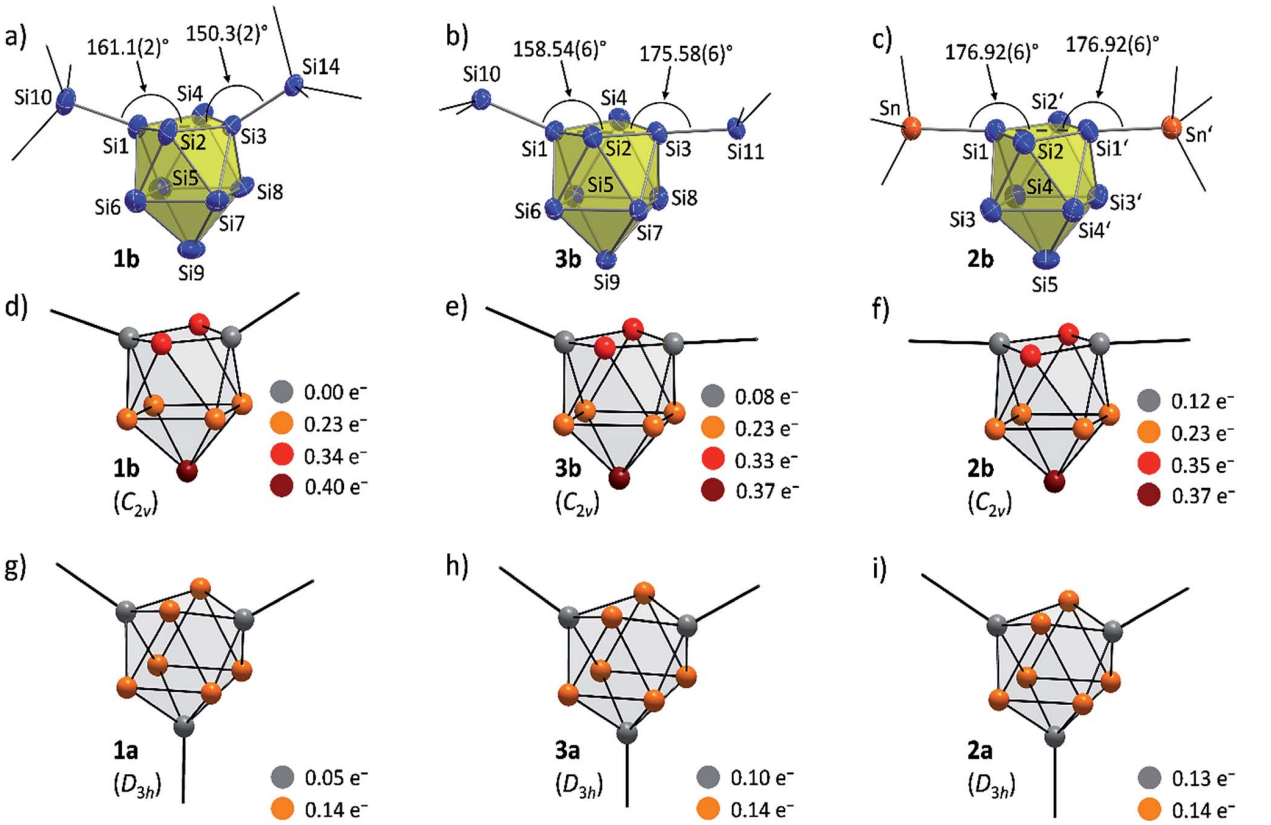

Fig. 4 Molecular structures: (a) $\{Si(TMS)_3\}_2Si_9^{2-}$ (**1b**); (b) $(SiH^tBu_2)_2Si_9^{2-}$ (**3b**);[30] (c) $(SnCy_3)_2Si_9^{2-}$ (**2b**, symmetry operation: (′) = $-x$, y, 0.5 − z); partial atomic charge distributions (DFT-PBE0/TZVP level of theory, all values in e^-): (d) $\{Si(TMS)_3\}_2Si_9^{2-}$ (**1b**); (e) $(SiH^tBu_2)_2Si_9^{2-}$ (**3b**); (f) $(SnCy_3)_2Si_9^{2-}$ (**2b**); (g) $\{Si(TMS)_3\}_3Si_9^-$ (**1a**); (h) $(SiH^tBu_2)_3Si_9^-$ (**3a**); (i) $(SnCy_3)_3Si_9^-$ (**2a**). Molecular structures: Si atoms in blue and Sn atoms in red-brown are shown as ellipsoids at 50% probability level; organic groups are shown as black sticks; H_{Si} atoms in **3b** are omitted.

Si5 (**2b**) with coordination number 4 form an umbrella-type coordination to the neighboring Si atoms. Most intriguingly, the atoms Si5 to Si8 in **1b** and Si3 to Si4 in **2b** each show, beside three shorter contacts of type 1, two longer contacts to atoms of the same kind (type 2). The corresponding Si–Si distances between 2.569(6)–2.738(5) Å in **1b** and 2.565(2)–2.664(2) Å in **2b** are in the typical region of unsubstituted Si atoms with an umbrella-type coordination sphere. Distances between such silicon atoms in known siliconoids as *e.g.* $(Tip)_5Si_6^-$ (2.5506(9) Å, Fig. 1b),[18] $(Tip)_6Si_6$ (2.7076(8) Å)[22] and $(Mes)_6Si_5$ (2.636(1) Å)[64] are comparable to the type 2 bonds.

A comparison of the molecular structures of the siliconoid di-anions **1b**, **2b** and **3b** (Fig. 3 and 4) shows specific differences for the arrangement of the two substituents at the respective Si_9 cluster core. As expected, the longest Si_9 cluster exo-bonds are detected for the stannyl derivative **3b** with Si_9–Sn bond lengths of 2.578(1) Å, while the Si_9–Si cluster exo-bonds in **1b** and **2b** are significantly shorter with values of 2.357(5)/2.339(5) Å (**1b**) and 2.349(2)/2.379(2) Å (**3b**) (Table 1). Si–Sn bonds in low-valent Si-compounds are scarce, but the Si_9–Sn bond lengths in **2b** compare well to the reported Si–Sn distance in the disilene $(Tip)_3(SnMe_3)Si_2$ (2.5675(6) Å).[65] The anion **2b** is located on a twofold symmetry axis, and the two equivalent Sn–Si1–Si1′ and Si1–Si1′–Sn′ angles are 176.92(6)°. In **2b**, the Sn atoms of the $SnCy_3$ ligands are almost in plane with the non-capped cluster square formed by the atoms Si1/Si1′/Si2/Si2. In the silyl derivatives **1b** and **3b**, the corresponding angles are smaller, and the exo-bonds are oriented towards the open face of the clusters [**1b**: Si10–Si1–Si3 with 161.1(2)°, Si1–Si3–Si14 with 150.3(2)°; **3b**: Si10–Si1–Si3 with 158.54(6)°, Si1–Si3–Si11 with 175.58(6)°]. The arrangement of the stannyl substituents in **2b** is consistent with the corresponding angles in the di-substituted Ge_9 derivative $(SnPh_3)_2Ge_9^{2-}$ [corresponding angles: 171.49(5)° and 172.22(5)°] in which one exo-bond is orientated towards the capped face of the cluster.[66]

This indicates a certain degree of interaction of the tin atoms with next-nearest neighbor silicon cluster atoms in **2b** as it was also indicated in the NMR experiments for the tin substituents in the disilene $(Tip)_3(Sn^tBu_2Cl)Si_2$.[65] Such an interaction is further supported by the formation of $(SnPh_3)Ge_9^{3-}$ in which the stannyl ligand is bonded to two Ge_9 cluster atoms.[66]

The highly dispersed ^{29}Si NMR signals in solution in a range from −8.70 to −360.72 ppm for **1a** and from −100.01 to −335.50 ppm for **2a** hint for an inhomogeneous electron distribution due to the different oxidation numbers. Such a broad range was observed before in $(Tip)_6Si_6$ (Tip = 2,4,6-triisopropylphenyl) with a tricyclic structure featuring silicon atoms with two, one, and no substituents outside the ring framework. Consequently, $(Tip)_6Si_6$ can be regarded as a tricyclic aromatic isomer of hexasilabenzene.[15] In contrast to $(Tip)_6Si_6$ with two Si atoms not attached to Tip substituents, bare Si_9^{4-} clusters reveal nine such atoms. Si_9^{4-} possesses a fully delocalized electronic system which fits the superatom model of a 40-electron cluster.[67–70] Ligand attachment to Si_9^{4-} allows for a step-wise transition to molecules with partially delocalized bonds.

In order to investigate the bond properties of the di- and tri-substituted Si_9 atom clusters we calculated the partial atomic charges [e^-] of the silicon cluster atoms of **1a**/**1b**, **2a**/**2b** and **3a**/**3b** (Fig. 4).[30] Comparison of the overall charge distributions shows that lower partial charges are located at substituted silicon atoms including substituent-specific charge differences underlining the electronic influence of the respective substituent on the cluster atoms (partial charges: $SnCy_3$ > SiH^tBu_2 > $Si(TMS)_3$). Interestingly, the partial charges at the unsubstituted Si atoms (prism faces) in the tri-substituted species **1a**/**2a**/**3a** are all identical with a value of 0.14e^- and show a homogeneous distribution of the extra negative charge at the cluster prism faces of the D_{3h} symmetric cluster. By contrast, the two extra

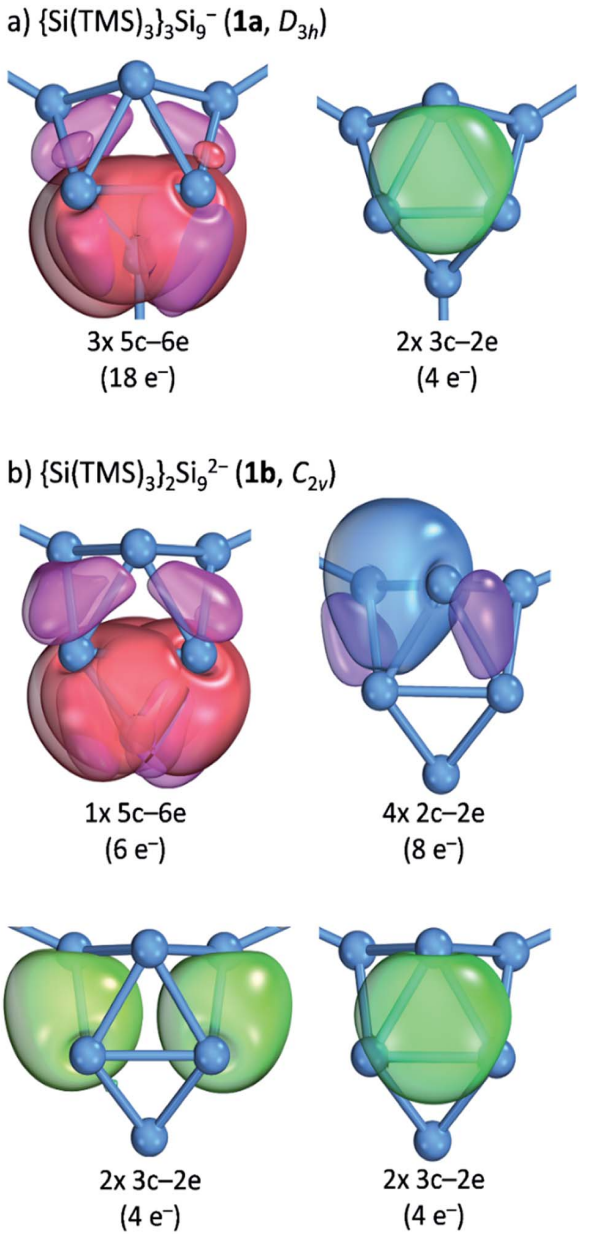

Fig. 5 Intrinsic bond orbital (IBO) analysis: (a) the D_{3h} symmetric cluster in $\{Si(TMS)_3\}_3Si_9^-$ (**1a**); (b) the C_{2v} symmetric cluster in $\{Si(TMS)_3\}_2Si_9^{2-}$ (**1b**). The plotted IBO isosurfaces enclose 80% of the total electron density of the IBO (DFT-PBE0/def2-TZVP level of theory). Details to cluster atom distributions to the respective bonds as well as to the 5c-6e bond in **1b** are shown in the ESI.‡

negative charges in the di-substituted C_{2v} symmetric clusters **1b**, **2b** and **3b** are distributed more versatilely on the cluster surfaces consisting of ligand-free Si atoms. The partial atomic charges of the silicon atoms in the capped cluster squares [**1b**/**3b**: Si5 to Si8; **2b**: Si3(′) and Si4(′)] are equal for all species with a value of $0.23e^-$ for each atom, whereas the highest partial charges at the square-capping silicon atoms, from which the substituents are detached during crystallization, is found in **1b** ($0.40e^-$, Si9 atom).

Further insight into the bonding situation within the cluster units is provided by an IBO analysis of **1a** and **1b** (Fig. 5) that manifests an influence of the third substituent on the bonding situation within the Si_9 cluster cores. The analysis shows a delocalization of the cluster valence electrons (total: $40e^-$) that is in accordance with a previous report for related tris-substituted nona-germanium clusters[71] stronger for D_{3h} symmetric **1a** than for C_{2v} symmetric **1b**. Delocalization in **1a** occurs by three 5c-6e (5 center-6 electron) bonds ($18e^-$) within the three capped square faces and by two 3c-2e bonds ($4e^-$) in the two prism faces. A comparison to the bonding situation in **1b** shows that only one delocalized 5c-6e bond ($6e^-$) is present here which is located within the capped square of the cluster from which cap the substituent is released. Most interestingly, causes the attachment of two ligands a high degree of bond localization in form of four covalent 2c-2e bonds ($8e^-$) in **1b** in the non-capped square of the cluster. Furthermore, two 3c-2e bonds (total $8e^-$) are present in the triangular faces of **1b**. The remaining 18 cluster valence electrons of **1a** and **1b** are located in the covalent cluster exo-bonds (**1a**: $6e^-$; **1b**: $4e^-$) and in six lone pairs which are distributed over the naked Si cluster atoms (**1a**: $12e^-$, six lone pairs: **1b**: $14e^-$, seven lone pairs). Similar bond delocalization was also reported for hexasilabenzene[15] in which theoretical analysis revealed the cyclic delocalization of six mobile electrons of the p-, s- and non-bonding type across the central four-membered ring and which was described as dismutational aromatic. The herein presented study to the charge distributions within substituted Si_9 clusters adds these cluster species as delocalized species to the known silicon molecules in the literature.

Furthermore, the crystals were characterized by Raman spectroscopy, and the measured vibrations are assigned by comparison to calculated Raman spectra of **1b** and **2b** (Fig. 6). Changes of intensities might be due to specific packing effects (calculations were performed on discrete anionic species) and to orientation effects of the single crystal. In both cases characteristic $\tilde{\nu}$(Si–Si) stretching vibrations of the Si_9 cluster cores were detected which agree well with the calculated values.

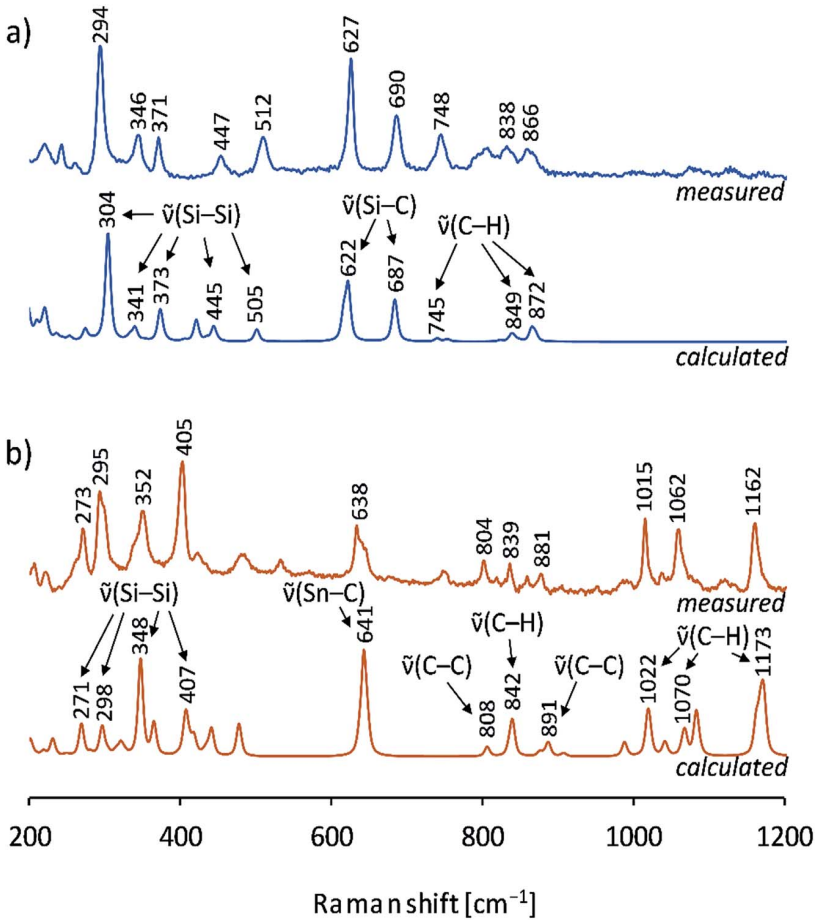

Fig. 6 Raman spectra of single crystals: (a) measured spectrum of a (K–222crypt)$_2$**1b** single crystal (blue, top), calculated spectrum of $\{Si(TMS)_3\}_2Si_9^{2-}$ (**1b**) by DFT-PBE0/TZVP (blue, bottom); (b) measured spectrum of a (K–222crypt)$_2$**2b** single crystal (red-brown, top), calculated spectrum of $(SnCy_3)_2Si_9^{2-}$ (**2b**) by DFT-PBE0/TZVP (red-brown, bottom); details of the calculations can be found in the ESI.‡

Interestingly, the peaks and the distribution range of the cluster vibrations are different for the two siliconoids (**1b**: 294, 346, 371, 447 cm^{-1}; **2b**: 273, 295, 352, 405 cm^{-1}), which indicates an influence of the respective substituent on the Si_9 intra-bonds. All vibrations for the stannyl derivative **2b** (range: 273–405 cm^{-1}) are found at lower wavenumbers than those of **1b** (range: 294–512 cm^{-1}). For **1b**, an Si_9–$Si(TMS)_3$ vibration for the cluster exo-bond was found at 512 cm^{-1}, whereas the Si_9–$SnCy_3$ exo-bonds are not detectable due to laser absorption effects in the spectrum below 200 cm^{-1}. Moreover, $\tilde{\nu}$[Si–C] and $\tilde{\nu}$[C–H] vibrations were observed for **1b** and $\tilde{\nu}$[Sn–C], $\tilde{\nu}$[C–C] and $\tilde{\nu}$[C–H] vibrations for **2b**, which also include the vibrations for the (K–222crypt) units in the single crystals.

Up to this study, the Raman spectra of Si_9 cluster compounds comprised the protonated cluster species $H_2Si_9^{2-}$ and Si_9^{4-} that show less Raman vibrations. The spectrum of $H_2Si_9^{2-}$ displays a prominent resonance at 386 cm^{-1} and a resonance of Si_9^{4-} as part of the solid phase $K_{12}Si_{17}$ at 390 cm^{-1}.[55] In contrast, multiple Si_9 vibrations are confirmed for the ligand-stabilized clusters **1b**/**2b**, and a possible correlation with the delocalized bonding situation from the IBO analysis is of interest for future reports.

Conclusions

The synthetic approach for silicon-rich molecules comprising silicon atoms with low oxidation state from the binary intermetallic precursor $K_{12}Si_{17}$ is established. For the first time a metal atom is attached to a Si_9 cluster core pathway allowing for the structural characterization of Cy_3Sn–(Si_9^{2-})–$SnCy_3$ (**2b**). In addition the anionic siliconoid $\{Si(TMS)_3\}_2Si_9^{2-}$ (**1b**) is structurally characterized. Both anions form *via* the tris-substituted derivatives $(SnCy_3)_3Si_9^-$ (**1a**) and $\{Si(TMS)_3\}_3Si_9^-$ (**2a**) that have been spectroscopically characterized. In contrast to known "molecular multi-step" approaches, the syntheses became feasible *via* a two-step reaction from elemental silicon. The molecular anions possess high numbers of unsubstituted Si cluster atoms and add as novel delocalized representatives to known silicon compounds in the literature. Moreover, the influence of the ligands on bond localization at the Si_9 cluster cores was pointed out.

Experimental section

General

All reactions and manipulations were performed under a purified argon atmosphere using standard Schlenk and glove box techniques. Thf was dried using the solvent purificator MBraun MB-SPS, and fluorobenzene was dried over CaH_2 prior to use. 222crypt was dried *in vacuo* prior to use. Liquid ammonia was dried and stored over sodium metal, and all other solvents (including deuterated solvents) were stored over molecular sieves (3 Å). All other chemicals were received commercially and used without further purification.

$K_{12}Si_{17}$ (*activated*)

The *Zintl* compound $K_{12}Si_{17}$ was synthesized by heating (heating rate: 2 °C min^{-1}) a stoichiometric mixture of 0.55 g K (14.0 mmol, 1 eq.) and 0.59 g Si (21.1 mmol, 1.5 eq.) in a sealed tantalum ampoule to 800 °C for 15 h and subsequent cooling (cooling rate: 0.5 °C min^{-1}) to room temperature. The ampoule was opened in a glove box, and the product was finely ground yielding 1.04 g $K_{12}Si_{17}$ (1.10 mmol, 94%) as a black solid. The solid was characterized by powder X-ray diffraction showing high purity for the solid phase (ESI‡). For the activation, 0.20 g $K_{12}Si_{17}$ (0.21 mmol, 1 eq.) and 0.15 g 222crypt (0.39 mmol, 1.9 eq.; 4,7,13,16,21,24-hexaoxa-1,10-diazabicyclo[8.8.8]hexacosan) were weighed into a Schlenk tube, and liquid ammonia was added at −78 °C (iPrOH/CO_2) to give a dark red solution. The solution was stirred at −78 °C for 2 h, and $K_{12}Si_{17}$ (*activated*) was obtained as a brown solid after the removal of liquid ammonia.

$(K–222crypt)^+$ salts of 1a and 1b

$K_{12}Si_{17}$ *activated* (batch with 200 mg $K_{12}Si_{17}$) was cooled to 0 °C (ice bath), and thf (12 mL) was added. 0.36 g $Si(TMS)_3Cl$ (1.26 mmol, 6 eq.) was added under continuous stirring as a pre-cooled thf solution (3 mL). The reaction mixture was stirred overnight and allowed to warm to room temperature. A brownish filtrate was obtained after filtration, and all volatiles were removed *in vacuo*. The residue was extracted with fluorobenzene (5 mL), and a red filtrate was obtained. After washing with hexane and vacuum drying, a light brown solid containing the $(K–222crypt)^+$ salt of **1a** was obtained (yield: 0.12 g, 40% based on $K_{12}Si_{17}$). The solid was characterized by ESI-MS in thf and NMR spectroscopy (^1H, ^{13}C, ^{29}Si) in solution (thf-d_8). For crystallization, a fluorobenzene solution of the solid (3 mL) was layered with hexane. Yellow block-shaped crystals of the $(K–222crypt)^+$ salt of **1b** suitable for single crystal X-ray diffraction were obtained after 10 d (10 mg, 10% based on (K–222crypt)**1a**). The crystals were investigated by Raman spectroscopy, and the K : Si ratio was confirmed by EDX analyses on single crystals.

Bulk material containing 1a. ESI-MS (negative mode, 4500 V, 300 °C): m/z = 996 $\{Si(TMS)_3\}_3Si_9^-$; ^1H NMR (500 MHz, thf-d_8) δ 3.64 (s, 12H, O–CH_2–CH_2–$O_{222crypt}$), 3.59 (t, J = 5.05 Hz, 12H, O–CH_2–CH_2–$N_{222crypt}$), 2.61 (t, 12H, J = 5.10 Hz, O–CH_2–CH_2–$N_{222crypt}$), 0.25 (s, 81H, SiMe_3); $^{13}C\{^1H\}$ NMR (75 MHz, thf-d_8) δ 71.47 (O–*C*H_2–*C*H_2–$O_{222crypt}$), 67.44 (O–*C*H_2–CH_2–$N_{222crypt}$), 55.01 (O–CH_2–*C*H_2–$N_{222crypt}$), 3.51 (Si*Me*$_3$); $^{29}Si\{^1H\}$ NMR (99 MHz, thf-d_8) δ −8.70 [Si(*TMS*)$_3$], −129.94 [*Si*(TMS)$_3$], −175.29 [*Si*–Si(TMS)$_3$], −360.72 [*Si*–Si–Si(TMS)$_3$].

Single crystals containing 1b. EDX analysis [single crystals of $(K–222crypt)_2$**1b**]: K : Si = 6.30% : 93.7% (calcd: 6.22% : 93.8%); Raman (532 nm): 294 [$\tilde{\nu}$(Si–Si) calcd 304], 346 [$\tilde{\nu}$(Si–Si) calcd 341], 371 [$\tilde{\nu}$(Si–Si) calcd 373], 447 [$\tilde{\nu}$(Si–Si) calcd 445], 512 [$\tilde{\nu}$(Si–Si) calcd 505], 627 [$\tilde{\nu}$(Si–C) calcd 622], 690 [$\tilde{\nu}$(Si–C) calcd 687], 748 [$\tilde{\nu}$(C–H) calcd 745], 838 [$\tilde{\nu}$(C–H) 849], 866 [$\tilde{\nu}$(C–H) calcd 872] cm^{-1}.

$(K–222crypt)^+$ salts of 2a and 2b

$K_{12}Si_{17}$ *activated* (batch with 200 mg $K_{12}Si_{17}$) was cooled to 0 °C (ice bath), and pyridine (12 mL) was added. 0.51 g (1.26 mol, 6 eq.) $SnCy_3Cl$ was added under continuous stirring as pre-cooled pyridine solution (3 mL). The reaction mixture was stirred

overnight and filtered under continuous cooling yielding a colored filtrate which was dried *in vacuo* and extracted with fluorobenzene (5 mL). The red filtrate was dried *in vacuo*, and a brown solid containing the $(K–222crypt)^+$ salt of **2a** was obtained (yield: 0.10 g, 27% based on $K_{12}Si_{17}$). The solid was investigated by ESI-MS in thf and NMR spectroscopy (^1H, ^{13}C, ^{29}Si, ^{119}Sn) in solution (thf-d_8). For crystallization, a fluorobenzene solution of the solid (3 mL) was layered with hexane. Yellow block-shaped crystals of the $(K–222crypt)^+$ salt of **2b** suitable for single crystal X-ray diffraction were obtained after 12 d (7 mg, 7% based on (K–222crypt)**2a**). The crystals were investigated by Raman spectroscopy, and the K : Si ratio was confirmed by EDX analyses on single crystals.

Bulk material containing 2a. ESI-MS (negative mode, 4500 V, 300 °C): m/z = 1357 $(SnCy_3)_3Si_9^-$, m/z = 996 $(SnCy_3)_2Si_9^-$; ^1H NMR (400 MHz, thf-d_8) δ 3.67 (s, 12H, O–CH_2–CH_2–$O_{222crypt}$), 3.61 (s, 12H, O–CH_2–CH_2–$N_{222crypt}$), 2.61 (s, 12H, O–CH_2–CH_2–$N_{222crypt}$), 1.94–1.30 (m, 69H, $H_{cyclohexyl}$); $^{13}C\{^1H\}$ NMR (126 MHz, thf-d_8) δ 71.58 (O–*C*H_2–*C*H_2–$O_{222crypt}$), 68.71 (O–*C*H_2–CH_2–$N_{222crypt}$), 55.09 (O–CH_2–*C*H_2–$N_{222crypt}$), 33.96 ($C_{cyclohexyl}$), 31.10 ($C_{cyclohexyl}$), 25.86 ($C_{cyclohexyl}$), 21.54 ($C_{cyclohexyl}$); $^{29}Si\{^1H\}$ NMR (99 MHz, thf-d_8) δ −100.01 [*Si*–Sn(Cy)$_3$], −335.50 [*Si*–Si–Sn(Cy)$_3$]; $^{119}Sn\{^1H\}$ NMR (112 MHz, thf-d_8) δ −70.50 [*Sn*(Cy)$_3$].

Single crystals containing 2b. EDX analysis [single crystals of $(K–222crypt)_2$**2b**]: K : Si : Sn = 15.5% : 44.1% : 40.4% (calcd: 13.8% : 44.5% : 41.8%); Raman (785 nm):, 273 [$\tilde{\nu}$(Si–Si) calcd 271], 295 [$\tilde{\nu}$(Si–Si) calcd 298], 352 [$\tilde{\nu}$(Si–Si) calcd 348], 405 [$\tilde{\nu}$(Si–Si) calcd 407], 638 [$\tilde{\nu}$(Sn–C) calcd 641], 804 [$\tilde{\nu}$(C–C) calcd 808], 839 [$\tilde{\nu}$(C–H) calcd 842], 881 [$\tilde{\nu}$(C–C) calcd 891], 1015 [$\tilde{\nu}$(C–H) calcd 1022], 1062 [$\tilde{\nu}$(C–H) calcd 1070], 1162 [$\tilde{\nu}$(C–H) calcd 1173] cm^{-1}.

Computational details

Quantum-chemical calculations at the DFT-PBE0/TZVP level of theory were carried out using the TURBOMOLE program package.[72–76] Intrinsic atomic orbitals (IAOs) and intrinsic bond orbitals were used to analyze the partial charges and bonding of the clusters, respectively.[77] Full computational details are available in the ESI.‡

Single crystal structure determination

For single crystal data collection, the crystals were fixed on a glass capillary and positioned in a cold stream of N_2 gas. Single crystal data collection was performed with a STOE StadiVari (Mo Kα radiation) diffractometer equipped with a DECTRIS PILATUS 300K detector. Structures were solved by Direct Methods (SHELXS-2014) and refined by full-matrix least-squares calculations against F^2 (SHELXL-2014).[78] The positions of the hydrogen atoms were calculated and refined using a riding model. Unless otherwise stated, all non-hydrogen atoms were treated with anisotropic displacement parameters. In **1b** some hypersilyl groups show rotational disorder and were refined at two split positions. In **2b**, one cyclohexyl group is found in two different orientations and was refined at two split positions. For visualization, the crystal structures have been plotted with Diamond.‡[79]

Electron dispersive X-ray (EDX) analysis

Single crystals of all compounds were analyzed with a SWIFT-ED-TM (Oxford Instruments) and a Hitachi TM-1000 Tabletop microscope (Hitachi High-Technologies) with the INCA system software.

NMR spectroscopy

^1H, ^{13}C and ^{29}Si NMR spectra were recorded on a Bruker AVIII Ultrashield 400 MHz or a Bruker AVIII 500 MHz Cryo system, ^{119}Sn NMR spectra were measured on a Bruker AVIII 300 MHz (*Bruker Inc*) instrument. The signals of the ^1H and ^{13}C spectra were calibrated on the rest proton signal of the used deuterated solvent thf-d_8. Chemical shift values are given in δ values by parts per million (ppm). The coupling constants J are stated in Hz. Signal multiplicities are abbreviated as follows: s – singlet, d – doublet, t – triplet, m – triplet. The spectra were evaluated with MestReNova.[80]

Electrospray ionization mass spectrometry (ESI-MS)

The preparation of the samples was done in a glove box. The spectra were measured on an *HCT* instrument (*Bruker Inc*). The data were analyzed using the program *Bruker Compass Data Analysis 4.0 SP 5*. The dry gas temperature was adjusted to 300 °C and the injection speed to 240 μL s^{-1}. For fragmentation experiments, the respective mass peaks were isolated (width: 40) and fragmented (amplitude: 2.0). Visualization of the spectra was carried out with the programs *OriginPro* (*Origin Lab Inc*) or *Microsoft Excel* (*Microsoft Inc*).

Raman spectroscopy

Raman spectra were recorded with an *inVia* Raman Microscope *RE04* with a *CCD* detector and 500 mW maximal power (Renishaw PLC; Software: *WiRE 4.2 build 5037*) at λ = 532 nm. For the measurements the samples were sealed in glass capillaries in a glove box.

Powder X-ray diffraction (PXRD)

The data were collected at room temperature on a STOE Stadi P diffractometer (Ge(111) monochromator, Cu Kα_1 radiation, λ = 1.54056 Å) with a Dectris MYTHEN 1K detector in Debye–Scherrer geometry. For the measurements the samples were sealed in glass capillaries (Ø 0.5 mm). The raw data were processed with *WinX-POW*,[81] *OriginPro* (*Origin Lab Inc*) was used for the visualization.

Conflicts of interest

There are no conflicts to declare.

Acknowledgements

The authors are thankful for the financial support by WACKER Chemie AG and Deutsche Forschungsgemeinschaft (DFG, FA 198/14-1). They thank Sebastian Geier and Christoph Wallach for the Raman measurements, Maria Müller for the EDX

analyses, Brigita Bratic for supporting the syntheses and Dr Annette Schier for proofreading. A. J. K. thanks the Academy of Finland for funding (grant 308089) and the Finnish IT Center for Science (CSC) for computational resources.

References

1 M. Ashuri, Q. He and L. L. Shaw, *Nanoscale*, 2016, **8**, 74–103.
2 M. G. Kanatzidis, *Adv. Mater.*, 2007, **19**, 1165–1181.
3 R. A. Bley and S. M. Kauzlarich, *J. Am. Chem. Soc.*, 1996, **118**, 12461–12462.
4 C. Eun-Chel, P. Sangwook, H. Xiaojing, S. Dengyuan, C. Gavin, P. Sang-Cheol and A. G. Martin, *Nanotechnology*, 2008, **19**, 245201.
5 L. T. Canham, *Appl. Phys. Lett.*, 1990, **57**, 1046–1048.
6 J. K. Rath, B. Stannowski, P. A. T. T. van Veenendaal, M. K. van Veen and R. E. I. Schropp, *Thin Solid Films*, 2001, **395**, 320–329.
7 M. L. Snedaker, Y. Zhang, C. S. Birkel, H. Wang, T. Day, Y. Shi, X. Ji, S. Kraemer, C. E. Mills, A. Moosazadeh, M. Moskovits, G. J. Snyder and G. D. Stucky, *Chem. Mater.*, 2013, **25**, 4867–4873.
8 L. Venema, *Nature*, 2011, **479**, 309.
9 D. N. Roark and G. J. D. Peddle, *J. Am. Chem. Soc.*, 1972, **94**, 5837–5841.
10 R. West, M. J. Fink and J. Michl, *Science*, 1981, **214**, 1343–1344.
11 A. G. Brook, F. Abdesaken, B. Gutekunst, G. Gutekunst and R. K. Kallury, *Chem. Commun.*, 1981, 191–192.
12 A. G. Brook, S. C. Nyburg, F. Abdesaken, B. Gutekunst, G. Gutekunst, R. Krishna, M. R. Kallury, Y. C. Poon, Y. M. Chang and W. N. Winnie, *J. Am. Chem. Soc.*, 1982, **104**, 5667–5672.
13 A. Sekiguchi, R. Kinjo and M. Ichinohe, *Science*, 2004, **305**, 1755–1757.
14 M. Denk, R. Lennon, R. Hayashi, R. West, A. V. Belyakov, H. P. Verne, A. Haaland, M. Wagner and N. Metzler, *J. Am. Chem. Soc.*, 1994, **116**, 2691–2692.
15 K. Abersfelder, A. J. P. White, H. S. Rzepa and D. Scheschkewitz, *Science*, 2010, **327**, 564–566.
16 K. C. Mondal, S. Roy, B. Dittrich, D. M. Andrada, G. Frenking and H. W. Roesky, *Angew. Chem., Int. Ed.*, 2016, **55**, 3158–3161.
17 D. Scheschkewitz, *Angew. Chem., Int. Ed.*, 2005, **44**, 2954–2956.
18 P. Willmes, K. Leszczyńska, Y. Heider, K. Abersfelder, M. Zimmer, V. Huch and D. Scheschkewitz, *Angew. Chem., Int. Ed.*, 2016, **55**, 2907–2910.
19 Y. Heider and D. Scheschkewitz, *Dalton Trans.*, 2018, **47**, 7104–7112.
20 T. Iwamoto, N. Akasaka and S. Ishida, *Nat. Commun.*, 2014, **5**, 5353.
21 G. Fischer, V. Huch, P. Mayer, S. K. Vasisht, M. Veith and N. Wiberg, *Angew. Chem., Int. Ed.*, 2005, **44**, 7884–7887.
22 K. Abersfelder, A. J. P. White, R. J. F. Berger, H. S. Rzepa and D. Scheschkewitz, *Angew. Chem., Int. Ed.*, 2011, **50**, 7936–7939.
23 K. Abersfelder, A. Russell, H. S. Rzepa, A. J. P. White, P. R. Haycock and D. Scheschkewitz, *J. Am. Chem. Soc.*, 2012, **134**, 16008–16016.
24 N. Akasaka, S. Ishida and T. Iwamoto, *Inorganics*, 2018, **6**, 107.
25 S. David, *Chem. Lett.*, 2011, **40**, 2–11.
26 Y. Ohmori, M. Ichinohe, A. Sekiguchi, M. J. Cowley, V. Huch and D. Scheschkewitz, *Organometallics*, 2013, **32**, 1591–1594.
27 K. Takeuchi, M. Ichinohe and A. Sekiguchi, *J. Am. Chem. Soc.*, 2008, **130**, 16848–16849.
28 M. Ichinohe, M. Toyoshima, R. Kinjo and A. Sekiguchi, *J. Am. Chem. Soc.*, 2003, **125**, 13328–13329.
29 T. Iwamoto, M. Tamura, C. Kabuto and M. Kira, *Science*, 2000, **290**, 504–506.
30 L. J. Schiegerl, A. J. Karttunen, W. Klein and T. F. Fässler, *Chem.–Eur. J.*, 2018, **24**, 19171–19174.
31 K. I. Leszczyńska, V. Huch, C. Präsang, J. Schwabedissen, R. J. F. Berger and D. Scheschkewitz, *Angew. Chem., Int. Ed.*, 2019, **58**, 5124–5128.
32 N. Wiberg, C. M. M. Finger and K. Polborn, *Angew. Chem., Int. Ed.*, 1993, **32**, 1054–1056.
33 T. M. Klapötke, S. K. Vasisht, G. Fischer and P. Mayer, *J. Organomet. Chem.*, 2010, **695**, 667–672.
34 T. Goebel, A. Ormeci, O. Pecher and F. Haarmann, *Z. Anorg. Allg. Chem.*, 2012, **638**, 1437–1445.
35 H. G. von Schnering, M. Schwarz, J. H. Chang, K. Peters, E. M. Peters and R. Nesper, *Z. Kristallogr. – New Cryst. Struct.*, 2005, **220**, 525.
36 L. A. Stearns, J. Gryko, J. Diefenbacher, G. K. Ramachandran and P. F. McMillan, *J. Solid State Chem.*, 2003, **173**, 251–258.
37 J. He, D. D. Klug, K. Uehara, K. F. Preston, C. I. Ratcliffe and J. S. Tse, *J. Phys. Chem. B*, 2001, **105**, 3475–3485.
38 V. Quéneau, E. Todorov and S. C. Sevov, *J. Am. Chem. Soc.*, 1998, **120**, 3263–3264.
39 C. Hoch, M. Wendorff and C. Röhr, *J. Alloys Compd.*, 2003, **361**, 206–221.
40 K. Wade, *Inorg. Nucl. Chem. Lett.*, 1972, **8**, 559–562.
41 K. Wade, *Chem. Commun.*, 1971, 792–793.
42 C. Lorenz, S. Gärtner and N. Korber, *Z. Anorg. Allg. Chem.*, 2017, **643**, 141–145.
43 C. B. Benda, T. Henneberger, W. Klein and T. F. Fässler, *Z. Anorg. Allg. Chem.*, 2017, **643**, 146–148.
44 S. Joseph, C. Suchentrunk, F. Kraus and N. Korber, *Eur. J. Inorg. Chem.*, 2009, **2009**, 4641–4647.
45 T. Henneberger, W. Klein and T. F. Fässler, *Z. Anorg. Allg. Chem.*, 2018, **644**, 1018–1027.
46 M. Waibel, F. Kraus, S. Scharfe, B. Wahl and T. F. Fässler, *Angew. Chem., Int. Ed.*, 2010, **49**, 6611–6615.
47 J. M. Goicoechea and S. C. Sevov, *Organometallics*, 2006, **25**, 4530–4536.
48 S. Joseph, M. Hamberger, F. Mutzbauer, O. Härtl, M. Meier and N. Korber, *Angew. Chem., Int. Ed.*, 2009, **48**, 8770–8772.
49 F. S. Geitner and T. F. Fässler, *Chem. Commun.*, 2017, **53**, 12974–12977.
50 M. W. Hull and S. C. Sevov, *Angew. Chem., Int. Ed.*, 2007, **46**, 6695–6698.
51 F. Li and S. C. Sevov, *Inorg. Chem.*, 2012, **51**, 2706–2708.

52 F. S. Geitner, J. V. Dums and T. F. Fässler, *J. Am. Chem. Soc.*, 2017, **139**, 11933–11940.
53 F. S. Geitner, W. Klein and T. F. Fässler, *Angew. Chem., Int. Ed.*, 2018, **57**, 14509–14513.
54 C. Lorenz, F. Hastreiter, J. Hioe, L. Nanjundappa, S. Gärtner, N. Korber and R. M. Gschwind, *Angew. Chem., Int. Ed.*, 2018, **57**, 12956–12960.
55 L. J. Schiegerl, A. J. Karttunen, J. Tillmann, S. Geier, G. Raudaschl-Sieber, M. Waibel and T. F. Fässler, *Angew. Chem., Int. Ed.*, 2018, **57**, 12950–12955.
56 L.-A. Jantke and T. Fässler, *Inorganics*, 2018, **6**, 31.
57 O. Kysliak, C. Schrenk and A. Schnepf, *Inorg. Chem.*, 2015, **54**, 7083–7088.
58 L. J. Schiegerl, F. S. Geitner, C. Fischer, W. Klein and T. F. Fässler, *Z. Anorg. Allg. Chem.*, 2016, **642**, 1419–1426.
59 K. Mayer, L. J. Schiegerl, T. Kratky, S. Günther and T. F. Fässler, *Chem. Commun.*, 2017, **53**, 11798–11801.
60 K. Mayer, L. J. Schiegerl and T. F. Fässler, *Chem.–Eur. J.*, 2016, **22**, 18794–18800.
61 O. Kysliak, T. Kunz and A. Schnepf, *Eur. J. Inorg. Chem.*, 2017, **2017**, 805–810.
62 L. G. Perla and S. C. Sevov, *J. Am. Chem. Soc.*, 2016, **138**, 9795–9798.
63 L. G. Perla, A. Muñoz-Castro and S. C. Sevov, *J. Am. Chem. Soc.*, 2017, **139**, 15176–15181.
64 D. Nied, R. Köppe, W. Klopper, H. Schnöckel and F. Breher, *J. Am. Chem. Soc.*, 2010, **132**, 10264–10265.
65 K. Abersfelder, T.-l. Nguyen and D. Scheschkewitz, *Z. Anorg. Allg. Chem.*, 2009, **635**, 2093–2098.
66 A. Ugrinov and S. C. Sevov, *Chem.–Eur. J.*, 2004, **10**, 3727–3733.
67 A. J. Stone, *Inorg. Chem.*, 1981, **20**, 563–571.
68 A. J. Stone and M. J. Alderton, *Inorg. Chem.*, 1982, **21**, 2297–2302.
69 W. A. de Heer, *Rev. Mod. Phys.*, 1993, **65**, 611–676.
70 P. Andre Clayborne and H. Häkkinen, *Phys. Chem. Chem. Phys.*, 2012, **14**, 9311–9316.
71 N. V. Tkachenko and A. I. Boldyrev, *Chem. Sci.*, 2019, **10**, 5761–5765.
72 *TURBOMOLE V7.3 2018, a development of University of Karlsruhe and Forschungszentrum Karlsruhe GmbH, 1989–2007*, TURBOMOLE GmbH, 2007.
73 R. Ahlrichs, M. Bär, M. Häser, H. Horn and C. Kölmel, *Chem. Phys. Lett.*, 1989, **162**, 165–169.
74 J. P. Perdew, K. Burke and M. Ernzerhof, *Phys. Rev. Lett.*, 1996, **77**, 3865–3868.
75 C. Adamo and V. J. Barone, *J. Chem. Phys.*, 1999, **110**, 6158–6170.
76 F. Weigend and R. Ahlrichs, *Phys. Chem. Chem. Phys.*, 2005, **7**, 3297–3305.
77 G. Knizia, *J. Chem. Theory Comput.*, 2013, **9**, 4834–4843.
78 C. B. Hübschle, G. M. Sheldrick and B. Dittrich, *J. Appl. Crystallogr.*, 2011, **44**, 1281–1284.
79 *Diamond Version 3.2k*, Crystal Impact GbR, 1997–2014.
80 *MestReNova v9.1.0*, Mestrelab Research S.L., 2014.
81 *WinXPOW v3.0.2.1*, STOE & Cie GmbH, 2011.

Electronic Supplementary Material (ESI) for Chemical Science.

Silicon Clusters with Six and Seven Unsubstituted Vertices *via* a Two-step Reaction from Elemental Silicon

Supporting Information

1. PXRD of the Zintl phase precursor $K_{12}Si_{17}$

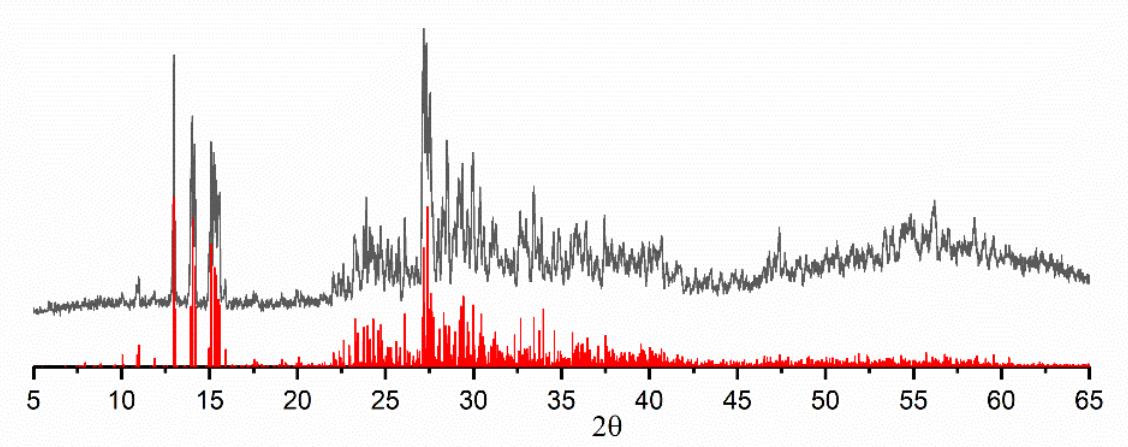

Figure SI 1. Powder X-ray diffractogram of the Zintl phase precursor $K_{12}Si_{17}$ (gray: *measd*.; red: *calcd*. from single crystal data).[1]

2. ESI-MS spectra

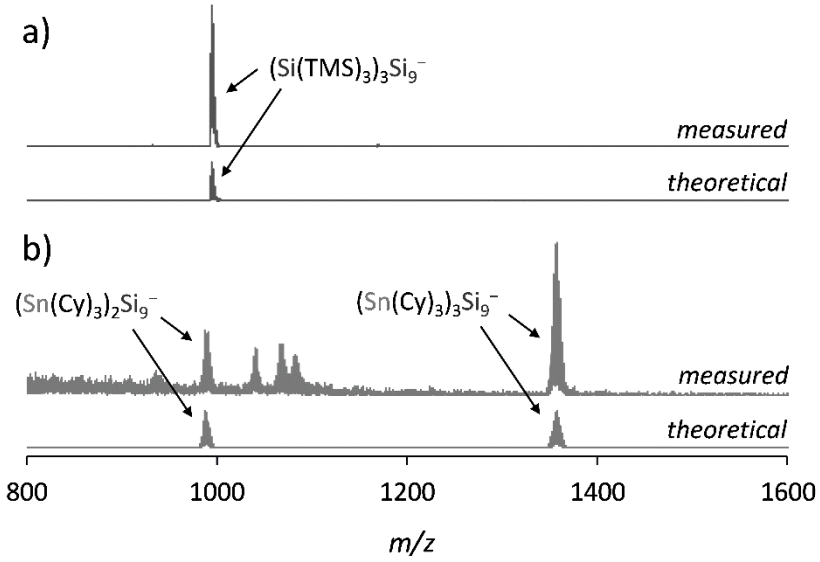

Figure SI 2. a) ESI-MS spectrum of the bulk material containing **1a** in thf (*m/z* = 996, **1a**); b) ESI-MS spectrum of the bulk material containing **2a** in pyridine (*m/z* = 1357, **2a**; *m/z* = 989, **2b**).

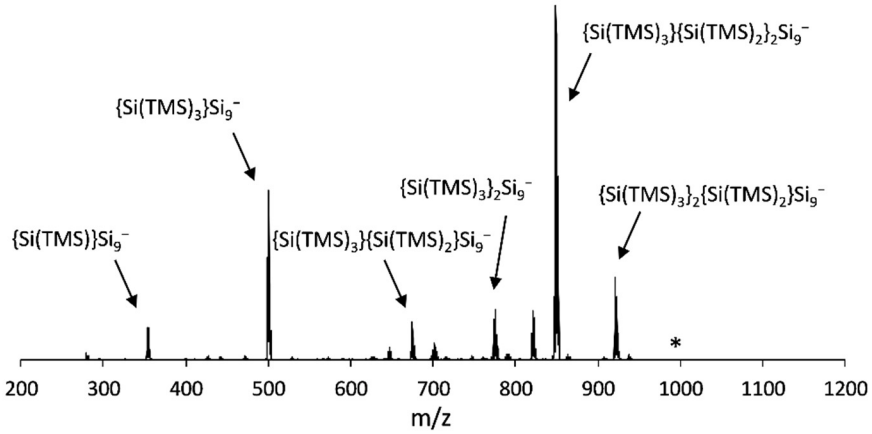

Figure SI 3. ESI-MS fragmentation spectrum of the $\{Si(TMS)_3\}_3Si_9^-$ (**1a**) mass peak (fragmented mass at *m/z* = 996: *) in thf; negative mode, 4000 V, 300 °C.

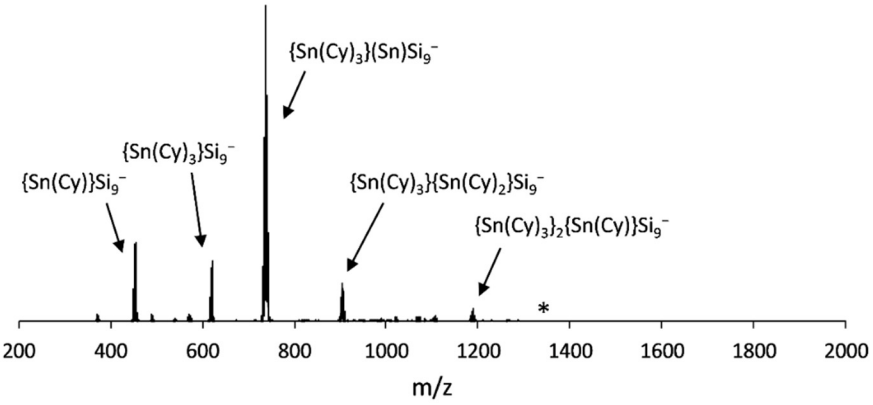

Figure SI 4. ESI-MS fragmentation spectrum of the $(SnCy_3)_3Si_9^-$ (**2a**) mass peak (fragmented mass at *m/z* = 1357: *) in pyridine; negative mode, 4500 V, 300 °C.

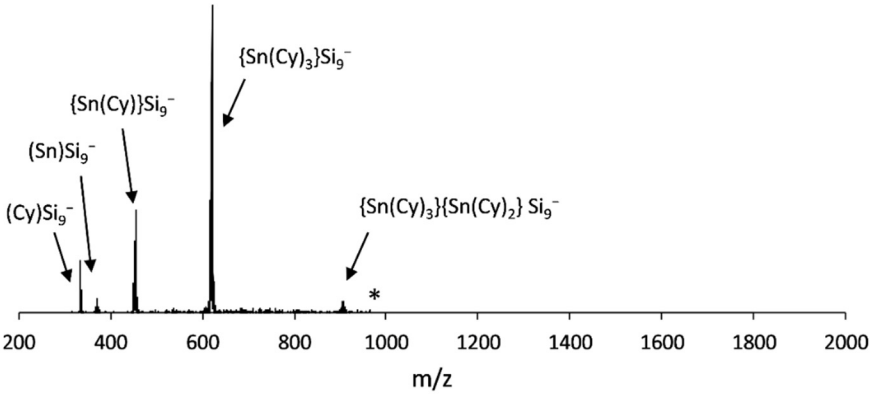

Figure SI 5. ESI-MS fragmentation spectrum of the $(SnCy_3)_2Si_9^-$ mass peak (fragmented mass at *m/z* = 989: *) in pyridine; negative mode, 3500 V, 300 °C.

3. NMR spectra

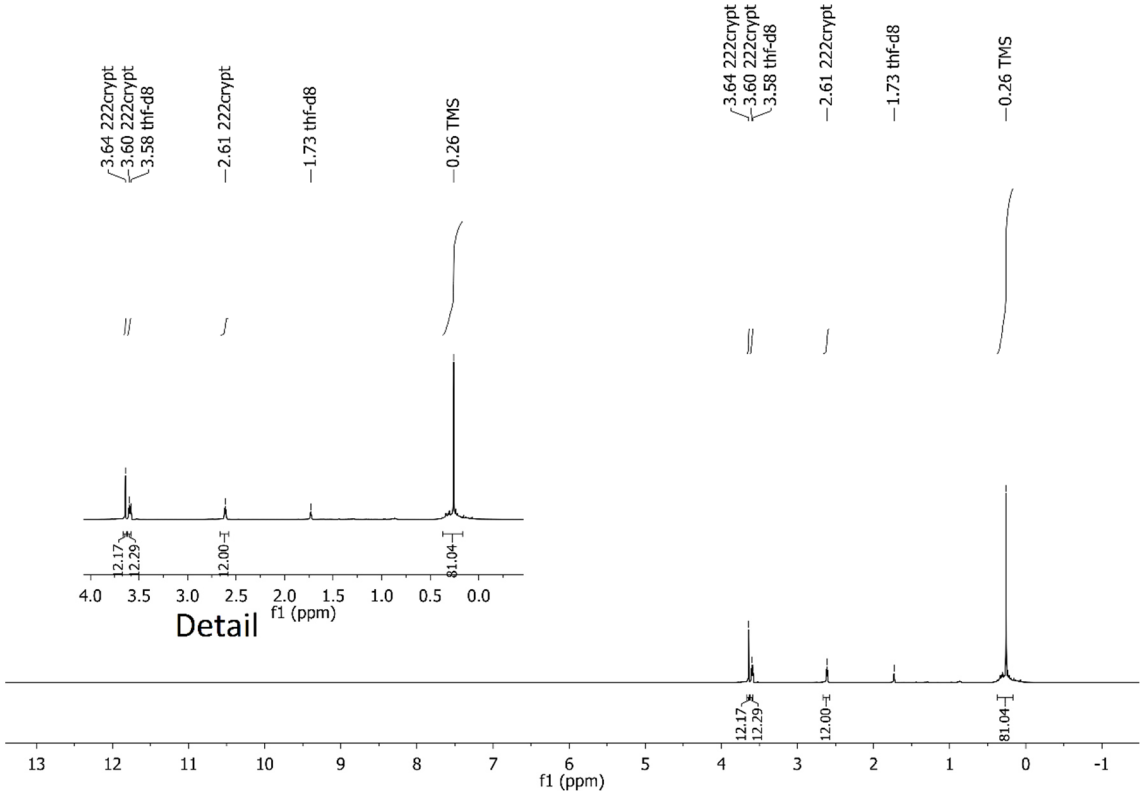

Figure SI 6. ^{1}H NMR (thf-*d8*) spectrum of the bulk material containing **1a**.

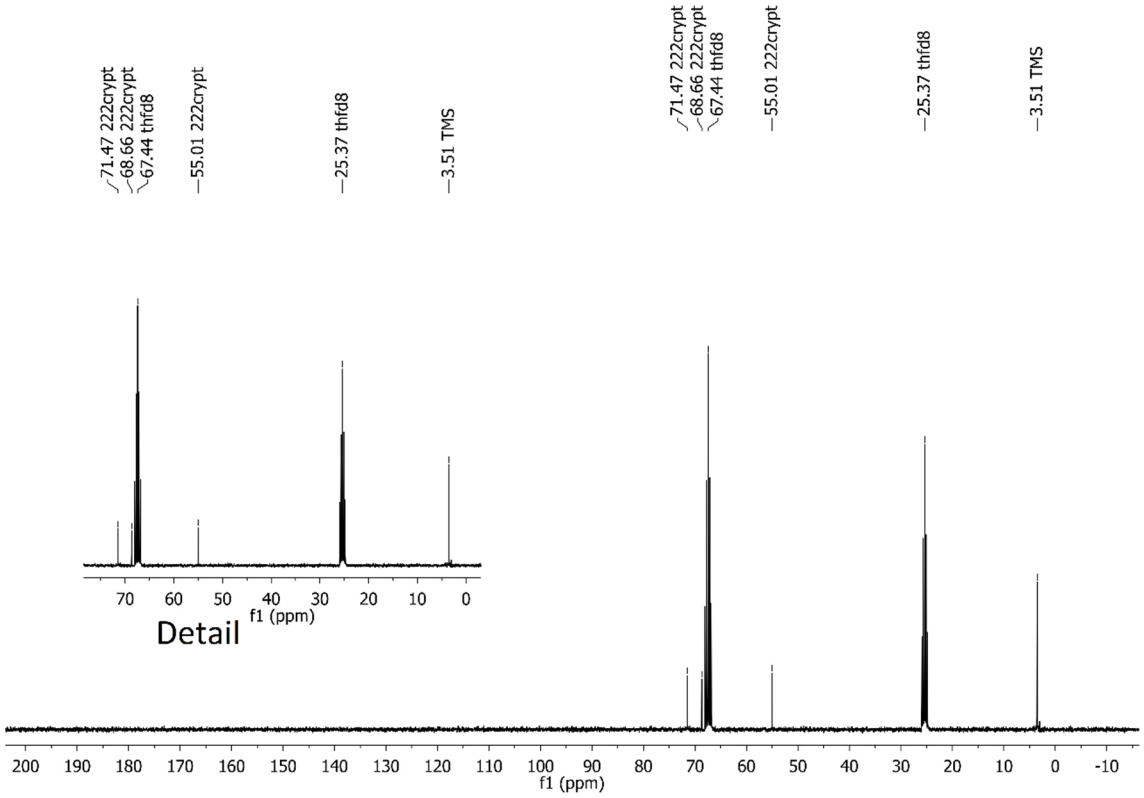

Figure SI 7. ^{13}C{^{1}H} NMR (thf-*d8*) spectrum of the bulk material containing **1a**.

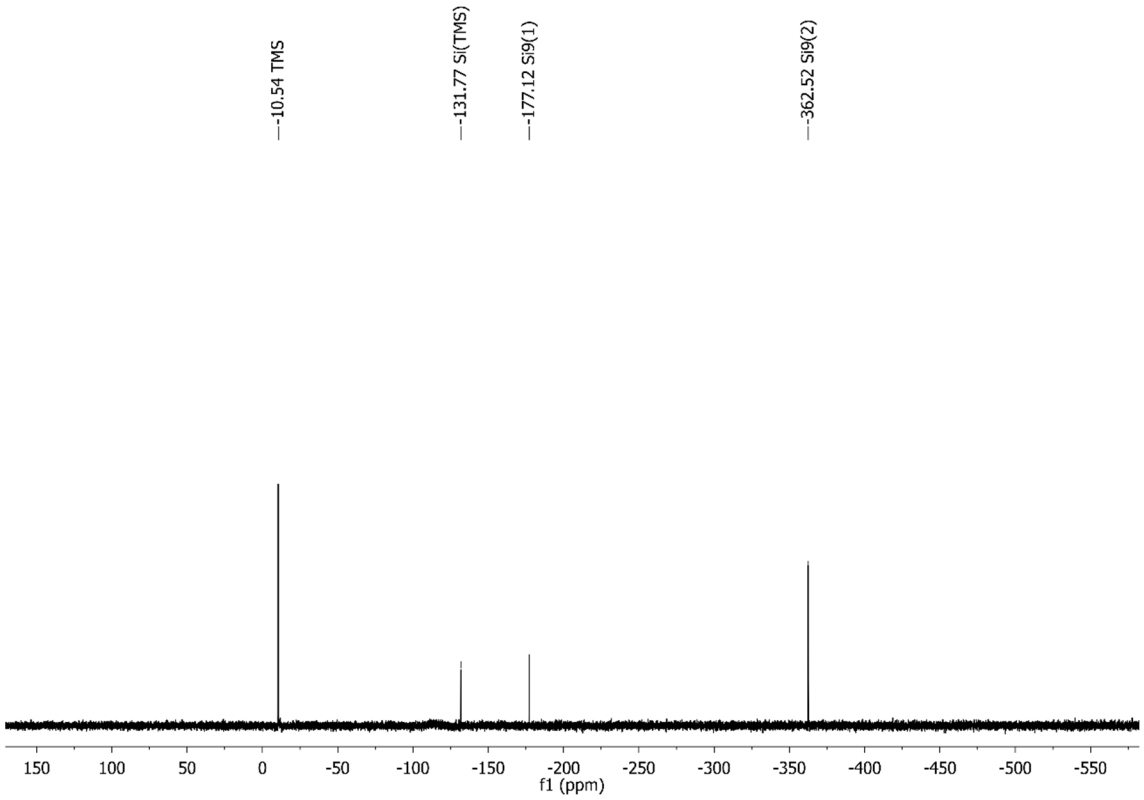

Figure SI 8. $^{29}Si\{^{1}H\}$ NMR (thf-*d8*) spectrum of the bulk material containing **1a**.

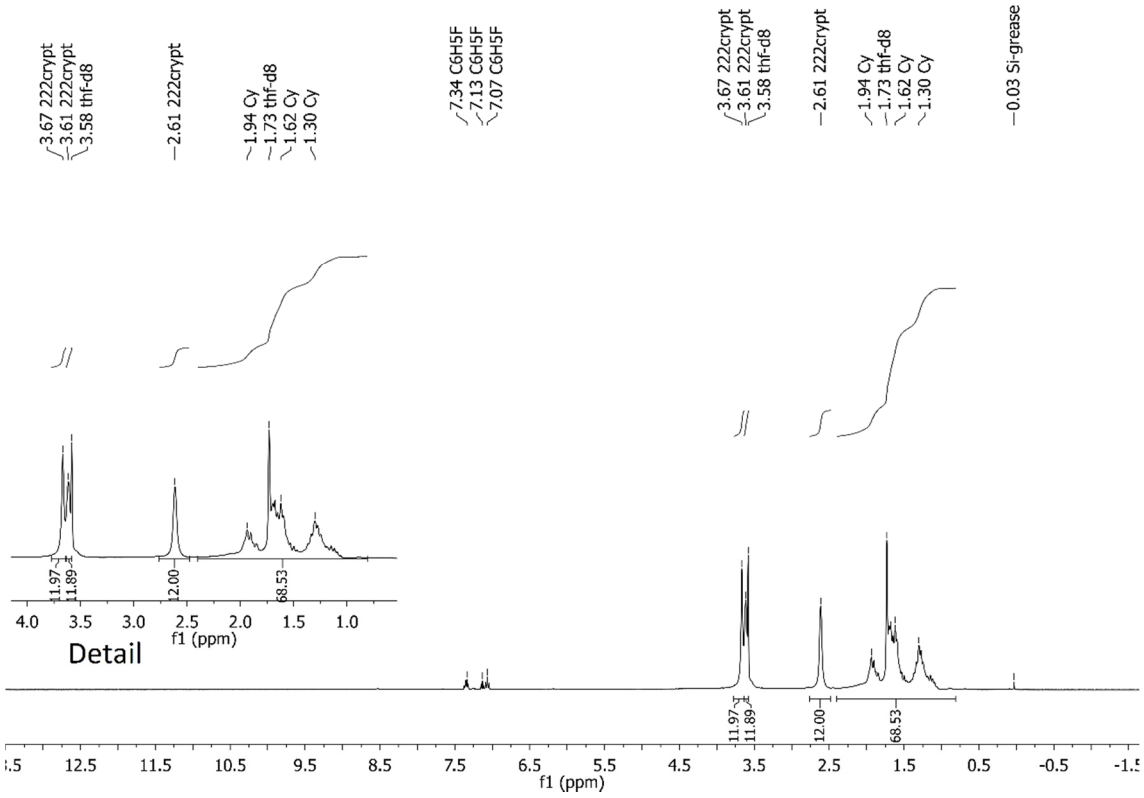

Figure SI 9. ^{1}H NMR (thf-*d8*) spectrum of the bulk material containing **2a**.

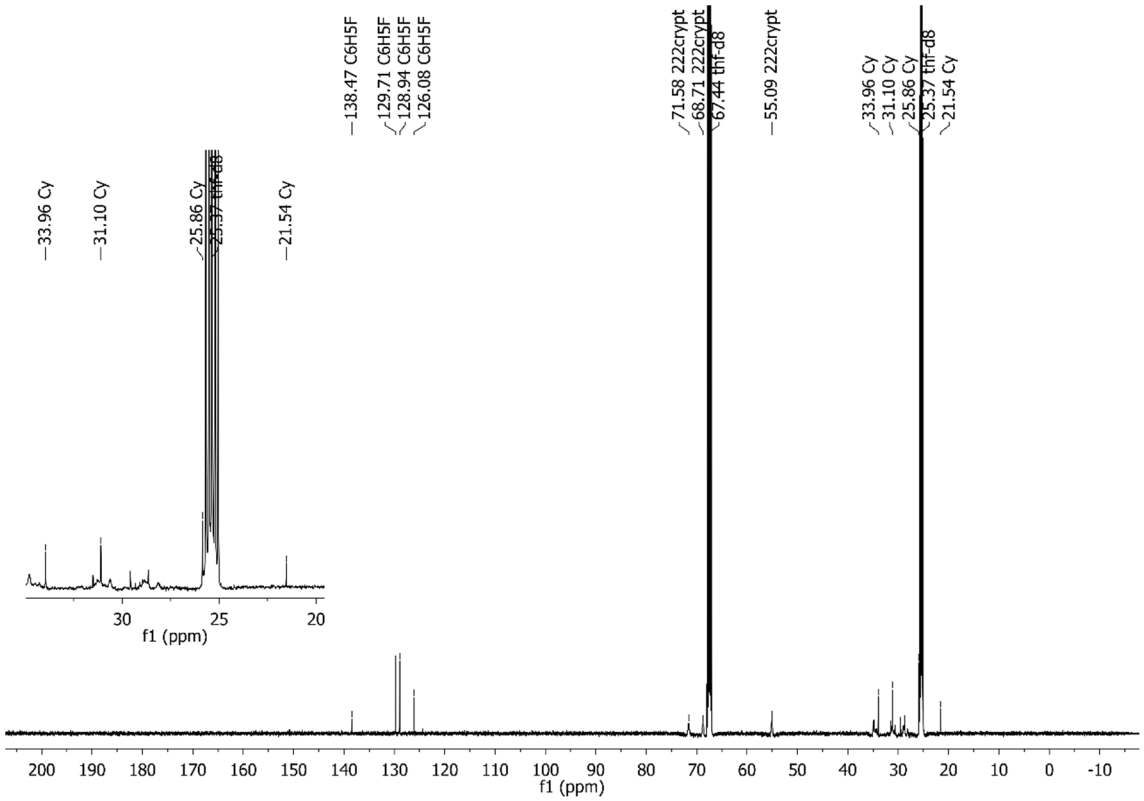

Figure SI 10. $^{13}C\{^{1}H\}$ NMR (thf-*d8*) spectrum of the bulk material containing **2a**.

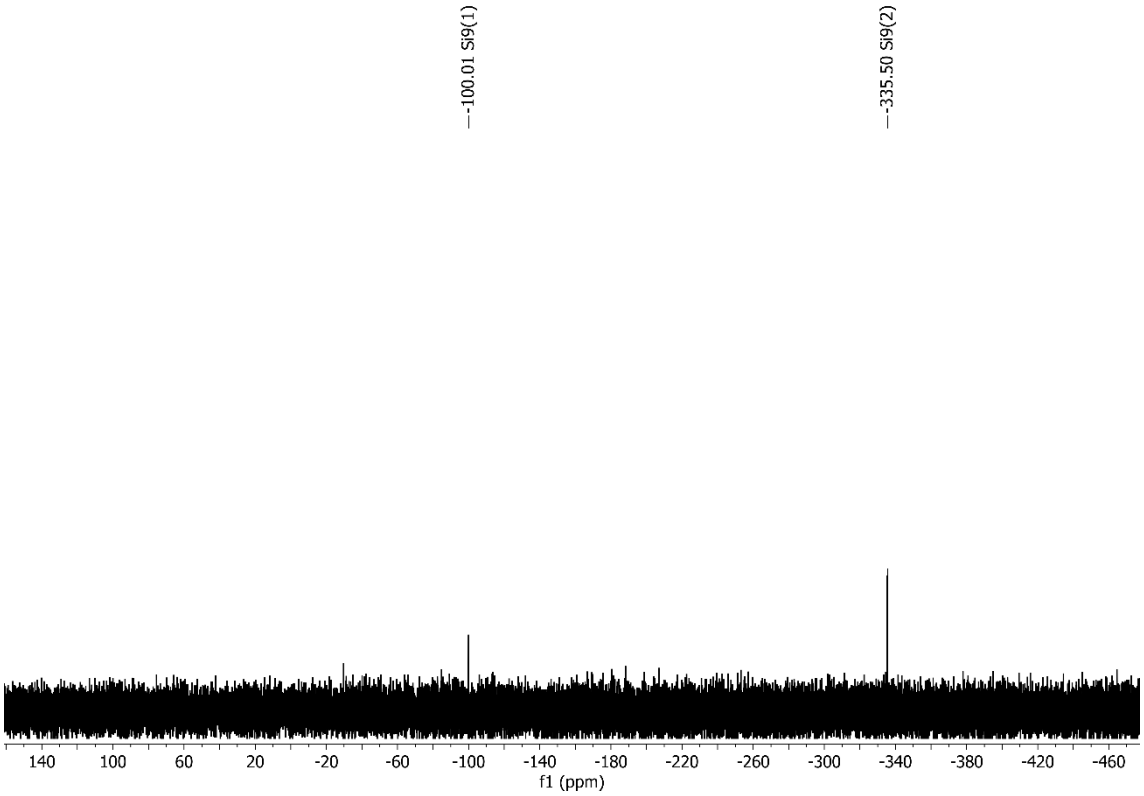

Figure SI 11. $^{29}Si\{^{1}H\}$ NMR (thf-*d8*) spectrum of the bulk material containing **2a**.

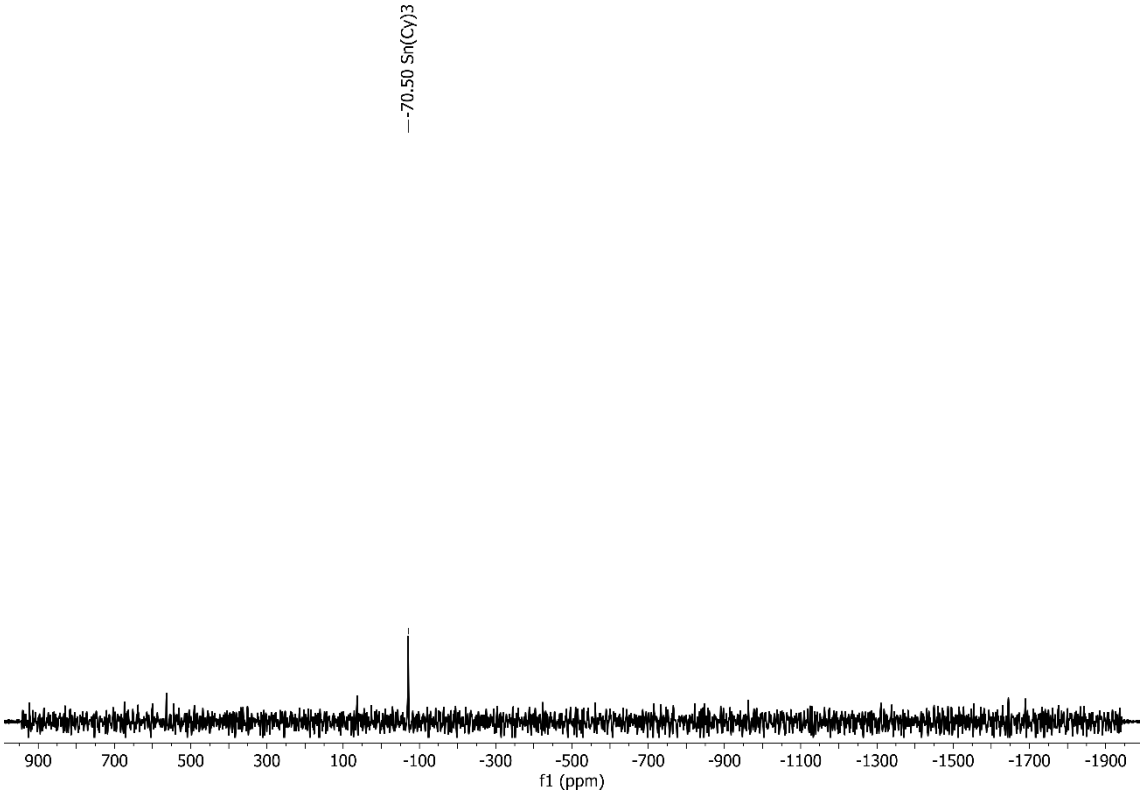

Figure SI 12. $^{119}Sn\{^{1}H\}$ NMR (thf-*d8*) spectrum of the bulk material containing **2a**.

4. Crystallographic details

Table SI 1. Crystallographic data and details of the structure determinations of (K-222crypt)$_2$**1b** and (K-222crypt)$_2$**2b**.

Compound	**(K-222crypt)$_2$1b ·C$_6$H$_5$F**	**(K-222crypt)$_2$2b**
formula	$C_{60}H_{131}FK_2N_4O_{12}Si_{17}$	$C_{72}H_{138}K_2N_4O_{12}Si_9Sn_2$
crystal shape	yellow block	yellow block
crystal size [mm]	0.4 x 0.2 x 0.3	0.4 x 0.2 x 0.1
fw (g·mol^{-1})	1675.41	1820.25
space group (no)	P_n (7)	$C2/c$ (15)
a (Å)	16.4939(9)	31.6324(14)
b (Å)	25.3561(17)	11.8423(7)
c (Å)	22.6197(12)	25.7817(12)
α (deg)	90	90
β (deg)	90.756(4)	108.231(3)
γ (deg)	90	90
V (Å^3)	9459.2(10)	9173.0(8)
Z	4	4
T (K)	120(2)	150(2)
ρ_{calc} (g·cm^{-3})	1.176	1.318
μ (mm^{-1})	0.366	0.806
measured reflections	60136	97474
R_{int}	0.0524	0.1068
	$-20 < h < 20$	$-38 < h < 38$
hkl range	$-27 < k < 29$	$-14 < k < 14$
	$-26 < l < 27$	$-31 < l < 31$
2 θ range	5.416 – 52.000	5.188 – 51.994
independent reflections	24142	9014
reflections [$I > 2\,\sigma(I)$]	12835	5313
parameters / restraints	1892 / 422	511 / 0
R_1 [$I > 2\,\sigma(I)$ / all data]	0.0729 / 0.1411	0.0444 / 0.0978
wR_2 [$I > 2\,\sigma(I)$ / all data]	0.1606 / 0.1880	0.0836 / 0.0997
goodness of fit	0.932	0.928
largest difference peak/hole [e Å^{-3}]	0.925 / −0.448	1.074 / −0.365
CCDC number	1896557	1896556

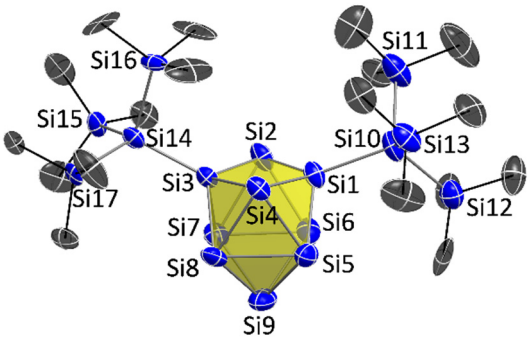

Figure SI 13. Molecular structure of $\{Si(TMS)_3\}_2Si_9^{2-}$ (**1b**) from the single crystal structure determination: Si and C atoms (in blue and black, respectively) are shown as ellipsoids at 50% probability level, H atoms are omitted, minor occupations of the disordered silyl groups are not shown.

Table SI 2. Selected interatomic distances from the single crystal structure determination of $(K\text{-}222crypt)_2$**1b**.

Atom 1	Atom 2	Distance [Å]	Atom 1	Atom 2	Distance [Å]
Si1	Si2	2.396(5)	Si4	Si8	2.488(5)
Si2	Si3	2.395(4)	Si4	Si5	2.485(6)
Si3	Si4	2.398(5)	Si5	Si6	2.772(6)
Si4	Si1	2.427(5)	Si6	Si7	2.569(6)
Si1	Si3	2.992(6)	Si7	Si8	2.738(5)
Si2	Si4	3.759(6)	Si8	Si5	2.585(6)
Si1	Si5	2.415(6)	Si5	Si9	2.468(6)
Si1	Si6	2.425(5)	Si6	Si9	2.470(6)
Si2	Si6	2.446(6)	Si7	Si9	2.427(6)
Si2	Si7	2.521(5)	Si8	Si9	2.475(7)
Si3	Si7	2.418(5)	Si1	Si10	2.357(5)
Si3	Si8	2.401(5)	Si3	Si14	2.339(5)

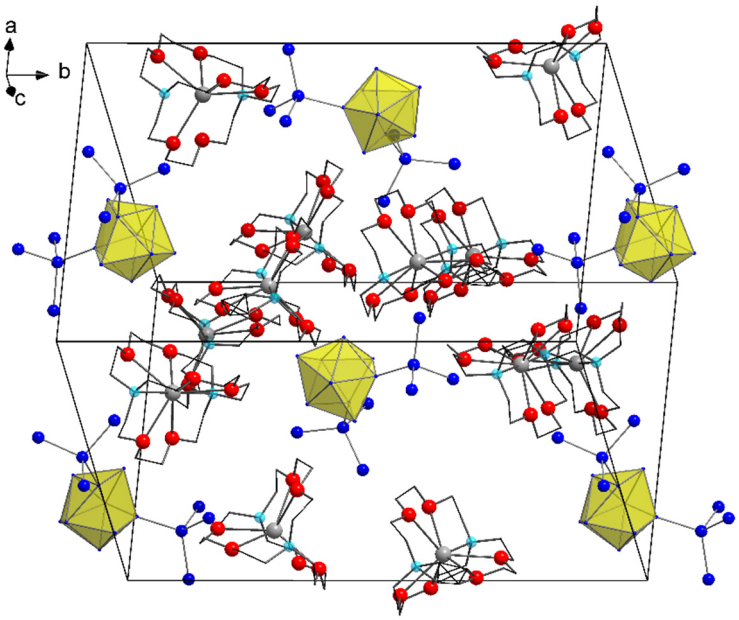

Figure SI 14. Extended unit cell of (K-222crypt)$_2$**1b** [Si_9 clusters are shown as yellow polyhedra, the Si atoms of the $Si(TMS)_3$ substituents (blue), K atoms (gray), O atoms (red), and N atoms (turquoise) are shown as balls, C atoms of 222crypt are shown as wire-sticks, TMS groups and H atoms of 222crypt are omitted].

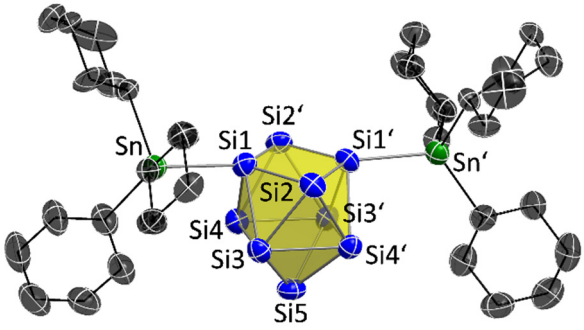

Figure SI 15. Molecular structure of $(SnCy_3)_2Si_9^{2-}$ (**2b**) from the single crystal structure determination: Si, Sn and C atoms (blue, green and black, respectively) are shown as ellipsoids at 50% probability level, H atoms are omitted, minor occupation of the disordered Cy group is not shown, symmetry operation (') −x, y, 0.5−z.

Table SI 3. Selected interatomic distances from the single crystal structure determination of (K-222crypt)$_2$**2b**.

Atom 1	Atom 2	Distance [Å]	Atom 1	Atom 2	Distance [Å]
Si1	Si2	2.430(2)	Si2'	Si4	2.466(2)
Si2	Si1'	2.433(2)	Si3	Si4	2.664(2)
Si1'	Si2'	2.430(2)	Si3'	Si4	2.565(2)
Si2'	Si1	2.433(2)	Si3'	Si4'	2.664(2)
Si1	Si4	2.457(2)	Si3	Si4'	2.565(2)
Si1	Si3	2.456(2)	Si4	Si5	2.436(2)
Si2	Si3	2.478(2)	Si3	Si5	2.432(2)
Si2	Si4'	2.466(2)	Si4'	Si5	2.436(2)
Si1'	Si4'	2.457(2)	Si3'	Si5	2.432(2)
Si1'	Si3'	2.456(2)	Si1	Sn	2.578(1)
Si2'	Si3'	2.478(2)	Si1'	Sn'	2.578(1)

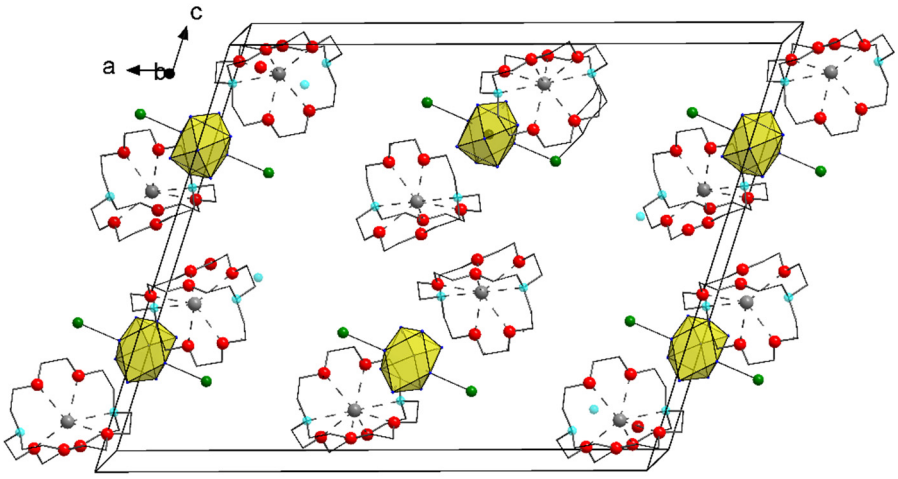

Figure SI 16. Extended unit cell of (K-222crypt)$_2$**2b** [Si_9 clusters are shown as yellow polyhedra, Sn atoms (green), K atoms (gray), O atoms (red), and N atoms (turquoise) are shown as balls, C atoms of 222crypt are shown as wire-sticks, Cy groups and H atoms of 222crypt are omitted].

5. Computational details

Quantum chemical calculations were carried out using the TURBOMOLE program package.[2, 3] We used the PBE0 hybrid density functional method[4, 5] and a triple-zeta-valence quality basis set with polarization functions (def2-TZVP for Si and Sn, def-TZVP for C and H).[6] Multipole-accelerated resolution-of-the-identity technique was used to speed up the calculations.[7-9] The COSMO continuum solvation model was used to counter the twofold negative charge of the dianions.[10] The molecular structures of the di- and tri-substituted clusters were fully optimized within C_{2v} and C_{3v} point group symmetry, respectively. In the 0 K calculations, the symmetry of the tri-substituted clusters is reduced from the ideal D_{3h} to C_{3v} because the ligands cannot rotate freely, but this does not affect the interpretation of the results. A hypothetical tetra-substituted cluster $\{Si(TMS)_3\}_4Si_9$ was optimized without any symmetry constraints. The optimized structures of the studied systems in XYZ format are reported below. Harmonic frequency calculations were carried out to confirm that the structures are true local minima (numerical frequency calculation with the COSMO solvent model). The structure **1b** had three imaginary vibrational modes corresponding to a rotation of methyl and TMS groups (140*i*, 63*i*, 55*i*). The rotational imaginary modes disappear by lowering the point group symmetry to C_2 (the ligands retain the same overall orientation as in the C_{2v} point group). In the Raman spectrum calculations (T = 298.15 K, experimental laser wavelength, unpolarized radiation, scattering angle of 90°),[11, 12] the COSMO solvent model was not used in the dynamic polarizability derivatives calculation. The Raman intensities are given relative to the most intensive peak. The harmonic frequencies of **2b** were scaled by a factor of 0.985 to facilitate comparisons with the experimental spectrum. The final Raman spectra were convoluted using Lorenzian peak profiles with FWHM of 10 cm^{-1}. The peak assignment was carried out by visual inspection of the normal modes (Jmol program package[13]). Intrinsic Atomic Orbitals (IAOs) and Intrinsic Bond Orbitals (IBO) were used to analyze the partial charges and bonding of the clusters, respectively.[14]

Table SI 4. Analysis of the Intrinsic Bond Orbitals (IBO) for **1a**. For each IBO, the atoms forming the IBO and their contributions in percentages are shown (in most cases, the contributions do not add up to 100%, because small contributions from other atoms are not listed separately). Each IBO contains two electrons. For the numbering scheme, see the figure below ([a] not a cluster atom).

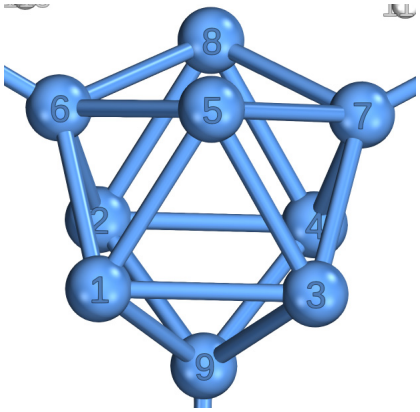

Atom 1	%	Atom 2	%	Atom 3	%
Lone pairs (12 electrons in total)					
1	91				
2	91				
4	91				
5	91				
8	91				
9	91				
Exo-bonds (6 electrons in total)					
9	51	[a]	46		
7	51	[a]	46		
6	51	[a]	46		
3c–2e bonds in trigonal prism faces (4 electrons in total)					
5	33	3	33	1	33
8	33	2	33	4	33
5c–6e system of the three trigonal prism faces and their capping atoms (18 electrons in total)					
6	46	2	31	8	18
6	49	5	33	8	9
6	47	1	35	8	9

Table SI 5. Analysis of the Intrinsic Bond Orbitals (IBO) for **1b**. For each IBO, the atoms forming the IBO and their contributions in percentages are shown (in most cases, the contributions do not add up to 100%, because small contributions from other atoms are not listed separately). Each IBO contains two electrons. For the numbering scheme, see the figure below ([a] not a cluster atom).

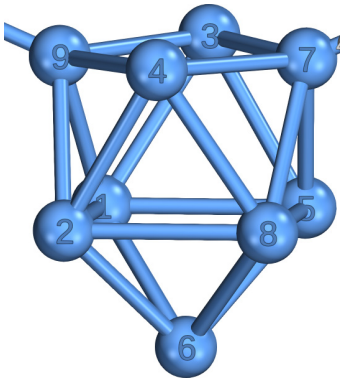

Atom 1	%	Atom 2	%	Atom 3	%
Lone pairs (14 electrons in total)					
1	94				
2	93				
3	93				
4	92				
5	92				
6	92				
8	92				
Exo-bonds (4 electrons in total)					
9	51	[a]	46		
7	51	[a]	46		
3c–2e bonds with one open-square atom and two closed square atoms (8 electrons in total)					
7	41	5	29	8	28
9	42	1	29	2	27
3	34	5	32	1	32
4	36	8	31	2	29
2c–2e bonds in open square, minor contribution from one closed square atom (8 electrons in total)					
9	48	4	39	2	6
7	48	4	39	8	6
7	49	3	39	5	5
9	49	3	39	1	5
5c–6e system of cap atom and the closed square (6 electrons in total)					
6	38	8	36	2	19
6	39	1	36	2	16
6	38	5	38	2	8

Table SI 6. Optimized XYZ coordinates of the studied systems [Å].

$\{Si(TMS)_3\}_2Si_9^{2-}$ (**1b**)				$(SnCy_3)_2Si_9^{2-}$ (**2b**)				$\{Si(TMS)_3\}_4Si_9$			
Si	-1.2743517	1.3358186	-3.1399453	Si	-1.2753634	1.344217	-2.7316151	Si	-0.3138832	0.7008659	1.0506022
Si	-1.2743517	-1.3358186	-3.1399453	Si	-1.2753634	-1.344217	-2.7316151	Si	-0.5741312	0.7450059	-2.5078788
Si	0	1.8459512	-1.0760077	Si	0	1.8552706	-0.6760474	Si	-0.5750799	-1.7152433	0.7111365
Si	0	-1.8459512	-1.0760077	Si	0	-1.8552706	-0.6760474	Si	-0.756453	-1.6634308	-2.0380319
Si	1.2743517	1.3358186	-3.1399453	Si	1.2753634	1.344217	-2.7316151	Si	1.7971899	-0.4427737	0.5577963
Si	0	0	-4.7236547	Si	0	0	-4.3102175	Si	1.0184658	1.4641647	-0.812898
Si	1.5434157	0	-1.1356343	Si	1.5380697	0	-0.7249815	Si	1.1733504	-2.3001762	-0.7980015
Si	1.2743517	-1.3358186	-3.1399453	Si	1.2753634	-1.344217	-2.7316151	Si	1.5677971	-0.4159911	-2.1895272
Si	-1.5434157	0	-1.1356343	Si	-1.5380697	0	-0.7249815	Si	-1.8768885	-0.0947712	-0.6231421
Si	3.7086121	0	-0.1981656	C	-5.0755216	0	-2.2975266	Si	2.3407775	-4.3215179	-0.9723541
Si	-3.7086121	0	-0.1981656	C	-5.8903127	-1.2548252	-2.6003642	Si	-4.1983681	-0.2052228	-1.150224
C	2.4237878	-1.9665689	2.416639	C	-5.8903127	1.2548252	-2.6003642	Si	2.3044001	3.3246248	-1.5607163
H	2.4171276	-2.9266684	2.9435383	H	-4.2008555	0	-2.9622829	C	4.7673778	-3.1875098	-3.2352091
H	2.5500531	-1.1739079	3.1577716	C	-6.378622	-1.2601555	-4.0487166	H	5.800384	-2.8753199	-3.4207675
H	1.4524988	-1.8301103	1.9340826	H	-6.7629604	-1.3009855	-1.9359048	H	4.5288542	-3.9945282	-3.9323332
C	2.4237878	1.9665689	2.416639	H	-5.3010975	-2.1574519	-2.4046945	H	4.110819	-2.3405517	-3.4508895
H	2.5500531	1.1739079	3.1577716	C	-6.378622	1.2601555	-4.0487166	C	1.183006	-4.431221	-4.287625
H	2.4171276	2.9266684	2.9435383	H	-6.7629604	1.3009855	-1.9359048	H	2.1522569	-4.0556817	-4.6224229
H	1.4524988	1.8301103	1.9340826	H	-5.3010975	2.1574519	-2.4046945	H	0.7417891	-5.0144234	-5.1027541
C	-2.4237878	1.9665689	2.416639	C	-7.1736172	0	-4.372602	H	0.5322742	-3.5748091	-4.0915075
H	-2.4171276	2.9266684	2.9435383	H	-6.9863387	-2.1515343	-4.2407083	C	-3.397398	-0.6809466	-4.6540158
H	-2.5500531	1.1739079	3.1577716	H	-5.5086598	-1.3209321	-4.7153339	H	-3.7576653	-1.1194529	-5.5914071
H	-1.4524988	1.8301103	1.9340826	H	-6.9863387	2.1515343	-4.2407083	H	-3.4042183	0.4059735	-4.7585025
C	-2.4237878	-1.9665689	2.416639	H	-5.5086598	1.3209321	-4.7153339	H	-2.3658564	-0.9988614	-4.4953278
H	-2.5500531	-1.1739079	3.1577716	H	-7.4743404	0	-5.4256289	C	-4.2738515	2.7999208	-2.9522751
H	-2.4171276	-2.9266684	2.9435383	H	-8.0998357	0	-3.7827334	H	-4.7024052	2.3108281	-3.8305392
H	-1.4524988	-1.8301103	1.9340826	C	5.0755216	0	-2.2975266	H	-4.5398524	3.8612686	-2.9919859
C	-3.6263509	-3.487787	0.0683775	C	5.8903127	1.2548252	-2.6003642	H	-3.1857386	2.7165578	-3.0155847
H	-4.4738061	-3.6054391	-0.6110065	C	5.8903127	-1.2548252	-2.6003642	C	0.0355155	4.5506996	-3.9724275
H	-2.7141388	-3.4292675	-0.5319469	H	4.2008555	0	-2.9622829	H	-0.74857	5.2725628	-4.224242
H	-3.5704276	-4.3797596	0.701547	C	6.378622	1.2601555	-4.0487166	H	0.8078778	4.609611	-4.7432741
C	-5.4531005	-2.0802038	2.0601931	H	6.7629604	1.3009855	-1.9359048	H	-0.3991971	3.5481619	-3.9967306
H	-6.2960268	-2.1309331	1.366389	H	5.3010975	2.1574519	-2.4046945	C	2.7742571	1.9396216	-4.8559195
H	-5.4626558	-2.9899159	2.6700776	C	6.378622	-1.2601555	-4.0487166	H	1.9538906	2.565197	-5.2139166
H	-5.613293	-1.2277826	2.7250504	H	6.7629604	-1.3009855	-1.9359048	H	3.4863453	1.8068717	-5.6779797
C	-5.4531005	2.0802038	2.0601931	H	5.3010975	-2.1574519	-2.4046945	H	2.3692786	0.9628074	-4.5869849
H	-5.613293	1.2277826	2.7250504	C	7.1736172	0	-4.372602	C	4.4022019	4.3474203	-4.0998782
H	-5.4626558	2.9899159	2.6700776	H	6.9863387	2.1515343	-4.2407083	H	4.9550427	4.9177437	-3.3523039
H	-6.2960268	2.1309331	1.366389	H	5.5086598	1.3209321	-4.7153339	H	5.0895242	4.1000952	-4.916146
C	-3.6263509	3.487787	0.0683775	H	6.9863387	-2.1515343	-4.2407083	H	3.618967	4.9905548	-4.5095504
H	-2.7141388	3.4292675	-0.5319469	H	5.5086598	-1.3209321	-4.7153339	C	5.0880793	1.6270116	-2.8682209
H	-4.4738061	3.6054391	-0.6110065	H	7.4743404	0	-5.4256289	H	5.7118822	2.1101744	-2.111971
H	-3.5704276	4.3797596	0.701547	H	8.0998357	0	-3.7827334	H	4.7058681	0.6920461	-2.451259
C	3.6263509	-3.487787	0.0683775	C	-4.4732429	1.8528295	0.7841204	H	5.7225505	1.3832961	-3.7266335
H	2.7141388	-3.4292675	-0.5319469	C	-5.930465	2.2257651	1.0526443	C	1.5584602	6.6434934	-2.3762868
H	4.4738061	-3.6054391	-0.6110065	C	-3.6669867	1.8916967	2.0822177	H	2.4062417	6.6328057	-3.0654906
H	3.5704276	-4.3797596	0.701547	H	-4.0519982	2.6107045	0.107916	H	0.8343247	7.3778625	-2.7447099
C	5.4531005	-2.0802038	2.0601931	C	-6.036144	3.5916436	1.7324847	H	1.9172512	6.9858097	-1.4030667

H	5.4626558	-2.9899159	2.6700776
H	6.2960268	-2.1309331	1.366389
H	5.613293	-1.2277826	2.7250504
C	5.4531005	2.0802038	2.0601931
H	6.2960268	2.1309331	1.366389
H	5.4626558	2.9899159	2.6700776
H	5.613293	1.2277826	2.7250504
C	3.6263509	3.487787	0.0683775
H	4.4738061	3.6054391	-0.6110065
H	2.7141388	3.4292675	-0.5319469
H	3.5704276	4.3797596	0.701547
Si	-3.8100533	-1.9511219	1.1415814
Si	-3.8100533	1.9511219	1.1415814
Si	3.8100533	1.9511219	1.1415814
Si	3.8100533	-1.9511219	1.1415814
Si	-5.4744897	0	-1.7733414
Si	5.4744897	0	-1.7733414
C	-7.1542498	0	-0.8869672
H	-7.7335085	0.8840649	-1.1683378
H	-7.7335085	-0.8840649	-1.1683378
H	-7.0558143	0	0.2001049
C	7.1542498	0	-0.8869672
H	7.7335085	-0.8840649	-1.1683378
H	7.7335085	0.8840649	-1.1683378
H	7.0558143	0	0.2001049
C	-5.3926925	-1.5376598	-2.8629191
H	-5.6042259	-2.4376295	-2.2804984
H	-6.1389061	-1.4662583	-3.6616264
H	-4.4024784	-1.6494906	-3.3130478
C	-5.3926925	1.5376598	-2.8629191
H	-6.1389061	1.4662583	-3.6616264
H	-5.6042259	2.4376295	-2.2804984
H	-4.4024784	1.6494906	-3.3130478
C	5.3926925	1.5376598	-2.8629191
H	5.6042259	2.4376295	-2.2804984
H	6.1389061	1.4662583	-3.6616264
H	4.4024784	1.6494906	-3.3130478
C	5.3926925	-1.5376598	-2.8629191
H	6.1389061	-1.4662583	-3.6616264
H	5.6042259	-2.4376295	-2.2804984
H	4.4024784	-1.6494906	-3.3130478

H	-6.3916427	1.4766218	1.7080342
H	-6.5120522	2.2298969	0.1264404
C	-3.7625999	3.2557437	2.7615302
H	-4.0503566	1.1265048	2.7710814
H	-2.6189885	1.6344938	1.8897541
C	-5.2147019	3.644373	3.0155615
H	-7.0850574	3.8272806	1.944338
H	-5.6737124	4.361916	1.0394857
H	-3.1997287	3.252161	3.7016502
H	-3.2936704	4.0088996	2.1151344
H	-5.2709811	4.6426676	3.4620784
H	-5.6477015	2.9492764	3.7469253
C	-4.4732429	-1.8528295	0.7841204
C	-3.6669867	-1.8916967	2.0822177
C	-5.930465	-2.2257651	1.0526443
H	-4.0519982	-2.6107045	0.107916
C	-3.7625999	-3.2557437	2.7615302
H	-4.0503566	-1.1265048	2.7710814
H	-2.6189885	-1.6344938	1.8897541
C	-6.036144	-3.5916436	1.7324847
H	-6.3916427	-1.4766218	1.7080342
H	-6.5120522	-2.2298969	0.1264404
C	-5.2147019	-3.644373	3.0155615
H	-3.1997287	-3.252161	3.7016502
H	-3.2936704	-4.0088996	2.1151344
H	-7.0850574	-3.8272806	1.944338
H	-5.6737124	-4.361916	1.0394857
H	-5.2709811	-4.6426676	3.4620784
H	-5.6477015	-2.9492764	3.7469253
C	4.4732429	1.8528295	0.7841204
C	3.6669867	1.8916967	2.0822177
C	5.930465	2.2257651	1.0526443
H	4.0519982	2.6107045	0.107916
C	3.7625999	3.2557437	2.7615302
H	4.0503566	1.1265048	2.7710814
H	2.6189885	1.6344938	1.8897541
C	6.036144	3.5916436	1.7324847
H	6.3916427	1.4766218	1.7080342
H	6.5120522	2.2298969	0.1264404
C	5.2147019	3.644373	3.0155615
H	3.1997287	3.252161	3.7016502
H	3.2936704	4.0088996	2.1151344
H	7.0850574	3.8272806	1.944338
H	5.6737124	4.361916	1.0394857
H	5.2709811	4.6426676	3.4620784
H	5.6477015	2.9492764	3.7469253
C	4.4732429	-1.8528295	0.7841204
C	5.930465	-2.2257651	1.0526443
C	3.6669867	-1.8916967	2.0822177
H	4.0519982	-2.6107045	0.107916

C	-0.7048758	5.0605775	-1.0582197
H	-1.2215759	4.1003589	-0.982593
H	-0.3659926	5.3448925	-0.0597628
H	-1.428512	5.8075995	-1.4000336
C	-4.3244096	3.0883498	0.0864603
H	-4.797256	2.776435	1.0200974
H	-3.2418648	3.0168355	0.213357
H	-4.5767308	4.1396071	-0.0854733
C	-6.8081663	2.1247603	-1.377676
H	-7.2336194	1.7612338	-0.4389159
H	-7.1235168	3.1654218	-1.5081526
H	-7.2345398	1.5378448	-2.1939263
C	-6.2816773	-0.8352832	-3.8258888
H	-6.3746004	0.2264952	-4.0676069
H	-6.501673	-1.4036305	-4.7361831
H	-7.0390402	-1.0834008	-3.0807693
C	-4.3908948	-3.1274886	-3.1161994
H	-3.4010871	-3.4193318	-2.7570315
H	-5.1400549	-3.5343427	-2.4328746
H	-4.547083	-3.583414	-4.0995369
C	5.1844698	-2.3555289	-0.3257038
H	4.6104132	-1.4397875	-0.4884078
H	5.096367	-2.621706	0.7299551
H	6.2369557	-2.1405628	-0.5385939
C	5.683622	-5.2514195	-1.1698584
H	6.7147167	-5.0114309	-1.4496447
H	5.6831463	-5.5572138	-0.1206084
H	5.3595667	-6.1032705	-1.7728744
C	2.428941	-6.9955837	-3.1799968
H	2.5656089	-7.6545647	-2.3192099
H	1.9613618	-7.577197	-3.981271
H	3.4165819	-6.6802951	-3.5264035
C	-0.3661097	-6.123556	-2.2684133
H	-0.3171126	-6.8340059	-1.4397137
H	-1.0076119	-5.2905989	-1.9691276
H	-0.8365077	-6.6272954	-3.1191211
Si	3.6748566	4.2342418	0.1443873
Si	2.1346847	-5.4381719	1.1092308
Si	-5.5243186	-1.3951195	0.4160382
Si	0.7266521	4.9554009	-2.270263
Si	3.6784033	2.7441466	-3.4173351
Si	4.5933021	-3.7420477	-1.4473988
Si	1.3431562	-5.5160052	-2.761315
Si	-4.5284007	-1.2571159	-3.2678117
Si	-4.9258576	2.046341	-1.3565056
C	-7.2151601	-1.7896795	-0.3164008
H	-7.1464883	-2.4760224	-1.1631361
H	-7.8229698	-2.2720864	0.456816
H	-7.7413717	-0.8899651	-0.6436326
C	5.0092565	5.3590313	-0.5627952

C	6.036144	-3.5916436	1.7324847
H	6.3916427	-1.4766218	1.7080342
H	6.5120522	-2.2298969	0.1264404
C	3.7625999	-3.2557437	2.7615302
H	4.0503566	-1.1265048	2.7710814
H	2.6189885	-1.6344938	1.8897541
C	5.2147019	-3.644373	3.0155615
H	7.0850574	-3.8272806	1.944338
H	5.6737124	-4.361916	1.0394857
H	3.1997287	-3.252161	3.7016502
H	3.2936704	-4.0088996	2.1151344
H	5.2709811	-4.6426676	3.4620784
H	5.6477015	-2.9492764	3.7469253
Sn	-4.1029826	0	-0.3312075
Sn	4.1029826	0	-0.3312075

H	5.5493627	5.8231413	0.2695066
H	5.7340032	4.8035042	-1.1622633
H	4.5907202	6.157782	-1.179276
C	2.8361145	-7.1772407	0.9464163
H	3.8770575	-7.1691396	0.6152735
H	2.7932555	-7.6784558	1.9190389
H	2.2576096	-7.7735703	0.2362082
C	2.6194958	5.2915913	1.2905116
H	3.1997038	5.6053034	2.1636933
H	2.2878691	6.1918964	0.7668222
H	1.7306269	4.7654612	1.6424511
C	4.5396315	2.8488817	1.0752522
H	5.2475884	2.3420031	0.4138778
H	5.0964754	3.2478693	1.9288077
H	3.8365619	2.0977927	1.4401188
C	3.101169	-4.5024674	2.4227974
H	2.9531179	-4.9751821	3.3990763
H	4.1722339	-4.5040468	2.2051477
H	2.771557	-3.4626572	2.4936687
C	0.337303	-5.5698689	1.6395258
H	-0.2530831	-6.1371618	0.9163555
H	0.2810819	-6.0844591	2.6044887
H	-0.1205993	-4.5836041	1.7501894
C	-4.707908	-3.029848	0.8592523
H	-5.2561732	-3.5144415	1.6734404
H	-4.7152834	-3.7012283	-0.0032132
H	-3.6697915	-2.9016364	1.1708697
C	-5.8276727	-0.3432538	1.944413
H	-6.4539113	0.5174562	1.6945797
H	-6.34872	-0.9298906	2.7077922
H	-4.8996181	0.0296424	2.3774706
Si	-0.3478224	1.0223006	3.4490829
Si	-1.2477162	-0.8666518	4.6016049
Si	1.7935345	1.3578834	4.4691071
Si	-1.6914262	2.9136182	3.9657574
C	2.4299373	3.1003855	4.1847355
H	2.6277931	3.2965292	3.1322672
H	1.7240743	3.8530922	4.5435909
H	3.3692163	3.2298265	4.732621
C	-3.5126727	2.4584524	3.8666625
H	-3.7688971	2.0459759	2.889742
H	-3.7787324	1.720564	4.6274562
H	-4.1278287	3.3492556	4.0296579
C	0.0248111	-2.2481996	4.6960391
H	0.3369006	-2.566653	3.6986914
H	0.9142576	-1.9466126	5.2537265
H	-0.4173957	-3.1107457	5.2053906
C	-2.8291643	-1.5413231	3.8578149
H	-3.6474728	-0.8276071	3.9662854
H	-2.714206	-1.78216	2.8010891

H	-3.1084965	-2.4571282	4.3894056
C	-1.3402274	4.3314113	2.7847043
H	-0.3067943	4.6740339	2.8782811
H	-1.5084992	4.0445407	1.744952
H	-1.9979701	5.1759879	3.0140219
C	3.123943	0.1296989	3.9698685
H	2.7967832	-0.9012396	4.121778
H	3.4179772	0.2319364	2.924681
H	4.0025847	0.306862	4.5999629
C	-1.7045478	-0.3463639	6.3567945
C	1.5843779	1.1604589	6.3332705
C	-1.3515077	3.5183563	5.716822
H	1.3767918	0.126919	6.6172661
H	-1.5391983	2.7423038	6.4620327
H	-2.0733201	-1.2326081	6.8850579
H	-2.0215962	4.3581215	5.9300048
H	0.8010218	1.7982616	6.7458435
H	-0.8677097	0.0604737	6.9242031
H	-2.5087186	0.393507	6.3528259
H	2.5334372	1.4488024	6.7986696
H	-0.3250267	3.8704857	5.8393604

6. References

1. C. Hoch, M. Wendorff and C. Röhr, *J. Alloys Compd.*, 2003, **361**, 206.
2. TURBOMOLE V7.3 2018, a development of University of Karlsruhe and Forschungszentrum Karlsruhe GmbH, 1989-2007, TURBOMOLE GmbH, since 2007.
3. R. Ahlrichs, M. Bär, M. Häser, H. Horn and C. Kölmel, *Chem. Phys. Lett.*, 1989, **162**, 165.
4. J. P. Perdew, K. Burke and M. Ernzerhof, *Phys. Rev. Lett.*, 1996, **77**, 3865.
5. C. Adamo and V. J. Barone, *J. Chem. Phys.*, 1999, **110**, 6158.
6. F. Weigend and R. Ahlrichs, *Phys. Chem. Chem. Phys.*, 2005, **7**, 3297
7. K. Eichkorn, O. Treutler, H. Öhm, M. Häser and R. Ahlrichs, *Chem. Phys. Lett.*, 1995, **240**, 283.
8. F. Weigend, *Phys. Chem. Chem. Phys.*, 2006, **8**, 1057.
9. M. Sierka, A. Hogekamp and R. Ahlrichs, *J. Chem. Phys.* , 2003, **118**, 9136.
10. A. Klamt and G. Schüürmann, *J. Chem. Soc., Perkin Trans. 2*, 1993, 799.
11. D. Rappoport and F. Furche, *J. Chem. Phys.*, 2007, **126**, 201104.
12. F. Furche and R. Ahlrichs, *J. Chem. Phys.*, 2002, **117**, 7433.
13. Jmol: an open-source Java viewer for chemical structures in 3D. http://www.jmol.org/.
14. G. Knizia, *J. Chem. Theory. Comput.*, 2013, **9**, 4834.